STRENGTHENING PRESTRESSED BEAMS USING PARAFIL ROPES AS EXTERNAL TENDONS

BY

AHMED HASSAN AHMED GHALLAB

B.Sc., M.Sc.

Submitted in accordance with the requirements for the degree of
Doctor of Philosophy

The University of Leeds

School of Civil Engineering

April, 2001

The candidate confirms that the work submitted is his own and that appropriate credit has been given where reference has been made to the work of others.

ACKNOWLEDGEMENTS

First words and foremost thanks to Allah, the most beneficent and merciful.

I will never be able to express my sincere appreciation and deepest thanks and gratitude to Professor A. W. Beeby, BSc., PhD, Ceng, MICE, MIStructE for his continuous guidance, supervision, valuable suggestions, encouragement and understanding throughout the research period and preparation of the thesis.

My deep thanks go to Mr. R. Bell, Mr. P. Richard, and Mr. M. Marsden for their technical advice and help during the testing and their valuable discussion.

I would like also to thank Mr. P. Flatt, and Mr. S. Holmes who helped in the preparation of the specimens and casting.

My appreciation and thanks are due to Mrs. D. Carr and Mr. J. Drake and all who offered me any direct or indirect assistance throughout the duration of research.

My special thanks to Mr. A. Badr, E. Etman and G.Ismail for the valuable discussion and the help they offered. Thanks go also to all my colleagues and friends, who I could not mention by name here because of the limited space, for their encouragement and support throughout the research period.

My appreciation to Linear Composite Limited for providing Parafil rope used in this research.

My appreciation and thanks are due to the Egyptian Government for providing the grant required for this study.

No words can express my thanks to my parents, whom I will never appreciate their rights what ever I do, my wife for her patience, understanding and encouragement, and my parents in law for their love and prayers.

Finally, my thanks go to my kids, Amr and Osama for their forgiveness for consuming their time during my study.

ABSTRACT

Many bridges in the world are classified as deficient and in need of rehabilitation or replacement. Some of them are deficient because their load-carrying capacity is inadequate for today's increased traffic load. To improve their efficiency and increase their load capacity, several methods can be used, one of them is the external prestressing. Also, to avoid corrosion problem that faced this type of strengthening, Fibre Reinforced Plastics (FRP) can be used instead of steel tendons. Within the different types of FRP, Parafil rope was established to be well suited for prestressing system, combining the benefits of light-weight, high strength, easy handling and efficient anchorage system.

Thirteen prestressed beams, one with internal prestressing steel only, and the rest strengthened externally using Parafil Ropes Type G were tested up to failure under two third point loading. Six factors were studied to investigate their effect on the behaviour of strengthened beams. These factors are the value of the external prestressing force and its eccentricity, deviator position, previous loading stage before strengthening, concrete strength and (span/depth) ratio. Also, analytical investigations were conducted to propose simple equations could be used in the analysis of this beam type, regarding its deflection and flexural strength with an acceptable accuracy.

The study indicated that, external prestressing using Parafil rope is a very powerful system for strengthening or rehabilitation of prestressed concrete structures. Also, providing external prestressing force by a moderate amount improves the stiffness, and both cracking and ultimate flexural strength of prestressed concrete beams without significant reduction in ductility even for cracked beams.

The modifications made to the methods used to calculate deflection and ultimate moment of bonded prestressed concrete, generalised these methods so, they can be used with beams have different types of prestressing tendons (bonded, internal unbonded, external unbonded or mixture of them). These methods, after modification, were found to give fairly accurate results.

Also, the novel equation described the relation between the increase in the external prestressing force and the deflection makes the analysis of the externally strengthened beams under service loads, less complicated with a reasonable accuracy.

TABLE OF CONTENTS

LIST OF FIGURES

Chapter 2: Literature Review

Chapter 3: Experimental Programme

Chapter 4: Test Results

Chapter 5: Discussion of Test Results

Chapter 6: Theoretical Analysis

LIST OF TABLES

Chapter 2: Literature Review

Chapter 3: Experimental Programme

Chapter 4: Test Results

Chapter 6: Theoretical Analysis

NOTATIONS

A_c = cross-sectional area of concrete;

A_e = area of external prestressing tendons

A_{ps} = area of internal prestressing steel

$$A_{ps.\text{int}} = A_{ps} + A_s \frac{f_{ys}}{f_{py}}$$

$$A_{ps.tot} = A_{ps,\text{int}} + A_e \frac{E_{pp}}{E_{ps}}$$

A_s = area of nonprestressed tensile steel

$A_{s'}$ = area of nonprestressed compressive steel

b_w = width of the web

B = width of the flange

c = depth from concrete extreme compressive fiber to neutral axis

d_e = depth from concrete extreme compressive fiber to centroid of external prestressing rope

d_{eu} = depth from concrete extreme compressive fiber to centroid of external prestressing rope at ultimate

d_p = depth from concrete extreme compressive fiber to centroid of prestressing steel

d_s = depth from concrete extreme compressive fiber to centroid of nonprestressed tensile steel

$d_{s'}$ = depth from concrete extreme compressive fiber to centroid of nonprestressed compressive steel

E_c = elastic modulus of concrete in compression

E_{ps} = modulus of elasticity of prestressing steel

E_{pp} = modulus of elasticity of Parafil rope

E_s = modulus of elasticity of nonprestressing steel

f'_c = cylinder strength of concrete;

f_{ct} = ultimate tensile strength of concrete

f_{ctm} = mean value of axial tensile strength of concrete

f_{cu} = cube strength of concrete

f_L = calculated stress due to live load

f_{pe} = effective prestress in prestressing steel

f_{pep} = effective prestress in Parafil rope

f_{pp} = ultimate stress in Parafil rope

f_{ps} = ultimate stress in prestressing steel

f_{pu} = ultimate strength of prestressing steel

f_{py} = yield strength of prestressing steel

f_r = modulus of rupture of concrete (MPa)

f_{TL} = total calculated stress in member

f_y = yield strength of nonprestressed tensile steel

h = total height of cross section

h_f = depth of flange

I = inertia of the cross section

I_e = effective moment of inertia

I_g = moment of inertia of uncracked cross section (neglecting the steel)

I_{cr} = moment of inertia of cracked cross section (neglecting concrete in tension)

I_{cra} = inertia of the cracked section relative to the centroidal axis

L_1 = length of loaded span or sum of lengths of loaded spans, affected by the same tendon

L_2 = length of tendon between end anchorages

K = multiplier deflection factor depending on the load type

K_D , K_L , K_P = multiplier deflection factors of dead load, live load and prestressing force

L = span length between end anchorages

L_o = equivalent plastic region length

L_p = width of plastic zone

M_a = applied moment

M_{cr} = cracking moment

M'_{cr} = net positive moment required to crack the section

M_d = moment due to dead load

M_{dec} = decompression moment (moment lead to zero stress on precompressed concrete extreme fibres)

M_L = moment due to live load

n_e = Parafil rope modular ratio

n_p = prestressing steel modular ratio

n_s = steel modular ratio

P_i = initial internal prestressing force

P_{ei} = effective internal prestressing force

P_x = initial external prestressing force

P_{ex} = effective external prestressing force

S_d = distance between deviators

y_b = distance from neutral axis to bottom fibre of the section

y_t = distance from neutral axis to top fibre of the section

β_1 = concrete compression block reduction factor

Δ = deflection at midspan in simple beam

Δ_I = deflection calculated on the basis of an uncracked section

Δ_{II} = deflection calculated on the basis of a cracked section

Δ_D = deflection of midspan due to dead load

Δ_L = deflection of midspan due to live load

Δ_P = deflection of midspan due to prestressing force

Δf_{ps} = tendon stress increase = $f_{ps} - f_{se}$

Δ_{eps} = increase in strain in prestressing steel above effective prestress

ε_{ce} = strain in concrete at level of prestressing steel due to f_{se}

ε_{cu} = ultimate concrete compression strain in top fiber.

ε_{ps} = strain in prestressing steel at ultimate

ε_{pu} = ultimate strain in prestressing steel

ε_s = strain in nonprestressed tensile steel at ultimate

ε_{se} = effective prestrain in prestressing steel

ρ_p = ratio of prestressing steel (A_{ps}/bd_p)

ρ_s = ratio of nonprestressed tensile steel (A_s/bd_s)

ϕ_{cr} = cracking curvature

ϕ_u = ultimate curvature

Ω = bond reduction factor before cracking

Ω_{cr} = bond reduction factor after cracking

Chapter 1

Introduction

1.1 INTRODUCTION

Many reinforced and prestressed concrete bridges throughout the world are deteriorated and/or distressed to such a degree that structural strengthening of the bridge or reducing the allowable loading on the bridge by loading posting is necessary to extend the service life of the bridge.

Hutchinson and Rahimi (1996) reported that, as a result of an European Community directive, all bridges in the United Kingdom are required to carry 40-tonne vehicles by 1999 or otherwise have a weight restriction order placed on them. A major assessment program for all bridges in the United Kingdom resulted in the need to upgrade over 10,000 of the total 60,000 reinforced concrete bridges.

In United States, among the 575,000 highway bridges, 230,000 were rated as structurally deficient or functionally obsolete and are thus candidates for replacement or significant rehabilitation work to extend their service lives. Another factor that adds to the urgency of the problem is that over the past 40 years there has been a steady increase in the weights of trucks legally permitted on highways. As a result, many bridges today are carrying loads up to 40% heavier than anticipated in their original design (*Crasto et al.* 1996). In another study made by *Whiteway* (2000), it was reported that in the United States alone, 600,000 road bridges are scheduled for repair

at an estimated cost of US$200 billion-four times the cost of their original construction.

External prestressing system can be an effective solution for improving the structural performance of many bridges suffering from deterioration, steel corrosion or in need strengthening, to cope with larger loads. Using prestressing will enhance the integrity of the existing structures, without adding to the weight.

However, several bridges built or strengthened by external steel tendons in Germany, France, USA, UK and other countries in the world did not behave satisfactory as most of these externally prestressed structures suffered from corrosion. (*Virlogeux* ,1993).

This problem can be solved by using fibre reinforced plastic elements (FRP) based on glass, aramid or carbon fibres, as an alternative to high strength prestressing steel due to its high-tensile strength and excellent corrosion resistance. One of these tendons is Parafil rope type G, which is considered as an efficient tendon for external prestressing.

However, several difficulties inhibit the use of FRP as external prestressing tendons over a wide range of structures. These difficulties can be summarized in two points as follows:

- The lack of data about the behaviour of prestressed members after having been externally strengthened using FRP tendons and the inadequacy of the recommendations pertaining to these members especially in most codes.

- Unsuitability of the design equations or analysis methods used in ordinary prestressed concrete for this type of members due to the lack of bond between the external tendons and concrete, and the loss in the tendon's eccentricity during loading.

1.2 OBJECTIVES OF THE PRESENT INVESTIGATION

The objective of this investigation can be summarised as follows:

- Study experimentally the influence of the following factors on the behaviour of prestressed concrete beams after being externally strengthened using Parafil rope type G with particular attention to crack formation, camber and deflection, losses in tendon's eccentricity, variation in internal and external prestressing force, and cracking and ultimate strengths.

    1. Value of external prestressing force
    2. Number of deviators
    3. Effective depth of the external prestressing force
    4. Previous loaded stage before being externally strengthened
    5. Concrete strength (f_{cu})
    6. Effective span / depth ratio (L/h)

- Obtain simple equations that can be used to calculate the cracking and ultimate strengths and be less complicated and time consuming.

- Modify some of the existing methods of deflection calculation to externally prestressed beams.

1.3 OUTLINE OF THE THESIS

For a better understanding of behaviour of externally prestressed beams and fibers, a review of literature related to the external prestressing system, FRP and Parafil rope was carried out and is presented in **chapter two**.

Chapter three is concerned with the manufacture and testing the specimens. Material characteristics, test equipment and test procedure are all incorporated.

The behaviour of test specimens and the test results are presented in **chapter four.**

Chapter five presents an extensive discussion of the test results as well as relations between some parameters.

A brief literature review of analytical methods used to calculate deflection and ultimate moment of bonded and unbonded prestressed concrete is presented in **chapter six**; which is then extended to describe the behaviour of the prestressed concrete beams after being externally strengthened.

Finally, **Chapter seven** includes a synopsis of the main observations and conclusions obtained from the experimental and analytical works, and a number of suggestions for further research.

Chapter 2

Literature Review

2.1 INTRODUCTION

This chapter is divided to two parts, the first part discussed the external prestressing system and the behaviour of the externally prestressed beams using external steel tendons, while in the second part several types of the commercial fibre reinforced plastics used in prestressing are compared and their properties are discussed. Also, the properties of Parafil rope and its anchorage are presented and discussed.

2.2 EXTERNAL PRESTRESSING

External prestressing is the form of prestressing in which the prestressing tendons are unbonded and are outside the concrete section, and their load is transferred to the concrete through end anchorages and deviators as shown in Figure (2.1). *Bruggeling* (1990) mentioned some reasons for the development of this type of prestressing as follows:

- The demand for methods to repair prestressed concrete bridges with corroded prestressing tendons or to strengthen concrete bridges or other structures already in use, due to the increase of traffic loads.

- The need for less complicated profile of prestressing tendons in the concrete structures. Simplifying tendon profiles has its effect on the concreting of the structure, the stressing of the tendons (friction problem) and the grouting of ducts (interaction between adjacent ducts)
- The growing interest in methods in which the influence of workmanship on the overall quality of the realized concrete structures is reduced.
- The need to maintain and repair concrete structures specially bridges, without harming the use of the structure, e.g. by closing off the traffic on the bridge or viaduct. In such cases, the use of external cables offers a very good solution.
- New development in bridge design and bridge construction are resulting in the use of external cables.

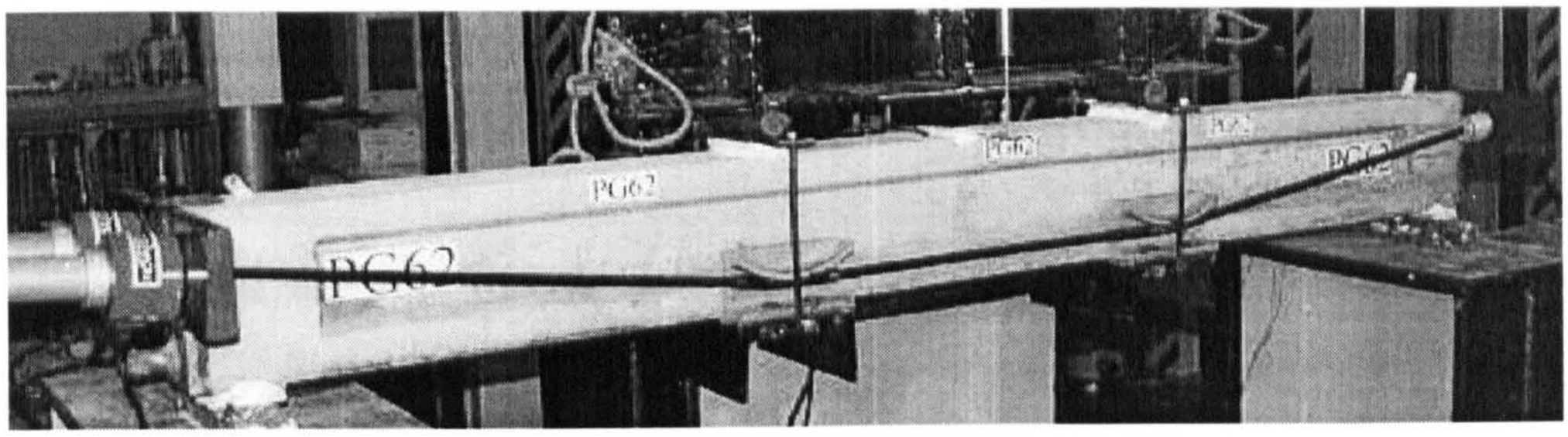

a) Outside a concrete section

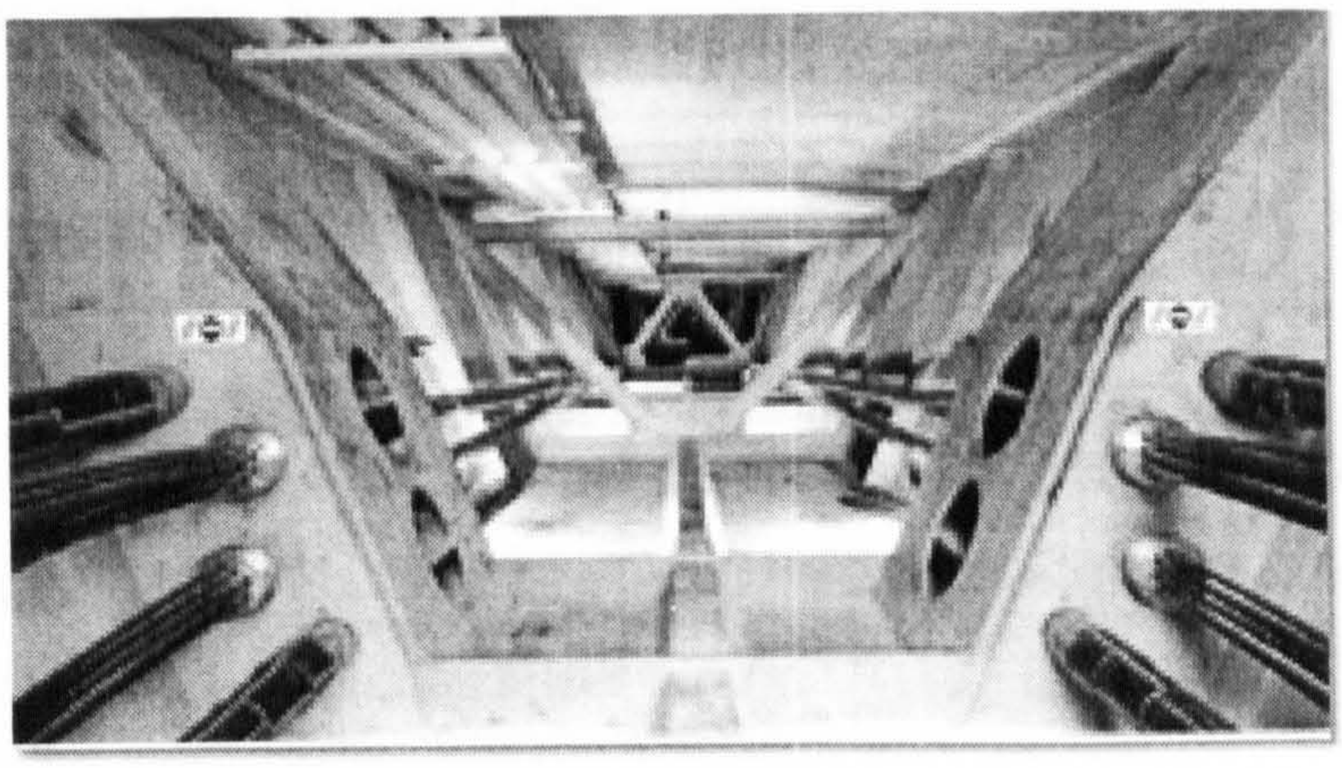

b) Inside a box section

Figure (2.1): External prestressing tendons layout

2.2.1 Requirements of Reinforcement for Prestressed Concrete:

- **High tensile strength**: Reinforcement used in prestressed concrete must have high tensile strength to enable it to counterbalance the high creep and shrinkage losses in concrete and have adequate residual stress to sustain the required prestressing force.
- **Low relaxation**: Stress relaxation in prestressing tendon is the loss of prestress when the wires or strands are subjected to essentially constant strain. So, the smaller the relaxation, the higher the effective prestressing.
- **High resistance to corrosion and deterioration of strands**: Corrosion decreases the cross section area of the tendon and hence, increases the applied stress. This stress can increase and be higher than the nominal strength of the tendons and lead to premature failure of the tendons and failure of the structural system.
- **Modulus of elasticity (Young's modulus)**: High modulus is needed to limit the extension of material during stressing, while the low modulus reduces losses due to creep and shrinkage of the concrete. During prestressing, the extension of tendons can be managed so using lower modulus will be advantage.

2.2.2 Method and System of Strengthening

Post-tensioning can be considered as one of the most efficient methods for strengthening. Strengthening using Post-tensioning requires a minimum of demolition and has only a minor impact on the overall structure with significant improvement in strength. This extends the life span of the structure at a very reasonable cost.

Strengthening using Post-tensioning can be achieved using either external tendons or internal tendons or both (*Vejvoda*, 1992). Various components constituting the system of external prestressing are as follows:

2.2.2.1 Tendons

Several types of tendons can be used to strengthen concrete members such as, steel, carbon fiber reinforced plastic (CFRP), aramid fiber reinforced plastic (AFRP), or glass fiber reinforced plastic (GFRP), etc.

2.2.2.2 Ducts and tendon geometry

The ducts form straight-line connections between the various "fixed points" (anchorages and deviators) and are used to protect the tendons from environmental attack or vandalism. For steel tendons, high density polyethylene sheaths are suitable as ducts, due to their high resistance to atmospheric effects (*Manjure*, 1996).

2.2.2.3 Deviators

Deviators are provided for the geometric requirements of the tendon and to accommodate the considerable force imposed by change in direction and to maintain the eccentricity of the tendon under ultimate bending conditions (*McKenna and Chan*, 1996). At deviation points, it is beneficial to provide as large a radius as possible. Excessively small radii of curvature should be avoided (*Manjure*, 1996).

To avoid unacceptable vibrations of the external tendons, the free length of the external tendons should be limited, a maximum distance of 7-8 m between two deviation points of a tendon has been recommended (*Bruggeling*, 1990). Also, in order to avoid second order effect due to beam deflection between the fixing points, *BD58/94* (1995) suggested the distance between the fixing points should not exceed 12 times the minimum depth of the beam. If the spacing between points where the tendons are held in position laterally exceeds 12m, checks shall be made to ensure that the first natural frequency of the tendons vibrating between fixing points is not in the range 0.8 to 1.2 times that of the bridge.

In order to reduce the stress concentration due to bending of the prestressing tendon at the deviators, *BD58/94* (1995) suggested the radius of curvature of tendons in the deviators not less than 5 times the tendon diameter for wire, or 10 times the diameter for strand. The total angle of deflection should not exceed 15°.

The deviators through which the tendons pass nominally straight are required to maintain the eccentricity of the tendon under ultimate bending conditions. The design forces on them are calculated by consideration of the angular change that will occur at failure of the beam as a whole (*McKenna and Ch*an, 1996)

2.2.2.4 Anchorages and diaphra ms

Anchorages are used to transfer the tendon forces to the structure. Different types can be used depending on the type and number of tendons used in the prestressing.

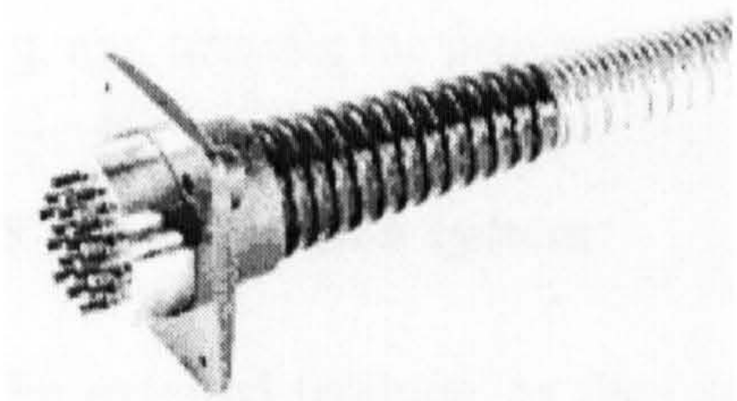

a) Multi strands anchorage

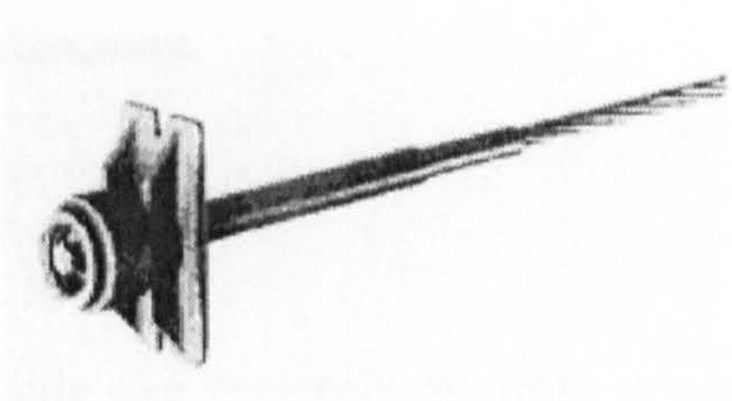

b) Single strand anchorage

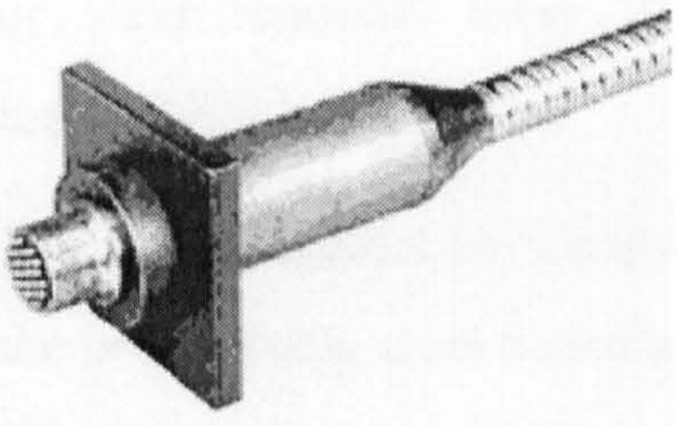

c) Multi wires anchorage

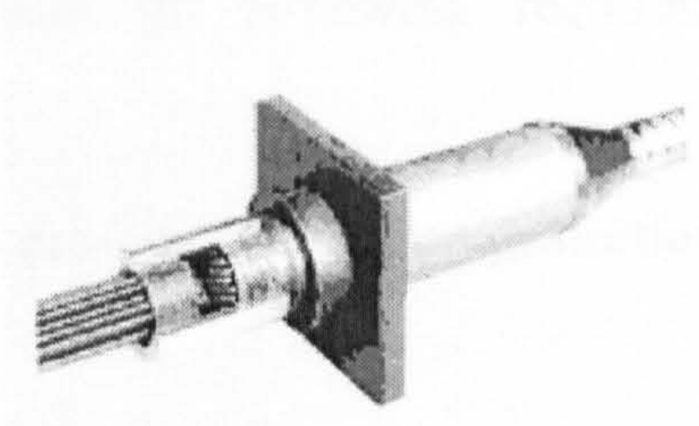

d) Button head wires anchorage

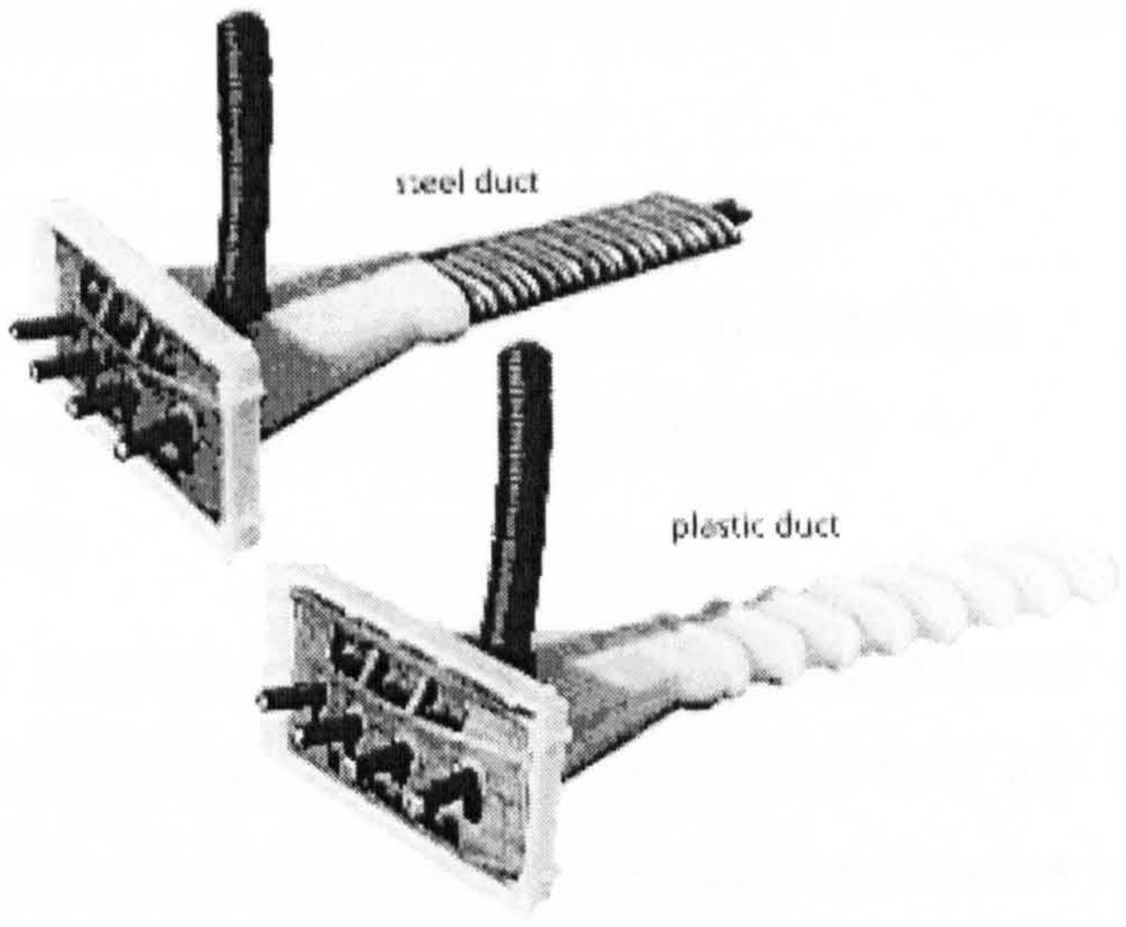

e) Four single-strand anchorage

Figure (2.2): Typical anchorages used in various steel prestressing systems

(*BBR*, 2001)

Figure (2.2) shows the steel anchorages, while Figure (2.8) shows anchorages of FRP. The difference between the steel anchorages and the FRP anchorages are related to the difference in their properties.

Diaphrams are generally provided for transfer the imposed loads onto the bearing, and transfer the prestressing forces to the structure.

2.2.2.5 The Protection system

The external tendons, as they are located outside the concrete section, are more susceptible to the atmospheric attack than the internal tendons embedded in the concrete. To protect the tendons, outer ducts filled with protective material should be used. For steel tendons, these ducts should fulfil the following requirements (*Bruggeling*, 1990):

- Resistance against environmental attack, to provide a corrosion protection to the prestressing steel over the whole length.
- Waterproof
- Compatibility with prestressing steel and its corrosion protection
- Resistance against damage during construction and installation
- Resistance against damage in service
- Fireproof in cases where fire cannot be excluded
- Controlled creep behaviour of the materials of the duct
- Resistance against transverse forces (deviations)
- Replaceability

In the case of external prestressing, grouting the external cables is easier to control because the ducts can be simply inspected as they are accessible. If some defects are determined they can be repaired because small holes can be drilled in the ducts to add new grout. The ducts used to protect steel tendons are commonly from steel with an internal cable sheathing made of polyethylene (*Bruggeling*, 1990).

For steel, several materials can be used to protect the tendons, such as cement grout, grease, wax, bitumen or plastics by injection in the ducts. Experience has

shown that the grouting of prestressing cables needs great care if later damage is to be avoided (*Eibl*, 1990).

These requirements of the protective sheath can be reduced when using FRP tendons, due to their high resistance to corrosion.

2.2.3 Losses in Post Tensioned Prestressing

The loss of stress in external prestressing tendons are less than those in internal prestressing tendons, as friction will be, for external tendons, at the deviator, and will be, for internal tendons, along the tendon length accompanied by warping effect if the tendons are not straight. Table (2.1) shows the types of losses in both external and internal prestressing tendons and its stage of occurrence.

Table (2.1): Types and stage of occurrence of losses in external and internal prestressing tendons

Type of prestress loss	***Stage of occurrence***	
	Internal prestressing	**External prestressing**
Elastic shortening of concrete	At sequential jacking	At sequential jacking
Shrinkage of concrete	After transfer	After transfer
Creep of concrete	After transfer	After transfer
Relaxation of tendons	After transfer	After transfer
Friction	At jacking*	At jacking **
Anchorage seating loss	At transfer	At transfer

*(location: at deviator points and along the length of duct tube)

**(location: at deviator points)

2.2.4 Behaviour of Externally Prestressed Beam

The behaviour of an externally prestressed beam is not only different than that of an internally bonded prestressed beam, due to lack of bond between the external tendons and the concrete but also different than that of an unbonded prestressed beam with internal tendons, due to the reduction in the tendon eccentricity especially at ultimate. However, the behaviour of externally prestressed beams, prior to cracking is similar to that of beams with conventional bonded tendons. While after cracking and as the load is increased there is a tendency for one crack to open more than the others, which eventually leads to failure. Thus, at failure, the externally prestressed beam can

be analyzed by assuming that the beam consists of a pair of rigid blocks, with all the rotation concentrated in a single hinge at the centre (*Burgoyne et a*l., 1996).

Harajli (1993) made a comparison between the behaviour of externally prestressed concrete beams and internally unbonded prestressed concrete beams. Harajli reported that in the case of a small area of prestressing tendon, the maximum moment strength of a prestressed beam with exterior cables is much less than that of interior cables. This is because the beam obtains a large deflection capacity, as the area of tension reinforcement is small.

Also, the rotation of the beam, as the load increased, causes the tendon to move relative to the compression flange, thus reducing the lever arm of the tendon and lowering the load capacity of the beam. Final failure was caused by explosive failure of the concrete in the compression zone, leading to complete collapse of the structure. (*Burgoyne* et *al.*, 1996. *Clark and Toms*, 1996).

After cracking and as failure approaches, the strain in unbonded tendons increases, but the increase is constant over the tendon length, or at least over the distance between deviators as shown in Figure (2.3). This strain is less than that of bonded tendons and less likely to reach yield. The lack of yield at failure means that the prestress in the tendons as well as the strength of the tendons has a significant effect on the strength of the structure, so a partial safety factor should be applied to the prestress (*Jackson*, 1996).

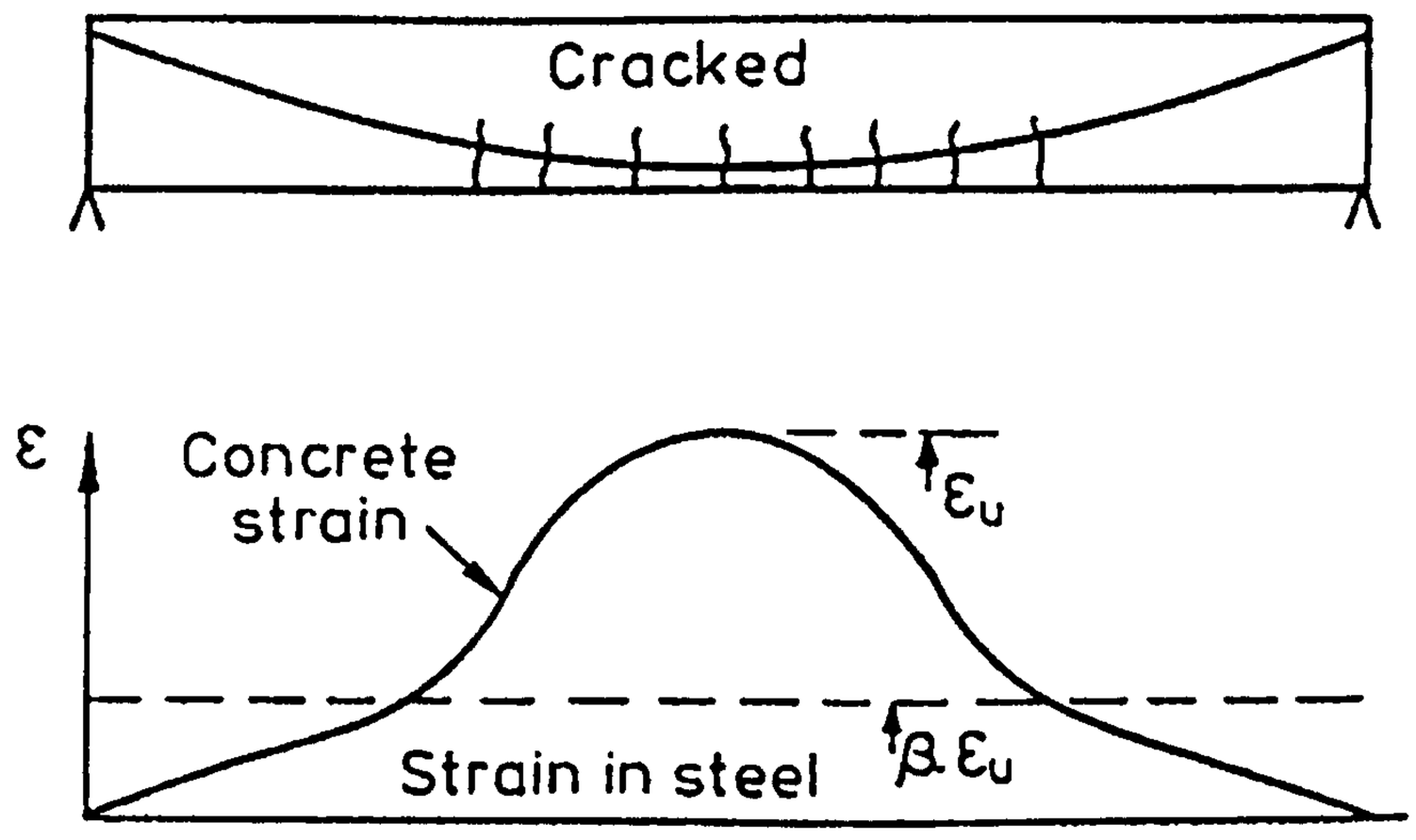

Figure (2.3): Strains in a cracked beam with an unbonded tendon

Yaginuma and Kitada (1988) studied the effect of (span/depth) ratio on the behaviour of externally prestressed beams. Yaginuma reported that for prestressed concrete beams with external tendons, the deflections up to maximum moment are similar to those of prestressed concrete beams with internal tendons regardless of supporting points (deviators) when (L/d) is small. However, when (L/d) is larger, the bending moment in externally prestressed concrete beams without supporting points tends to decrease greatly at all stages after the onset of cracking in comparison with other prestressed concrete beams.

Tan and Ng (1997) compared the behaviour of externally prestressed concrete beam with draped tendons and identical beam with straight tendons, and they concluded that the beam with draped tendons had less stiffness, wider spread of cracks, greater tendon stress and more ductility at failure.

2.2.5 Effect of External Prestressing on Shear Behaviour of the Beam

External prestressing system can be used to improve the shear capacities of existing structures. As a result of prestressing, there will be an increase in the cracking load as well as the shear strength. Also, strengthening may be obtained even in a previously cracked RC specimen by introducing external prestressing (*Kondo et al.*, 1994).

To check the shear strength, an externally prestressed beam can be considered as a reinforced beam subjected to an external load and using the enhancement for axial load for a column, or by considering it as a bonded prestressed beam, both approaches are always safe and usually over-safe. (*Jackson*, 1996).

Also, tests show that the shear cracking load predicted either by using elastic theory (which was applied to the uncracked section irrespective of whether the section was cracked in flexure), or by plastic theory (which incorporated an effectiveness factor that was a function of prestress) gave a good prediction of shear capacity. Also, section shape and tendon type (internal or external) had no effect on the accuracy of the prediction of the shear-cracking load (*Clark and Toms*, 1996)

2.2.6 Effect of Loss of Tendon Eccentricity and Tendon Profile

The difference between the behaviour of externally prestressed concrete beams and internally unbonded prestressed concrete beams, as mentioned before, is mainly caused by the secondary effect, namely "loss of tendon's eccentricity", induced by the large deflection of beam under bending load as shown in Figure (2.4). An externally prestressed concrete beam with a large distance between deviators gives a significantly lower flexural strength than that of internal unbonded prestressed concrete beam. (*Matupayont* et *al.*, 1994).

An externally prestressed beam with a straight horizontal tendon profile is relatively less effective in increasing the flexural resistance as compared to a deviated profile, because of the progressive reduction of the depth of the straight external tendons with increasing member deformation as failure is approached (*Harajli*, 1993. *Yaginuma and Kitada*, 1988). Also, tests carried out by *Tan and Ng* (1997) on beams with straight tendons and a span-depth ratio of 15 indicated that the provision of a single deviator at the section of maximum deflection resulted in satisfactory service and ultimate load behaviour.

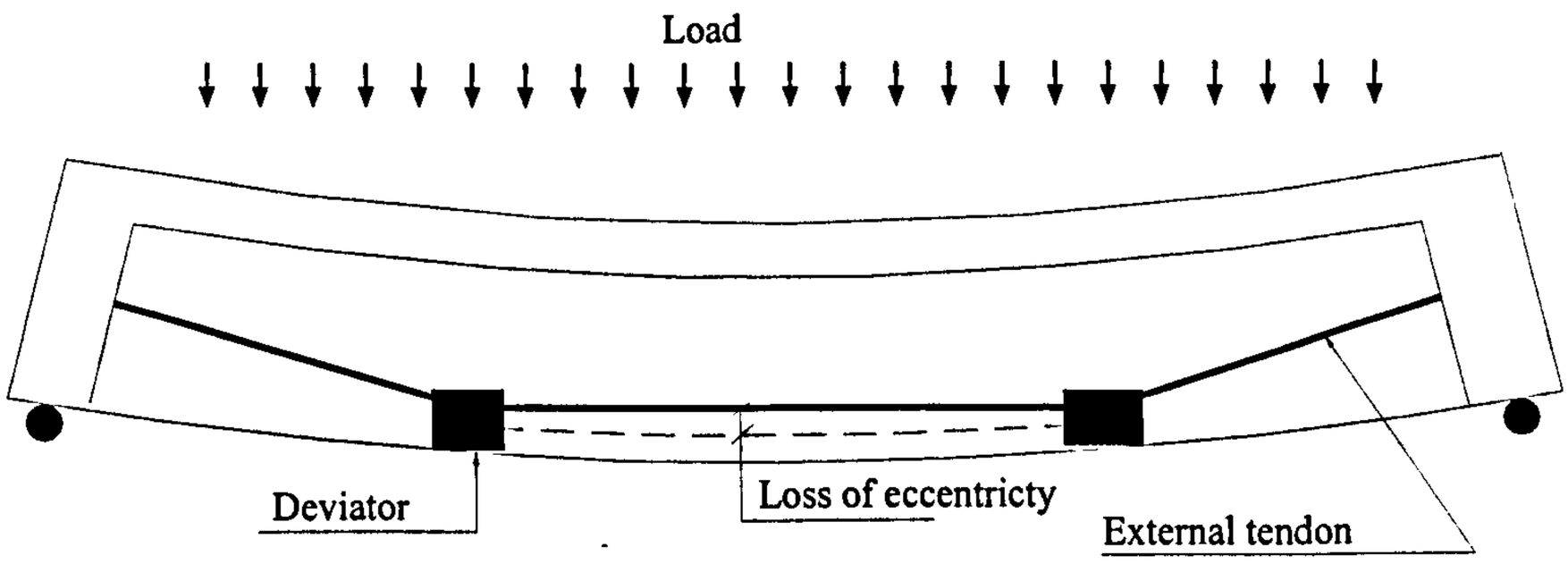

Figure (2.4): Loss of tendon eccentricity in external prestressed beam

Songkiat et al. (1994) stated that "it is found that the externally prestressed concrete beam possessing a proper arrangement of deviators to eliminate the loss of tendon's eccentricity (that is deviator at mid span in the simple beam) shows the same flexural behaviour as that of the internal unbonded PC beam".

Harajli et al. (1999), studied the effect of deviators on the response of externally prestressed members, using a straight horizontal tendon profile having constant effective eccentricity. Three different configurations of deviators along the span were evaluated (tendon without deviators, tendons with one deviator at the mid-span and tendons with two deviators). Also, three different values of external prestressing force for each configuration were applied. They reported that:

- For a horizontal tendon profile, and in the presence of deviator(s), the influence of the second order effects on the response of externally prestressed members is minimal.

- Single-draped profile (when used one deviator) produced lower nominal moment capacity and post elastic deflection than did the other draped profiles (when used two or more deviators).

- With increasing distance between deviators, the nominal moment capacity increased up to $\alpha=L_d/L= 0.25$ where L_d= distance between the two deviators and L= effective span, then decreased depending on the extent of the second order effect. The undraped profile ($\alpha=1.0$) produced the lowest nominal moment resistance.

2.2.7 Effect of Steel Area:

For an externally prestressed concrete beam with a straight horizontal profile or a deviated profile, providing the same prestressing force, the use of a larger tendon area gave similar service load behaviour but a higher ultimate strength and less ductile behaviour near failure (*Tan and Ng*, 1997).

2.2.8 Effect of Prestressing Force:

Use of a smaller effective prestressing force leads to larger stress in external tendons, larger crack widths, and service load deflections, but more ductile behaviour at ultimate (*Tan and Ng*, 1997).

2.2.9 Effect of Loading Type:

Tests of prestressed beams with single deviator and without deviators under different type of loading (concentrated, two-third points and uniform loading) were investigated by *Harajli et al.* (1999). The results showed that, because a single concentrated loads developed the smallest equivalent plastic hinge length at failure, they tended to mobilize the lowest postelastic deflection at failure in comparison with uniform load or third point loading. Also, since the nominal reduction in the tendons' depth is related to the ductility of the member, the difference in the nominal moment capacity acquired using tendons with or without deviators was least significant for concentrated loads.

2.2.10 External Prestressing and Fatigue

External prestressing causes a significant improvement in the fatigue life of the strengthened beams due to the lack of bond between concrete and tendons, which results in a decrease in the stress ranges and mean stress levels.

2.2.11 External Prestressing as Restrengthening Materials

The use of external prestressing tendons to strengthen cracked concrete is completely different from that used initially in the construction for several reasons. Firstly, when used for strengthening, the external tendons represent only a part of the total flexural reinforcement, the remaining reinforcement being the original reinforcement in the member. Secondly, not all the prestressing force will be transmitted to the concrete in the case of strengthening a cracked element, because part of this force will be used to close the cracks (*Farkas and Akasha*, 1998).

Harajli (1993) studied the effect of repeated loading on strengthened precracked reinforced beams. He reported that providing external prestressing by a relatively moderate amount resulted in an increase in the nominal flexural resistance by a significant value, without significant reduction in ductility or ultimate flexural deformation of the member. Also, external prestressing was shown to:

- Reduce the crack widths or close the cracks completely

- Reduce significantly the service load deflections induced under cyclic fatigue loading
- Lead to stiffer service load-deflection response and, hence, reduce the live load deflections.

Cairns and Rafeeqi (1997) studied the effect of loading arrangement (shear span/effective depth), effective depth of external reinforcement and geometric ratio of bonded reinforcement on the behaviour of externally strengthened beams and reported that:

- Retrofitting of external reinforcement could attain an increase in flexural capacity of up to 85%, with some reduction in ductility. However, structural cracking gave ample warning of structural distress.
- The increase in strength is higher for lightly reinforced beams.
- The enhancement in serviceability performance arising from the addition of external unbonded reinforcement, is less than the improvement obtained at the ultimate limit state.

2.2.12 Behaviour of Prestressed Beams Containing External and Internal Prestressing Tendons

During construction, the bridge's span must be built before the external prestressing tendons are installed, and its weight must be balanced by some construction equipment or by an adapted system of tendons. This system can be internal or external cables according to the method of construction.

It was found that using a mixture of internal unbonded tendons and external prestressing tendons improves flexural behaviour and increases the ultimate strength relative to external tendons alone (*Yaginuma*, 1994). Also, the block length, the tensile force ratio of the external to total tendon forces and the existence of deviators significantly affect the ultimate strength and the total tensile force of tendons (*Saito and Yaginuma*, 1998).

2.3 FIBRE REINFORCED PLASTICS (FRP) AS EXTERNAL PRESTRESSING TENDONS

Using steel as external prestressing tendons increases the chance of corrosion. This problem can be overcome by using fibre reinforced composites instead of steel as the external prestressing tendons.

Composite materials typically consist of fibres and a matrix material. Several high strength fibres exist for possible use as non-metallic tendons in prestressed structures. The most popular fibres used for prestressing tendons are glass, aramid and carbon fibres. The fibres may be used individually, as rope (e.g. Parafil rope), or encased in a resin such as epoxy to form bars. The physical performance of the fibre reinforced composite depends on several factors such as fibre type, matrix type, adhesion between the fibre and the matrix, manufacturing techniques, etc.

In the following sections, the most common types of fibres and matrices used in prestressed concrete are presented.

2.3.1 Fibres

A fibre is a long fine filament of matter with a diameter generally of the order of 5 to 25 μm and an aspect ratio of length to diameter between a thousand and virtually infinity for continuous fibres (*Kim*, 1995). Fibres used in prestressing tendons, are high-strength fibres, and have a nearly linear stress-strain relation to failure as shown in Figure (2.5). the fibre strength is considerably higher than steel, while the modulus of elasticity for most fibres, is lower than steel. Also, its strain at failure is significantly less than steel and has no ductility as is commonly associated with the yielding of steel. The functional requirements of fibres impregnated in matrix are as follows (*Faza and GangaRao*, 1993):

- A high modulus of elasticity to give stiffness to the composite.
- A high ultimate strength.
- A low variation of strength between individual fibres.
- Stability during handling.
- A uniform diameter.

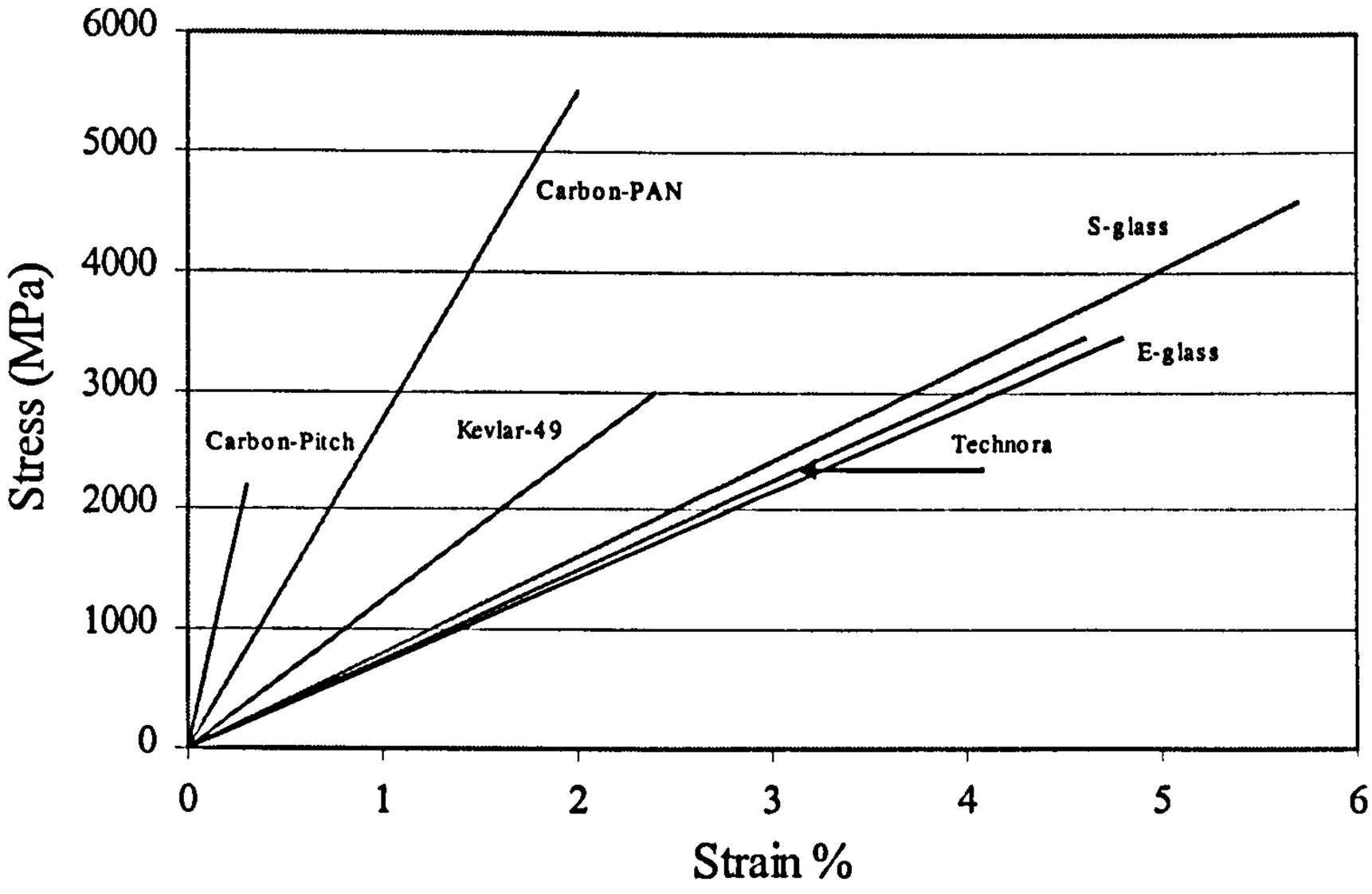

Figure (2.5): Stress-Strain curves of different types of fibres

It should be noted that, a bar made from fibres encased in resin has less tensile strength than the individual fibre has. This is for several reasons (*Dolan*, 1990):

- Individual fibres behave analogously to a long chain. The chain is only as strong as its weakest section which thus defines its total strength. Interaction between twisted fibres or between fibres encased in resin prevents the multiple fibre bundles from failing at the lowest possible load. Thus, the strength of a fibre bundle is lower than the strength predicted for individual fibres, but greated than the lowest possible fibre strength.
- The tensile load is assumed to be carried uniformly between all the fibres in the bundle. In fact, the pultrusion process or the anchoring of individual fibre bundles creates differential initial stresses and provides varying strain conditions in the individual fibres within the bundle. At high stress conditions the most highly strained fibres fail first and load is transferred to the remaining fibres. The differential strains in the fibres lead to a progressive collapse of the fibre bundle at strength less than that predicted by summing the strength of individual fibres.
- The shear strength of composite fibres is 5 to 10 percent of their tensile strength. The transfer of axial load to the anchor at the tendon end creates a

high transverse shear. The internal shear between the surface of the tendon and the inner fibres may be sufficient to initiate progressive failure of the tendons.

- Fibre strength deteriorates when subjected to sustained high load levels just as a concrete cylinder will fail at less than the short term loading strength when subjected to high-sustained loads.

The most common types of fibres commercially used in prestressed concrete are as follows:

2.3.1.1 Glass Fibres (GFRP)

Glass fibres are the most common of all reinforcing fibres for FRP. Two main types used for glass fibers are generally used, namely, E-glass, which was developed for electrical applications, and S-glass, which was developed for structural applications. At the time of writing, a new glass fiber, Z-glass, is being introduced to the market, with the claim of high resistance to alkalis. Young's modulus of glass fibre ranges between 72-85 GPa while its tensile strength ranges between 3400-4580 MPa (*Vaughan*, 1998).

2.3.1.2 Carbon Fibres (CFRP)

The production of commercial carbon fibres begins with organic precursors such as rayon, Polyacrylonitrile (PAN), and isotropic and liquid crystalline pitches. Depending on variables such as precursor, heat treatment and degree of stretch during processing, the strength and elastic constants of carbon fibres can vary greatly (*Bakis*, 1993). Young's modulus of carbon fibre ranges between 230-830 GPa while its tensile strength ranges between 2200-5650 MPa (*Lafdi and Wright*, 1998).

Carbon fibres, in general, are not affected by moisture, atmosphere, solvents, bases or weak acids at room temperature.

2.3.1.3 Aramid Fibres (AFRP)

Aramid is a generic term for 'aromatic polyamide fibres'. Aramid is an organic, man-made fibre with a high degree of crystallinity. Aramid fibres have a highly anisotropic structure that leads to low longitudinal shear modulus, poor transverse

properties, and low axial compressive strength. Also, the interfacial bond strength between aramid fibres and epoxy resins is normally lower than what is experienced with carbon fibre composites (*Jang*, 1994). However, aramid has high fatigue resistance, static and dynamic, high specific strength, toughness and creep resistance combined with moderate cost. Young's modulus of aramid fibre ranges between 54-143 GPa while its tensile strength ranges between 2900-4590 MPa (*Clements*, 1998).

2.3.2 Matrix

Ceramic matrix, Carbon-Carbon matrix, Metal matrix, polymer matrix are different types of binders can be used to bind the fibers together. However, Polymer matrix is considered as the popular one.

A polymer is a long chain molecule made by connecting many smaller molecules called monomers by the chemical process known as polymerization. Polymers are generally characterized by low elastic modulus and low strengths. They are generally quite brittle, particularly at low temperatures, and most are of no structural value at temperatures in excess of 200 °C. The fibres control all the mechanical properties of the composite in the longitudinal direction, while the matrix controls most of the properties in the transverse direction.

The matrix resin comprises approximately 30% to 40% of the composite and fulfils a variety of critical functions (*Arnold et al.*, 1991. *Faza and GangaRao*, 1993. *Rostasy*, 1993):

- Binds the fibres together and separates them.
- Protects the fibres from premature wear such as abrasion and environmental corrosion.
- Transfers stresses to the fibres efficiently by adhesion and /or friction
- Plays a critical role in preventing the fibres from buckling due to compressive loading.
- Distributes the applied load and acts as a stress transfer medium from broken to unbroken fibres, so that when an individual fibre fails, the composite structure does not lose its load-carrying capability.

Polymers used in FRP can be classified as thermoset and thermoplastic. A comparison between both types is shown in Table (2.2).

Table (2.2): Comparison between thermoset and thermoplastic polymers

	Thermoset polymers	***Thermoplastic polymers***
Polymer molecules	Highly cross-linked (each molecular chain is chemically bound to its neighbour)	Linear cross-linked (molecules lying next to each other, holding by electrostatic attraction)
Effect of heat	Undergoes a chemical change that results in a substantially infusible and insoluble material	Can be repeatedly softened upon heating and hardened upon cooling
Advantages	▪ Their historical availability ▪ The existence of a large database for commercially available resin systems ▪ Better chemical resistance ▪ High application temperatures ▪ Better resistance to creep ▪ Low material costs	▪ Versatile bonding methods such as ultrasonic or heat welding ▪ High damage tolerance ▪ Possibility to reprocess scrap material. ▪ More ductile and tough than cross-linked ▪ Easy quality control, less batch-to-batch variability
Disadvantages	▪ Cured once and can never be reformed, recured or reused.	▪ Possible environmental stress cracking, solvent susceptibility and creep (except for semicrystalline polymers) ▪ Processing problems (tooling costs, high temperatures and pressures required) ▪ Higher thermal coefficient of expansion than thermost polymers at equivalent fibre volume fraction ▪ Limited database, particularly for long-term performance, including fatigue and creep behaviour
Types (examples)	Epoxy, Polyesters, Polyimides, Vinylesters.	Polypropylene, Polyamide, Nylons, PEEK.
Cost	Lower raw materials cost (with some exceptions)	More expensive than thermoset polymers

Some properties of the matrix resin which most influence the performance of the composite structure are (*Arnold et al.*, 1991):

- Elastic modulus (stiffness)
- Strength-tensile, compressive, and shear
- Yield and ultimate elongation
- Resistance to aggressive organic liquids

- Fracture toughness and, accordingly, damage tolerance
- Thermal, oxidative, and moisture resistance

2.3.3 Interface

The interface between the fibre and the matrix is an anisotropic transition region exhibiting a gradation of properties through which the transfer of stresses between fibre and matrix occurs. It must provide adequate chemically and physically stable bonding between the fibres and the matrix. Its functional requirements vary considerably according to the performance requirements of the composite during its various stages under service conditions (*Faza and GangaRao*, 1993).

2.3.4 Properties of Fibre Rein forced Plastics (FRP)

FRP bars are strongly anisotropic, with the longitudinal axis being the strong axis. Also, unlike steel, the mechanical properties of FRP vary significantly from one product to another. Factors such as volume and type of fiber and resin, fiber orientation and quality control during the manufacturing play a major role in the characteristics of the product. Furthermore, the mechanical properties of all composites, are affected by loading history and duration, temperature and moisture (*Ehsani*, 1993. *Rostasy*, 1993). The short term and long term properties of GFRP, AFRP, and CFRP are discussed as follows, while Table (2.5) shows a comparison between their properties .

2.3.4.1 Short- term behaviour

2.3.4.1.1 Tensile strength and modulus of elasticity

Ultimate strength and modulus of elasticity are the most important short-term properties of prestressing tendons. The tensile strength of FRP is generally higher than that of prestressing steel strands and depends on several factors such as the fibre tensile strength, ratio of fibre volume, size and cross-sectional area of the fiber and the bond performance between the fibers and the resin matrix. Due to the low strength of the matrix, the strength and the modulus of elasticity of FRP elements mainly relate to the fibres (*Rostasy*, 1993).

The tensile strength will drop when the diameter is increased because the bond performance of the fibres and matrix will decrease, even though the number of fibres will increase. However, the tensile strength fluctuation coefficient is 2-7%, which indicates a small-scale strength of dispersion (*Mochizuki. et al*, 1993)

Figure (2.6) shows typical stress-strain relationships for different types of FRP and high tensile steel. It should be noted that when comparing the several commercial FRP bars with prestressing steel the ratio of fibre volume must be taken into consideration.

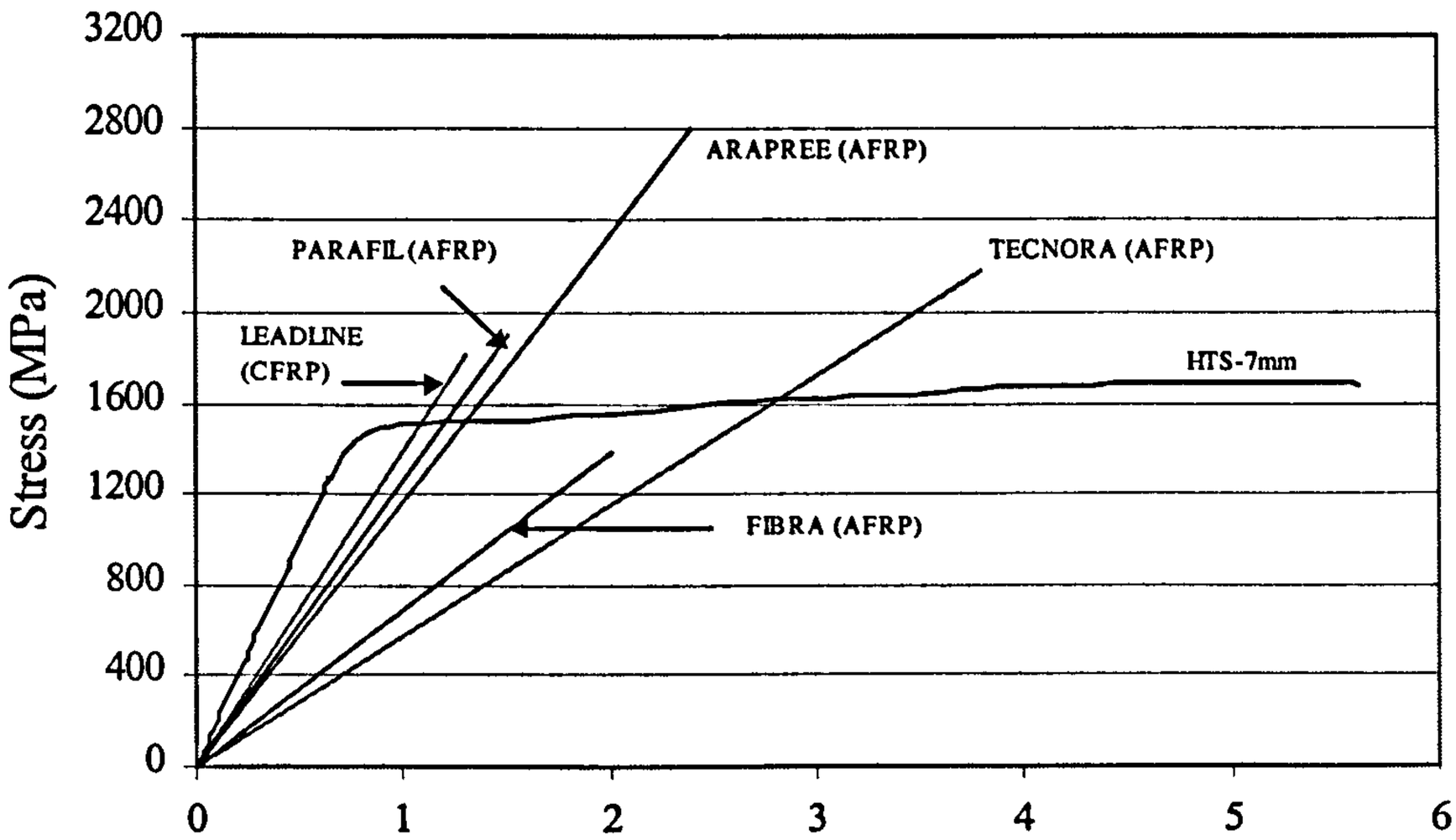

Figure (2.6): Stress-Strain curves of different types of FRP

2.3.4.1.2 Bending of FRP :

Maruyama and Honma (1993) carried out tests on CFRP and AFRP to check the effect of the bent portion of the rod on its tensile strength. Three radius values were examined 5, 15 and 25-mm respectively. They reported that:

- CFRP and AFRP rods all ruptured at the beginning of the bent portion on the loading side.
- The tensile strength of the bent portion of FRP rods tended to decrease hyperbolically as the radius of the curvature of the processed portion decreased.

- The rate at which tensile strength decreased varied with bend radius , fibre type, and bending method employed

Also, experiments on GFRP rods show that sharper bends, similar to 90^{o} or 180^{o} hooks, cannot be performed in the field. Attempts to bend a straight bar or straighten a bent bar will result in a very large stresses in the outermost fibers at those locations, leading to fracture of the bar (*Ehsani*, 1993).

2.3.4.1.3 Bond

Bond between FRP bar and concrete depends on several factors such as surface roughness of FRP bar, indentations of FRP, chemical adhesion, thickness and mechanical properties of the polymeric layer, etc. Bond between FRP bars and concrete can be divided into three parts as that between steel and concrete as follows:

- Friction
- Chemical adhesion
- Mechanical interlock

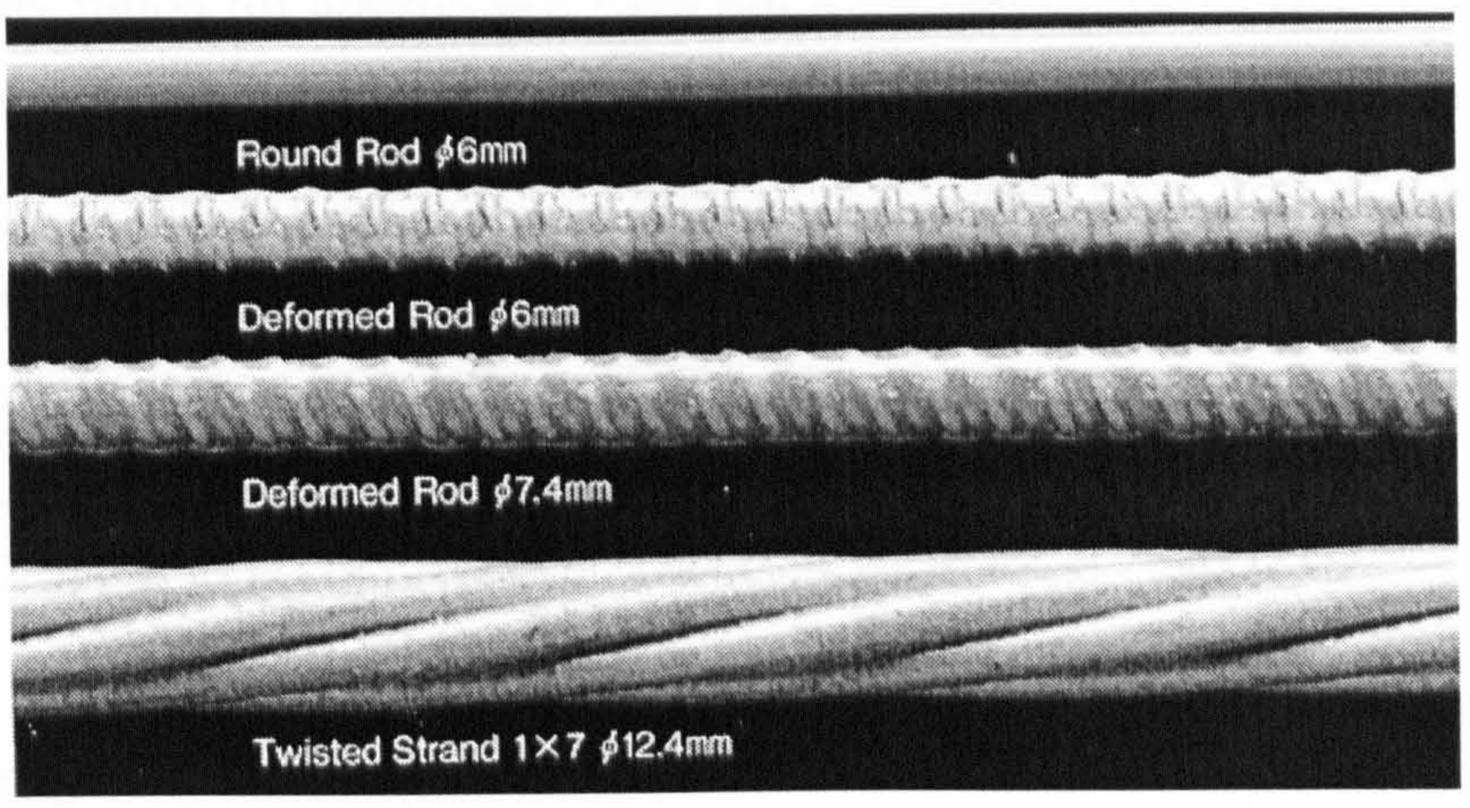

Figure (2.7): Different shape of FRP element.

An experimental study to determine the instantaneous and long term transfer length of fibre glass and steel pretensioned concrete specimens was carried out by *Issa et al.* (1993) who concluded that the bond between fibre glass and concrete is superior to that between steel and concrete. However, *Tighiouart et al.* (1998) studied the bond strength of glass fibre in reinforced concrete and reported that glass fibre has lower bond strength value than steel bars, this also was concluded by *Ehsani et al* (1993).

This discrepancy may be explained by reference to the bond mechanism between FRP bars and concrete, noting that bond between FRP bars and concrete is not a fibre property but it is a matrix property. So, a change to the matrix type or surface roughness will certainly change the bond properties. This is not only for GFRP but also for AFRP and CFRP. *Benmokrane et al* (2000), who investigated the bond between AFRP and CFRP bars and concrete, reported that the surface geometry of FRP rods and the properties of filling grouts influenced the pullout behaviour and bond strength of grouted FRP rods.

Also, *Ehsani et al.* (1997) carried out tests to investigate the transfer bond length of both AFRP and CFRP and reported that the transfer length for FRP tendons is generally shorter than that for steel.

2.3.4.1.4 Fire resistance

Tests indicated that at 350 °C carbon FRP retains 35% of its normal temperature breaking load and 40% of its normal temperature tensile elastic modulus. The corresponding ratios for aramid are 15% and 40% respectively. The rate of decrease in elastic modulus is thus about half that of the breaking load (*Alsayed et al*, 2000). (Reduction in strength of prestressing steel usually starts from 150 °C, and only 50% of its original tensile strength (i.e. 20 °C) is retained when the temperature is about 400 to 450 °C (*Bardhan-Roy*, 1982)).

2.3.4.2 Long-term behaviour

2.3.4.2.1 Creep

Prestressing tendons in a prestressed concrete member are essentially subjected to long-term static tensile stresses. These stresses increase tendon strain and can result in failure due to creep rupture. Creep of FRP materials is highly dependent on the level of the sustained load. Also, the volume of fibers and the matrix of FRP have a significant influence on the creep performance of the composites.

Glass fibres have excellent resistance to creep. If a rod is loaded to a value less than 70% of its short-term strength, then creep is of no significance (*Wolff and*

Miesseler, 1993). Also, for a high quality GFRP rod, the additional strain caused by creep were estimated to be only 3% of the initial elastic strains (*Ehsani*, 1993).

Based on their experimental tests conducted on 10-mm diameter AFRP rods *Saadatmanesh and Tannous* (1999) concluded that the specimens exhibited good creep characteristics in air and in alkaline solution and, to a lesser degree, in acidic solution, at sustained loads corresponding to 40 % of the ultimate strength.

Also *Benmokrane et al* (2000), examined the effect of tendon type and constituent, grout type, and bond or fixed anchor length on CFRP and AFRP uplift and sustained loading behaviour when used as ground anchor tendons. They reported that creep behaviour appeared to control the long-term uplift capacity of prestressed FRP ground anchors. The recommended working load for post-tensioned FRP ground anchors is 0.40 f_{pu} for AFRP rods and 0.50 f_{pu} for CFRP rods, where f_{pu} is the ultimate load or strength of the anchor tendon

2.3.4.2.2 Relaxation

Stress relaxation is defined as the loss of stress (with time) at constant strain. Relaxation of FRP rods is dependent on several factors as concluded by *Saadatmanesh and Tannous* (1999), after testing 10-mm diameter AFRP rods in air and in direct exposure to three different chemical solutions. *Saadatmanesh and Tannous* concluded that the relaxation losses increase with increase in temperature, and are lower in air than in solutions. Also, the relaxation losses were higher in acidic solution than in alkaline solution.

CFRP has the least relaxation among FRPs. The final relaxation loss of GFRP remains limited to 3.2 % at an initial stress level of 0.5 f_{pu} (extrapolated to 57 years) (*Taerwe*, 1993), while relaxation loss of AFRP after 100 years extrapolated from 5000 hours-relaxation test results is in the range of 10% to 15% (*Dolan*, 1993).

2.3.4.2.3 Fatigue

Tests showed that the fatigue strength of ARFP and CFRP were superior to high-strength prestressing wire. In contrast to this GFRP has a lower fatigue strength

(*Rostasy*, 1993). However, the fatigue life of FRP materials is dependent on the applied load, stress range, specimen shape, fibre reinforcement, percentage contents of fibres and resin and the number of fatigue cycles (*Uomoto and Ohga*, 1996). Also, test results revealed that the presence of moisture and increase in temperature could have an adverse effect on the fatigue life of composite materials (*Alsayed et al.*, 2000).

2.3.4.2.4 Durability

FRP rods expose to natural weathering will deteriorate but the degree of deterioration will be dependent on several factors such as (*Hollaway*, 1993):

- Type of the gel coat used to protect the exposed surface of polymer composites.
- Ultraviolet component of the sunlight and its wavelength.
- The action of the weather on the composite in different climates and situations
- The provisions of the required level of quality control to ensure suitable production environment, a correct fabrication procedure and an adequate cure for the resin.

Some factors, which have an effect on the durability of FRP bars, are discussed as follows:

Alkaline effect

Tests show that CFRP is not affected by alkaline solutions, while unprotected GFRP made with E- or S-glass fibres is detrimentally affected by alkaline solutions and sea water, and may fail by corrosion induced creep rupture. AFRP are far less sensitive to alkaline solutions than GFRP (*Rostasy*, 1993).

Takewaka and Khin (1996) tested seven different kinds of FRP rod for durability in the high alkaline solution simulating the pore water of concrete under different prestress conditions and different exposing periods. They concluded that:

- Not only GFRP rod but also CFRP and AFRP rods are probably deteriorated by the alkaline action of the pore solution in concrete.

- The loss of the strength of CFRP and AFRP rods in an alkaline environment varies according to the types of rod, though they have the same kinds of fiber and matrix resin. The strength of some types of rod does not decrease at all [fibre: carbon (PAN TR Besfit) - matrix: Epoxy Resin (Novolak)], while in other types of rod 20 to 30% decreased [fibre: carbon (Pan TR-30) - matrix: Epoxy Resin (Bisphenol A)].
- The decrease of strength of the CFRP rod resulting from immersion in the alkaline solution is attributed to the deterioration of the matrix resin , and that of AFRP rod is probably due to the combined deterioration of both the aramid fibre itself and the matrix resin
- There is a fairly high possibility of stress rupture on GFRP rod immersed in the alkaline solution, though the duration varies according to the tensile stress levels.

Also, *Uomoto and Ohga* (1996) reported that alkali could penetrate into GFRP rods using vinylester resins as matrices, due to the very thin thickness of resin protecting fibres and poor alkaline resistance of glass fibres.

Sea water and ultraviolet effect

Both GFRP and CFRP have better resistance to the ultraviolet rays than AFRP. Tested carried out by *Uomoto and Ohga* (1996) on different types of FRP show that tensile strength of AFRP rods reduced by about 30% under both inland and marine environment conditions at the age of 3 years. While that of GFRP was about 1% at the age of 3 years. The reduction of the tensile strength of CFRP was about 9% at the age of 1 year and no reduction after that. *Uomoto and Ohga* attributed the reduction in the tensile strength of AFRP to the deterioration of aramid fibre used in the AFRP rods by ultraviolet rays.

2.3.5 The prestressing tendon and its anchorage

The prestressing force, in post-tensioned prestressed concrete, is transferred from the tendons to the anchorage mainly by shear stress and lateral pressure. When using FRP as prestressing tendons, special anchorages are needed because the shear strength of FRP is very low. Also, FRP elements are very sensitive to transverse pressure and

specially to notches, which may sever the outer fibres. To overcome these problems, special anchorages are made for FRP tendons. These anchorages should fulfil the following requirements (*ISIS Canada*, 1997):

- Develop a minimum of 95% of the ultimate tensile strength of the tendon (the anchorage efficiency)
- Fatigue failure of the anchorage components should not occur.
- Creep in the anchorage must be minimal.

The most common types of FRP anchorage systems, as shown in figures (2.8-2.9), can be classified into (*ISIS Canada*, 1997):

- **Split wedge anchorage system** where a metal wedge in a conical housing is used to grip the tendon. The wedges compress the perimeter of the tendon and teeth in the wedges grip it.
- **Plug-in-cone anchorage system**. A bundle of tendons is placed in a conical housing socket and a solid cone is driven into the bundle centre to splay out the tendons and grip them individually between the spike itself and the socket.
- **Resin-sleeve anchorage system**. An epoxy resin is injected between a cylindrical steel shell and the tendons.
- **Resin-potted anchorage system** where the resin-sleeve anchorage system is modified to this geometry to achieve better anchorage.
- **Soft-metal overlay anchorage**. The gripping pressure is transferred to the FRP rods through a soft metal tube.
- **Swaged anchor** where the rod/cable is embedded in a resin and transverse stress is generated along a steel shell using bolts and nuts.

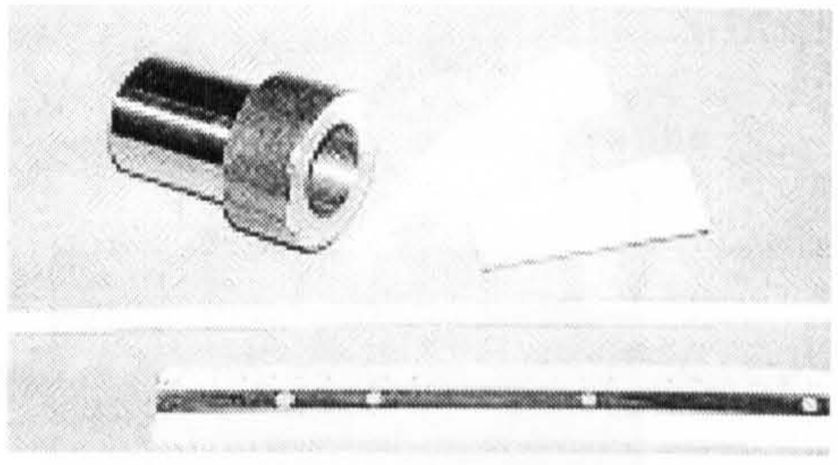

Arapree tendon

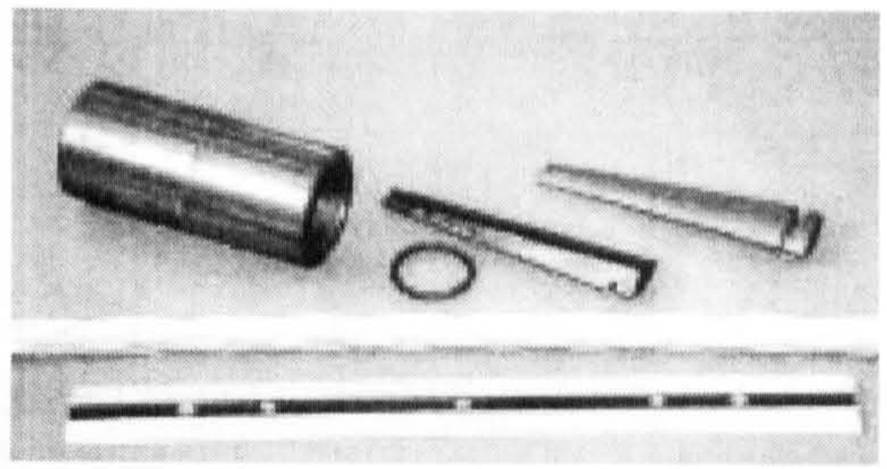

Fibra tendon

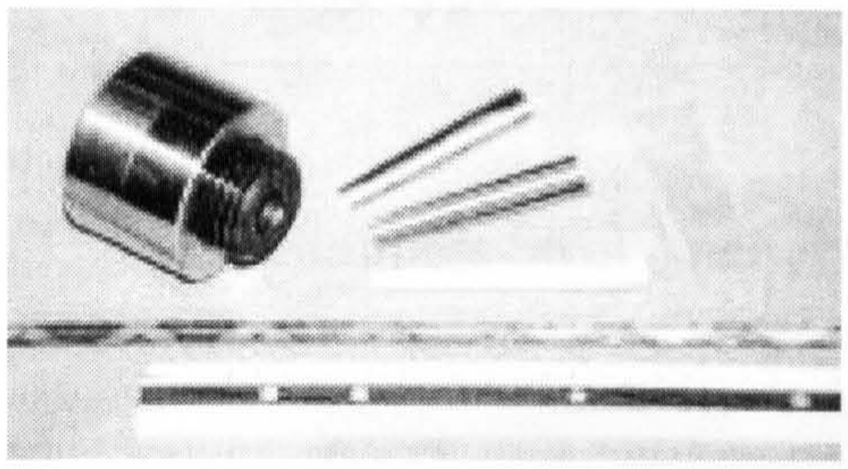

Leadline tendon

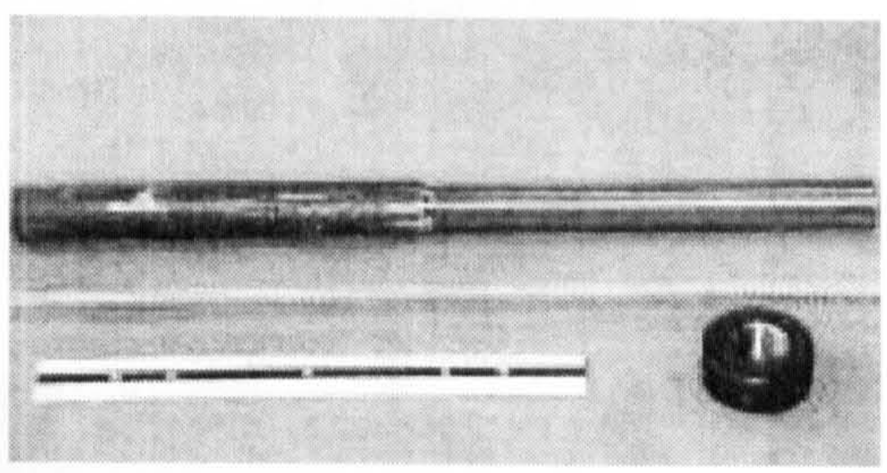

Technora tendon

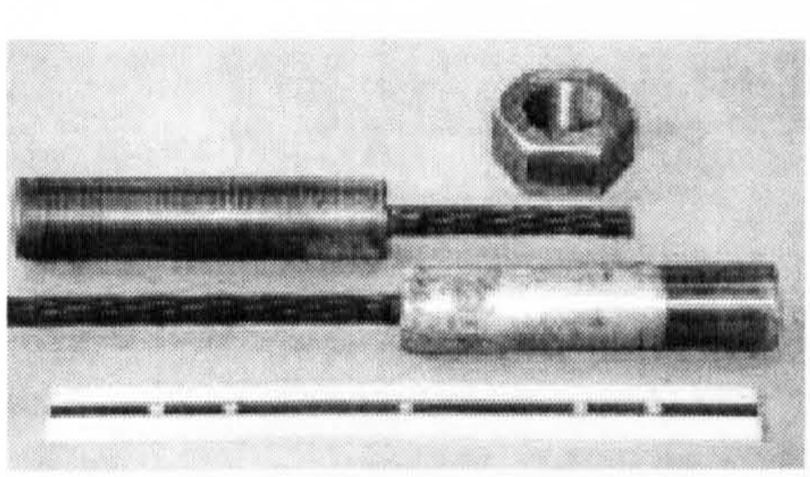

CFCC tendon

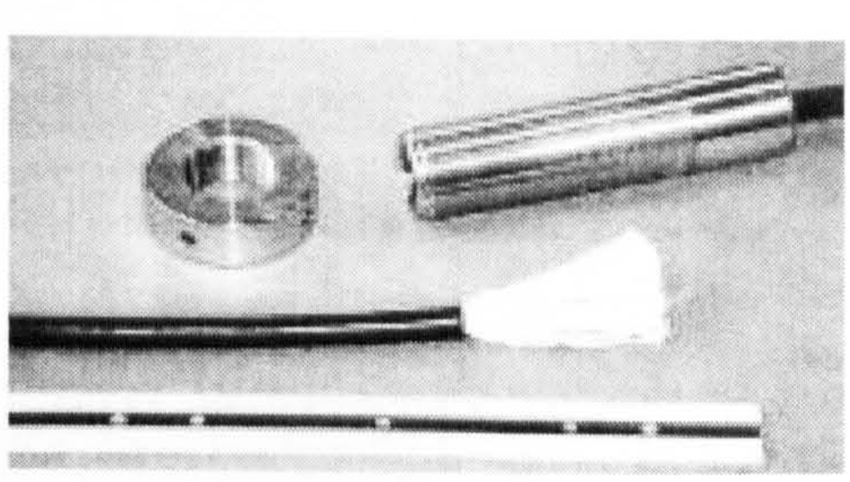

Parafil tendon

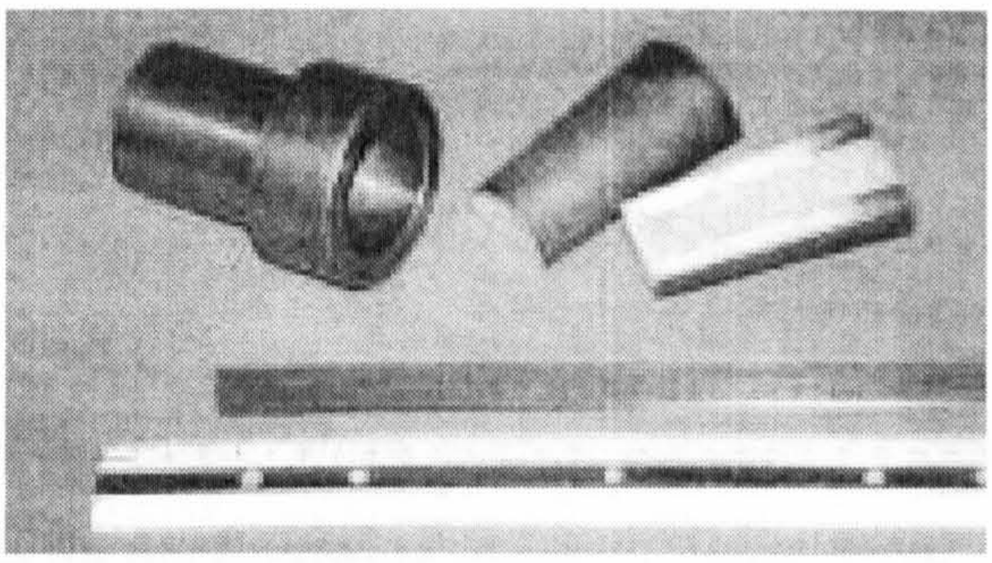

Carbon stress tendon

Figure (2.8): Anchor components for different FRP tendons (*Nanni et al*, 1996)

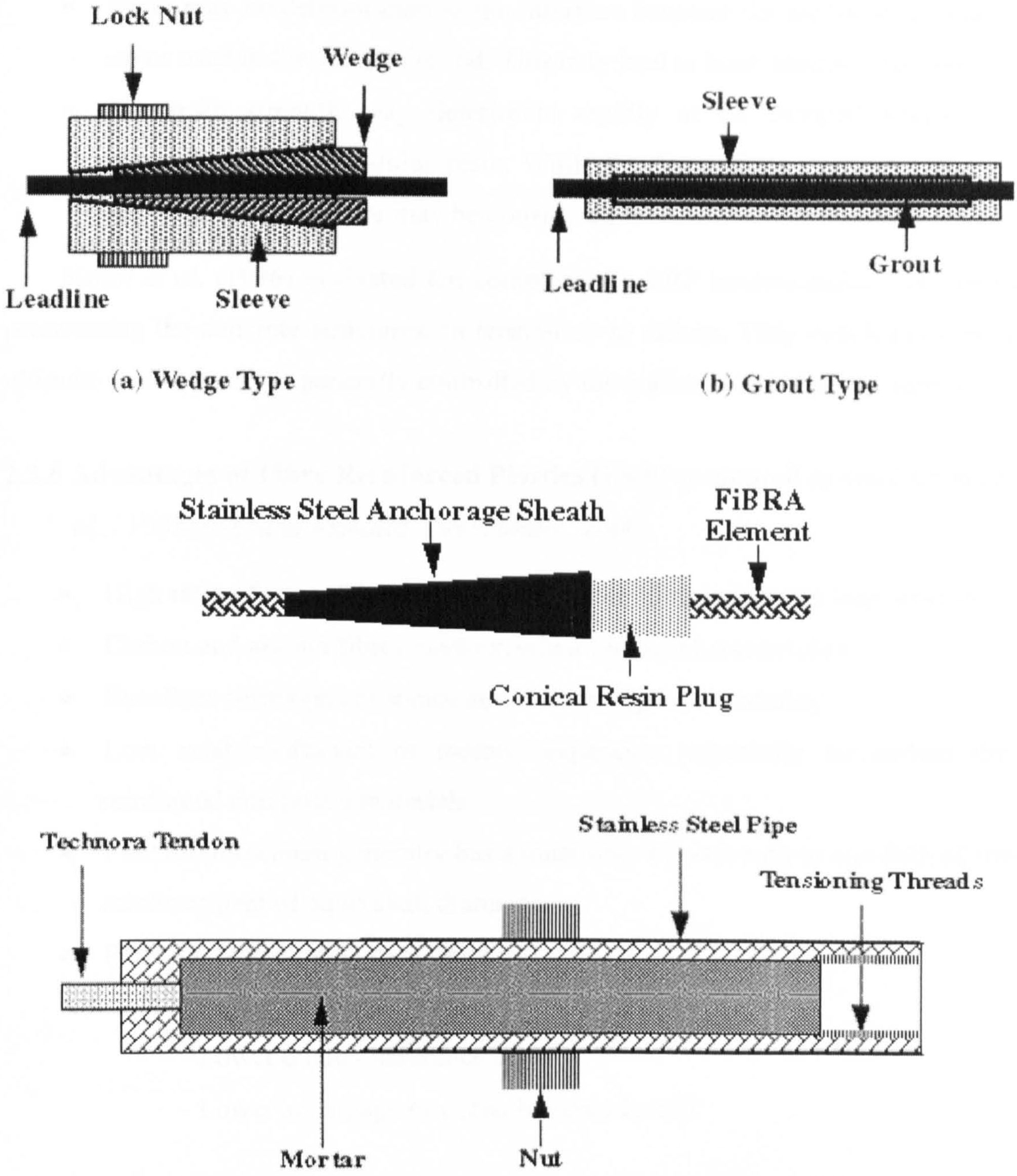

Figure (2.9): Anchor components for different FRP tendons (*ISIS Canada*, 1997)

Several problems appeared, when anchor depends on resin to transfer the rod load, after long periods for the following reasons (*Dolan*, 1990):

- Creep of the resin may lead to apparent relaxation due to tendon shortening.
- Deterioration of the resin may lead to a loss of anchor capacity.

- There may be deterioration at the interface between the anchor resin and the resins used in the composite rod. This may lead to bond failure in the anchor.
- The resin strength may deteriorate rapidly at an elevated temperature, especially the low modulus resin. While the fibres are not affected, thermal protection of the anchor may be considered.

Nanni et al. (1996) evaluated ten commercially FRP tendon-anchor systems for prestressing the concrete structures, in tension up to failure. They concluded that the ultimate load capacity is generally controlled by the anchor rather than the tendon.

2.3.6 Advantages of Fibre Reinforced Plastics (FRP) compared to steel (*Arnold et al.*,. 1991. *Erki and Rizkalla,* 1993. *Meier*, 2000).

- High ratio of strength to mass density (10 to 15 times greater than steel's)
- Carbon and aramid fibres have excellent fatigue characteristics
- Excellent corrosion resistance and electromagnetic neutrality
- Low axial coefficient of thermal expansion, especially for carbon fibre reinforced composite materials
- FRP reinforcement generally has a mass only one-seventh to one-fifth of steel reinforcement of equivalent diameter.
- Potential lower component costs:
    - Lower fabrication costs
    - Lower quality assurance costs
    - Lower scrappage rate (can be reproduced)

2.3.7 Disadvantages of FRP reinforcement (*Erki and Rizkalla, 1993*).

- Higher cost than steel.
- Low modulus of elasticity when used in ordinary reinforced beams.
- Low failure strain
- Special attention must be paid to anchorages when FRP reinforcement used for prestressing.
- Long-term strength of FRP reinforcement can be lower than short-term static strength (e.g. the long-term strength of GFRP is approximately 70 % of its short-term strength)

- Ultra-violet radiation can deteriorate FRP rods
- Aramid fibres can be deteriorated due to water absorption
- The low durability in acidic or alkaline environments.

2.3.8 Factors Which Affect the Performance of FRP When Used as Bonded Tendons

The performance of FRP tendons when used as internal bonded prestressing tendons is affected by several factors. Some of these factors are as follows:

2.3.8.1 Bond

FRP bars, in a general, have a shorter transfer length than steel; they have higher bond stresses. This in conjunction with a low cover value may lead to splitting cracks along the FRP element (*Rostasy*, 1993). The bond between FRP bars and concrete, as mentioned before, depends strongly on the matrix type and surface texture of the FRP element and on the tensile and compressive strength of the concrete. Any deterioration in the surface of FRP bars or in the bond between the fibres and the resin matrix will reduce the bond strength and hence, the efficiency of FRP bars as reinforcement to the concrete.

This deterioration could be due to moisture absorption, alkaline environments, cyclic loading, etc. The following subsections discuss some of factors which may reduce the bond between FRP bars and concrete:

2.3.8.1.1 Moisture

Water acts as a plasticizer when absorbed by the matrix, softening the material and reducing some properties of the laminate. Moisture may also migrate along the fibre-matrix interface, affecting the adhesion. Moisture in composites reduces matrix-dominated properties, such as transverse strength, fracture toughness and impact resistance. Debonding can occur due to formation of discontinuous bubbles and cracking in the matrix. Mechanical properties can be reduced even further if heat is present or if the composite is under cured or has a large amount of voids. Moisture absorption is usually dependent on the matrix, but aramid fibres will also absorb water

(*Whitaker et al*, 1998). Also, after testing FRP bars conditioned in aqueous solutions for 14 and 84 days at a temperature of 80 °C, *Bank et al.* (1998) recommended polyester resin should not be used for FRP bars due to its severe degradation. Also, it was reported that, radial and circumferential cracking was observed in the resin matrix. Circumferential cracking can lead to a failure phenomenon whereby the core of unidirectional fibres are debonded from the outer surface of the rod which remains bonded to the concrete.

2.3.8.1.2 Cyclic loading

Katz (2000) studied the effect of cyclic loading on the bond between FRP rods (with different resin matrices) and concrete immersed in water at 60 and 20 °C to accelerate deterioration effects. *Katz* reported that the reduction in the bond strength was approximately 70% after loading. Also, three mechanisms of failure were identified:

- Abrasion of the surface of the rod, which, in the case of uniform resin throughout the rod, may lead to a reduction of 20-30% in the bond strength
- Delamination of the outer layer of the resin at the surface of the rod, which may lead to a reduction of up to 60% in the bond strength.
- Abrasion of cement particles entrapped between the rod and the concrete, which serves as the main source of "bond" for smooth rods

2.3.8.1.3 High temperature

FRP bars showed a reduction of between 80 and 90% in the bond strength as the temperature increased from 20 to 250 °C. While, in comparison, ordinary deformed steel bars showed a reduction of only 38% in the same temperature range. The reduction in bond strength of FRP bars was attributed to the polymer in the surface of the bar only and the reduction in concrete properties was not the cause of the loss of bond strength at high temperature (*Katz et al.*, 1999). This severe reduction in bond strength at the high temperature can lead to the failure of members.

2.3.8.2 FRP tendon's strain

During the life of a structure, cracking of concrete can occur for several reasons , such as increase in concrete stress above its tensile strength, environmental attack, etc. When cracks occur on the tension face of a bonded prestressed concrete element, the tendons may be subjected to very high strains at the crack location. In the case of steel tendons, local debonding between steel and concrete may occur and steel is able to deform locally in a ductile manner to lessen such localised high strain. This continues until the average strain along the debonded length of the bar is less than the high strain as shown in Figure (2.10).

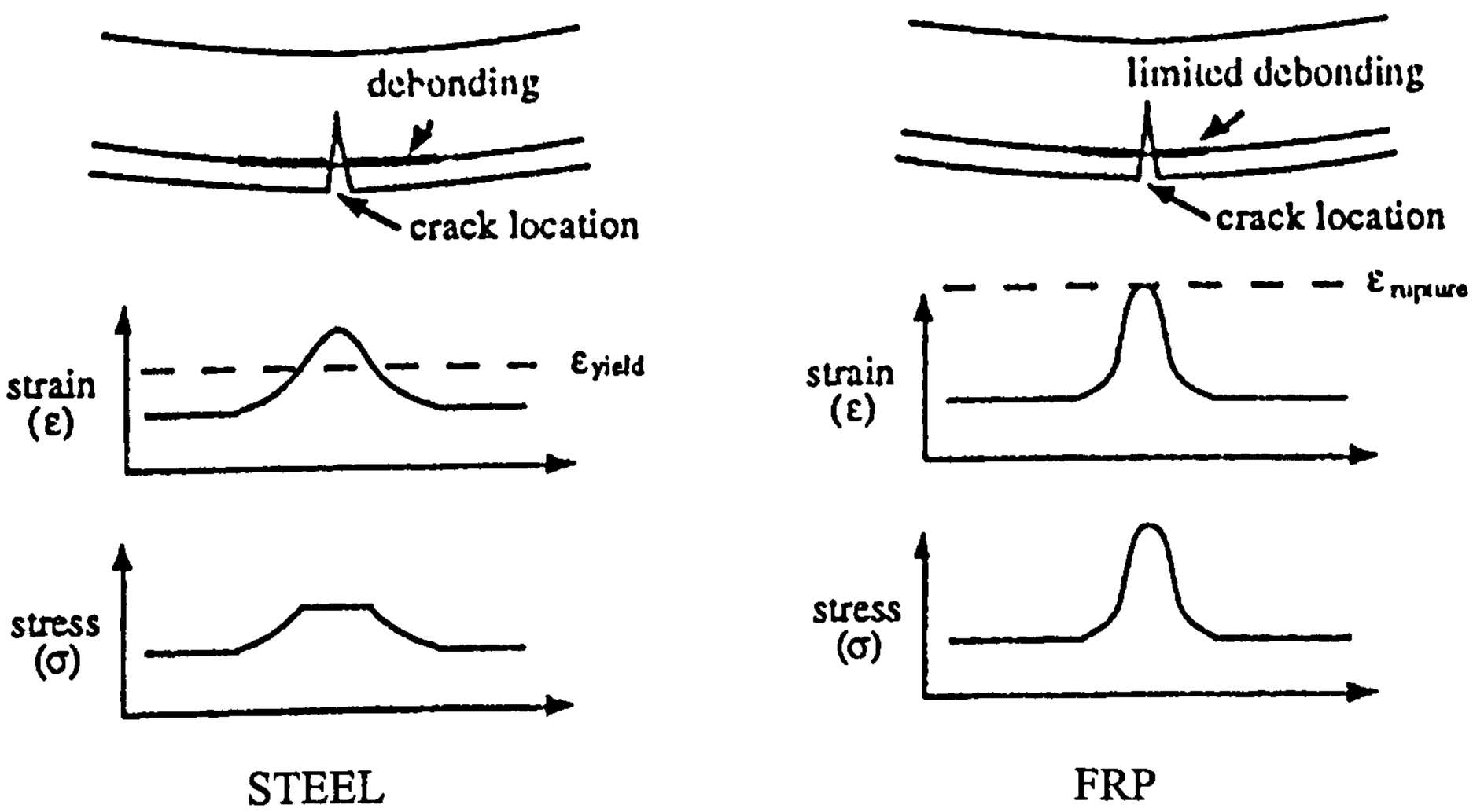

Figure (2.10): Strains and Stresses at the crack locations

When using FRP as prestressing tendons, it should be noted that:

- FRP has a linear elastic response right up to failure with little or no ductility.
- FRP has a limited strain capacity which is less than steel (typically 0.015 or above).

However, as FRP is expensive, it is preferred to use FRP close to its strain capacity, but during prestressing, much of the fibre strain capacity is absorbed in prestressing. This leaves the tendon very sensitive to additional strain induced by beam curvature or cracking of concrete, and may lead to failure of the concrete structure.

For unbonded tendons, when the beam is subjected to its ultimate load, and concrete strains increase to a very high value, the tendon will not see that peak strain, since it will continue to be subjected to an average value as shown in Figure (2.11). Though this value is affected by contact between tendons and deviators (where some sizeable friction effects may arise), the tendon strain will remain much lower than the local concrete strain (*Burgoyne*, 1993).

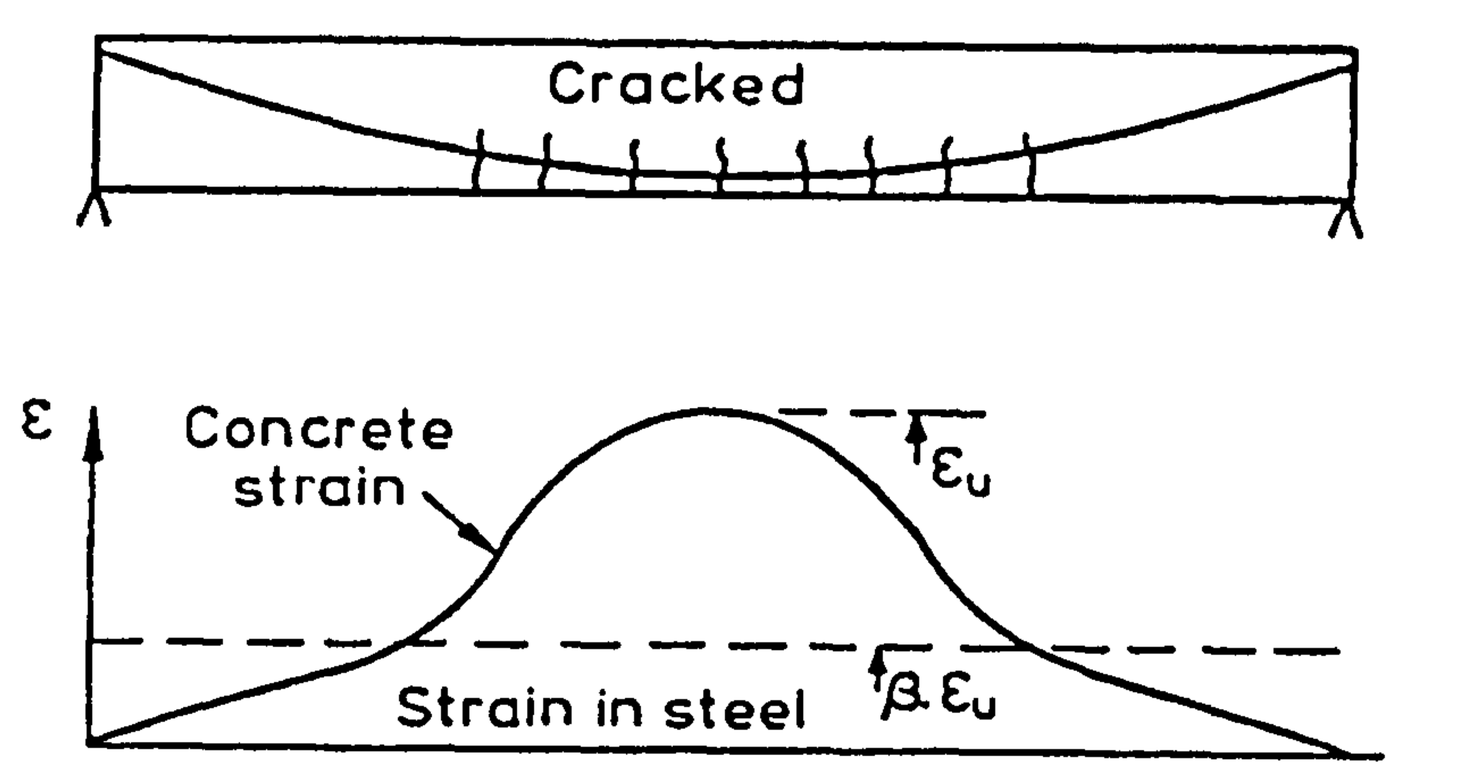

Figure (2.11): Strains in a cracked beam with an unbonded tendon

2.3.8.3 Coefficient of thermal expansion

FRP bars have two coefficients of thermal expansion (CTE), one in the longitudinal direction and the other in the transverse direction. For most commercially produced FRP bars, the longitudinal coefficient of thermal expansion is generally close to that of concrete, while the transverse coefficient of thermal expansion is higher than that of concrete and may be 10 times that of concrete.

In reinforced concrete, as both steel and concrete have the same coefficient of thermal expansion, internal strains due to temperature variation will not occur between steel and concrete. But, when using FRP bars, this problem appears, as the coefficient of thermal expansion of FRP is different than that of concrete. CFRP, for example, has a longitudinal coefficient of thermal expansion of almost zero. While GFRP and hardened concrete have the same longitudinal coefficient of thermal expansion, its transverse coefficient of thermal expansion (GFRP) is over five times higher (*Abdalla and Elbadry*, 1997). Also, the longitudinal coefficient of thermal expansion of AFRP approaches zero (this leaves a difference from the surrounding

concrete of approximately 12 x 10^{-6}/°C) and its transverse coefficient of thermal expansion is about (4 to 5) times that of the surrounding concrete (*Gerritse*, 1993).

The difference between the longitudinal coefficient of thermal expansion of FRP bar and concrete at high temperature leads to internal slip between the concrete and FRP bars results in a reduction of failure strength of the section. Also, this difference results in a marginal change in prestressing force (dependent on the temperature variation), and should be taken into consideration especially at high or low temperatures (*Gerritse*, 1993).

Also, the difference in the thermal expansion in the transverse direction may cause significant bursting stresses within the concrete around the bars under temperature increase, or separation of the bars from the concrete under temperature decrease (*Abdalla and Elbadry*, 1997)

2.3.9 Behaviour of Prestressed Concrete Beams Strengthened by External FRP Posttensioned Tendons:

Jerrett and Ahmad (1996) tested four (203 x 406 x 5490 mm) steel prestressed beams strengthened by external CFRP post-tensioned tendons. The beams were each prestressed with either one or two (13 mm) 7 wire steel prestressing strand and tested under four points loading. External post tensioning for strengthening was provided by two 8-mm diameter CFRP (Leadline) tendons, deviated by 4.8 degrees at each of two points. Effective steel prestress of the beams varied from 985 to 1130 MPa . The post-tensioning stress in the CFRP tendons varied from 1240 to 1500 MPa. Due to the external prestressing, the average strength was increased by 115% for the beams with single steel strands and 46% for beams with double steel strands.

Saeki et al. (1993), tested artificially cracked prestressed concrete beams externally strengthened using aramid ropes, under both static and repeated loading. Fatigue tests of strengthened beams were conducted under the condition of two million cycles, the stress level being up to 33% of the ultimate statical strength of beam and cable tension force being 34% of tensile strength. The change of rigidity of beam was found to be no significant difference between before and after fatigue tests,

and the ultimate bending strength of beams after fatigue test was nearly same value as that of beams before testing.

2.3.10 Using FRP Materials in Prestressed Concrete Structures (*Minosaku*, 1992. *Khalifa et al.*, 1993. *Taerwe and Matthys*, 1999. *Rizkalla and Labossiere*, 1999)

Due to their lightweight, high tensile strength and excellent corrosion resistance FRP are used in a wide range of structures such as bridges, piers, radar stations, etc. FRP reinforcements have been used in pedestrian and road bridges. Bridge types range from simply supported slabs to the most sophisticated systems, such as cable-stayed bridges.

2.3.10.1 Application of CFRP in a post-tensioned prestressed concrete bridges:

- CFRP strands were used as a part of the tendons in a post- tensioned prestressed concrete highway bridge erected in 1991 in a German factory area. The bridge is approximately 80-m long and 11.2 m wide. Large capacity multi-cable of 19 CFRP strands of 12.5 mm diameter were used and anchored by a wedge system.
- CFRP rods were used as tendons in a simple two-span prestressed concrete highway bridge erected in 1989 in Kitakyusyu City in Japan. The bridge is 35.8 long and 12.3 wide. The tendons consisted of eight multi-cables bundled with eight CFRP rods of 8-mm diameter. A wedge- type steel anchorage was used for the multi-cables.
- CFRP stirrups as well as CFRP prestressing cables were used in Taylor Bridge in 1997 . The bridge is located in Manitoba, Canada. The total length of the bridge is 165 m, divided into five equal spans. In addition GFRP reinforces portions of the barrier walls.
- In the cable-stayed Storchen Bridge in Winterthur, Switzerland, two 35 m long CFRP stay cables have been incorporated with 22 steel stay cables. The total length of this road bridge is 124 m.
- In Denmark, the Herning cable-stayed Bridge, with a total length of 80 m, is built with the exclusive use of CFRP stay cables. The bridge deck is post-tensioned with six CFRP tendons (12.5 mm) seven-wire strands from Tokyo Rope. And a 40-m segment of the bridge deck is reinforced with CFRP bars and stirrups. The

other 40-m segment will be reinforced with a conventional steel and stainless steel reinforcement.

2.3.10.2 Application of AFRP in a post-tensioned prestressed concrete bridges:

- AFRP bands were used as tendons in a post-tensioned prestressed concrete suspended slab bridge. 54.5 m long and 2.1 m wide pedestrian bridge built 1990 at a golf course in Mito City in Japan. The cross section of AFRP bands is 4.86 x 19.5 mm. Eight of the bands were combined to make a single cable, and 16 cables were used. Cables were anchored by inserting eight AFRP bands into a sleeve (material: SCM435) and filling it with expansive mortar. Cable bundling nine CFRP rods of 8-mm diameter was used for ground anchors.

2.3.10.3 Application of GFRP in a post-tensioned prestressed concrete bridges:

- GFRP rods were used as multi-cables in the Ulenberg-Stasse bridge. The bridge was built in 1986 in Dusseldorf in Germany. The bridge is a 2-span continuous girded highway bridge, one span is 21.3 m long and the other is 25.6 m long, both are 15 m wide. 59 multi-cables consisting of 19 GFRP rods with a diameter of 7.5 mm. The tendons are anchored by adhesion to a mortar containing quartz and polyester resin, which was injected to avoid alkali reaction of the glass fibres.
- The Schiessbergstrasse bridge in Leverkusen, Germany was built in 1990. It is a three span, solid concrete slab bridge with two sides spans of 16.3 m each and a 20.4 m middle span. The slab is 9.7 m wide and the deck is 1.12 m thick. Twenty-seven glass fibres prestressing tendons were used in a post-bonding process. Optical fibre sensors were also integrated for remote observation of the stresses.
- GFRP were used in construction of the Notsh Road Bridge in Karnten, Austria began in 1990. The bridge is very similar to the Schiessbergstrasse Bridge, but has different span lengths and was designed to be partially prestressed using 27 glass fibre tendons. The side spans are 13 m, the main span is 18 m, and the slab thickness is 0.75 m. The bridge is equipped with optical fibre sensors as well as chemical sensors.

2.4 PARAFIL:

Parafil ropes were the first products lunched by Linear Composites Ltd. in 1969. They consist of a closely packed core of high strength synthetic fibres lying parallel to each other, and encased in a tough and durable polymeric sheath. Fibres used in the core of Parafil rope differ from type to type as shown in Table (2.3) (*LCL*, 2000)

Table (2.3): *Comparison between types of Parafil ropes.*

Rope type	***Fibre type***	***Sheath type***
Type A	Polyester	Different types can be used with each rope: 1- polyethylene 2- Polyethylene-EVA copolymer 3- Polyester elastomer 4- Flame retardant
Type F	Standard modulus aramid (Kevlar 29)	
Type G	High modulus aramid (Kevlar 49)	

The sheath is used to hold the fibres together, maintain the circular profile of the rope and protect the core from ultraviolet radiation and external abrasion. The especially formulated Polyethylene sheath is most commonly used and is perfectly satisfactory for most purposes, but the Polyethylene-EVA copolymer sheath is more flexible. Higher resistance to heat and abrasion can be obtained from the Polyester elastomer.

The avoidance of twist, and of fibres crossing each other enables maximum use to obtain from the tensile strength and stiffness of the fibres. It also avoids the complication and sometimes adverse properties of more formal rope structures e.g. high creep and low tension-tension fatigue performance (*Kingston*, 1988). Also, aligning the yarns parallel to each other has the added advantage that they do not rub over each other on loading, so no inter-yarn abrasion occurs within the main body of rope. The only abrasion that occurs is within the termination, or where the path of the rope is deviated over a sheave (*Burgoyne et al.*, 1989).

2.4.1 Properties of Parafil rope type G:

The structural behaviour of Parafil rope depends mainly on the fibres due to the lack of bond between the fibres and the sheath. This enables the full benefit of Kevlar

fibres and eliminates problems which appear when the fibres held in a matrix as discussed before.

2.4.1.1 Short term properties:

2.4.1.1.1 Tensile strength:

The stress-strain relationship for Parafil rope is shown in Figure (2.12). The strength of Parafil rope exceeds that of prestressing steel, while its elastic modulus represents approximately two thirds that of steel. However, tensile strength of the rope decreases with the increasing rope diameter.

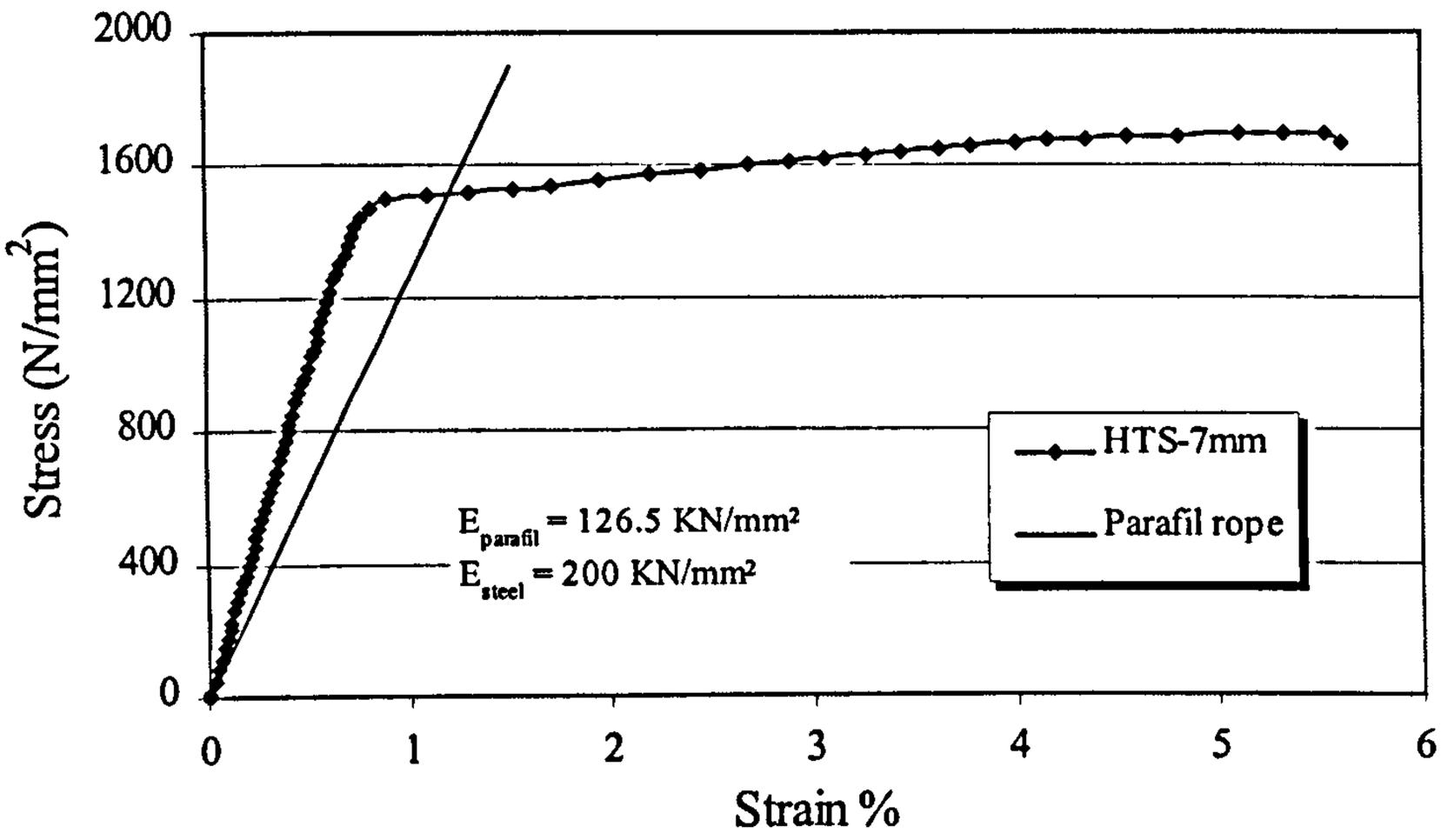

Figure (2.12) Stress-strain curves of Parafil rope and high tensile steel

Parafil rope has a linear stress-strain relationship with a nominal strength of 1962 MPa and a strain at failure of about 1.5%.

2.4.1.1.2 Effect of the rope length and curvature

Tests carried out by *Chambers* (1986) on 6-tonne Type G ropes with lengths of 2.9 m and 10.9 m, revealed that the rope strength remained unaffected by length. Also, stretching the rope around a deflector with a deflection angle up to 15^{o} and a radius of curvature of 50 times the diameter had no effect on their strength.

2.1.1.1.1 Effect of rope size

As discussed before, the strength of a group of fibres will be less than the strength of individual fibre, due to the bundle effect and the weaker fibres fail at a lower load than the stronger ones, leaving the total load-carrying capacity reduced. This process has to be applied twice in Parafil ropes; they are made as a bundle of parallel yarns, which are in turn made from about 1000 individual filaments. The filaments themselves have strengths of about 3500 MPa; the yarns have a strength of about 2900 MPa, and the ropes have a minimum strength of about 1930 MPa (*Burgoyne*, 1993). Figure (2.13) shows the relation between the tensile strength and rope size.

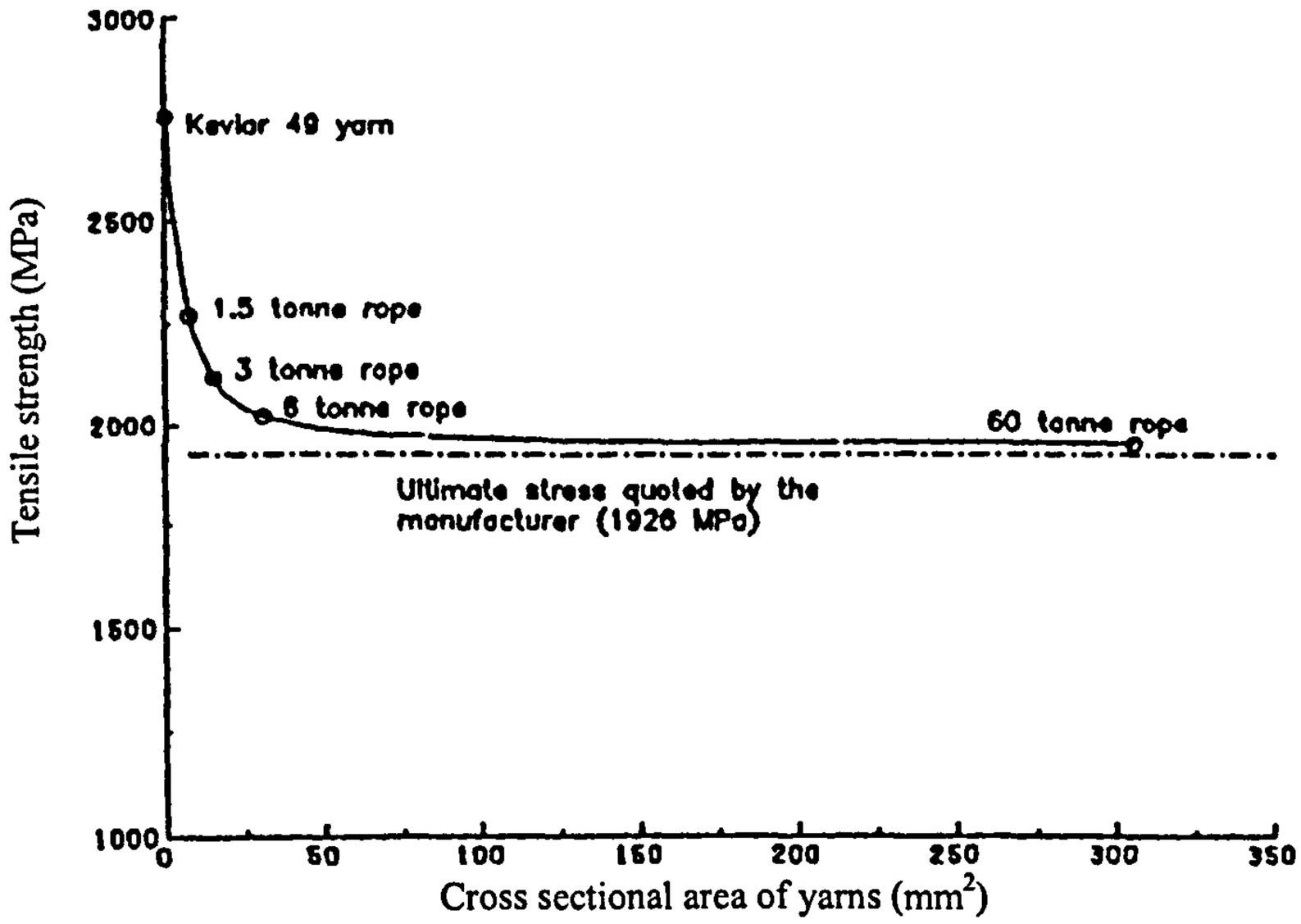

Figure (2. 13): effect of rope size on the tensile strength of Parafil rope type G

2.4.1.1.3 Effect of temperature

Parafil based on aramid fibres has been tested at temperatures between –40 °C and + 80 °C and showed no detectable change in properties. Moreover aramid fibres exposed to a temperature of 150 °C for long periods of time show no detectable change in residual strength when tested at normal temperatures. Aramid fibres show a strength loss of only 5% after 20 hours' exposure at 200 °C when tested at normal temperatures. While at a temperature of 250 °C, the drop is much more accentuated, resulting in a residual strength of about 65% after 20 hours exposure. However, at

about 460 °C, the kevlar 49, which constitute the core of Parafil rope decomposes with a significant weight loss. Figure (2.14) shows the relation between the percentage of tensile strength and the time of exposure, even though these results are for resin impregnated strands of kevlar, the results are broadly applicable to bare yarns. (*Guimaraes*, 1988).

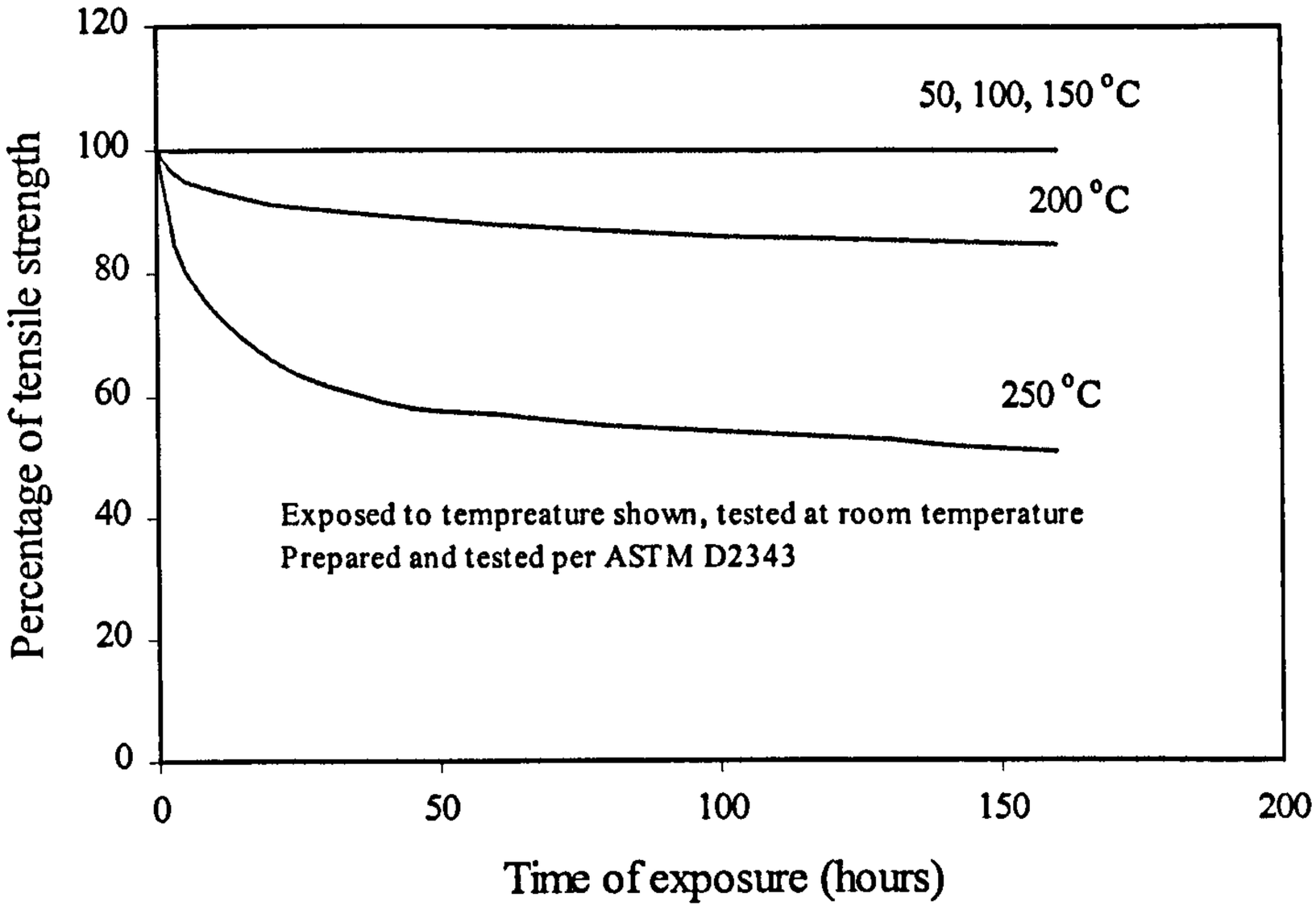

Figure (2. 14): The effect of temperature on the tensile strength of resin impregnated strands of Kevlar 49 (*DU PONT*, 1981)

The relation between the coefficient of thermal expansion (CTE) and the ratio (initial strain/ultimate strain) is linear for a stress level varying from 3% to 45% of the tensile strength of the yarns; at a ratio of 33% the coefficient of thermal expansion will be $-5.7 \times 10^{-6}/°C$. Also, the coefficient of thermal expansion decreases as this ratio increases (*Guimaraes*, 1988).

2.4.1.1.4 Bond

As there is no bond between the yarns that constitute the core of Parafil rope and the surrounding sheath, so the bond between the sheath and the concrete, if it exists, will have a negligible effect on the core. Hence, the Papafil rope has to be considered only as unbonded tendons.

2.4.1.1.5 Long term properties:

Since prestressing tendons are subjected to high permanent stress, the long-term time dependent properties are extremely important. The properties of prime significance are creep, stress-rupture and stress relaxation.

2.4.1.1.6 Creep

Parafil ropes will creep to failure at high stress level. *Chambers* (1988) investigated the behaviour of 60 tonnes nominal breaking load (NBL) rope subjected to different sustained stress values (68% - 95% of normal breaking stress). Chambers concluded that there is a linear relationship between applied stress and the logarithm of the "time to break" which leads to the prediction that a rope subjects to 50% of its NBL will fail after about 100 years.

Also, the total creep strains are of the order of 0.13%, which can be compared with a rope extension when stressed to about 50% of its NBL of about 0.8%. Thus, we can expect to lose something like 16% of the initial prestress force in a Parafil tendon (*Burgoyne*, 1993).

Guimaraes and Burgoyne (1992) studied the creep behaviour of Parafil rope type G of 1.5 and 3.0 tonne NBL and reported that applying a pretensioning load to Parafil rope has the effect of reducing the creep strain of ropes in subsequent loading.

2.4.1.1.7 Stress relaxation

The stress-relaxation relationship of Parafil rope type G shows a linear relation. *Chamber* (1988) studied the stress relaxation of Parafil rope type G of 60 tonne NBL and based on a numerical equation he calculated the predicted relaxation after 100 years as shown in Table (2.4) and Figure (2.15).

Table (2.4): *Predicted relaxation at 100 years*

Nominal initial stress % NBL	***Predicted relaxation at 100 years (% NBL)***
30	7
40	7.4
50	7.8
60	8.2*
70	8.6*

* at these stresses, over long periods of time, Parafil may fail due to stress-rupture.

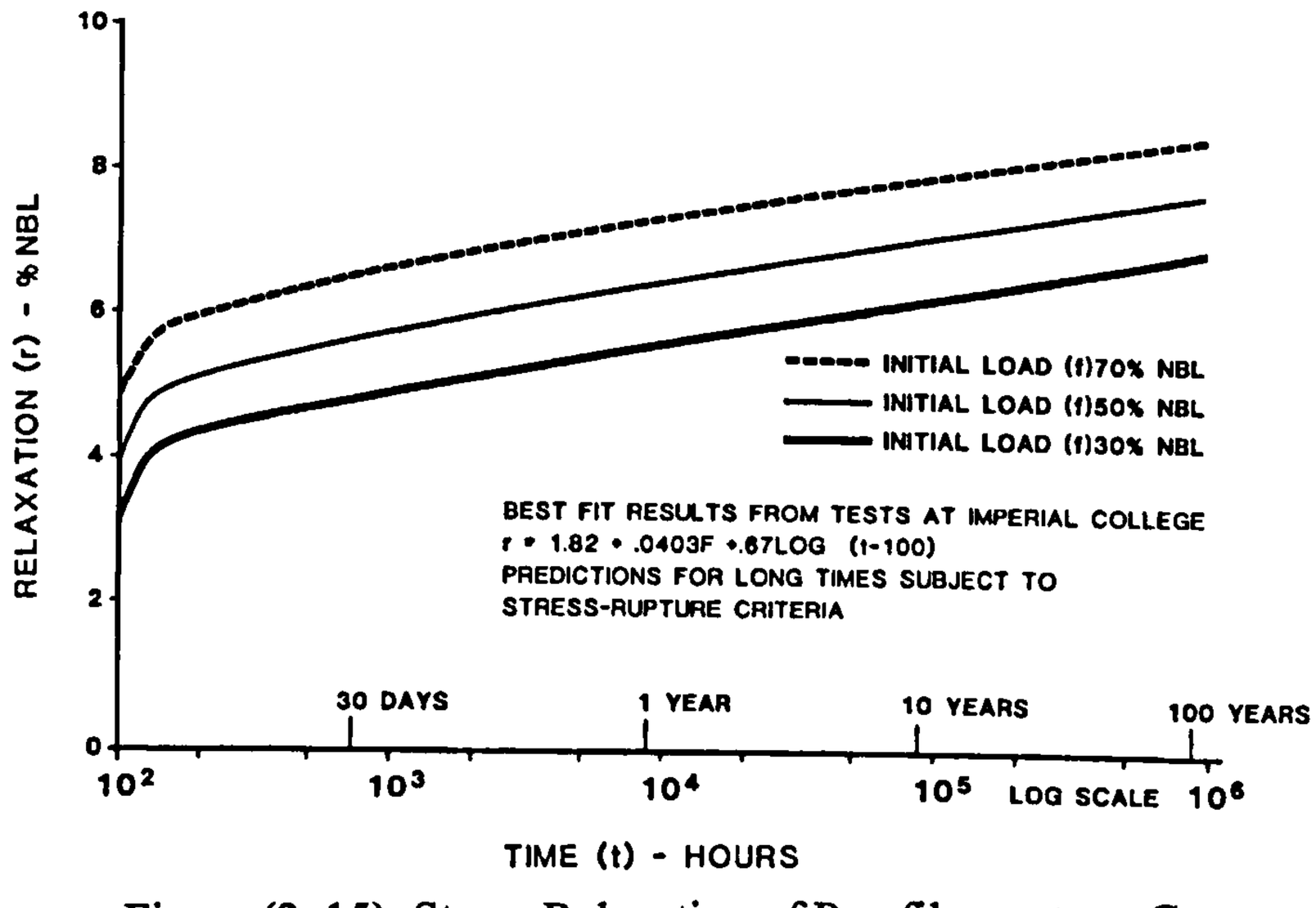

Figure (2. 15): Stress-Relaxation of Parafil rope type G

It should be pointed out that the total loss of prestressing force in a member prestressed with Parafil is very similar to that in a beam prestressed with steel. This is because, whilst the losses due to the relaxation of the tendon are higher than steel, as explained above, the losses due to the elastic shortening, creep and shrinkage of the concrete are less because the Young's modulus of Parafil rope is lower than that of steel (about 2/3). Also the anchorage system of Parafil rope does not cause any loss due to anchorage slip. Therefore, the total losses will be very similar (*Chambers*,1988. *Burgoyne*, 1993).

2.1.1.1.2 Fatigue performance

The fatigue characteristics of aramid fibres are very good. The resistance of Kevlar to tension-tension fatigue is better than that of steel. When fatigue failure of

Kevlar do occur, they are normally due to fretting of fibres over one another. This can only occur at the terminations, or at loading points, and the variation in force in prestressing tendons, especially when unbonded, is extremely low. Thus, it is not believed that fatigue is a problem in prestressing applications (*Burgoyne*, 1993).

2.4.1.1.8 Resistance to environmental effects

The tendons can be expected to have high durability in normal environments. Kevlar is degraded by ultraviolet light, but this is shielded by the sheath and is not a problem. Kevlar fibres also suffer hydrolytic attack by strong acids and alkalis, but the tendons would not be bonded to the concrete, so the fibres will not come into contact with the alkaline concrete. In any event, the sheath will act as a barrier to ingress of chemicals. DuPont have reported that Kevlar is not degraded by either fresh or salt water at normal pH levels (*Burgoyne*, 1993).

2.4.2 Anchorages of Parafil ropes

Parafil ropes are anchored by means of a spike and barrel fitting, which grips the fibres between a central tapered spike and an external matching barrel as shown in Figure (2.16). This has the advantage that as the rope is loaded, the spike is drawn into the barrel, thereby clamping the rope even more tightly. To attach the termination, the end of the rope is passed through the terminal body, and the sheath is removed over the length of the spike; the yarns are then spread out evenly around the terminal, then the spike is pushed in the centre of the end of the rope while the rope itself is slowly pulled down until the cut end of the sheath is level with the back end of the termination. To reduce the creep losses the rope should be pretensioned to a load in excess of that to be applied in practice.

This system has a number of advantages over wedge systems which grip the outside of a tension member (*Burgoyne*, 1993):

- The gripping force between the spike and the barrel has to pass through every fibre (Figure 2.17) which means that each fibre can develop an equal friction force against its neighbours or the fitting. Thus there is no tendency for some of the fibres to carry a disproportionate amount of the load, which would

cause early failure of those fibres, and hence the rope. Systems, which rely on external wedges, have a tendency to develop hoop compression around the outside of the tension member, leaving the inner fibres less well gripped.

- There is no resin in the system, which means that the effectiveness of the termination is not affected by temperature or creep.
- The system is easy to fit, on site if necessary.
- There are no size effects; terminations for large ropes are linearly scaled versions of the terminations for small ropes. The mechanics of operation remain the same.
- The terminations can develop the full strength of the parent rope as shown from test results.

Also, the possibility to change the material of terminations; (aluminum, galvanized steel, stainless steel, etc.), make it suitable for all environmental conditions.

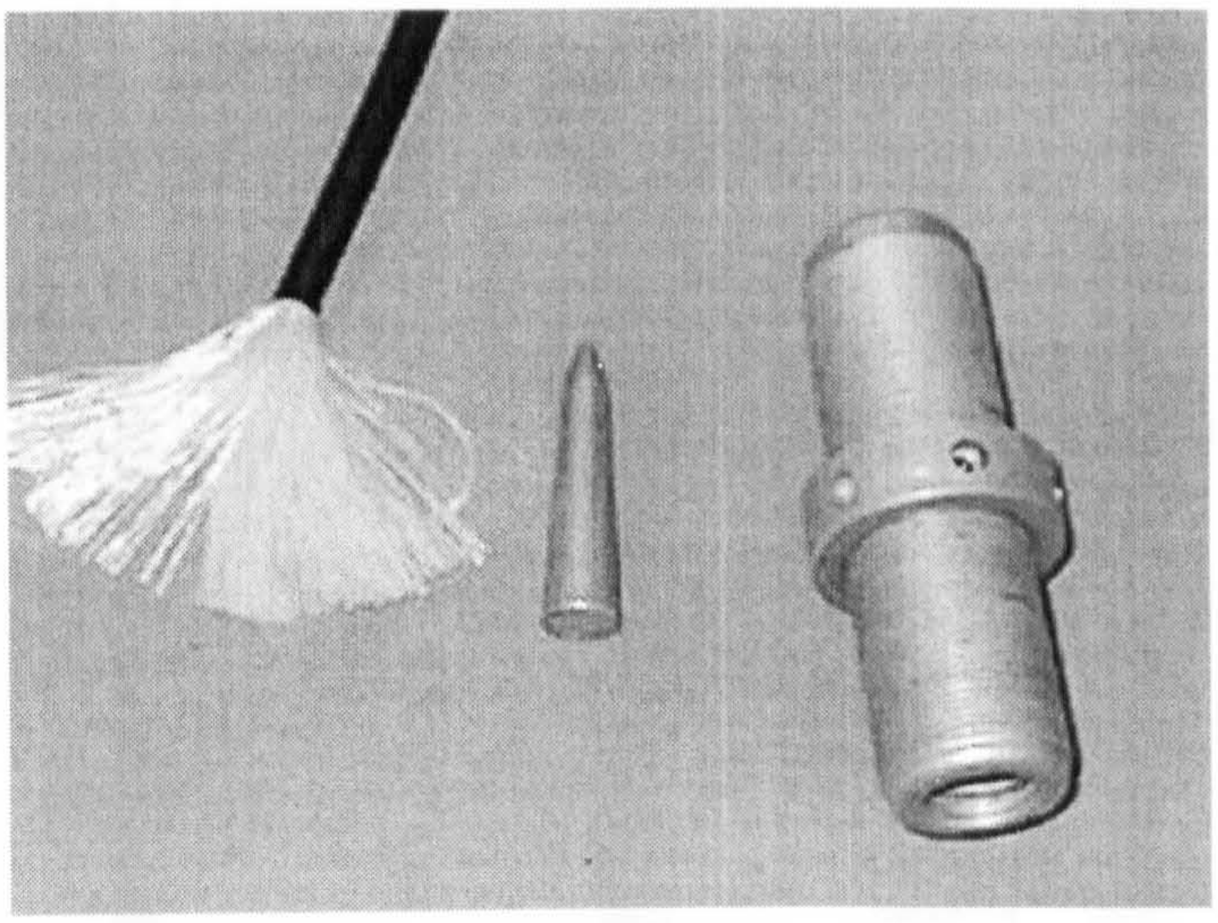

Figure (2.16): Parafil rope and its anchorage

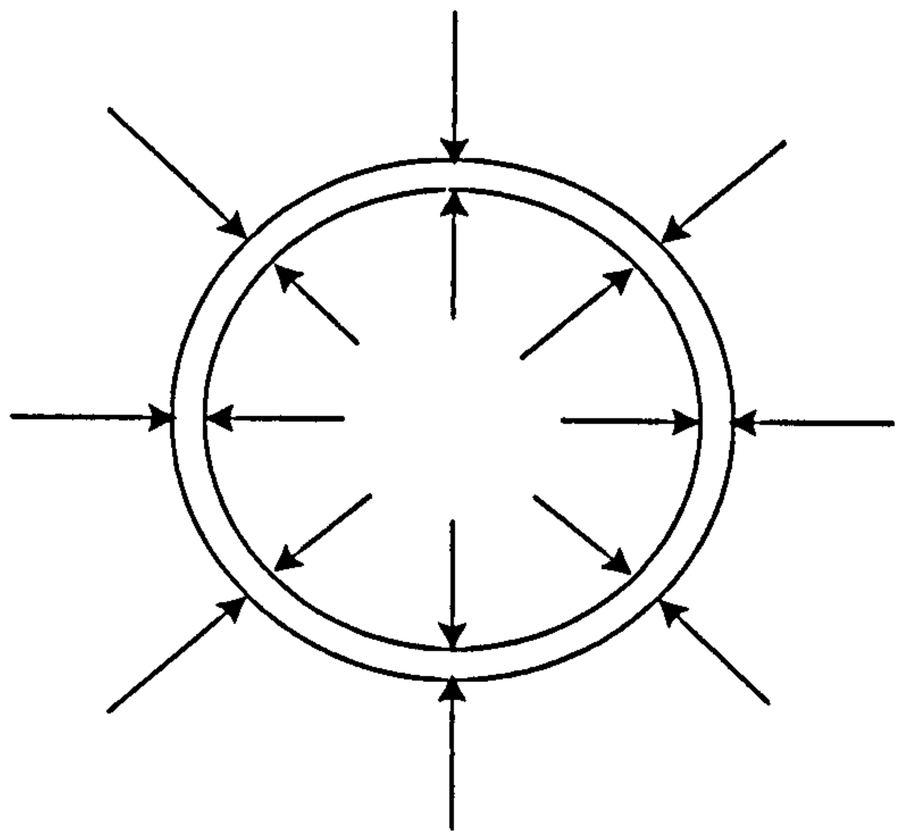

Figure (2.17): Gripping forces within termination

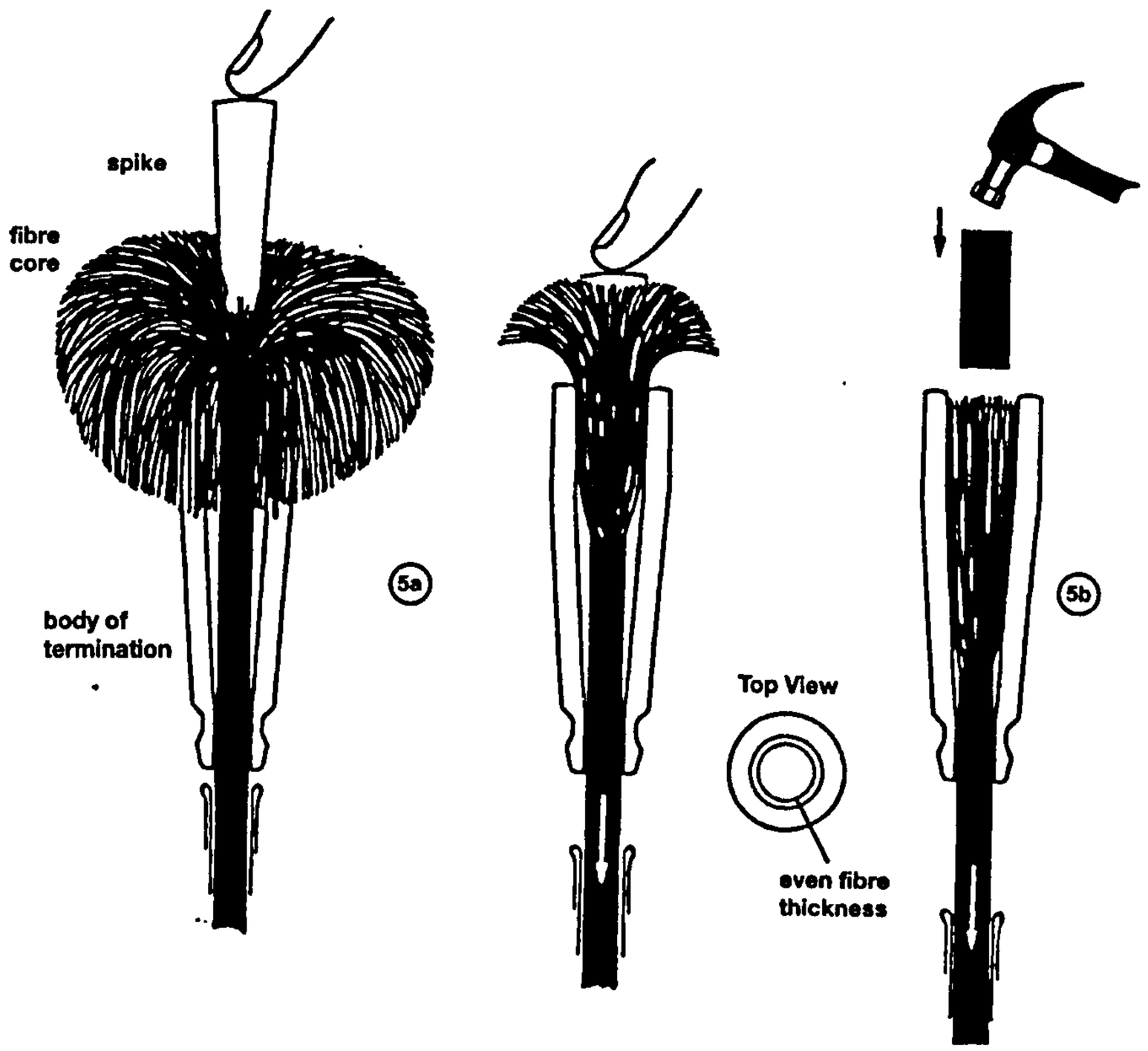

Figure (2.18): Installation procedure for Parafil rope

Table (2.5): *Comparison between GFRP, AFRP and CFRP**

Factor	***GFRP***	***AFRP***	***CFRP***
Types	▪ E-glass (good strength, electrical and weathering properties) ▪ S-glass (more expensive than E-glass , but has a higher strength, Young's modulus and temperature resistance) ▪ S-2 as S-glass but with different coating ▪ T-glass (has higher strength, higher modulus, higher heat resistance and less thermal coefficient than E-glass, also has improved impact strength and electrical properties and improved thermal and chemical resistance ▪ R-glass (has higher tensile strength and modulus relative to E-glass, and gives beneficial results with higher resistance to fatigue ,ageing, temperature and corrosion	▪ Arapree: are fabricated from high moduls Twaron fibres with epoxy resin. ▪ FiBRA: aramid fibres with flexible/elastomeric and rigid resins. ▪ Technora: are made from poly-para-phenylene-3,4-oxidiphenylene terephthalamide (PPODTA) fibres and vinylester resin.	▪ Leadline: are pultruted using unidirectional carbon fibres at 65% fibre volume fraction with an epoxy resin ▪ Carbon fibre composite cable (CFCC): are made from PAN based carbon fibre in epoxy or bismaimide resins ▪ Nippon steel advanced carbon fibre composite (NACC): is made using both PAN and Pitch based carbon fibers.
Tensile strength	▪ 0.55 -1.67 GPa	▪ Arapree: 2.8-3 GPa ▪ FiBRA: 1.39 GPa ▪ Technora: 2.18 GPa	▪ Leadline: 1.78-1.83 GPa ▪ CFCC: 1.8 Gpa ▪ NACC: 0.79-2.02 GPa
Modulus of elasticity in longitudinal direction	▪ 41-55 GPa (approximately 25% of that of the steel). ▪ The properties of glass fibres are isotopic. Thus ,the axial and transverse modulus of elasticity are the same	▪ Arapree: 125-130 GPa ▪ FiBRA: 68.6 GPa ▪ Technora: 54 GPa ▪ Properties are anisotropic	▪ Leadline:147 GPa ▪ CFCC: 137 GPa ▪ NACC: 118-206 GPa ▪ Properties are anisotropic

Table (2.5): *Comparison between GFRP, AFRP and CFRP**

Factor	***GFRP***	***AFRP***	***CFRP***
Ultimate strain %	3% - 5.5%	▪ Arapree: 2.4 % ▪ FiBRA: 2 % ▪ Technora: 3.8 %	▪ Leadline: 1.5-1.7% ▪ CFCC: 1.6 % ▪ 0.3 (HM)- 2.0 (LM)
Creep	▪ Glass fibres have excellent resistance to creep. Creep rupture diminishes if (Psustained / P short term) ≤ 60%	▪ Has lower creep resistance than steel , GFRP and CFRP	▪ has high resistance to creep (at 1000 hrs creep strain ≅ 0.006%)
Relaxation	▪ Has a good resistance to relaxation (better than steel, but less than carbon)	▪ Lower resistance to relaxation than steel.	▪ Has an excellent resistance to relaxation
Fatigue (Dynamic behaviour)	▪ GFRP'S fatigue strength is lower than that of steel. GFRP bars do not fatigue when stressed to no more than 50% of their ultimate strength	▪ AFRP has an excellent fatigue strength	▪ CFRP has better fatigue strength than that of steel.
Transverse Shear strength	quite low in comparison with their longitudinal properties		
Coefficient of thermal expansion (CTE) in the longitudinal direction	6-12 x 10^{-6} / ^{0}C	▪ Arapree: 1.8 x 10^{-6}/ ^{0}C ▪ FiBRA: -5.2 x 10^{-6}/ ^{0}C ▪ Technora: -3 x 10^{-6}/ ^{0}C	Carbon fibre has low longitudinal and transverse CTE) ≅ 0.6x 10^{-6} / ^{0}C
Specific gravity (SG) t/m^3	(1.5-2.0)	(1-1.5)	(1.5-2.2)
Effect of humid Environment	▪ Glass fibres do not absorb water	▪ aramid fibres absorb water and can be deteriorated due to water absorption.	carbon fibres have excellent moisture resistance
Magnetic permeability	Electro-magnetic neutrality.	as GFRP	less than steel strand

Table (2.5): *Comparison between GFRP, AFRP and CFRP**

Factor	***GFRP***	***AFRP***	***CFRP***
Chemical attack	▪ GFRP bars have high resistance to acids ▪ GFRP bars can deteriorate rapidly in an alkaline environment.	▪ AFRP has excellent resistance to chlorides ▪ Due to chemical attack, AFRP strength (after 100 years) ≅ 85% of the initial strength.	▪ Carbon fibres exhibit a good resistance to both highly acid and highly alkaline environments.
Impact resistance	Less than AFRP	has excellent impact resistance	carbon fibres have a low impact resistance due to their low ultimate strain
Electrical conductivity	GFRP bars have excellent electrical insulating properties.	as GFRP	can be highly conductive to electricity
Ultraviolet (UV) effect	Almost no deterioration	Aramid fibers are strong UV absorbers and deteriorate when exposed to ultraviolet light.	Almost no deterioration
Fracture	Almost completely brittle and fracture without any reduction in cross-sectional area.	Aramid fibres fracture in ductile manner, although the overall strain to failure is still small	as GF
Workability	▪ Using thermosetting resins, bars cannot bend sharply (90^0 or 180^0) in the field ▪ Can be cut easily in the field with portable saw	▪ AFRP reinforcement made in the form of rods, tendons and ropes	▪ CFRP reinforcement made in the form of rods, tendons and ropes
Cost	Some types are cheaper than steel	Higher than steel	higher than aramid fibres

* *Clements,* 1998. *Karbhari,* 1998. *Vaughan,* 1998.

Chapter 3

Experimental Programme

3.1 INTRODUCTION

To study the benefit of using Parafil rope Type G as external prestressing tendons for strengthening or rehabilitation prestressed concrete beams and to understand the behaviour of these beams after strengthening, thirteen prestressed concrete beams were tested up to failure, over a period of over one year. One had internal prestressing steel only, and twelve had internal prestressing steel and were strengthened using external prestressing Parafil Rope Type G. All beams were of I-section with an overall depth of 180 mm. Some of the main factors affecting the behaviour of strengthened prestressed beams, during service and ultimate stage, were examined. These factors are:

- Value of external prestressing force
- Number of deviators
- Effective depth of the external prestressing force
- Previous loaded stage before being externally strengthened
- Concrete strength (f_{cu})
- Effective span / depth ratio (L/h)

In this chapter, details of test specimens, materials used, instrumentation and testing procedures are described. Figure (3.1) shows the sequence of stages of beam preparations prior to testing.

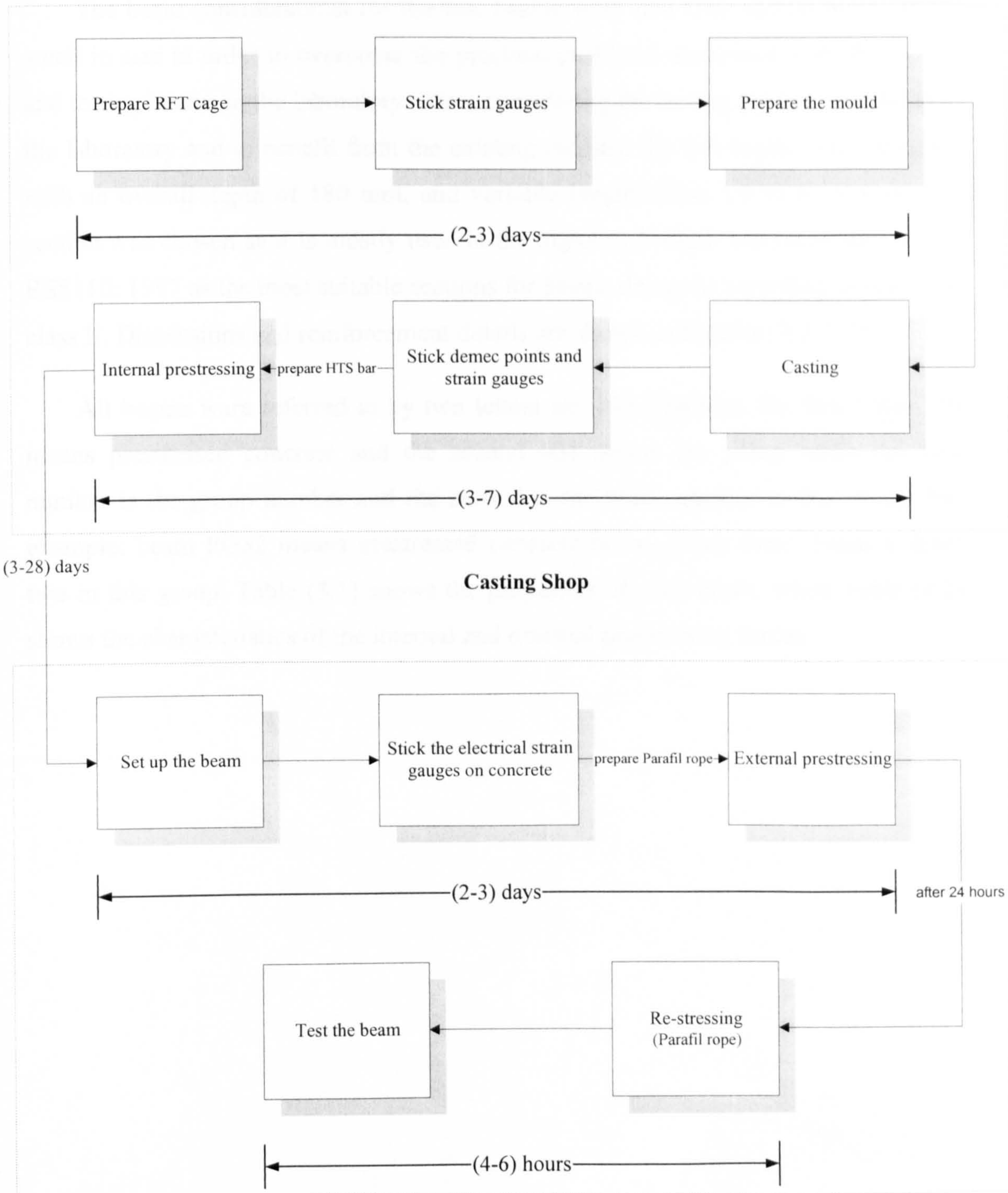

Figure (3.1): Stages of beam preparation till testing

3.2 DESCRIPTION OF TEST BEAMS

3.2.1 Test Beams

The basic considerations for the test beams were that they should be relatively small in size in order to overcome the practical problems associated with fabricating and testing beams in the laboratory. Also, considering the testing facilities available in the laboratory and to benefit from the existing moulds, the test beams were designed with an overall depth of 180 mm, and variable length (from 1.9 m to 3.90 m). I-section was chosen as it is mostly used in the highway bridges and recommended by BS8110: 1997 as the most suitable sections for beams designed according to class I or class II. Dimensions and reinforcement details are shown in Figures (3.2- 3.3).

All beams were referred to by two letters and two numbers, the first letter (P) means prestressed concrete and the second (G) means the group while the first number is the group number and the second is the beam number in this group. For example; beam PG32 means prestressed concrete beam, group three, beam number two in this group. Table (3.1) shows the properties of each beam, while Table (3.2) shows the characteristics of the internal and external prestressing forces.

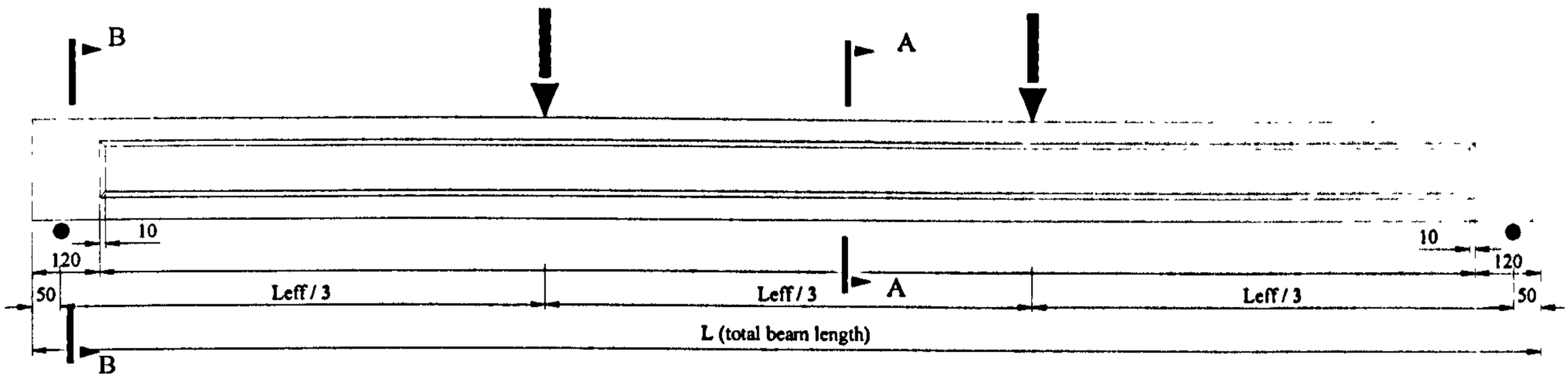

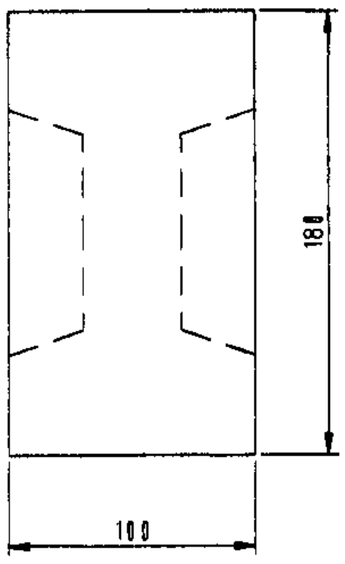

Sec (B-B)

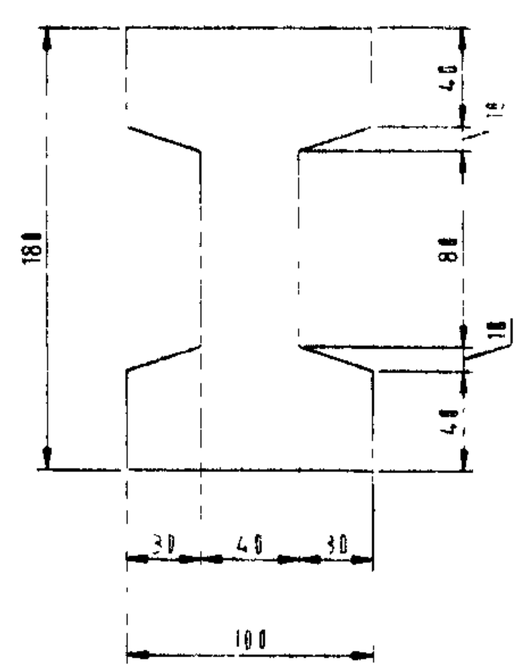

Sec A-A

Figure (3.2): Beam dimensions

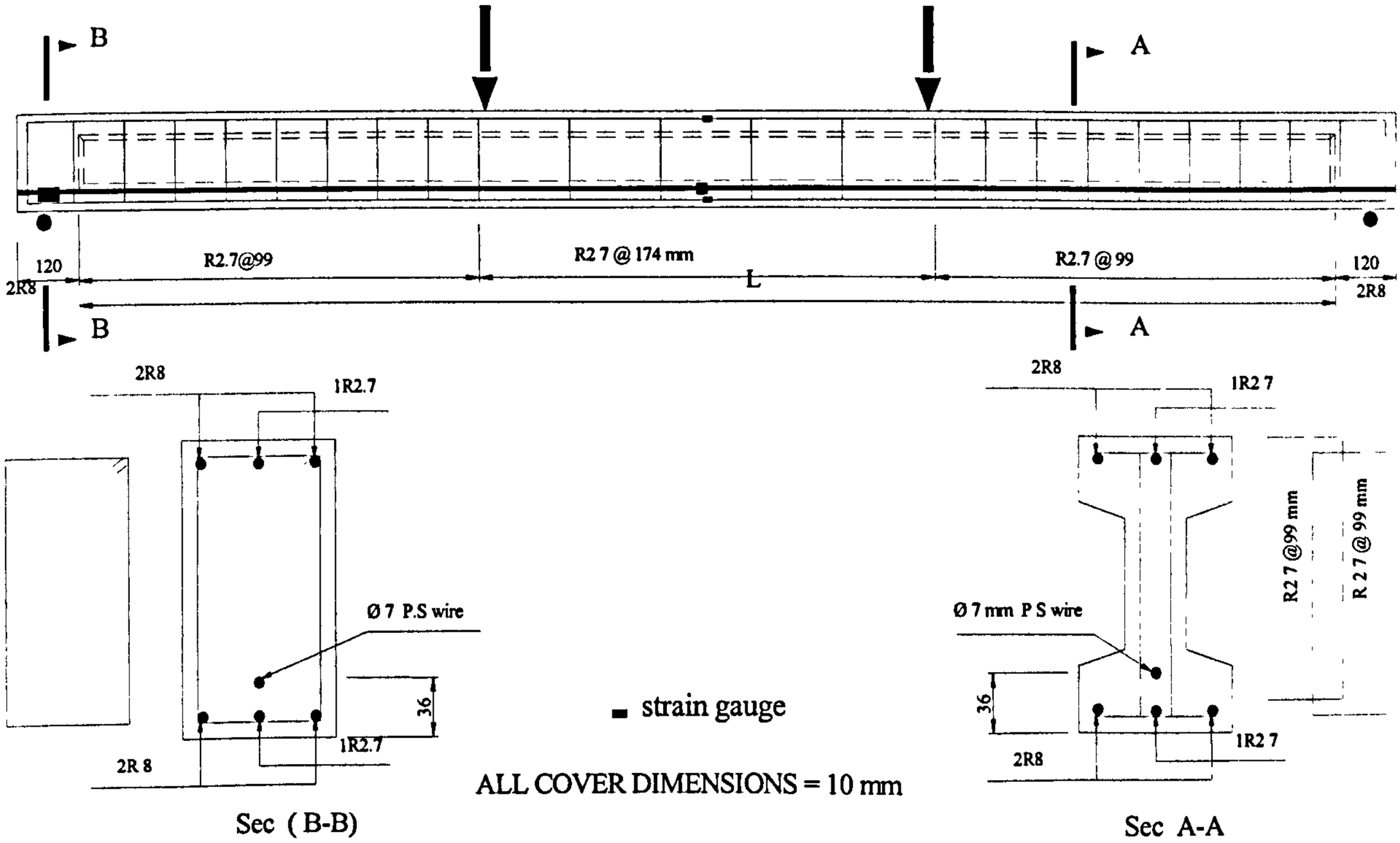

Sec (B-B)

Sec A-A

Figure (3.3): Reinforcement details of beam test

Table (3.1): *Details of test beams*

Beam no.	***Dimensions***		***Internal prestressing***		***External prestressing***	
	Length (L_o) (mm)	**Depth (mm)**	**f_{cu} (MPa)**	**Date ***	**f_{cu} (MPa)§**	**Date***
B1	2700	180	42.37	7 days	55.37	26 days
PG11	2700	180	42.2	7 days	55.77	40 days
PG12	2700	180	42.6	7 days	53.3	34 days
PG13	2700	180	43.13	7 days	55.03	33 days
PG21	2700	180	38.8	7 days	47.7	33 days
PG31	2700	180	47.9	11 days	54.2	36 days
PG32	2700	180	40.87	6 days	57.13	34 days
PG41	2700	180	38.5	6 days	52.2	32 days
PG42	2700	180	32.73	6 days	45.7	31 days
PG51	2700	180	37.2	6 days	43.3	9 days
PG52	2700	180	63.5	6 days	79.27	34 days
PG61	3900	180	33.83	7 days	48.93	37 days
PG62	1900	180	37.87	8 days	47.47	30 days

* From casting date. § At test date

Table (3.2): *details of prestressing forces*

Beam no.	***Internal prestressing force***			***External prestressing force***		
	$P_{initial}$ (KN)	**$P_{effective}$ (KN)**	**Eccentricity (mm)**	**$P_{effective}$ (KN)**	**Number of deviators**	**Eccentricity (mm)**
B1	40.62	37.85	151.5	-------	-------	-------
PG11	42.07	38.76	151.5	60.35	2	142.9
PG12	44.38	41.21	149.5	48.98	2	142.9
PG13	43.44	40.27	150.5	72.27	2	142.9
PG21	43.55	39.36	150.5	60.01	1	142.9
PG31	41.73	39.25	151.5	60.52	2	160.9
PG32	42.87	39.08	151.5	61.03	2	192.9
PG41	45.63	40.80	151.5	60.3	2	142.9
PG42	41.14	37.07	151.5	60.57	2	142.9
PG51	40.53	38.54	150.5	60.53	2	142.9
PG52	43.46	40.75	151.5	60.13	2	142.9
PG61	42.5	40.1	149.5	60.16	2	142.9
PG62	43.64	41.16	151	60.73	2	142.9

3.2.2 Mix Design

Beam width and the prestressing force exerted on the beam during the internal prestressing after about 7-days from casting, are two factors that govern the concrete mix design. Due to the narrow section, a reasonable workability for the concrete was needed and concrete strength after 7-days should be able to tolerate the prestressing force safely. For these reasons (for all beams except beam PG52 that had a different mix), three trial mixes were made to choose the suitable one for casting. That mix gave nominal 28-days cube strength of 55 MPa and having a slump of 185 mm was selected. Although, beam PG51 had the same mix as the previous beams but it had

lower concrete strength (43.3 MPa) at test date, as it was tested after three days from internal prestressing, this for two reasons:

- High concrete strength at internal prestressing was needed to overcome the problems that appeared if a lower concrete strength was used (bursting cracks at end block or flexural cracks along the beam span).
- To achieve the required concrete strength at the time of external prestressing.

In order to get almost the same effective prestressing force at test date as the other beams, the initial prestressing force of beam PG51 was reduced by a value equal the difference between the average losses at test date and at three days.

For beam PG52, another mix was selected to give 80 MPa cube strength after 28 days. To achieve the required workability, a water reducer was used

The ingredients of these mixes were as follows:

- **Cement**: Ordinary Portland cement (OPC) with no additives was used throughout the whole series of tests.
- **Fine aggregate**: Ordinary concreting sand of zone III, having a maximum size of 0.5 mm was used.
- **Coarse aggregate**: supplied from the same zone, with 10-mm maximum size.

Table (3.3): Properties of concrete mixes

Mix no.	*Cement*	*Gravel*	*Sand*	*Water*	*Slump (mm)*	*plasticier*
I	1	2.86	1.94	0.54	185	--------
II	1	2.4	1	0.34	High slump	1 %

3.2.3 Steel:

3.2.3.1 Longitudinal non-prestr essed steel

Two 8-mm hot-rolled mild steel bars (notation R8) were provided at the bottom flange as tensile reinforcement, and at the top flange to facilitate the formation and location of the reinforcing cage. The results of tensile tests on sample bars are given in Table (3.4), and the typical stress-strain curve is shown in Figure (3.4).

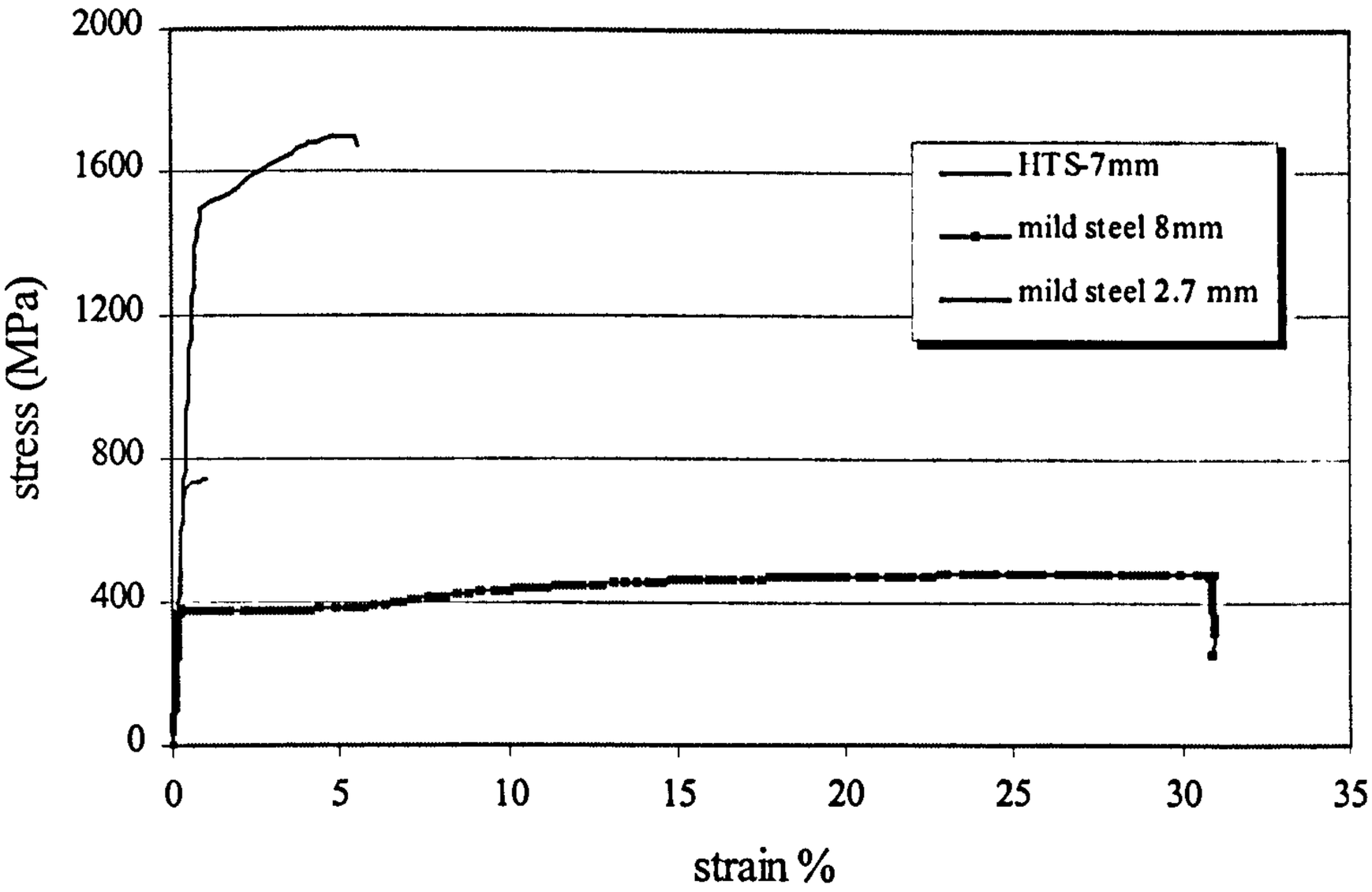

Figure (3.4): Stress-Strain curves of steel reinforcement

3.2.3.2 Internal Prestressing Steel:

Prestressing tendons used in this study were 7-mm diameter, plain cold-drawn, high tensile steel wire with a specified characteristic strength of 1690 MPa. The properties and dimensions of the steel wire conformed to the requirements of BS 5896:1980. A typical stress-strain relationship of the wire, obtained from tensile tests, is shown in Figures (3.4-3.5), and its mechanical properties are given in Table (3.4).

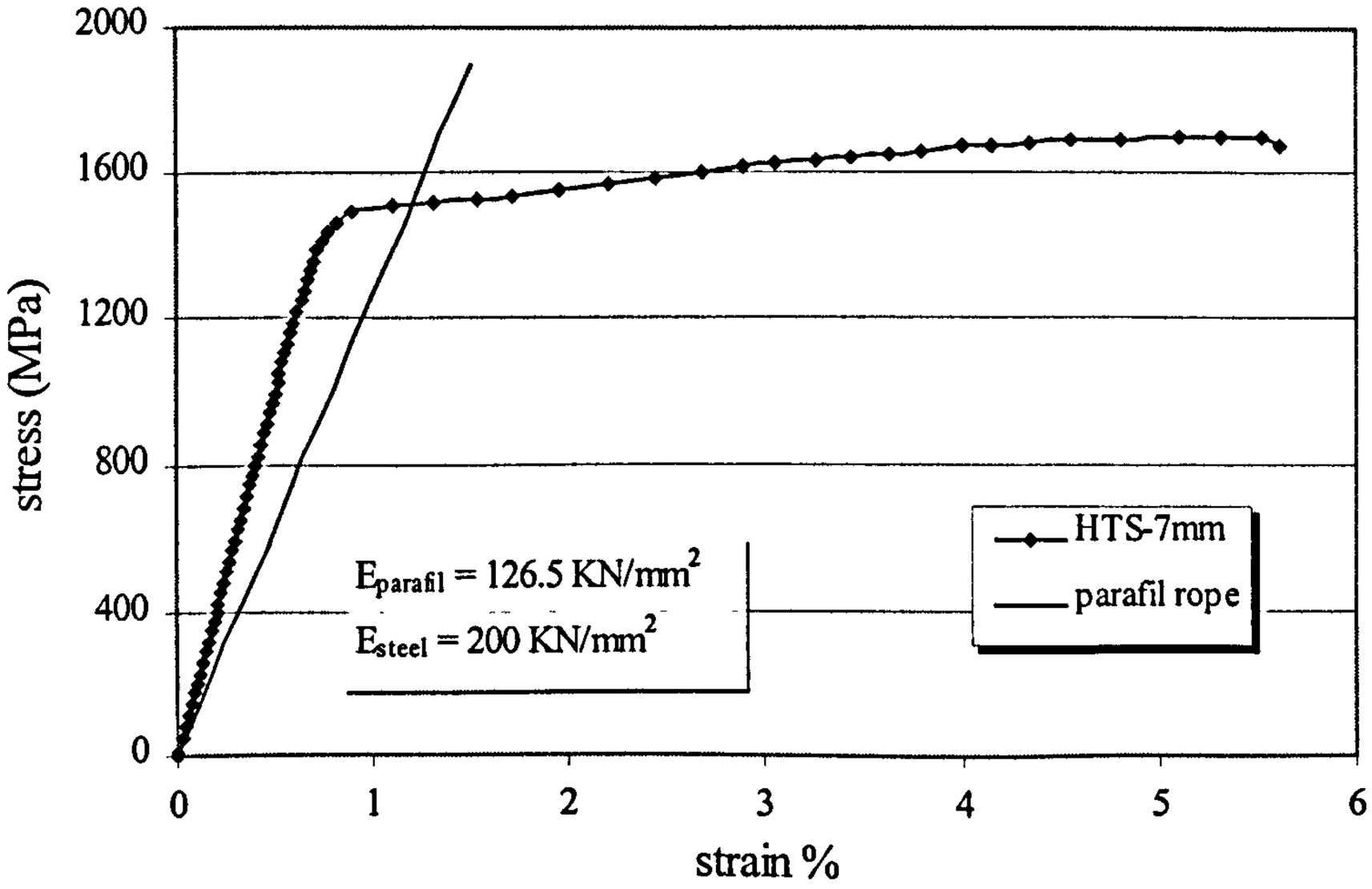

Figure (3.5): Stress- Strain curves

3.2.3.3 Shear Reinforcement

Shear reinforcement was provided by 2.7-mm mild steel as shown in Figure (3.3). Also, they were used to hold the longitudinal mild steel in position. In each beam, shear reinforcement at a spacing of about 99 mm was used throughout the shear span on both sides except at the support regions where two 8-mm hot-rolled mild steel links were used to resist bursting force results from the prestressing force.

3.2.4 External Prestressing Tendons

External prestressing tendons were composed of two Parafil ropes Type G with a diameter of 11 mm. The properties of the Parafil rope are shown in Table (3.4) and Figure (3.5).

Table (3.4): *Properties of steel and Parafil Rope*

	stirrups	***Mild steel***	***High tensile steel***	***Parafil Rope***
Diameter (mm)	2.67	8	7	11/ (7.6)*
Area (mm^2)	5.6013	50.265	38.5	30.55 **
Yield strength (N/mm^2)	----	368	1470	----
Young's modulus (KN/mm^2)	200	200	200	126.5
Ultimate strength (N/mm^2)	709	468	1660	1900
Ultimate strain (ε_{ult} %)	0.464	21.54	5.2	1.5

*Outside sheath diameter / fibres core diameter. ** Based on area of fibres in the core

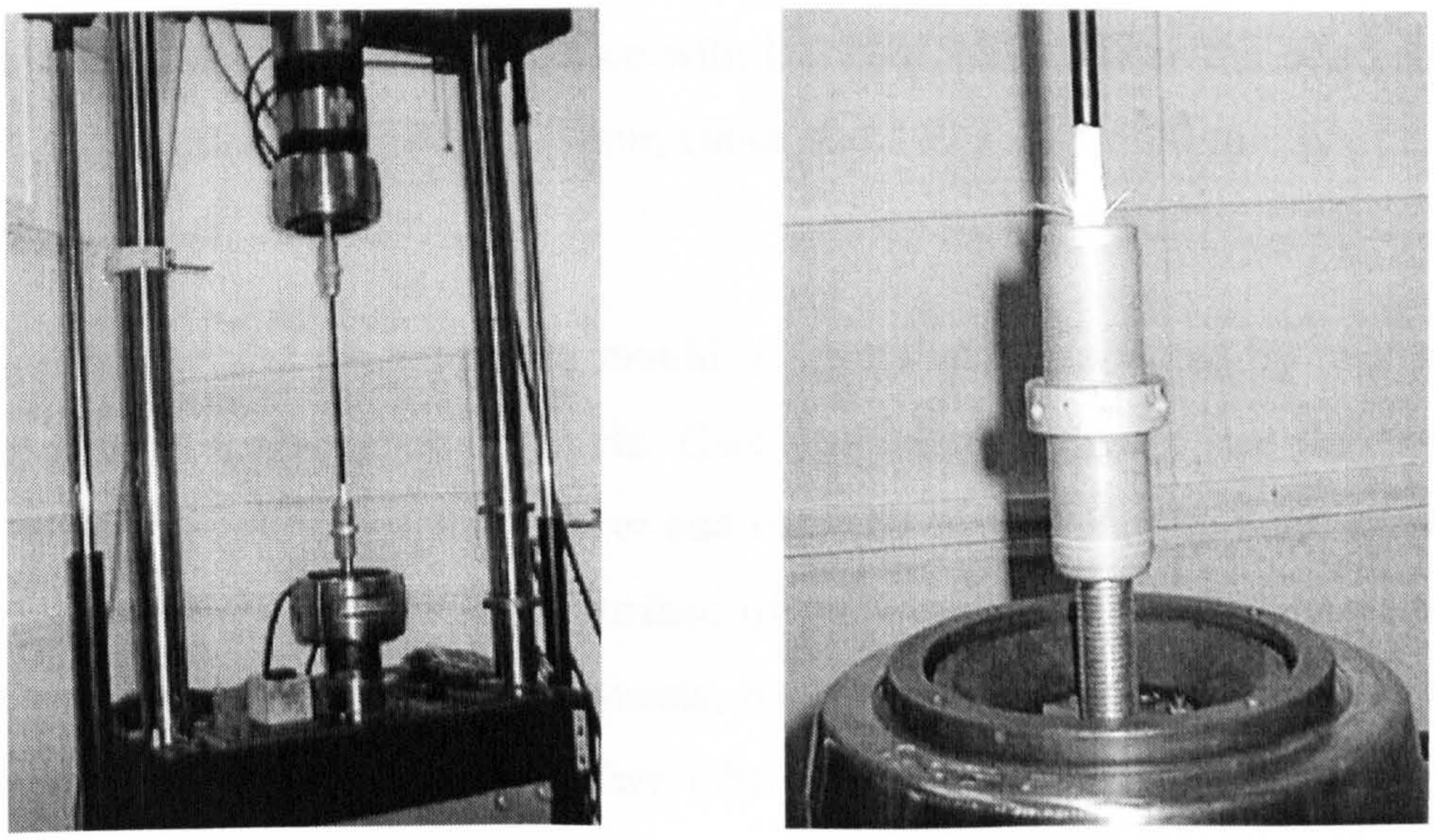

Figure (3.6): Testing of Parafil Rope

The moulds were constructed on the vibrating table bed. The sides of the mould consisted of two steel channels 180 mm deep, placed back to back and bolted to a horizontal bed. Varnished wood sections were attached to the inside faces to form the web shape. Steel plates with accurately located holes were placed at the ends of the unit to keep the 20-mm diameter inflatable rubber duct in the correct position. The beams were cast one at a time, in one mould 2.7 metres long. Only group six was cast in another mould due to the change in length.

3.2.5 Casting and Placing

Before placing the reinforcing cage in the mould, the sides of the mould were given a coat of mould oil then the reinforcing cage was located accurately by means of spacers at regular intervals to maintain the required concrete cover (10 mm).

The duct for the tendons was formed by an inflated rubber tube of 20-mm diameter held rigidly in position by locating rings fixed to the sides of the mould at the required level. For grouting requirements, two inclined plastic tubes, one at each end were placed on the top surface of the rubber tube and protruded above the beam surface as shown in Figure (3.7). For each concrete mix, all the constituent materials were weighed in the required proportions before being fed into a mixer of 250-kg dry weight capacity. The materials were turned over for about a minute before the addition of the required quantity of water, which was followed by a further two minutes of mixing to ensure a uniform workable mix. Slump tests on the fresh concrete were carried out in accordance with BS 1881:1983 before the concrete was placed. Control tests comprising 100-mm cubes and 500 x 100 x100 mm prisms were cast from each mix.

The concrete was placed in the mould in layers and compacted by means of a vibrating table at a frequency of 50 Hz. Care was taken to ensure that the concrete flowed freely around the inflated rubber and between the reinforcing bars, especially in the bottom flange. The exposed surface of the beams and specimens were then covered with wet burlap and plastic sheets, the former of which was watered daily. The mould was stripped and the rubber tube was deflated one day before internal prestressing.

3.2.6 Control Tests:

Concrete strength as well as modulus of rupture of each beam was determined according to BS 1881:1983. Specimens used to determine the concrete strength and modulus of rupture were as follows:

- **Cube test**: six 100-mm cubes were used to obtain the concrete compressive strength. Three cubes were tested on the day of internal prestressing and three on the day of test.
- **Modulus of rupture**: tests were carried out on four 100x100x500 mm prisms, two on the day of internal prestressing and two on the day of test.

3.3 INTERNAL PRESTRESSING PROCEDURE

3.3.1 Preparation of Beams

About one week after casting, the beams were internally stressed. One day prior to the time of stressing the following procedure was carried out. Grids on each beam were marked in pencil for strain measurements. Stainless steel demec studs for the 100-mm demountable mechanical extensometers were attached at the positions on beam surface as shown in Figure (3.16).

3.3.2 Components of The Internal Prestressing System:

- **Duct**: duct was formed using an inflated rubber tube of 20-mm diameter. After casting and concrete hardened this tube deflated and removed outside the beam, leaving a straight duct through the beam with the required eccentricity.
- **End plates**: Two steel end plates with dimensions (100 mm width x 100 mm height, 10 mm thickness) were used, one at each end, to transfer and spread the prestressing force to the beam.
- **Anchors**: Two 7-mm steel anchors were used, one at each end, to transfer the prestressing force to the concrete and fix the prestressing wire in position as shown in Figure (3.7)

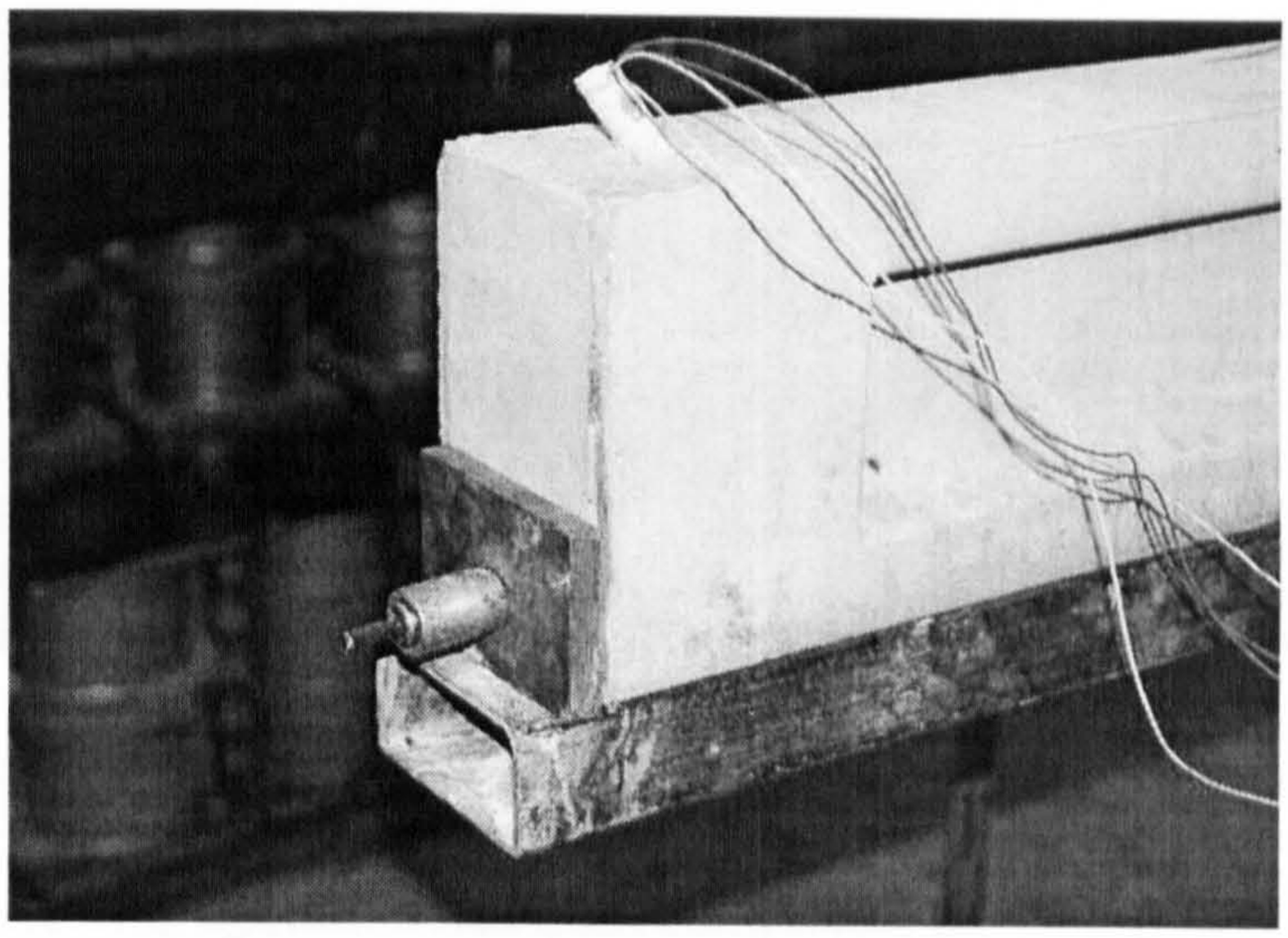

Figure (3.7): Anchor, end plate and grouting tube for internal prestressing process.

3.3.3 Prestressing Process:

The stressing operation was carried out about one week after casting, when concrete strength was about 40 MPa. Before stressing, initial measurements on the gauge points and initial deflection were taken. The prestressing wire was cleaned and degreased, then threaded through the duct, care being taken to prevent twisting inside the duct. The end bearing plates were placed over the ends of the prestressing beam and the wire at the remote end was locked using anchor grips.

A force of 6 KN was applied to the wire by means of mono-wire jack to secure the end plates in position accurately and take up the wire slack. Tension in the wire was then increased to 45 KN. The extension of the wire was measured and checked against the calculated value. The force applied by the jack was measured by the jack pressure gauge, which had previously been calibrated by the manufacturer. This force was also checked against the readings obtained from the electrical strain gauges on the wire. When the desired force had been attained, the split wedges were hammered into position and the jack pressure released, then the beam was grouted. This procedure was repeated for all beams.

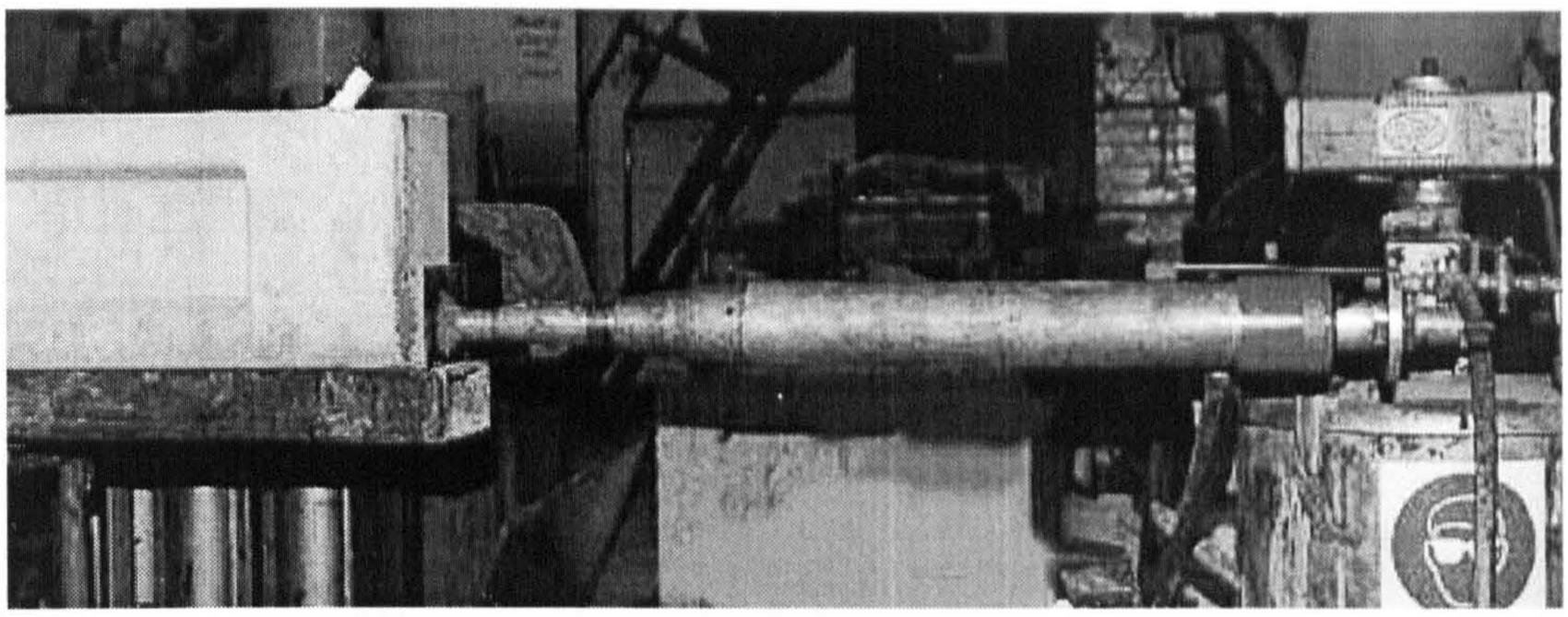

Figure (3.8): The hydraulic jack during internal prestressing process.

After the stressing operation had been completed, the Demec and electrical strain gauge measurements and mid- span deflection were taken. Then the projecting wire was cut off and the beam was lifted and transferred to the lab where it would be tested.

Prestressing force was determined from the strain on the wire. This strain was measured using the extension of the hydraulic jack and electrical strain gauges mounted on the prestressing wire. In each beam, strain measured via the hydraulic jack extension was slightly higher than that of the strain gauge. This difference between the strain gauge value and jack reading value (during stressing the wire) can be attributed to following reasons:

- The gradual seating of the anchorages that normally accompanies the increase in stress in the prestressing steel.
- The slippage between the wire and the anchor during stressing.

These resulted in, particularly for short-span members of the type used in this research, increased hydraulic jack extension reading and hence, increased computed strain values. Due to this, the strain gauge reading was adopted as the actual value. Typical relationship between prestressing force and gauge strain reading is shown in Figure (3.9).

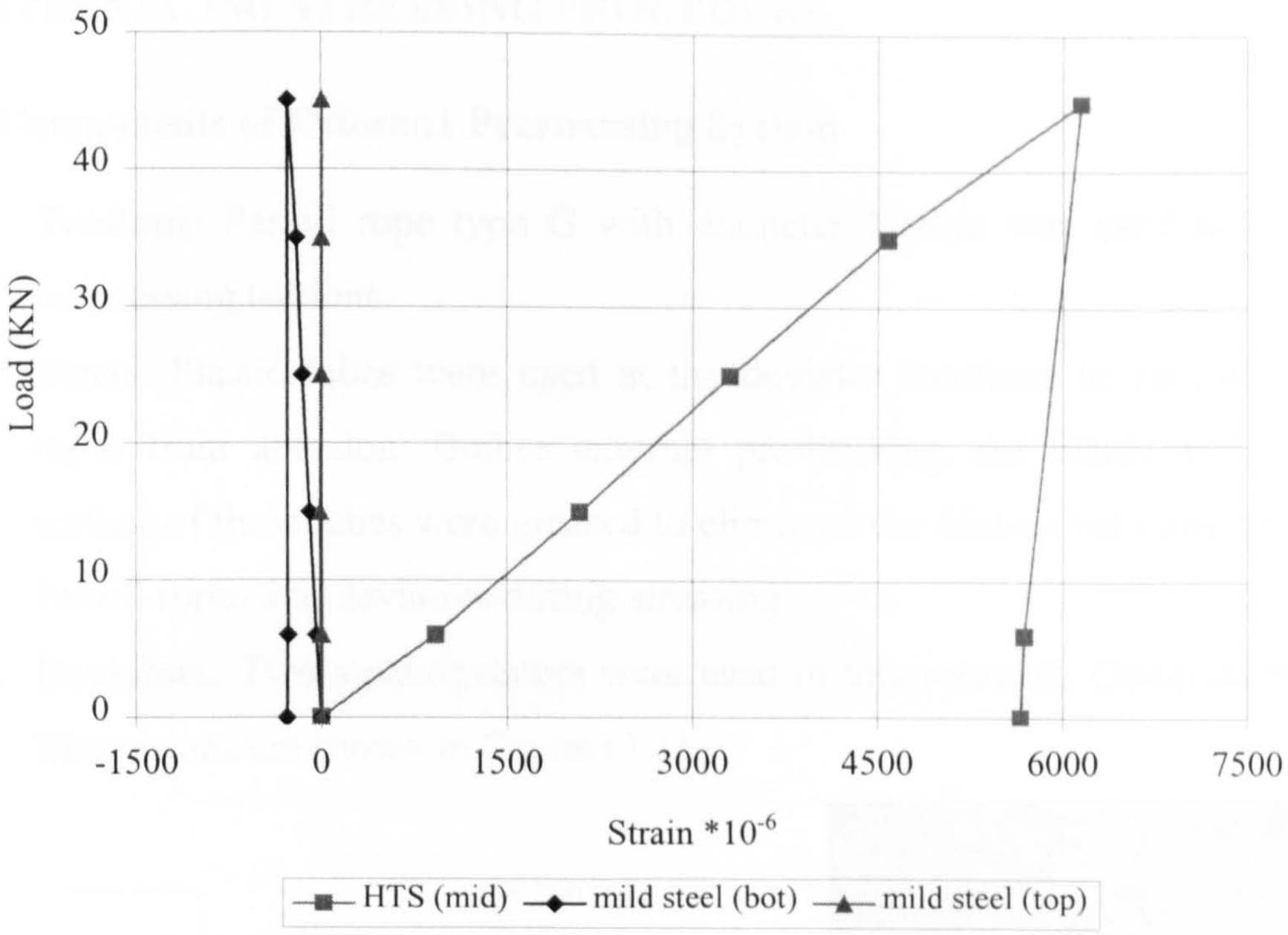

Figure (3.9): Steel strain during internal prestressing.

3.3.4 Grouting Procedure

After tensioning, the beam was grouted. First, the duct was thoroughly washed by blowing water and then dried by blowing compressed air under high pressure through it. Then the ends of the beam were sealed with sealant material and the duct was grouted, with a mixture of two parts of rapid-hardening Portland cement to one part of water, at a pressure of 0.35-0.42 MPa. After grouting, the beam was removed to the lab, and stored till the testing day.

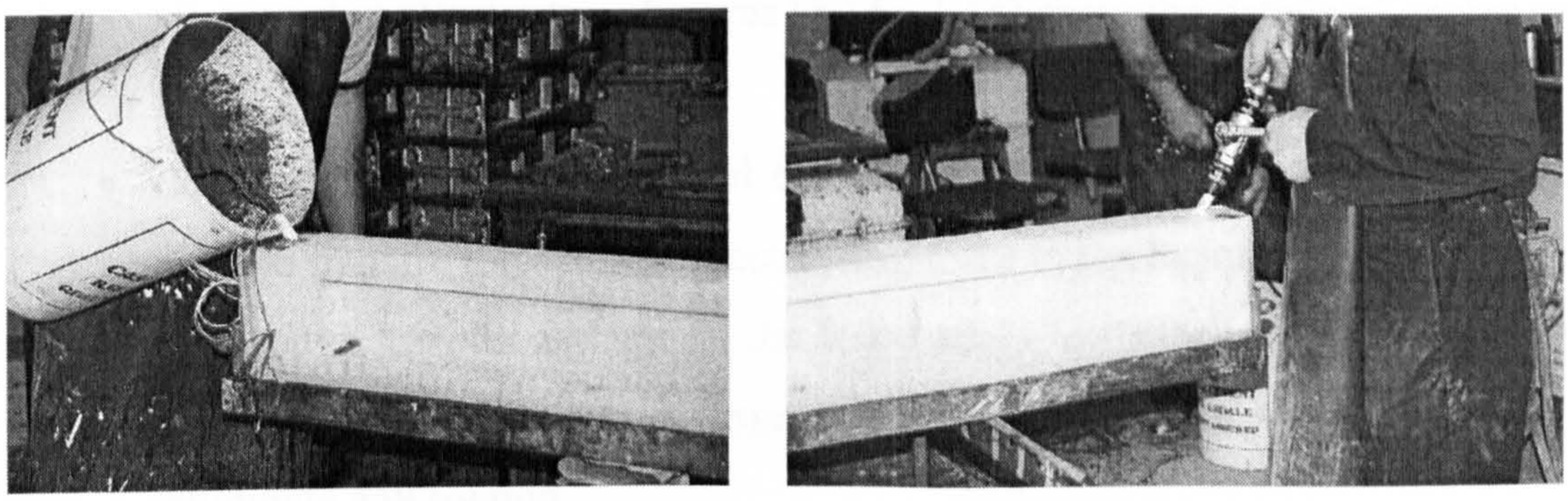

Figure (3.10): Grouting process.

3.4 EXTERNAL PRESTRESSING PROCEDURE

3.4.1 Components of External Prestressing System

- **Tendons**: Parafil rope type G with diameter 11-mm was used as external prestressing tendons.
- **Ducts**: Plastic tubes were used at the deviator locations to protect Parafil ropes from abrasion. Before external prestressing, the inside and outside surface of these tubes were greased to eliminate the friction between them and Parafil ropes and deviators during stressing.
- **Deviators**: Two steel deviators were used in this research. Components and Dimensions are shown in Figure (3.11).

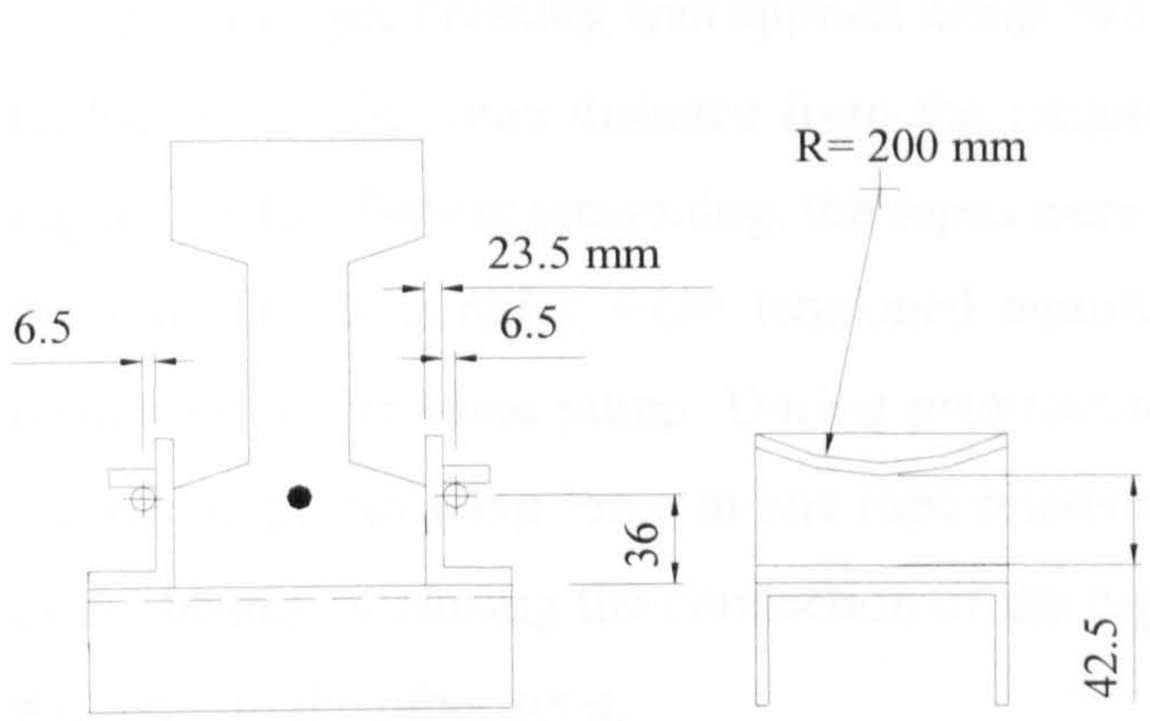

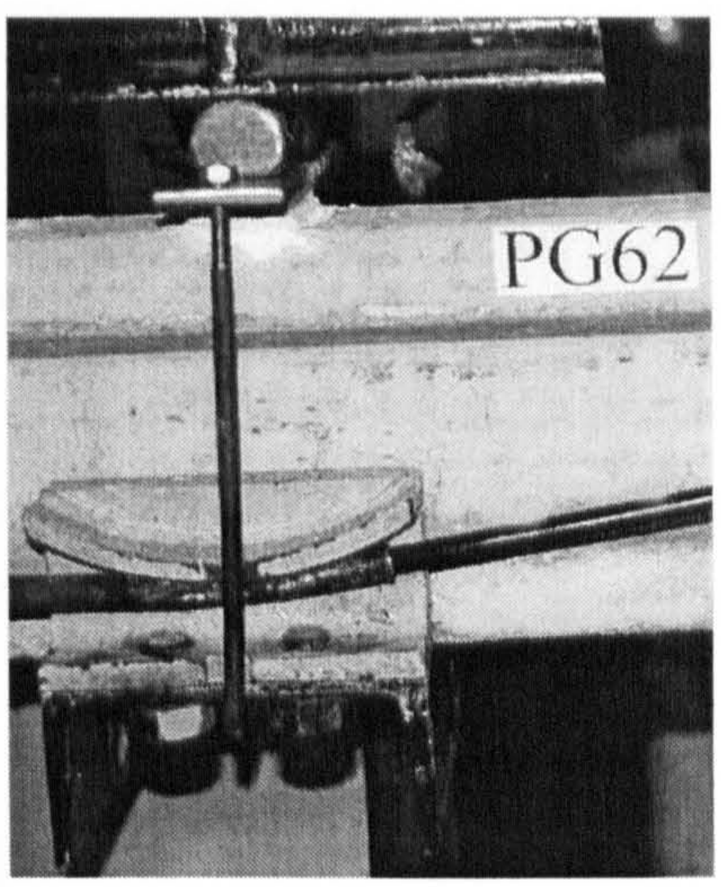

Figure (3.11): Details of deviator.

- **Anchorages**: Four aluminium anchors were used to transfer the rope forces to the end plates then to the beam. Details of anchorage method were discussed in chapter two. Figures (3.13 - 3.14) show the details of anchorage-beam connection.
- **End plates**: Two tapered steel end plates as shown in Figure (3.12) were used to transfer the external prestressing force to the beam. Dimensions were selected to transfer and spread the force safely to the beam at the end blocks and to keep the ropes away from contact with the beam surface in order to eliminate any friction.

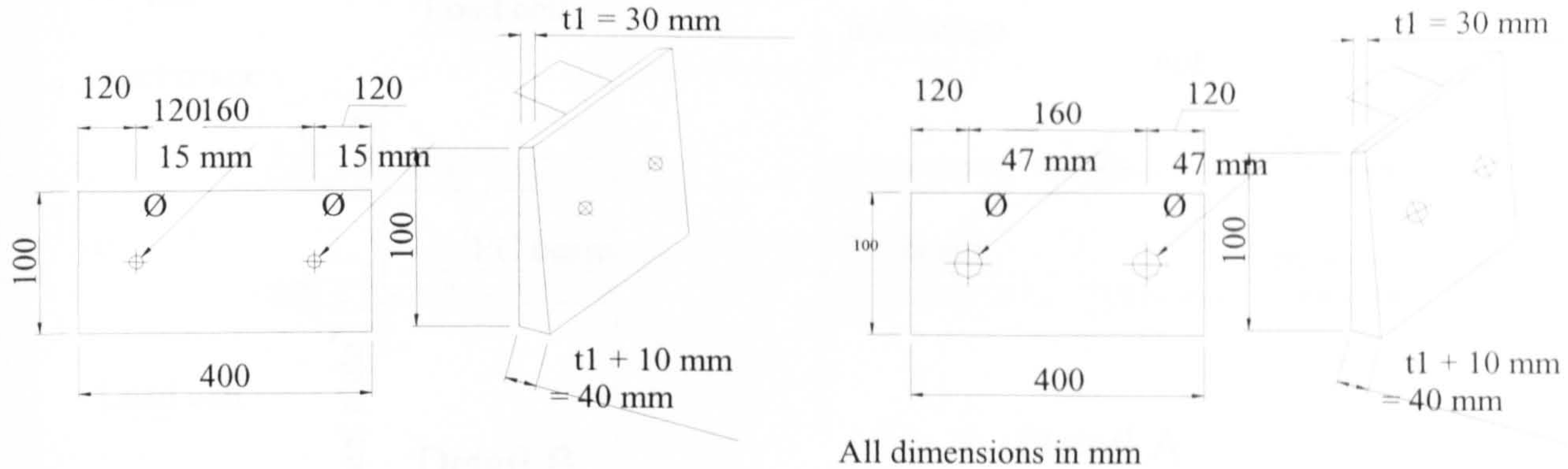

Figure (3.12): dimensions of the end plates

3.4.2 External Prestressing Process:

External prestressing was applied using two (11-mm diameter) Parafil ropes type G, located at the same distance from the longitudinal axis of the beam as shown in Figure (3.13). Before tensioning, the ropes were greased at the deviators to reduce the friction. The two ropes were tensioned simultaneously using two hydraulic jacks connected to the same pump. During prestressing, precautions were taken to prevent increasing prestressing force in one rope relative to the other to avoid biaxial bending of the beam, by closing the connection of the higher force to the pump and increasing the force in the other rope.

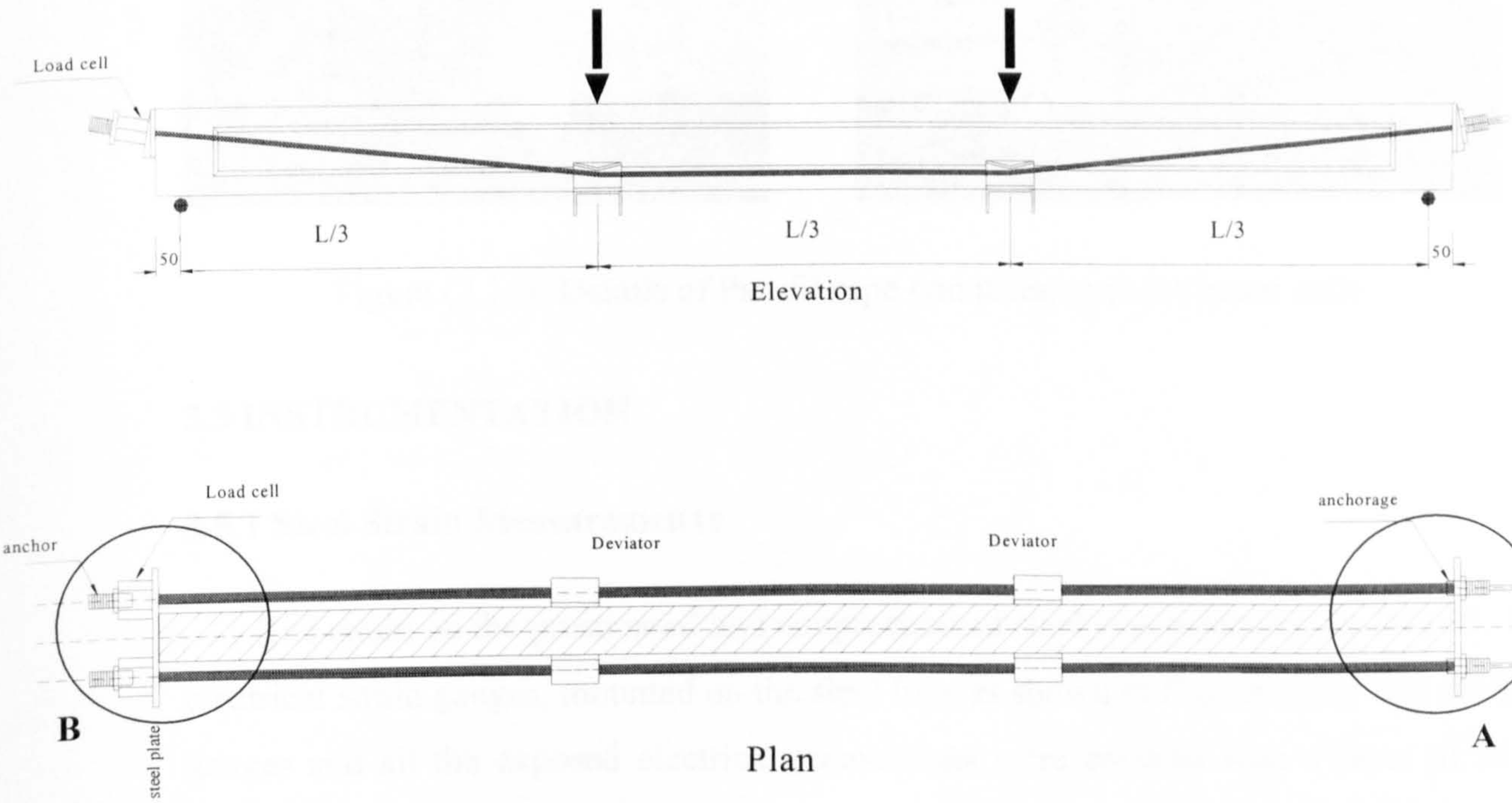

Figure (3.13): External prestressing process

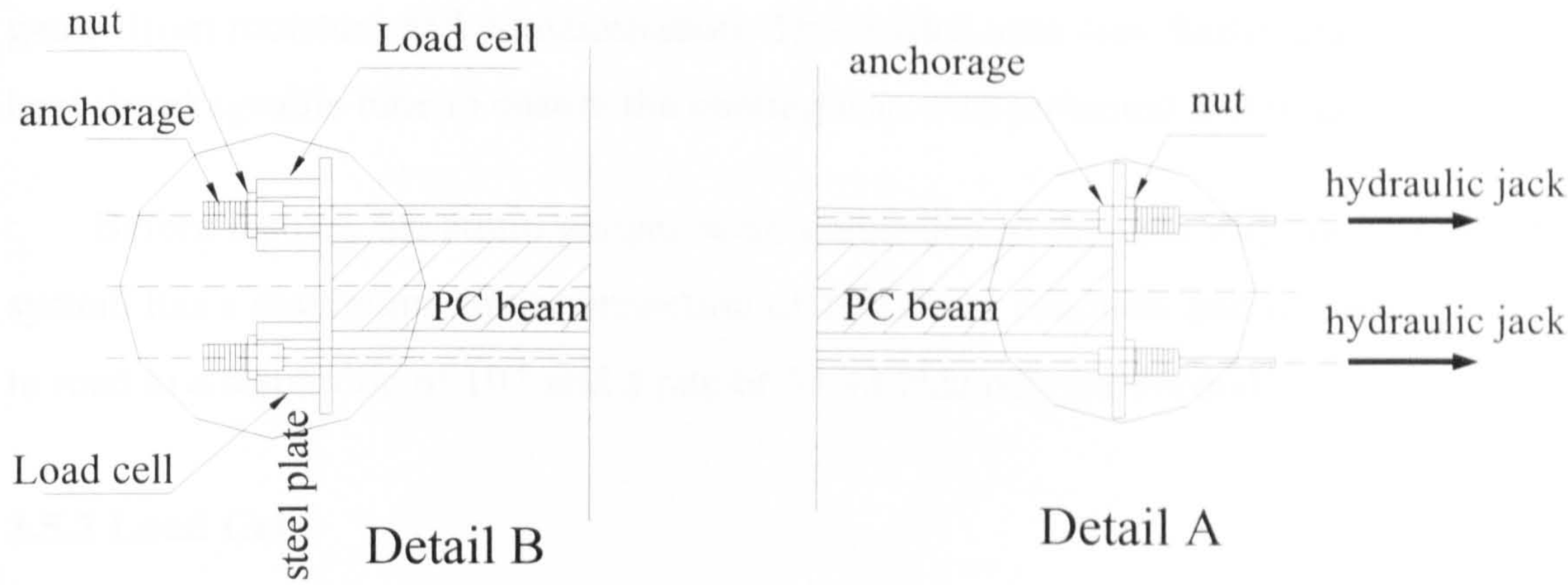

Figure (3.14): Details of external prestressing anchorage.

After reaching the required force, the ropes were locked by tightening the anchorage nuts against the end plate. The losses due to anchorage draw in were almost zero. After twenty-four hours, the ropes were re-tensioning to compensate for creep, then the test started. The external prestressing force during the prestressing process and testing was measured in both ropes using two 100 KN- load cells at the end of the ropes as shown in Figures (3.14 and 3.15).

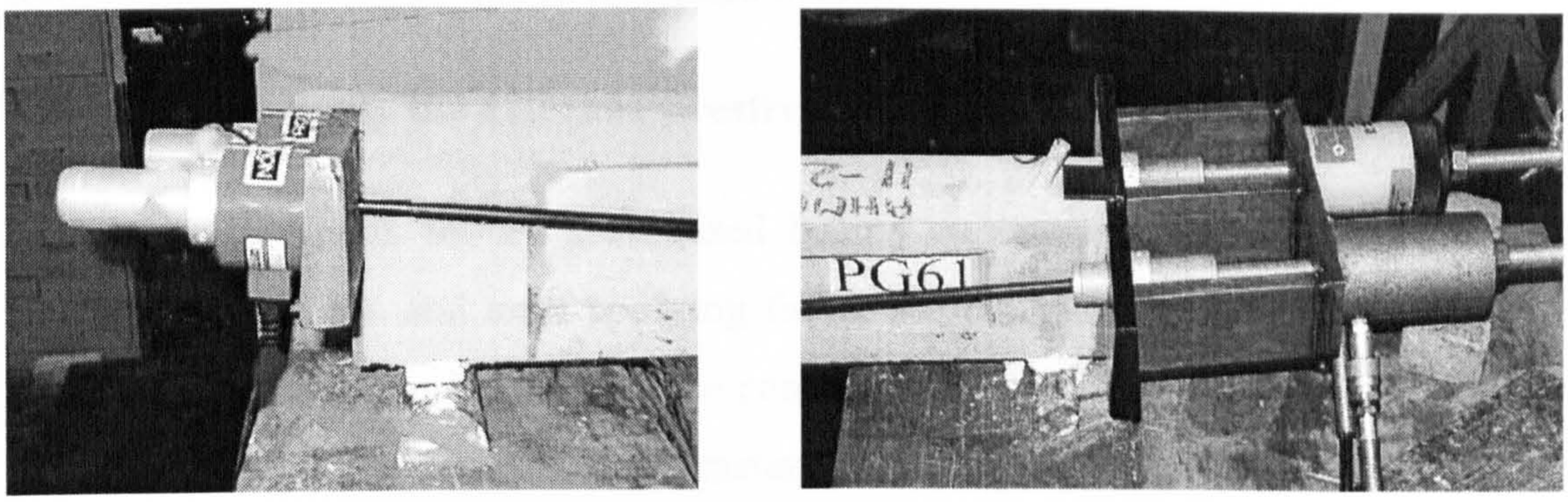

Figure (3.15): Details of Parafil rope connections at the beam ends.

3.5 INSTRUMENTATION

3.5.1 Steel Strain Measuremen ts

The strain on the prestressed and nonprestressed steel was measured by four PL-5 electrical strain gauges, mounted on the steel bars as shown in Figure (3.3). The strain gauges and all the exposed electrical connections were covered with a layer of M-Coat that provided insulation against any possible electrical leakage and sealed the

gauge from moisture and contamination. The treated area was finally enclosed with a heat shrinkageable tube to ensure the coating was well protected and isolated.

Before testing, the strain gauges were connected to the data logging system. The system has a maximum input connection of 100 strain channels and was programmed to read to a resolution of 10^{-6} and a rate of 33.33 channels per second.

3.5.2 Load Cells

Two 100 KN load cells with sensitivity of 0.01 KN were used to measure the prestressing force in each rope during external prestressing and test. Before used, the load cells were calibrated, then fixed at the rope end as shown in Figure (3.12). Both load cells were connected to the same data logging system.

3.5.3 Concrete Strains

Two types of strain gauges, mechanical and electrical, were used to measure longitudinal concrete strains as discussed below:

3.5.3.1 Before apply the external prestressing force

Concrete strains for all prestressed beams were measured during the internal prestressing process and until applying the external prestressing force using demec points, glued with epoxy cement to the concrete. The strain between the demec points was measured by a demec extensometer with gauge length 100-mm. The gauge resolution was 14.8-microstrain. Strain of each prestressed beam was measured on seven levels distributed from top to bottom on one side at the mid-span as shown in Figure (3.16). These provided the data for determining the initial strains (at transfer of prestressing force) and strains just before apply the external prestressing force.

3.5.3.2 After applying the external prestressing force.

For safety reasons, and due to the external rope obstacle, concrete strains could not be measured during test using the demec extensometer. So electrical strain gauges were used at the middle, to measure concrete strains during and after applying the external prestressing force as shown in Figure (3.16).

Before fixing the electrical strain gauges, a thin layer of epoxy resin was applied. After it had cured, the surface was made smooth with a fine grain sandpaper prior to being cleaned. The gauges were fixed with super glue adhesive, then connected to the data logging system.

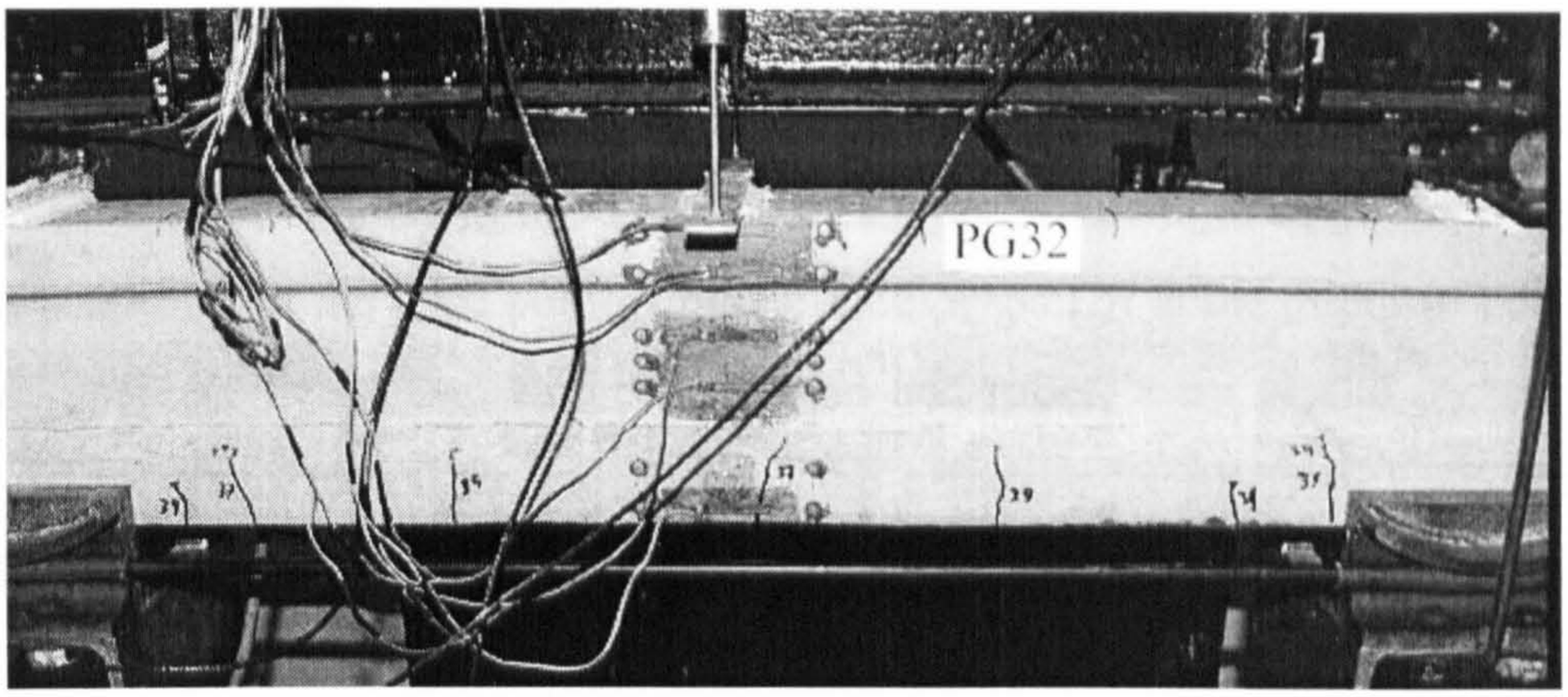

Figure (3.16): locations of demec points and electrical strain gauges.

3.5.4 Deflection Measurement

Deflection of the test beams was measured at the middle during internal prestressing using mechanical dial gauges with an accuracy of 0.01 mm. During the external prestressing and testing process, four linear voltage differential transducers (LVDTs) were used to measure the deflection, two at the middle and two at the concentrated loads as shown in Figure (3.17). All LVDTs were calibrated before used and connected to the data logging system.

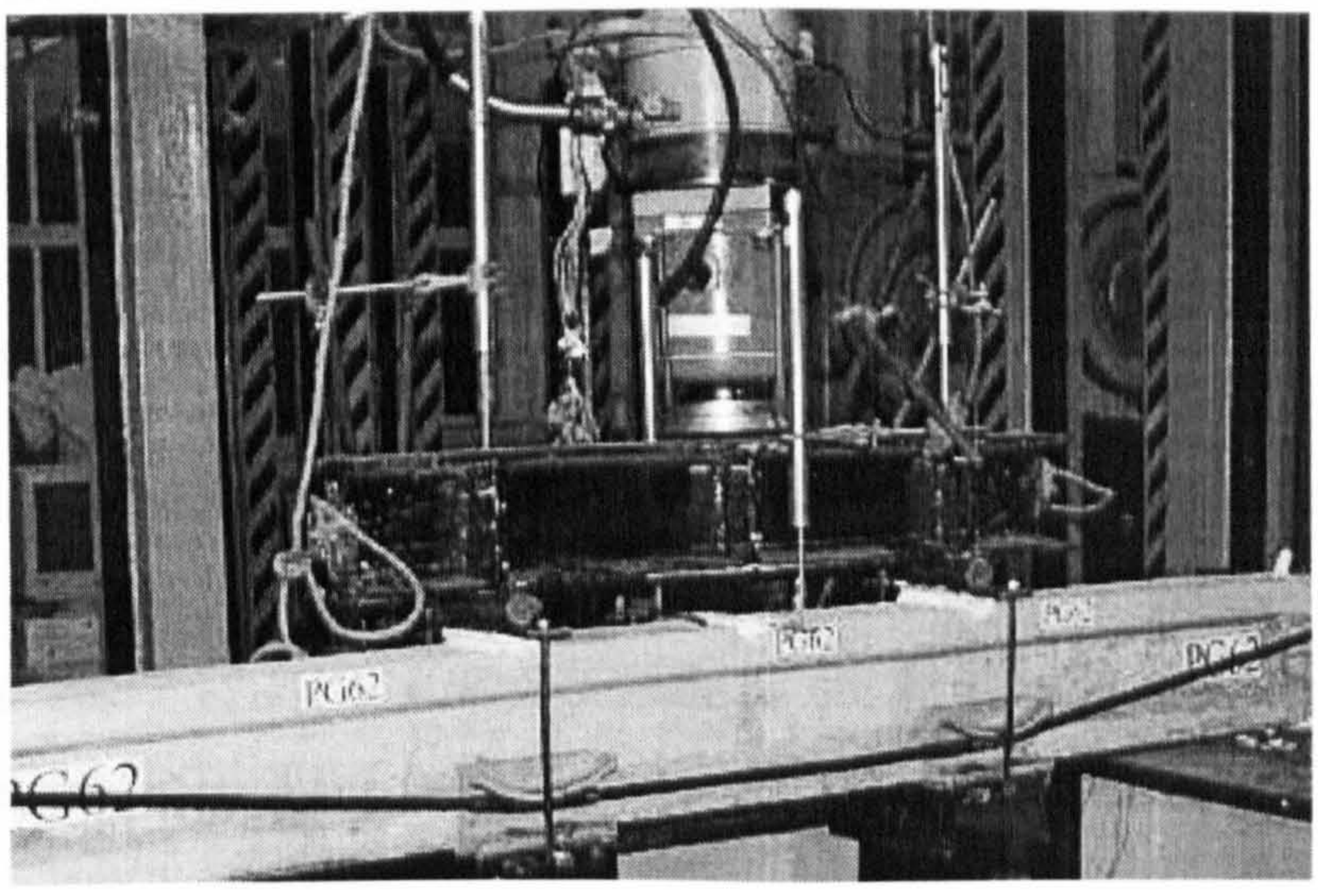

Figure (3. 17): loading system and positions of LVDTs

3.6 BEAM TESTING

3.6.1 Preparation of Beams for Testing

After about one month from casting, each beam was externally prestressed and loaded to failure. Before being externally prestressed, the beam was set up and carefully aligned in a test rig with the required effective span, supported on two steel rollers designed to simulate hinged and roller supports. Then the deviators were fixed in their positions (at the third points of the effective span or at the middle). To support the load spreader beam, two supports, hinged and roller, were placed on top of the beam, at a distance equal to one third of the effective length from each end. The spreader beam was then placed in position, and the LVDTs' were adjusted vertically at their locations. Then the load cells, LVDTs, steel and concrete strain gauges were connected to the data logging system.

After beam set up and before applying the external prestressing force, the beam was inspected carefully for any cracks due to shrinkage or mishandling during transportation, and strain and deflection readings were taken. Then the beam was externally prestressed. During and after applying the external prestressing force, steel and concrete strains, external prestressing force, as well as the deflection, were recorded.

One day after, the external prestressing force was readjusted, the beam was inspected carefully for any cracks, and the strain and deflection readings were retaken. Then the hydraulic jack was carefully centred over the spreader beam as shown in Figure (3.17).

3.6.2 Testing Procedure

Following external prestressing the specimens were subjected to an incremental load till failure. During loading, all measurements, such as beam deflections (at middle and at load positions), strains in internal mild and high tensile steel bars, and force in the external ropes were recorded at each increment.

Before cracking, the load was applied in increments between 1 and 2 KN until the first crack appeared. Then the incremental load was increased to 3 KN and then

reduced to 0.5 KN near failure. After each increment of load had been added, the cracking pattern was inspected and marked. In the higher loading range the tendency of beam to creep was more noticeable and the load had to be maintained for a longer period of time to obtain reasonably steady strain and deflection readings. Load increments were added until failure took place. The time required to load the beam to failure was usually between two and three hours. Control cubes and prisms were tested on the same day.

3.6.3 Testing Procedure of Group G4

To study the effect of the previous loading stage before externally prestressed, beams in group four (G4) were loaded to different stages. Beam PG41 was loaded until the flexural cracks appeared at the bottom flange (at about 0.36 P_{ult} of B1), then unloaded and strengthened by external prestressing and tested after one day. Beam PG42 was loaded to 0.6 P_{ult} of B1, by which load several flexural and diagonal cracks had appeared along the span. The beam was then unloaded, externally prestressed and tested one day after.

The difference between this group and other beams was only in the pre-loading before externally prestressed.

3.7 REMARKS:

During testing beam PG13, the pump controlled the hydraulic jack load malfunctioned and beam PG13 subjected to impact load for a short period before the load was removed. The test was stopped for four days till the pump was fixed. During that period the external prestressing force was still applied to the beam.

Chapter 4

Test Results

4.1 INTRODUCTION

The behaviour of prestressed concrete beams after strengthening by external prestressing is different from that of ordinary prestressed concrete beams. This is mainly due to effect of the external prestressing force and the change in its effective depth during loading.

To understand the behaviour of such type of beam, and determine the main factors affect on this behaviour, thirteen prestressed beams were tested, twelve of them after external prestressing using Parafil Rope, up to failure.

In this chapter, the behaviour of test beams during tests and the tests results are presented and discussed.

4.2 RESULTS OF BEAM TESTS

The beams were divided into six groups according to the factors that were taken into consideration in this investigation as shown in Table (4.1). Properties of these beams at test day are shown in Table (4.2)

Table (4.1): *Factors and group number*

Group no.	***Factors***	***Beam no.***
G1	Value of external prestressing force	PG11- PG12- PG13
G2	Number of deviators	PG21– PG51
G3	Effective depth of the external prestressing force	PG11- PG31– PG32
G4	Previous loaded stage before being externally strengthened	PG11– PG41– PG42
G5	Concrete strength (f_{cu})	PG11– PG51– PG52
G6	Effective span length / depth ratio (L/h)	PG11– PG61– PG62

Table (4.2): *Properties of test beams at test day*

Beam no.	f_{cu} ***(MPa)***	$\left(\frac{L}{h}\right)$*	***Internal prestressing force***			***External prestressing force***		
			P_i § (KN)	P_e ‡ (KN)	ecc. (mm)	P_{ex} (KN)	ecc. (mm)	number of deviators
B1	55.37	14.4	40.62	37.85	151.5	-----	-----	----
PG11	55.77	14.4	42.07	38.76	151.5	60.35	142.9	2
PG12	53.3	14.4	44.38	41.21	149.5	48.98	142.9	2
PG13	55.03	14.4	43.44	40.27	150.5	72.27	142.9	2
PG21	47.7	14.4	43.55	39.36	150.5	60.01	142.9	1
PG31	54.2	14.4	41.73	39.25	151.5	60.52	160.9	2
PG32	57.13	14.4	42.87	39.08	151.5	61.03	192.9	2
PG41	52.2	14.4	45.63	40.80	151.5	60.3	142.9	2
PG42	45.7	14.4	41.14	37.07	151.5	60.57	142.9	2
PG51	43.3	14.4	40.53	37.86	150.5	60.53	142.9	2
PG52	79.27	14.4	43.44	40.75	151.5	60.13	142.9	2
PG61	48.93	20	42.50	40.1	149.5	60.16	142.9	2
PG62	47.47	10	43.64	41.16	151	60.73	142.9	2

* L = effective span length § initial prestressing force ‡ effective prestressing force at test day

4.2.1 Cracking Patterns

Cracking of the beam with internal bonded tendons only, began at the location of high flexural moment then spread over the beam length as the load increased. Cracks in the middle were almost vertical, while those in the shear span were inclined due to the effect of shear stress as shown in figure (4.1).

In the externally prestressed beams cracks also occurred in the pure flexural zone, then spread, as the load increased; only a few diagonal cracks appeared in the shear span. These diagonal cracks started first near the concentrated load at the bottom flange then spread towards the support. They extended into the web towards the concentrated load, as the load increased.

Comparing the two types of beams it can be seen that:

- Cracks widths (using visual observation) in the externally prestressed beam were smaller than in the internally prestressed beam. However, there is no appreciable difference in the number or spacing of the main cracks over a beam length of constant moment.

- In both types, during the working stage, well-distributed cracks developed along their span. The width of the cracks increased consistently as the load increased, with no sign of deformation concentrating at a single crack location.

- Diagonal cracks of the internal bonded prestressed beam distributed along the shear span further than those of the externally prestressed beams.

The cracking load at which the cracks were visually observed is used to compare the cracking patterns of the externally prestressed beams.

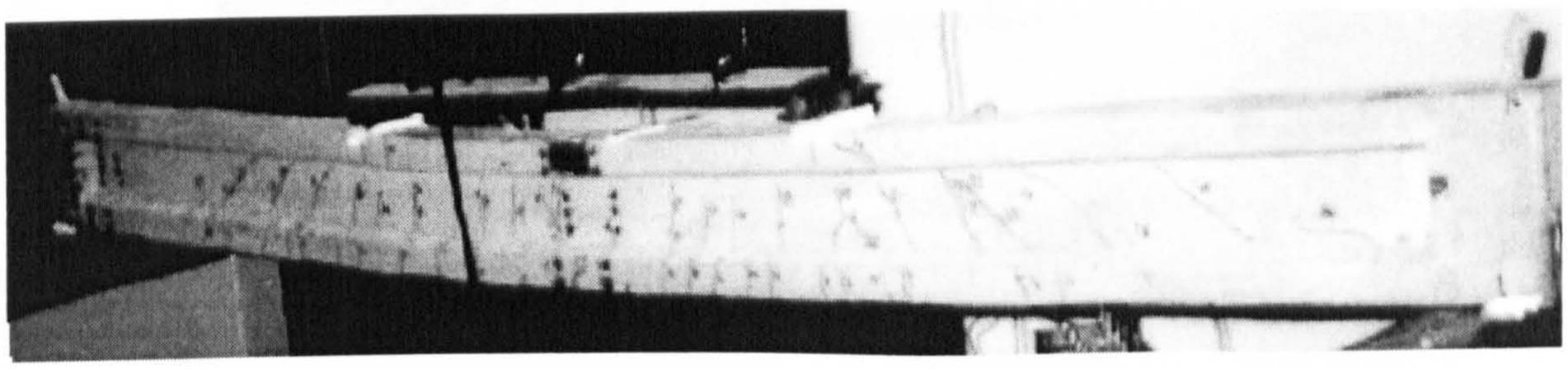

Figure (4.1): Cracks pattern of internal prestressing beam

4.2.1.1 Group 1 (Value of the external prestressing force)

Figures (4.2–4.3) show the flexural and shear cracks of beams in group one (G1). The number and the distance between the flexural cracks of beams PG12, PG11 and PG13 (P_{ext} = 48.98, 60.35, 72.27 KN) are slightly different. Flexural cracks of beam PG11 appeared at a load (28 KN) higher than that of beam PG12 (25 KN) and lower than that of beam PG13 (33 KN). The same observation was obtained when comparing cracks in the shear span, the higher the external prestressing force, the higher the load at which cracks appeared (31, 36, 39 KN for PG12, PG11 and PG13). Also, as the external prestressing force increased, the number of diagonal cracks decreased and the crack widths (using the visual observation) decreased as well.

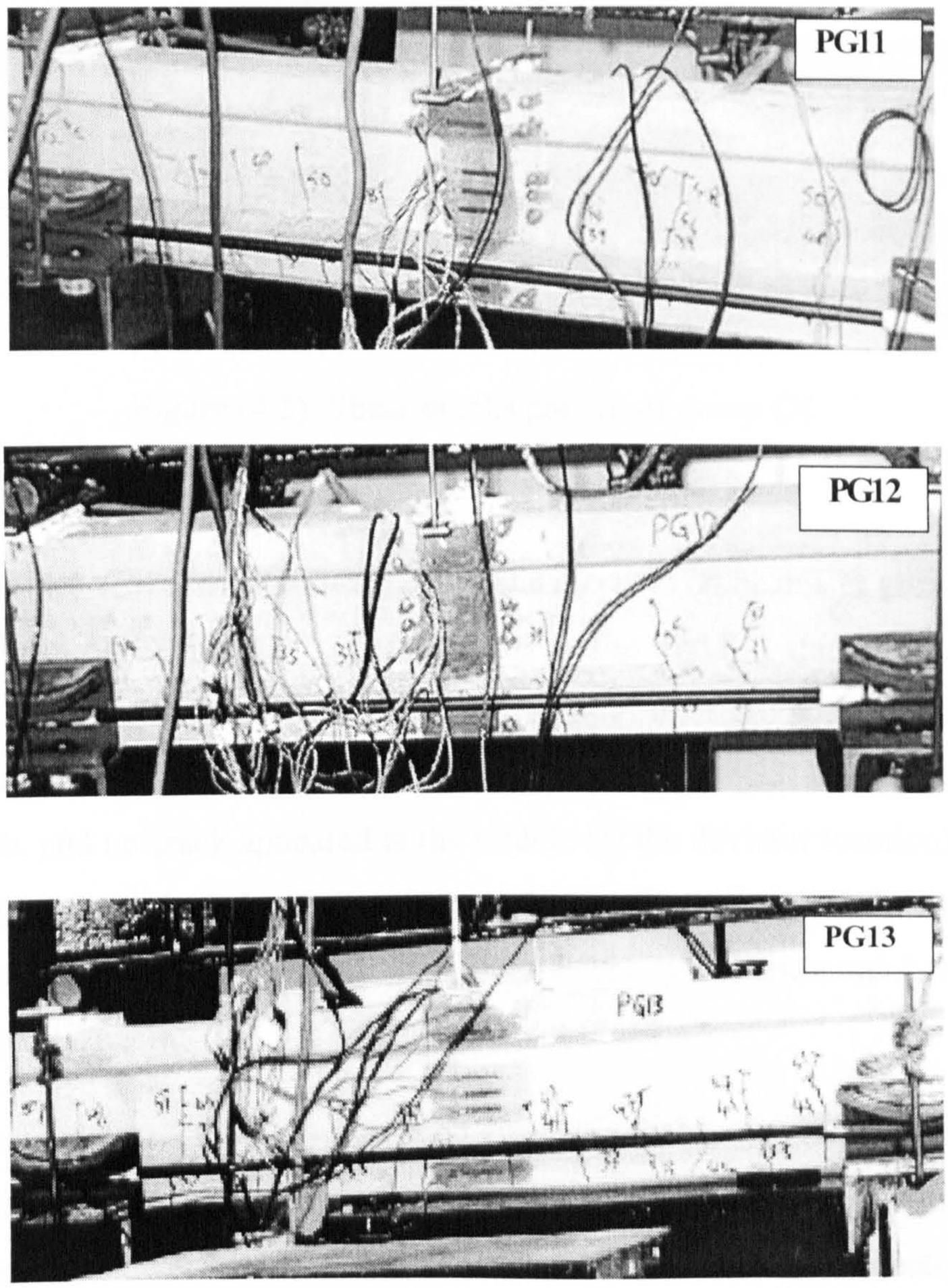

Figure (4.2): Flexural cracking pattern of group G1

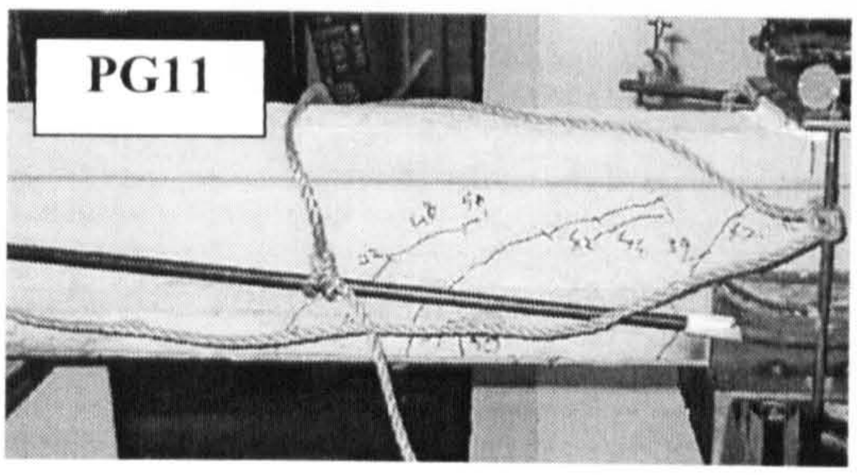

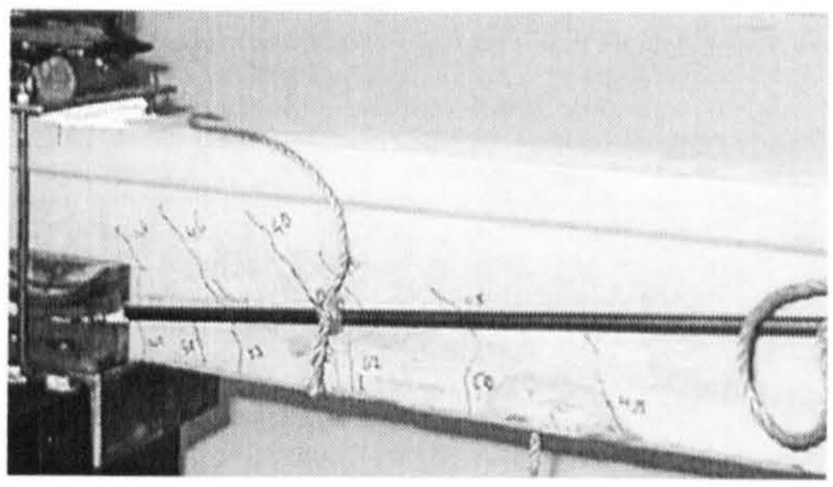

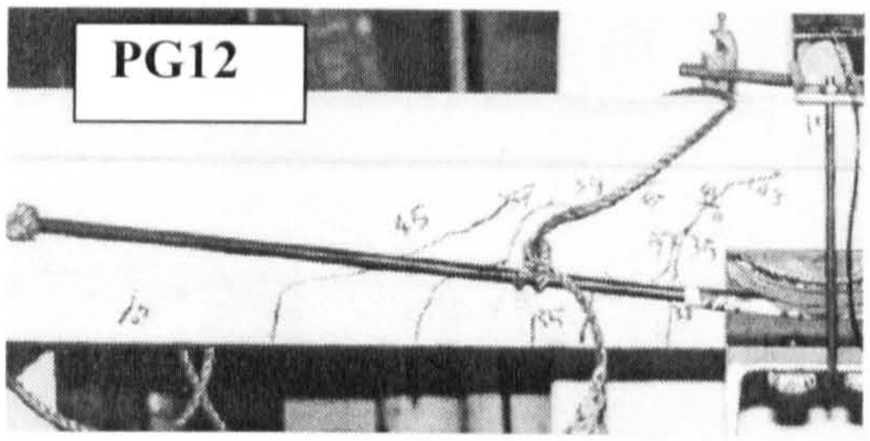

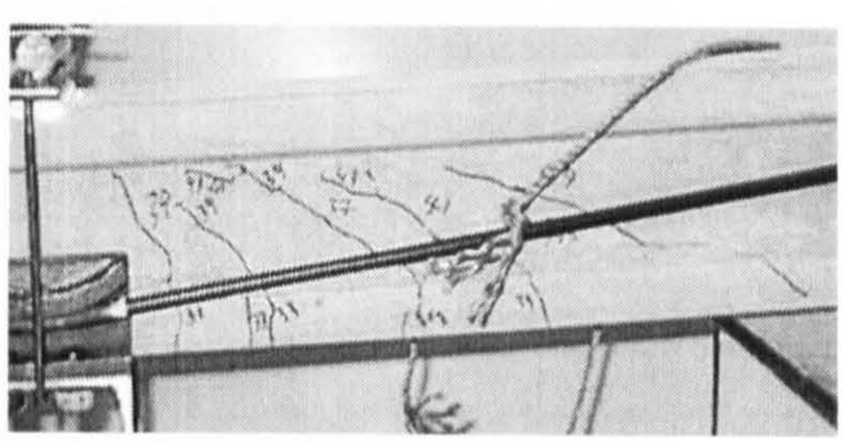

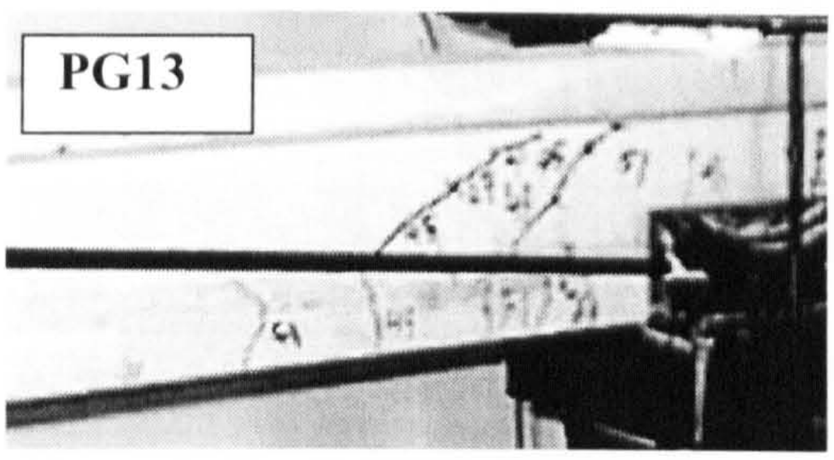

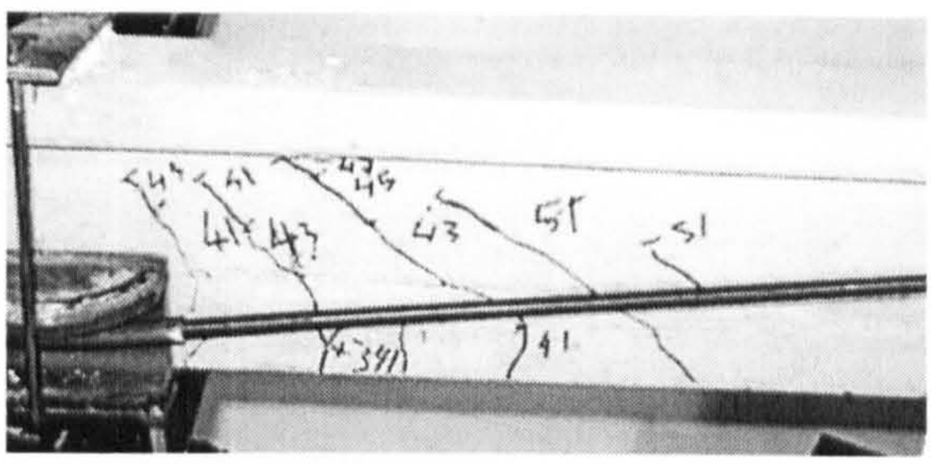

Figure (4.3): Shear cracks pattern of group G1

4.2.1.2 Group 2 (Number of deviators)

Figures (4.4-4.5) show the flexural and shear cracks on beams in group two (G2). Flexural cracks of Beam PG21 (one deviator at the middle) started to appear at a lower load than that of beam PG51 (two deviators at the third span). The number of flexural cracks in beam PG21 was less than that of beam PG51 but extended higher into the web, and no crack appeared at the middle (at the deviator location), where the prestressing moment had the highest value. Diagonal cracks on both sides of beam PG21, appeared also at load below that of beam PG51, with higher number and spread over a longer distance

Flexural cracks on both beams in this group were visually observed at almost the same load (25 and 26 KN for PG21 and PG51). While the diagonal cracks on beam PG21 appeared at lower load than that of beam PG51 (29, 36 KN) respectively.

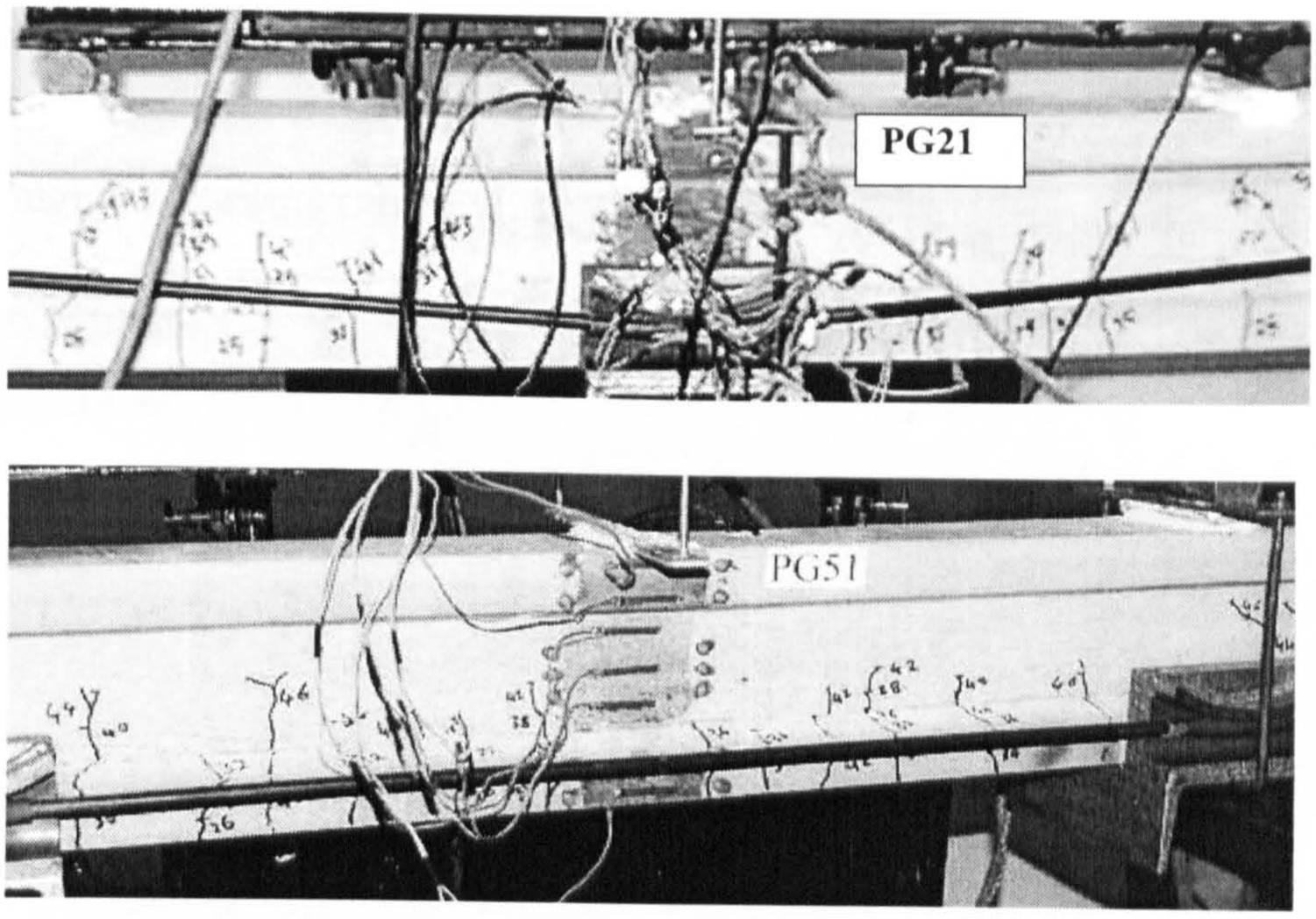

Figure (4.4): Flexural cracking pattern of group G2

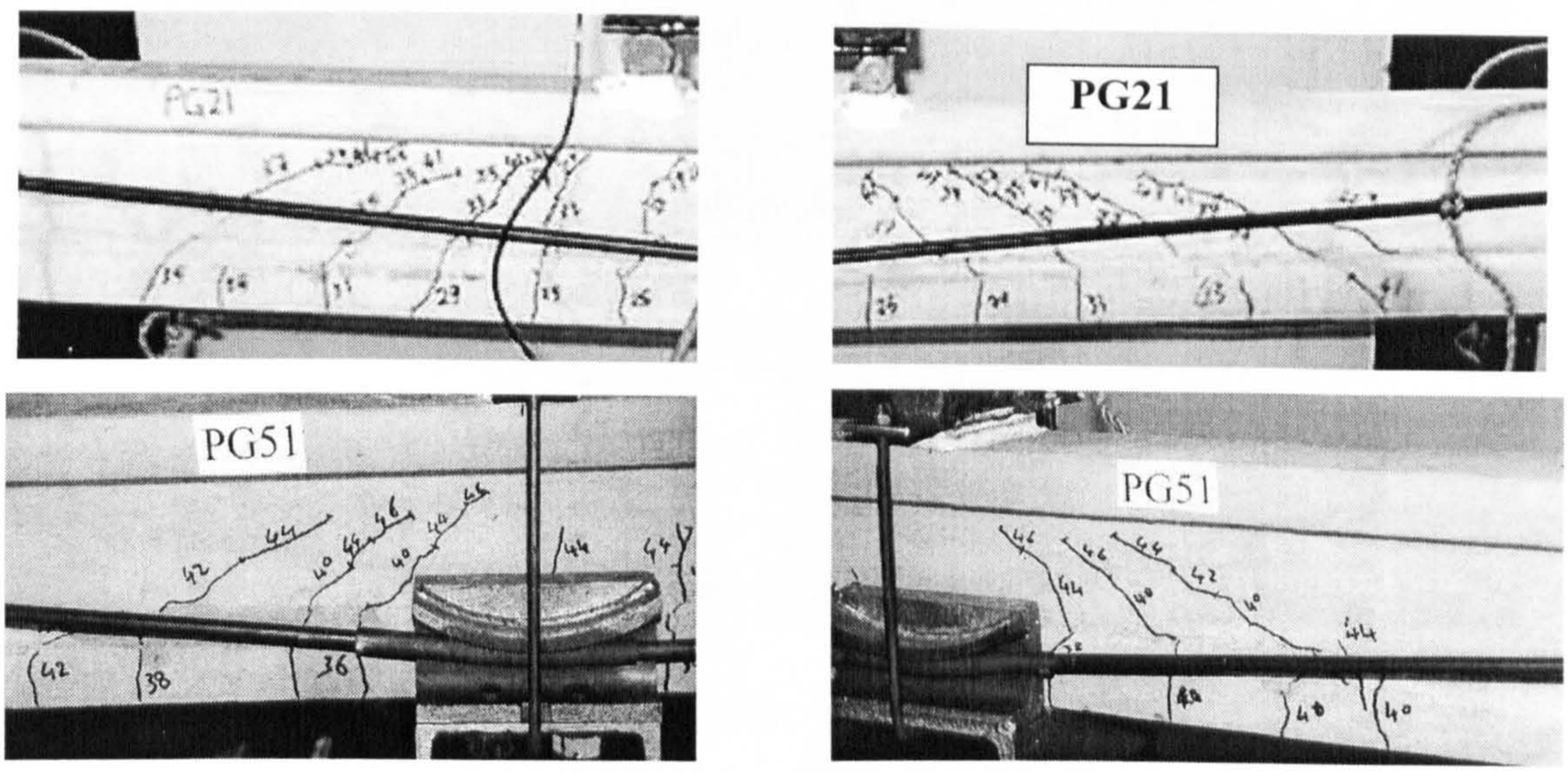

Figure (4.5): Shear cracks pattern of group G2

4.2.1.3 Group 3 (Effective depth of the external prestressing force)

Figure (4.6) shows the flexural and shear cracks of beams in group three (G3). The flexural cracks patterns of beams PG11, PG31 and PG32 (e/h = 0.794, 0.894 and 1.072), were almost the same. However, the flexural cracks on beam PG11 with lower eccentricity appeared earlier and extended more rapidly than the other beams. Flexural cracks appeared at loads 28, 31 and 35 KN for beam PG11, PG31 and PG32 respectively.

During loading, diagonal cracks appeared and spread within the shear span. That of the beam with lower eccentricity (PG11) appeared at lower load and extended faster through the web than those of PG31 and PG32 (36, 37, 41 KN respectively).

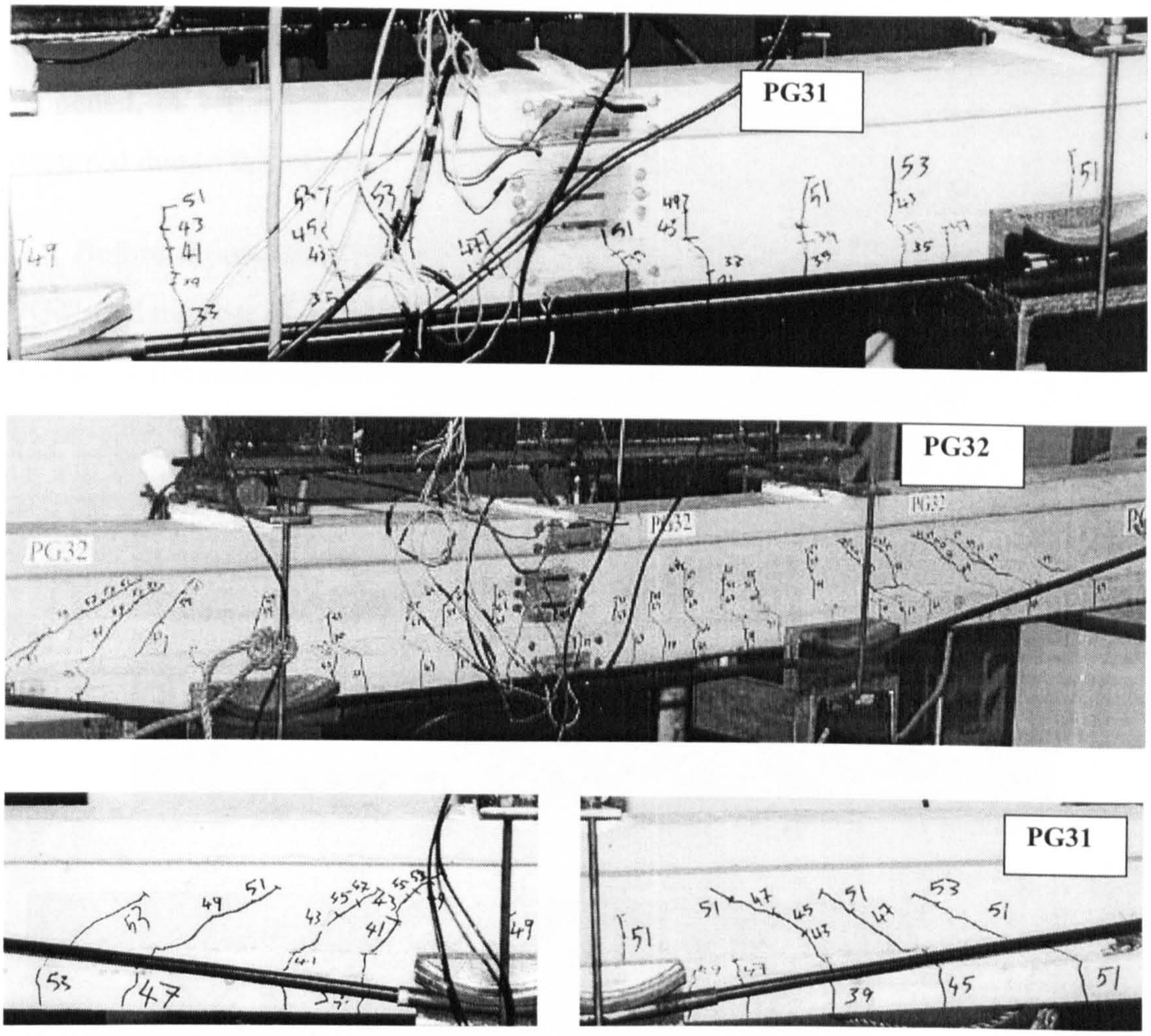

Figure (4.6): Cracks pattern of group G3

4.2.1.4 Group 4 (Previous load stage before being externally strengthened)

Beam PG41 was loaded until the flexural cracks appeared at the bottom flange at load 12 KN (about 0.36 P_{ult} of B1) as shown in figure (4.7), then unloaded, strengthened and tested after one day. Beam PG42 was loaded up to 20 KN (about 0.6 P_{ult} of B1), by which load several flexural and diagonal cracks had appeared along the span as shown in figure (4.7). The beam was then unloaded, externally prestressed and tested after one day.

After external prestressing, the cracks on beams PG41 and PG42 were completely closed and could not be seen even with a magnifier lens. Then during the

testing these cracks started to reopen at a load about double the previous cracking load (22 and 24 KN for PG41 and PG42), then new flexural cracks appeared at higher loads. In beam PG41, shear cracks appeared at higher load (32 KN) and spread on both sides of the shear span. Failure occurred due to the extension of new flexural crack near to the middle of the span. During testing beam PG42 after all cracks reopened, new flexural and shear cracks started to appear on both sides and failure occurred due to the extension of previous crack at the middle of the flexural span.

Before failure, the flexural cracks on beam PG42 extended higher than those of PG41 and number of the new shear cracks (after strengthening) was less. Figures (4.8-4.9) show the cracking pattern of beam PG41 and PG42 after strengthening.

Figure (4.7): Cracks pattern of beams PG41 & PG42 before external prestressing

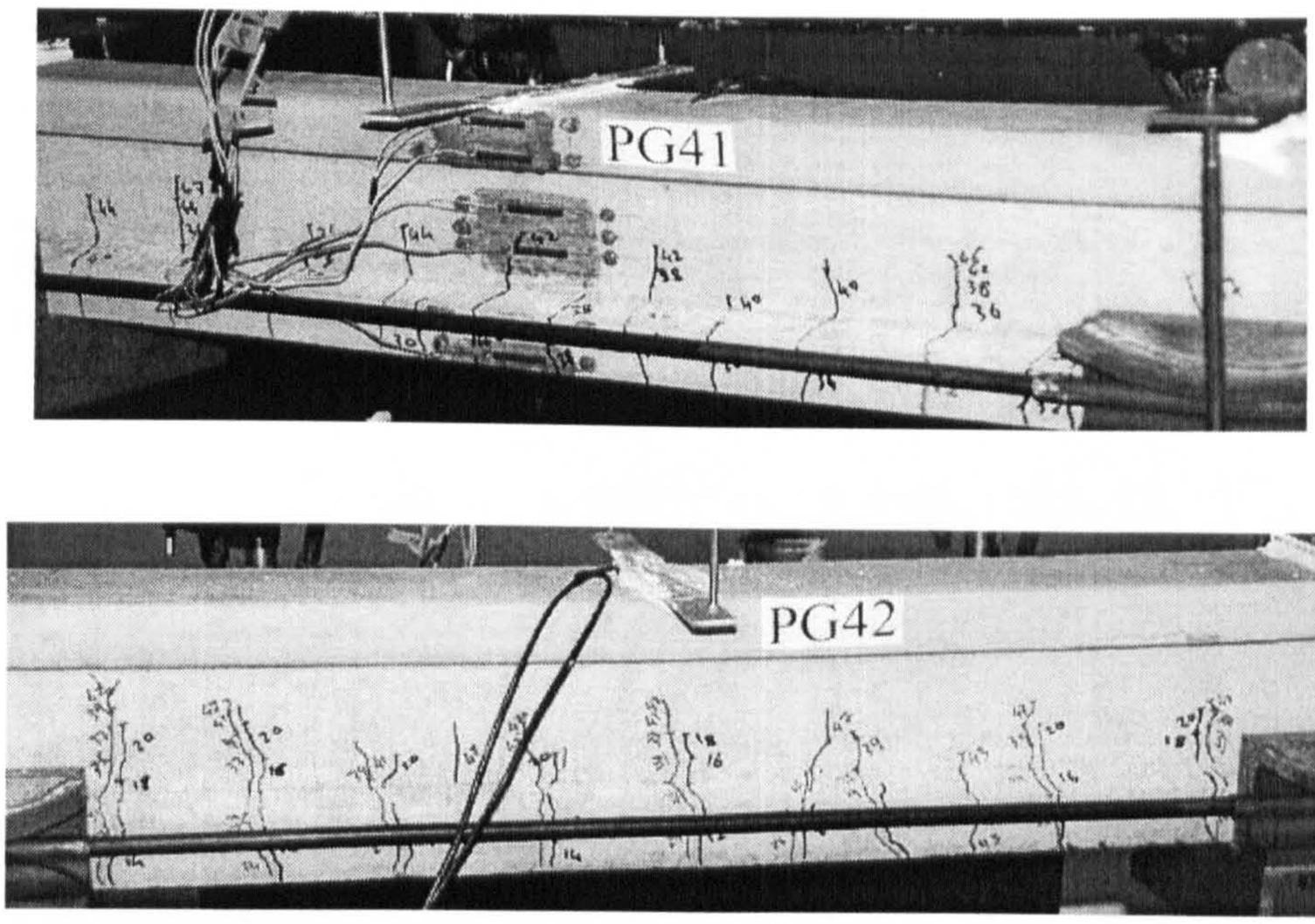

Figure (4.8): Flexural cracks pattern of beams PG41 & PG42 after external prestressing

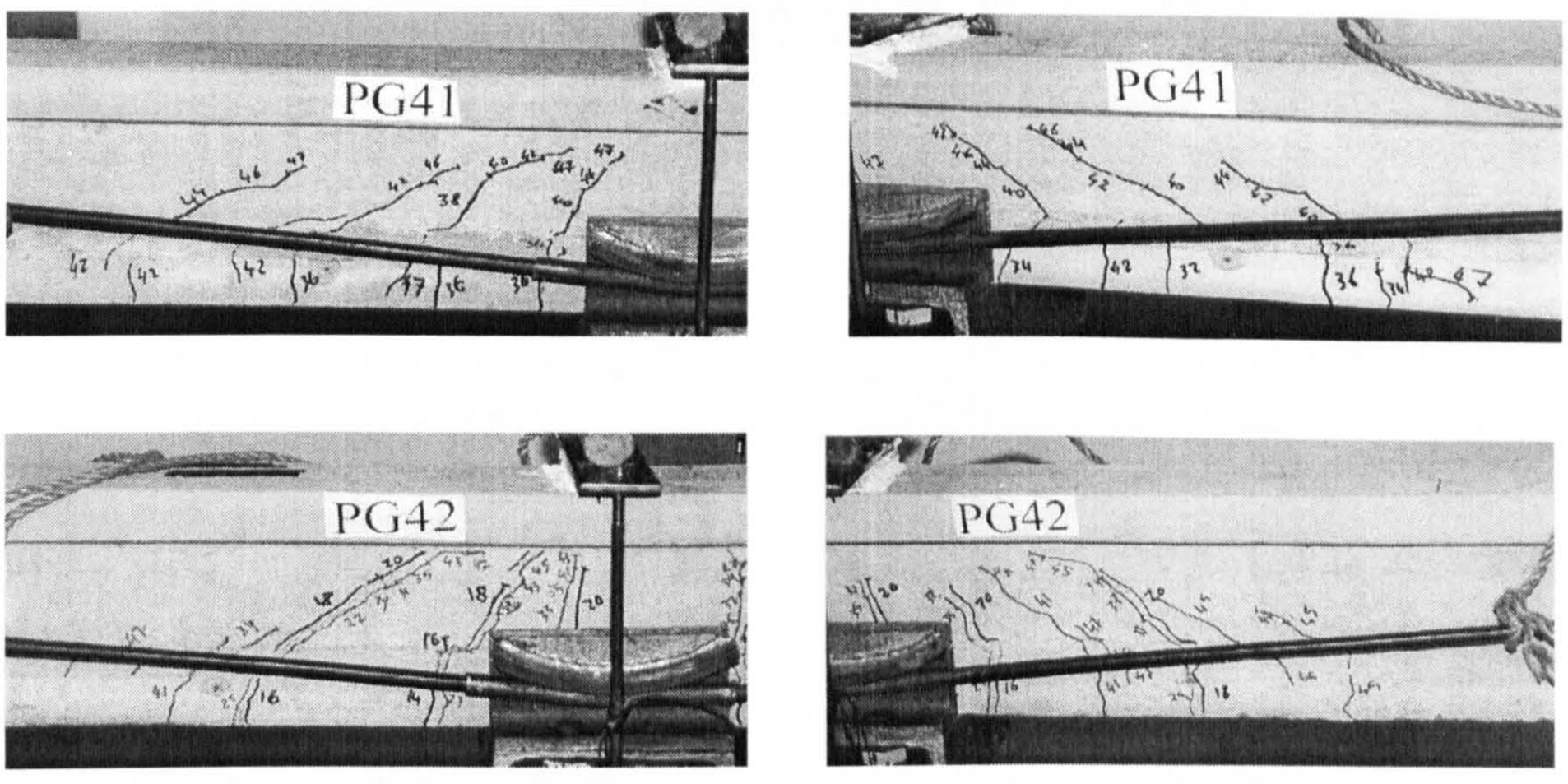

Figure (4.9): Shear cracks pattern of beams PG41 & PG42 after external prestressing

4.2.1.5 Group 5 (Concrete strength)

The flexural cracks on beam PG51 with low concrete strength (f_{cu}=43.3 MPa), were less extensive than those on beams PG11 and PG52 (f_{cu}= 55.8 and 79.3 MPa) and only a few cracks extended through the web. The flexural cracks appeared at loads 26,28 and 29 KN for beams PG51, PG11 and PG52 respectively. However, the cracks in the shear span occurred at almost the same load for all beams (36, 36 and 35

KN respectively). The cracking pattern of beams PG51 and PG52 are shown in figures (4.10-4.11).

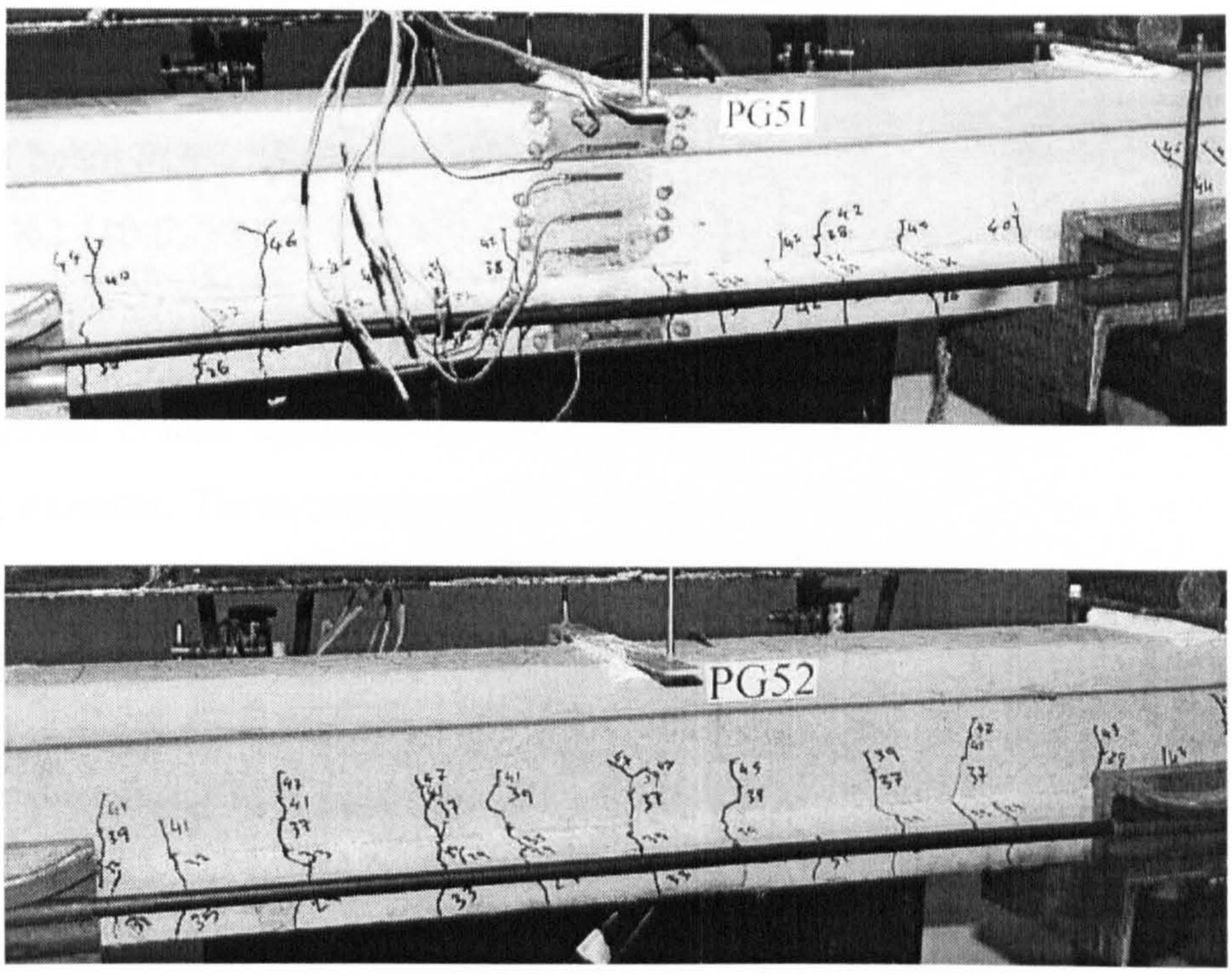

Figure (4.10): Flexural cracks pattern of group G5.

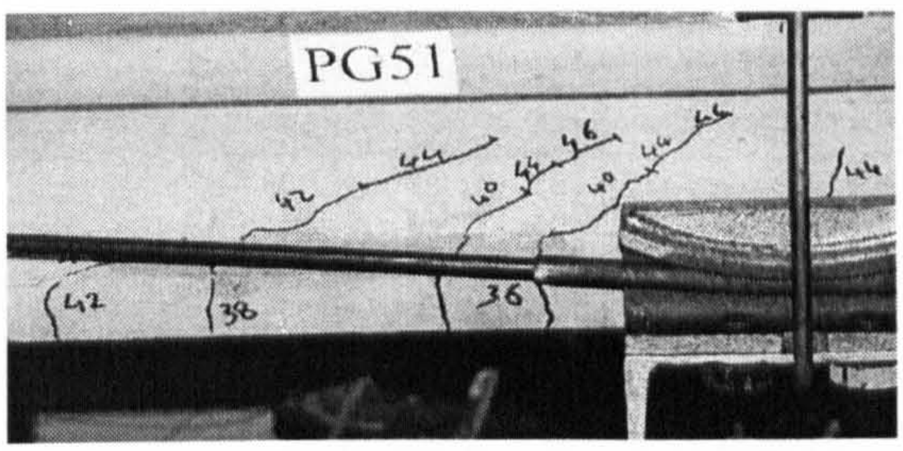

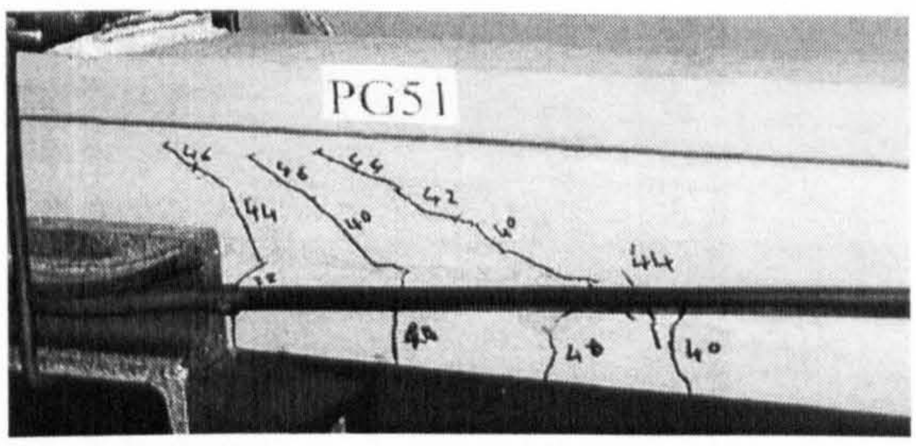

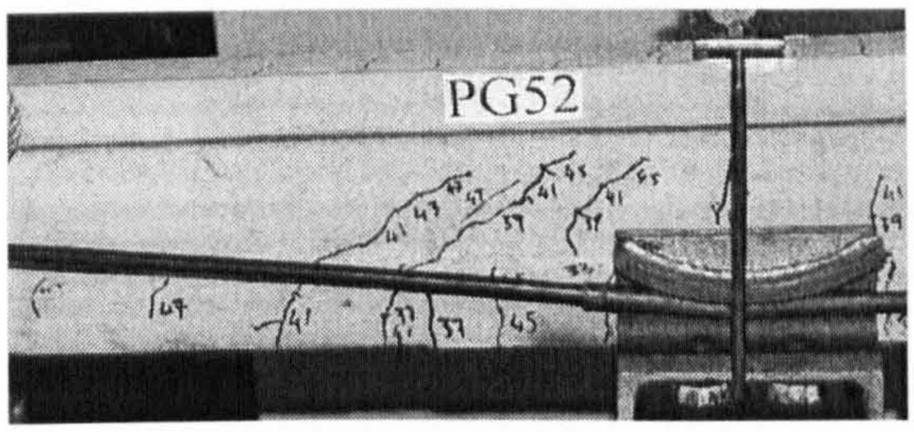

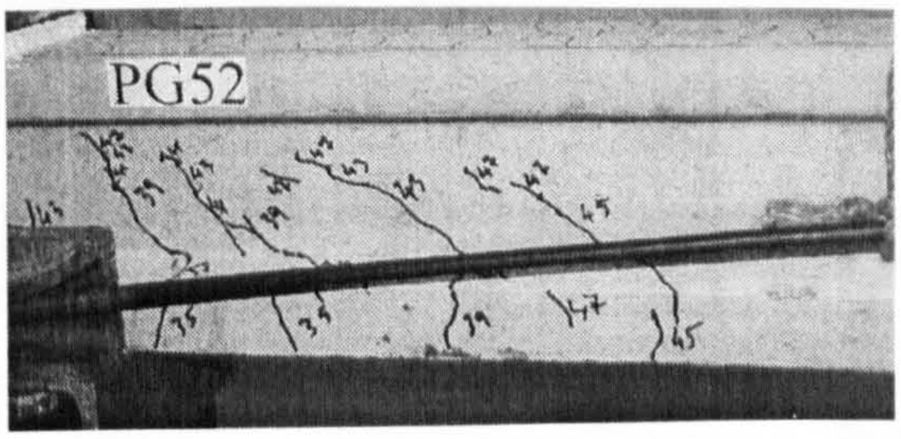

Figure (4.11): Shear cracks pattern of group G5.

4.2.1.6 Group 6 (Effective span/ depth ratio (L/h))

Figure (4.12) shows the cracking pattern of beams PG61 and PG62. In all three beams, PG61 (L/h=20), PG11 (L/h =14.4) and PG62 (L/h =10), flexural cracks appeared in the middle then propagated and extended as the load increased. Flexural cracks of beam PG61 appeared at a lower moment than that of beam PG11 and that of beam PG62 (10.8, 12.18, 13.2 KN.m respectively). Also, the cracks widths of beam PG61 were wider than those of beams PG11 and PG62.

Diagonal cracks appeared on both sides at a higher moment than the flexural cracking moment. These moments were 13.8, 15.7, 15 KN.m for PG61, PG11, PG62 respectively. The cracks in the shear span of PG62 appeared on the web then extended in the flange, while those on the other beams, appeared on the bottom flange then extended through the web. Also, cracks in the shear span of PG62 were steeper than those of PG61 and covered more than the half shear span. The average distance between the diagonal cracks of PG62 was less than that of PG61 and PG11.

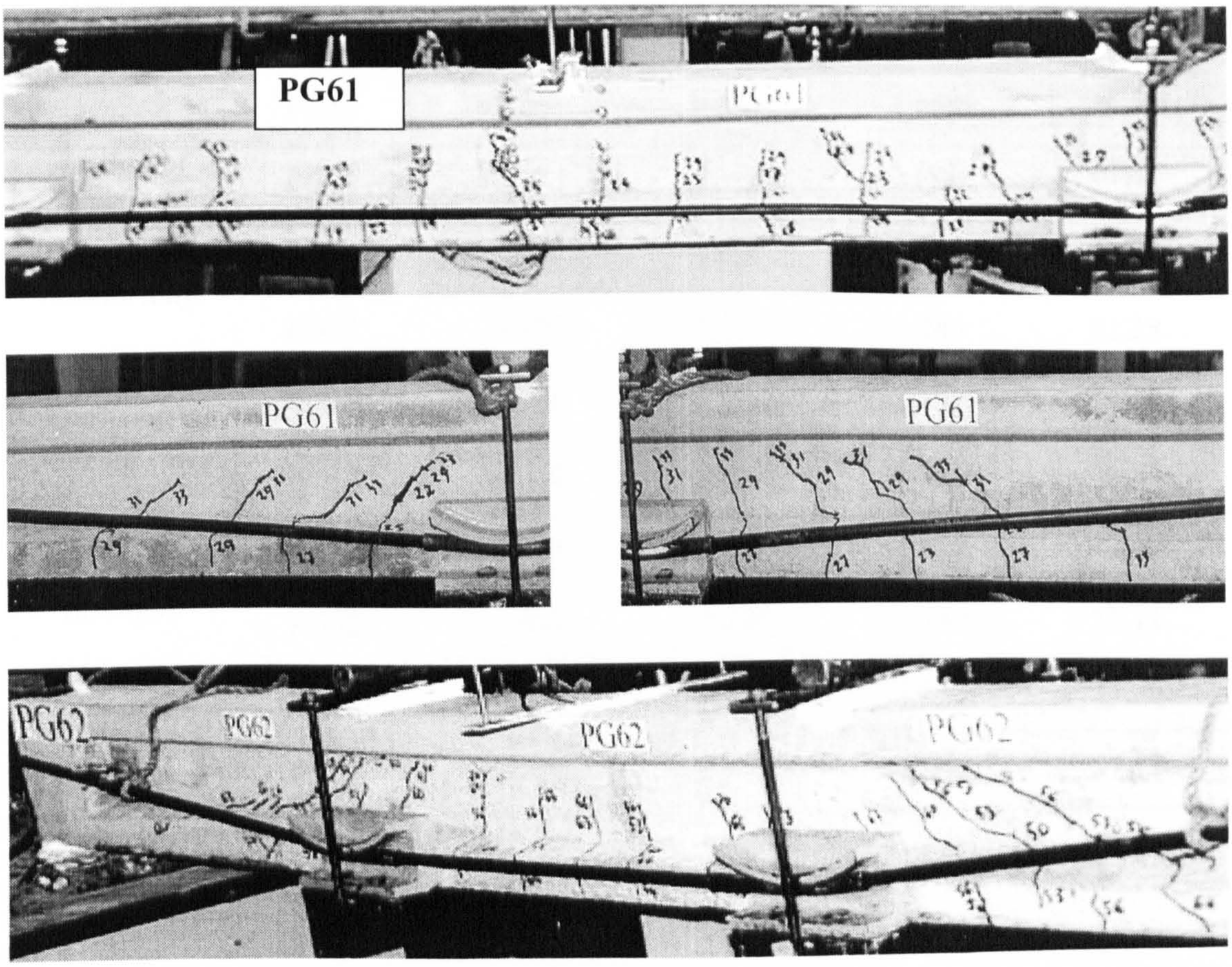

Figure (4.12): Cracks pattern of group G6.

4.2.2 Load-Deflection Behaviour

4.2.2.1 During prestressing

During the external prestressing process, camber increased as the prestressing force increased. After reaching the target prestressing force, the beams were left for about twenty-four hours before testing. During that period, there was an increase in the camber accompanied by decrease in the external prestressing force due to creep. Table (4.3) shows camber of tested beams while, Figures (4.13-4.18) show the relation between the camber and the external prestressing force. Camber is given a (-ve) sign while deflection is given (+ ve) sign.

Table (4.3): *Camber of beam tests at different stages*

Factor	***Beam no.***	***Camber (mm)***			***Increase in camber % ****
		External prestressing	***Creep***	***Total***	
External prestressing force value	PG12	-1.333	-0.405	-1.738	27.68
	PG11	-1.172	-0.324	-1.496	30.38
	PG13	-1.400	-0.561	-1.961	40.07
Number of deviators	PG21	-0.582	-0.314	-0.896	53.98
Eccentricity	PG31	-1.867	-0.628	-2.495	33.63
	PG32	-3.995	-1.249	-5.244	31.28
Previous cracking stage	PG41	-1.286	-0.445	-1.731	34.59
	PG42	-1.730	-0.464	-2.195	26.84
Concrete Strength	PG51	-1.278	-0.540	-1.818	42.22
	PG52	-0.984	-0.346	-1.330	35.11
(L/h) ratio	PG61	-2.491	-0.942	-3.433	37.80
	PG62	-0.601	-0.344	-0.945	57.17

* Relative to camber due to external prestressing only.

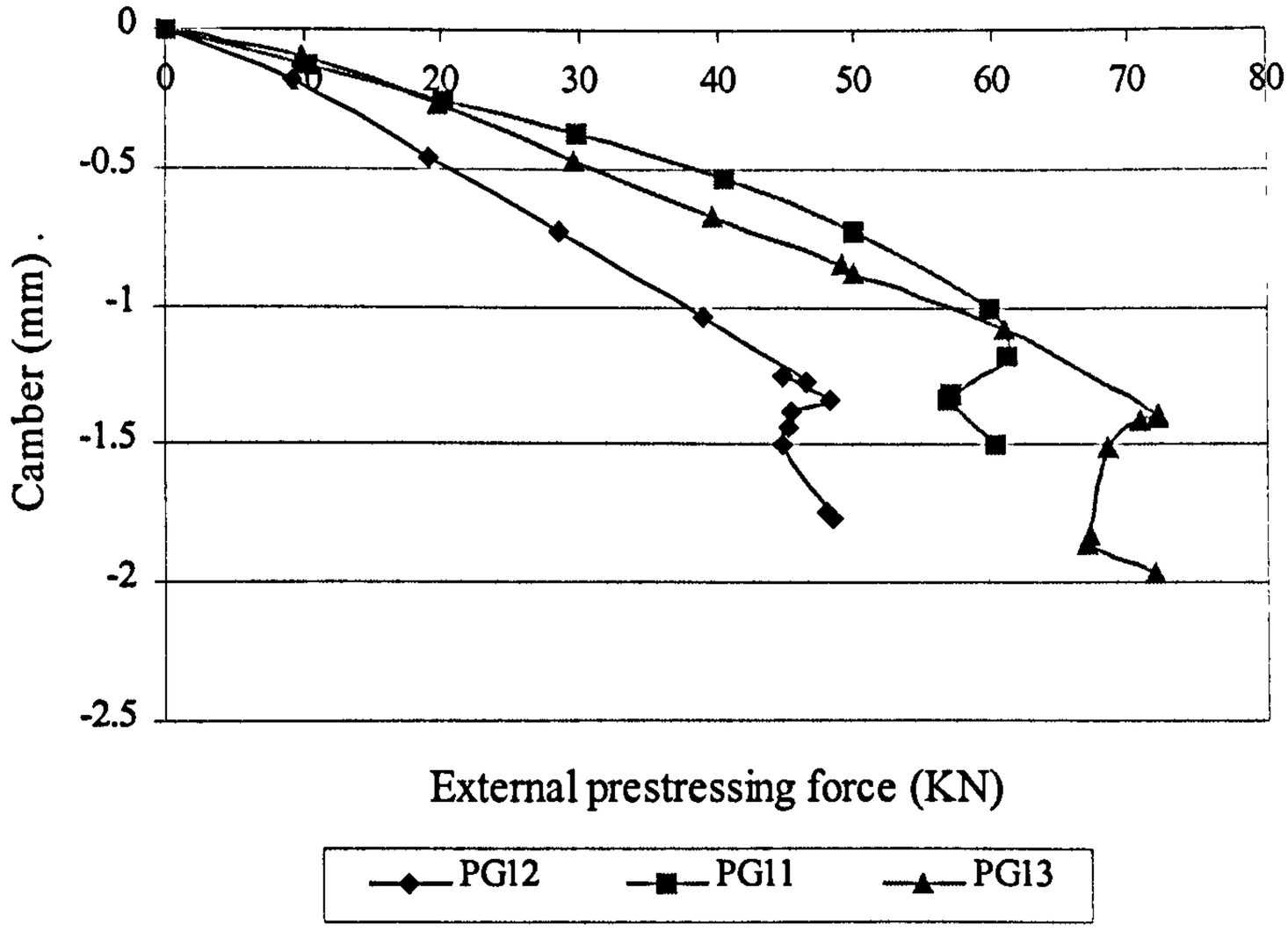

Figure (4.13): Camber – External prestressing force curve of group G1

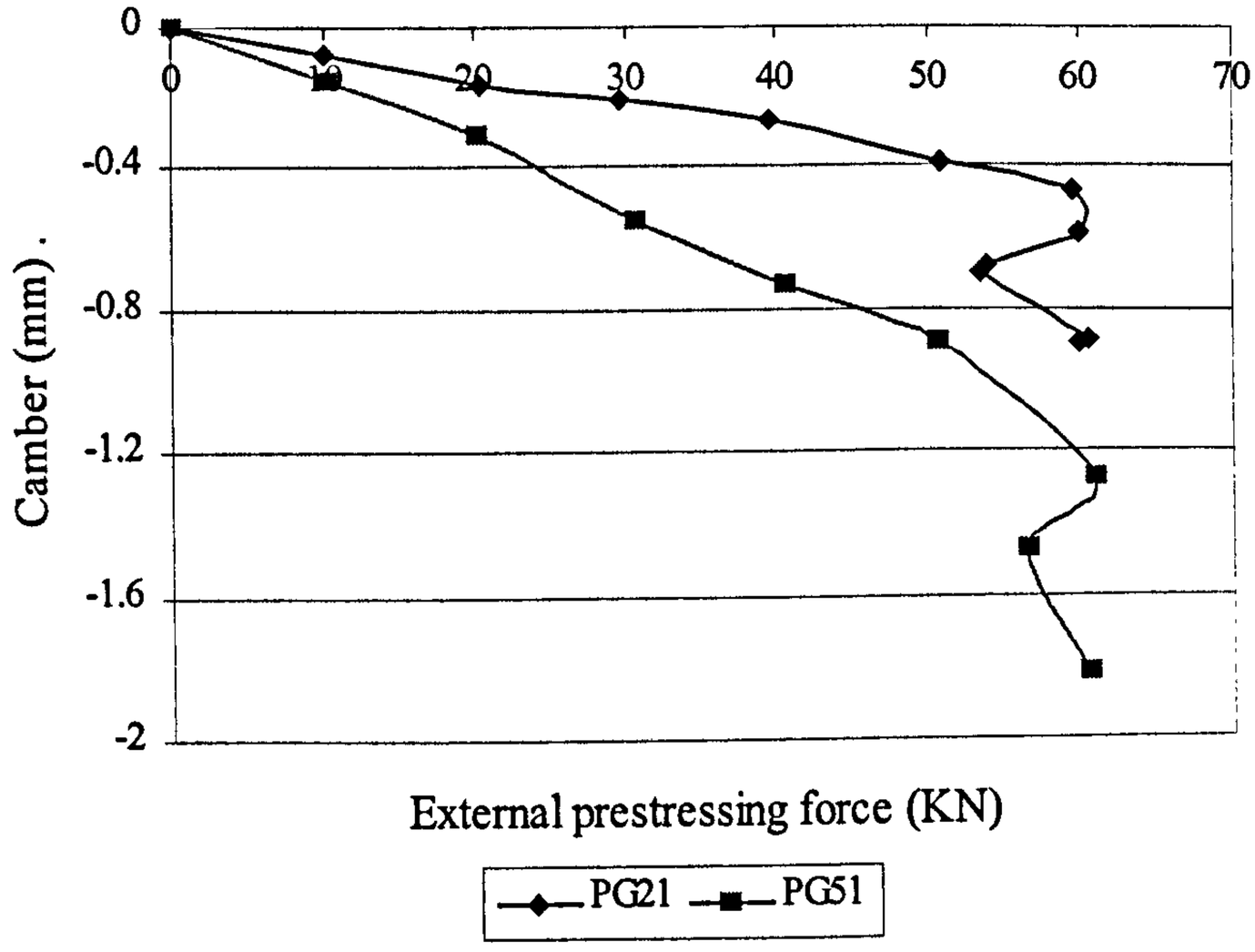

Figure (4.14): Camber – External prestressing force curve of group G2

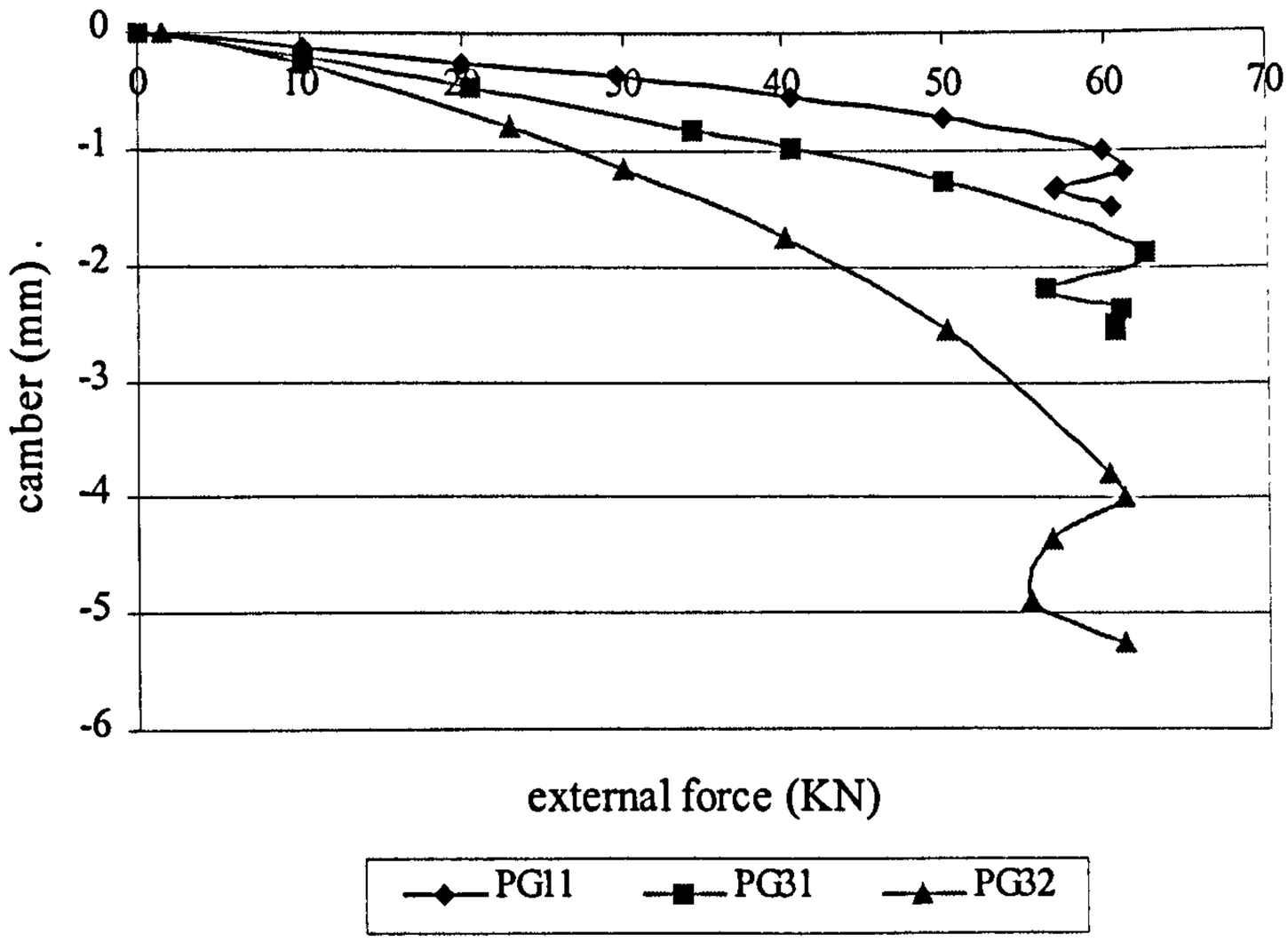

Figure (4.15): Camber – External prestressing force curve of group G3

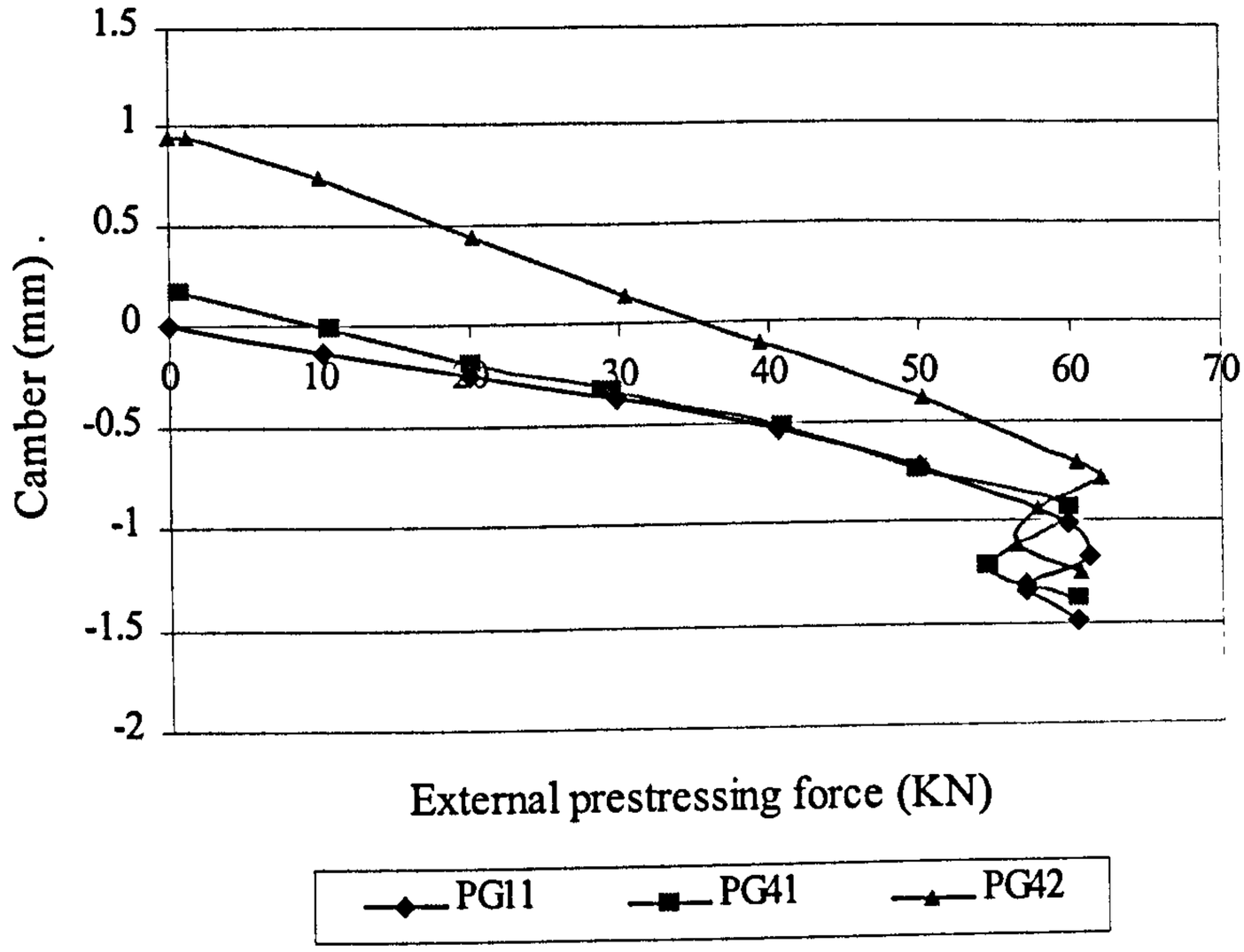

Figure (4.16): Camber – External prestressing force curve of group G4

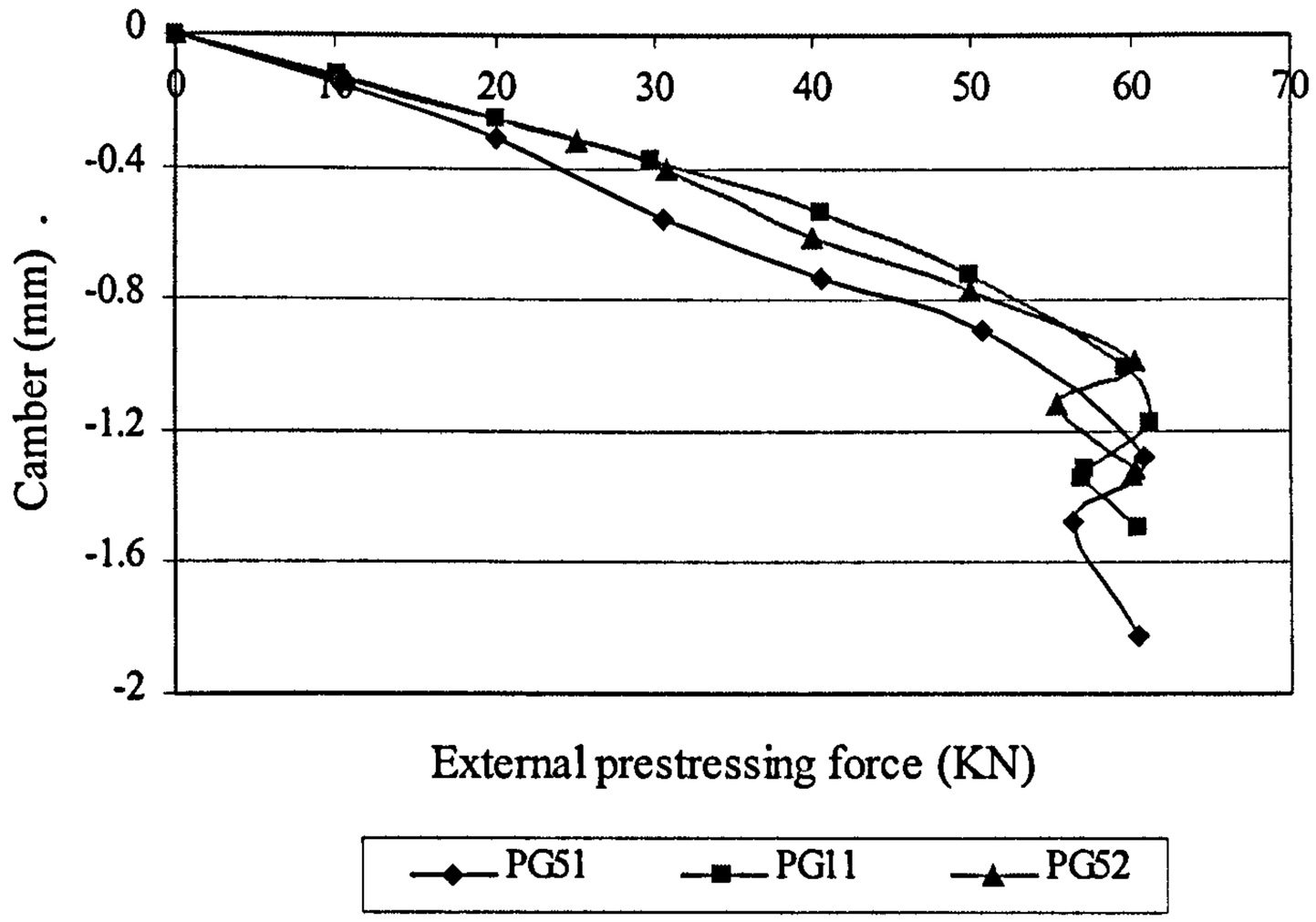

Figure (4. 17): Camber – External prestressing force curve of group G5

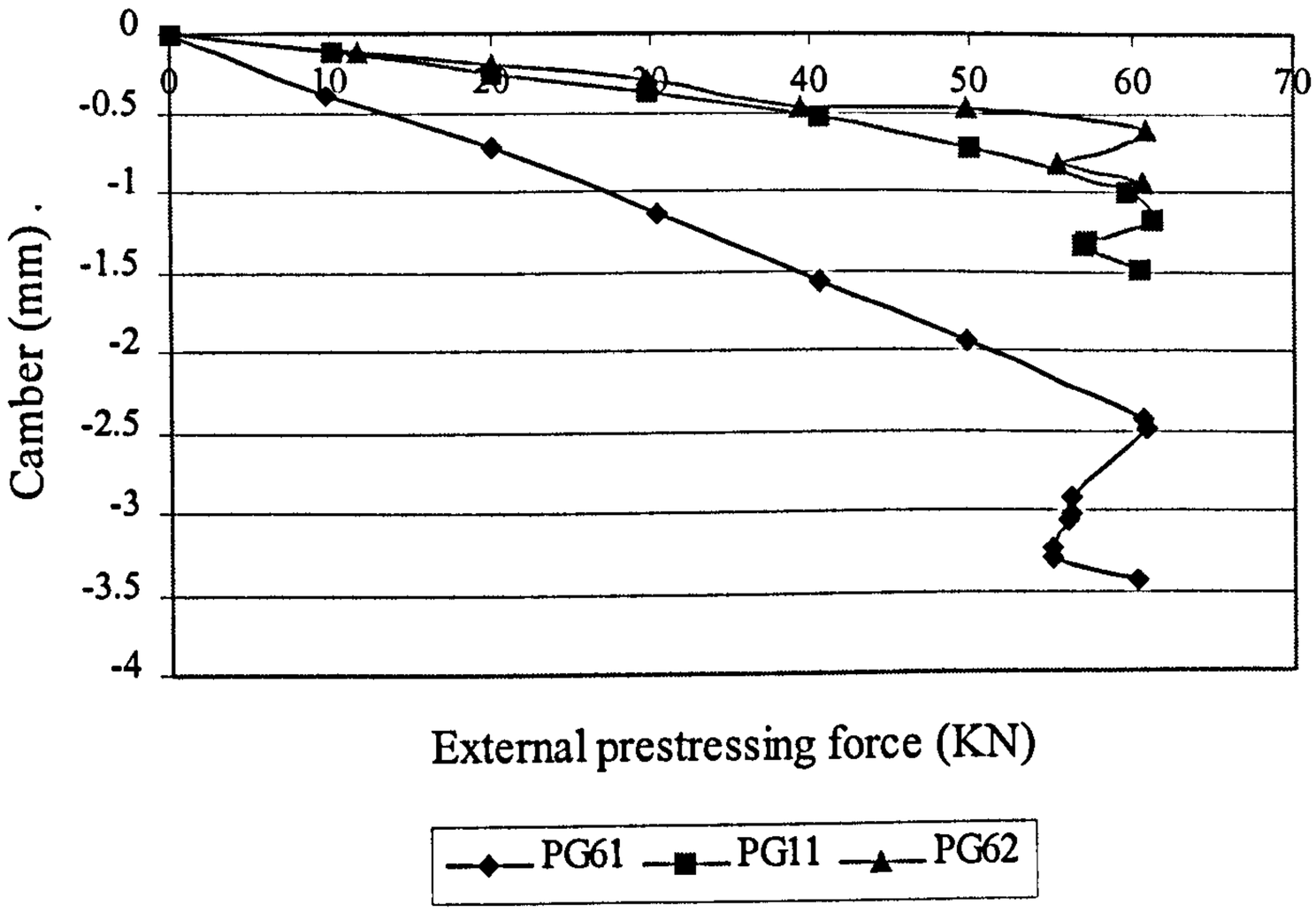

Figure (4. 18): Camber – External prestressing force curve of group G6

4.2.2.2 During testing

The deflection of all beams was measured during external prestressing and loading up to failure, and the relations between moment and deflection were drawn. From these curves, three stages were observed. In the first stage, the curves show the linear elastic behaviour associated with an uncracked section, all curves are linear up to the cracking load and the extent of this stage is a function of the modulus of rupture of the concrete, and the magnitude and eccentricity of the effective prestressing force.

The second stage of the load-deflection curve is characterised by a constantly increased rate of change rate of deflection with the applied load and represents the behaviour of the beam after the concrete is cracked (working stage). The relationship between deflection and load remains linear. However, the gradient of the line does not represent the stiffness but rather a steadily decreasing stiffness with increasing load as the cracking spreads.

The third stage is characterised by a greatly increased rate of increase in deflection with load. The transition from the second stage to the third stage is the result of yielding of the bonded non-prestressed steel.

The relation between load and deflection can be approximated by three straight segments as seen in figure (4.19)

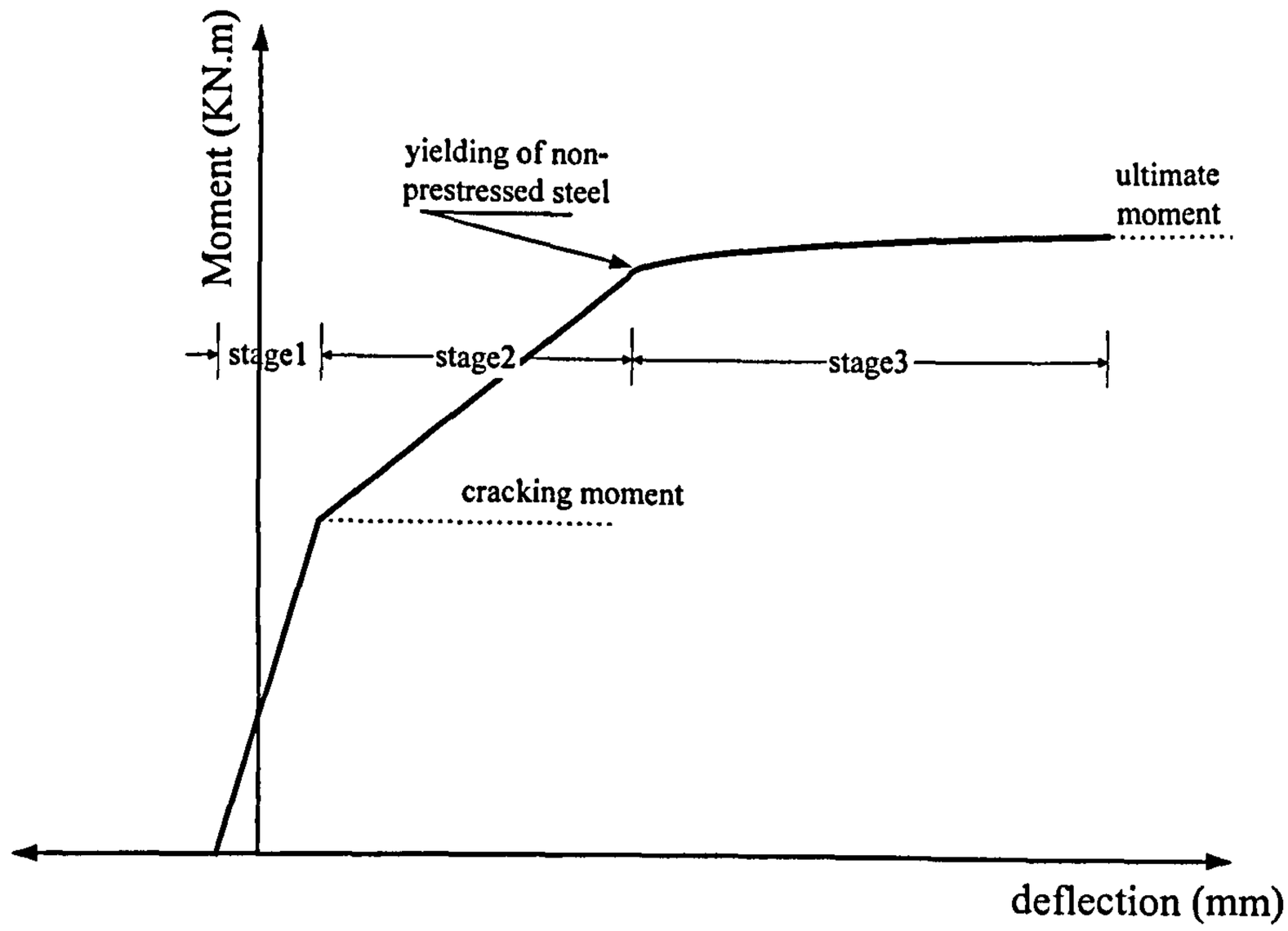

Figure (4.19): Simplified load-deflection curve for external prestressed beam

Also, comparing the load-deflection curves of the externally prestressed beams with that of the beam with internal prestressing only, it can be seen that, the internal prestressed beam (B1) had higher deflections and ductility than the external prestressed beams, but was less stiff after the cracking stage.

The flexural stiffness for all beams before cracking was higher than after cracking, then reached its minimum value at ultimate stage after yielding of the internal tension reinforcement.

While the gradient of the load-deflection curve during stages two and three were not strictly a stiffness, they nevertheless providing a useful indication of the improvement in stiffness provided by the external prestressing. These gradients have therefore been adopted as a basis for comparison.

4.2.2.2.1 Group 1 (Value of the external prestressing force)

Figure (4.20) shows the relation between moment and deflection for beams PG12, PG11, PG13 (P_{ext} = 48.98, 60.35, 72.27 KN) respectively, while Table (4.4) shows the value of deflections and slope of load-deflection curve at each stage. It can be seen that, the camber due to the external prestressing force, slightly increased as external prestressing force increased. And, as expected, the load-deflection

characteristics were largely similar up to the cracking load. Beyond that, beam PG13 registered a smaller deflection at any particular load than the other two beams, while beam PG12 had higher deflection at any load.

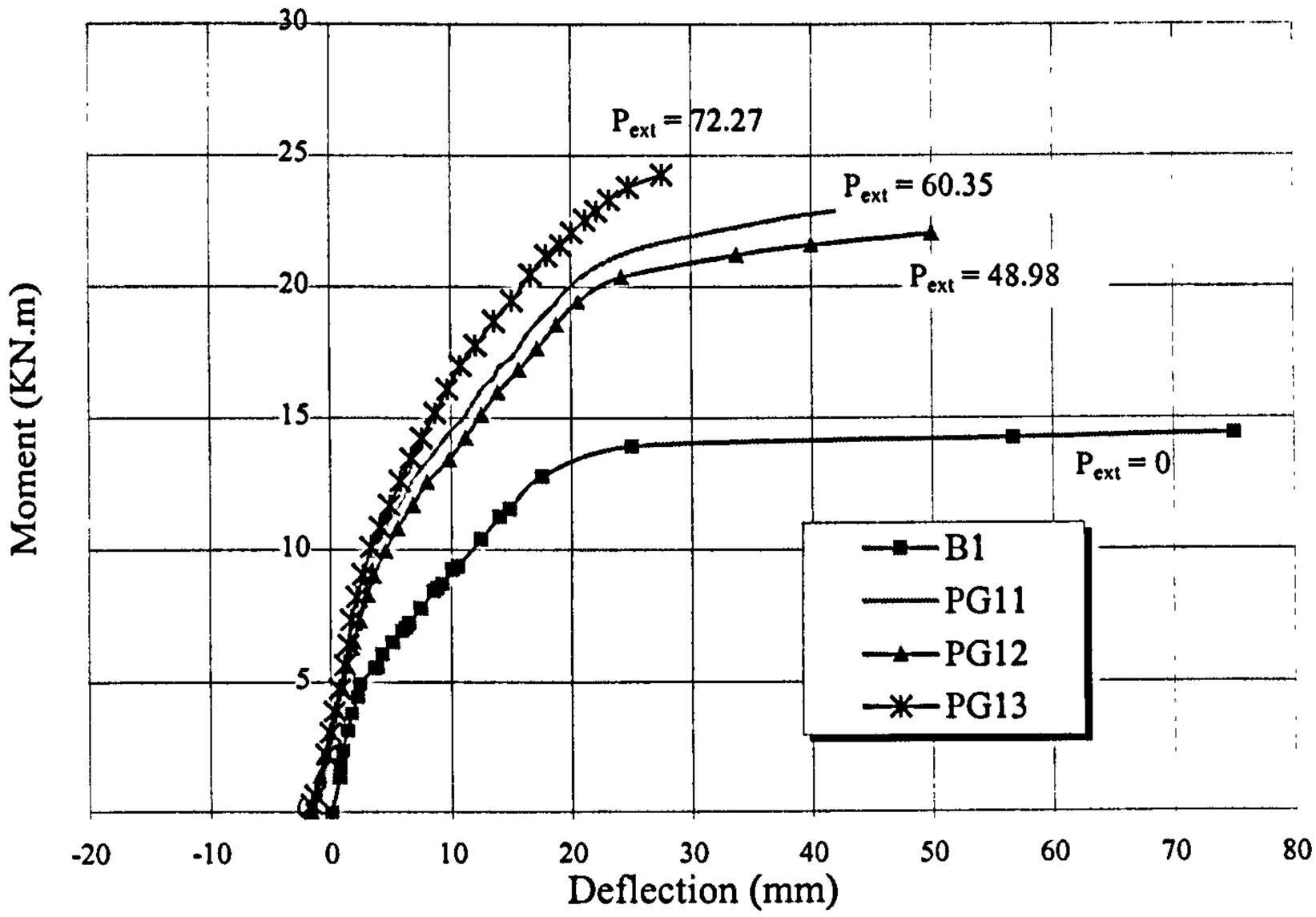

Figure (4.20): Moment -deflection curve of group G1

Table (4.4): *Deflection and slope of load-deflection curve of group G1.*

Beam no.	***Deflection (mm)***				***Slope of P-Δ curve (N/mm)***		
	External prestressing	Cracking load*	Yielding load*	Ultimate load*	Stage (1) $0 \rightarrow P_{cr}$	Stage (2) $P_{cr} \rightarrow P_y$	Stage (3) $P_y \rightarrow P_{ult}$
B1	-----	2.544	17.584	75	4.673	1.282	0.022
PG12	-1.738	4.144	21.169	52.965	4.219	1.327	0.116
PG11	-1.496	5.426	24.059	44.078	4.678	1.363	0.189
PG13	-1.961	4.794	26.237	29.035	4.897	1.520	0.393

* Since applying load

Comparing the beams before and after cracking, it can be seen that there was a slight improvement in the gradients as the external prestressing force increased. Reduction in slope of load-deflection (P-Δ) relation at working and ultimate stages relative to the slope before cracking of beam PG12 were (68.55 %, 97.26 %), beam PG11 were (71%, 96%) and beam PG13 were (68.96 %, 91.97 %) respectively.

4.2.2.2.2 Group 2 (Number of deviators)

Figure (4.21) shows the relation between moment and deflection of PG21 (one deviator at the middle) and PG51 (two deviators at the third span), while Table (4.5) shows the value of deflections and slope of load-deflection curve at each stage. It can be seen that the camber of beam PG51 was higher than that of beam PG21, (The same result was obtained when comparing beam PG21 and beam PG11).

During prestressing, the effective depth of PG51 increased as the camber increased, but during loading, the effective depth decreased as the load increased. The reduction became significant after cracking had occurred and more so after the yielding of the internal reinforcement.

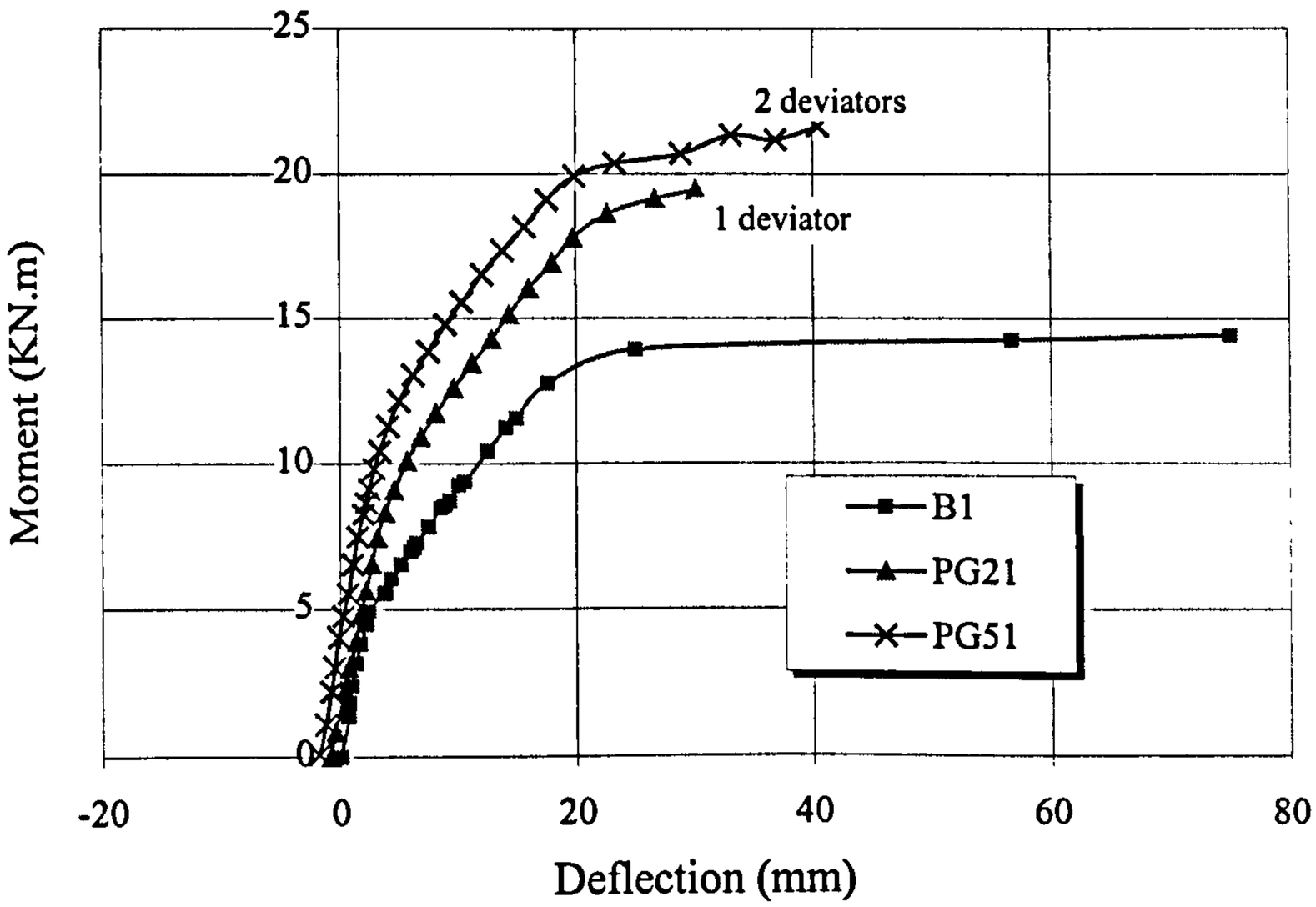

Figure (4.21): Moment -deflection curve of group 2

Before cracking, the difference in deflection of the beams at any moment is small, while after cracking PG21 registered higher deflection. At failure, beam PG51 failed with greater deflection than beam PG21.

Before and after cracking the stiffness of beam PG51 was slightly higher than that of beam PG21. However, at ultimate, the stiffness of beam PG21 was slightly higher. Reductions in slope of the load-deflection (P-Δ) relation at working and

ultimate stages of PG21 were 68.6 % and 94%, while that of PG51 were 73%, 97% respectively.

Table (4.5): *Deflection and slope of load-deflection curves of group G2.*

Beam	***Deflection (mm)***				***Slope of P-Δ curve (N/mm)***		
	External prestressing	cracking load*	Yielding load*	Ultimate load*	Stage (1) $0 \rightarrow P_{cr}$	Stage (2) $P_{cr} \rightarrow P_y$	Stage (3) $P_y \rightarrow P_{ult}$
PG51	-1.818	4.710	21.692	42.296	5.0413	1.3611	0.1915
PG21	-.896	4.668	20.637	31.019	4.2339	1.3278	0.2556

* Since applying load

4.2.2.2.3 Group 3 (Effective depth of the external prestressing force)

Figure (4.22) shows the relation between the moment and deflection of PG11, PG31, and PG32 (e/h = 0.794, 0.894 and 1.072) respectively, while Table (4.6) shows the value of the deflections and slopes of load-deflection curves at each stage. It can be seen that, camber due to external prestressing force, significantly increased as the eccentricity of the external prestressing force increased. Also, the rate of increase in deflection of all beams before cracking was almost the same, except for beam PG31 which was internally prestressed after 11 days.

After cracking, and at ultimate, the beam with the lowest eccentricity (PG11) had the highest deflection at any load, due to the rapid reduction in its inertia. However, the rate of increase in deflection is slightly different in working and ultimate stages.

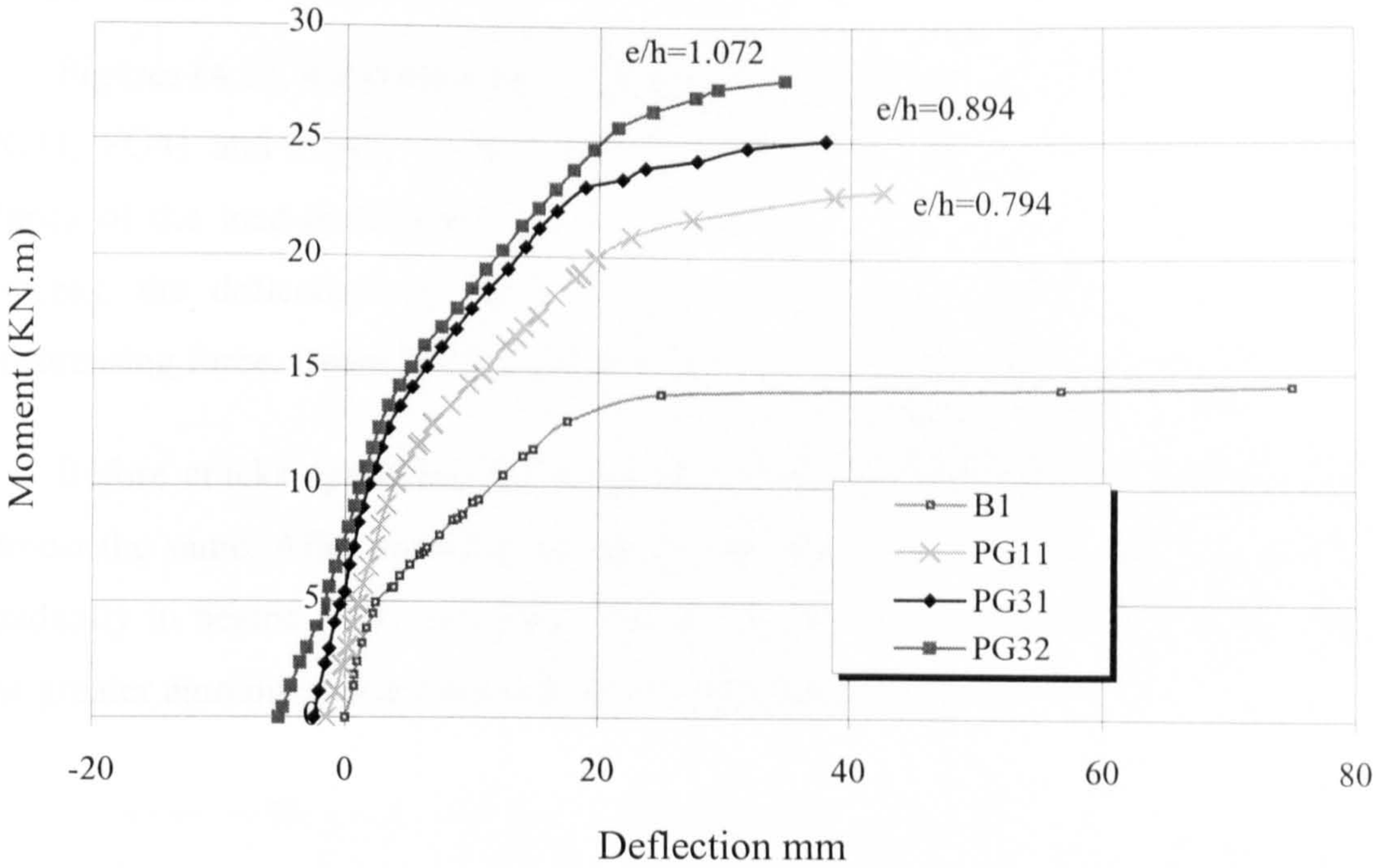

Figure (4.22): Moment -deflection curve of group 3

Table (4.6): *Deflection and slope of load-deflection curves of group G3*

Beam no.	***Deflection (mm)***				***Slope of P-Δ curve (N/mm)***		
	External prestressing	cracking load*	Yielding load*	Ultimate load*	Stage (1) $0 \rightarrow P_{cr}$	Stage (2) $P_{cr} \rightarrow P_y$	Stage (3) $P_y \rightarrow P_{ult}$
PG11	-1.496	5.426	24.059	44.078	4.678	1.363	0.189
PG31	-2.495	5.317	21.477	40.559	5.063	1.576	0.209
PG32	-4.296	8.606	26.734	39.922	4.217	1.553	0.235

* Since applying load

After cracking, the stiffness of all beams decreased as can be seen from figure (4.22). However, PG31, PG32 had slightly higher load-deflection (P-Δ) gradients than PG11 at working and ultimate stages. Reduction in slope of the P-Δ relation at these stages relative to the uncracked stage were (71%, 96%) of PG11, (70 %, 95.9%) of PG31 and (65%, 94.5%) of PG32.

4.2.2.2.4 Group 4 (Previous load stage before externally strengthened)

Figures (4.23, 4.24) shows the relation between moment and deflection of beams PG11, PG41 and PG42, while Table (4.7) shows the values of the deflections and slopes of the load-deflection curves at each stage. During the external prestressing process, the deflection of PG11, PG41 and PG42 reduced due to the external prestressing force. Beam PG42 strengthened after 0.6 P_{ult} had the highest camber.

Before cracks appeared, the deflection of the externally prestressed beams was almost the same. After cracking the rate of increase of deflection with load increased gradually in beams PG41 and PG11 but the increase was sharper with PG42, due to the greater amount of cracking before strengthening.

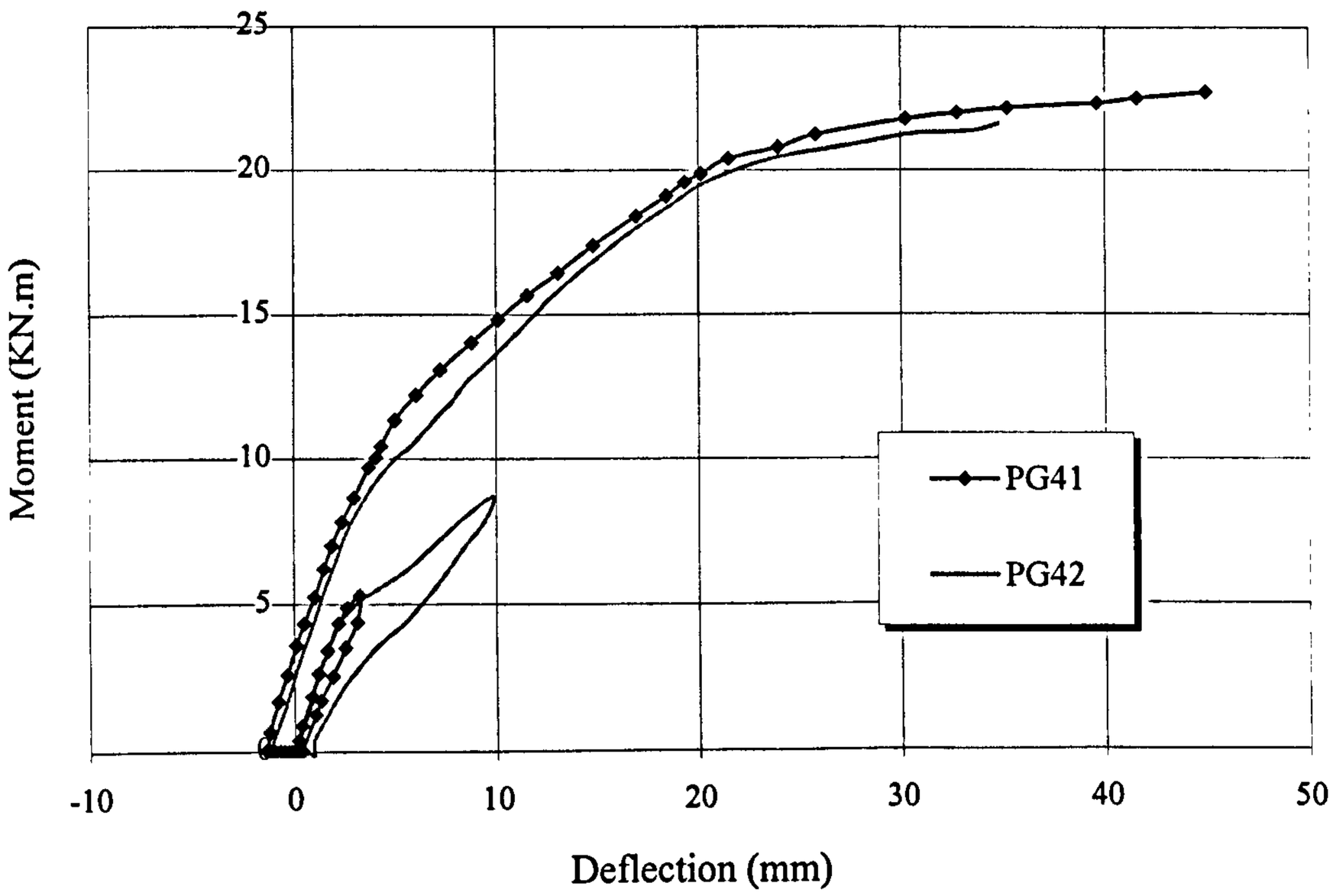

Figure (4.23): Moment -deflection curve of group G4 before and after strengthening

Comparing the slope of the moment-deflection curves before and after the external prestressing was applied, it can be seen that there was an increase in this rate in beam PG41 by about 30% and 250% in beam PG42. Also, after strengthening and before cracks reopening the slope of load-deflection curve was almost the same for all beams, While after cracking the slope of PG42 more sharply decreased than that of PG11 and PG41. The average stiffness after cracking in the working and ultimate stages almost the same of all beams.

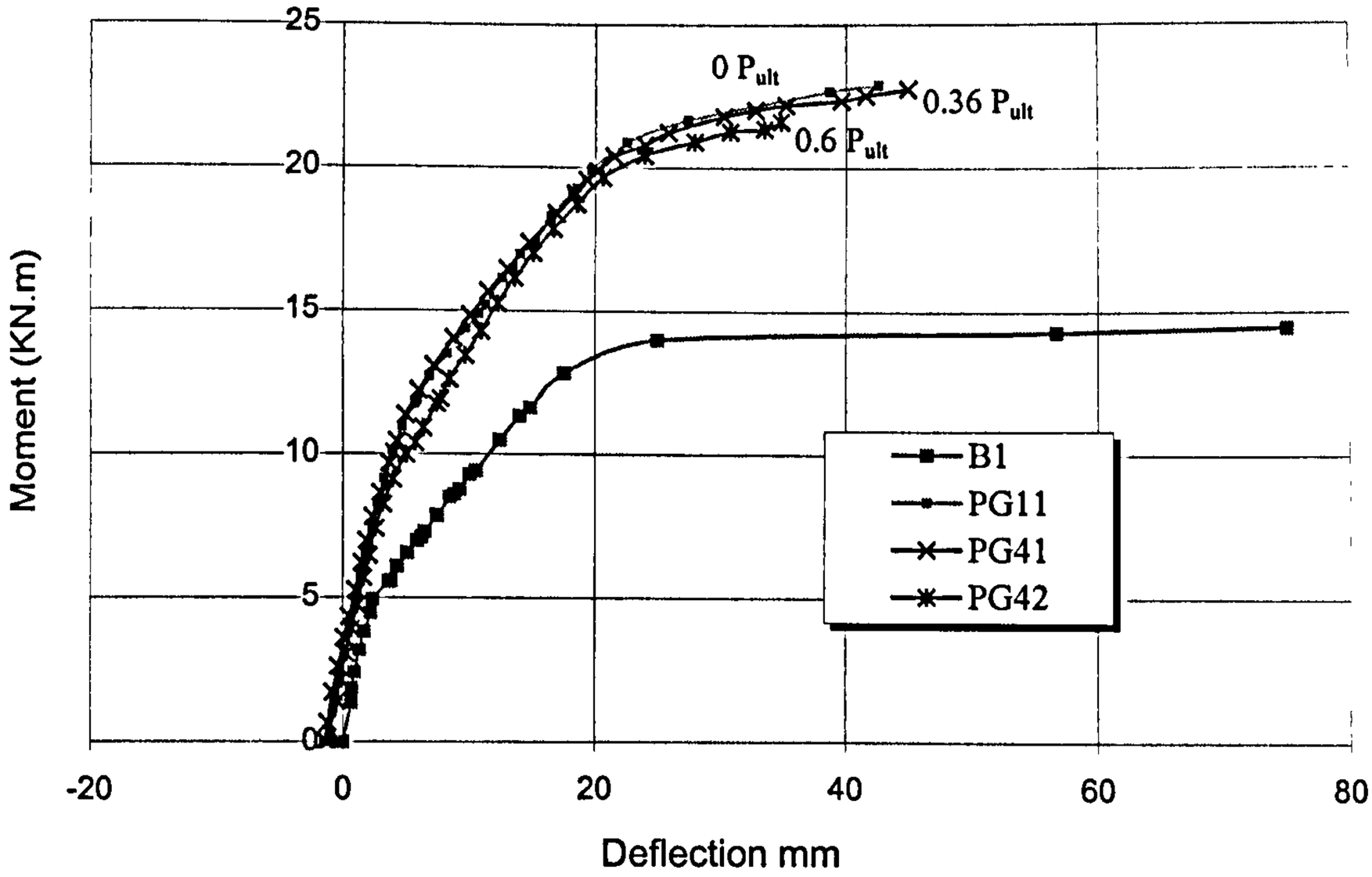

Figure (4. 24): load-deflection curve of group G4 after strengthening

Table (4.7): *Deflection and slope of load-deflection curves of group G4*

Beam no.	***Deflection (mm)***				***Slope of P-Δ curve (N/mm)***		
	External prestressing	cracking load*	Yielding load*	Ultimate load*	Stage (1) $0 \rightarrow P_{cr}$	Stage (2) $P_{cr} \rightarrow P_y$	Stage (3) $P_y \rightarrow P_{ult}$
B1	-----	2.2544	17.584	75	4.6732	1.2823	0.022
PG11	-1.496	5.4259	24.059	44.078	4.6776	1.3633	0.1889
PG41	-1.731	4.3647*	22.894	46.314	4.5689	1.3755	0.17
PG42	-2.195	4.455*	21.869	36.028	4.5129	1.5953	0.2096

* after external prestressing. ** Since applying load

§ (P/Δ) of PG41 and PG42 before cracking and external prestressing =(4.37,4.74)

§ (P/Δ) of PG41 and PG42 before external prestressing =(3.47, 1.28)

4.2.2.2.5 Group 5 (Concrete strength)

Figure (4.25) shows the relation between moment and deflection of beams PG51, PG11 and PG52 (f_{cu}= 43.3, 55.8 and 79.3 MPa) respectively, while Table (4.8) shows the value of the deflections and slopes of the load-deflection curves at each stage. It can be seen that camber due to external prestressing force slightly increased as concrete strength decreased, due to the reduction in Young's modulus and hence reduction in stiffness as the concrete strength decreases.

The moment-deflection characteristics of the externally prestressed beams were largely similar up to the cracking load. Beyond that, beam PG52 registered a slightly smaller deflection at any particular load than the other two beams. However, at failure PG52 had a higher deflection.

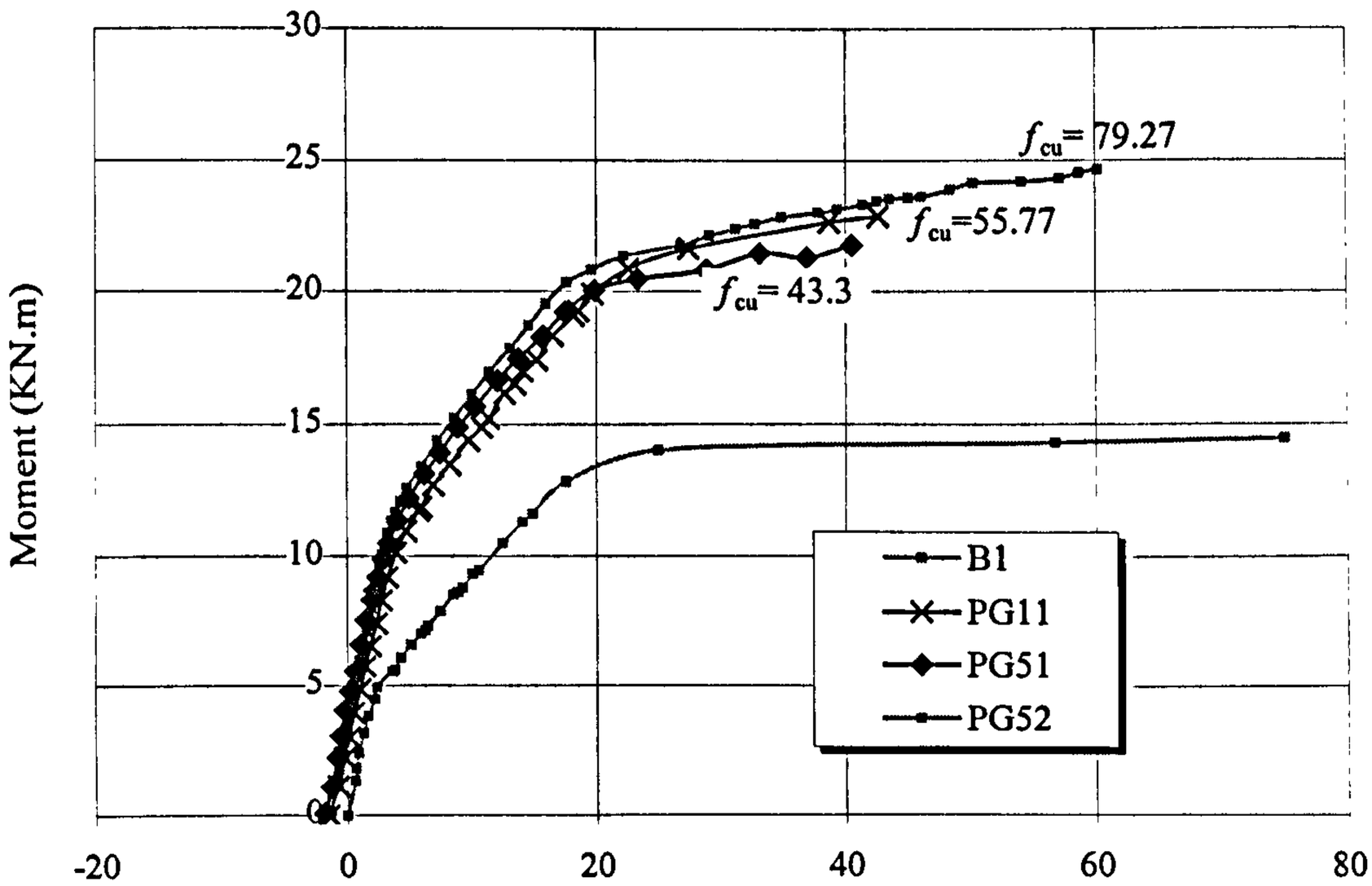

Figure (4.25): Moment-deflection curve of group G5

Table (4.8): *Deflection and slope of load-deflection curves of group G5*

Beam no.	***Deflection (mm)***				***Slope of P-Δ curve (N/mm)***		
	External prestressing	Cracking load*	Yielding load*	Ultimate load*	Stage (1) $0 \rightarrow P_{cr}$	Stage (2) $P_{cr} \rightarrow P_y$	Stage (3) $P_y \rightarrow P_{ult}$
PG51	-1.818	4.710	21.692	42.296	5.041	1.361	0.192
PG11	-1.496	5.426	24.059	44.078	4.678	1.363	0.189
PG52	-1.330	4.59445	18.9886	61.51775	5.5743	1.4862	0.1915

* Since applying load

Before and after cracking, the beam with the highest concrete strength had slightly higher stiffness. However, beam PG51 had higher stiffness than beam PG11 before cracking and almost the same stiffness after cracking. Reduction in the slope of

the load-deflection relation at working and ultimate stages of PG11 were 71 % and 96%, while that of PG51and PG52 were 73%, 97% and 73%, 97.5% respectively.

4.2.2.2.6 Group 6 (Effective span length / depth ratio (L/h))

Figure (4.26) shows the relation between the moment and deflection of beams PG61, PG11, PG62 (L/h= 20, 14.4, 10) respectively, while Table (4.9) shows the values of the deflections and slopes of the load-deflection curves at each stage. To compare the deflection behaviour of these beams, the deflection of each beam was divided by the square of the effective beam length (L^2). Figure (4.27) shows the relation between moment and deflection after modification.

From the moment-deflection curves, it can be seen that the camber due to the external prestressing force increased as (L/h) increased. Also, before cracking the deflection increased as (L/h) increased. After cracking, this difference became greater and reached its maximum value at the ultimate stage. Beam PG62 (L/h=10) registered smaller deflection at any particular load than the other two beams, while beam PG61 (L/h=20) had the highest deflection at any load.

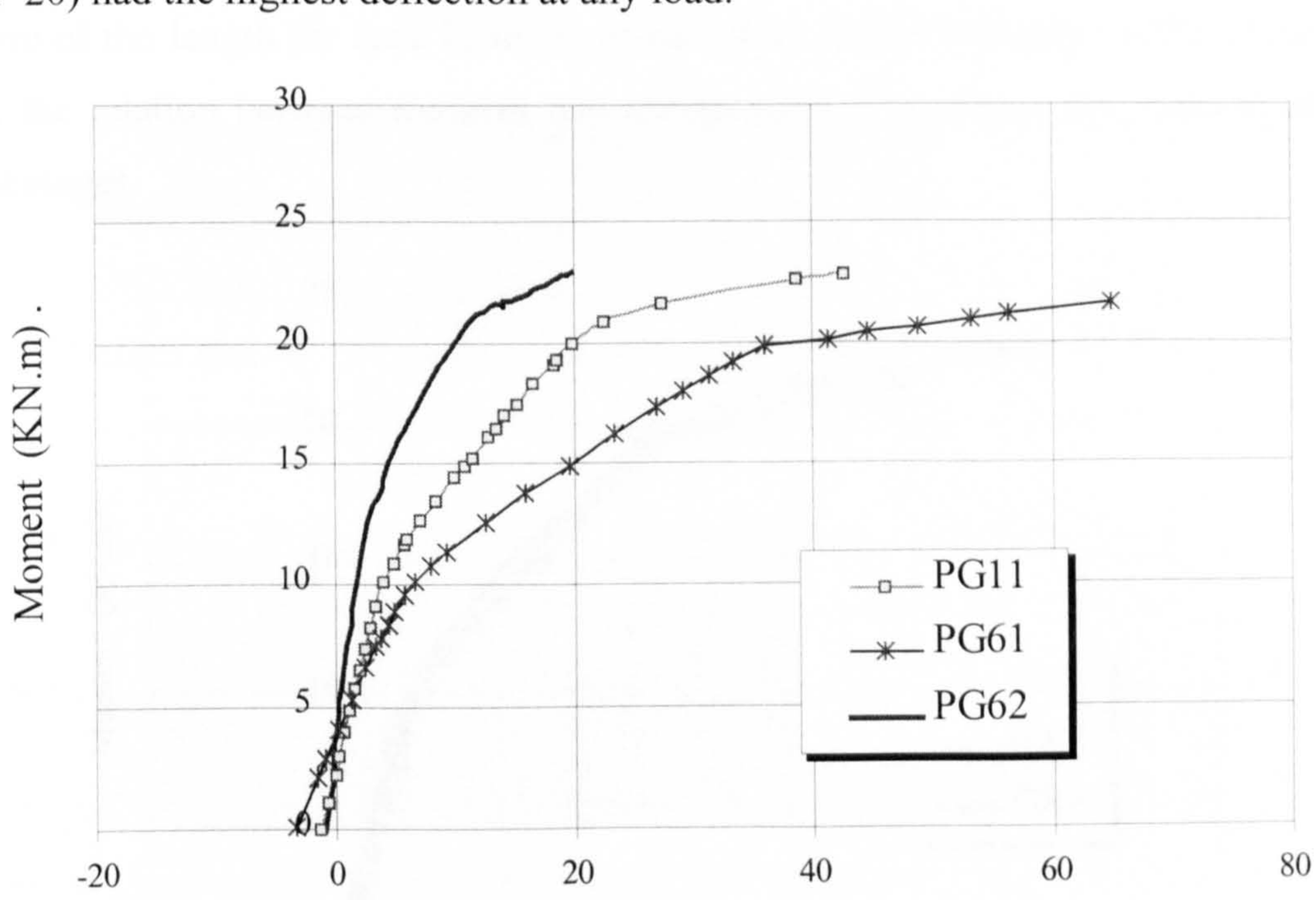

Figure (4.26): load-deflection curve of group 6

Table (4.9): *Deflection and slope of load-deflection curves of group G6*

Beam no.	***Deflection (mm)***				***Slope of P-Δ curve (N/mm)***		
	External prestressing	cracking load*	Yielding load*	Ultimate load*	Stage (1) $0 \rightarrow P_{cr}$	Stage (2) $P_{cr} \rightarrow P_y$	Stage (3) $P_y \rightarrow P_{ult}$
PG61	-3.433	9.076	39.323	62.76	1.846	0.599	0.128
PG11	-1.496	5.426	24.059	44.078	4.678	1.363	0.189
PG62	-0.945	2.788	12.425	20.807	13.241	3.516	0.752

* Since applying load

Comparing stiffnesses of the test beams, it can be seen that beams with lower (L/h) ratios had the highest stiffness at all stages. After cracking, the stiffness decreased and reached its minimum value at the ultimate stage. The reduction in slope of the load-deflection relation at working and ultimate stages of beam PG11 were (71%, 96%), beam PG61 were (67.54 %, 93.01%) while those of beam PG62 were (73.34%, 94.32%) respectively.

The relation between moment and deflection after dividing deflection by the square of the length for each beam in group G6 is shown in figure (4.27). It can see that, the relation between moment and (deflection/L^2) is almost the same in all the three stages.

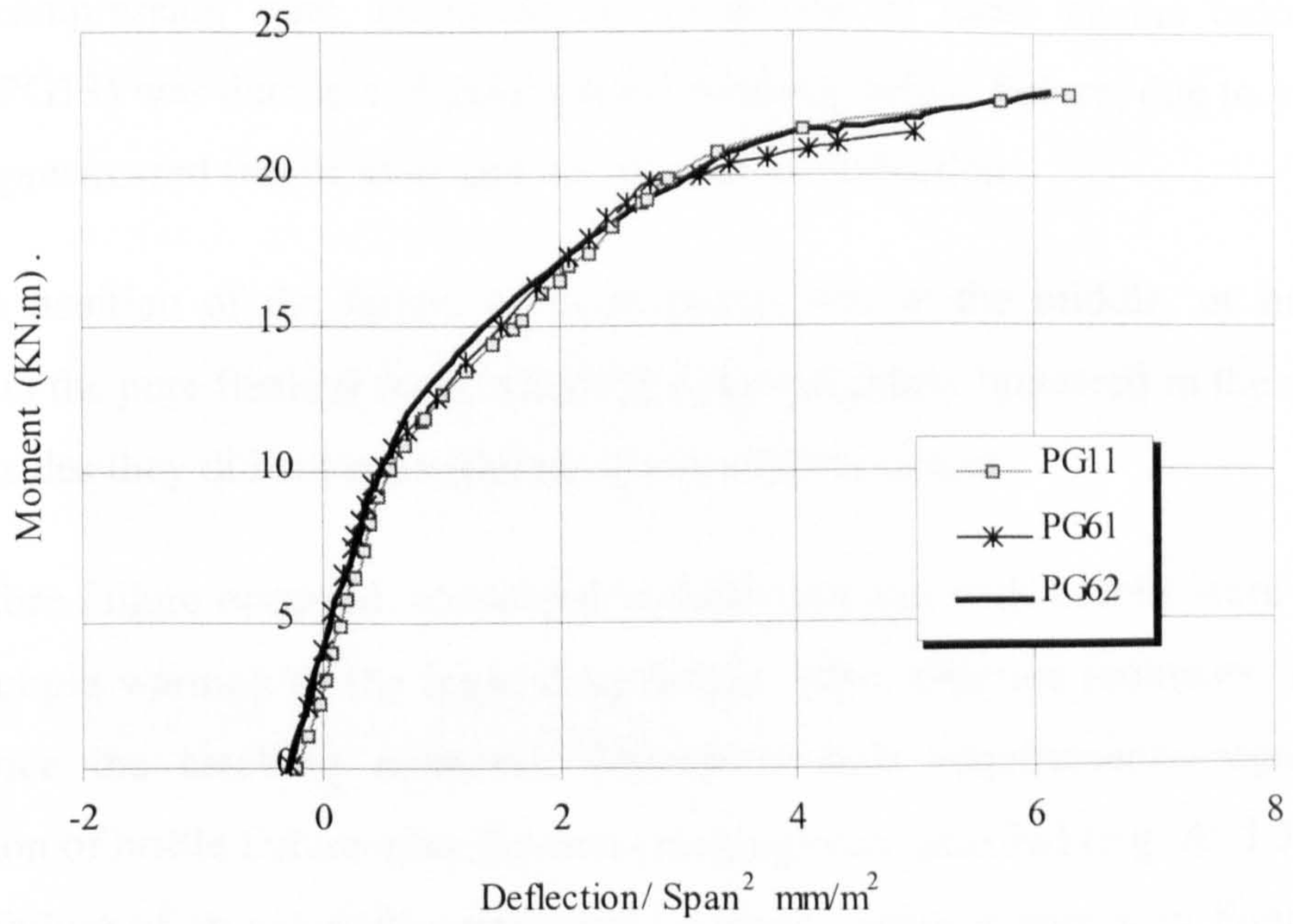

Figure (4.27): Moment-deflection curve of group G6 after modification

Table (4.10): *(Deflection/L^2) and slope of(P-Δ/L^2)curve of group G6*

	Deflection/L^2 (mm/m^2)				***Slope of P-Δ/L^2 curve (N/mm)/m^2***		
	External prestressing	cracking load	Yielding load	Ultimate load	Stage (1) $0 \rightarrow P_{cr}$	Stage (2) $P_{cr} \rightarrow P_y$	Stage (3) $P_y \rightarrow P_{ult}$
PG61	-0.27	0.700	3.034	4.843	0.142	0.046	0.010
PG11	-0.221	0.803	3.559	6.520	0.692	0.202	0.028
PG62	-0.292	0.860	3.835	6.422	4.087	1.085	0.232

4.2.3 Mode of Failure

Mode of failure of the internally prestressed beams with or without external prestressing, started by yielding of the non prestressed steel and ended by concrete crushing, except for beam PG13 which had a high external prestressing force and failed due to concrete crushing while the steel was still in the elastic stage.

In the internally prestressed beam, flexural cracks formed in a regular pattern without any sign of formation of a plastic hinge, and the crack widths were wider than any other beam. Its failure was ductile and occurred at the middle.

In all externally prestressed beams the failure was destructive and accompanied by concrete spalling at the tension face, crushing at the compression face and buckling of the compression steel. However, the behaviour of these beams before failure (except PG13) was ductile and gave a good warning before failure, due to yielding of the non-prestressed tensile steel and the increase in deflection.

The position of the failure of these beams was at the middle, or near to the middle, in the pure flexural zone. Although diagonal cracks appeared in the shear span on both sides they did not cause failure in any of these beams.

Before failure occurred, considerable deflection and wide cracks were observed, giving ample warning of the impending failure. Also, ultimate moments were more than twice the cracking moments. Therefore, code requirements regarding the prevention of brittle failure after flexural cracking were satisfied (e.g. ACI 318-99). A typical failure of an externally prestressed concrete beam is shown in Figures (4.28-4.32).

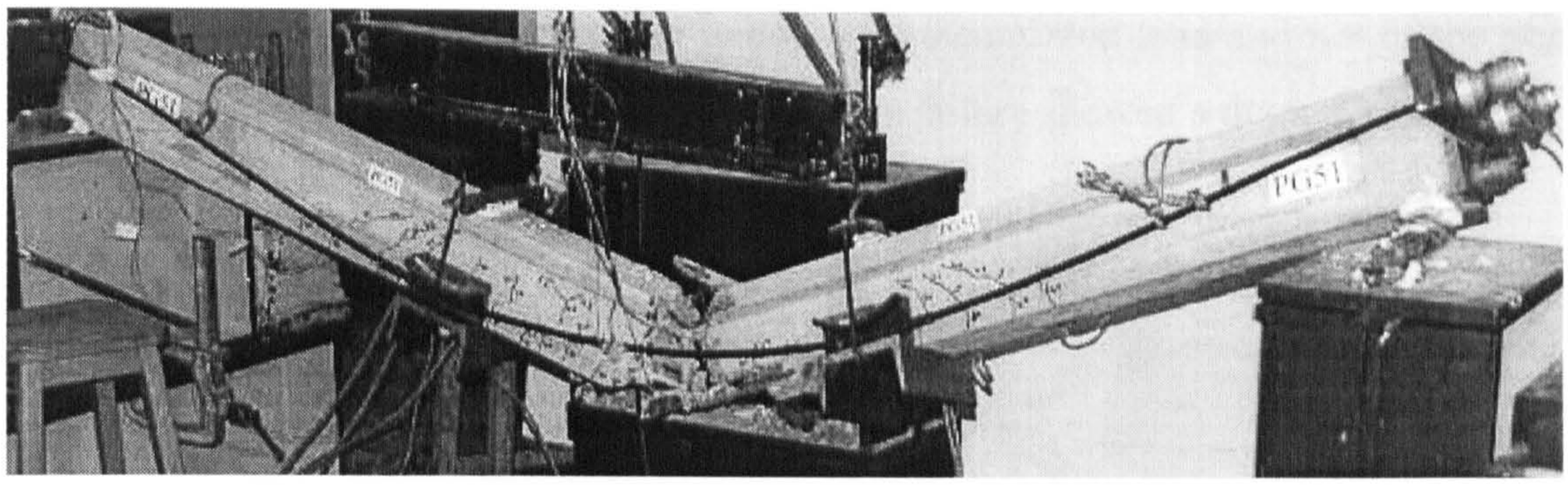

Figure (4.28): Typical flexural failure of external prestressed beam

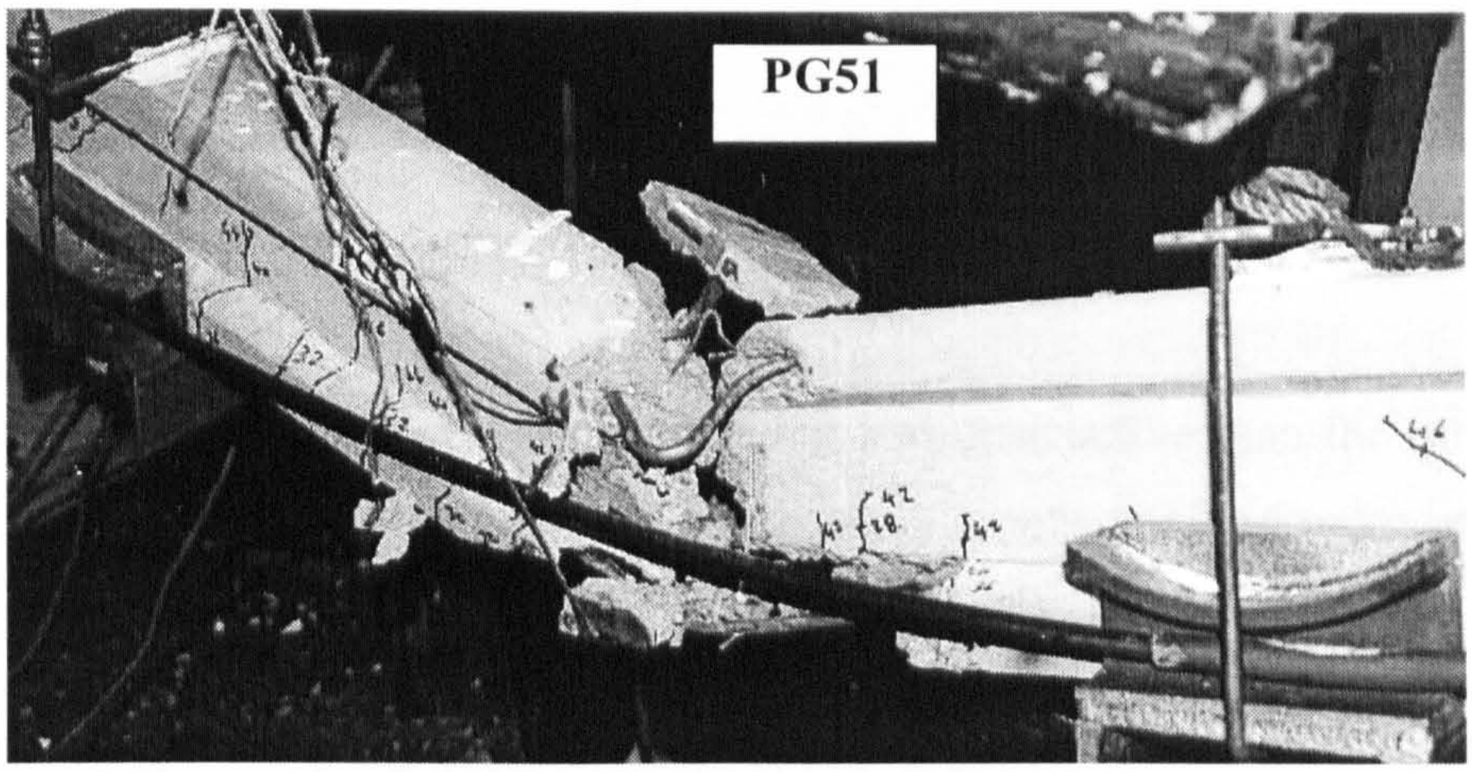

Figure (4.29): Close-up of flexural failure of external prestressed concrete beam

Beam PG13 had a brittle failure as its failure was due to concrete crushing and was not accompanied by increase in deflection, or yielding of steel. Therefore, it had the least ductility among all beams with the same length. Failure occurred in the flexural zone near to the concentrated load.

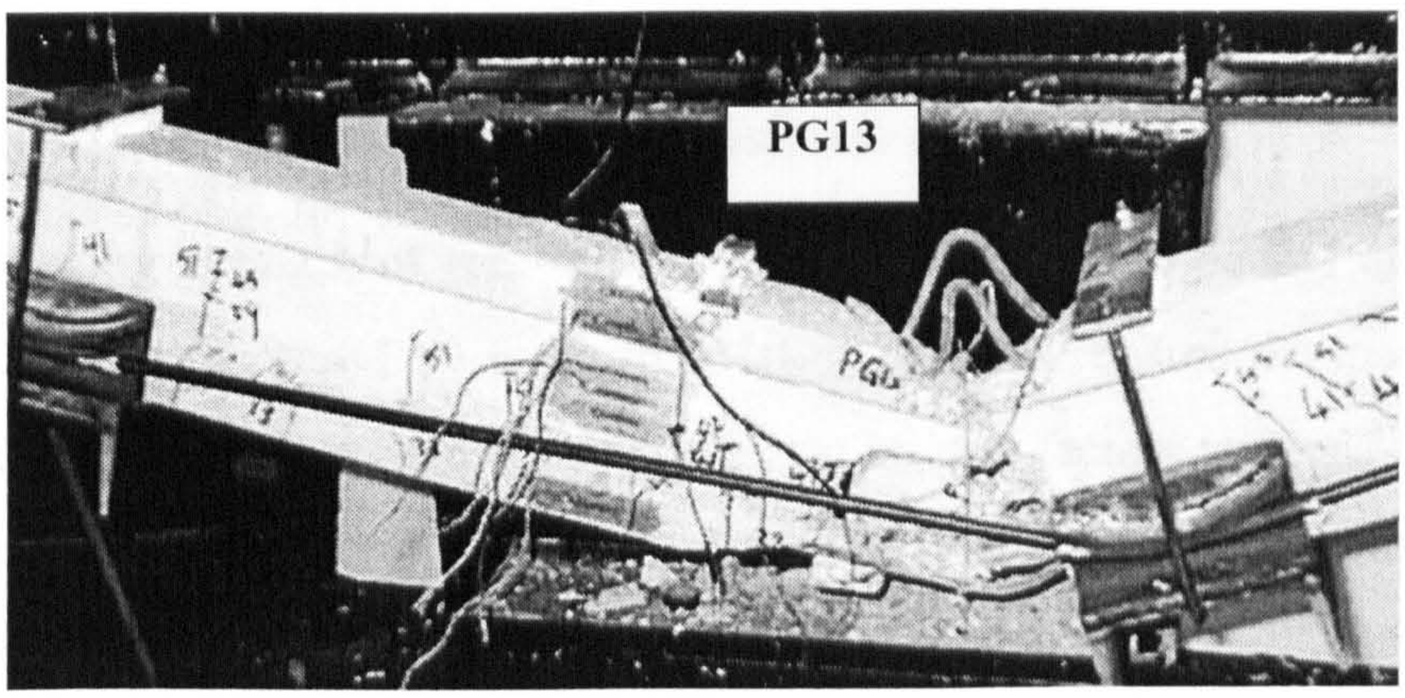

Figure (4.30): Failure of beam PG13

Failure of beam PG21 occurred under the concentrated load and not in the pure flexural zone as in the other beams. However, its failure showed a ductile trend.

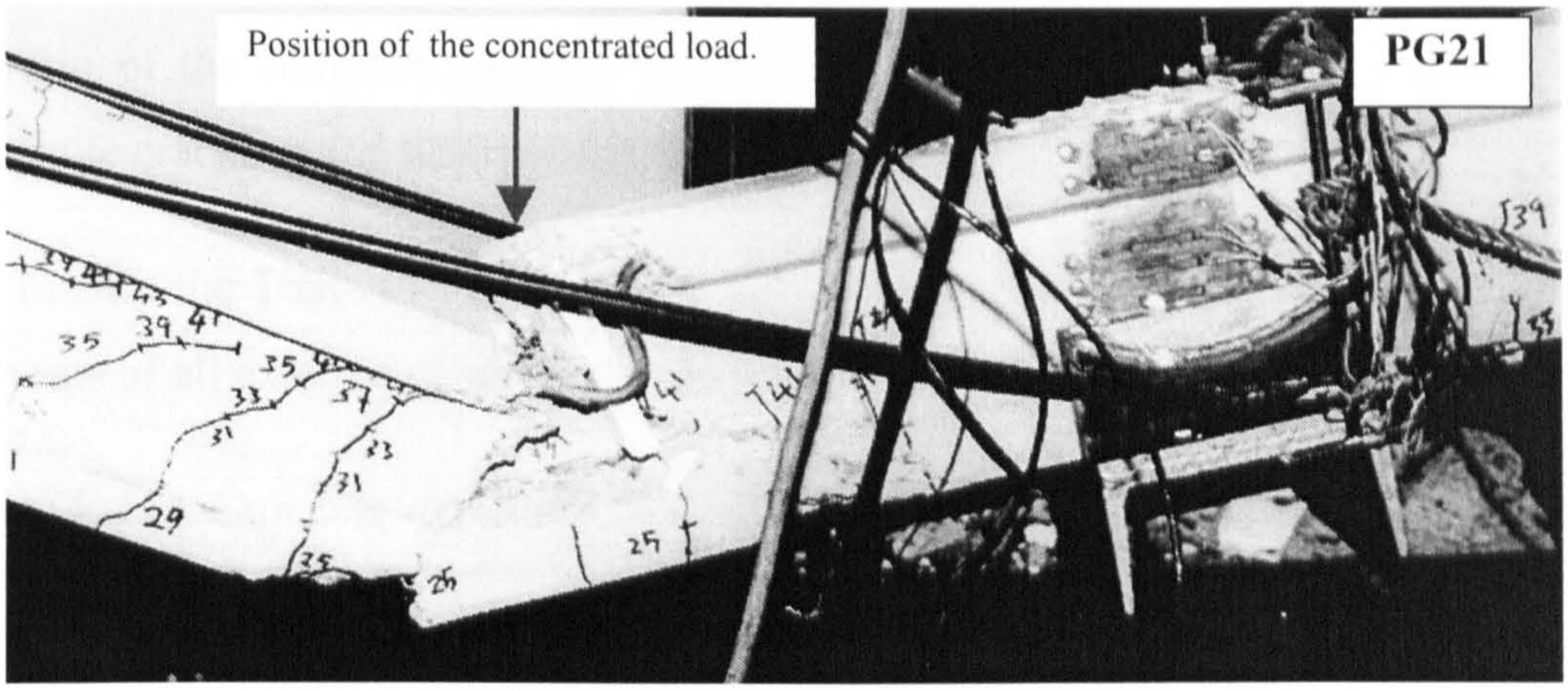

Figure (4.31): Failure of beam PG21

Failure of beam PG62 was less ductile but less destructive than the other beams. Failure occurred near to the deviator, and the shear cracks covered most of the shear span length on both sides.

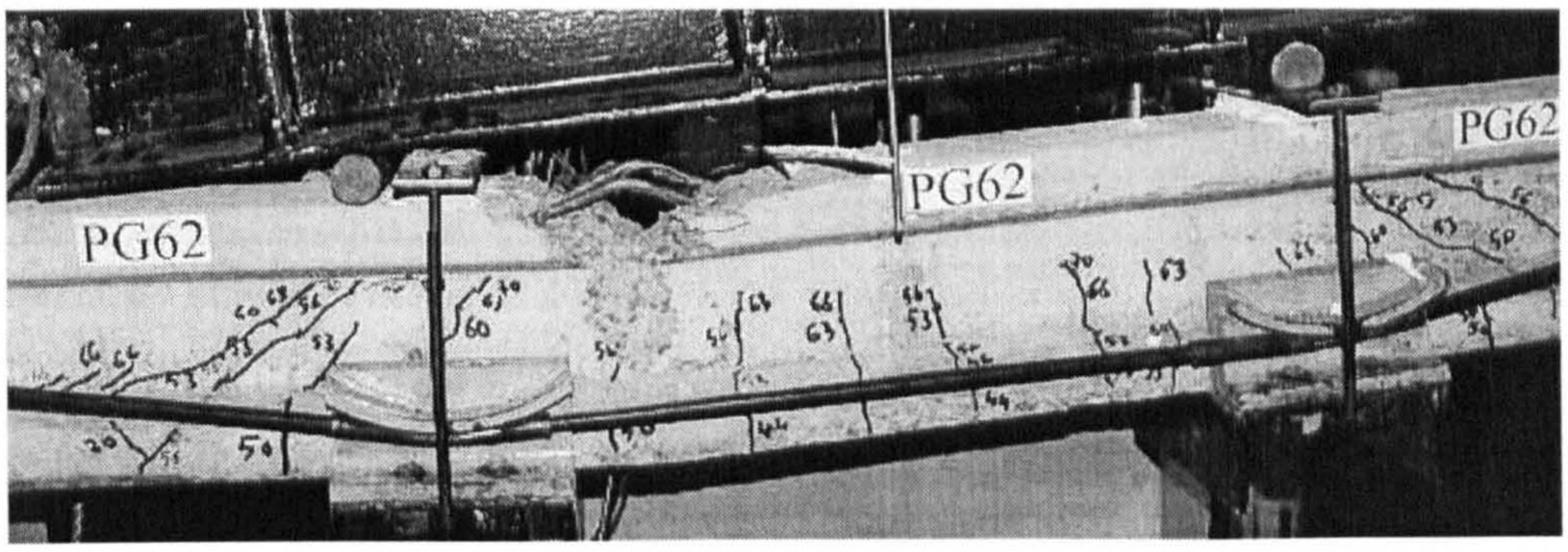

Figure (4.32): Failure of beam PG62

4.2.4 Cracking and Ultimate Moments Resistances

The cracking strength of the internal prestressed concrete beams after external strengthening was increased by more than 100% in many beams compared with an unstrengthened beam. This increase depended on several factors such as, the value of the external prestressing force, the position of the deviator and the eccentricity of the external prestressing force.

Also, an appreciable increase in the ultimate strength was obtained by the addition of the external prestressing, although the unbonded ropes did not reach their ultimate stress in any test. Table (4.11) shows the cracking and ultimate moments and the ratio of the ultimate moment relative to that of beam B1, while Figure (4.33) shows the cracking and ultimate moments of all beams.

Finally the Table (4.11) shows the ratio of increase in the cracking and ultimate moments of all external prestressed beams were relative to those of beam B1.

Table (4. 11): *Cracking and ultimate moments of beam tests*

Factor	***Beam no.***	M_{cr} ***(KN.m)***	M_{ult} ***(KN.m)***	M_{ult}/M_{cr}	$M_{cr}/M_{cr(B1)}$	$M_{ult}/M_{ult(B1)}$
Internal only	B1	4.96	14.49	2.92	1.00	1.00
External prestressing force value	PG12	9.09	22.14	2.44	1.83	1.53
	PG11	10.14	22.88	2.26	2.04	1.58
	PG13	10.18	24.40	2.40	2.05	1.68
Number of deviators	PG21	8.35	19.58	2.34	1.68	1.35
Eccentricity	PG31	11.70	25.23	2.16	2.36	1.74
	PG32	13.53	27.84	2.06	2.73	1.92
Previous cracking stage	PG41	(4.87/8.66)*	22.75	**(4.67/2.63)***	(0.98/1.75)*	1.57
	PG42	(4.35/8.27)*	21.62	(4.97/2.62)*	(0.88/1.67)*	1.49
Concrete Strength	PG51	9.87	21.79	2.21	1.99	1.50
	PG52	10.88	24.66	2.27	2.19	1.70
(L/h) ratio	PG61	9.60	21.60	2.25	1.94	1.49
	PG62	10.77	22.95	2.13	2.17	1.58

* Before and after external prestressing.

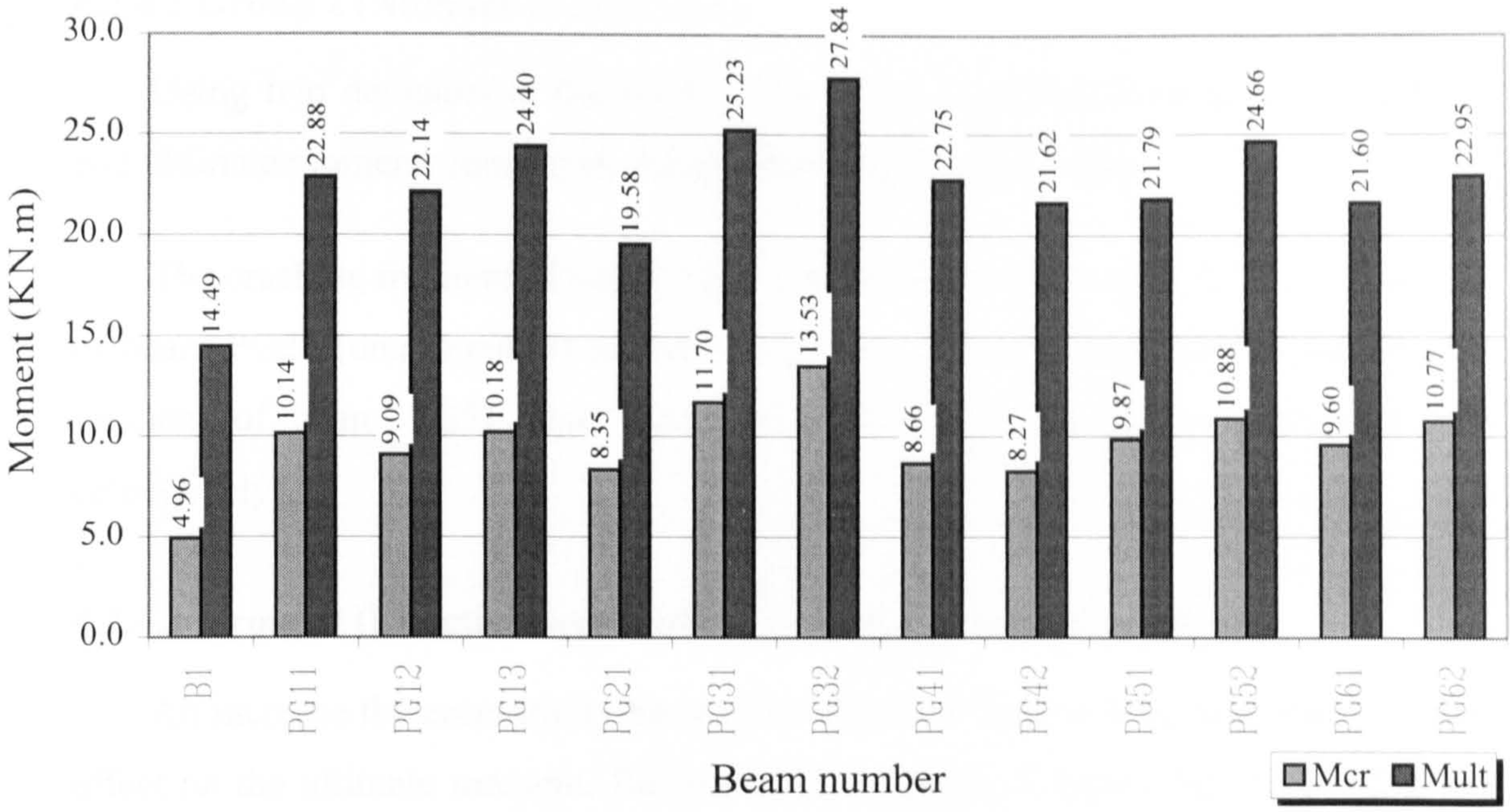

Figure (4. 33): Cracking and ultimate moments of test beams

4.2.4.1 Group 1 (Value of the external prestressing force)

Both cracking and ultimate moment increased as the external prestressing force increased. However, the increase in the cracking moment was higher than the increase in the ultimate moment.

The cracking moment of beams PG12, PG11 and PG13 (P_{ext} = 48.98, 60.35, 72.27 KN) increased by 83 %, 104 %, and 105 % respectively, while the ultimate moment increased by 53%, 58% and 68% respectively.

Comparing the beams PG11 and PG13 to beam PG12, it can be seen that the increase in the cracking moment of PG11 and PG13 were 11.6% and 12%, while the increase in the ultimate moments were 3.3% and 10.2%.

The increase in the cracking moment of beam PG13 was almost the same as that of beam PG11. This may be due to the impact load that accidentally applied to beam PG13 during testing. However, this impact load seemed to have no effect on the ultimate moment.

4.2.4.2 Group 2 (Number of deviators)

Using two deviators at the third points of the span increased both the cracking and ultimate moments more than using one deviator at the middle.

The cracking moment of beam PG51 (two deviators) increased by 99% while that of beam PG21 (one deviator) increased by 68%. Also, the increased in the ultimate moment of beam PG51 was higher than that of beam PG21 (50% and 35% respectively).

4.2.4.3 Group 3 (Effective depth of the external prestressing force)

An increase the eccentricity has a great effect on the cracking moment and lower effect on the ultimate moment. Resistance to cracking of beams PG11, PG31, PG32 (e/h = 0.794, 0.894 and 1.072) increased (compared to that of B1) by 104%, 136%, and 173% respectively. While, their ultimate moments increased by 58%, 74% and 92% respectively. Also, it can be seen that increased eccentricity of beam PG11 by 35% (that of PG32) increased the cracking moment by 33.4% and the ultimate moment by 21.7%.

4.2.4.4 Group 4 (Previous load stage before externally strengthened)

Both beams PG41, PG42 were loaded before being externally prestressed. The cracking moments before externally prestressing were 4.87 and 4.35 KN.m respectively. This difference was due to the variation in the concrete strength (52.2, 45.7 MPa) and the internal prestressing force (40.8, 37.1 KN). After strengthening and during loading, the pre-existing cracks reopened at a moment 8.66 and 8.27 KN.m respectively. Due to the external prestressing force, the cracking moments increased above than that before external prestressing, by 78% and 90 %, while the nominal moments increased (compared to that of beam B1) by 57% and 49%

Because the concrete tensile strength after cracking diminished and the resistance to cracks reopening is due to the external and internal prestressing forces only, the cracking moment of both beams PG41 and PG42, after externally strengthened, were almost the same. While at ultimate, the effect of previous cracking on the ultimate moment resistance of the beam is negligible as can be seen when comparing beams

PG11 and PG41 (had almost the same ultimate moments, 22.88 and 22.75 KN.m respectively) or comparing beams PG42 and PG51, (had almost the same moments 21.62 and 21.79 KN.m respectively).

4.2.4.5 Group 5 (Concrete strength)

Increased concrete strength slightly increased both cracking and ultimate moments. Comparing beams PG51, PG11 and PG52 (f_{cu}= 43.3, 55.8 and 79.3 MPa), it can be seen that the increase in the concrete strength of PG11 and PG52 relative to that of PG51 were 28.8% and 83.1%. This resulted in an increase in the cracking moments of PG11 and PG52 by 2.74% and 10.23% respectively and an increase in the ultimate moments by 5% and 13.17% respectively.

4.2.4.6 Group 6 (Effect of span/depth ratio)

Comparing the cracking and ultimate moments of beams PG62, PG11 and PG61 (L/h =10, 14.44 and 20), it can be seen that, both the cracking and ultimate moments were slightly affected by the increased in the (L/h) ratio, as the increase in the cracking moments of PG11 and PG62 compared to that of PG61, were 5.63% and 12.2%, while the increase in the ultimate moments were 5.93% and 6.25% respectively.

4.2.5 High Tensile Steel (HTS) Strain:

The strain on the internal high tensile steel (HTS) was measured using two strain gauges fixed to the surface of the wire at the middle and at the end. The stress was then determined from the stress-strain curve for the wires. Table (4.12) shows the stresses at different stages. During the external prestressing, the stress in the HTS reduced due to the compressive stress produced by the external prestressing force. During this stage, until cracks due to the applied load appeared, the reduction or increase in steel strain can be determined from the concrete strain at the same level assuming perfect bond between concrete and steel. A good agreement between the strain gauge reading on the steel and that calculated from the concrete strain distribution was observed.

Table (4.12): *Stresses of internal prestressing steel (HTS) at different stage*

Beam no.	***Net stress (MPa)***			***Total stress (MPa)***		
	due to internal prestressing	due to losses	due to external prestressing	after internal prestressing	after losses	after external prestressing
B1	1055	-72	0	1055	983	983
PG11	1092.6	-85.8	-75.06	1092.6	1006.8	931.74
PG12	1152.8	-82.4	-48.32	1152.8	1070.4	1022.08
PG13	1128.4	-82.4	-137.48	1128.4	1046	908.52
PG21	1131.2	-109	-55.48	1131.2	1022.2	966.72
PG31	1083.8	-64.4	-87.96	1083.8	1019.4	931.44
PG32	1113.4	-98.4	-110.76	1113.4	1015	904.24
PG41	1185.2	-125.4	-73.28	1185.2	1059.8	986.52
PG42	1068.6	-105.8	-88.96	1068.6	962.8	873.84
PG51	1052.8	-51.7	-73.8	1052.8	1001.1	927.3
PG52	1128.2	-69.8	-42.02	1128.2	1058.4	1016.38
PG61	1103.8	-54	-70.02	1103.8	1049.8	979.78
PG62	1133.4	-64.4	-51.84	1133.4	1069	1017.16

Figures (4.34-4.39) show the relation between moment and high tensile steel strain at mid-span of each beam. From them it can be seen that the increase in strain in the tensile reinforcement with applied load shows a trend similar to the load-deflection response.

Before cracking, the increase in steel strain was linear and relatively low up to the flexural cracking load, but after cracking, the rate of increase in strain increased and close to ultimate the rate increased rapidly.

After cracking, different types of reading were observed depending on the crack locations relative to the strain gauge fixed on the wire surface. If cracks occurred on both sides of the strain gauge, its reading decreased as the load increased and probably become (-ve) depending on the distance between the cracks and the strain gauge. If the strain gauge was near the crack, its reading was very high.

Due to the previous point, it was difficult and inaccurate to compare the steel strain of beams of each group. However, it can be seen that the increase in the steel strain after cracking was higher in internally prestressed beam than that in the externally prestressed beams.

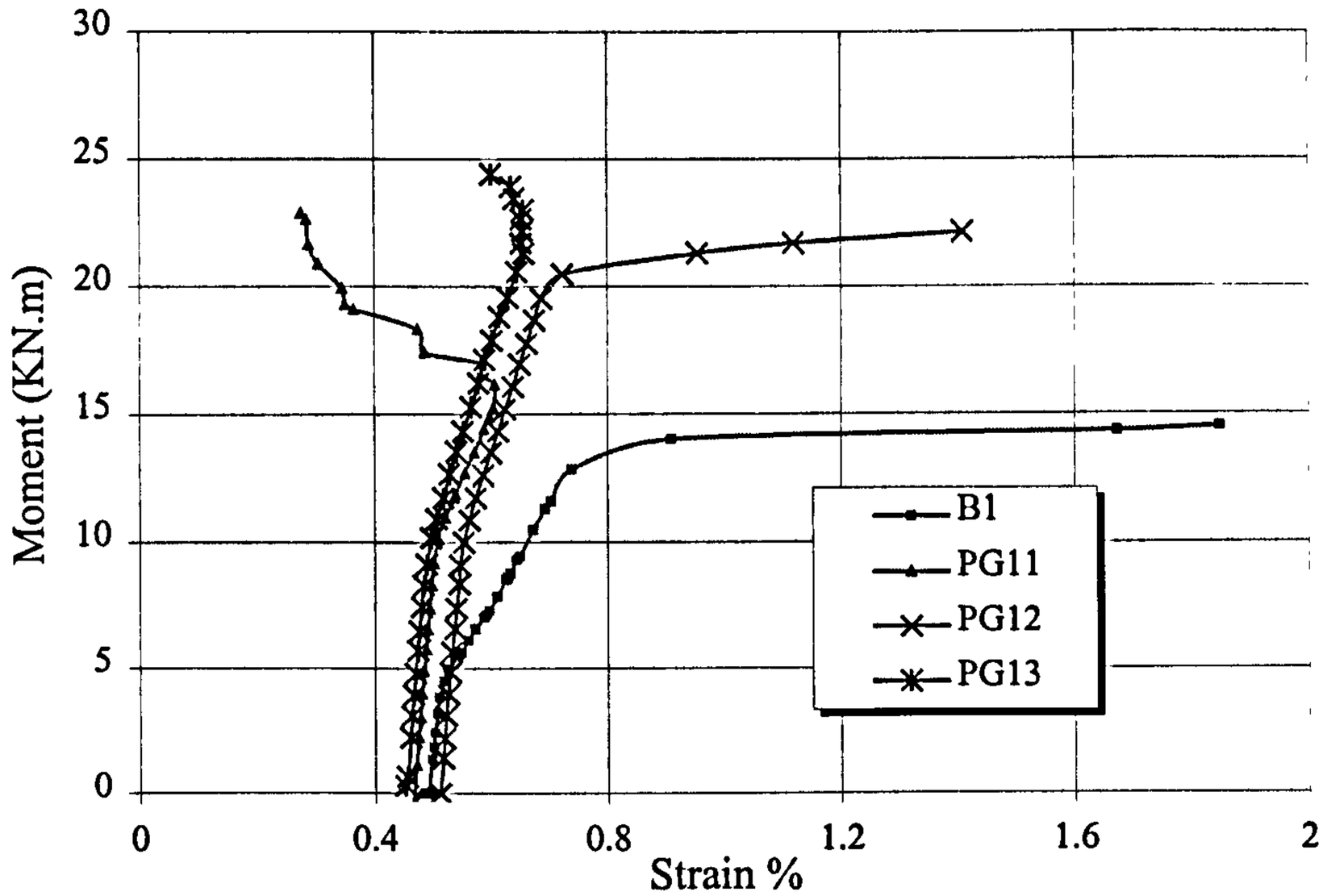

Figure (4.34): Moment-Strain relationship of group G1

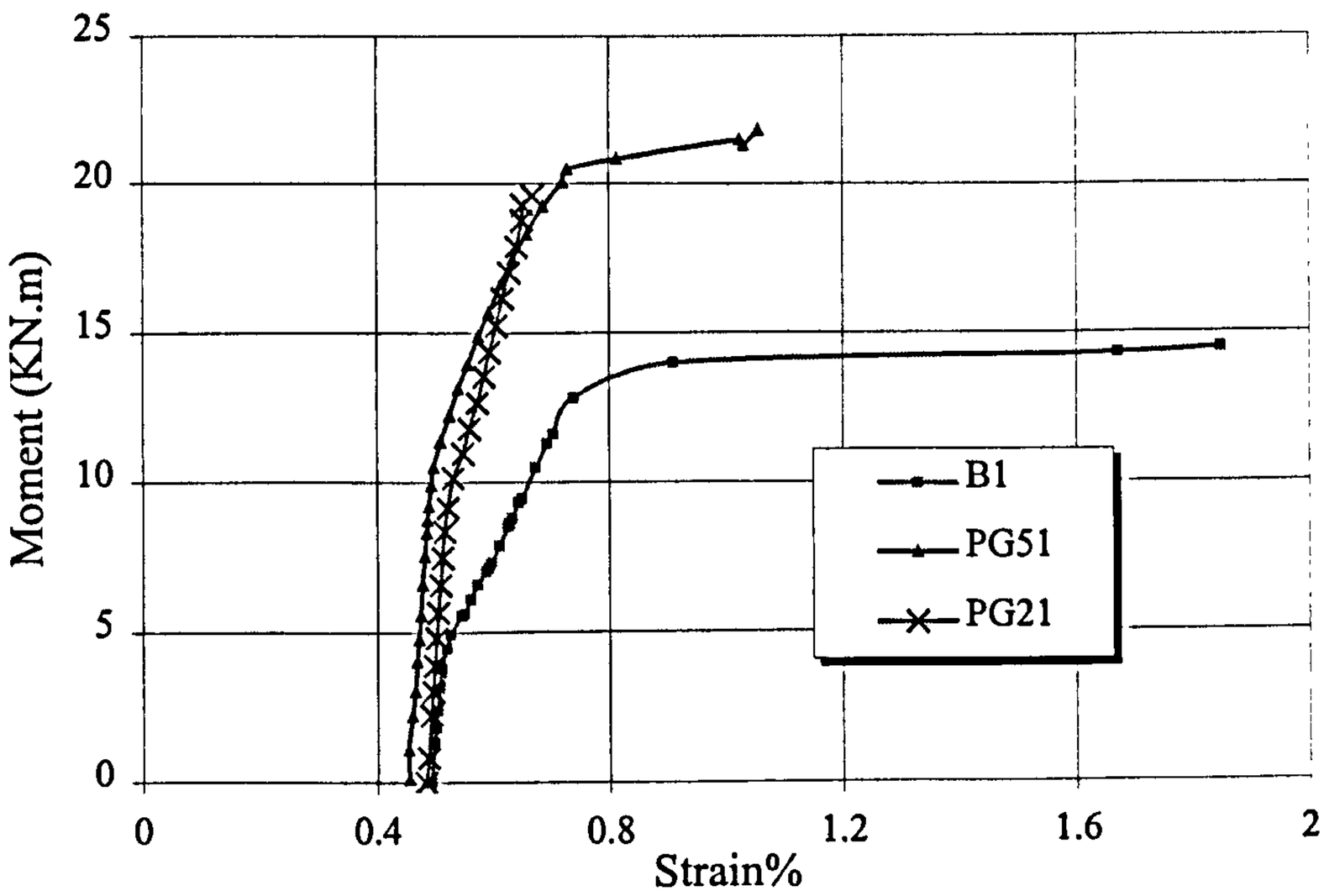

Figure (4.35): Moment-Strain relationship of group G2

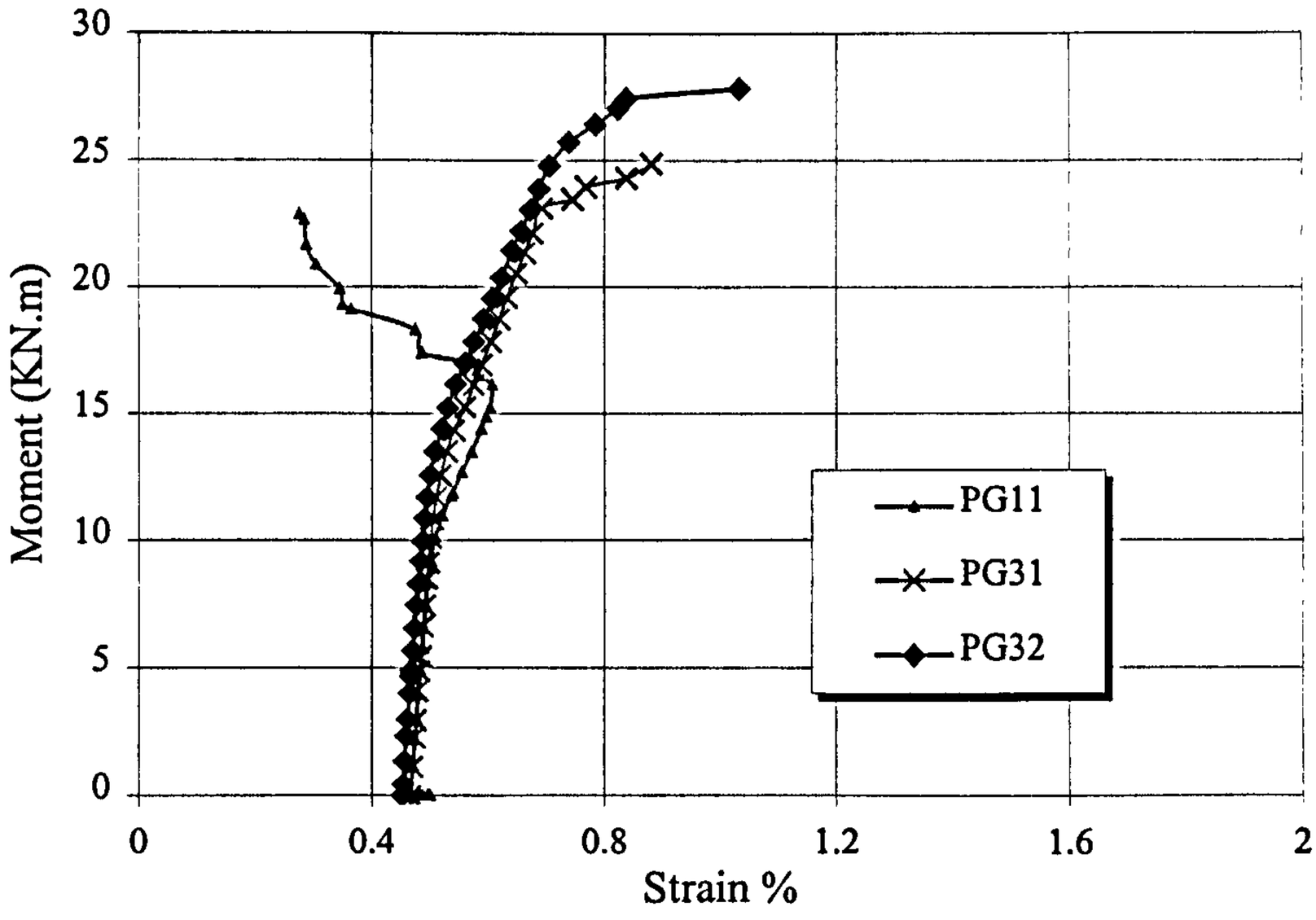

Figure (4.36): Moment-Strain relationship of group G3

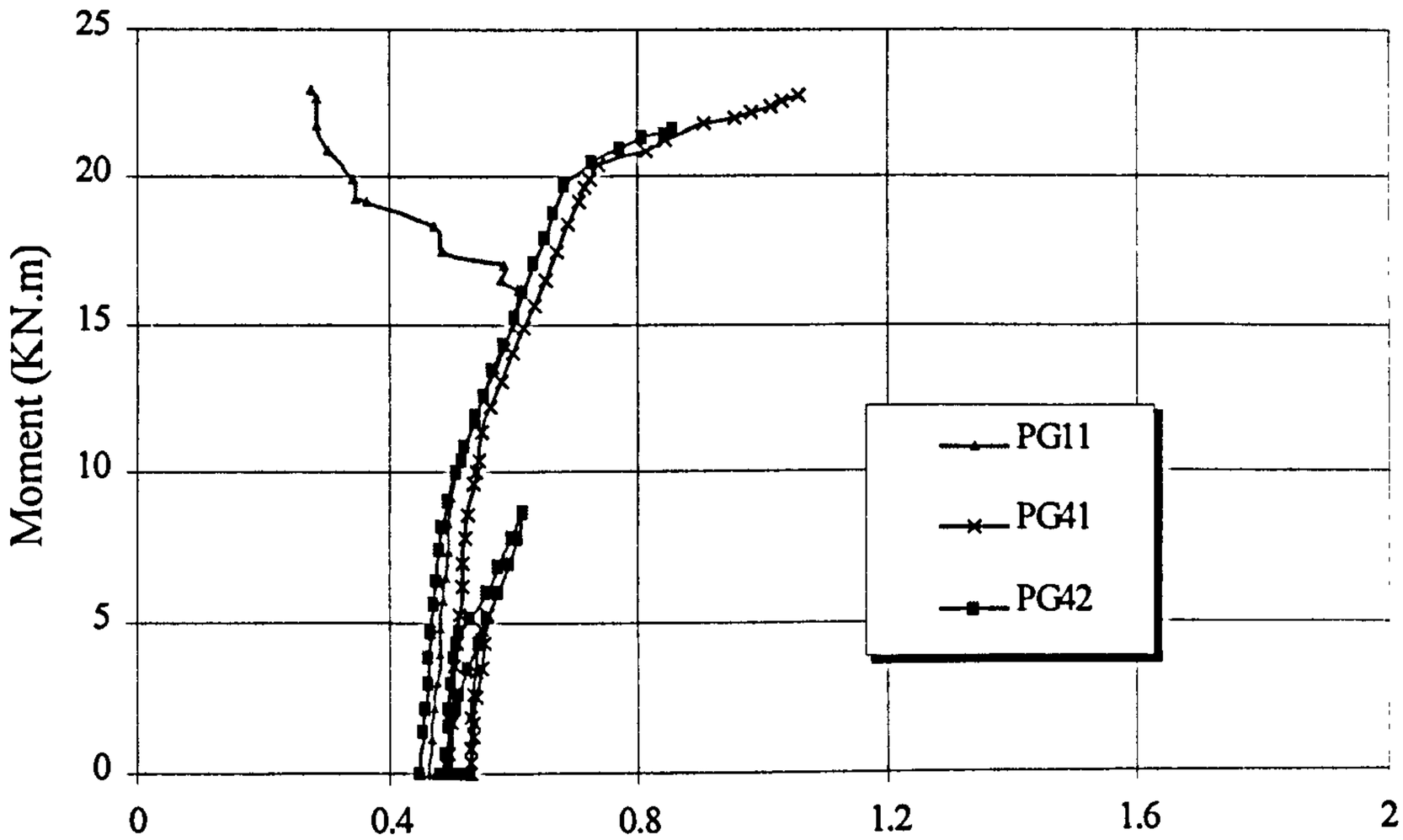

Figure (4.37): Moment-Strain relationship of group G4

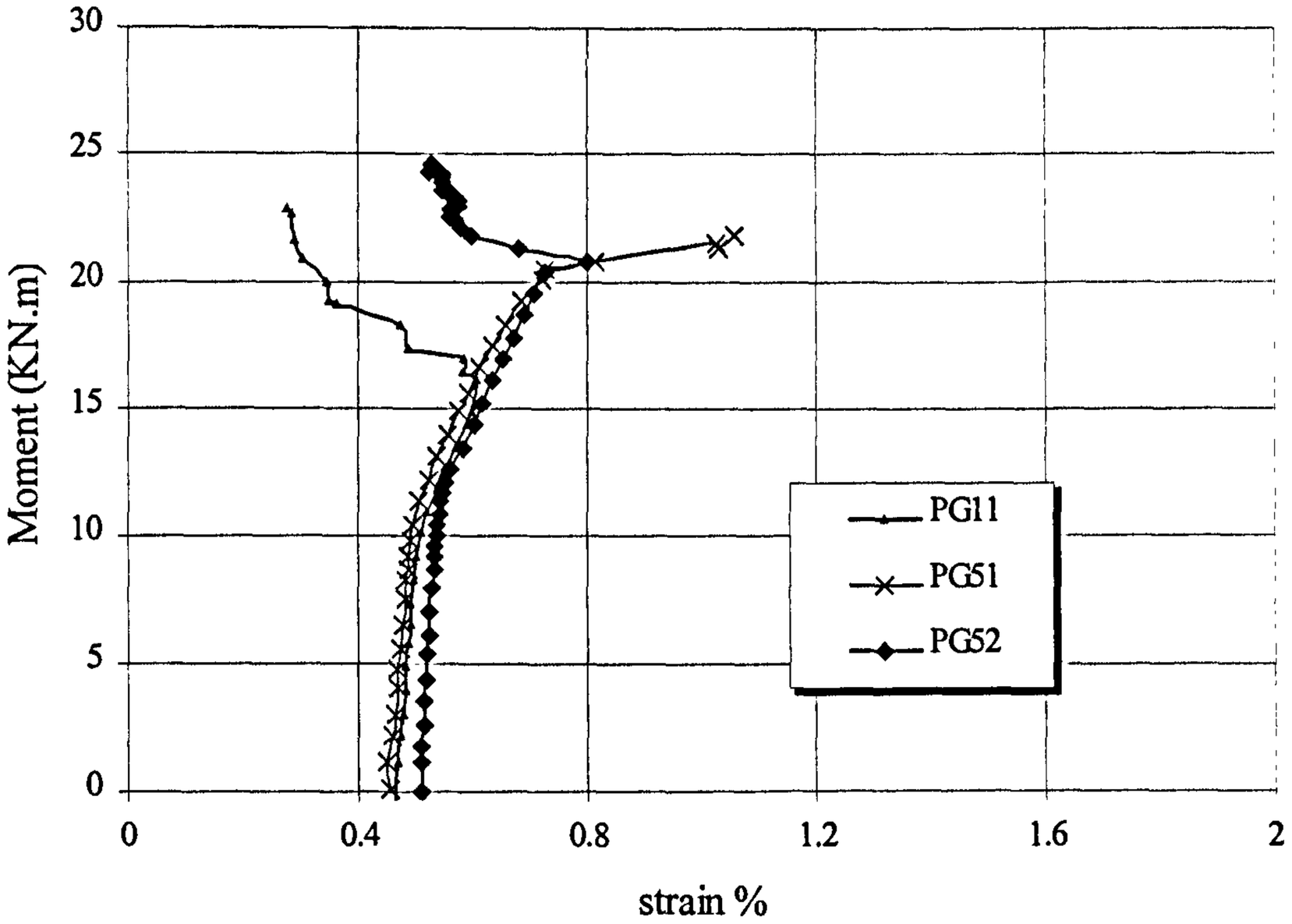

Figure (4.38): Moment-Strain relationship of group G5

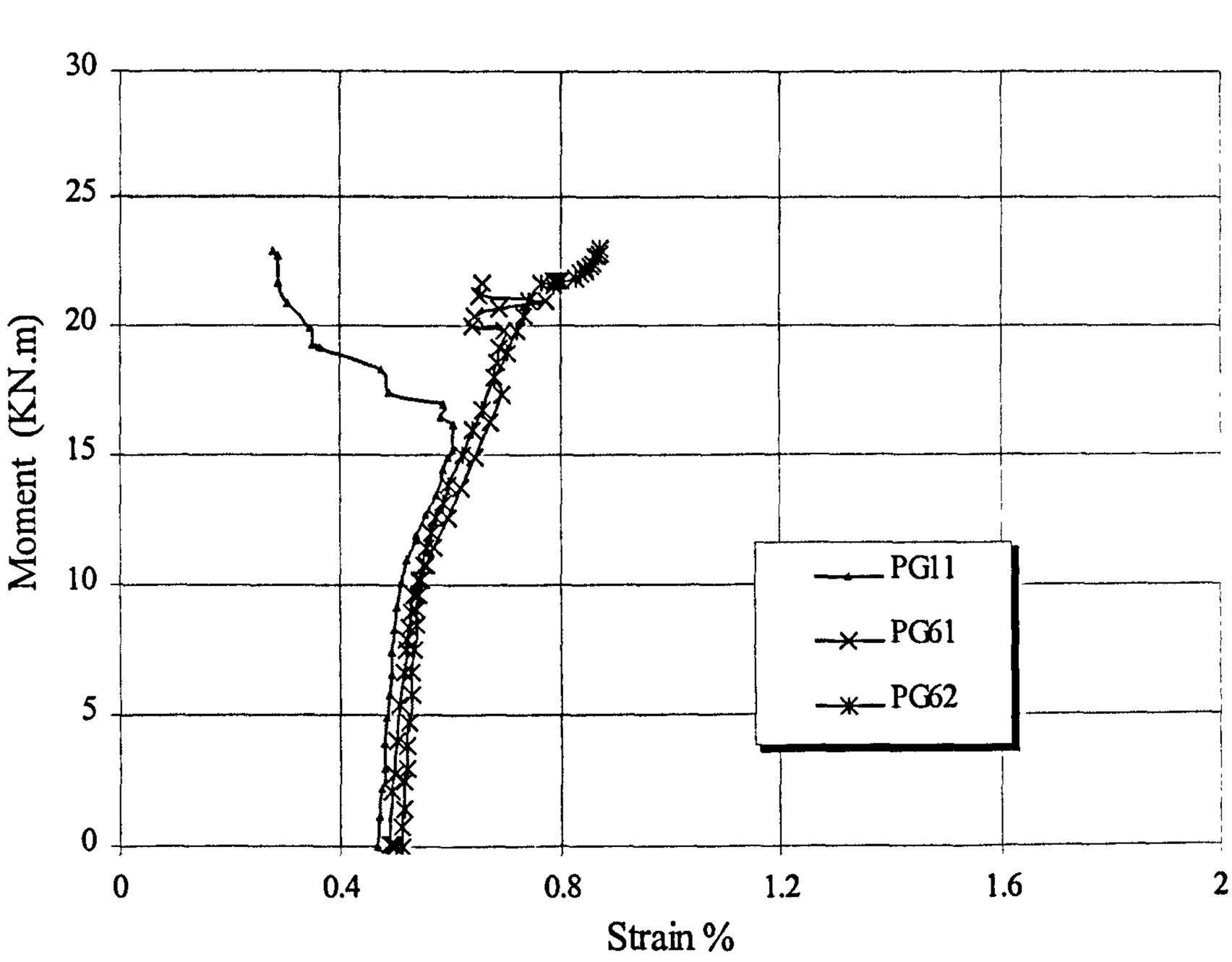

Figure (4.39): Moment-Strain relationship of group G6

Figure (4.40) shows the relation between load and HTS strain near the beam end of group G1. It can be seen that strain of each beam almost constant during test and slightly increased before failure. This was due to the effect of external prestressing force that prevents bond destruction between steel and concrete. Also, it can be seen that, the higher the external force the less the bond destruction.

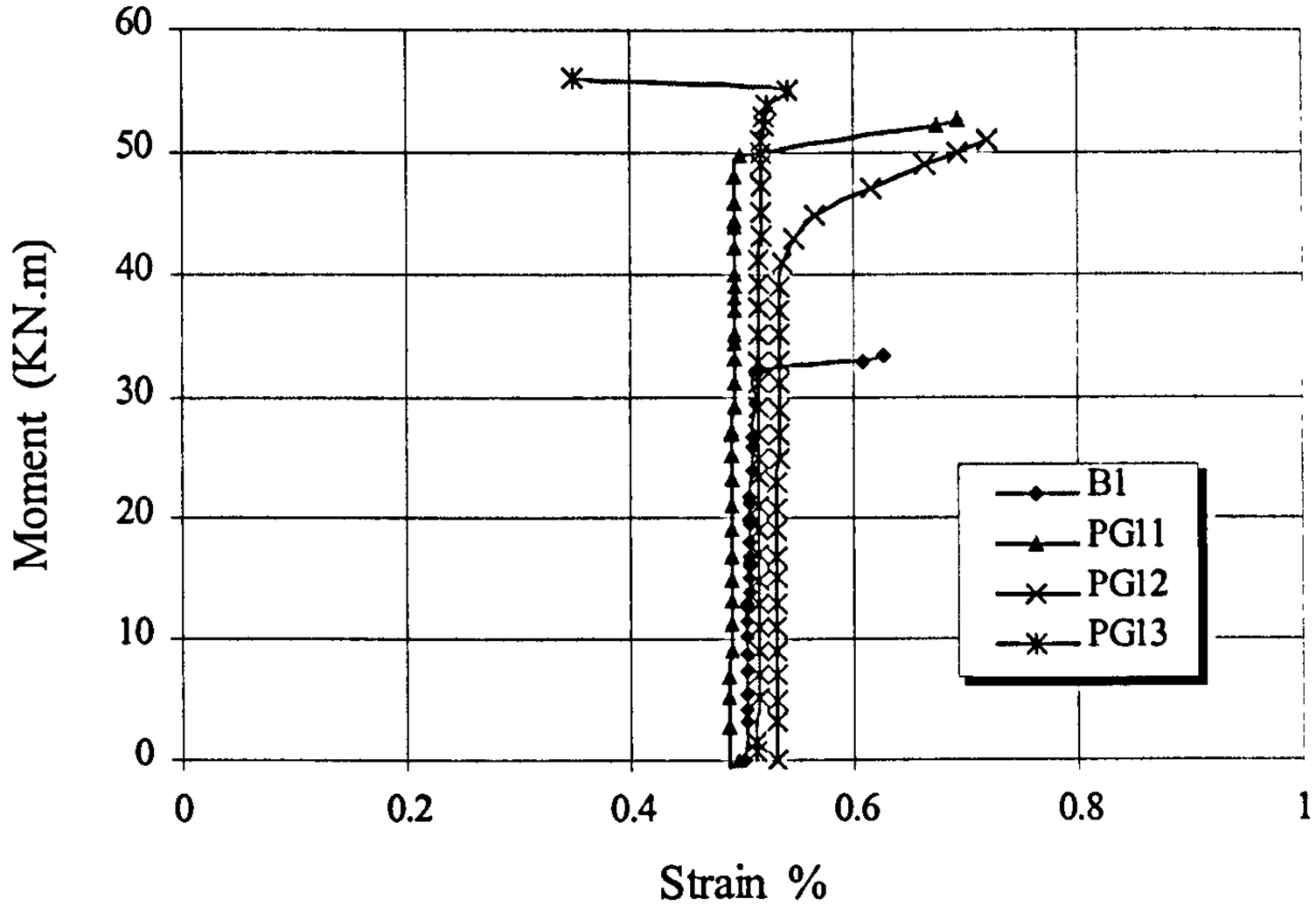

Figure (4.40): Moment-Edge strain relationship of group G1

4.2.6 External Prestressing Force (Parafil Rope Load)

The increase in the external prestressing force was measured using two load cells as stated in the previous chapter. The relation between the applied moment and the external prestressing force had a shape similar to that between the applied moment and deflection.

During loading three stages were observed. Before cracking, the increase in the external prestressing force was linear and relatively low up to the flexural cracking moment. After cracking, the external prestressing force tended to increased as the applied load increased and the relation between the increase in the external prestressing force and the moment was linear up to the yielding moment.

Then at ultimate, the rate of increase in the external prestressing force reached its maximum value as the external prestressing force tended to increase rapidly with any slight increase in the applied load. However, the force in any rope never reached the

nominal breaking load of the Parafil rope and no rope fractured during any test. Table (4.13) shows the value of the external prestressing force at specific load stages, while Table (4.14) shows the ratio of increase in the external prestressing force at different load stages.

Table (4.13): *External prestressing force value at different loads*

Factor	*Beam no.*	*Initial rope load (KN)*	*Rope load at different stages (KN)*		
			P_{cr}	P_y	P_{ult}
External prestressing force value	PG12	47.98	49.05	56.82	67.76
	PG11	60.35	61.37	71.43	82.49
	PG13	69.93	73.94	82.64	86.47
Number of Deviators	PG21	60.01	60.42	66.25	72.44
Eccentricity	PG31	60.52	63.07	73.14	83.82
	PG32	61.03	65.65	79.7	88.47
Previous cracking stage	PG41	60.3	61.35	70.08	81.96
	PG42	60.57	61.81	70.73	77.6
Concrete Strength	PG51	60.53	61.66	69.67	79.75
	PG52	60.13	61.21	69.2	92.64
(L/h) ratio	PG61	60.16	60.95	69.49	78.99
	PG62	60.73	61.77	72.83	81.67

Table (4.14): *Percentage of the increase in the external prestressing force at different loads*

Factor	***Beam no.***	***Rope load at different stages %****			***% of rope load to ultimate rope load §***
		P_{cr}	P_y	P_{ult}	
External prestressing force value	PG12	2.23	18.42	41.23	54.15
	PG11	1.69	18.36	36.69	65.92
	PG13	5.73	18.18	23.65	69.10
Number of Deviators	PG21	0.68	10.40	20.71	57.89
Eccentricity	PG31	3.97	20.85	38.5	66.98
	PG32	7.57	30.59	44.96	70.7
Previous cracking stage	PG41	1.74	16.22	35.92	65.50
	PG42	2.05	16.77	28.12	62.01
Concrete Strength	PG51	1.87	15.10	31.75	63.73
	PG52	1.80	15.08	54.07	74.03
(L/h) ratio	PG61	1.31	15.51	31.30	63.135
	PG62	1.71	19.92	34.48	65.27

*Relative to the external prestressing force before test.
§ Maximum rope load (at ultimate) / breaking rope load (from test).

4.2.6.1 Group 1 (Value of the external prestressing force)

Figure (4.41) shows the relation between the applied load and the increase in the Parafil rope load up to failure of beams PG12, PG11, PG13 (P_{ext} = 48.98, 60.35, 72.27 KN) respectively. Before cracking the increase in the rope load was small, while after cracking there was a rapid increase in the rope load in all beams. The increase in rope load of beam PG13 was higher before cracking than the other beams, and lower at ultimate.

At ultimate, the rate of increase in rope load increased as the initial external prestressing force decreased. While the ultimate rope load increased as the initial external prestressing force increased.

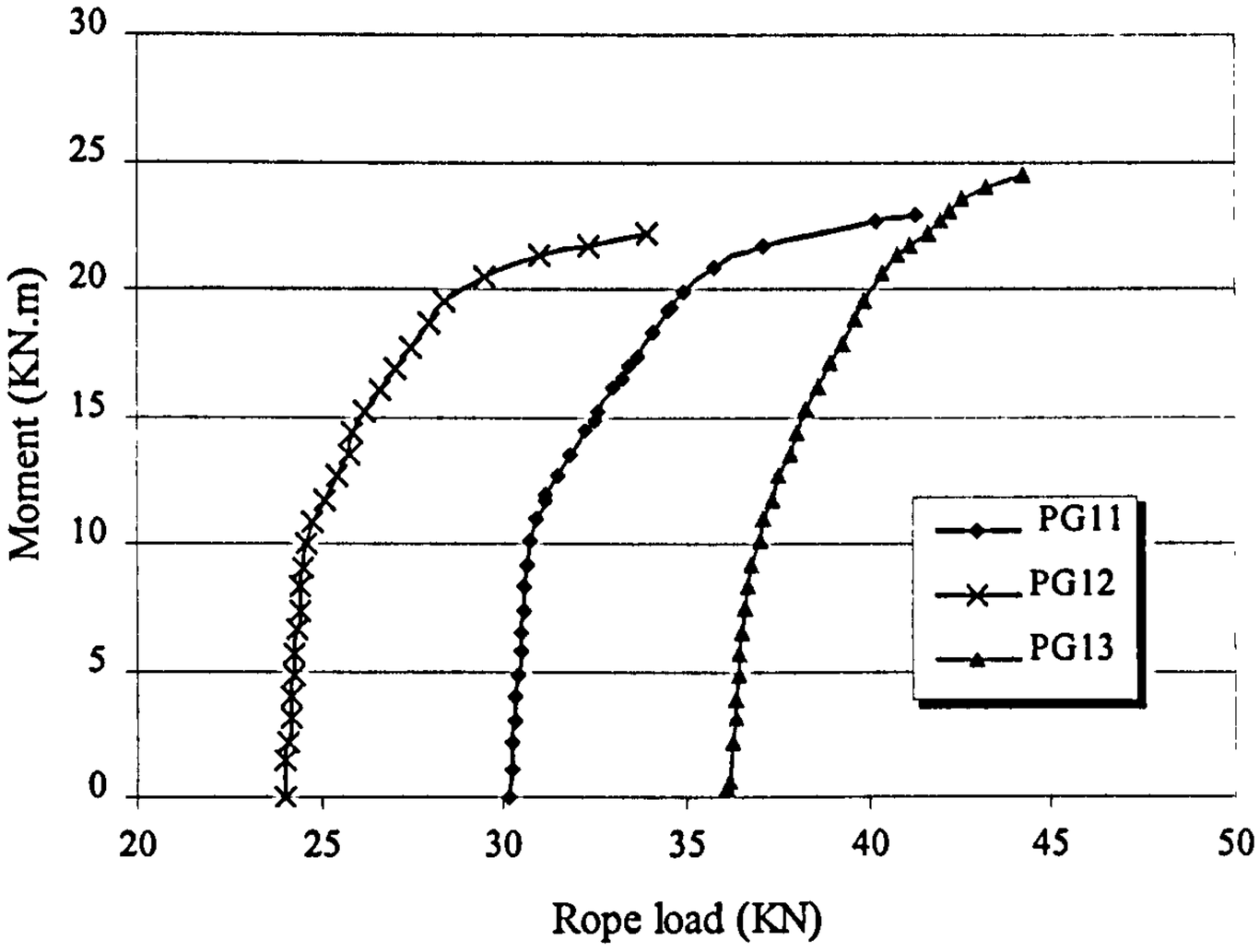

Figure (4.41): Relation between applied load and average rope load of group G1

4.2.6.2 Group 2 (Number of deviators)

Figure (4.42) shows the relation between the applied load and the increase in the Parafil rope load up to failure of beams PG21 and PG51. Before cracking the rate of increase in rope load of beam PG51 (two deviators at the third span) and beam PG21 (one deviator at the mid span) were slightly different. This was also observed after cracking and during the working load stage. However, at ultimate, the increase in rope load of beam PG51 was higher than that of beam PG21.

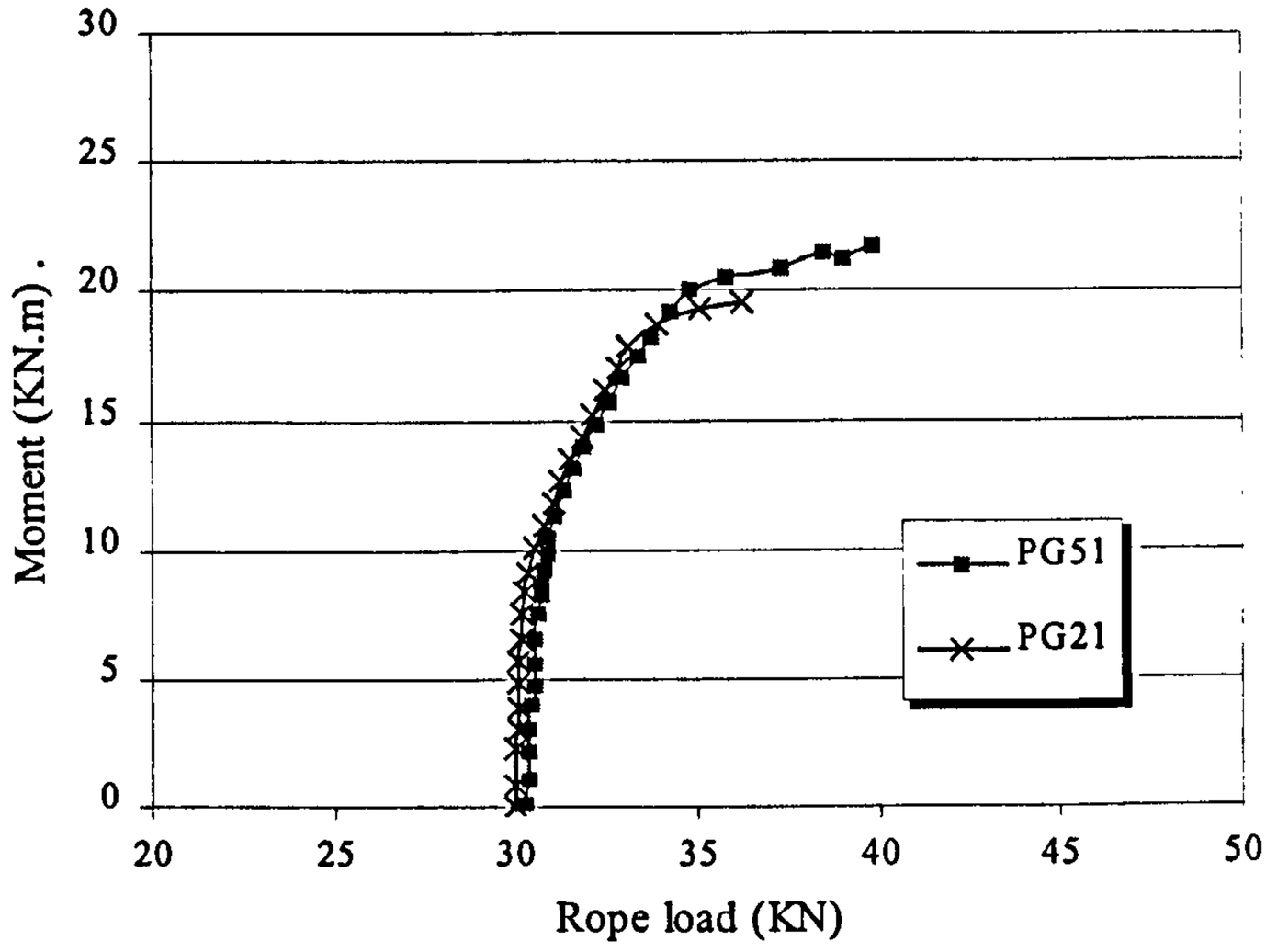

Figure (4.42): Relation between applied load and average rope load of group G2

4.2.6.3 Group 3 (Effective depth of the external prestressing force)

Figure (4.43) shows the relation between the applied load and the increase in Parafil rope load up to failure of beams PG11, PG31 and PG32 (e/h = 0.794, 0.894 and 1.072). Before and after cracking the rate of increase in the rope load increased as the rope eccentricity increased. This because rope stress change is relative to its distance from the neutral axis; the greater the distance the higher the stress.

Also, from Table (4.14), it can be seen that the increase in rope load of beam PG32 was higher at any load than the other test beams except beam PG52 at ultimate.

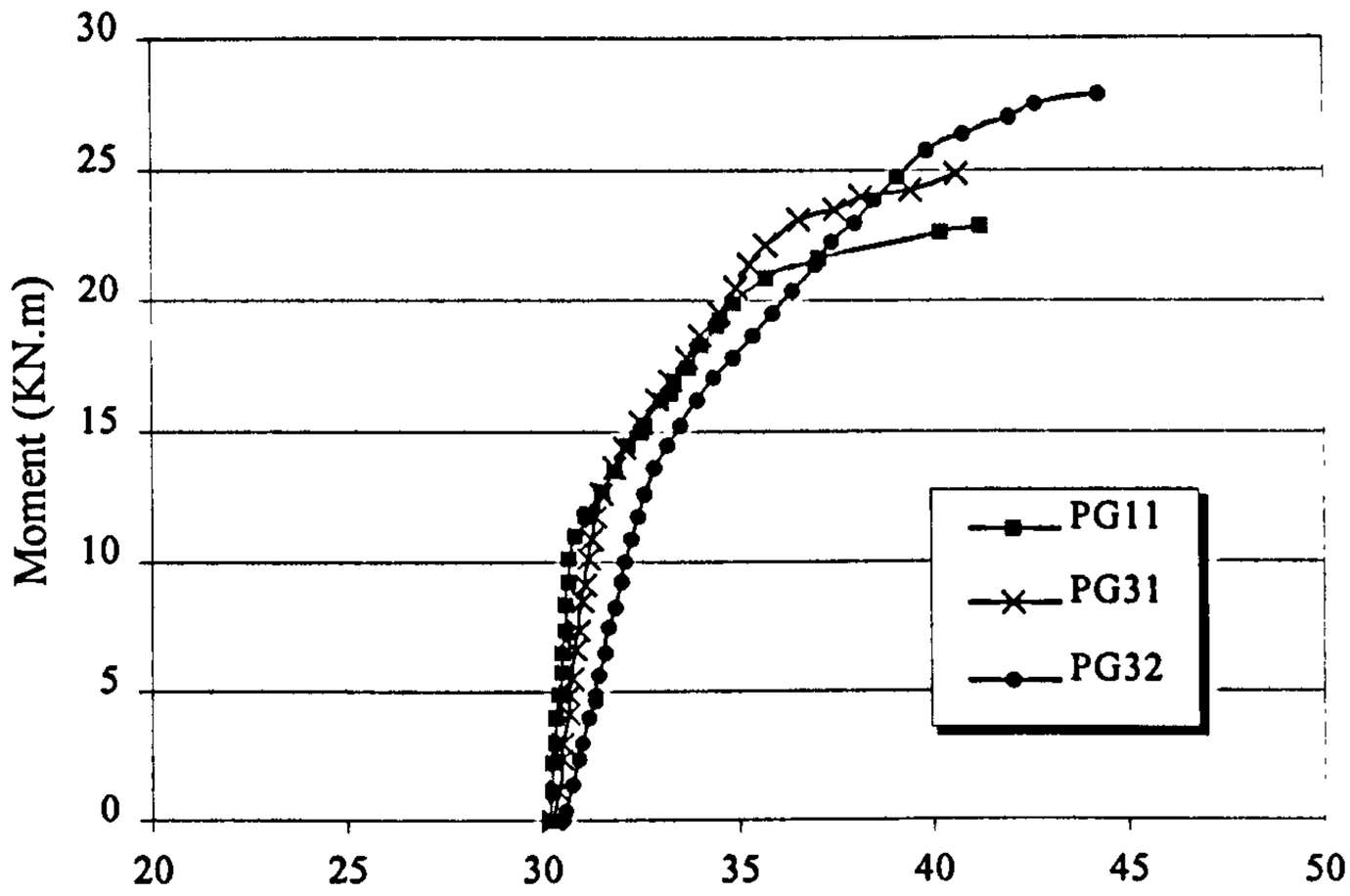

Figure (4.43): Relation between applied load and average rope load of group G3

4.2.6.4 Group 4 (Previous load stage before externally strengthened)

Figure (4.44) shows the relation between the applied load and the increase in the Parafil rope load up to failure of beams PG11, PG41 and PG42. Before and after cracking, the increase in the rope load was almost the same in all beams but at ultimate that of beam PG42 was lower compared to PG11 and PG41.

The rate of increase in the rope load in beam PG42 after cracking was higher than that in PG11 and PG41, due to cracks opening fully as soon as the bottom stress changed to tension.

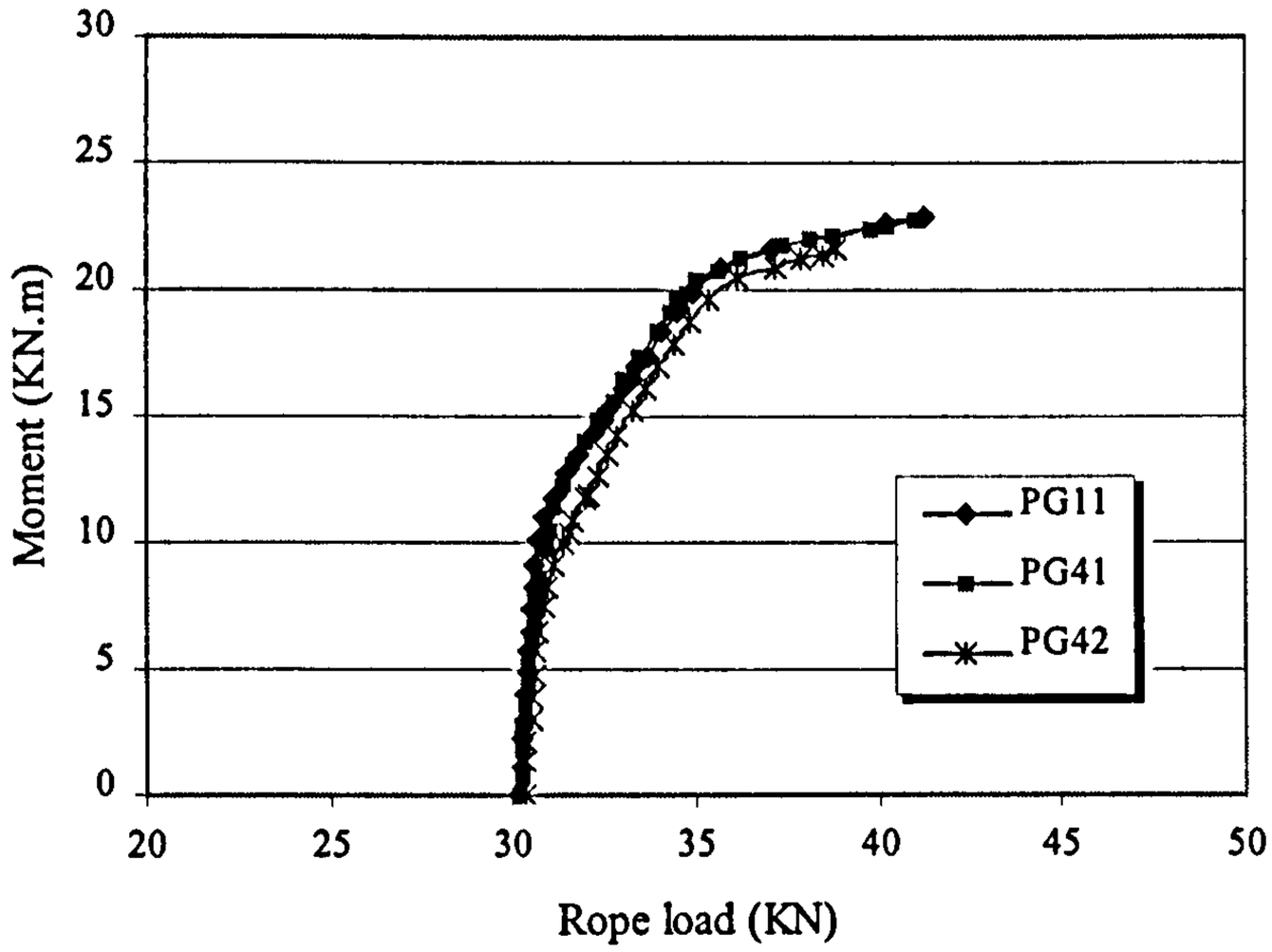

Figure (4.44): Relation between applied load and average rope load of group G4

4.2.6.5 Group 5 (Concrete strength)

Figure (4.45) shows the relation between the applied load and the increase in the Parafil rope load up to failure of PG51, PG11 and PG52 (f_{cu}= 43.3, 55.8 and 79.3 MPa) respectively. Before cracking and at the working stage the increase in the rope load was almost the same for all beams. At ultimate, beam had higher strength had higher increase in rope load.

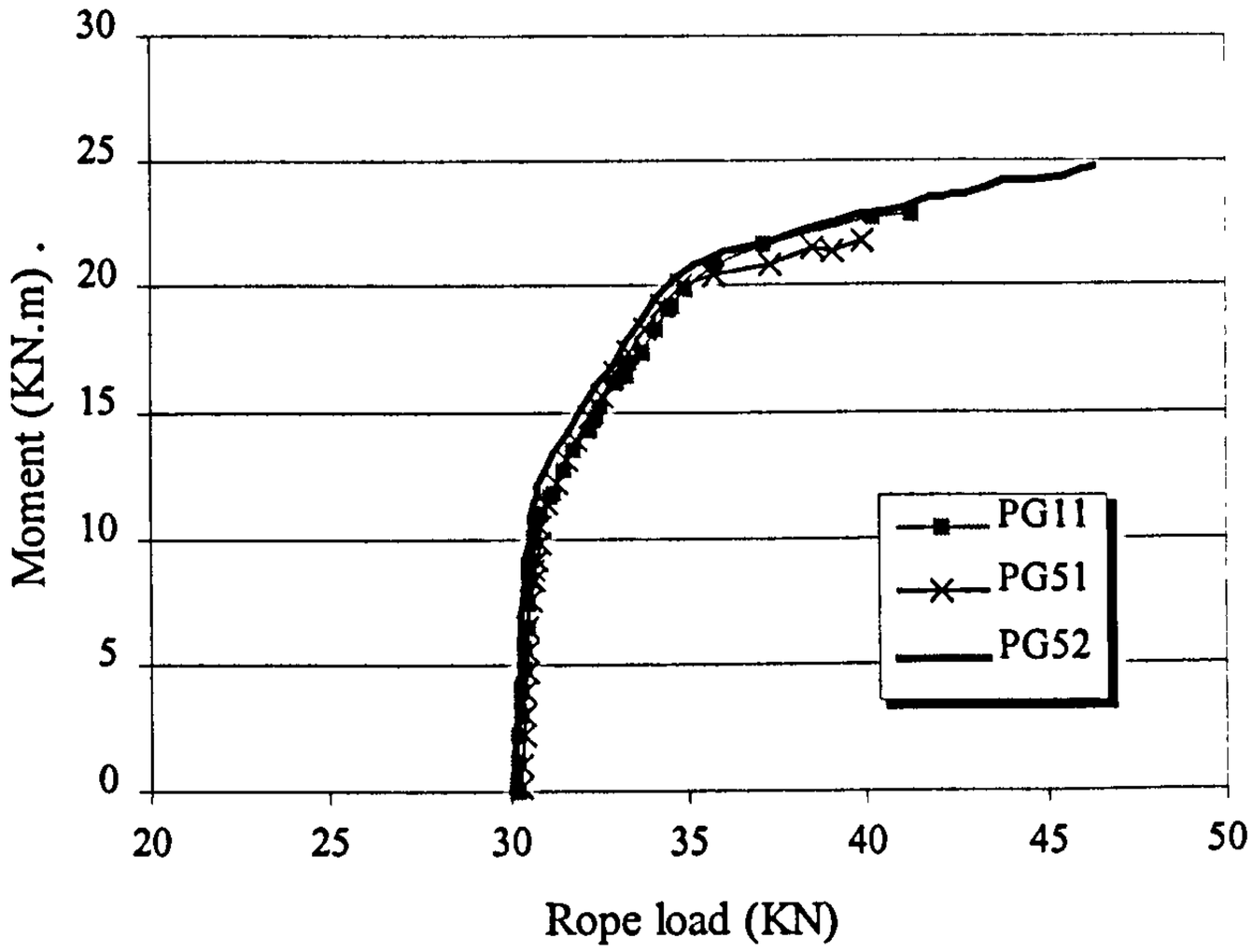

Figure (4.45): Relation between applied load and average rope load of group G5

Also, from Table (4.14), it can be seen that beam PG52 (which had the highest concrete strength) had the highest increase in rope load at ultimate among the other test beams. This because the increase in concrete strength enables the section to resist higher load and that resulted in higher increase in rope load.

4.2.6.6 Group 6 (Effective span length / depth ratio (L/h))

Figure (4.45) shows the relation between the applied load and the increase in the Parafil rope load up to failure of PG62, PG11, PG61 (L/h= 10, 14.4, 20) respectively. Before, after cracking and up to failure, the increase in rope load of all beams was slightly different. However, beam PG61 had a slight lower increase in the rope load during all load stages comparing to PG11 and PG62.

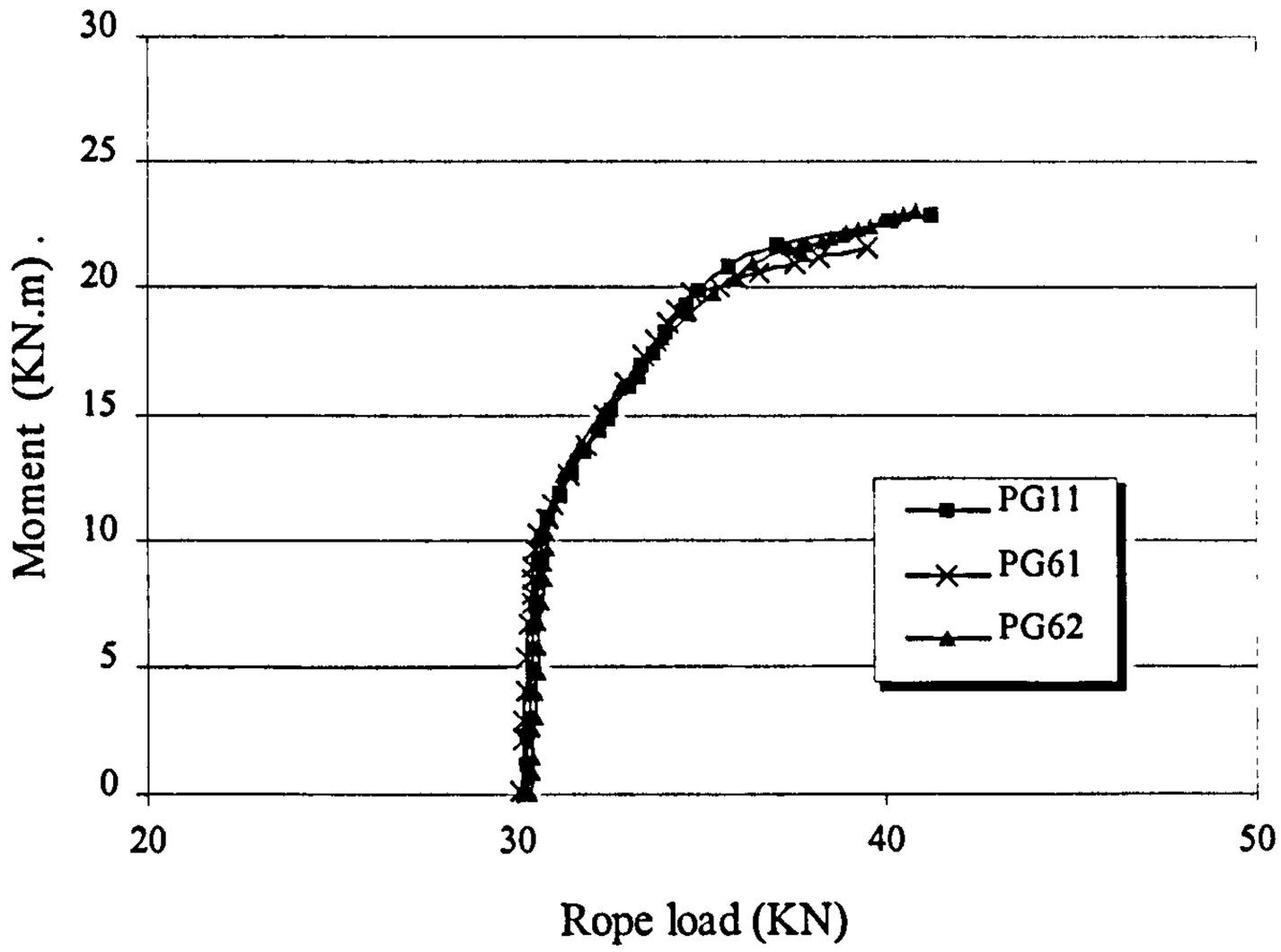

Figure (4.46): Relation between applied moment and average rope load of group G6

4.2.7 Changes in Rope Eccentricity (Second Order Effect)

Changes in rope eccentricity during external prestressing process and loading were calculated by measuring deflection at the middle and at the deviator locations, then the increase or decrease in the rope eccentricity was determined from the difference between the deflection at middle and the average deflection at the deviators.

During the external prestressing process, there was an increase in the eccentricity at the middle, while during loading, this eccentricity decreased as the load increased. Before cracking, the loss in rope eccentricity was small, but after cracking, it was increased as load increased then rapidly increased at the ultimate stage.

Before cracking, and because the deflection and hence the loss in rope eccentricity were small, the measured value of losses in the rope eccentricity were not accurate, and more sensitive LVDTs were needed. However, after cracking, the losses in the rope eccentricity were significant especially at ultimate and the error in measuring can be negligible.

Figures (4.47–4.51) show the relation between load and losses in rope eccentricity of each group, while Table (4.15) shows the value of losses in rope eccentricity at different stages during loading for all test beams.

Losses of rope eccentricity of beam PG12 could not be measured due to a fault in LVDTs reading at deviator locations during testing. Comparing all the beams, it can be seen that, at ultimate beam PG52 had the highest losses while beam PG62 had the smallest value. Also, the loss in rope eccentricity at ultimate increased as:

- External prestressing force decreased.
- Rope eccentricity decreased.
- The precracking stage decreased.
- Concrete strength increased.
- (Span/depth) ratio increased.

Table (4.15): *Losses in rope eccentricity at different loading stages*

Factor	***Beam no.***	***Total losses in rope eccentricity (mm)****				***% losses in rope eccentricity****			
		Ext. prest.	P_{cr}	P_y	P_{ult}	Ext. prest	P_{cr}	P_y	P_{ult}
External prestressing force value	PG11	-0.28	0.298	2.503	6.88	-0.196	0.209	1.752	4.815
	PG12	N/A	N/A	N/A	N/A	N/A	N/A	N/A	N/A
	PG13	-0.87	-0.39	1.832	2.026	-0.609	-0.273	1.282	1.418
Number of deviator	PG21	0.0	0.0	0.0	0.0	0.0	0.0	0.0	0.0
Eccentricity	PG31	-0.39	0.078	1.614	5.127	-0.242	0.051	1.065	3.186
	PG32	-0.78	0.152	1.943	4.715	-0.404	0.079	1.007	2.444
Previous cracking stage	PG41	-0.64	0	2.1	6.336	-0.448	0	1.47	4.434
	PG42	-0.36	0.116	2.021	4.325	-0.252	0.081	1.414	3.027
Concrete Strength	PG51	-0.13	0.29	2.655	7.087	-0.091	0.203	1.858	4.959
	PG52	-0.38	0.024	1.928	11.71	-0.266	0.017	1.349	8.195
(L/h) ratio	PG61	-0.56	0.236	4.649	10.163	-0.392	0.165	3.253	7.112
	PG62	-0.18	-0.19	0.629	1.868	-0.126	-0.133	0.44	1.307

* Measured from the initial eccentricity of rope location from the top concrete surface.

** Relative to the initial eccentricity of rope from top concrete surface

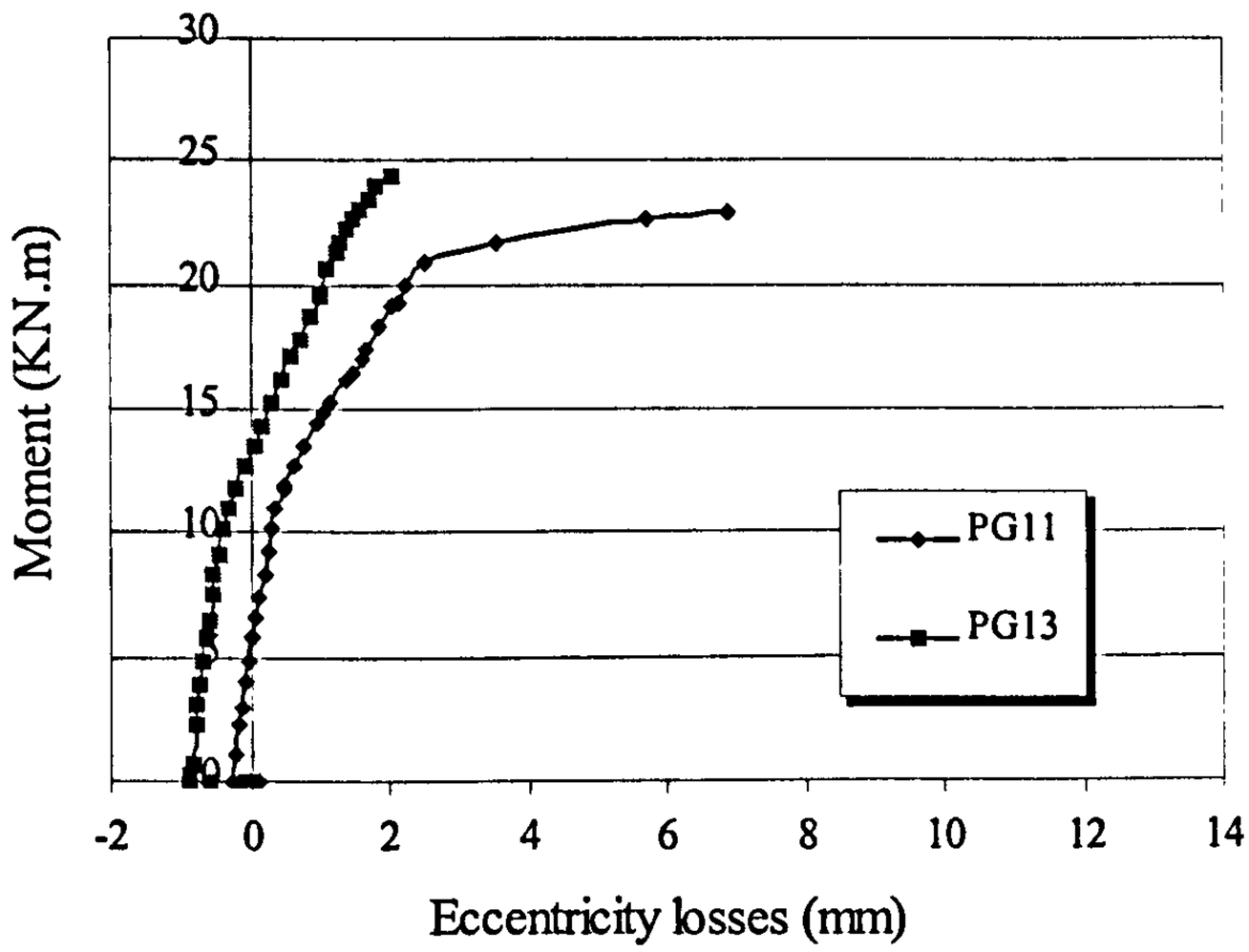

Figure (4.47): Relation between applied load and losses in rope eccentricity of group G1

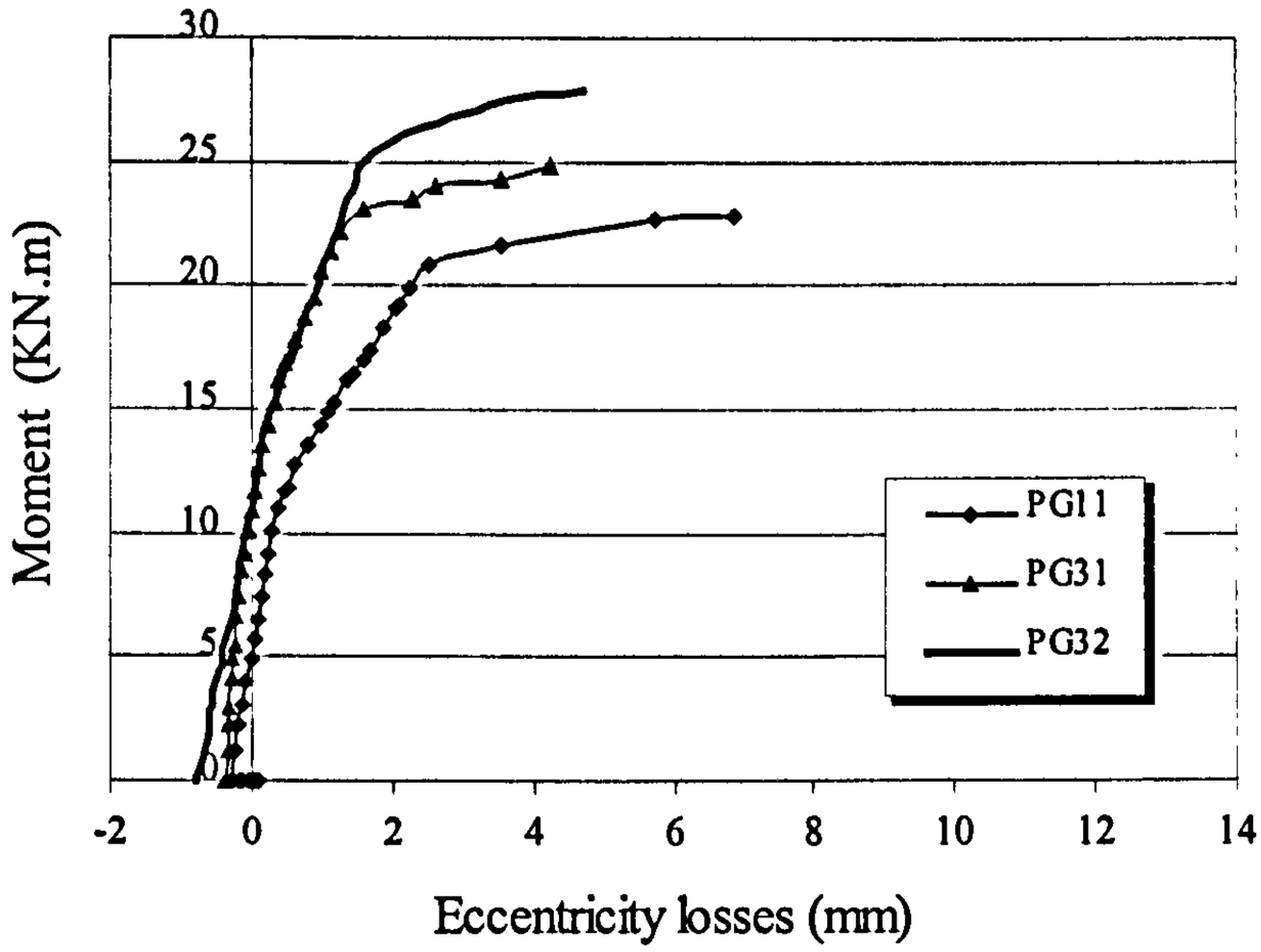

Figure (4.48): Relation between applied load and losses in rope eccentricity of group G3

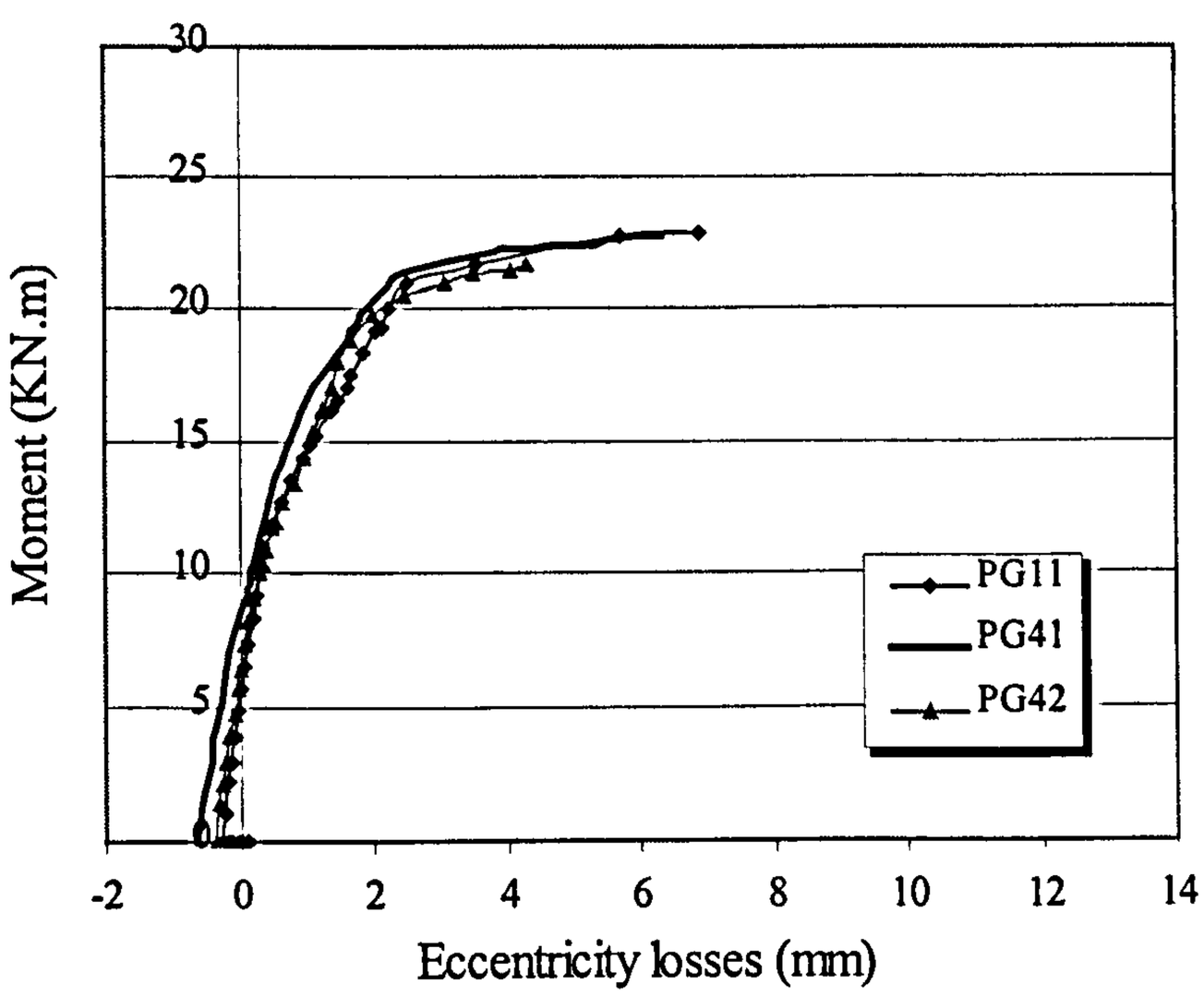

Figure (4.49): Relation between applied load and losses in rope eccentricity of group G4

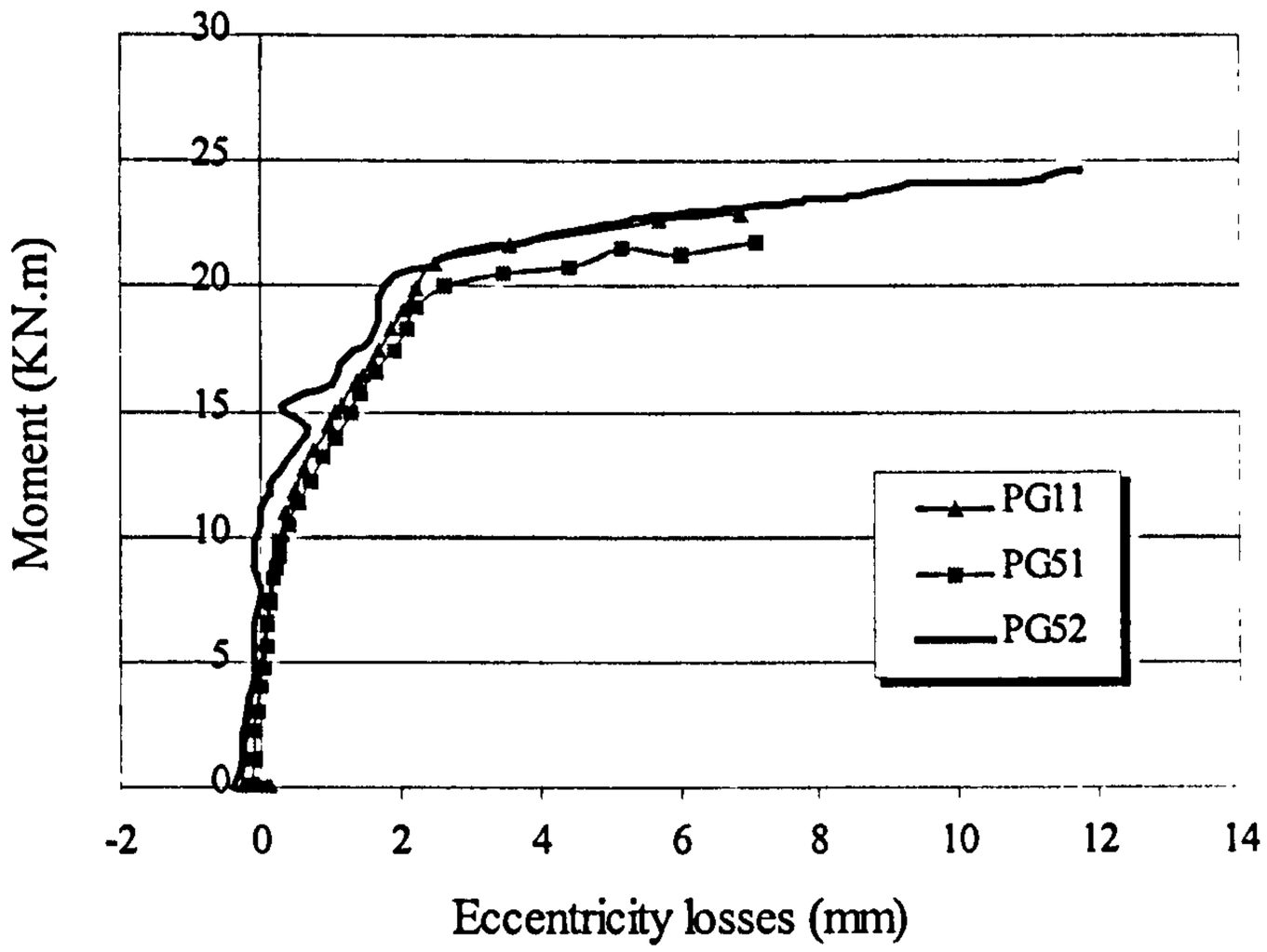

Figure (4.50): Relation between applied load and losses in rope eccentricity of group G5

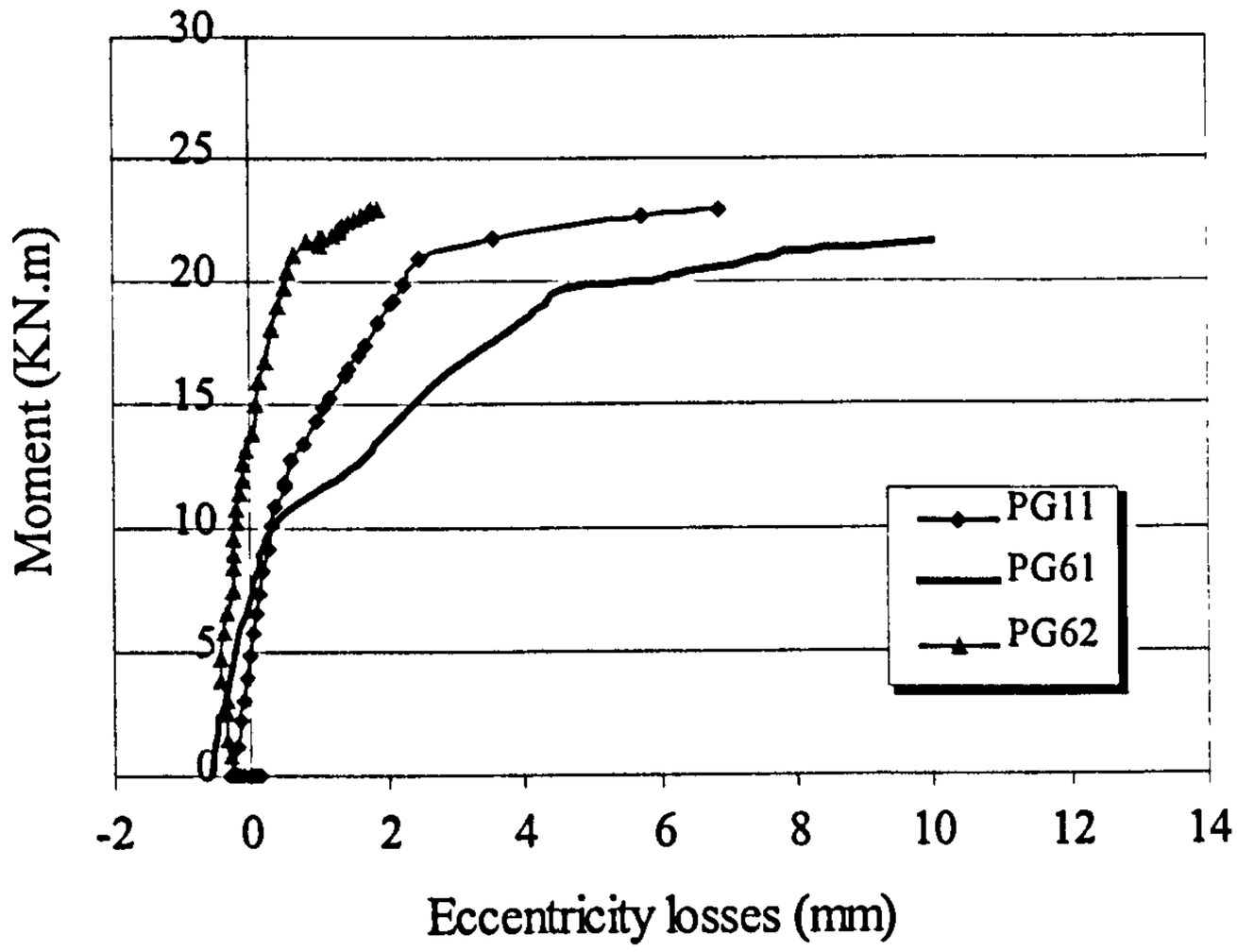

Figure (4.51): Relation between moment and losses in rope eccentricity of group G6

4.2.8 Concrete Strain

The concrete strains on all beams were measured at the middle, using demec points mounted on the concrete surface, during internal prestressing, and using electrical strain gauges during the external prestressing and testing.

For accurate results, concrete strains need to be measured at least over the whole distance between the concentrated loads. So, the results obtained during beam testing may not have the sufficient accuracy to determine the concrete strain distribution during loading. However, it will give an indication of the behaviour of concrete before and after strengthening.

4.2.8.1 After internal prestressing

The concrete strain distribution on all beams, due to the internal prestressing force was linear as shown in figure (4.52). As the difference between the prestressing force applied to all beams was small, concrete strains were almost the same, with a high compressive value at bottom and small tensile or compressive value at top.

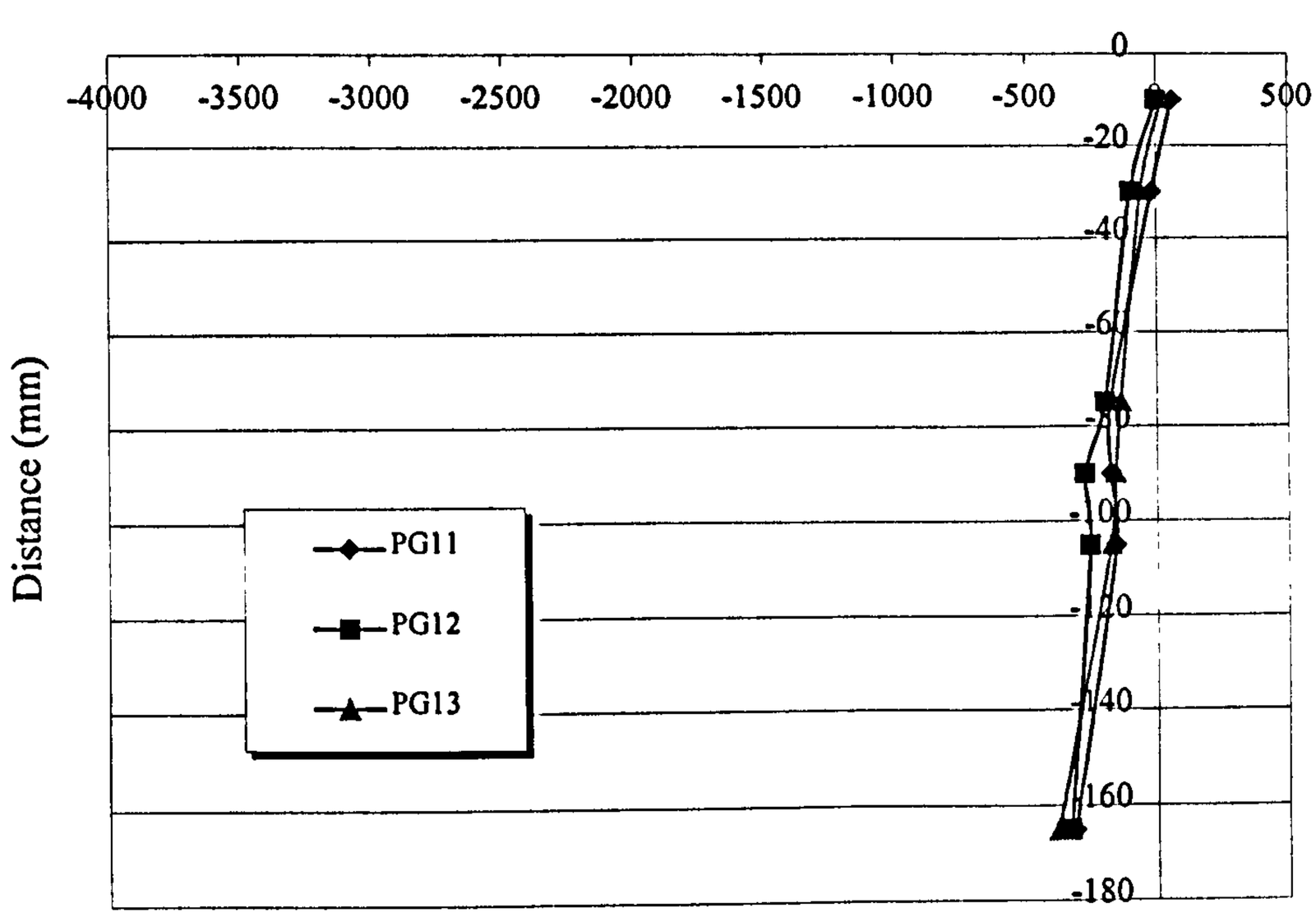

Figure (4. 52): Strain distribution at mid-span after internally prestressing of G1

4.2.8.2 Losses effect

After internally prestressing the concrete strain changed slightly. The value of losses varied among the beams due to the variation of the environmental conditions such as temperature, humidity, etc. the concrete compressive strain increased at bottom, while at top the tensile concrete strain reduced or changed to compressive.

Beam PG51 had smaller losses than the other beams as it was tested only nine days after casting. Beam PG61 had the least losses although it was tested after thirty-one days, this can be attributed to the increase in its length, where the losses due to shrinkage and creep had less effect (losses α 1/beam length).

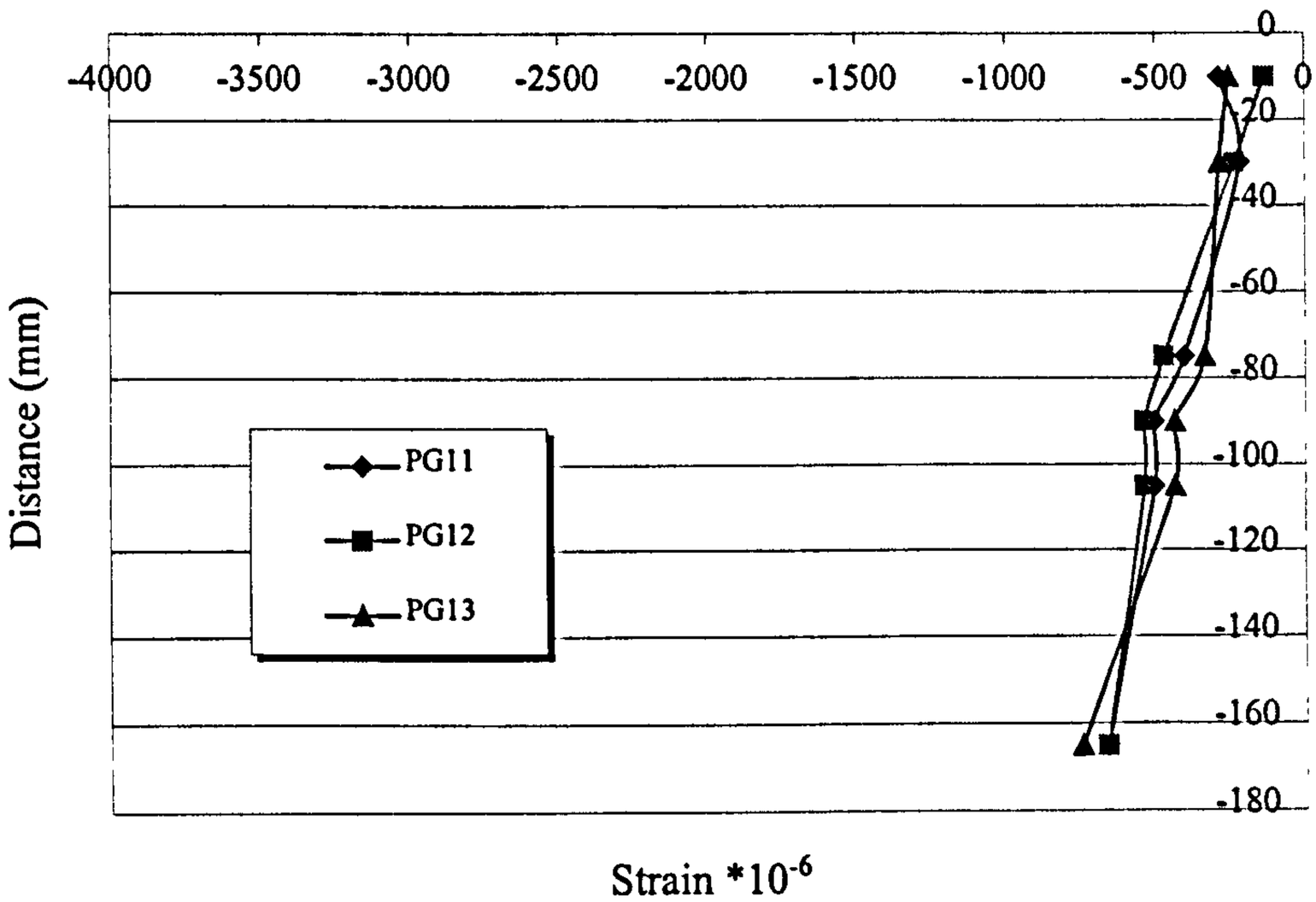

Figure (4. 53): Strain distribution at mid-span after losses of G1

4.2.8.3 Group 1 (Value of the external prestressing force)

The external prestressing force caused an increase in the bottom compressive concrete strain as external force increased, while the top concrete strain changed only slightly. Before the ultimate stage, PG13, with the maximum external prestressing force had the highest compressive strain while PG12 with the lower external prestressing force had the smallest value.

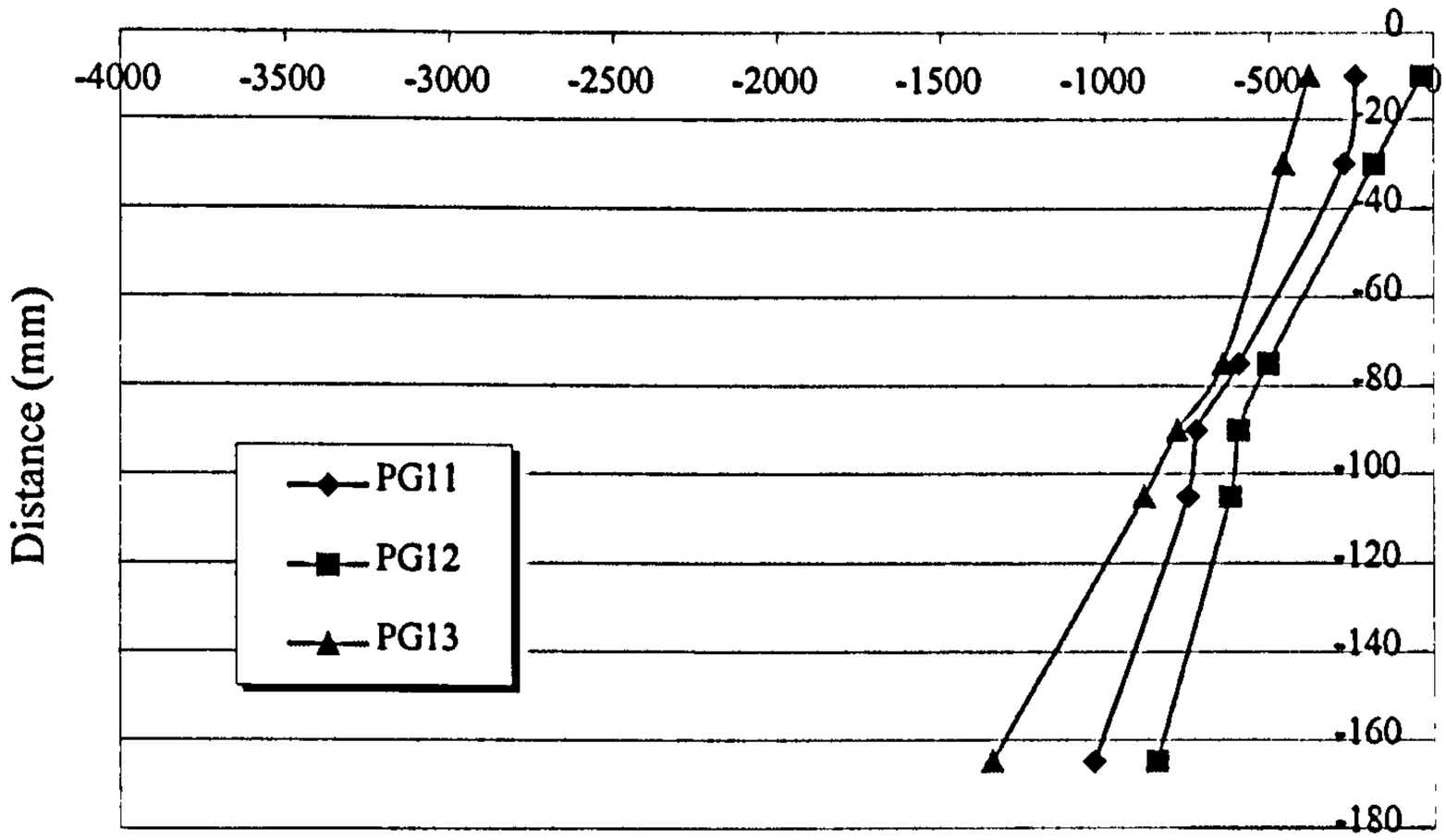

Figure (4.54): Strain distribution at mid-span after external prestressing of G1

At ultimate the increase in compressive concrete strain of PG11 was higher than that of PG12, while the top concrete strain of PG13 increased rapidly after yielding till failure (within a short period) and could not be measured just before the sudden failure.

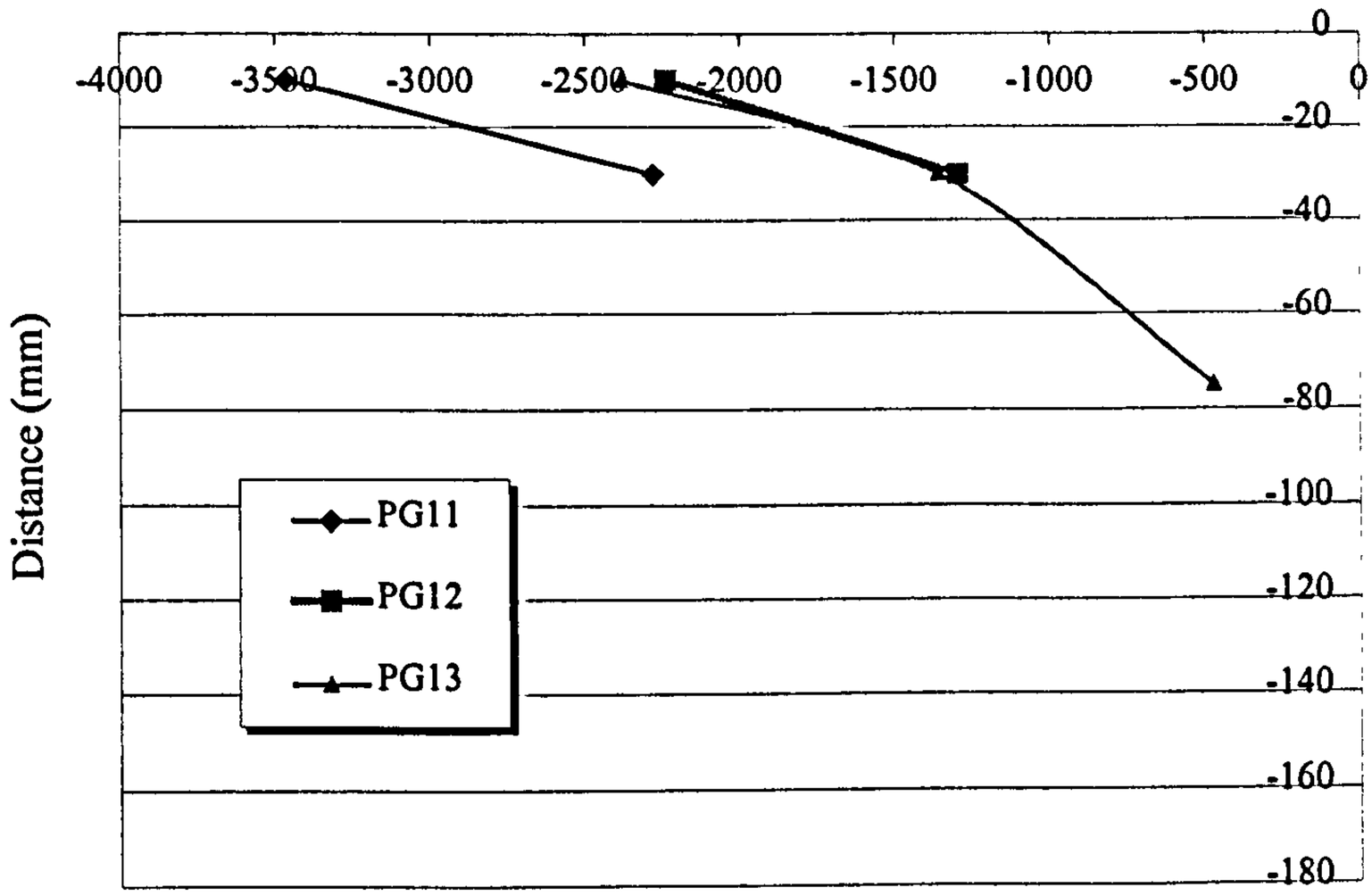

Figure (4.55): Strain distribution at mid-span at ultimate of G1

4.2.8.4 Group 2 (Number of deviators)

The concrete strain due to the external prestressing force changed slightly between beam PG51 (with two deviators) and beam PG21 (with one deviator). The bottom compressive strain in beam PG51 was higher than that in beam PG21. This is due partly to the increase in the inclined angle of the external prestressing force of PG21, so its horizontal component is less than that of PG51 and partly to the increase in the eccentricity of the external prestressing force of PG51 during prestressing

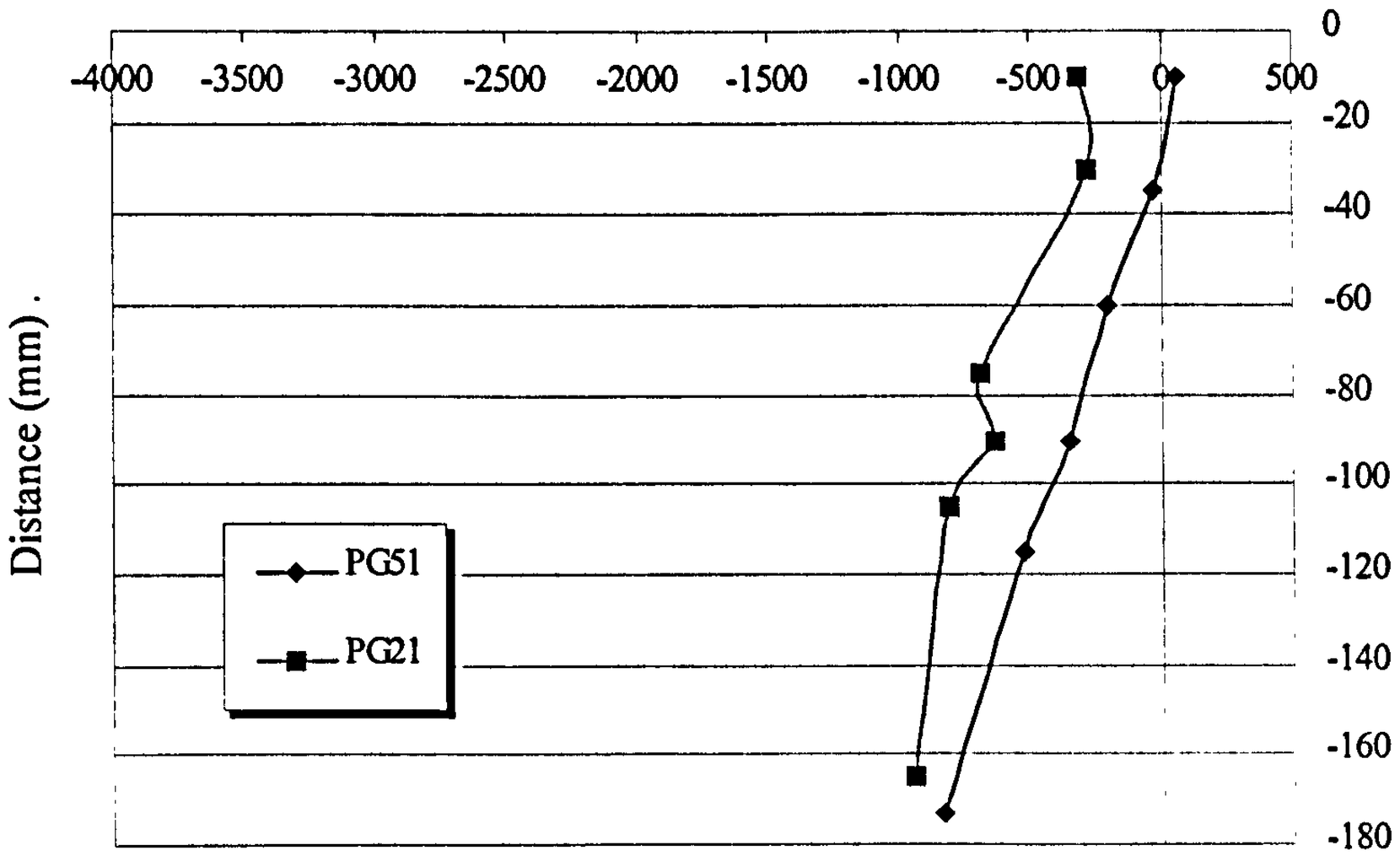

Figure (4.56): Strain distribution at mid-span after external prestressing of G2

At cracking the bottom tensile strain was almost the same for all beams. While at yielding and ultimate stages, the increase in the top compressive strain of PG51 was higher than that of PG21.

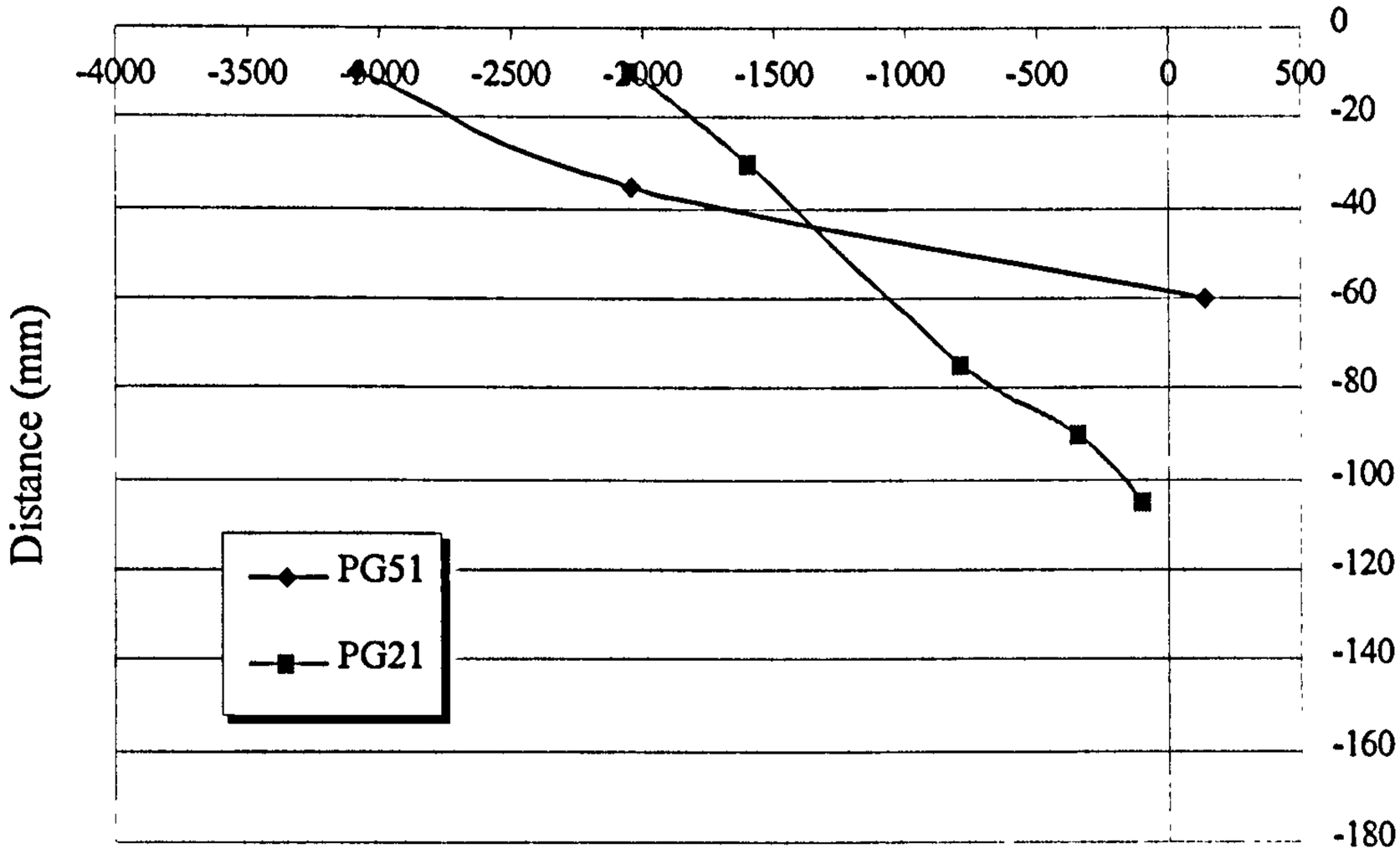

Figure (4.57): Strain distribution at mid-span at ultimate of G2

4.2.8.5 Group 3 (effect of eccentricity of the external prestressing force)

During external prestressing, the top compressive concrete strain reduced as the external prestessing eccentricity increased, while the compressive strain slightly changed (this could have been expected to increase as the eccentricity increased).

During loading, beam PG11 (e/h=0.794) had a greater compressive strain at all loads than the other beam. However, at ultimate, beam PG32 (e/h=1.072) with high eccentricity, had higher compressive strain and curvature. While beam PG31 (e/h=0.894) had less than that of beam PG11, even though it had higher eccentricity, this may be as the failure of beam PG31 was not at the middle (where strain was measured) but slightly away from it. The compressive strain at low eccentricity (0.794) was almost linear and tent to be nonlinear as the eccentricity increased

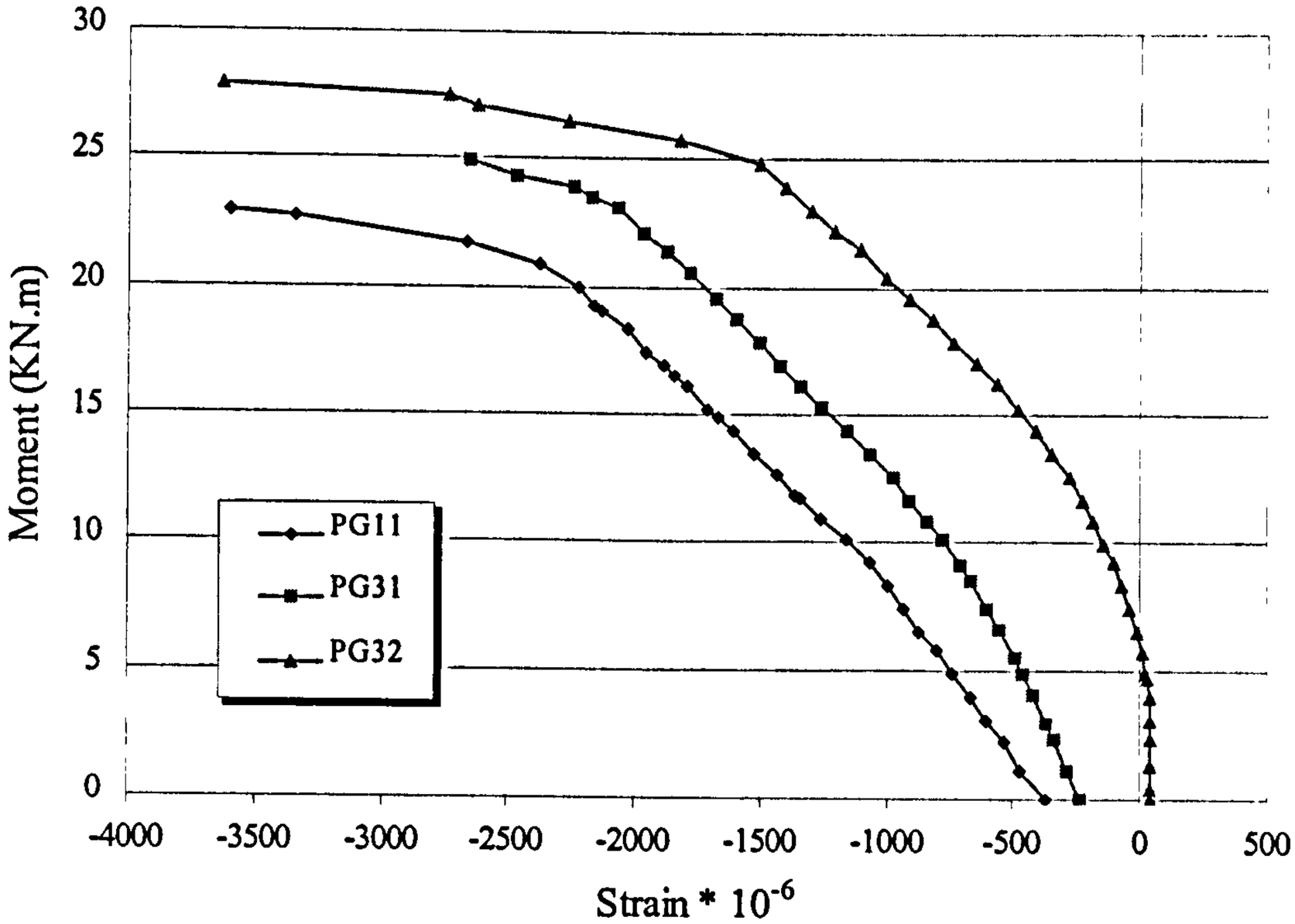

Figure (4.58): Top concrete strain during testing

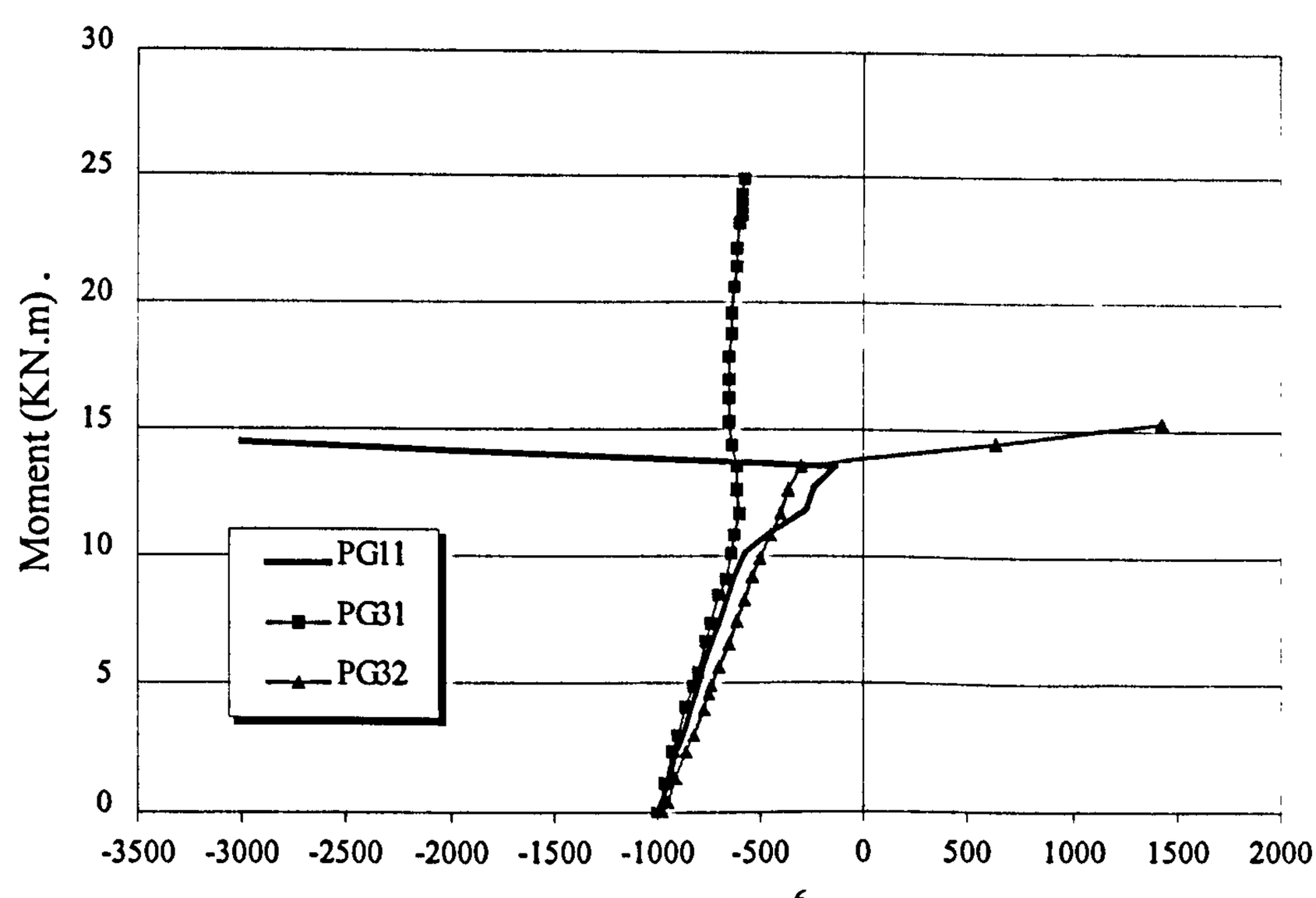

Figure (4.59): Bottom concrete strain during testing

4.2.8.6 Group 4 (Previous load stage before externally strengthened)

PG41 and PG42 were loaded to different cracking stages before the external prestressing. Due to loading and unloading, strain in concrete after unloading was reduced relative to that before loading. During loading, cracks extended in the web of beam PG42 (loaded to 0.6 P_{ult} of B1) therefore the concrete strain could not be measured on the lower part of its section.

After strengthening, the net concrete strain distribution due to the external prestressing force in the uncracked part of beams PG41, PG42 and PG11 were almost the same. This was because the prestressing force closed the cracks and enabled the section to behave as one unit again.

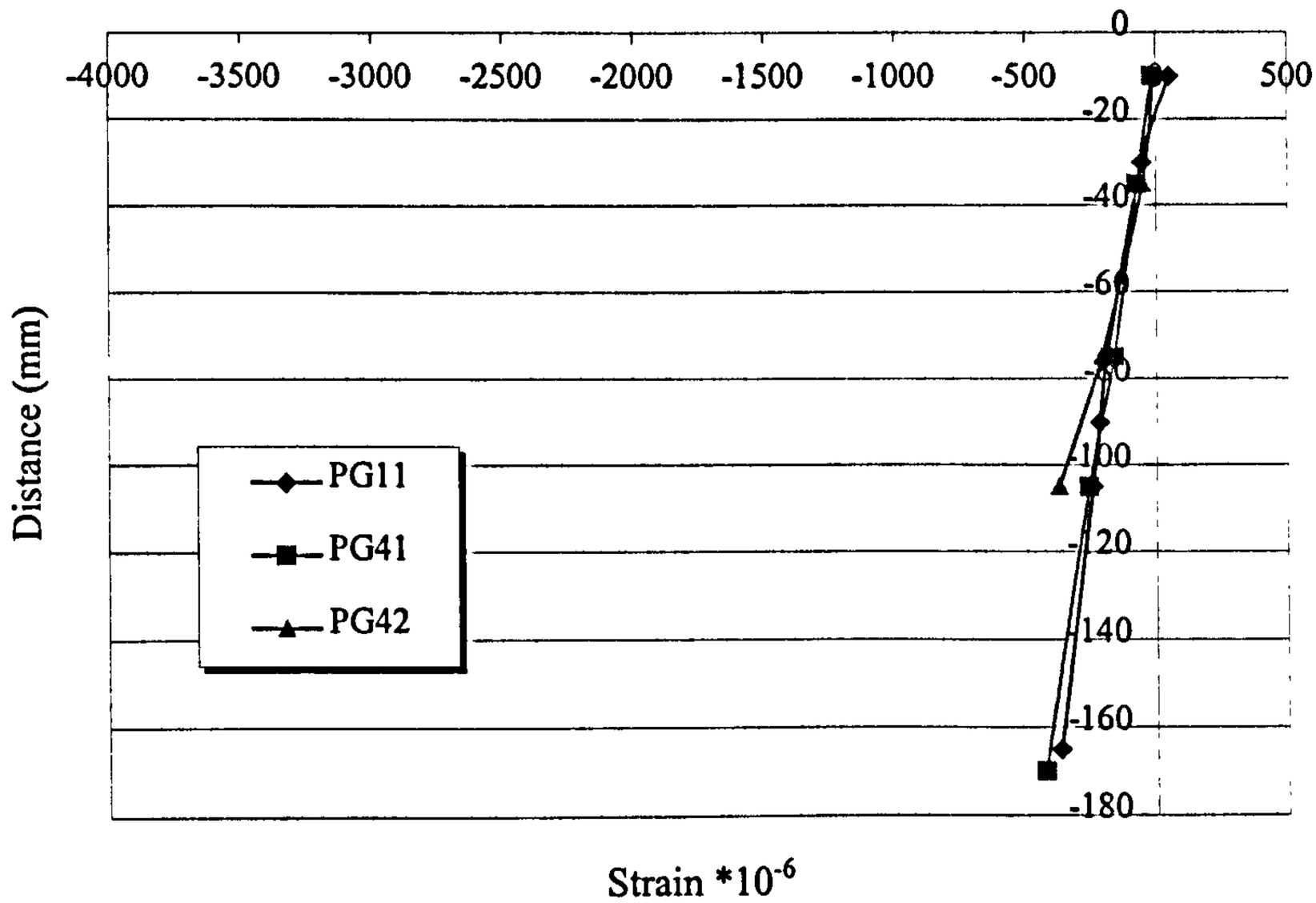

Figure (4.60): Net strain distribution at the mid-span due to external prestressing of G4

During loading, beam PG42 had smaller concrete compressive strains than the other beams. This is because the cracks in the web produced by prior loading had resulted in an inelastic extension.

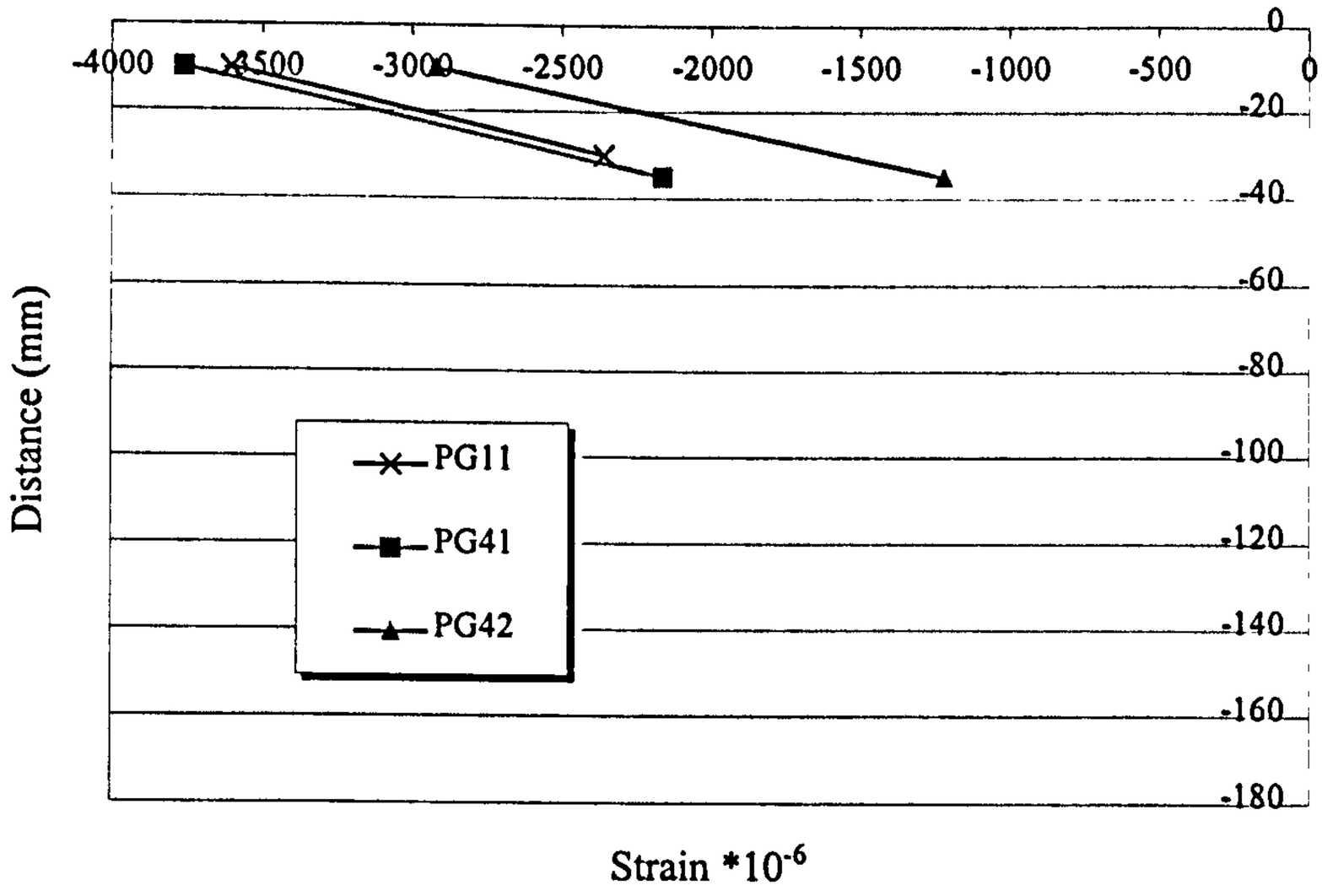

Figure (4.61): Strain distribution at mid-span at ultimate of G4

4.2.8.7 Group 5 (Concrete strength)

The concrete strains due to the external prestressing force in beams PG11, PG51 and PG52 were slightly different. Comparing the beams at ultimate, it can be seen that beam PG52 had less compressive strain than PG11. This is because the strain in the concrete reduced as the concrete strength increased. However, Beam PG51 had less strain than that of beam PG11 and PG52, although its concrete strength was less. There are two reason for this:

- The losses in beam PG51 were lower than that of beams PG11 and PG52, resulting in decreased the compressive strains in beam PG51.

- Beam PG51 was tested after three days from internal prestressing. Therefore, the effect of the prestressing force on its Young's modulus was less than on that of beam PG11 (Young's modulus reduced when subject to compression force and $E_{c(effective)} \alpha$ 1/duration loading time). Also, strain of beam with low Young's modulus is lower than that with high Young's modulus at the same stress.

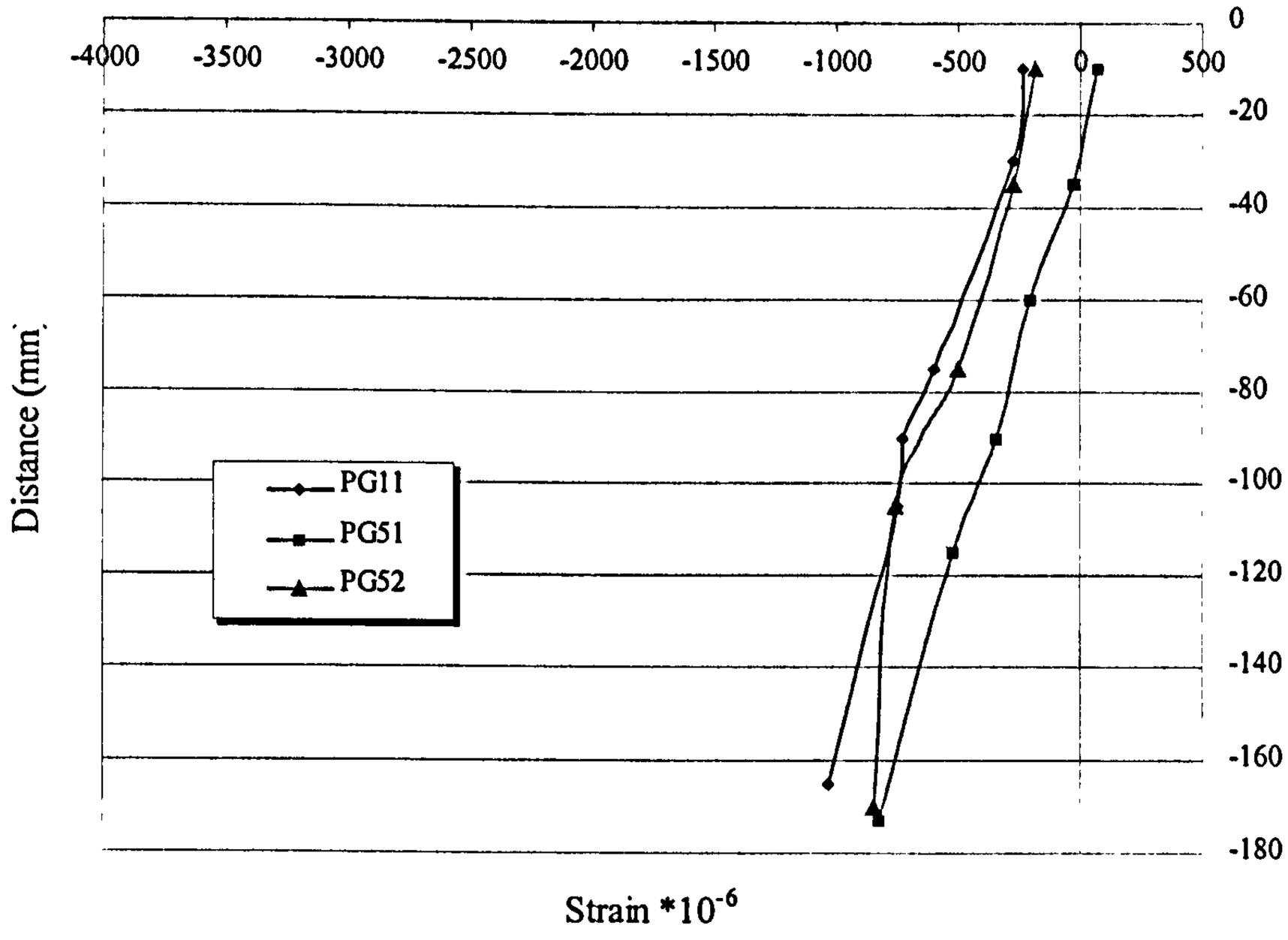

Figure (4.62): Strain distribution at mid-span after external prestressing of G5

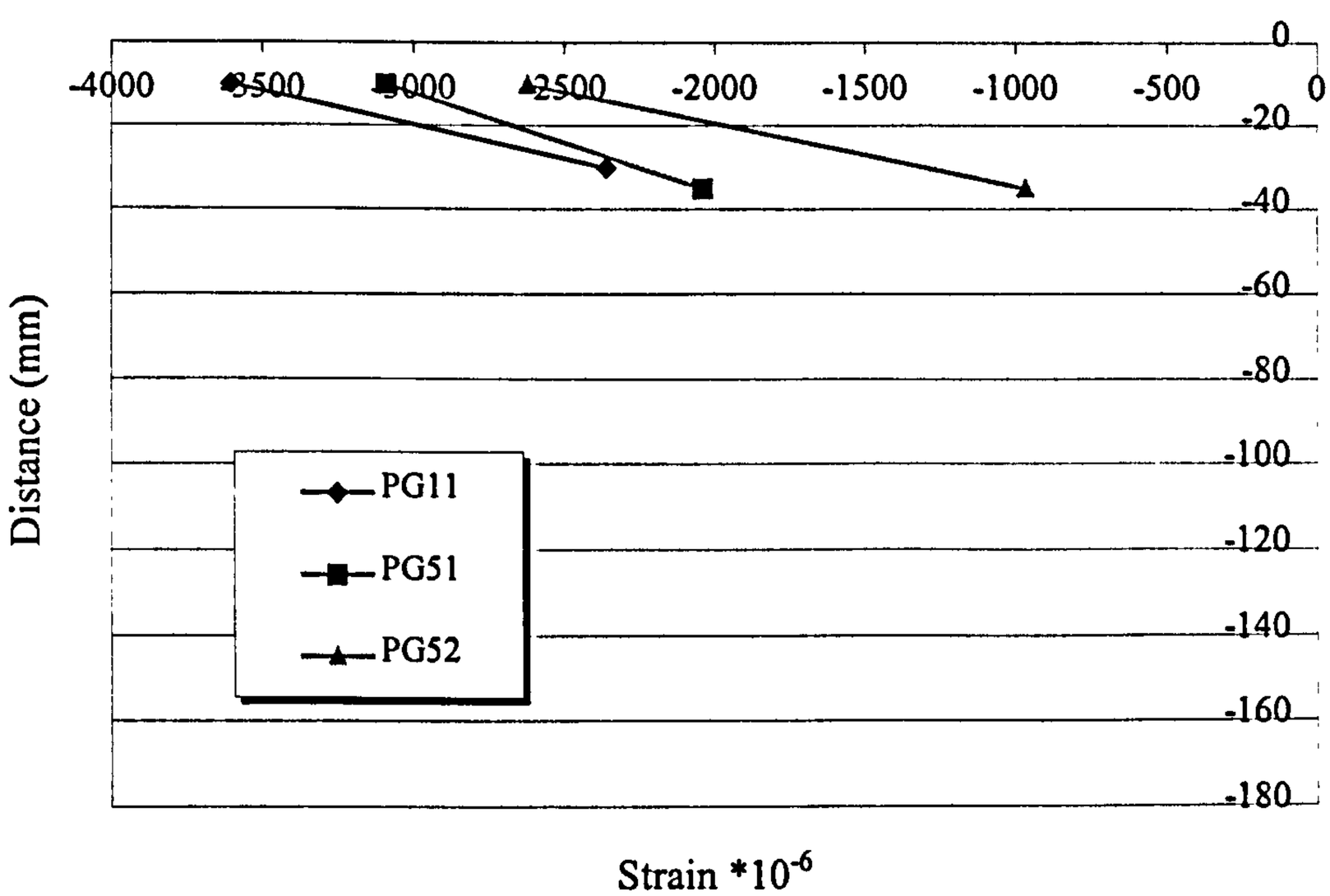

Figure (4.63): Strain distribution at mid-span at ultimate of G5

4.2.8.8 Group 6 (Effective span length / depth ratio (L/h))

The strain on beam PG61 was measured as on the other beams, at the middle. This was not ideal and it would have been better to measure the strain over greater length for better accuracy. However, the results can be used for comparison.

Before cracking, due to the external prestressing force, beam PG61 had less strain and less curvature. This was observed during loading till just before ultimate stage. This can be attributed to the effect of its length (L/h= 20), that resulted in reduced losses and deformation during loading. However, at ultimate, beam PG61 had the greatest curvature of all the beams of group G6 and had higher strains than that of beam PG62 (L/h=10). This may be because the failure of beam PG62 was not at the middle (where strain was measured) but near to the concentrated load.

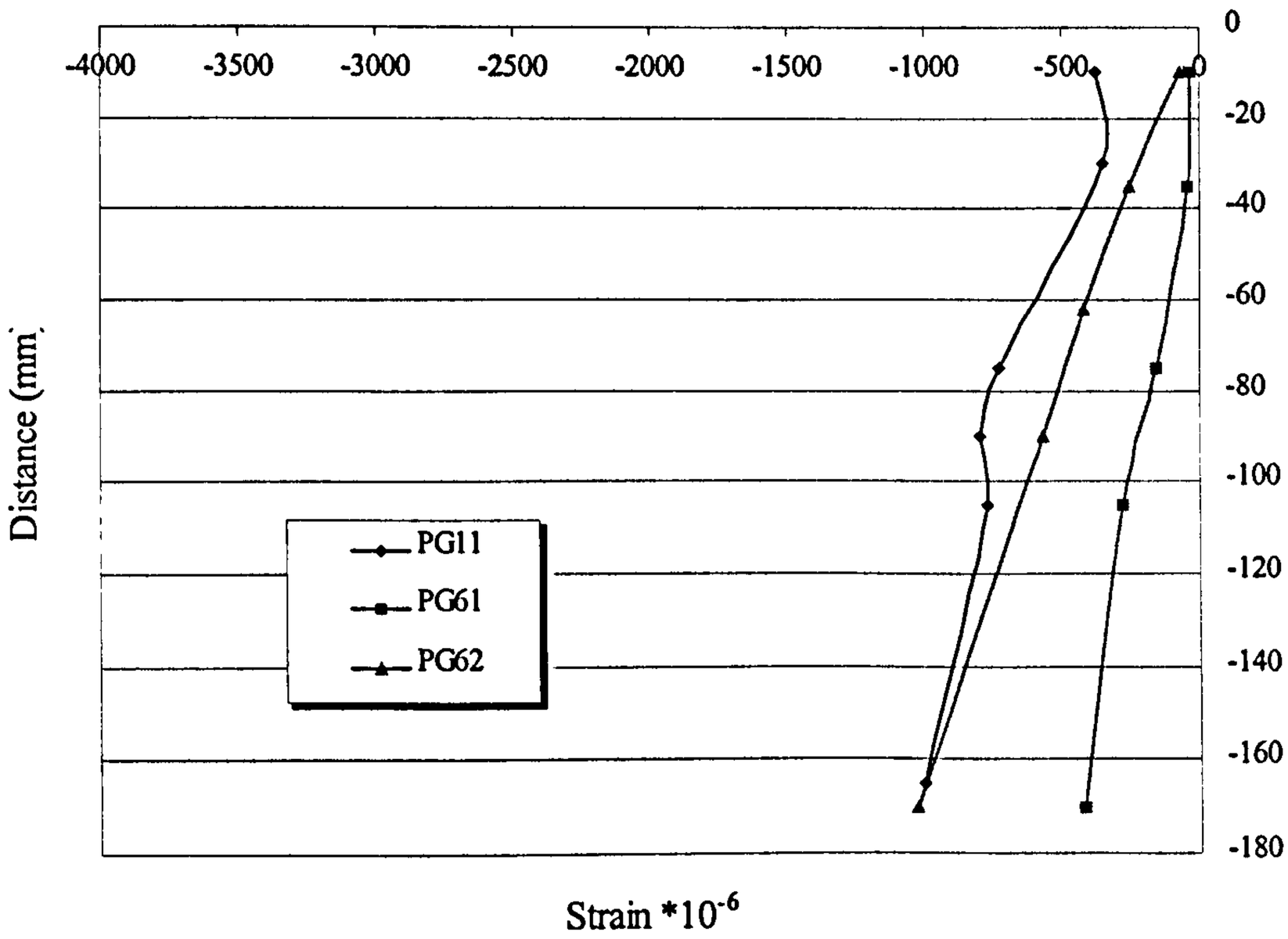

Figure (4.64): Middle strain distribution after external prestressing of G6

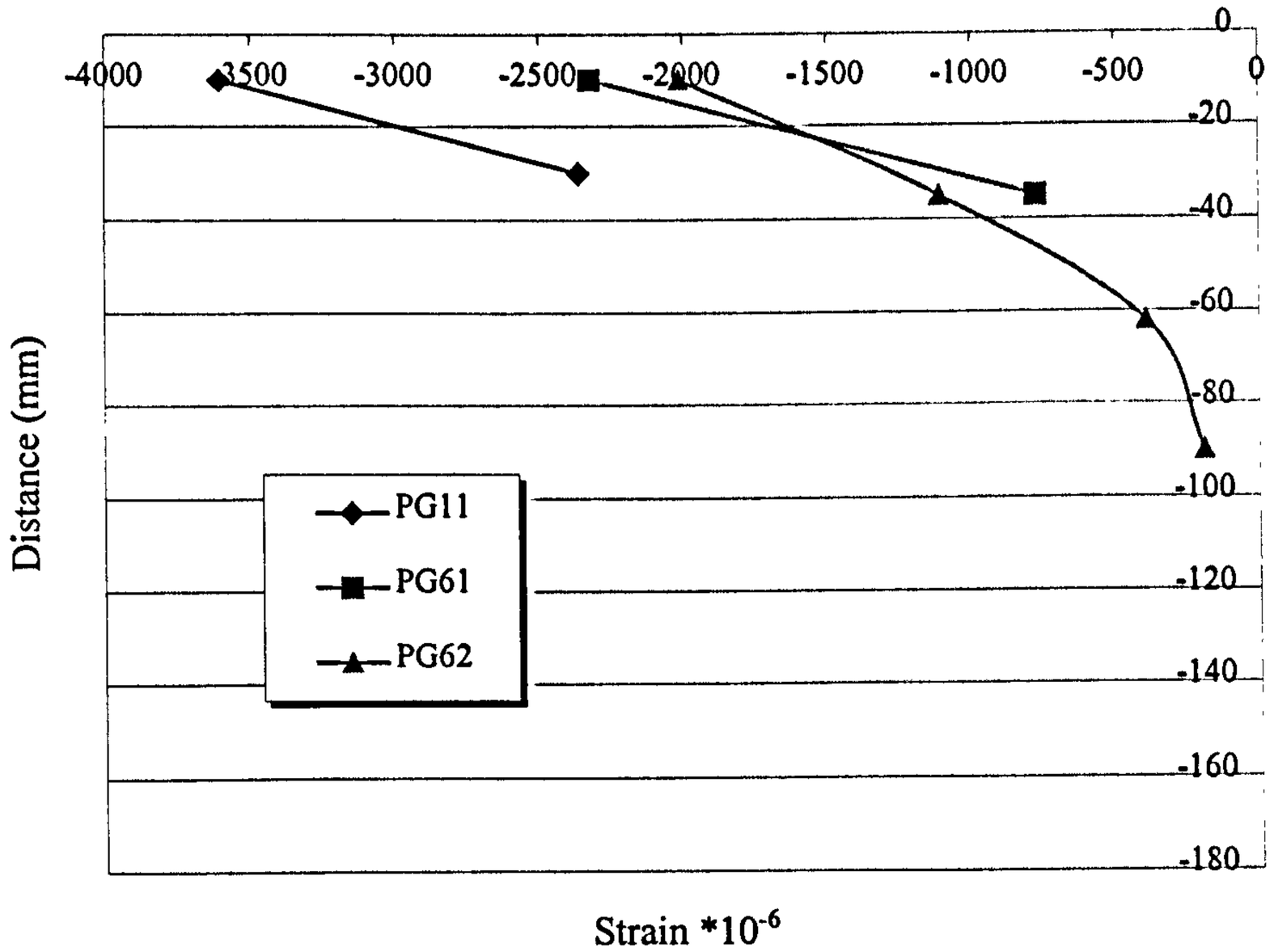

Figure (4.65): Middle strain distribution at ultimate of G6

Chapter 5

Discussion of Test Results

5.1 INTRODUCTION

Results of thirteen prestressed beams (twelve externally strengthened using Parafil Rope) were presented in the previous chapter. Discussion of the test results regarding the effect of factors taken into consideration on the behaviour of the strengthened beam during its life span is presented in this chapter.

This includes the cracking patterns, moment–deflection response, increase in external prestressing force at ultimate and service loads and flexural strength of all the tested beams.

First, a comparison between the general behaviour of prestressed concrete beams with and without external prestressing is presented. Then the effect of each factor on the behaviour of the strengthened beams is discussed. Then the relation between the external prestressing force and both the deflection and the internal prestressing force is obtained. Finally, a summary of the effect of each factor on the behaviour of externally prestressed concrete beams is presented.

5.2 GENERAL BEHAVIOUR

5.2.1 Behaviour of Internally Prestressed Concrete Beam

Figure (5.1) shows a diagrammatic sketch of the relation between moment and deflection of an internally prestressed beam. During the internal prestressing process, the camber increased as the prestressing force increased, depending on several factors such as, concrete strength, supports positions and eccentricity of the internal prestressing force.

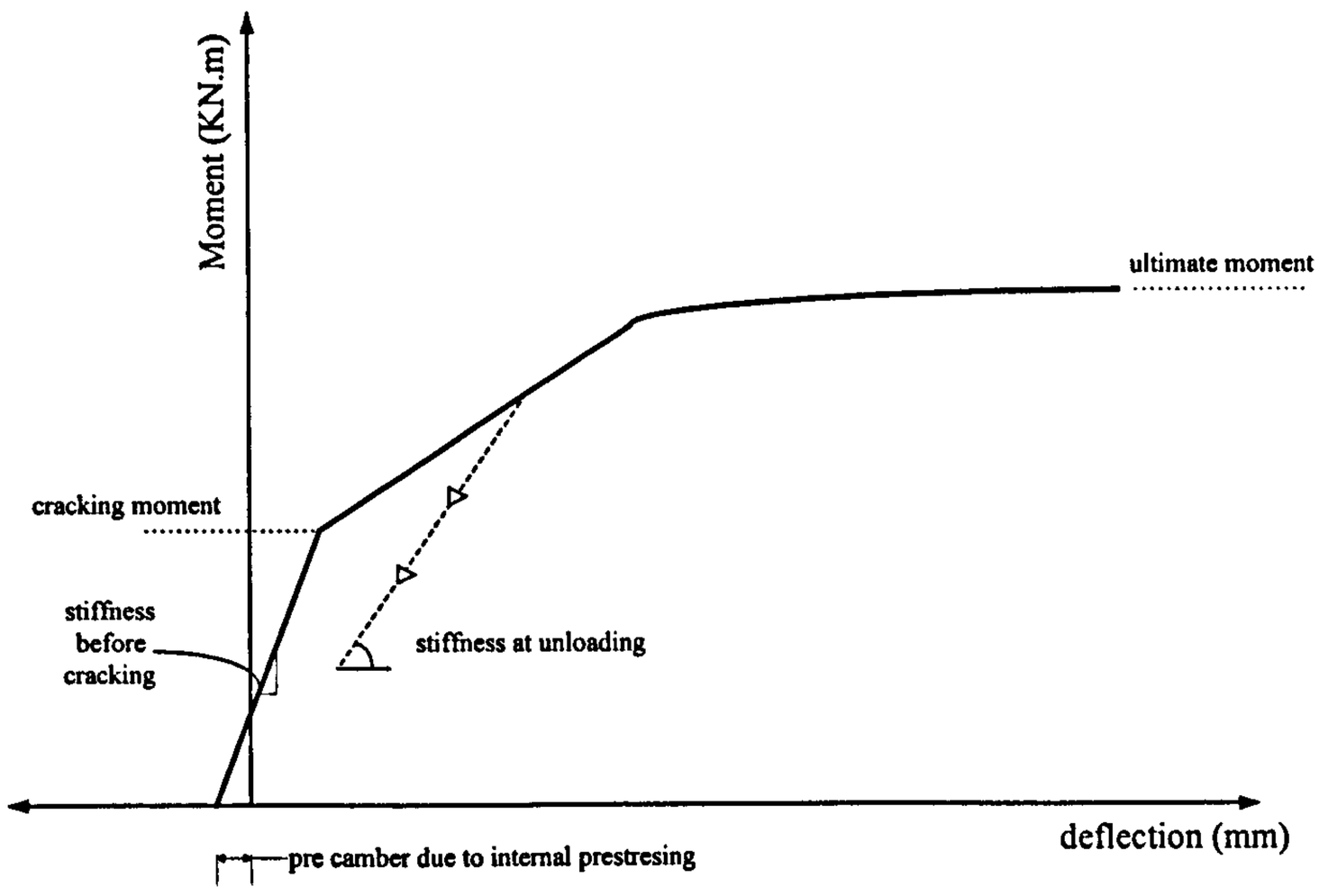

Figure (5.1): Diagrammatic sketch of moment-deflection relationship of internally prestressed concrete beam

During loading, the relation between load and deflection shows three phases of behaviour. In the first stage, before cracking, this relation was linear and the increase in deflection and in internal prestressing steel stress was relatively small. Stiffness in this stage is dependent on the inertia of the cross section.

In the second stage; after cracking, there was a constant changing rate of increase in deflection with the applied load accompanied by a reduction in stiffness due to the spread of cracking. The slope of load-deflection response in this stage was about 27% of that before cracking. Flexural cracks appeared first in the pure flexural zone, then the shear cracks appeared in the shear span. These cracks extended and propagated as the load increased. The transfer of the tensile stress carried by the concrete to the

reinforcement after cracking increased the steel stress, nevertheless, during this stage, the prestressed steel was still in the elastic range of its stress-strain curve and the concrete strain in compression was linear.

In the third stage, the load–deflection curve was nearly flat and the slope of load-deflection was less than 0.5% of that before cracking. Crack widths increased as the load increased. Also, the reinforcement stress was in the inelastic range.

During unloading of beam PG42, there was a significant reduction in stiffness. Also, after unloading, cracks on the beam surface were not completely closed and could still be seen.

5.2.2 Behaviour of Internally Prestressed Concrete Beams After Being Externally Strengthened

During loading, both internally prestressed and externally strengthened concrete beams show well distributed cracks, because of the presence of nonstressed steel (this was also observed during testing several internally prestressed beams without mild steel in the department, where just one or two flexural cracks appeared). Crack widths on the strengthened beams were smaller than on the internally prestressed beams because the additional compression force prevented cracks from opening.

Cracks, in the shear span of the internally prestressed beam extended and distributed more than those on the strengthened beams and their number were higher. This is because the vertical component of the external compression force reduced the shear force while the horizontal component reduced the principal tensile stress in the shear span.

Figure (5.2) shows the general relation between moment and deflection of internally prestressed beam after strengthening with external prestress. Due to the external prestressing force, additional camber was produced, and previous cracks, if they existed, were completely closed. This improves the beam stiffness and helps protect the internal steel from environmental attack thus extending the structural life.

From Table (4.3), it can be seen that camber due to the external prestressing force depends mainly on the eccentricity of the external prestressing force and (span/depth)

ratio, while the increase in external prestressing force, previous loading stage and concrete strength have a slight effect.

During loading, the relation between load and deflection of the strengthened beams show three types of behaviour, similar to the internally prestressed beam. In the first stage, this relation was linear and the increase in deflection was relatively small. Stiffness of both beam types (internally prestressed and strengthened, cracked or uncracked) were almost the same. So, the inertia of the full section can be used in deflection calculation after strengthening even though the section was pre-cracked.

After cracking, there was a reduction in stiffness and the rate of increase in deflection constantly changed. However, the stiffness of the strengthened beams was higher than the stiffness of the internally prestressed beam. This can be attributed to the reduced propagation and extension of the cracks in the strengthened beams due to the external compressive force.

In the third stage, the stiffness of the strengthened beam was very small and the slope of the load-deflection curve was only about 4% of that before cracking, even though the stiffness of the strengthened beam was still higher than that of the internally prestressed beam at the same stage. This ratio slightly increased as the external prestressing force increased and decreased as the concrete strength increased. In this stage, the internal reinforcement stress was in the inelastic range while the external rope did not reach its maximum load.

The cracking moment of strengthened beams was higher than that of the internally prestressed beam due to the effect of the additional compressive stress (produced by the external prestressing force) which counteracted the tensile stress due to external moment and hence delayed the cracking.

The ultimate moment of the strengthened beam was significantly higher than that of the internally prestressed beam due to the additional prestressing moment provided by the external prestressing.

During loading there was an increase in the external prestressing force, even though this increase was less than the increase in the internal prestressing force. This

is because the increase in the effective external prestressing force is dependent on the total deformation of the member rather than the section deformation (as the bonded prestressing force). So, it can be said that factors which affect the beam's deformation have an effect on the increase in external prestressing force as well.

Before cracking, the increase in external prestressing force was small due to the small deflection at this stage, while, after cracking there was a more rapid increase in external prestressing force due to the more rapid increase in deflection. At ultimate, the beam with the higher concrete strength had a higher deflection and higher ultimate moment and hence had a greater increase in the external prestressing force.

Comparing all beams before cracking it can be seen that the difference between the increase in external prestressing force is negligible, due to the small deflection at this stage. So, the error resulting from using the effective external prestressing force in flexural strength calculations during the uncracked stage can be neglected.

Also, because the external ropes were not bonded to the concrete, there was a reduction in its eccentricity during loading resulting a reduction in the lever arm as the deflection increased.

Since the loss of eccentricity is simply equal to the deflection of the beam relative to the deflectors, it is obvious that the relation between loss and load will be similar to the relation between load and deflection and will depend on the same parameters. So, factors, which increase deflection, are expected to increase the loss in rope eccentricity as well.

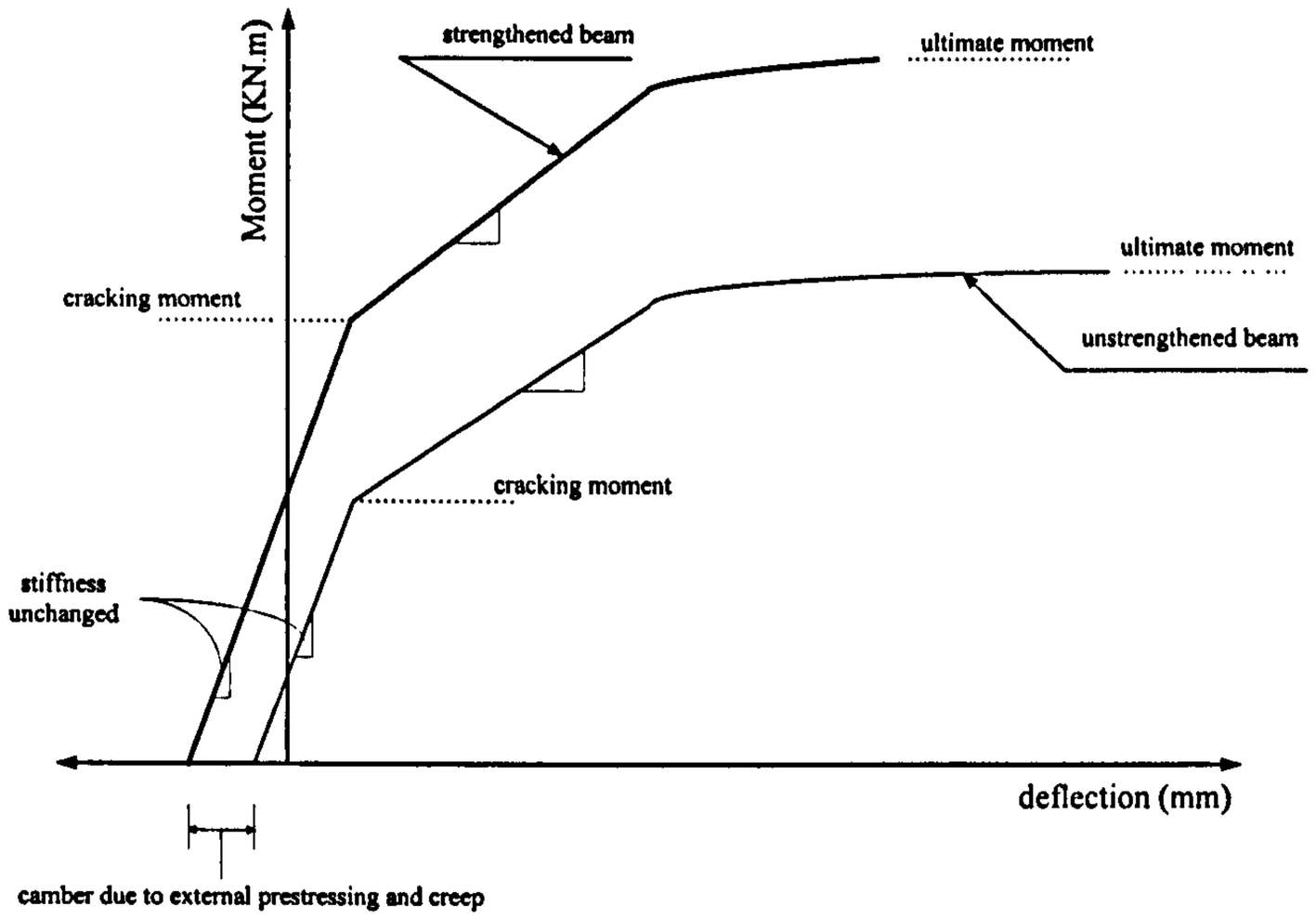

Figure (5.2): Diagrammatic sketch of moment-deflection relationship of internally prestressed concrete beam after strengthening

5.3 DISCUSSION OF RESULTS OF TEST BEAMS

The effect of each factor considered in this study, on the behaviour of the strengthened beam is discussed as follows:

5.3.1 Effect of External Prestressing Force

Increasing the external prestressing force increased the compressive stress at the tension side and hence reduced the net tensile stress. This improves the cracking resistance of the beam and enables the beam to resist higher load.

5.3.1.1 Cracking patterns

Increasing the external prestressing force delayed the appearance of flexural cracks and decreased the rate of crack propagation. Also, increasing the external prestressing force increased its vertical component and hence increased shear-cracking load and reduced number of diagonal cracks.

5.3.1.2 Load-deflection behaviour

As can be seen from Figure (4.20) and Table (4.4), after cracking, deflection of beams in group G1, decreased and the slope of load-deflection increased as the

external prestresseing force increased. This is because the stiffness after cracking increased as the external prestressing force increased.

Also from Figure (5.3) it can be seen that the external prestressing force at cracking seems to have no effect on deflection while at ultimate, the deflection is inversely proportional to the external prestressing force.

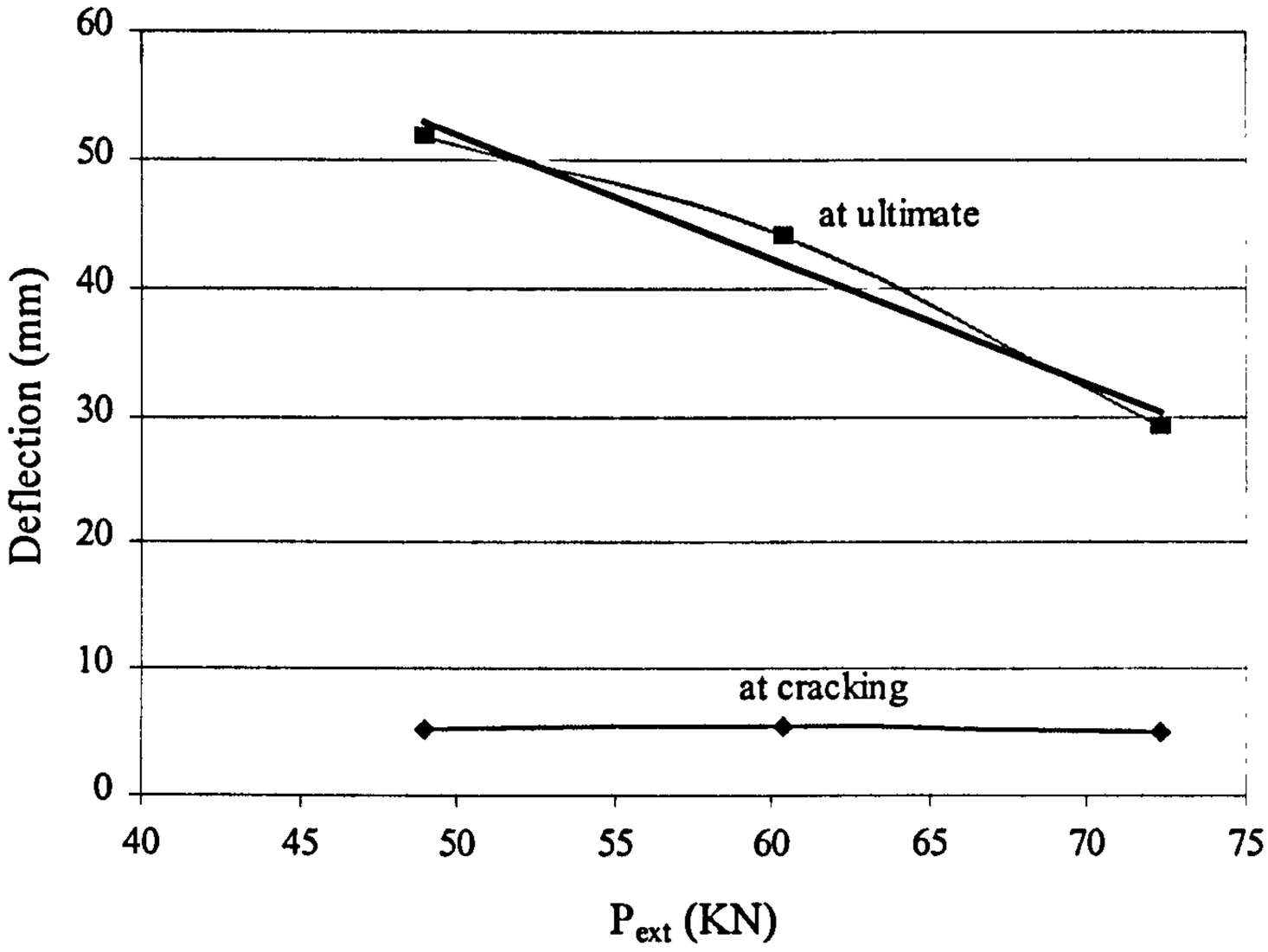

Figure (5.3): Deflection-External prestressing force relationship

5.3.1.3 Cracking and ultimate moments

Although increasing the external prestressing force increased the cracking moment, the cracking moment of beam PG13 was almost the same as that of beam PG11. This may be due to the impact load that was accidentally applied to beam PG13 during testing and may have produced cracks (which could not be seen due to the external prestressing force) so the cracking strength was due to the prestressing force only. However, at ultimate stage, this impact load seemed to have had no effect on the ultimate moment of beam PG13 as its ultimate moment was higher than those of PG12 and PG11.

The ultimate moments of PG12, PG11 and PG13 were slightly different, and increasing the external prestressing force by 47.6% (PG13 compared to PG12) just increased the ultimate moment by 6.6%. This is because the ultimate moment, which

depends mainly on the prestressing tendons (areas and stresses) in tension and concrete in compression, was controlled by the concrete strength. The failure of the strengthened beams were due to concrete crushing, while the stress in the Parafil Rope never reached its ultimate strength.

From Figure (5.4) it can be seen that both cracking and ultimate moments vary linearly with the external prestressing force and the rate of increase in moment at both cracking and ultimate moments are almost the same and is small.

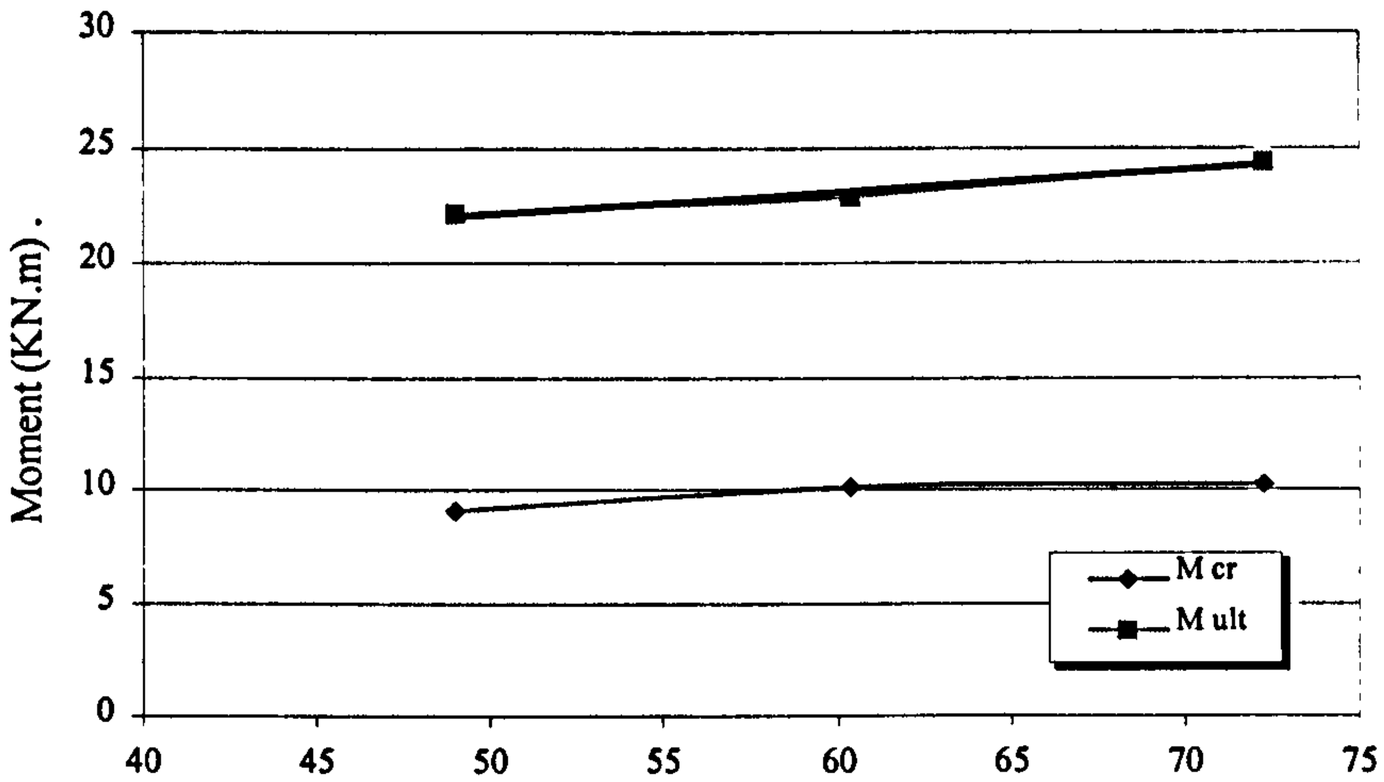

Figure (5.4): Moment-External prestressing force relationship

5.3.1.4 External prestressing force (Parafil Rope Load)

During loading, the increase in external prestressing force of beam PG13 was higher before cracking than the other beams. This may be due to the previous impact load. However, at ultimate, because the failure of beam PG13 was a brittle failure while those of beams PG11 and PG12 were ductile, the increase in external prestressing force of PG13 was smaller than those of beams PG11 and PG12.

From Figure (5.5) it can be said that the value of the initial external prestressing force has a negligible effect on the increase in external prestressing force at cracking, while at ultimate the rate of increase in the external prestressing force decreases as the initial prestressing force increases.

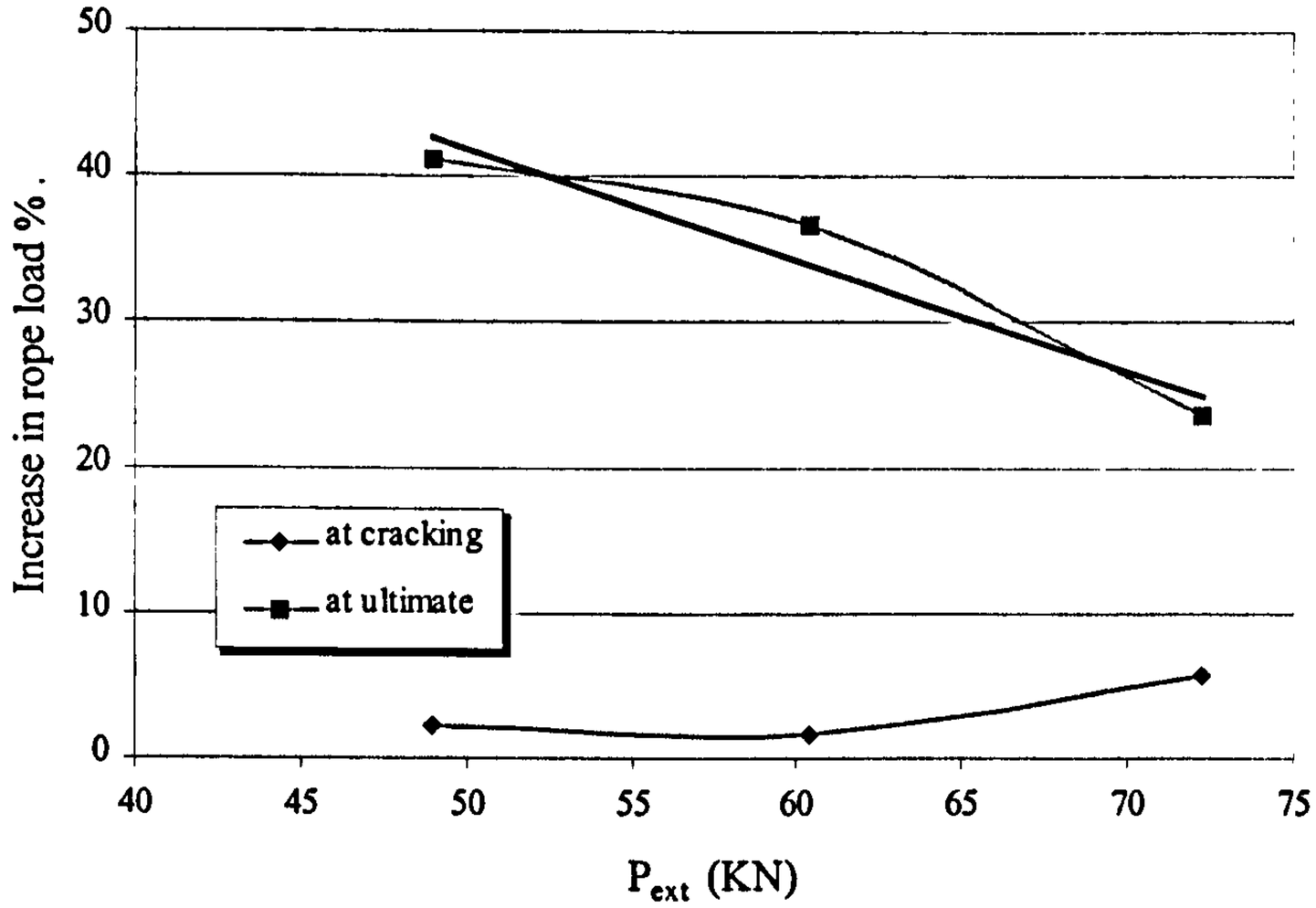

Figure (5.5): Relation between the increase in External prestressing force and the initial external prestressing force

5.3.1.5 Change in rope eccentricity

As can be seen from Figure (5.6), increasing the external prestressing force decreased the loss in rope eccentricity, especially at ultimate, due to the less ductile behaviour.

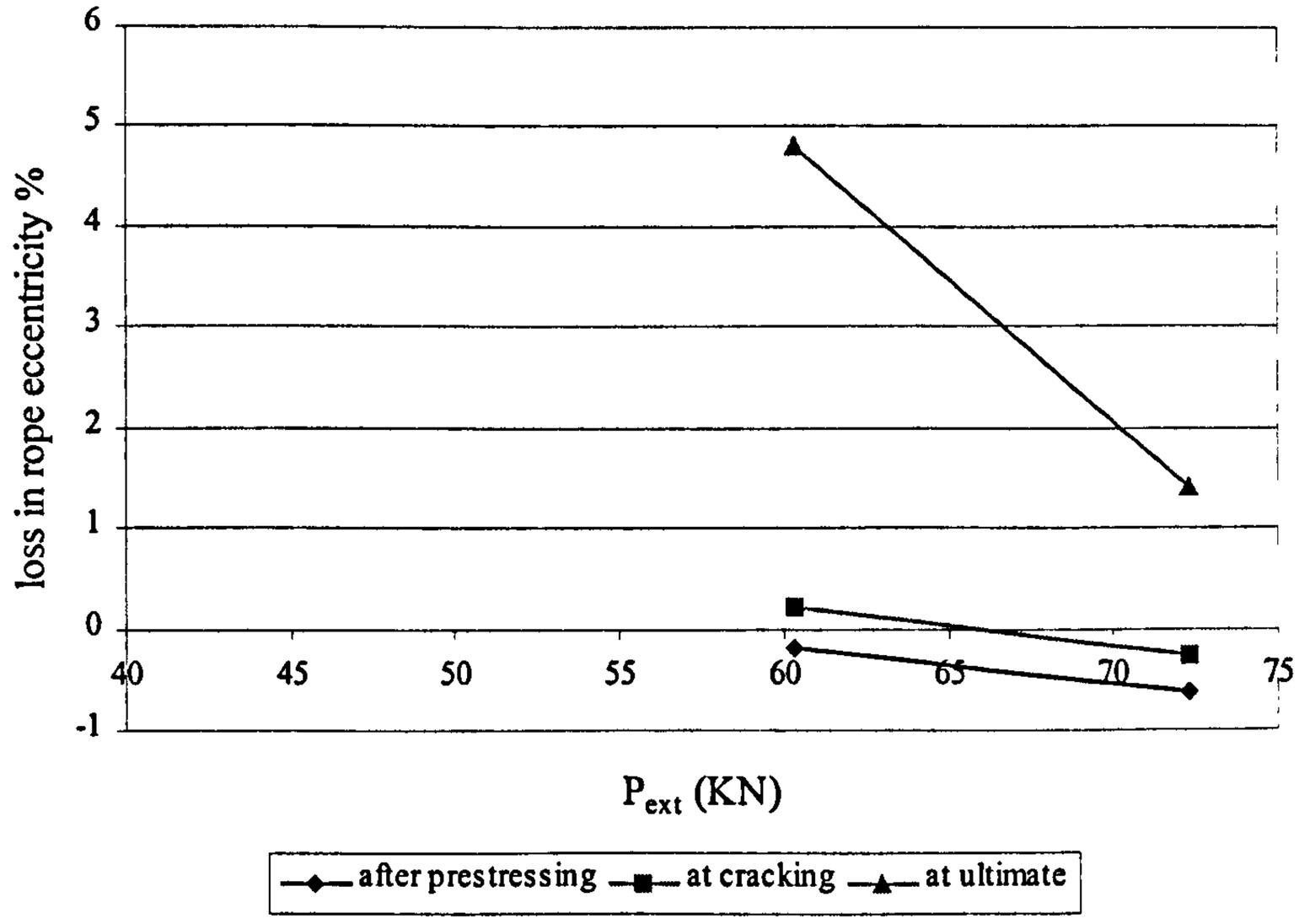

Figure (5.6): Relation between losses in Rope eccentricity and external prestressing force

5.3.2 Group 2 (Number of Deviators)

The prestressing moment can be considered constant between the deviators when using two deviators at the third span (PG51), while it decreases with distance from the deviator when using one deviator at the mid span (PG21). In the case of two-concentrated loads and deviators at third span as used in this study, the critical section is at the middle while, in case of beam with one deviator is at the concentrated load.

5.3.2.1 Cracking patterns

The flexural cracks on beam PG21 extended higher than those on beam PG51 due to the reduction in prestressing moment, especially at the concentrated loads. Also, the cracks in the shear span on beam PG21, as stated in chapter four, appeared at a load below that of beam PG51, with a higher number and spread over a longer distance as shown in Figure (4.5). This is because the inclination angle (and hence the vertical component of the prestressing force) and the bending moment (and hence, the compressive prestressing stress) were less in PG21 due to the reduction in the eccentricity of the external prestressing force.

5.3.2.2 Load-deflection behaviour

After prestressing, the camber due to the external prestressing force for beam PG51 was about 120% larger than that for beam PG21. In theory, assuming linear elastic behaviour and that everything else is the same (including internal and external prestressing force and flexural stiffness of the members), the camber due to external prestressing would be expected to be about 82% higher for the two deviators than for the one deviator used in this investigation. The difference between the actual and theoretical values can be attributed to the difference in concrete strength as well as the increase in the eccentricity of the external prestressing force of beam PG51 during prestressing at the mid span.

During loading and before yielding, PG21 registered higher deflections than PG51, due to the greater extension of the cracks on it. To determine the effect of deviator position on the deflection of strengthened beams, several tests are required. However, from the available test results it can be said that deflection at cracking is not

affected by the position of the deviator, while at ultimate, it depends on the location of failure. Figure (5.7) shows the relation between deflection and ratio of the distance of deviator from the support to the span.

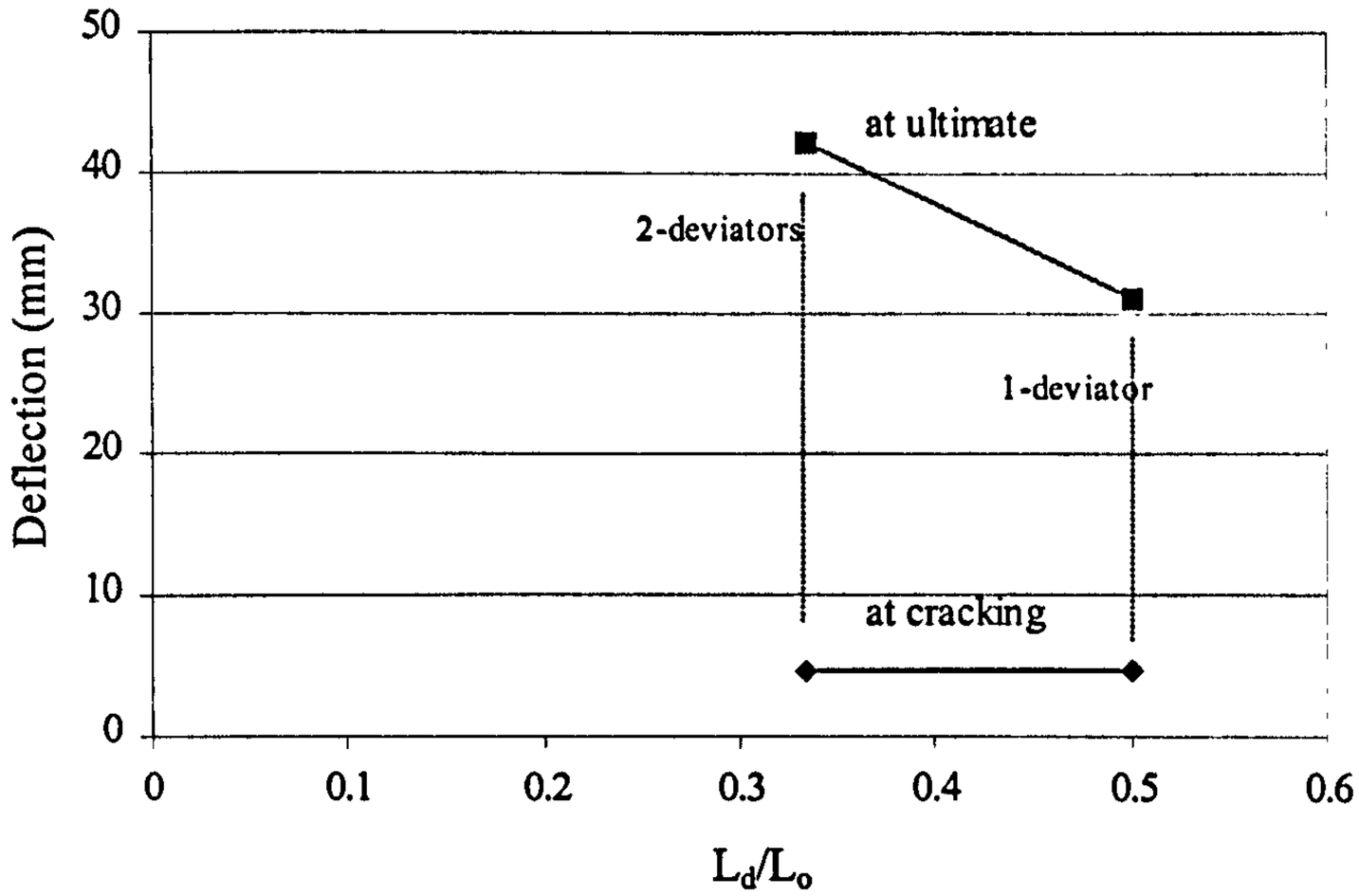

Figure (5.7): Deflection- (Distance of deviator/ span) ratio relationship

5.3.2.3 Cracking and ultimate moments

Both the cracking and ultimate moments of PG51 were higher than those of PG21, as can be seen in Figure (5.8), even though beam PG51 had less concrete strength. This is because both the first crack and the failure occurred in PG21 at the concentrated load (where the prestressing moment is less) and those of PG51 occurred in the constant flexural zone.

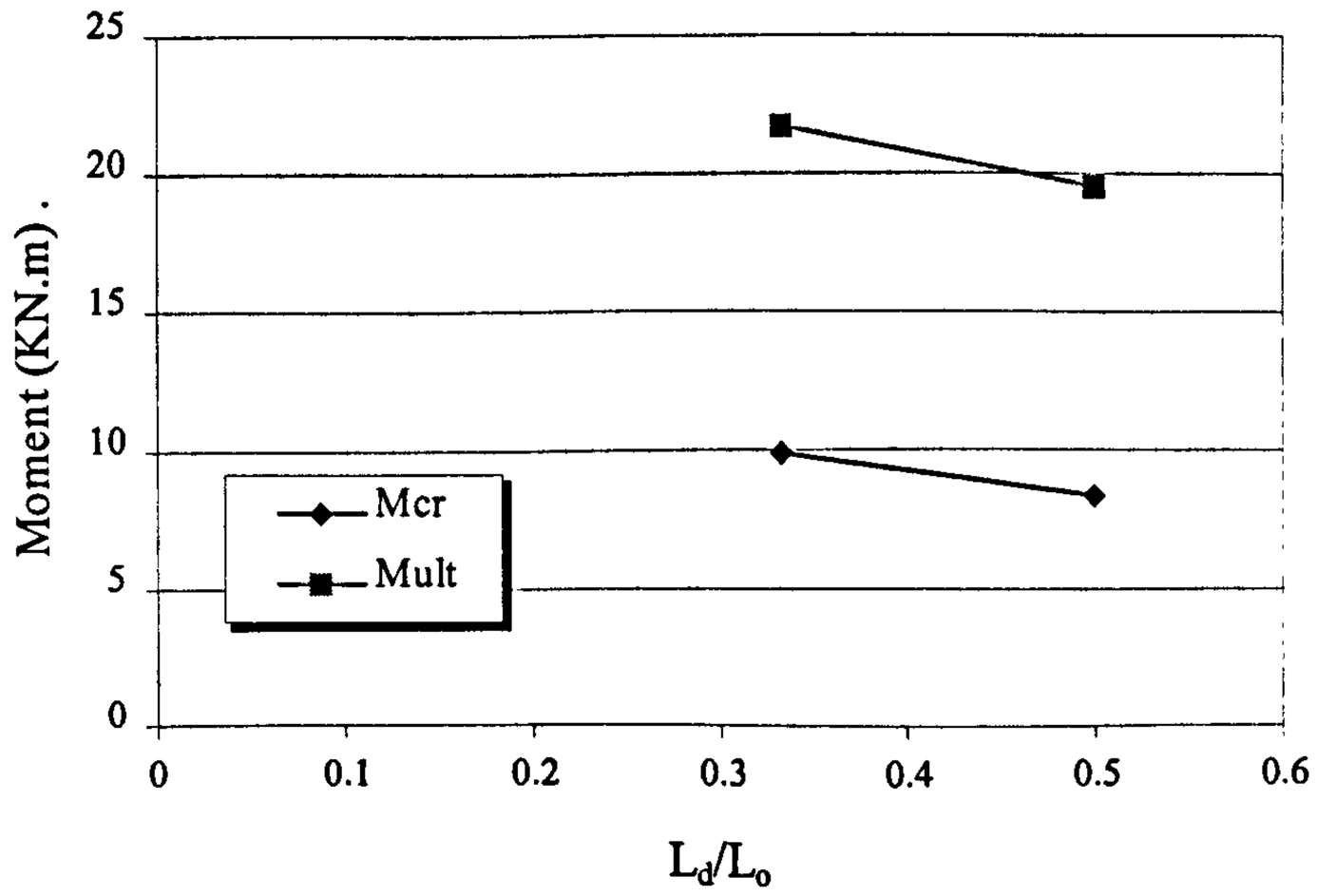

Figure (5.8): Moment- (Distance of deviator/ span) ratio relationship

5.3.2.4 External prestressing force (Parafil Rope Load)

At ultimate the increase in external prestressing force of beam PG51 was higher than that of beam PG21. This can be attributed to the more ductile failure of PG51 compared to that of PG21. Both curves in Figure (5.9) show a trend of increased external prestressing force when using two deviators at the third span compared with using one deviator at the mid span.

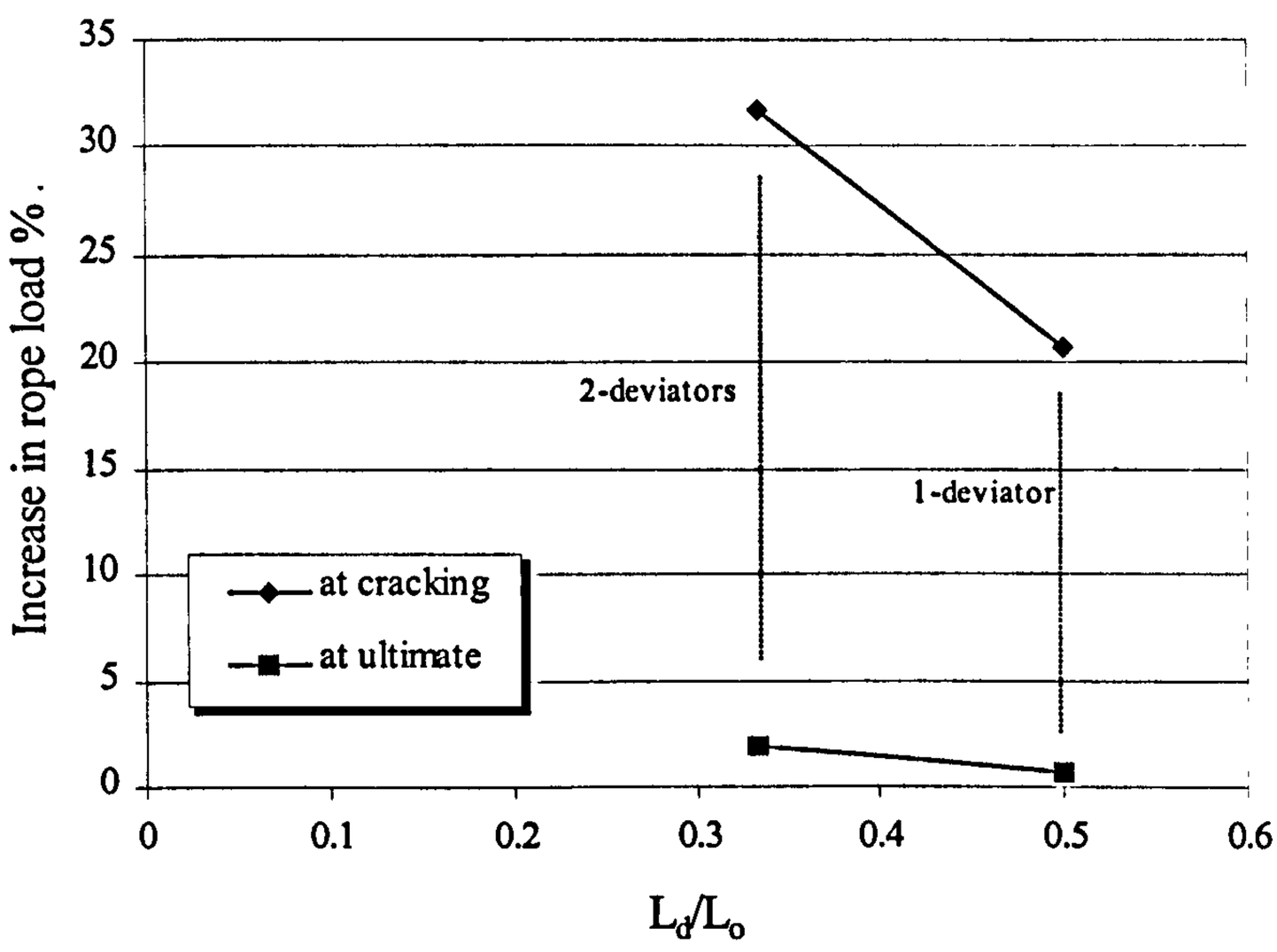

Figure (5.9): Relation between the increase in External prestressing force and (Deviator distance/Span distance) ratio

5.3.3 Group 3 (Effective Depth of The External Prestressing Force)

Increasing the eccentricity of the external prestressing force increased the prestressing moment and enabled the section to tolerate more loads. Also, increasing the eccentricity increased the compressive stress that prevented cracks from extending and decreased the reduction in inertia and stiffness after cracking.

5.3.3.1 Cracking patterns

Due to the increase in compressive stress, the flexural cracks on beam PG32 appeared later and extended more slowly than on the other beams. The same was observed when comparing the cracks in the shear span, those of PG32 appeared later

and extended more slowly. This, also, due to the increase in the compressive stress as well as the increase in the vertical component of the external prestressing force.

5.3.3.2 Load-deflection behaviour

After prestressing, the beam with the higher eccentricity had the higher prestressing moment and higher camber. After cracking, the beam had higher eccentricity had a greater stiffness and a smaller deflection. However, beam PG31 had almost the same deflection during the working stage as beam PG32. This may be because it had higher concrete strength when internally prestressed than PG11 and PG32 (47.9, 42.2 and 40.87 MPa respectively). This may well have increased its Young's modulus and reduced its ductility (*Bennett*, 1973).

From Figure (5.10) it can be seen that deflection at cracking increases slightly as (e/h) increases, while at ultimate, the deflection decreased as (e/h) increased.

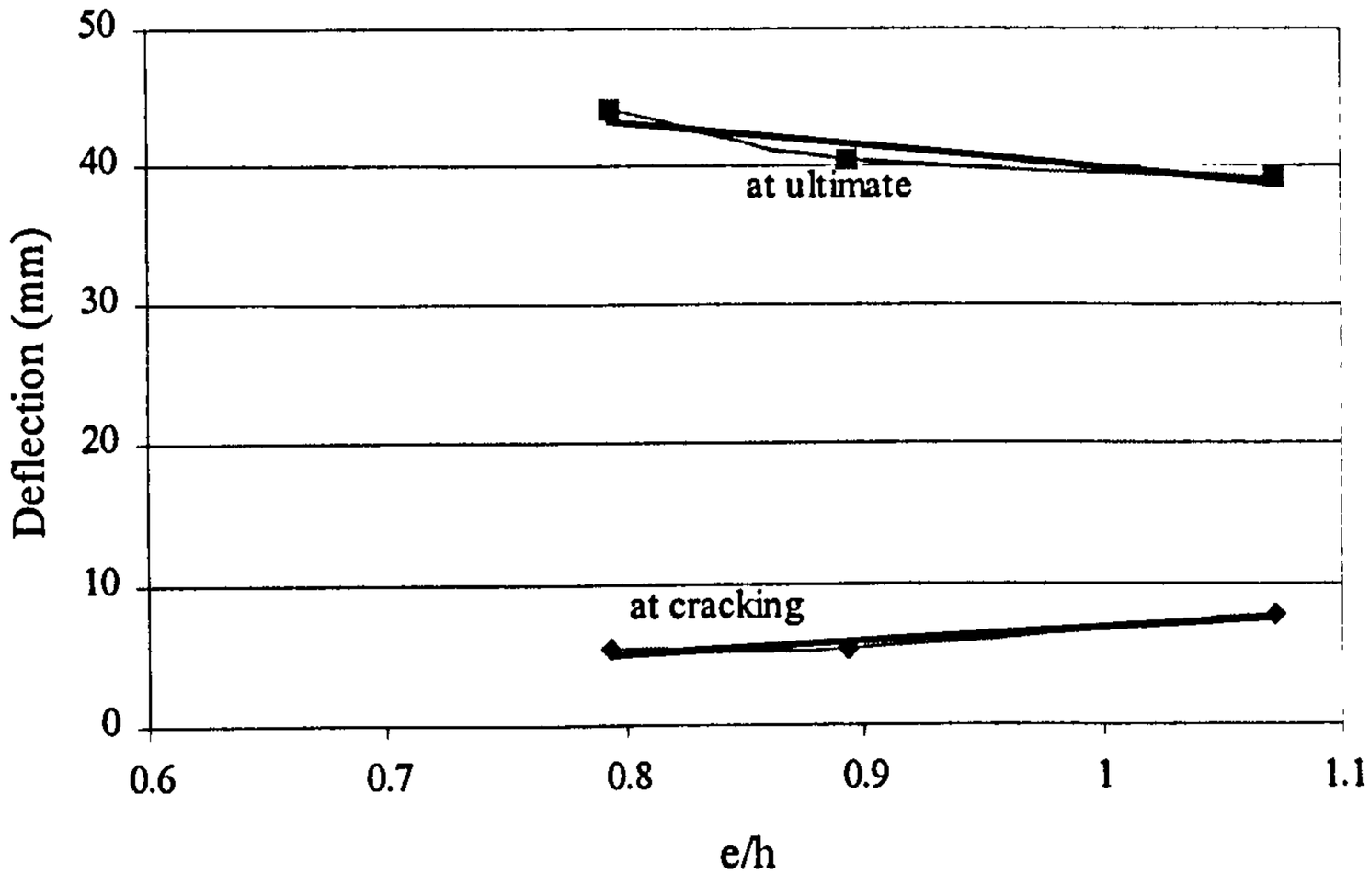

Figure (5.10): Deflection- (External prestressing force eccentricity/ depth) ratio relationship

5.3.3.3 Cracking and ultimate moments

The increase in the eccentricity of the external prestressing force can be considered to be the main factor in increasing the cracking and ultimate moments. An increase in the eccentricity by about 35% (PG32 compared to PG11) increased the cracking moment by about 33.45 and the ultimate moment by about 21.7%.

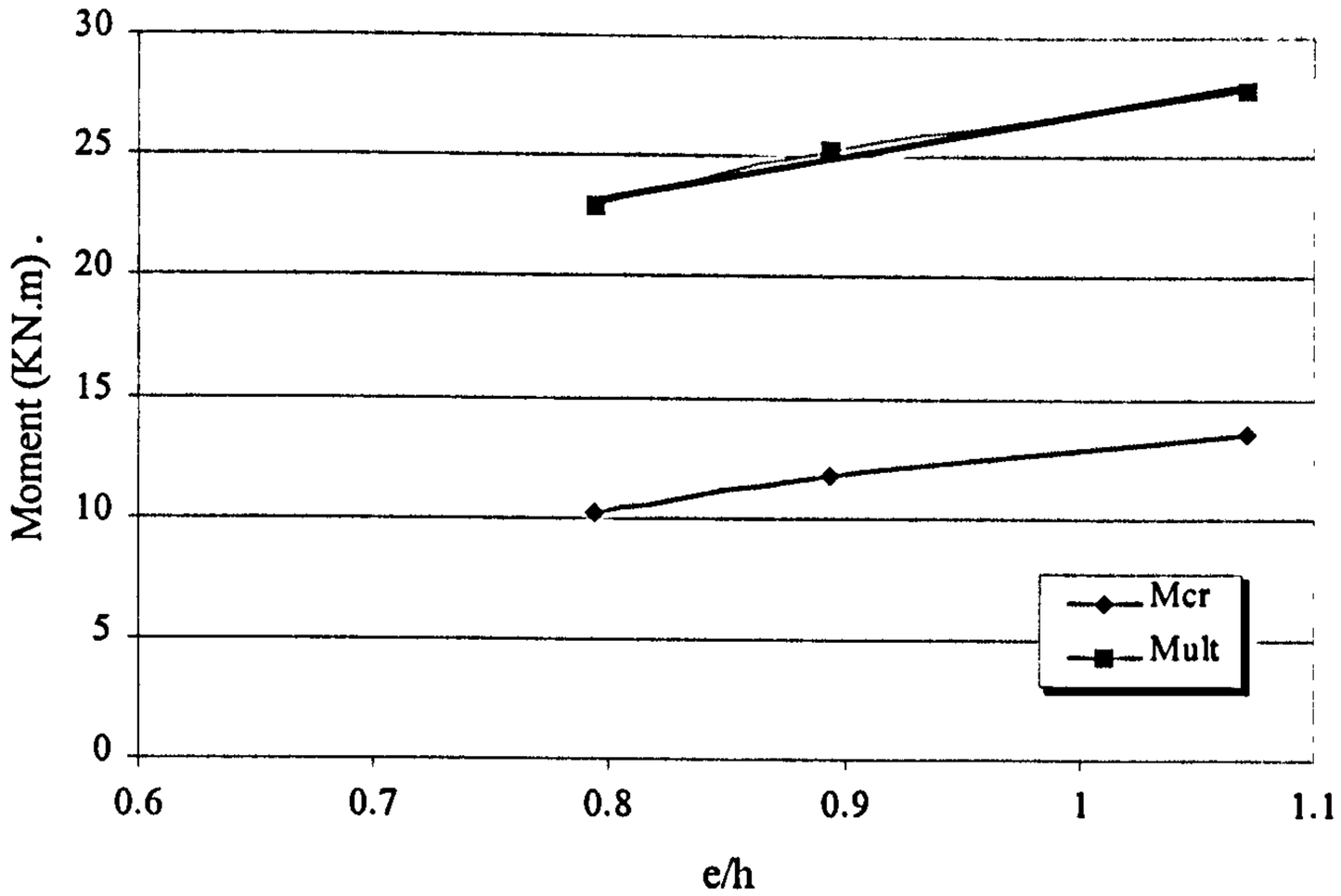

Figure (5.11): Moment- (External prestressing force eccentricity/depth) ratio relationship

5.3.3.4 External prestressing force (Parafil Rope Load)

The change in the external prestressing force increased as the eccentricity increased. This was observed before, after cracking and at ultimate as can be seen from Table (4.13) and Figure (5.12). This is because the change in rope stress is relative to its distance from the neutral axis; the greater the distance the higher the stress. Also, the rate of increase in the external prestressing force is slightly greater at ultimate than at cracking.

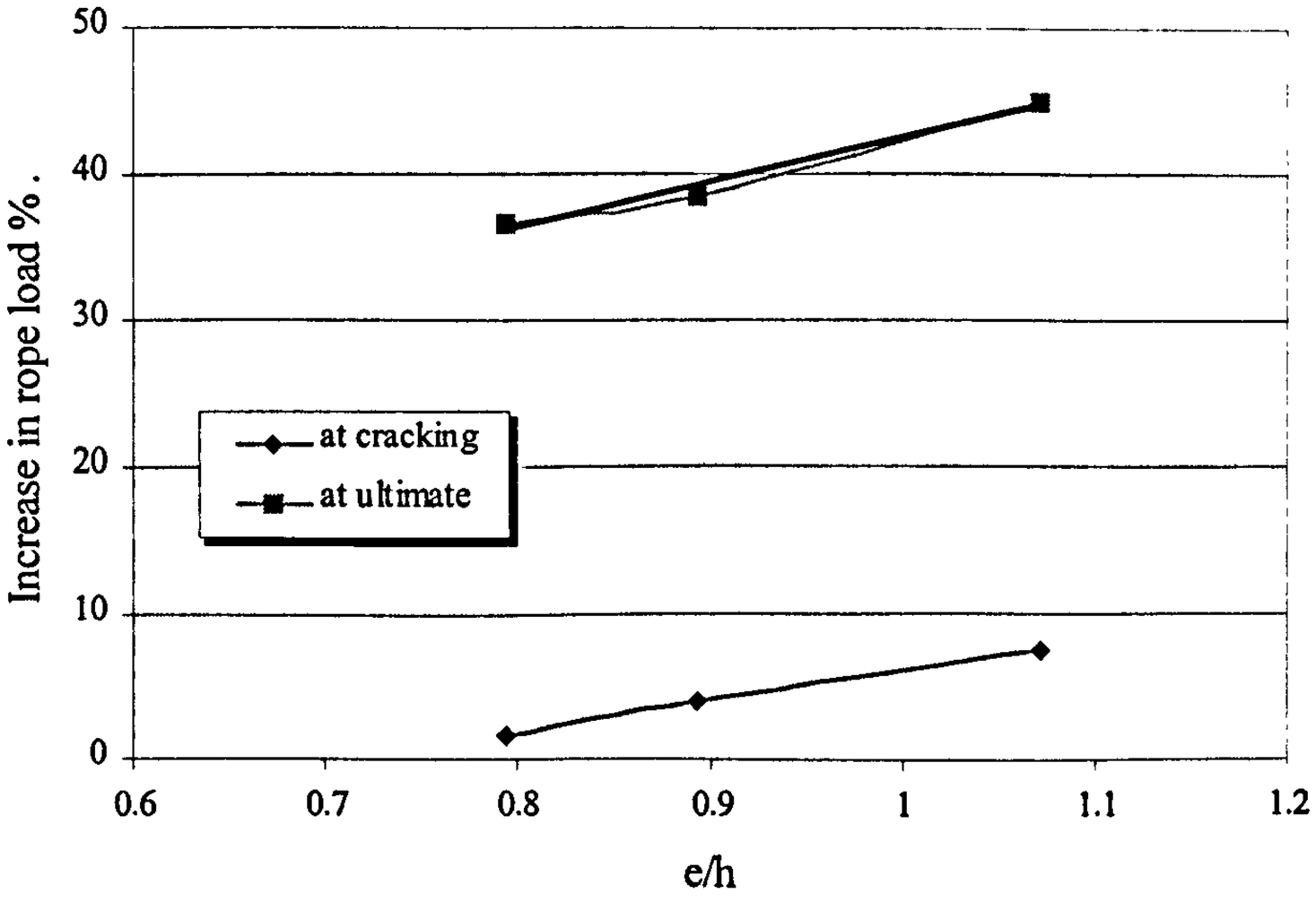

Figure (5.12): Relation between the increase in External prestressing force and (eccentricity of the external prestressing force/ depth) ratio

5.3.3.5 Change in rope eccentricity

Due to prestressing, the gain in camber increased slightly as the eccentricity increased due to the increase in prestressing moment. While at ultimate the ratio of loss in eccentricity decreases as the eccentricity increases as shown in Figure (5.13).

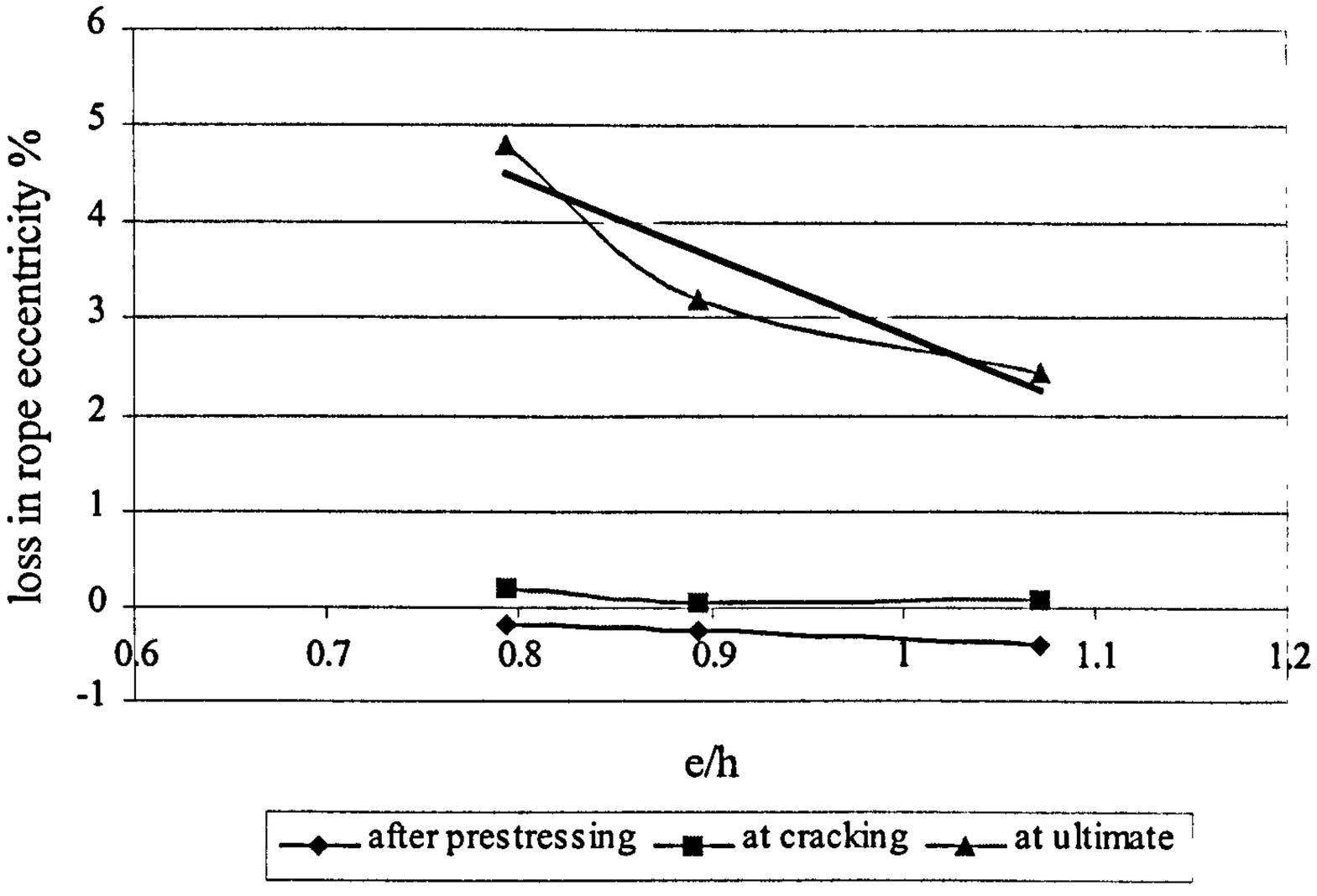

Figure (5.13): Relation between losses in Rope eccentricity and (rope-eccentricity/depth) ratio

5.3.4 Group 4 (Previous Cracking Stage Before Externally Strengthened)

The stiffness of the pre-cracked beams was increased because the prestressing force closed the previous cracks, but at the working stage, the stiffness of the strengthened beams rapidly reduced as the previous cracking increased.

5.3.4.1 Cracking patterns

Before failure, the flexural cracks on beam PG42 extended higher than those of PG41 and PG11 and the number of the new shear cracks (after strengthening) was less, due to the greater degree of cracking prior to strengthening that reduced its cracking resistance.

5.3.4.2 Load-deflection behaviour

During external prestressing beam PG42 had a slightly higher camber due to its reduced stiffness. After strengthening there was a significant improvement in the beam stiffness (as can be seen when comparing the slope of load-deflection of beam PG42 before and after strengthening (1.28 and 4.5 respectively). Also, after strengthening all beams had almost the same load-deflection slopes. Therefore, their deflection before cracking was almost the same.

After cracking, the slope of PG42 decreased more sharply than that of PG11 and PG41. This can be attributed to the extension of the cracks of beam PG42 before strengthening, up to about the middle of the height of its cross section. Then after external prestressing and during loading these cracks fully opened as soon as the bottom stress changed to tension, hence, the reduction in stiffness would be more rapid and accompanied by a more rapid increase in deflection. The gradient of the load-deflection response of beam PG42 in the second stage after strengthening was higher than in the second stage before strengthening (1.6, 1.28 respectively). So, there is a slight improvement in beam stiffness in the working stage.

From Figure (5.14), it can be seen that the deflection at cracking is only slightly affected by the pre-loading stage, while at ultimate it can be said that deflection decreased as the degree of cracking before strengthening increased.

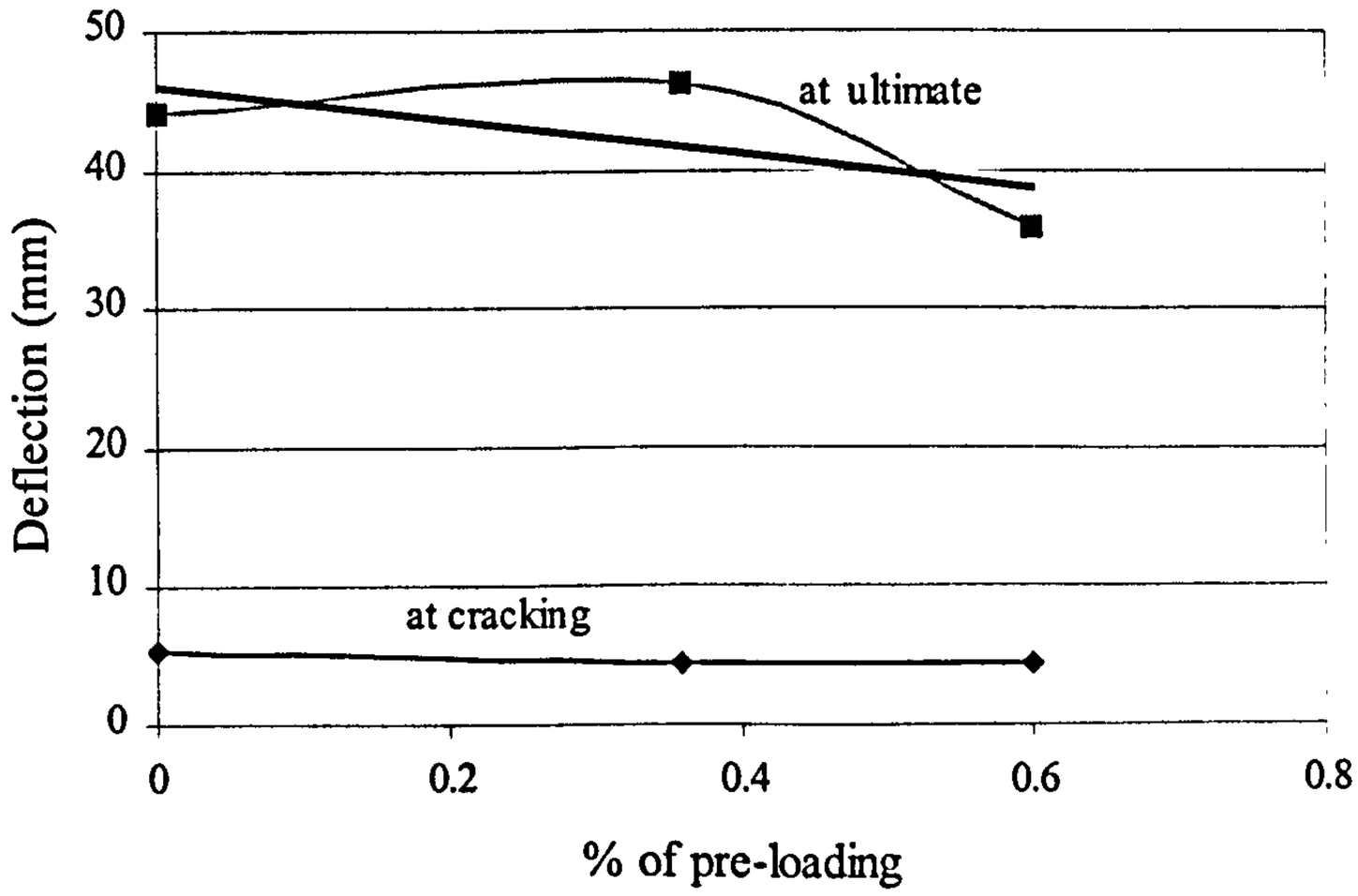

Figure (5.14): Deflection- % of pre-loading relationship

5.3.4.3 Cracking and ultimate moments

External prestressing significantly increased the cracking and ultimate moments of both the uncracked beam (PG11) and the beam with severe cracks (PG42). The increase in the moment of resistance can be attributed to the external prestressing moment (increase in cracking moment of beam PG41 was 3.79 kN.m and that of beam PG42 was 3.92 kN.m greater than that before externally prestressed). It is worth noting that the cracking moment of beams PG41 and PG42, after strengthening, were almost the same (8.66 and 8.27 kN.m), even though they had different concrete strength. Also, the resistance moment due to the concrete tensile strength can be calculated as the difference between the cracking moment of beam PG11 and that of beam PG41 after strengthening, as they had almost the same properties, which is equal 1.48 kN.m. The difference between the ultimate moments can be attributed to the difference between the concrete strength and the internal prestressing force; increasing the concrete strength and/or the internal prestressing force increased the ultimate moment.

From Figure (5.15) it can be seen that the cracking moment of the pre-cracked beam decreases very slightly (as discussed) while ratio of pre-loading increases. At ultimate, it can be said, the effect of the percentage of pre- loading can be neglected if the internal reinforcement does not reach yield before strengthening. So, the pre-cracked beam, after strengthening, can be analyzed at ultimate stage in the same way as the uncracked strengthend beam

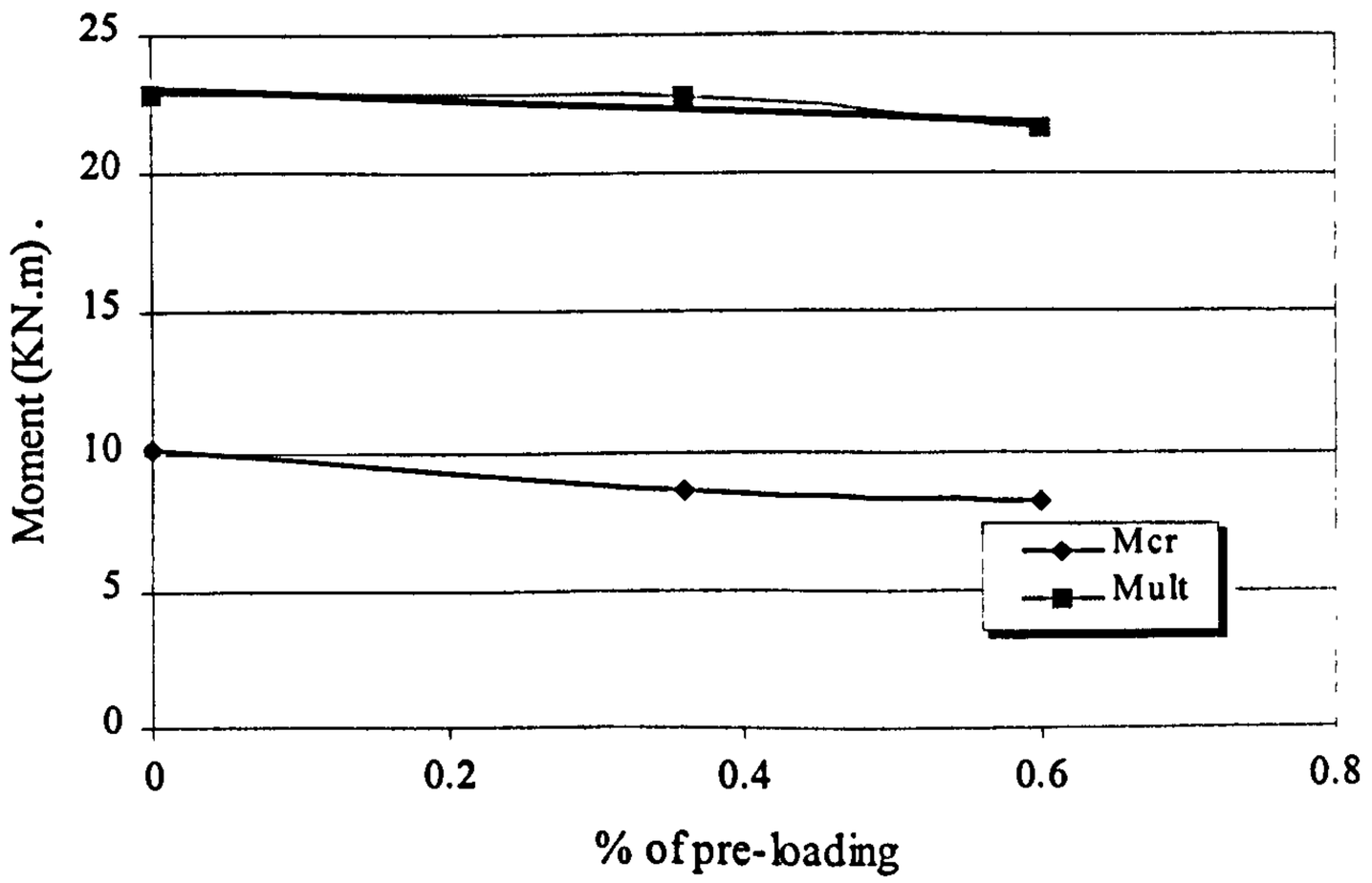

Figure (5.15): Moment - % of pre-loading relationship

5.3.4.4 External prestressing force (Parafil Rope Load)

Before cracking and due to the improvement in stiffness of beams PG41 and PG42 by the external prestressing, the increase in external prestressing force was almost equal that of beam PG11 and slightly increased as the ratio of pre-loading increased. After cracking, the increase in external prestressing force in beam PG42 (as shown in Figure 4.44) was higher than those in beams PG11and PG41 at any load. This can be attributed to the drop in its stiffness as soon as the bottom stress changed to tension.

At ultimate the increase in the ratio of pre-loading slightly decreased the external prestressing force as can be seen when beam PG11 and beam PG41 are compared or when PG51 and PG42 are compared. It appears from Figure (5.16) that the increase in the pre-loading stage significantly decreased the increase in external prestressing force. This is because the difference between the increase in external prestressing force of PG11 and PG42 is partly due to reduction in stiffness due to pre-cracking, and partly due to the difference in concrete strength (f_{cu} =55.77 and 45.7 MPa for PG11and PG42 respectively). This can be confirmed when comparing the difference between the increase in external prestressing force of beams PG51 and PG42, (both had almost the same concrete strength, f_{cu} =43.3 and 45.7 MPa respectively), and the ratio of increase in their external prestressing forces as shown in Table (4.14) were 31.75 and 28.12 (Figure 5.17).

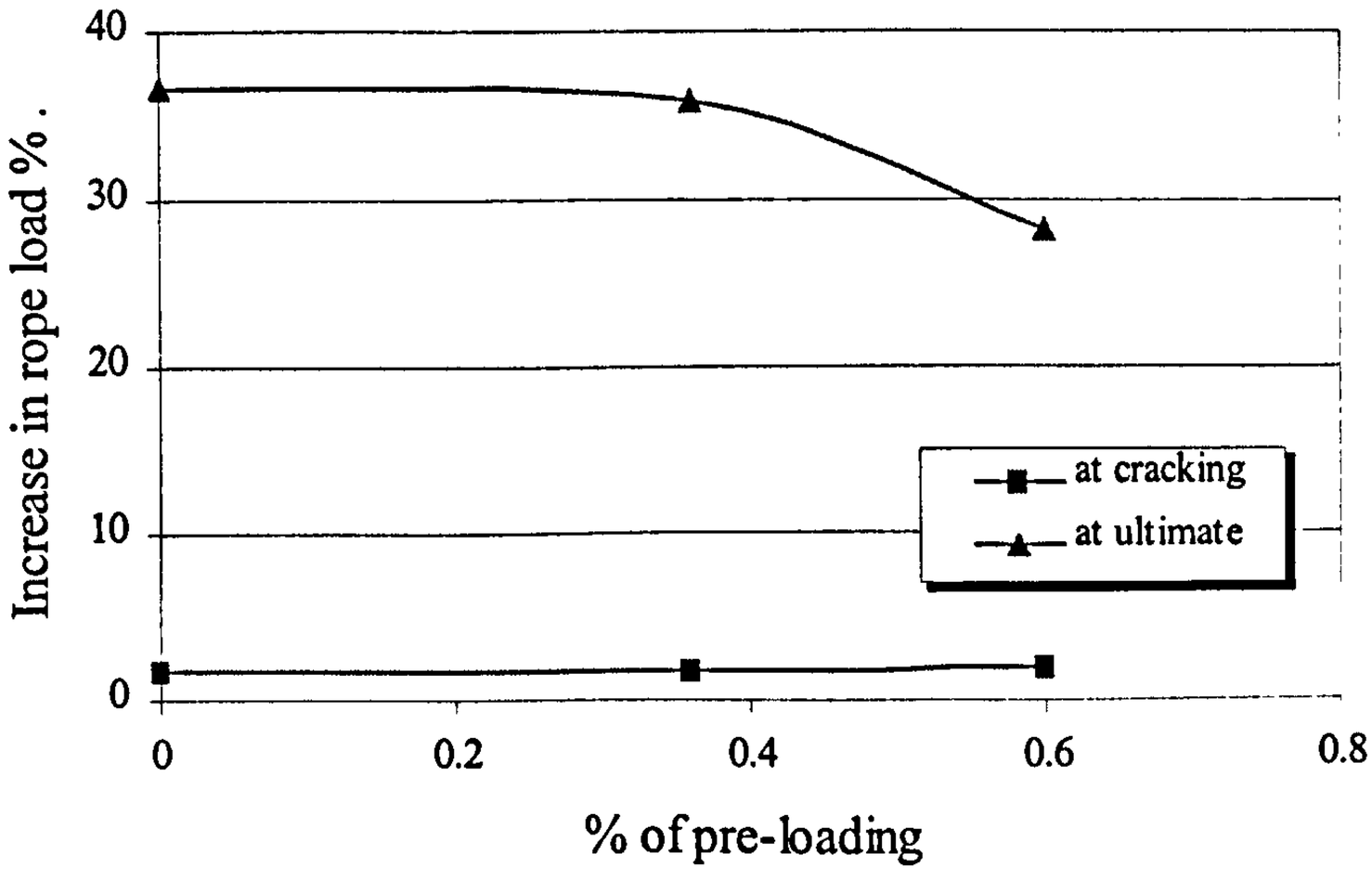

Figure (5.16): Relation between the increase in External prestressing force and ratio of pre-loading

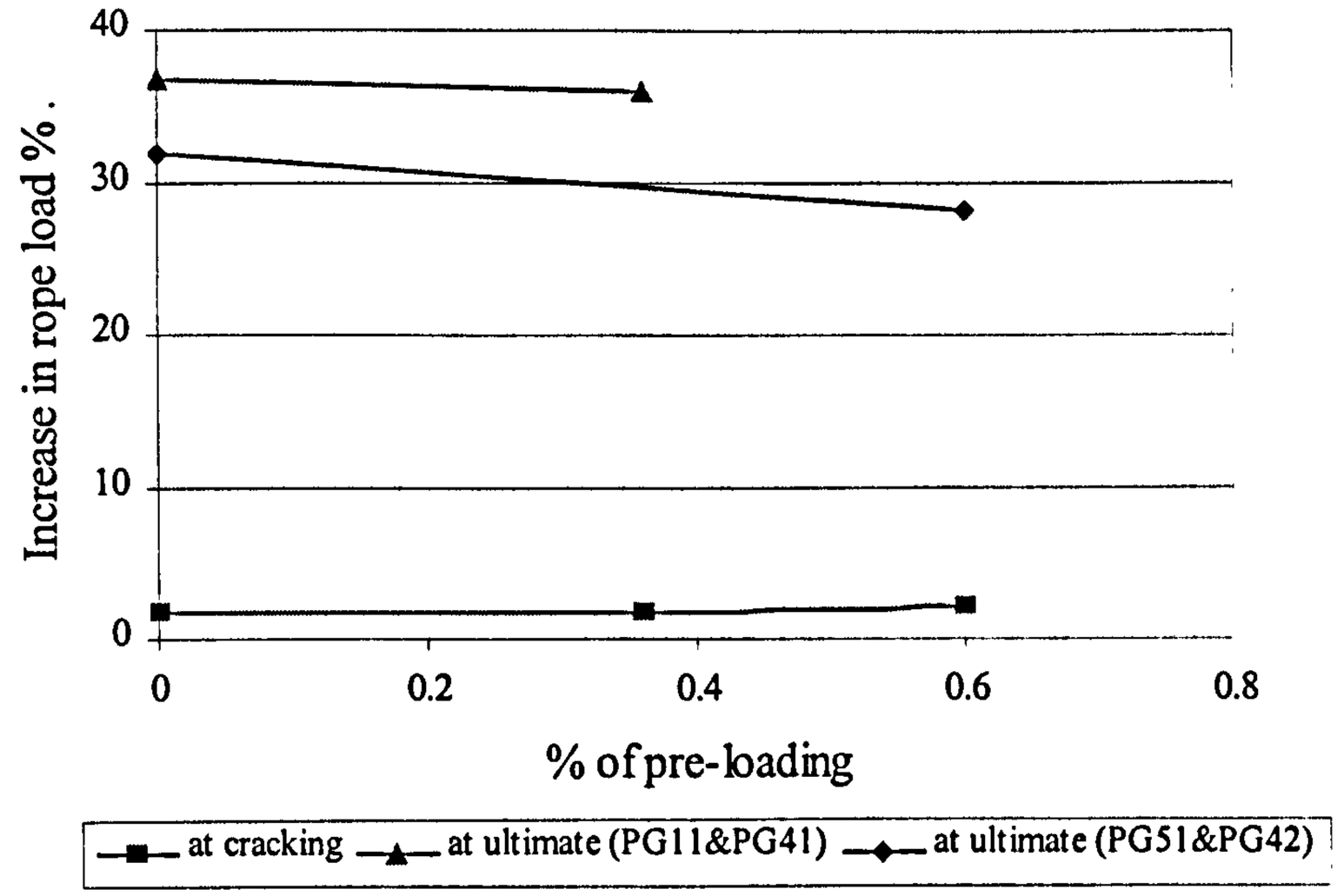

Figure (5.17): Relation between the increase in External prestressing force and ratio of pre-loading

5.3.4.5 Change in rope eccentricity

The relation between the losses of rope eccentricity and the pre-loading stage is shown in Figures (5.18 and 5.19). After strengthening, there was a slight difference in losses in eccentricity of all beams, due to the improvement in stiffness of the pre-cracked beams, while at ultimate the losses of the pre-cracked beams decreased due to its less ductile failure.

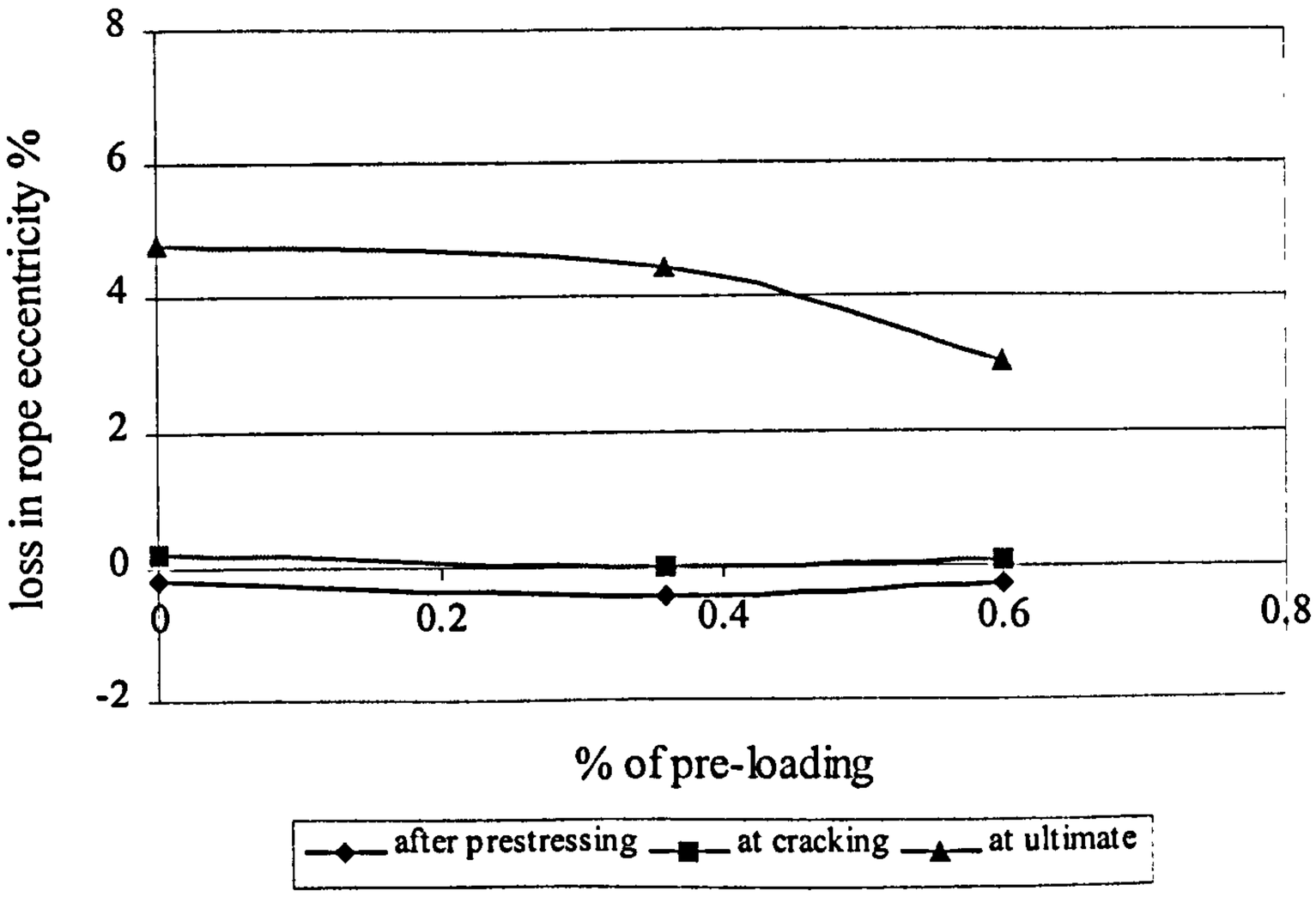

Figure (5.18): Relation between losses in Rope eccentricity and pre-loading ratio

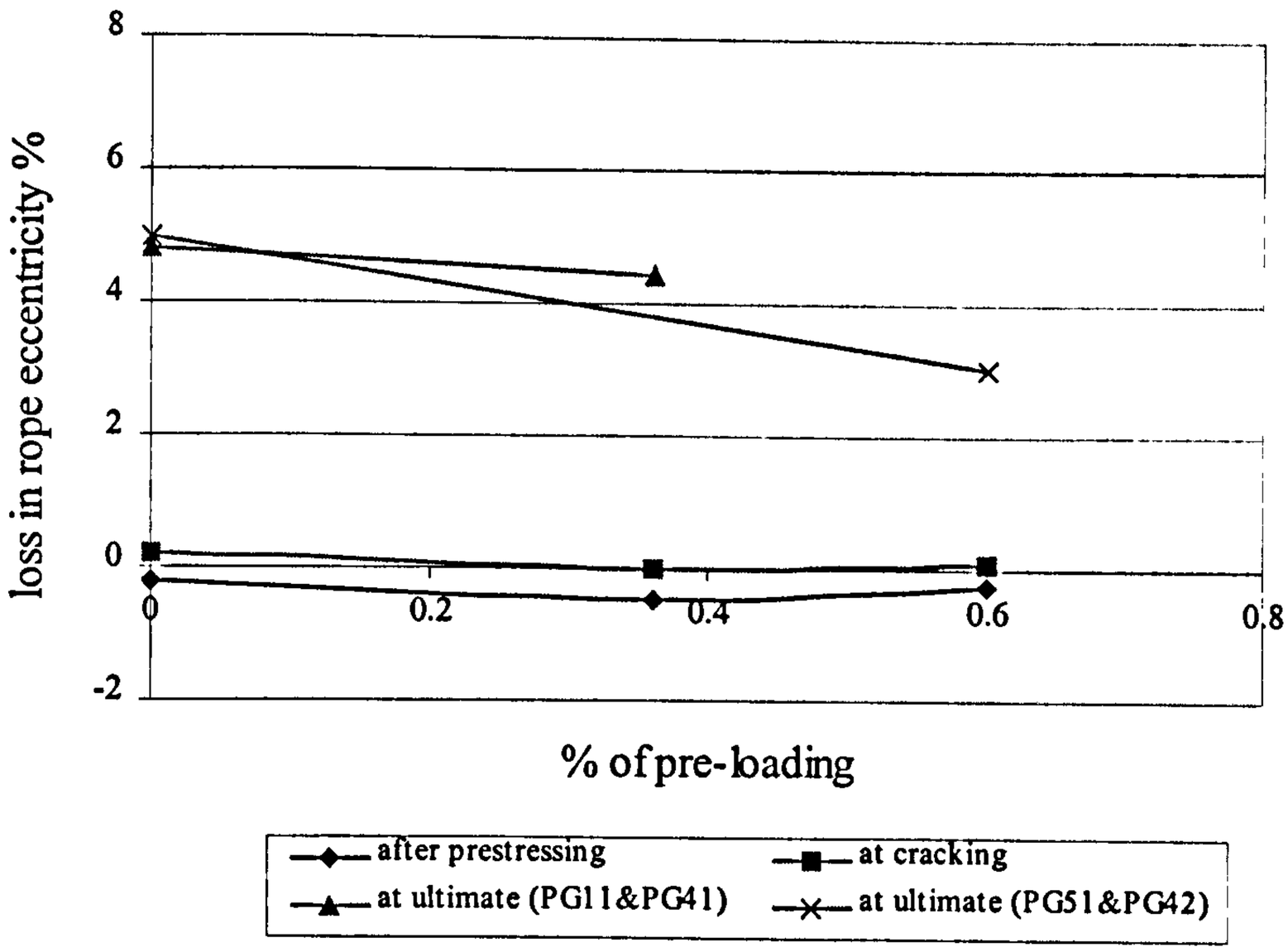

Figure (5.19): Relation between losses in Rope eccentricity and pre-loading ratio

5.3.5 Group 5 (Effect of Concrete Strength)

Increasing the concrete strength enabled the beam to resist higher compressive stresses and a higher ultimate moment, allowing more extensive yield of the steel before the concrete reached its ultimate capacity, and more ductile failure.

5.3.5.1 Cracking patterns

Flexural cracks on beam PG51 were less extensive than those on PG11 and PG52. This can be attributed to the fact that, concrete can resist more load before the deformation concentrates at a single crack location, as the concrete strength increases.

Cracks in the shear span appeared at almost the same load. This is probably because, while the difference in concrete strength is high, the variation in tensile strength was not great.

5.3.5.2 Load-deflection behaviour

The camber due to the external prestressing slightly decreased as the concrete strength increased. This is because Young's modulus increases (and hence stiffness) as the concrete strength increases. This also was observed after strengthening and

during loading, where the beam with the higher concrete strength (PG52) had a slightly lower deflection. However, beam PG51 had higher stiffness (and lower deflection) before cracking than beam PG11. This can be attributed to the effect of the time of loading on the Young's modulus ($E_{c(effective)}$ α 1/time loading) and as beam PG51 was tested after four days from the internal prestressing, so its effective Young's modulus was higher than that of beam PG11. Therefore, its stiffness was higher before cracking. After cracking it had almost the same stiffness. At failure PG52 had a higher deflection. This appears to be due to the higher strength concrete permitting more extensive yield of the steel before the concrete reached its ultimate capacity and hence, more rotation before failure. This agrees with remarks of *Skogman et al.* (1988) and tests carried out by *Pendyala et al.* (1996).

From Figure (5.20) it can be seen that, while the deflection at cracking was only slightly affected by the increase in concrete strength, it increased at ultimate as the concrete strength increased.

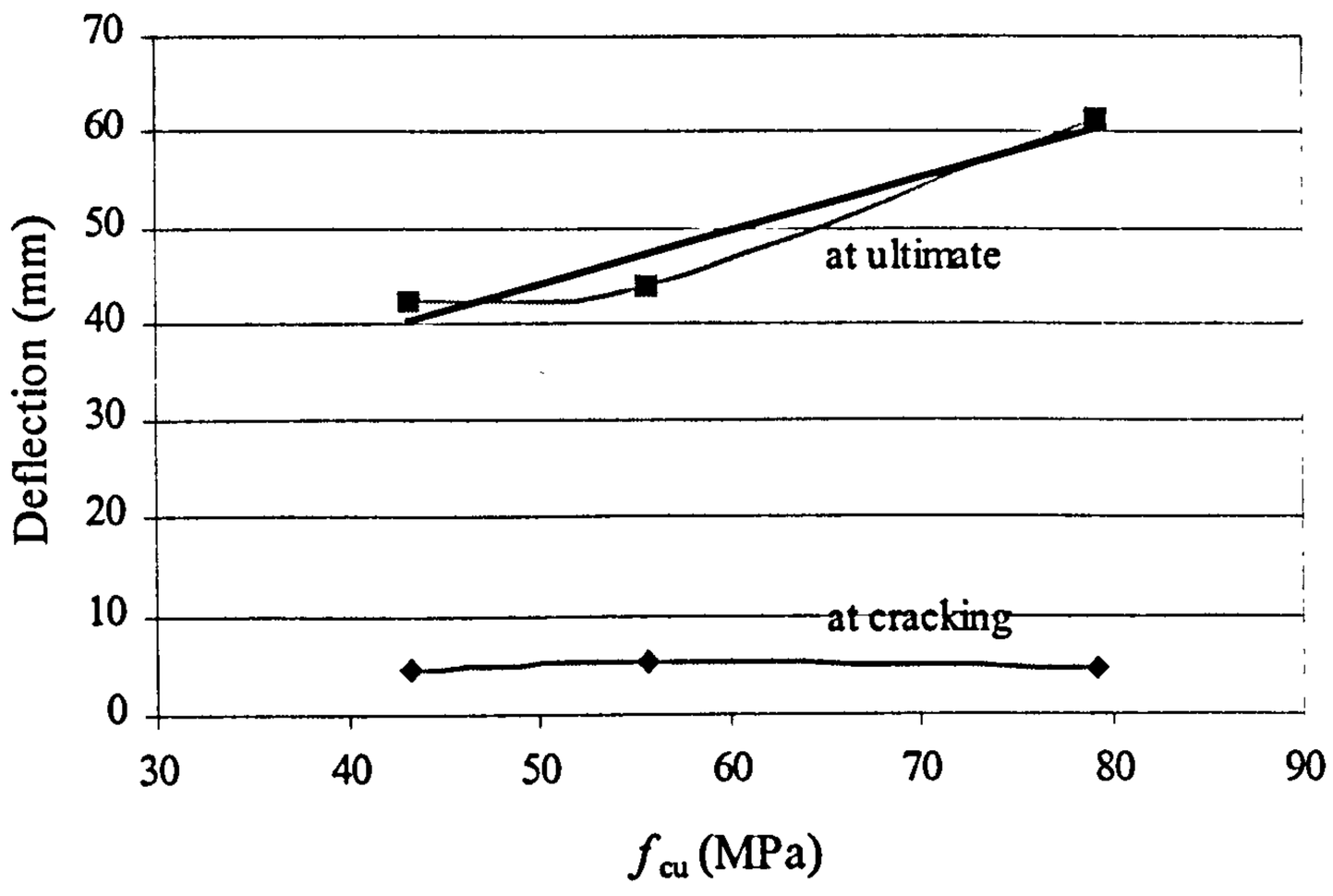

Figure (5.20): Deflection- Concrete strength relationship

5.3.5.3 Cracking and ultimate moments

The cracking moment was slightly affected by the variation in concrete strength as can be seen from Figure (5.21). The difference between the cracking moments of PG51 and PG52 (f_{cu}= 43.3 and 79.3 MPa) was 1.01 KN.m.

The ultimate moment is also marginally affected by the change in concrete strength. This is because failure of these beams started by yielding of steel bars and ended by concrete crushing due to the excessive compressive strain. So, increasing the concrete strength enables it to resist higher compressive stress, resulting in a slightly higher ultimate moment.

Finally, it can be said that an increase the ultimate moment can be more easily achieved by increasing the eccentricity of the external prestressing force than by increasing the concrete strength. An increase the eccentricity of PG11 by about 12.6% resulted in higher moment (25.23 KN.m that of PG31) than that achieved by increasing its concrete strength by about 42.1% (24.66 KN.m that of PG52).

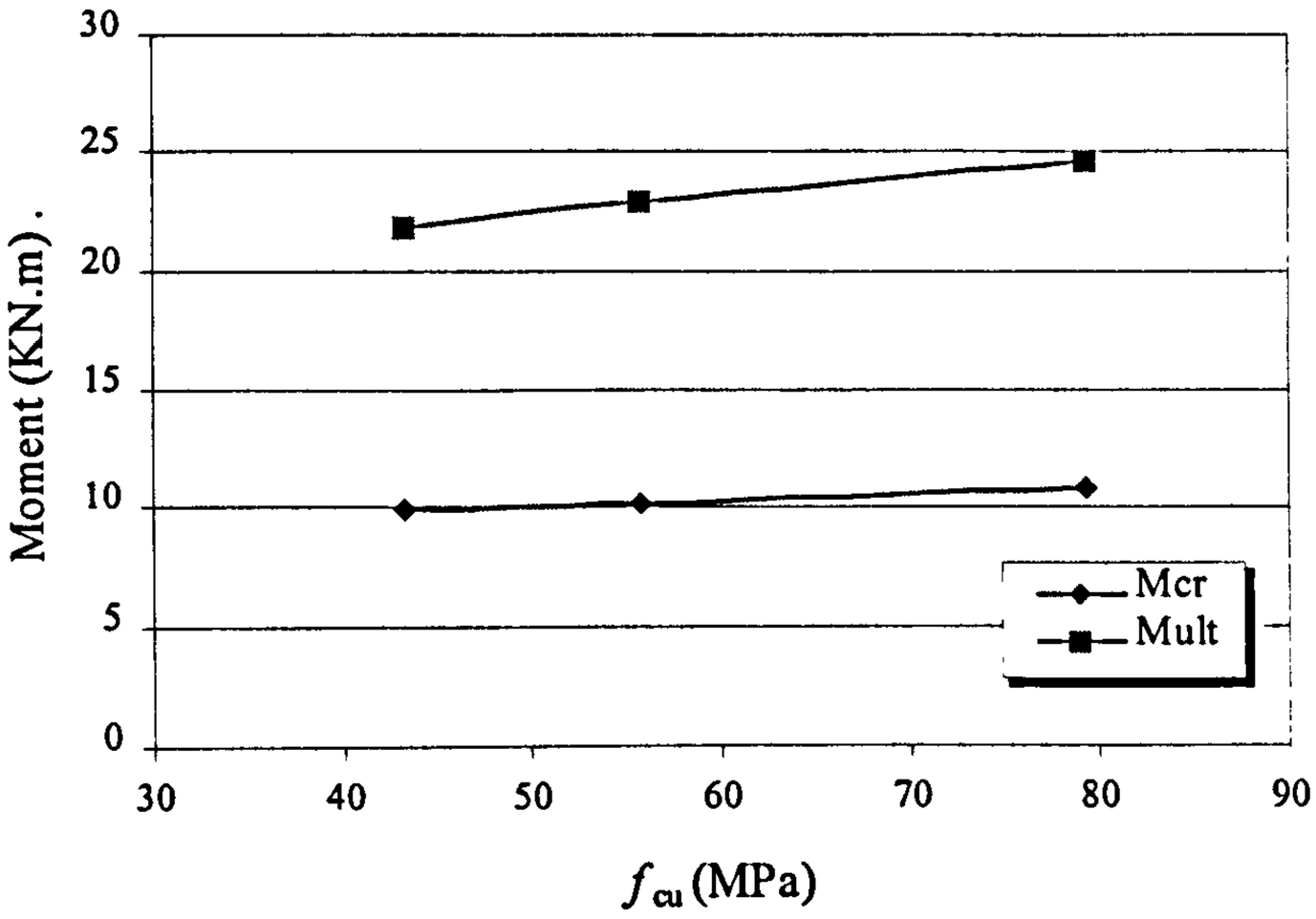

Figure (5. 21): Moment- Concrete strength relationship

5.3.5.4 External prestressing force (Parafil Rope Load)

At cracking there was a slight difference between the increase in external prestressing force of beams PG51, PG11 and PG52 as shown in Figure (5.22). At ultimate, however, the higher strength beams had a greater increase in the external prestressing force, due to its more ductile failure. So, comparing the effect of the concrete strength with the effect of the other factors considered in this study on the external prestressing force, it can be said that concrete strength is the main factor affecting the increase in external prestressing force at ultimate.

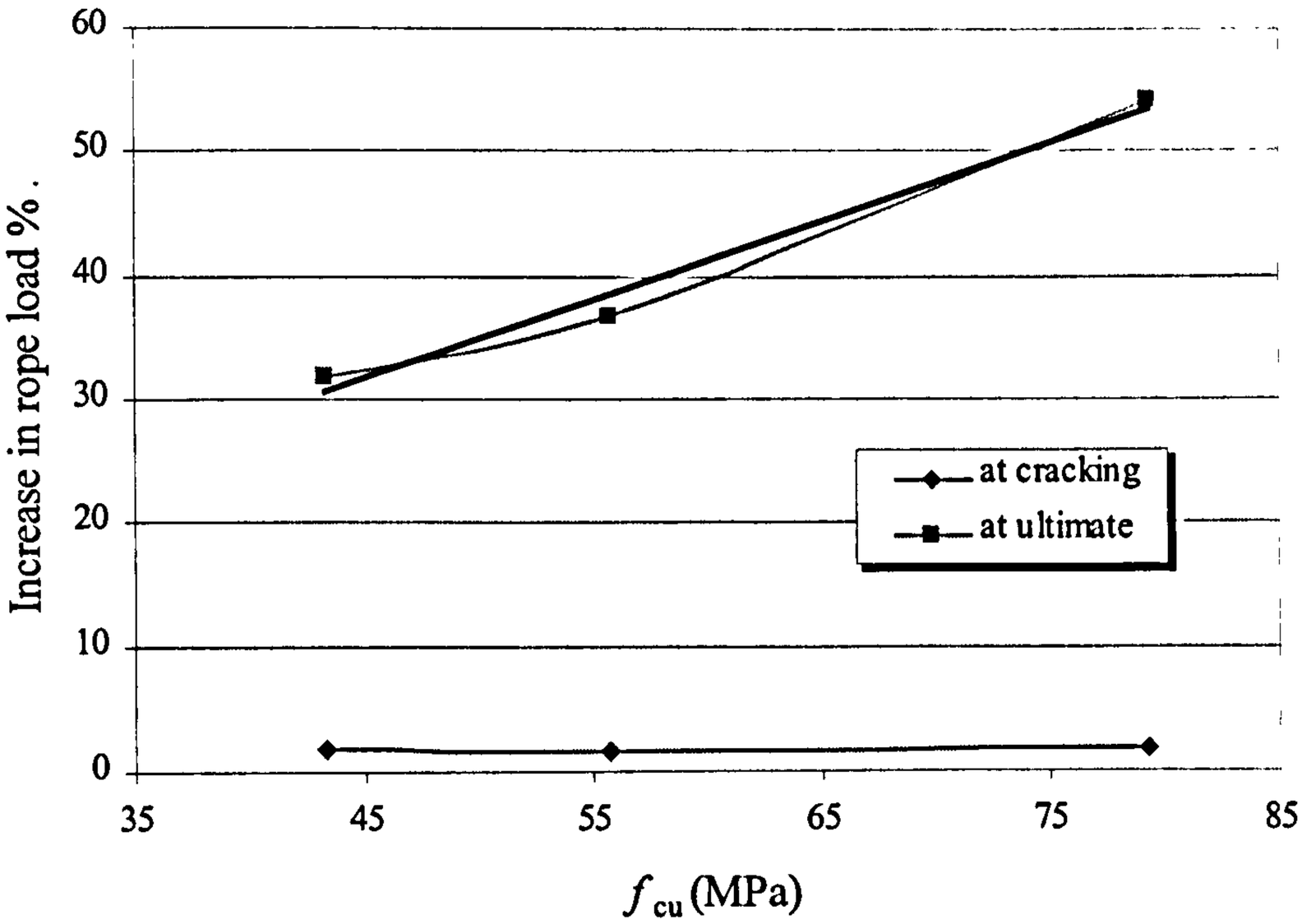

Figure (5.22): Relation between the increase in External prestressing force and the concrete strength

5.3.5.5 Change in rope eccentricity

From Figure (5.23) it can be seen that the ratio of loss in rope eccentricity at cracking is negligible, while at ultimate this ratio increased as the concrete strength increased due to the ductile failure of the higher strength concrete beam.

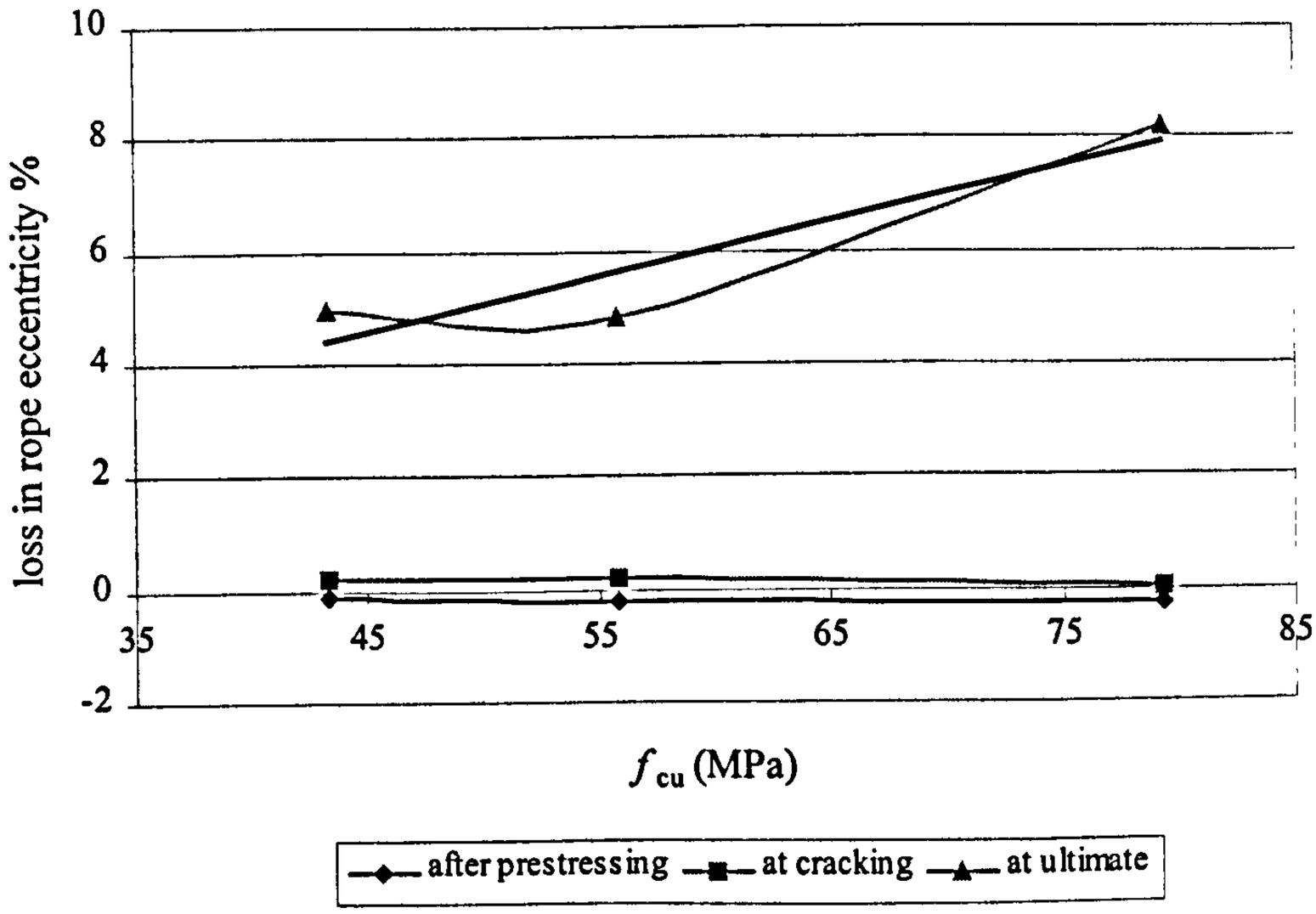

Figure (5.23): Relation between losses in Rope eccentricity and concrete strength

5.3.6 Group 6 (Effective Span/Depth Ratio (L/h))

Increased (L/h) ratio decreased the beam stiffness and hence increased the deflection and the loss in eccentricity of the external prestressing force. This decreased the prestressing moment especially at ultimate.

5.3.6.1 Cracking patterns

The cracks in the shear span were steeper as (L/h) decreased and appeared in the web first (PG62), because the member tended to behave as flexural member rather than shear flexural member as (L/h) ratio increased. This resulted in a decrease in the effect of the shear stress on the crack directions. This can be observed, as the first crack in the shear span of PG62 was a web shear crack while it was flexural cracks (at the bottom flange) on PG61.

5.3.6.2 Load-deflection behaviour

As expected during prestressing, camber increased as (L/h) ratio increased. This also was observed before and after cracking; beam had higher (L/h) ratio had higher deflection as it had less stiffness.

From Figure (5.24) it can be seen that, deflection at cracking, increased slightly as the (span/depth) ratio increased, while it increased significantly at ultimate. The deflection increased in both stages proportionally with (L/h).

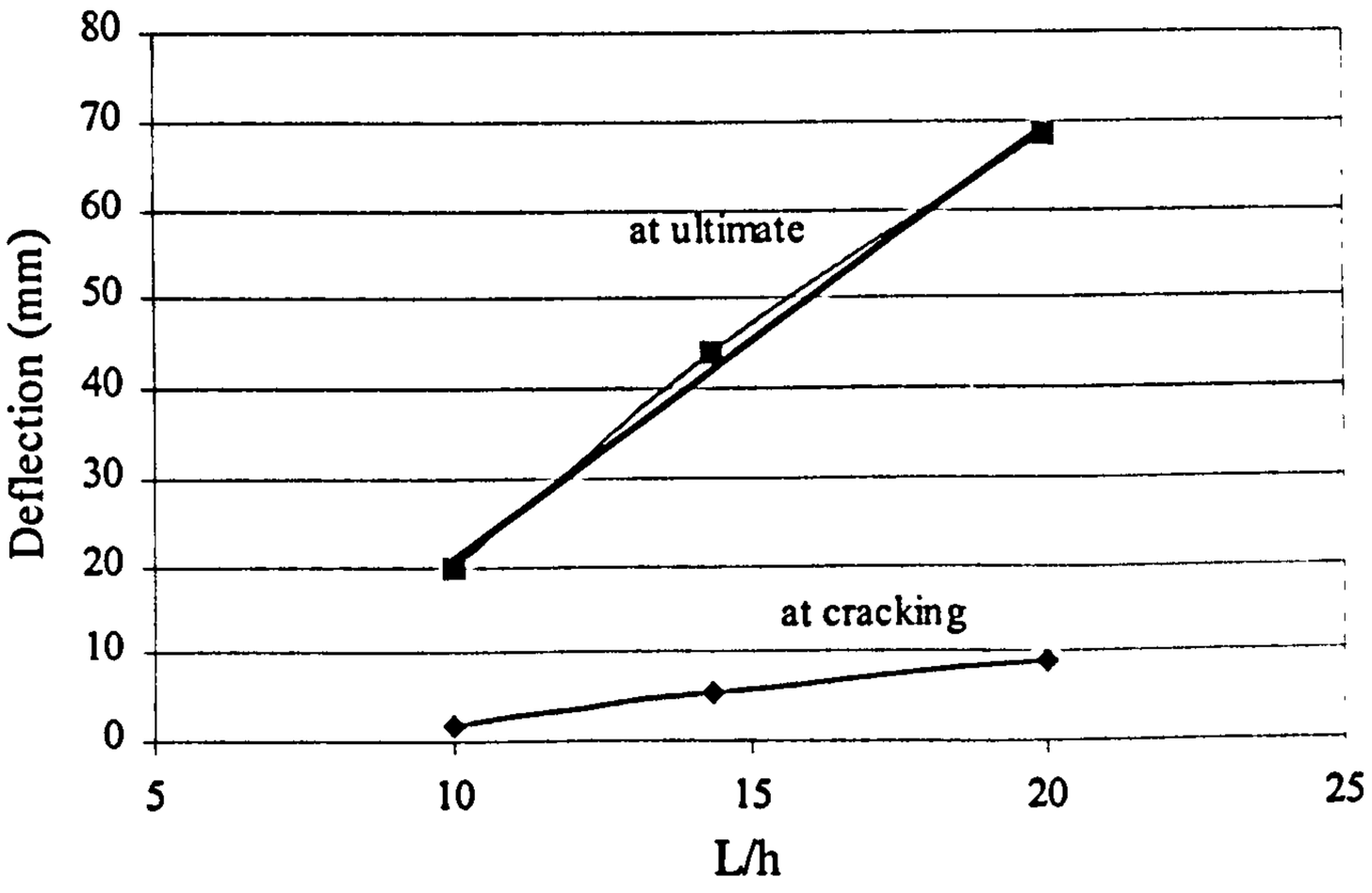

Figure (5.24): Deflection- (Span / depth) ratio relationship

5.3.6.3 Cracking and ultimate moments

Both the cracking and ultimate moments were slightly affected by the variation in (L/h) ratio with a trend to decrease as the (L/h) ratio increased, as seen in Figure (5.25), due to the reduction in the prestressing moment. However, the effect of (L/h) ratio within the range taken in this investigation on the cracking and ultimate moments is small, as the ratio of the difference between the ultimate moments was less than 7%.

Beam PG11 had almost the same ultimate moment as beam PG62 because its concrete strength was higher, resulting in an increased ultimate moment, as discussed before.

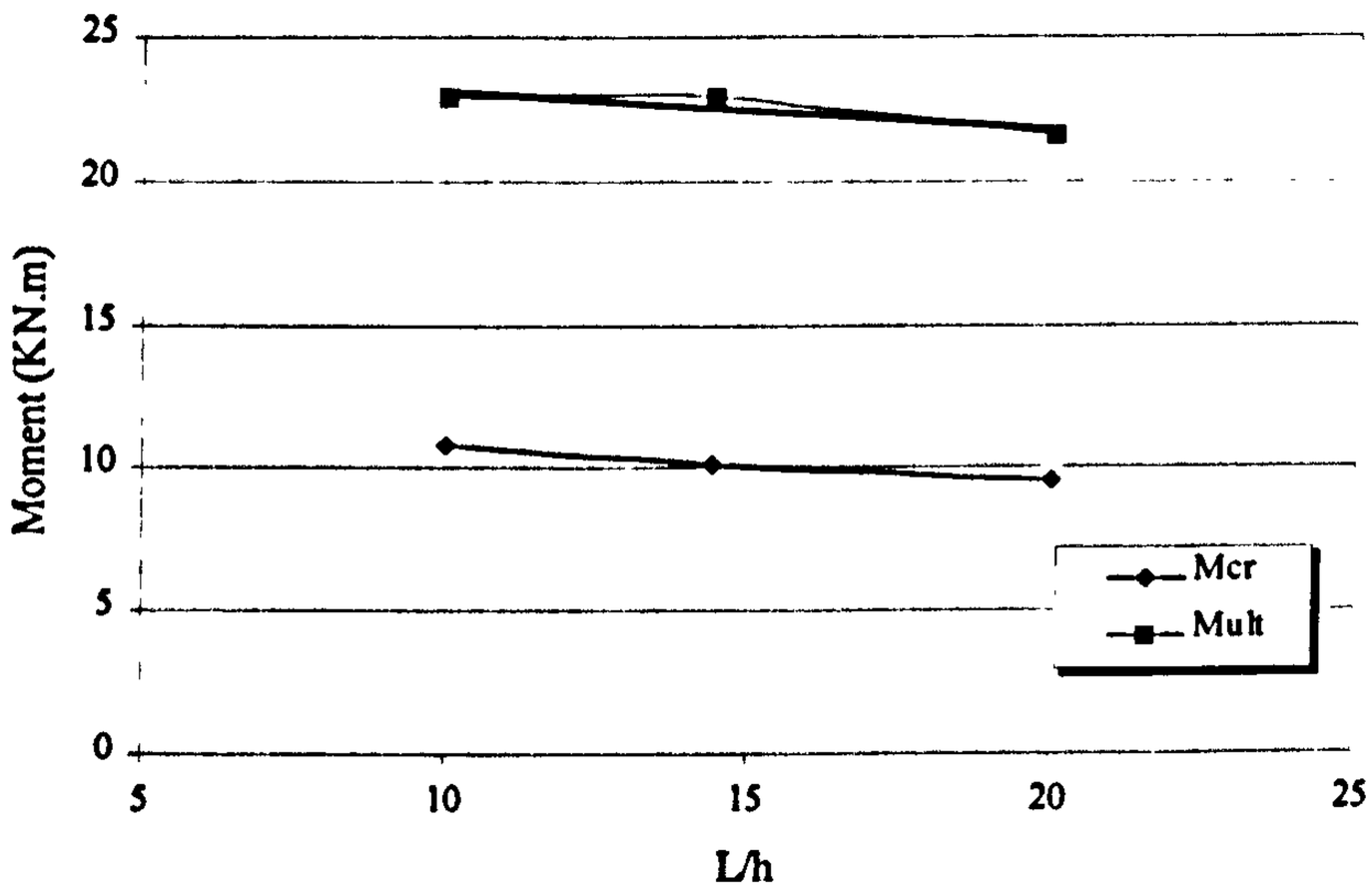

Figure (5. 25): Moment - (Span / depth) ratio relationship

5.3.6.4 External prestressing force (Parafil Rope Load)

Before cracking the relation between moment and external prestressing force for all beams was almost the same and the differences between the increases in external prestressing force were negligible, as shown in Figure (5.26), due to the small deflection at this stage.

After cracking there was a rapid increase in the external prestressing force in all beams, due to the reduction in stiffness of the cracked beam and increase in accompanied deflection at this stage. During the working and ultimate stages, the difference between the increase in external prestressing force of all beams was small.

Thus the increase in external prestressing force is only slightly affected by (span/depth) ratio between (span/depth) ratios of 10 and 20.

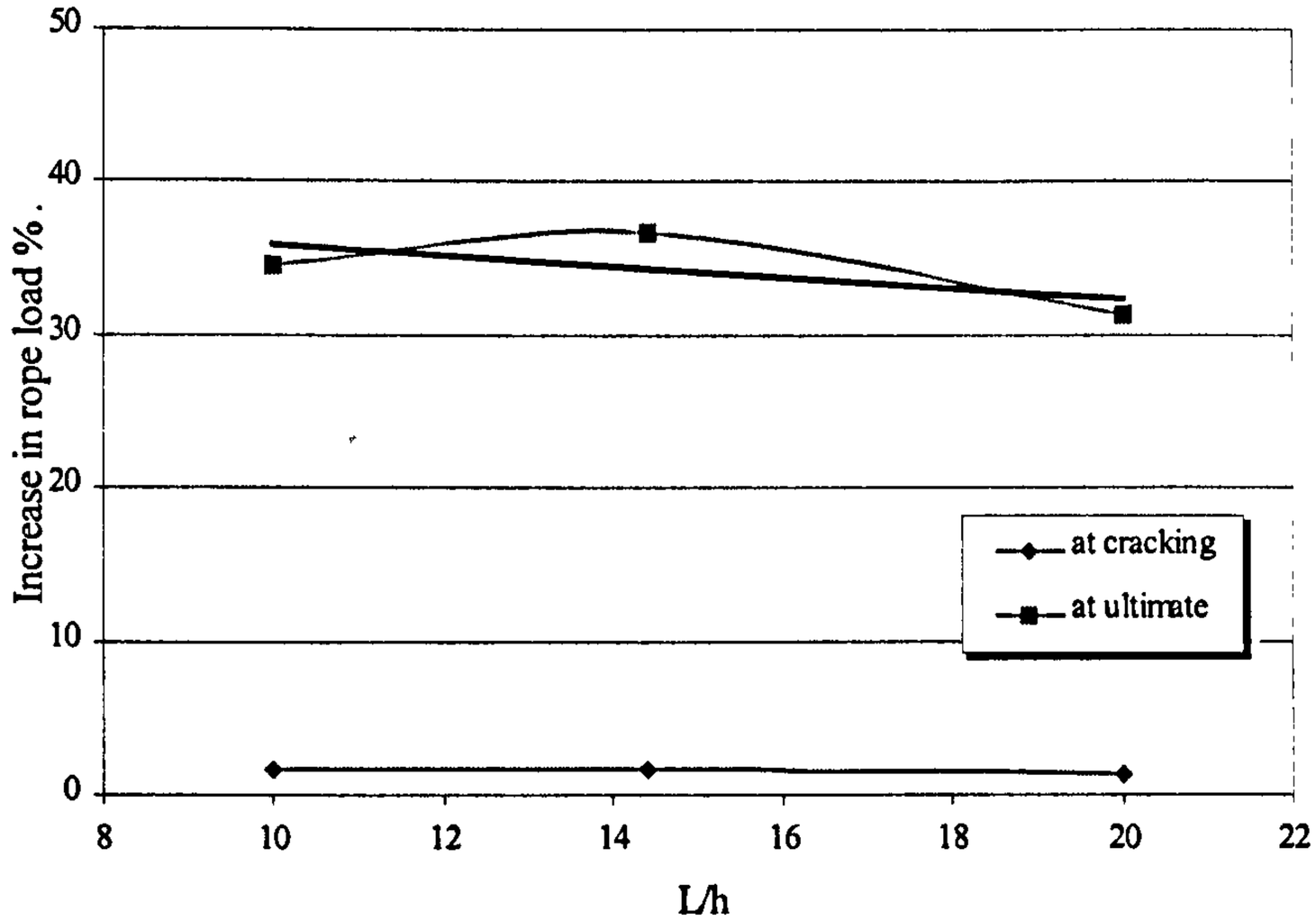

Figure (5.26): Relation between the increase in External prestressing force and (Span/depth) ratio

5.3.6.5 Change in rope eccentricity

The loss in eccentricity of the external prestressing force varied slightly before cracking with (L/h) ratio. However at ultimate the beam with a higher (L/h) ratio had higher losses due to its higher deflection and the longer distance between the deviators. The loss in rope eccentricity at ultimate seems to be linearly proportional with (L/h) ratio as can be seen in Figure (5.27).

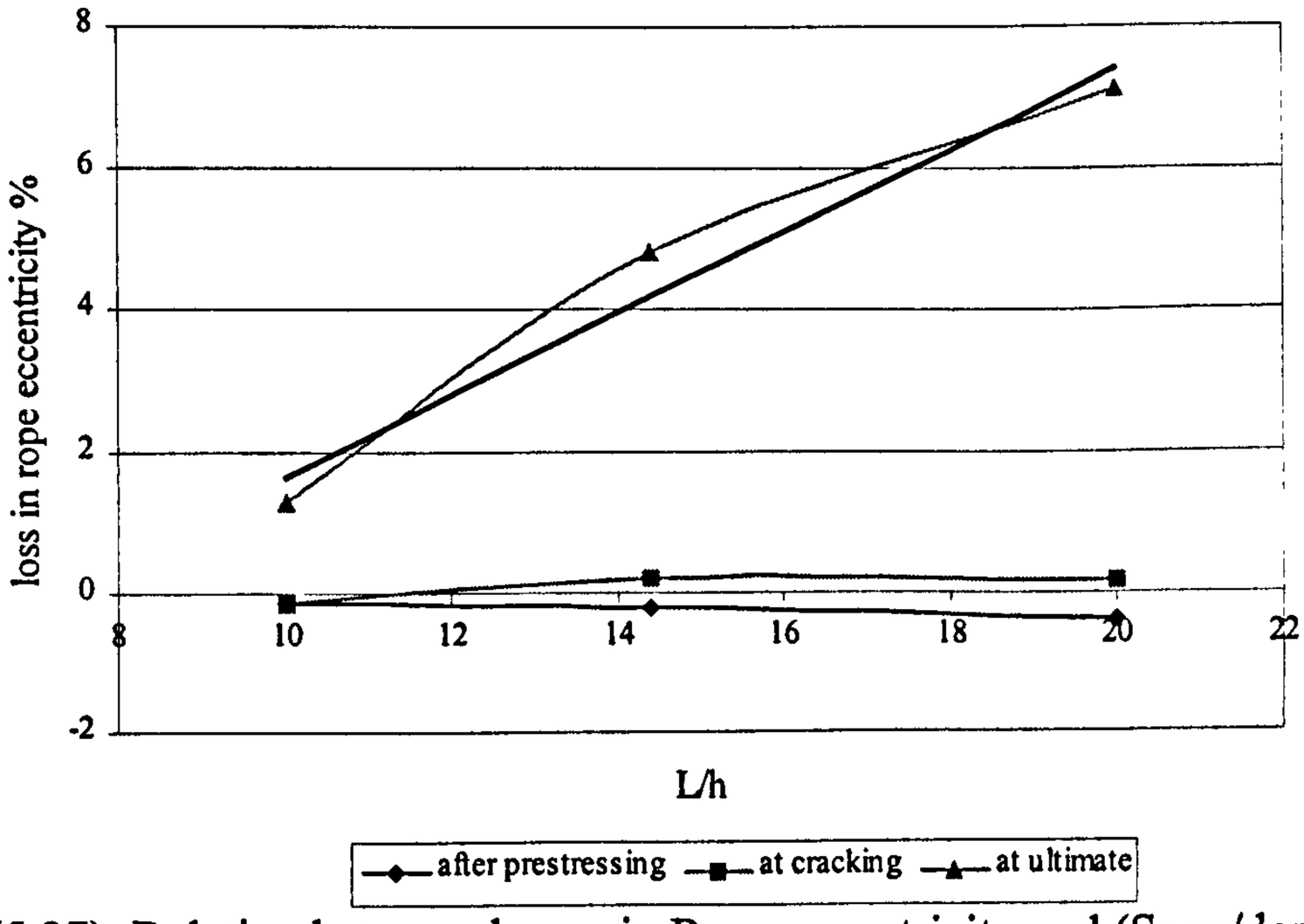

Figure (5.27): Relation between losses in Rope eccentricity and (Span/depth) ratio

5.3.7 Relation Between The External Prestressing Force and Other Parameters

5.3.7.1 Relation between external prestressing force and deflection

The increase in external prestressing force (as stated before) depends on deformation of the member. Hence the change in external prestressing force is expected to be proportional to the deflection. Figures (5.28–5.31) show the relation between deflection and external prestressing force up to failure. These Figures show a bilinear relation between deflection and external prestressing force for all beams, before and after cracking. So, it can be said that, the factors affecting the deflection affect the external prestressing force in a similar manner.

Before cracking, the slope of the relation between deflection and external prestressing force was higher than that after cracking and the increase in deflection was accompanied by a relatively small increase in external prestressing force. After cracking, the external prestressing force rapidly increased as the deflection increased and the relation between deflection and external prestressing force was almost linear up to failure.

The main factors as shown in Figures (5.28–5.31), influencing the relation between deflection and external prestressing force are:

- Position of the Deviator (one deviator at the mid-span or two deviators at the third span).
- Eccentricity of the external prestressing force.

Although Figure (5.33) gives an impression that the (span/depth) ratio has a major effect on the relation between deflection and external prestressing force, however, by dividing deflection by (L^2) where L is the span, the relation between (deflection/ L^2) and external prestressing force seems to be almost the same for all beams in group G6 as shown in Figure (5.34). So, the effect of (span/depth) ratio on the relation between deflection and external prestressing force can be neglected if the relation between the (deflection/L^2) and external prestressing force is used instead of deflection and external prestressing force.

Also, the initial value of the external prestressing force, precracking stage and concrete strength seems to have only a slight effect on the slope of the relation between deflection and external prestressing force.

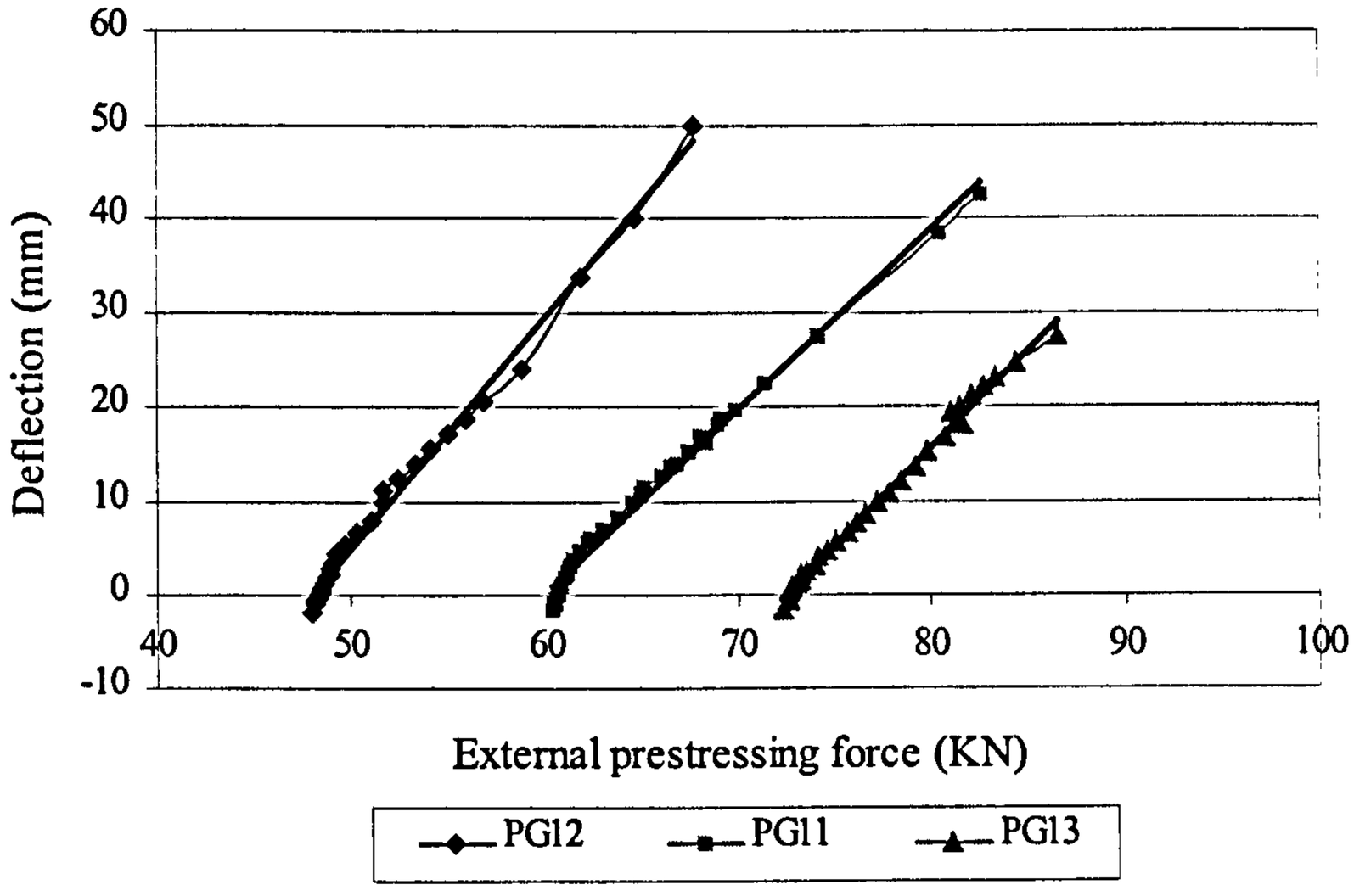

Figure (5.28): Relation between deflection and increase in external prestressing force for group G1

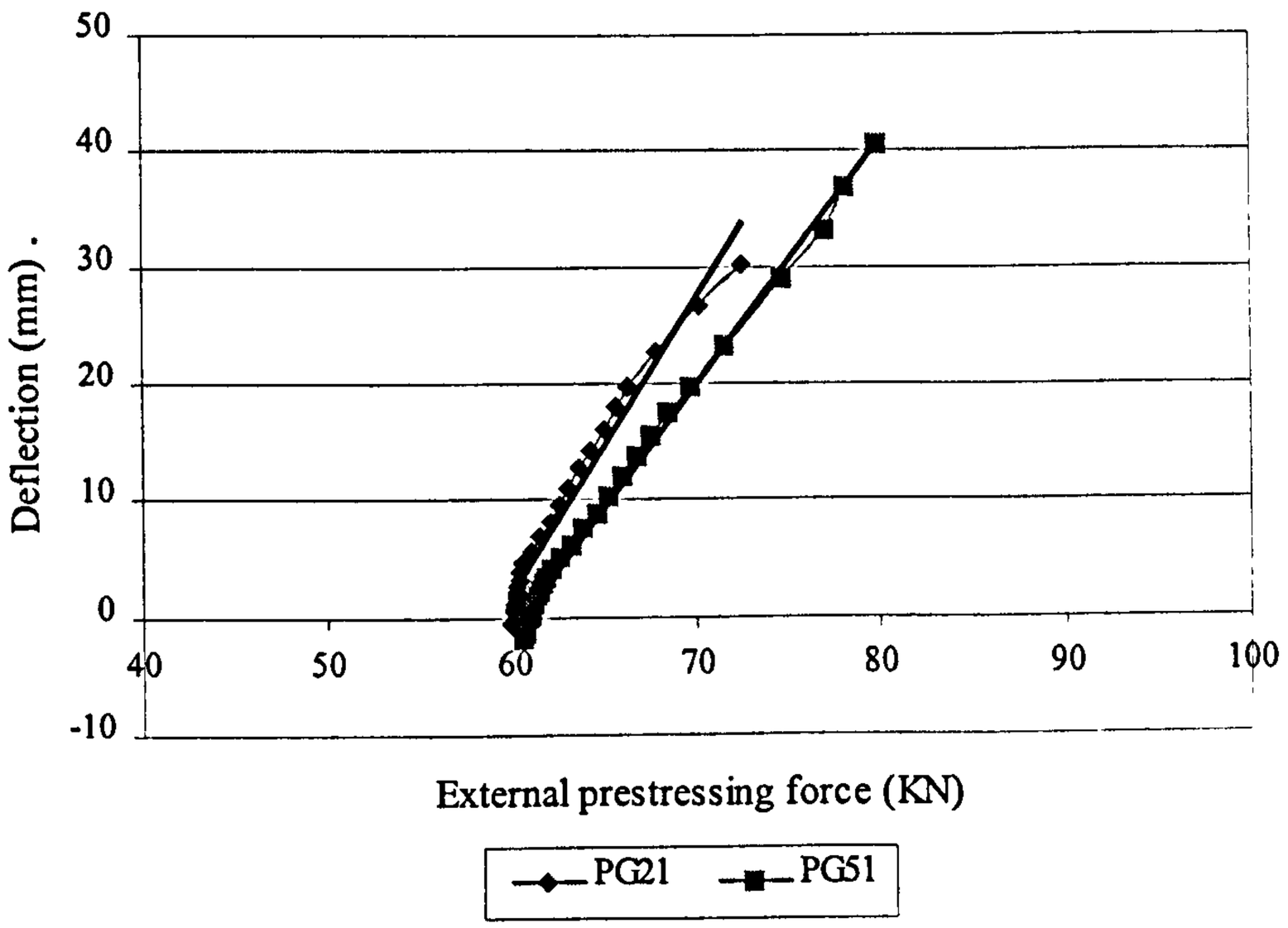

Figure (5.29): Relation between deflection and increase in external prestressing force for group G2

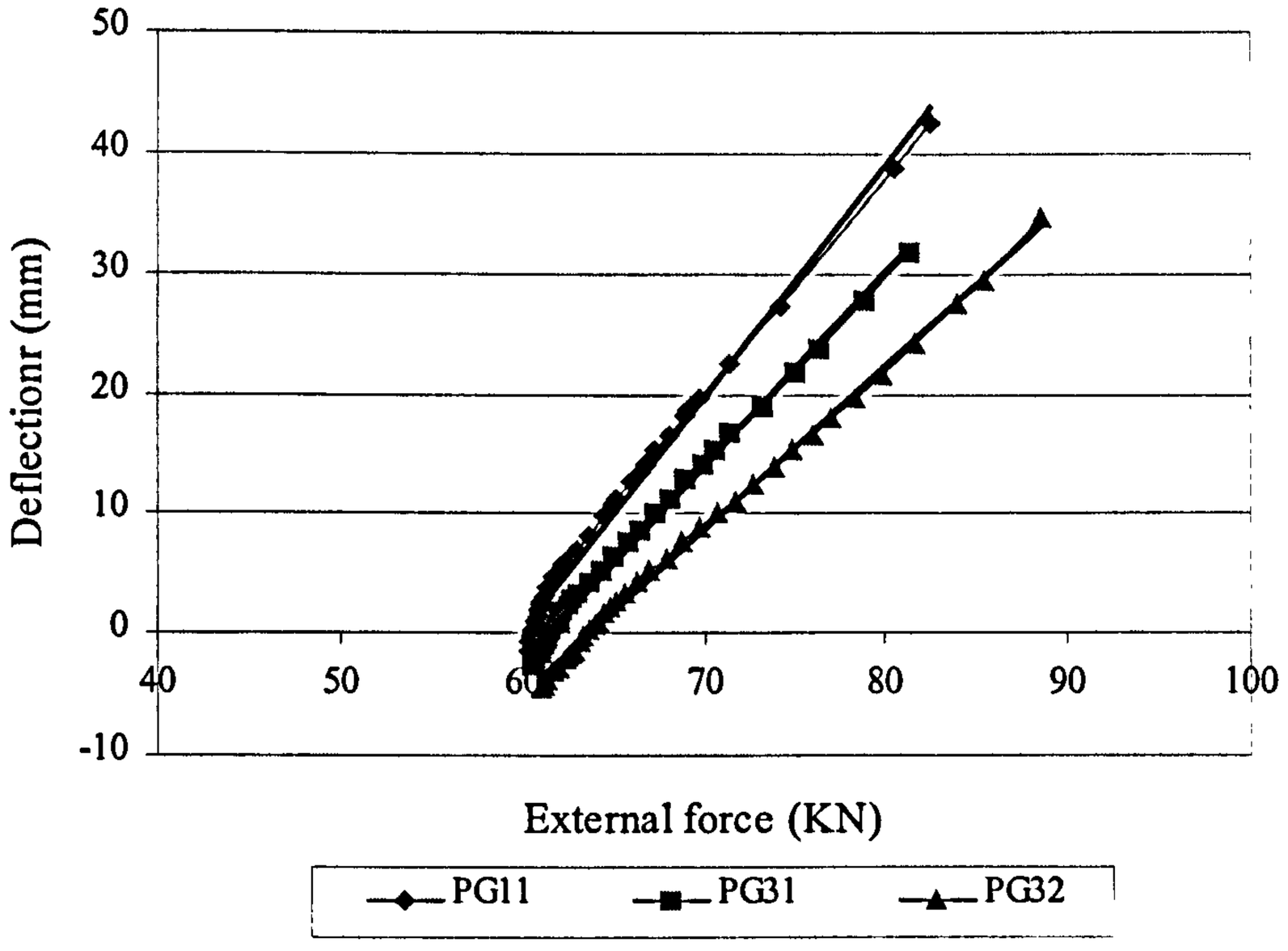

Figure (5.30): Relation between deflection and increase in external prestressing force for group G3

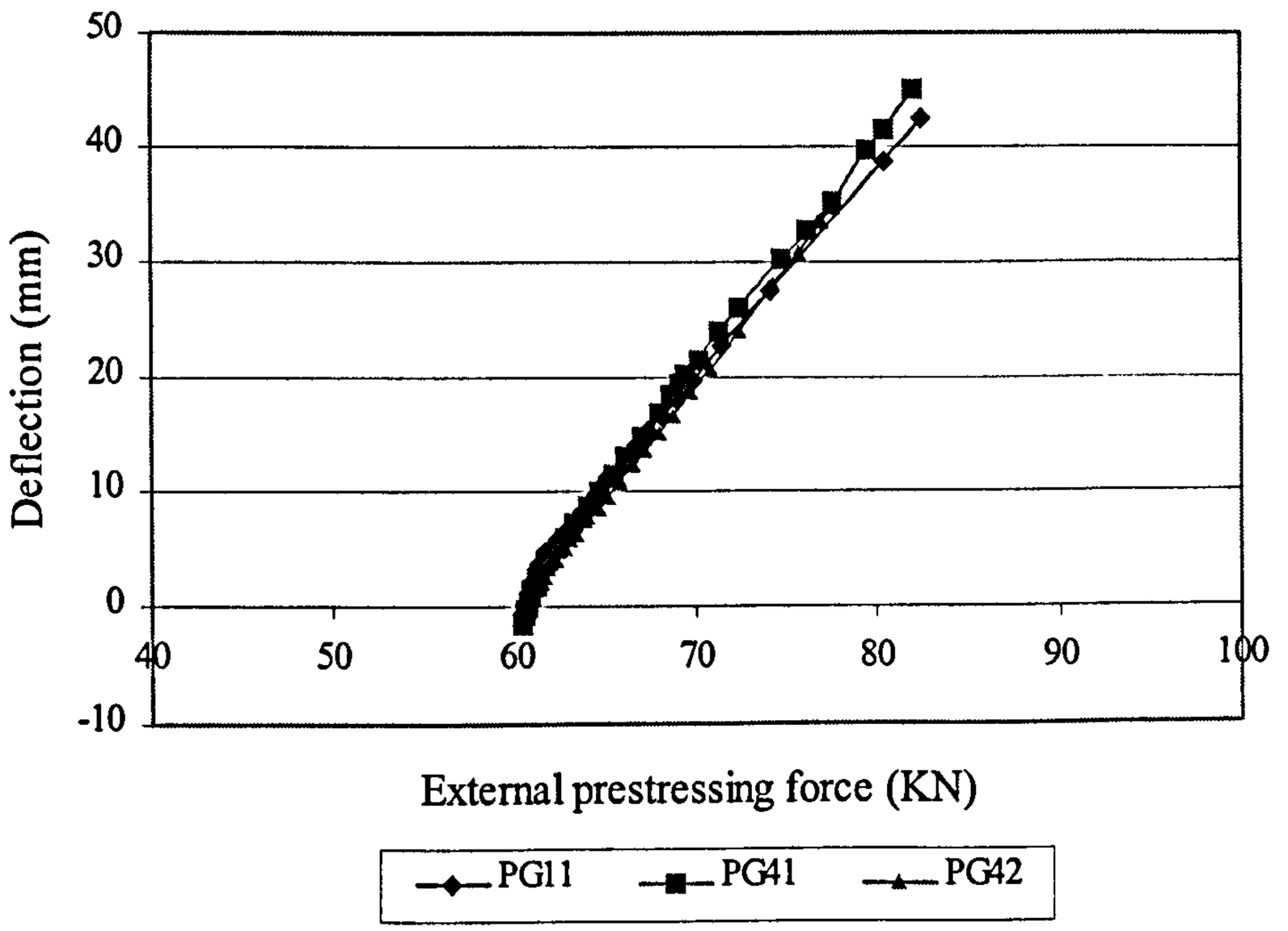

Figure (5.31): Relation between deflection and increase in external prestressing force for group G4

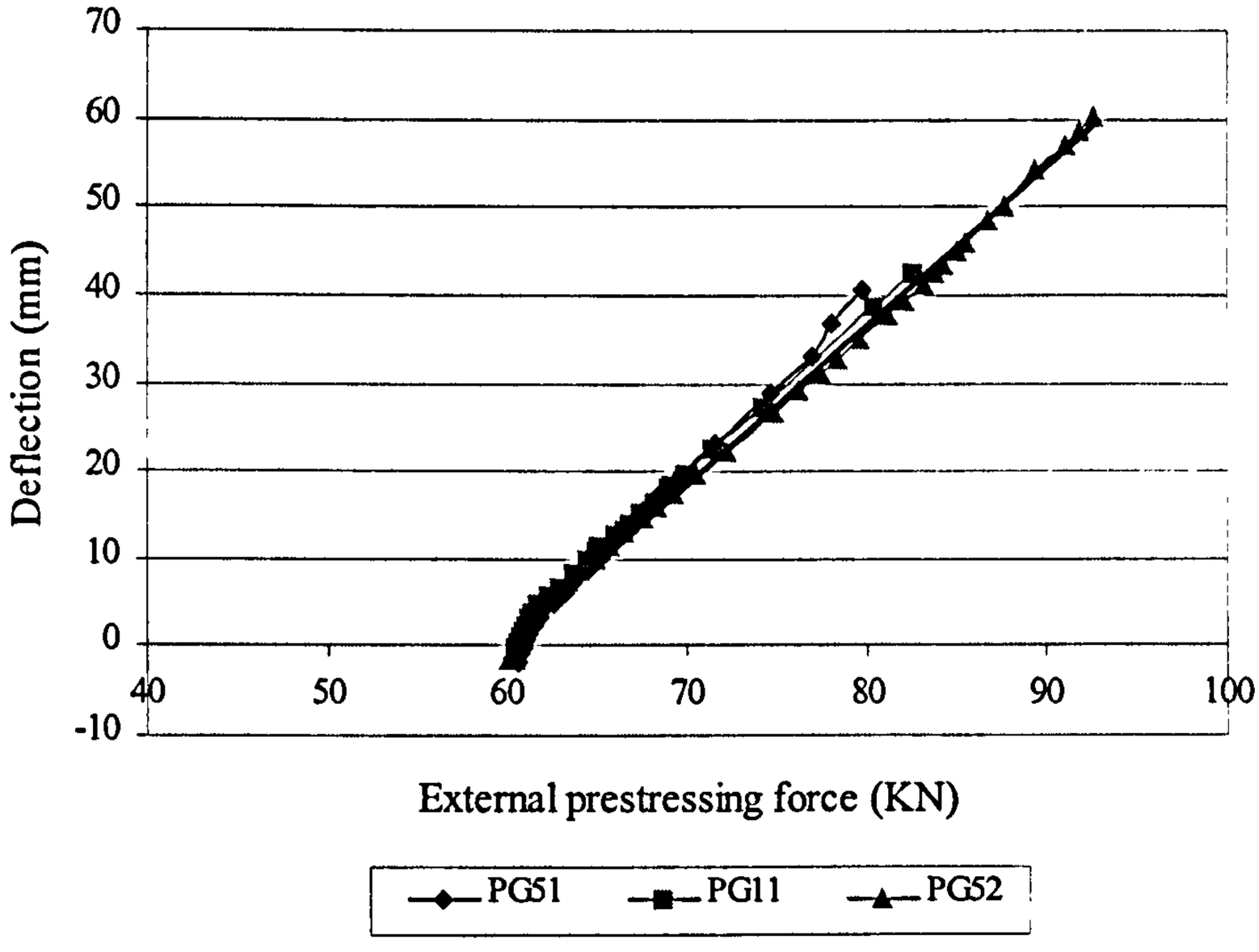

Figure (5.32): Relation between deflection and increase in external prestressing force for group G5

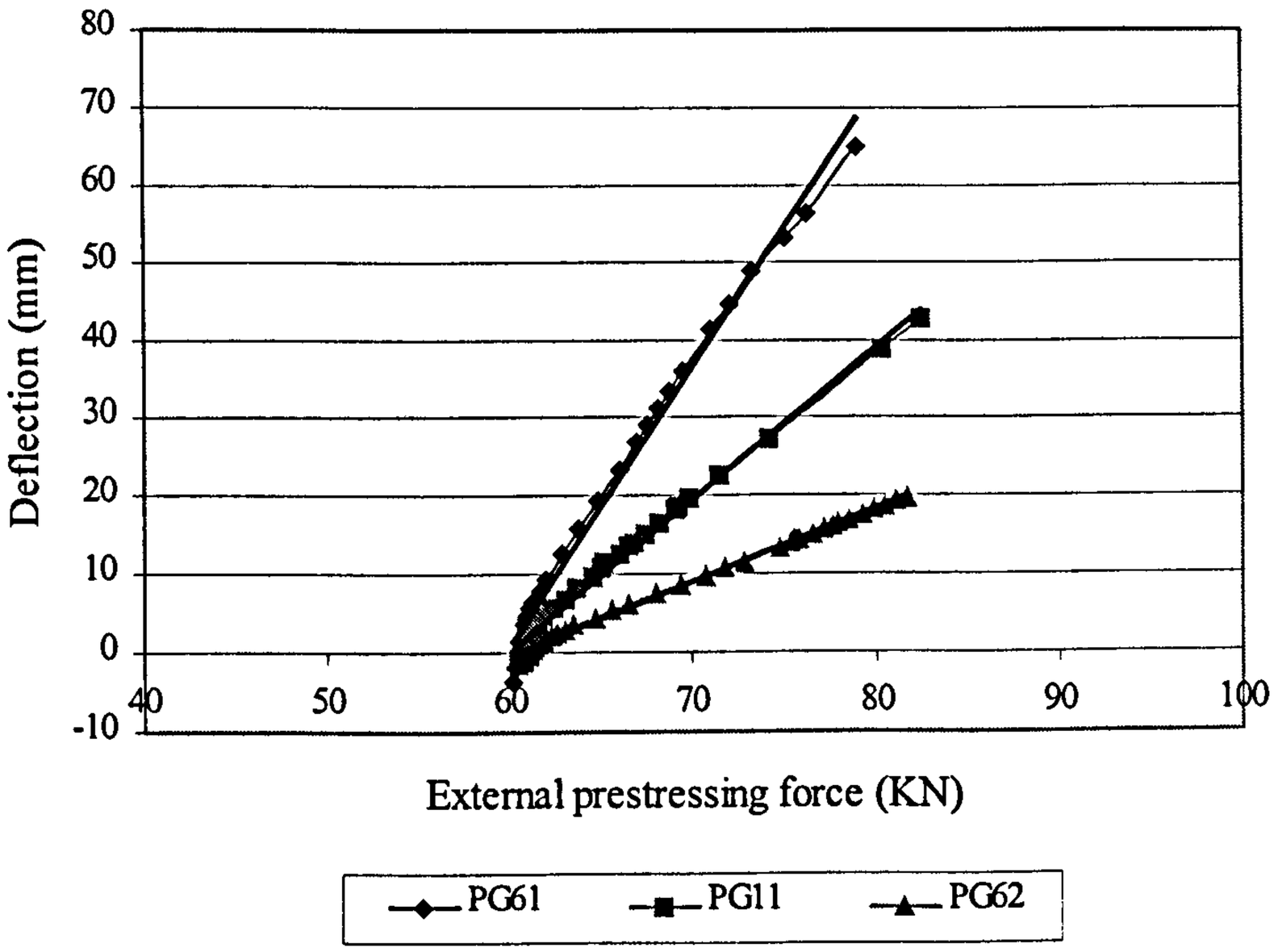

Figure (5.33): Relation between deflection and increase in external prestressing force for group G6

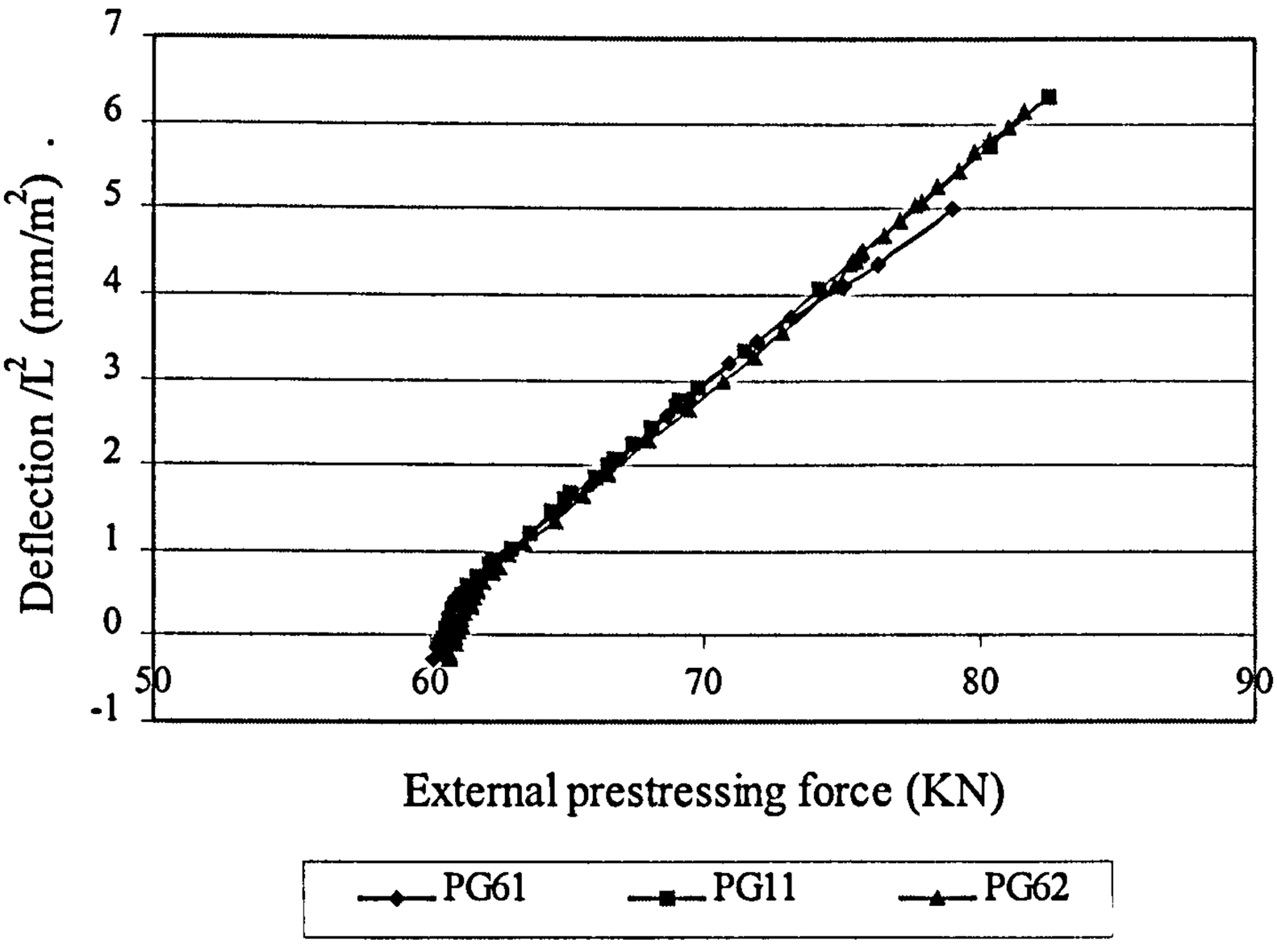

Figure (5.34): Relation between (deflection/ L^2) and increase in external prestressing force for group G6

Following the previous discussion, the relation between (deflection/L^2) and ratio of the increase in external prestressing force for all strengthened beams during loading was drawn as shown in Figure (5.35). From it, the following regression equation was obtained

$$\frac{\Delta_i}{L^2} = 16.21\left(\frac{P_i}{P_o}\right) - 16.183 \qquad 5.1$$

Where Δ_i is the deflection at any load.

P_i is the external prestressing force corresponding to deflection (Δ_i)

P_o is the effective external prestressing force

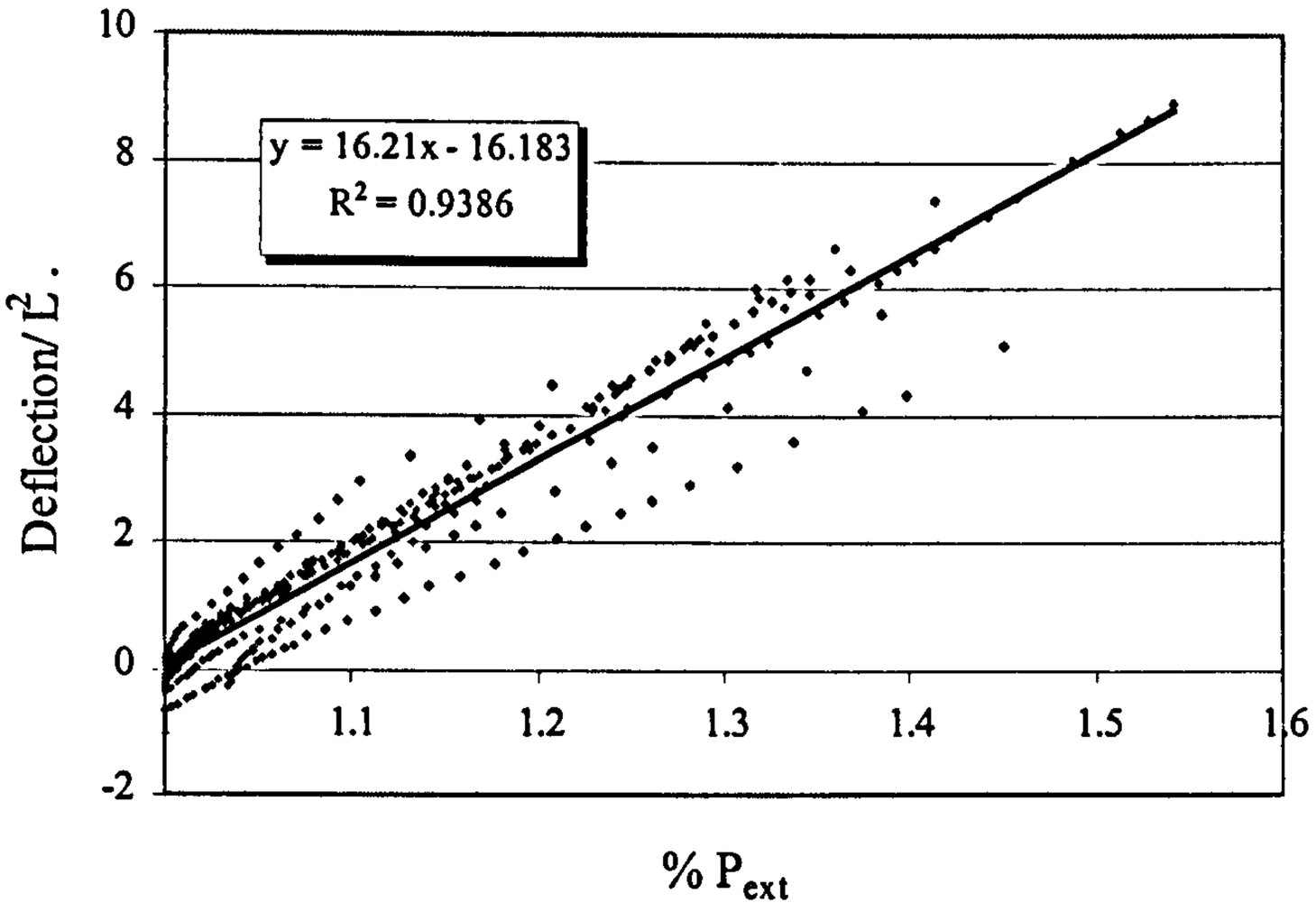

Figure (5.35): Relation between (deflection/L^2) and ratio of increase in external prestressing force for all beams

To get more accurate relation between (deflection/L^2) and ratio of the increase in external prestressing force after cracking to the intial prestressing force, it was decided to limit this relation to beams with two deviators at the third span and eccentricity less than the section height. Then a new regression equation, to describe this relation after cracking, was obtained

$$\frac{\Delta_i}{L^2} = 16.27\left(\frac{P_i}{P_o}\right) - 16.077 \qquad e/h \leq 1.0 \qquad 5.2$$

To check the accuracy of equation 5.2 to calculate the external prestressing force after cracking, the deflections of the beams were calculated using the *Branson & Trost* method (1982) after modification as will be discussed in chapter six (Theoretical Analysis). The ratio of the increase in external prestressing force was then calculated from equation 5.2. the relation between the theoretical and the actual ratios of the increase in external prestressing force is shown in Figure (5.37). A good correlation between the theoretical and the actual values can be seen.

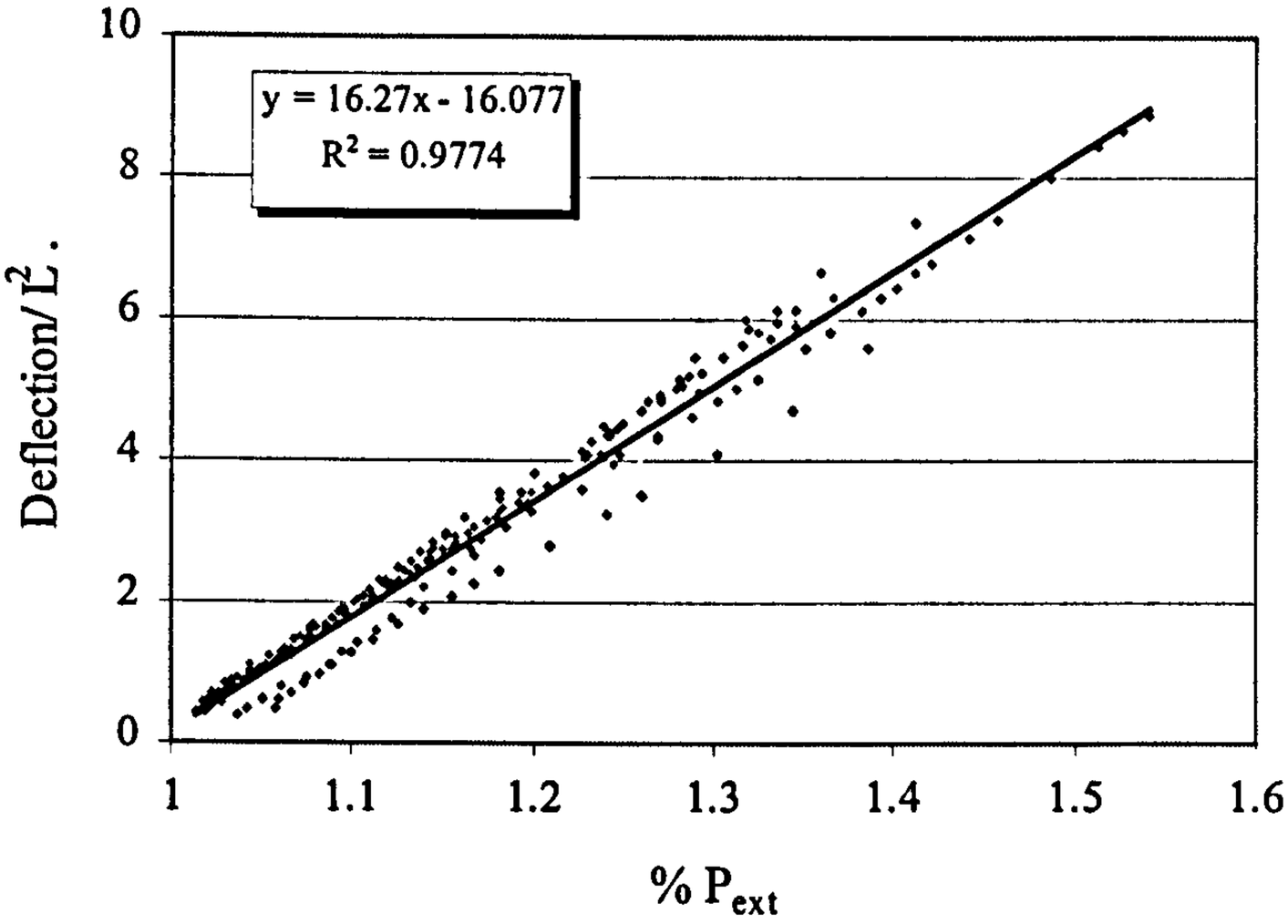

Figure (5.36): Improved relation between (deflection/L^2) and ratio of increase in external prestressing force

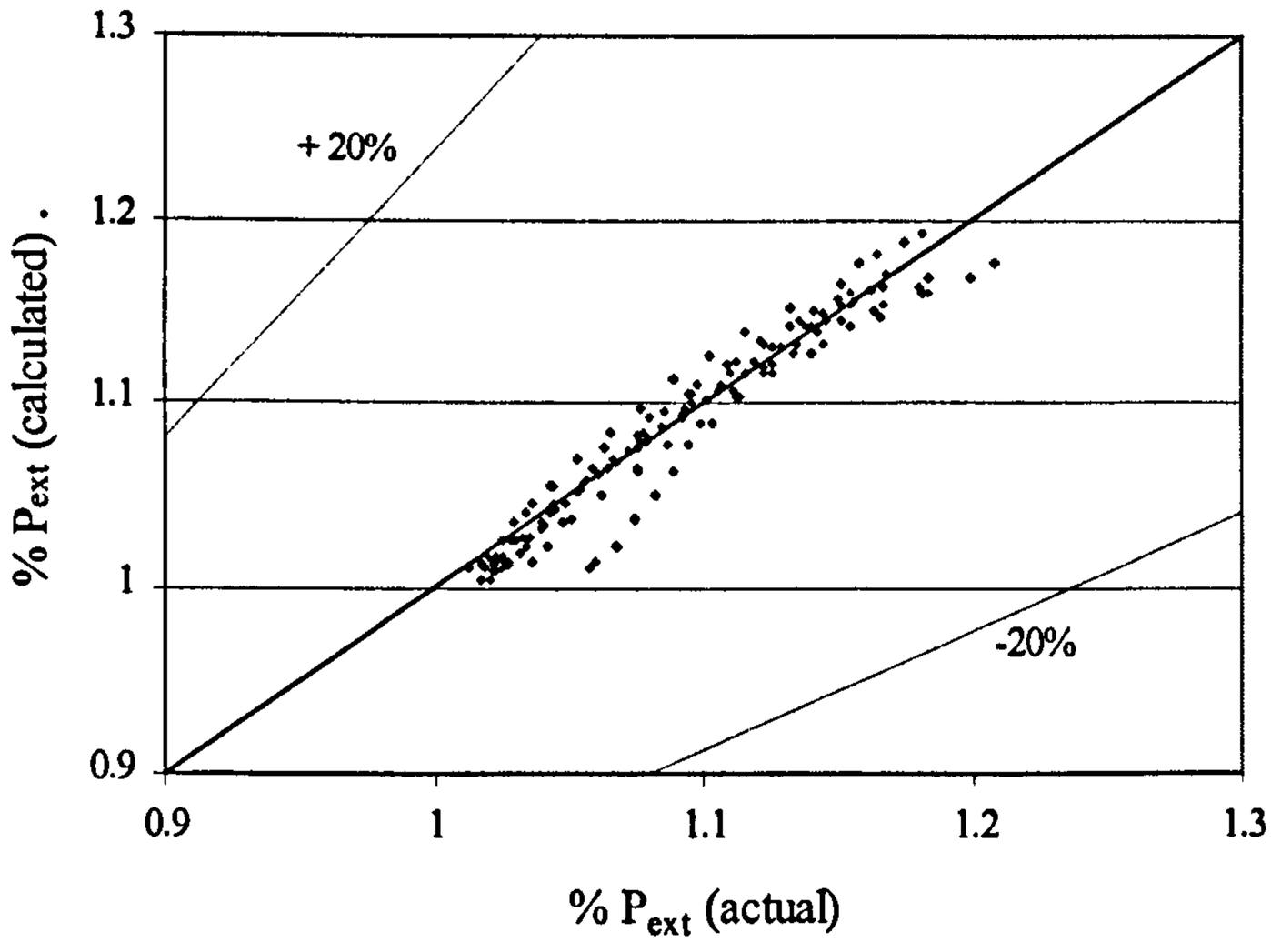

Figure (5.37): Relation between theoretical and actual ratios of increase in external prestressing force

5.3.7.2 Relation between Internal and External prestressing forces

The relations between the increase in external prestressing force and the increase in internal prestressing force for the test beams are shown in Figures (5.38-5.43). This relation was linear up to the yielding of the internal prestressing steel and the rate of increase in internal prestressing force was higher than the rate of increase in the external prestressing force. However, after yielding of the internal prestressing steel,

the external prestressing force increased significantly more rapidly than the internal prestressing force. This can be attributed to the following reasons:

- After yielding of the internal prestressing steel, even though there was a high increase in strain of the internal prestressing steel, the corresponding increase in stress (force) was small.
- Yielding of the steel was accompanied by a significant increase in deflection resulted in rapid increase in external prestressing force.

The value of the external prestressing force, deviator location, pre-cracking stage and (L/h) ratio, before yielding of the internal prestressing steel, have no effect on the relation between the increase in external prestressing force and the increase in internal prestressing force. While the increase in the eccentricity of external prestressing force or the concrete strength and the increase in (eccentricity/depth) ratio have a slight effect.

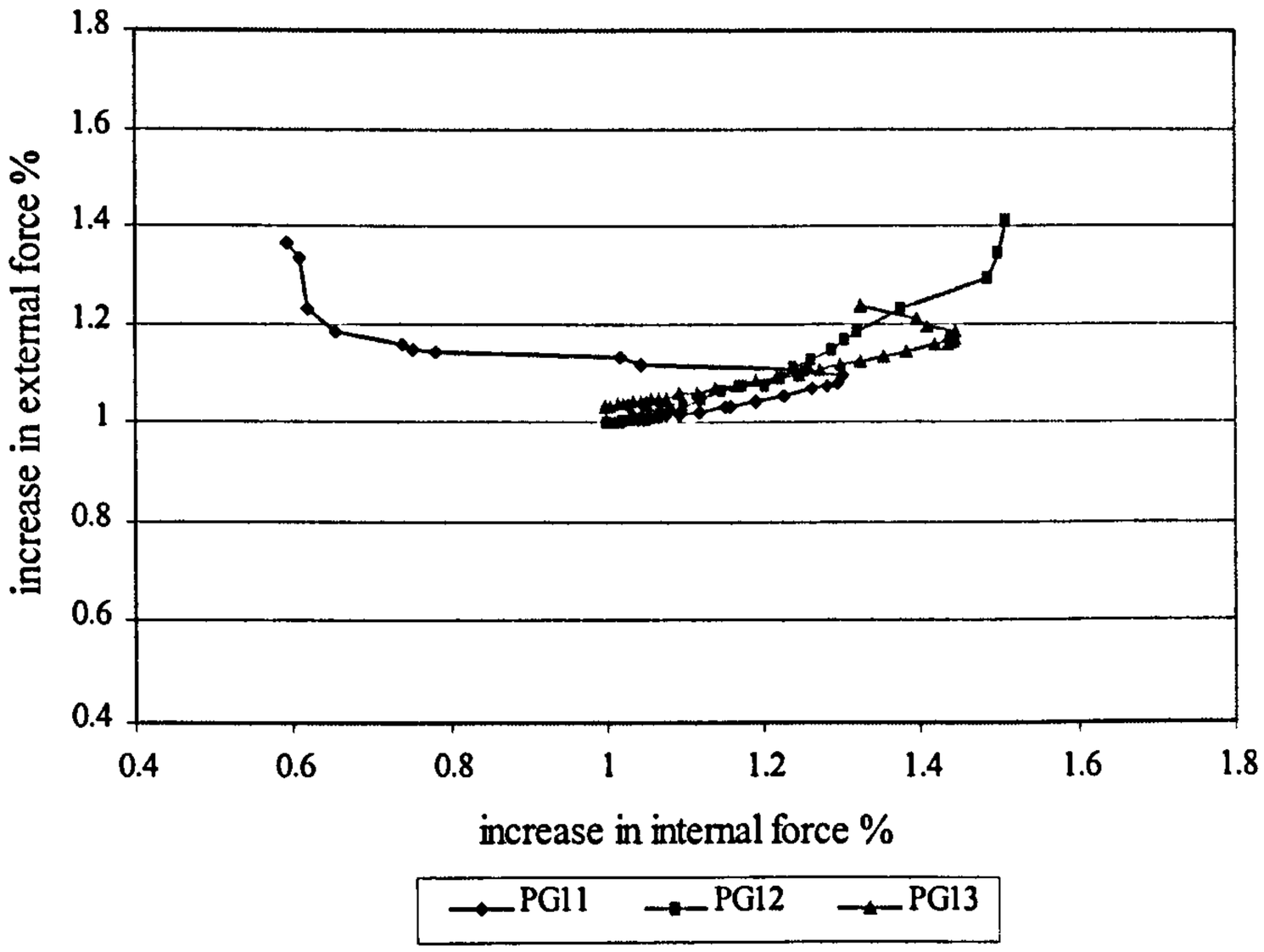

Figure (5.38): Relation between the increase in external prestressing force and the increase in the internal prestressing force for group G1

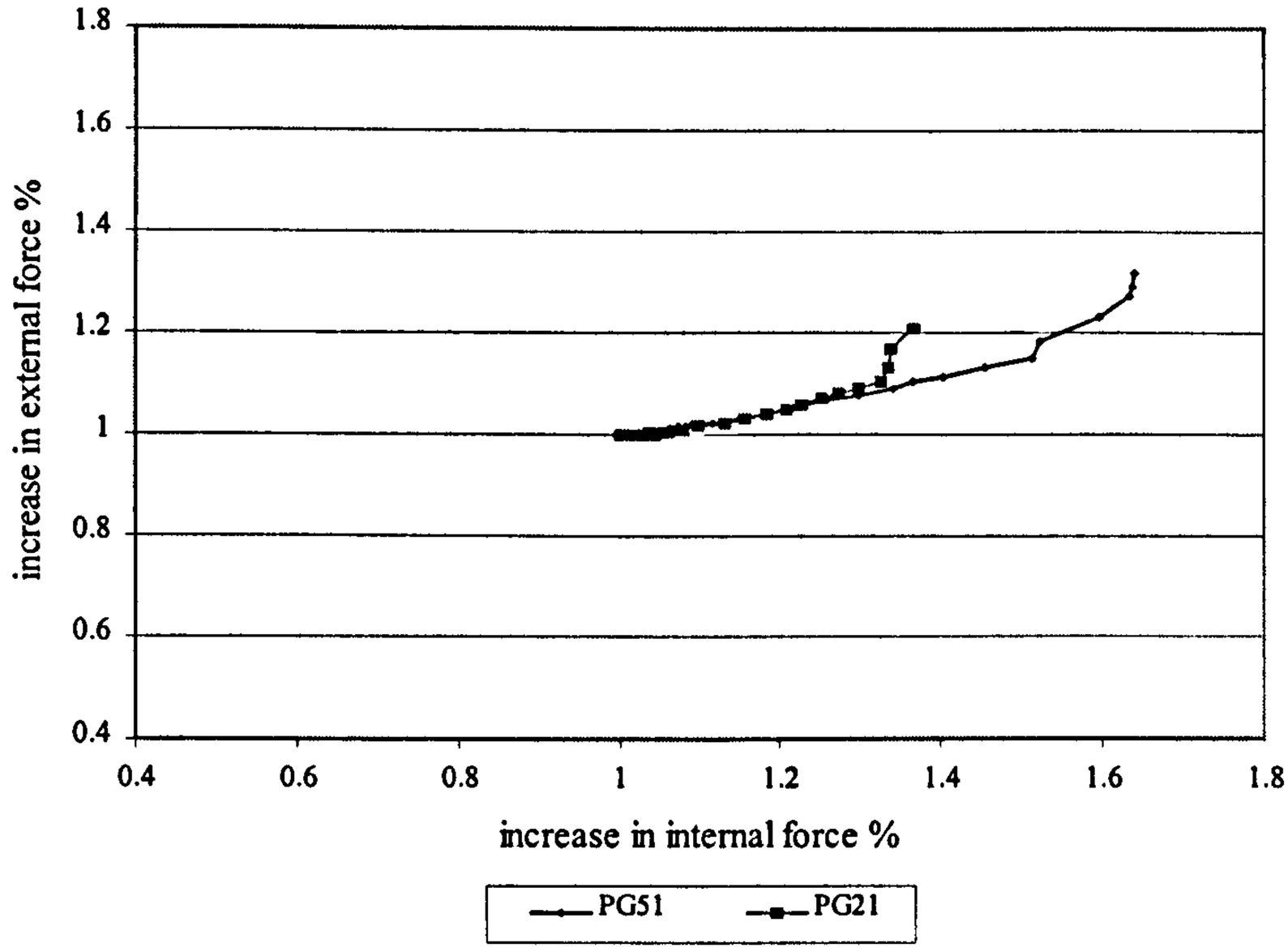

Figure (5.39): Relation between the increase in external prestressing force and the increase in the internal prestressing force for group G2

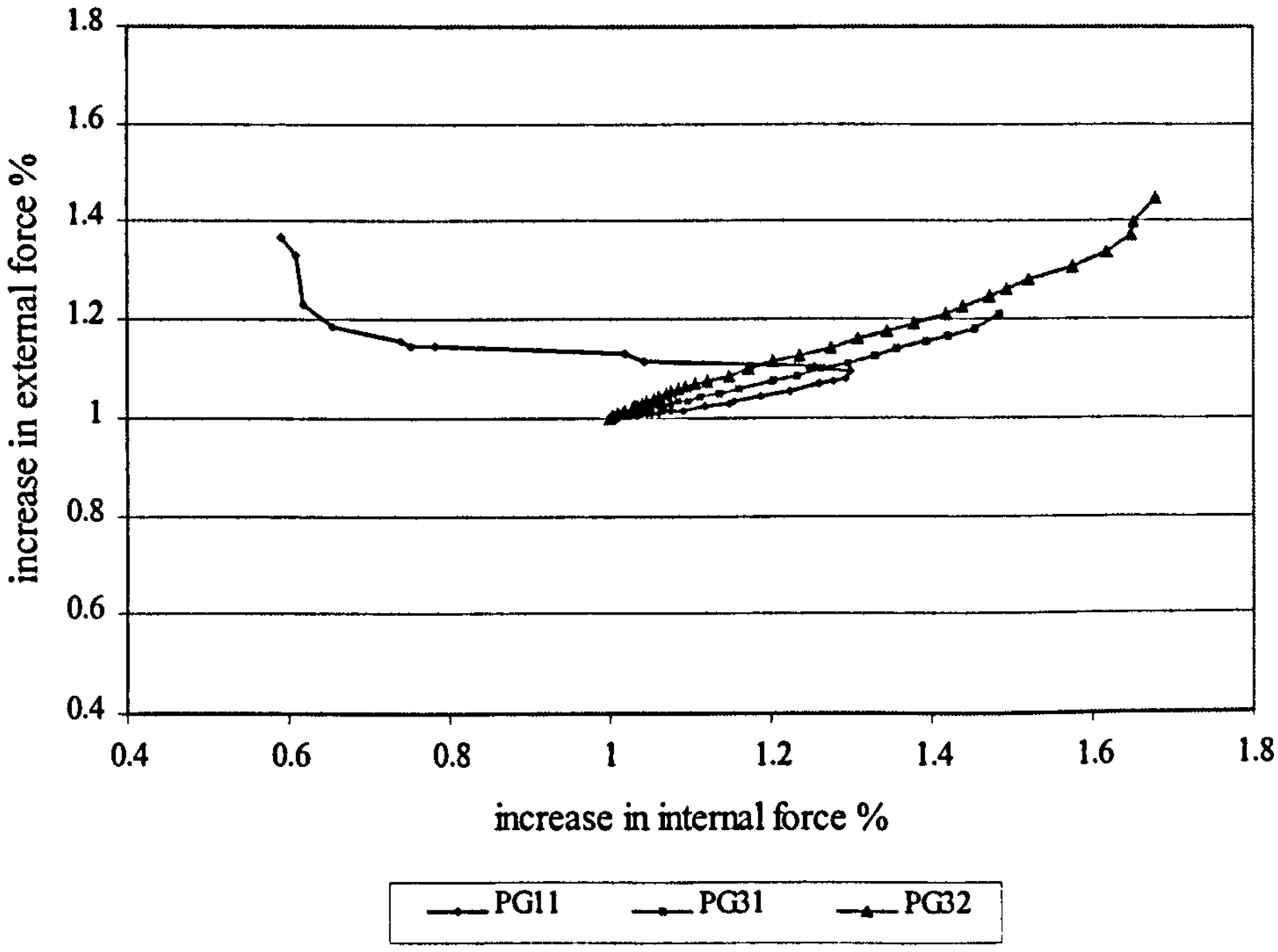

Figure (5.40): Relation between the increase in external prestressing force and the increase in the internal prestressing force for group G3

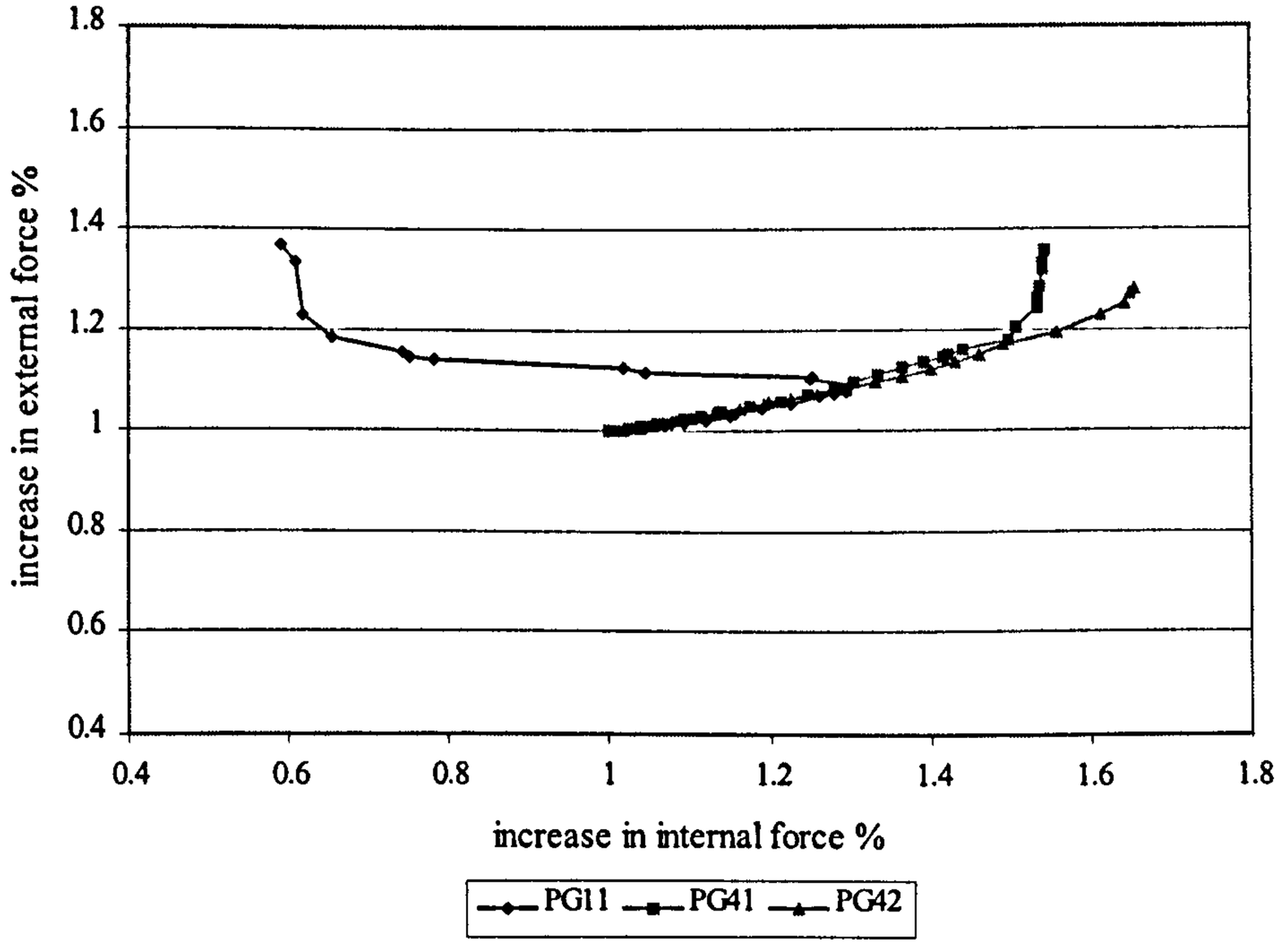

Figure (5.41): Relation between the increase in external prestressing force and the increase in the internal prestressing force for group G4

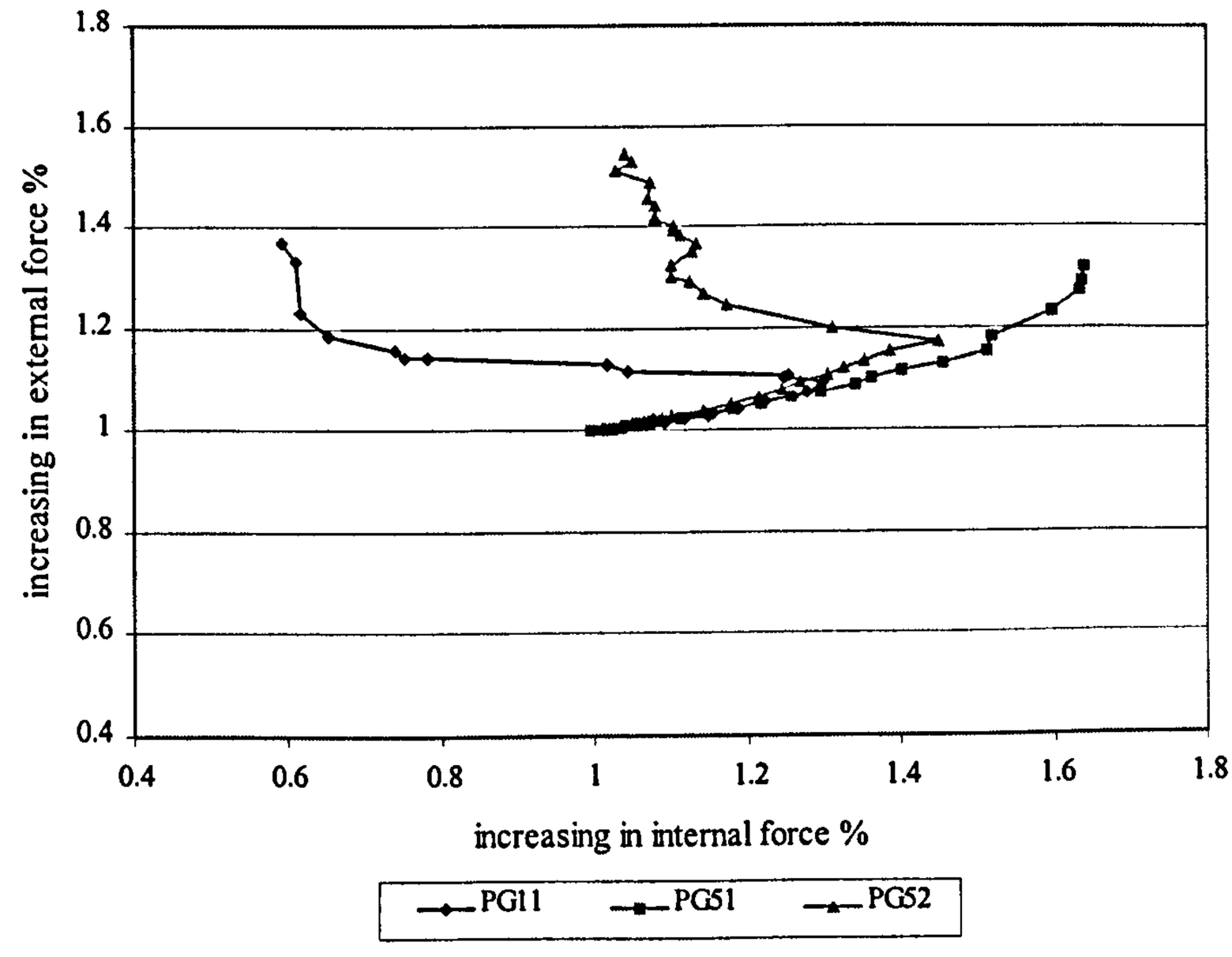

Figure (5.42): Relation between the increase in external prestressing force and the increase in the internal prestressing force for group G5

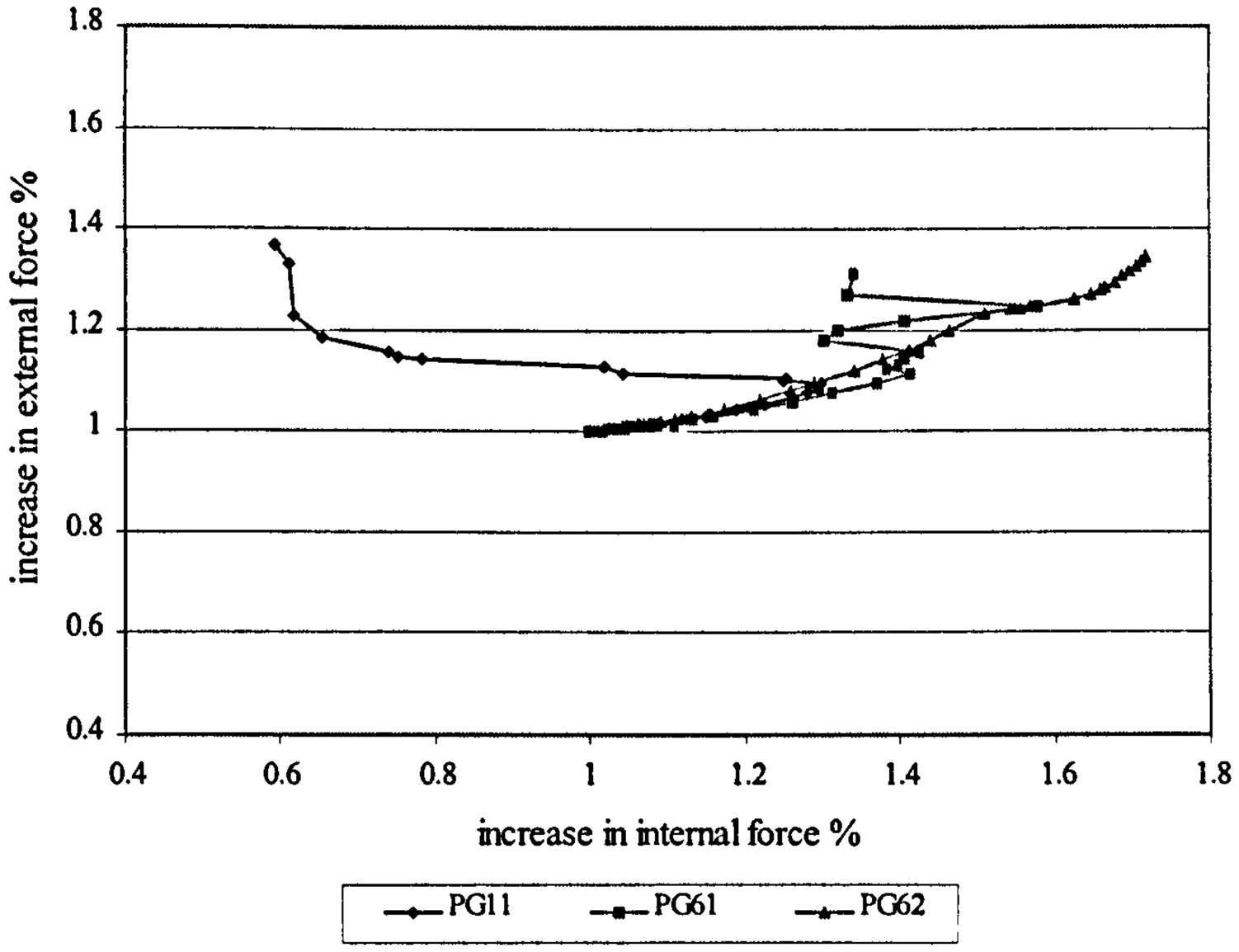

Figure (5.43): Relation between the increase in external prestressing force and the increase in the internal prestressing force for group G6

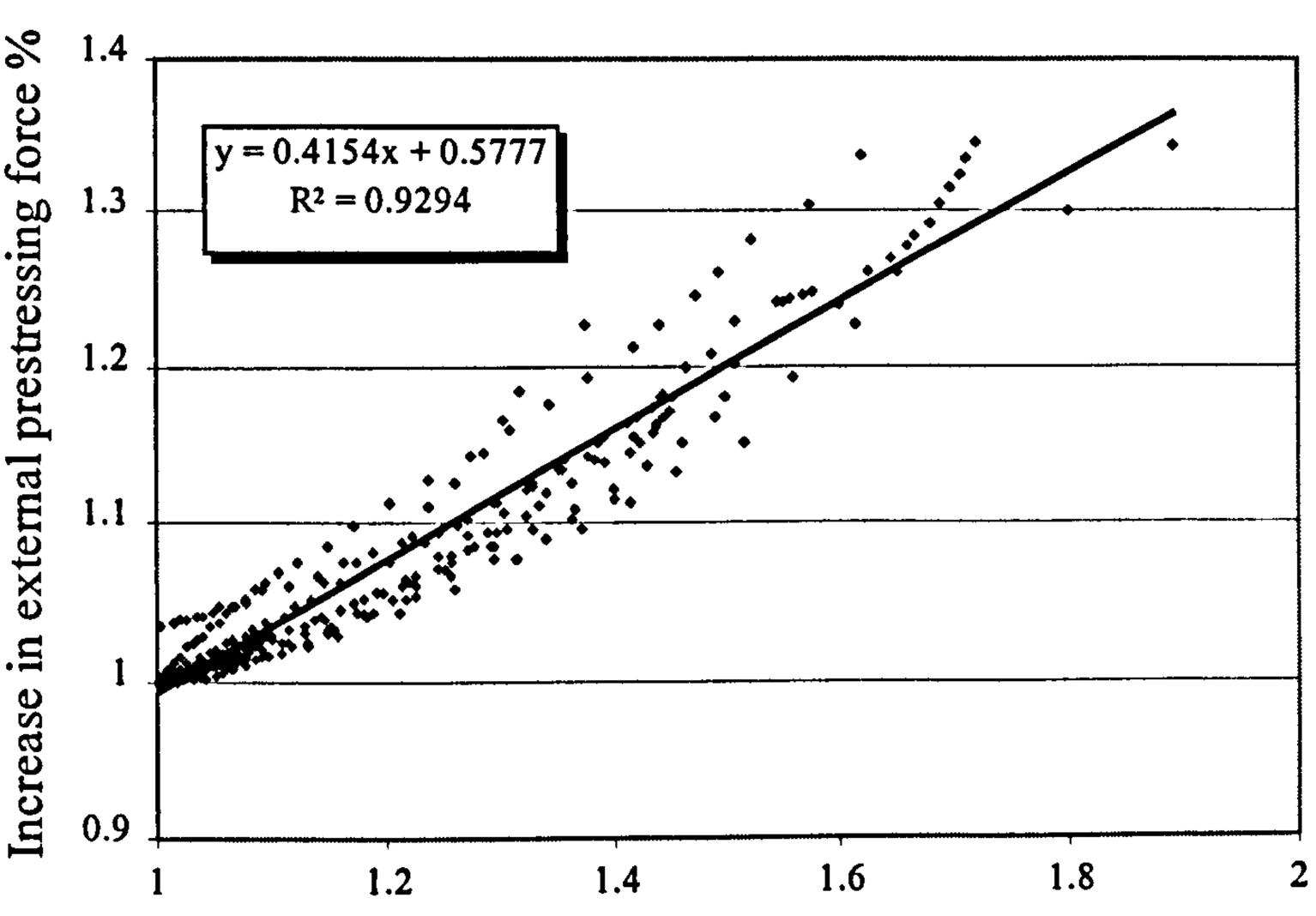

Figure (5.44): Relation between the increase in external prestressing force and the increase in the internal prestressing force

5.4 SUMMARY

The effect of the factors taken into consideration on the behaviour of strengthened prestressed beams can be summarized as follows:

5.4.1 Group 1 (Value of The External Prestressing Force)

To study the effect of initial value of the external prestressing force on the behaviour of prestressed concrete beams after externally strengthened, three identical beams with different external prestressing force PG12, PG11 and PG13 (P_{ext} = 48.98, 60.35, 72.27 KN) were tested up to failure. Increasing the external prestressing force increased the compressive stress at the tension side and hence reduced the net tensile stress. This resulted in delaying the cracking and reducing its extension.

After cracking the rate of reduction in the inertia (stiffness) decreased as the external prestressing force increased. This resulted in decreasing deflection after cracking in both working and ultimate stages as the external prestressing force increased.

The effect of increase in the external prestressing force can be summarized as follows:

- Increased cracking moment resistance
- Improved stiffness after cracking
- Decreased ductility after cracking
- Increased ultimate moment resistance
- Increased shear cracking load and reduced number of diagonal cracks. This is likely to increase the shear strength.

5.4.2 Group 2 (Number of deviators)

Two identical beams (one with one deviator at mid span and the other with two deviators at the third span) were tested to study the effect of deviator location on behaviour of the strengthened prestressed beams. The prestressing moment can be considered constant between the deviators when using two deviators at the third span, while it decreases with distance from the deviator when using one deviator at the mid

span. This resulted in a decrease the prestressing moment especially at the concentrated load and decreased the cracking and ultimate moments. Also, using two deviators increased the inclination angle of the external prestressing force and hence its vertical component which thus reduced the shear force. So, using two deviators resulted in:

- Higher cracking moment resistance
- Better spread of the flexural cracks and preventing formation of the plastic hinge at early stage
- Higher stiffness after cracking
- Higher ductility at ultimate
- Higher ultimate moment resistance

5.4.3 Group 3 (Effective depth of the external prestressing force)

Three identical beams with different eccentricity of the external prestressing force (e/h = 0.794, 0.894 and 1.072) were tested to study the effect of eccentricity of the external prestressing force on the behaviour of strengthened beam. Increasing eccentricity of the external prestressing force increased the prestressing moment and enabled the section to tolerate more load. Also, increasing the eccentricity increased the compressive stress that prevented cracks from extending. This resulted in decreasing the reduction in inertia and stiffness after cracking. The effect of the increase of the external prestressing force eccentricity can be summarized as follows:

- Increased camber and creep deformation
- Increased cracking moment resistance
- Decreased ductility especially after cracking
- Increase ultimate moment resistance
- Increase shear strength and reduced spread of the cracks in the shear span

5.4.4 Group 4 (Previous loading stage before strengthening)

The effect of the previous loading stage before strengthening on the behaviour of externally prestressed beams was studied using three beams loaded up to different stages relative to the ultimate strength before being externally prestressed, as follows (0 P_{ult},, 0.36 P_{ult} , 0.6 P_{ult}). After externally prestressing, previous cracks were

completely closed by the external prestressing force, this improved stiffness of the pre-cracked beam.

The load level before strengthening had a significant effect on the cracking resistance. This is because, the concrete tensile strength, before strengthening, was diminished after cracking and, after strengthening, the cracking moment resistance was due to the prestressing moment only. However, the previous loading stage had almost no effect on the ultimate moment of resistance (assuming the internal prestressing steel did not reach its yielding stage). So, the pre-cracked beam, after strengthening, can be analyzed at the ultimate stage in the same way as the uncracked strengthend beam. The effect of the external prestressing force can be summarized as follows:

- Increased moment at which cracks reopen.
- Improved stiffness
- Improved serviceability behaviour.
- Increased ultimate moment resistance.

5.4.5 Group 5 (Effect of concr e te strength)

The effect of concrete strength on the behaviour of strengthened beams was studied using three identical beams with different concrete strengths (f_{cu}= 43.3, 55.8 and 79.3 MPa). Increasing the concrete strength enabled them to resist higher compressive stress and a higher ultimate moment , allowing more extensive yield of the steel before the concrete reached its ultimate capacity. The effect of concrete strength can be summarized as follows:

- Slightly increased cracking moment resistance.
- Increased ultimate moment resistance
- Improved ductility at failure.
- Increased crack widths especially at ultimate.

5.4.6 Group 6 (Effective span length/depth ratio (L/h))

The three beams of group 6 had the same depth but different (span/depth) ratios (L/h= 10, 14.4, 20). They were tested to examine the effect of (L/h) ratio on the behaviour of prestressed concrete beams after external prestressing.

Increased (L/h) ratio decreased the beam stiffness and hence increased the deflection. Also, the loss in eccentricity of the external prestressing force increased as (L/h) ratio increased. This decreased the prestressing moment especially at ultimate. The effect of increase of (L/h) ratio can be summarized as follows:

- Slightly decreased cracking moment.
- Decreased stiffness and increased deflection at any load.
- Increased flexural crack widths, with less spread of cracks in the shear span.
- Increase ductility at failure.
- Slightly decreased ultimate moment.

Chapter 6

Theoretical Analysis

6.1 INTRODUCTION

The efficiency of any strengthening method is dependent on the ability to determinate the behaviour of the strengthened member either in the working stage (i.e. deflection) or in the ultimate stage (i.e. nominal strength). This is especially true in bridges where both the deflection and nominal strength are of interest in order to limit the maximum permitted load or smooth driving.

To reach these goals, unless a nonlinear computer analysis program is used, calculation of the cracking as well as the ultimate moments of such a beam will be very tedious. Also, several factors that affect the precision of the deflection calculation can not be known with a high accuracy, especially in the field, such as the concrete strength, effect of creep and shrinkage, value of the internal prestressing force, etc.

Therefore, simple equations are needed to determine the service and ultimate behaviours of strengthened flexural members with a reasonable accuracy. Also, it

should be able to be done in a reasonably short time, instead of requiring complicated equations especially in the design stage.

In this chapter, methods that being used in cracking moment, deflection and ultimate moment calculations for prestressed concrete beams with steel tendons will be modified to take the effect of the external prestressing force and be suitable for Parafil rope.

6.2 CRACKING LOAD

Before cracking, the increase in both the internal and the external prestressing force and the reduction in the eccentricity of the external prestressing force are small and can be neglected. Hence, the cracking moment can be calculated using the same equations used for bonded prestressed concrete beams. The full section inertia was considered in the calculation even where the beam was precracked as in group G4 (due to the improvement in the stiffness as shown from moment-deflection curves). The cracking moment due to live moment only was calculated as follows:

$$f_r = -\left(\frac{P_{ei}+P_{ex}}{A}\right)-\left(\frac{P_{ei}e_i+P_{ex}e_e}{I}\right)y_b+\frac{M_{cr}y_b}{I}+\frac{M_d y_b}{I} \qquad (6.1)$$

Or

$$M_{cr} = f_r\frac{I}{y_b}+\left(\frac{P_{ei}+P_{ex}}{A}\right)\frac{I}{y_b}+P_{ei}e_i+P_{ex}e_e-M_d \qquad (6.2)$$

Where

P_{ei} =effective internal prestressing force

P_{ex} =effective internal prestressing force

A = area of the cross section = $Bh-(B\text{-}b_w)*(h\text{-}2h_f)$

I = inertia of the cross section = $\frac{Bh^3}{12}-\frac{(B-b_w)(h-h_f)^3}{12}$

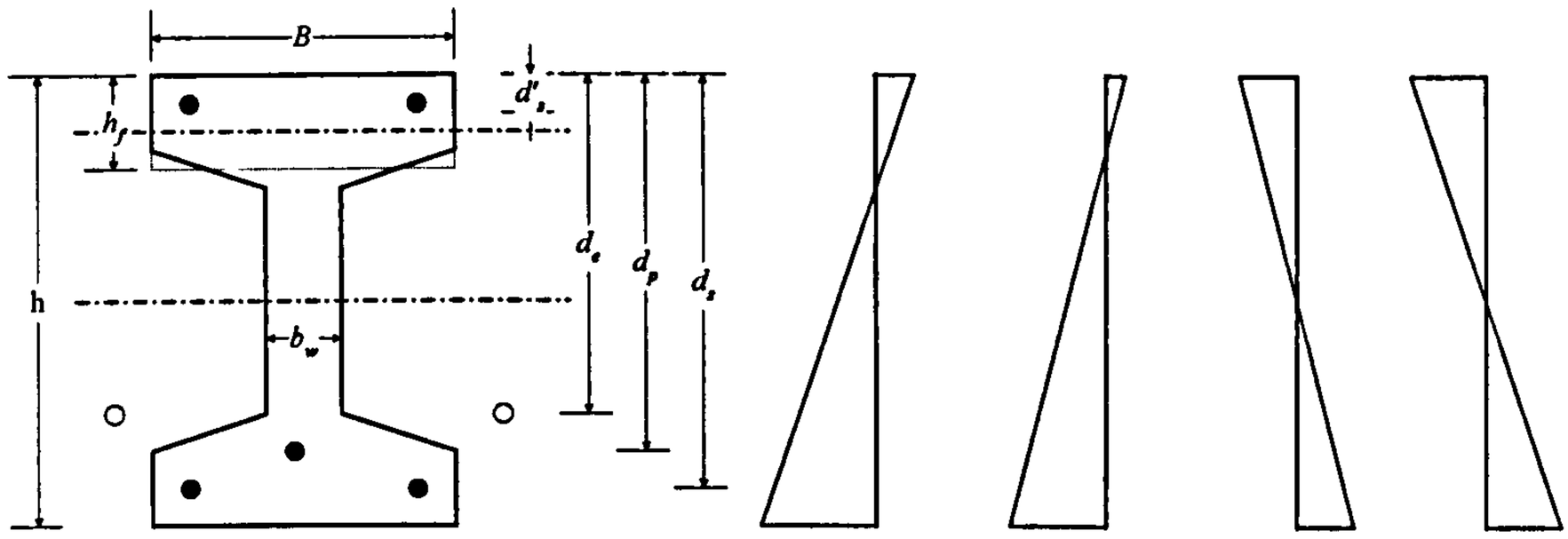

Figure (6.1): Stress distribution due to different loads

Table (6.1) shows the actual and calculated cracking moments using f_{ctm} and f_r (mean value of axial tensile strength of concrete and modulus of rupture of concrete respectively) of all beams, while Figure.(6.1) shows the relation between them. It can be seen there is a good agreement between the calculated and the actual values. The calculated cracking moment was found to be higher than the actual moment, this is due to the difficulty in accurately determining the concrete tensile strength and neglecting the reduction in eccentricity of the external prestressing force. However, the average difference is less than 10%.

From Table (6.1) it can be seen that:

- The actual cracking moment of beam PG13 was found to be slightly lower than the calculated moment. This maybe due to the previous impact load that was applied to it in the first stage.

Also, the cracking moment of beam PG21 (one deviator at the middle) was calculated at the concentrated load (critical section) and not at the middle as the other beams.

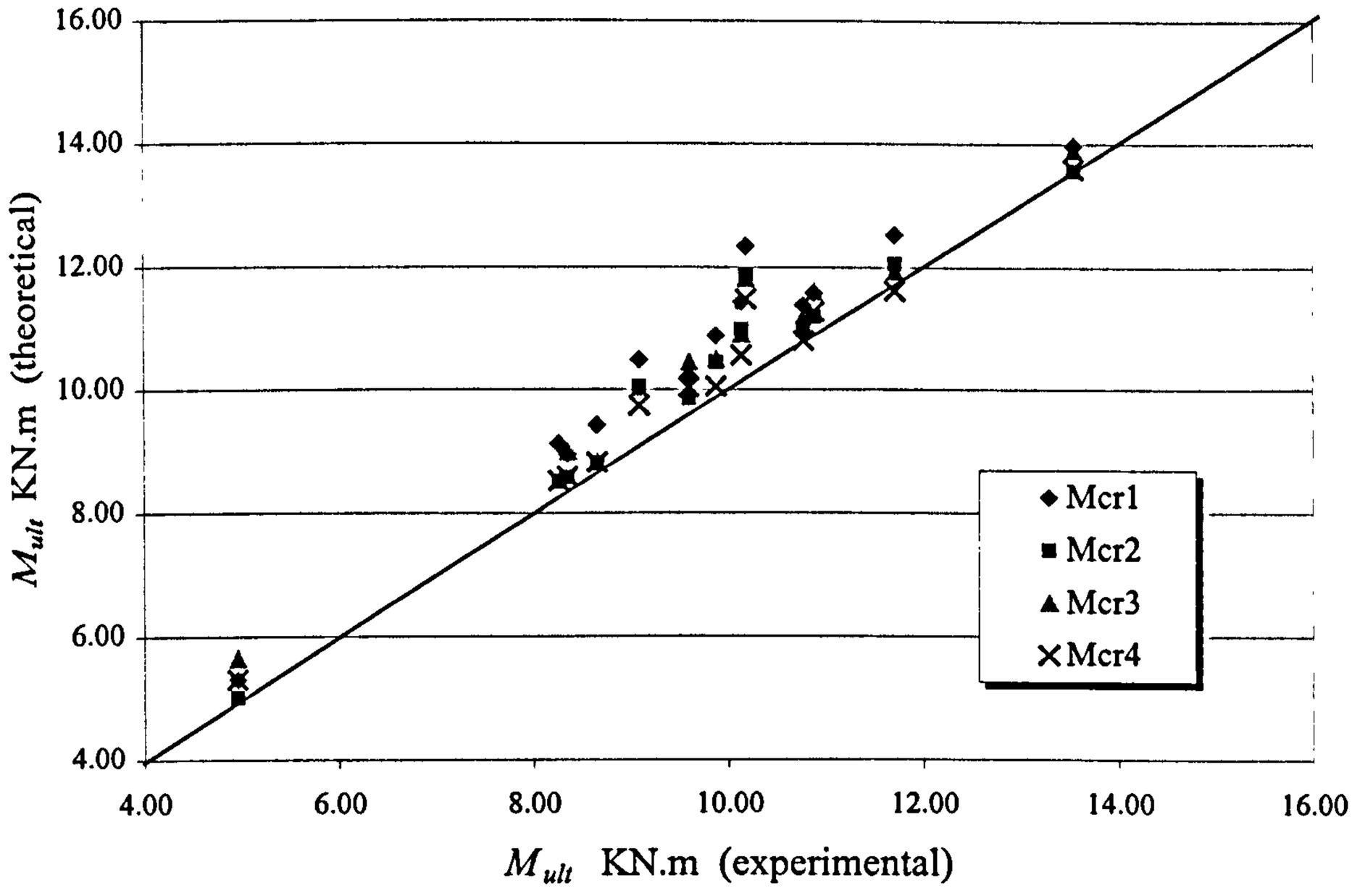

Figure (6.2): Comparison between the actual and the calculated cracking moments

Table (6. 1): *Actual and calculated cracking moments.*

Beam no.	**Cracking Moment (KN.m)**					**Ratio of calculated moment to actual moment**			
	Actual	M_{cr1}	M_{cr2}	M_{cr3}	M_{cr4}	M_{cr1}/M_{act}	M_{cr2}/M_{act}	M_{cr3}/M_{act}	M_{cr4}/M_{act}
B1	4.96	5.31	5.03	5.64	5.31	1.07	1.01	1.14	1.07
PG11	10.14	11.44	10.98	10.9	10.56	1.13	1.08	1.08	1.04
PG12	9.09	10.48	10.05	10.03	9.74	1.15	1.11	1.10	1.07
PG13	10.18	12.34	11.87	11.81	11.48	1.21	1.17	1.16	1.13
PG21	8.35	8.97	8.58	8.99	8.59	1.07	1.03	1.08	1.03
PG31	11.7	12.53	12.06	11.92	11.62	1.07	1.03	1.02	0.99
PG32	13.53	13.97	13.57	13.89	13.6	1.03	1.00	1.03	1.01
PG41	8.66	9.43	8.83	8.83	8.83	1.09	1.02	1.02	1.02
PG42	8.27	9.12	8.52	8.52	8.52	1.10	1.03	1.03	1.03
PG51	9.87	10.95	10.51	10.54	10.12	1.11	1.06	1.07	1.02
PG52	10.88	11.58	11.2	11.6	11.28	1.07	1.03	1.07	1.04
PG61	9.6	10.21	9.85	10.44	10.04	1.06	1.03	1.09	1.05
PG62	10.77	11.39	10.97	11.19	10.8	1.06	1.02	1.04	1.00

- M_{cr1} = based on experimental results of f_r and transformed section.
- M_{cr2} = based on experimental results of f_r and full section.
- M_{cr3} = based on theoretical f_r and full section.
- M_{cr4} = based on theoretical f_{ctm} and full section.

6.3 DEFLECTION

The deflection of prestressed concrete beams depends on several factors, such as concrete cracking, long term behaviour of concrete, shape and period of the applied load and other factors that can not be determined accurately especially in the field.

So, the method used in the deflection calculation should not be too complicated or time consuming nor give a false feeling of accuracy, while not to be so simple that it gives a wrong value by neglecting several factors.

Deflection of prestressed concrete beams due to live load can be calculated from the general equation as follows:

$$\Delta_L = K\frac{M_L L^2}{EI} \tag{6. 3}$$

Where :

K = multiplier deflection factor depending on the load type

E = concrete elastic modulus

I = moment of inertia as a general (uncracked or cracked)

Before cracking, the gross moment of inertia (I_g) or more accurately the transformed moment of inertia, can be used to determine the deflection, though using the transformed moment of inertia does not result in a significant gain in accuracy.

After cracking and due to the tension stiffening, the moment of inertia lies between the gross and fully cracked inertia depending on the value of applied moment relative to the cracking moment. Several methods have been developed to take the effect of variation in stiffness caused by cracking along the span, some of them calculate the deflection from integration of curvature along the span, others use the effective moment of inertia or bilinear relation between load and deflection.

In this chapter a brief review of some methods that are used in deflection calculation is presented and discussed and then extended to introduce the effect of the external prestressing force. However, methods that need iteration or integration are not included.

6.3.1 Deflection of Bonded Prestressed Concrete Beams

The equation for I_e (effective moment of ineria) originally proposed by *Branson* for reinforced concrete members, is expressed as follows:

$$I_e = \left(\frac{M_{cr}}{M_a}\right)^3 I_g + \left(1 - \left(\frac{M_{cr}}{M_a}\right)^3\right) I_{cr} \leq I_g \qquad (6.4)$$

Where M_{cr} and M_a are the cracking and applied moment at the beam critical section, I_g and I_{cr} are the gross moment of inertia of uncracked (neglecting the steel) and cracked sections (neglecting concrete in tension) respectively.

Branson has recommended the use of I_e for prestressed and partially prestressed cracked members using bonded tendons or unbonded tendons after modification.

However, although the concept of the I-effective method was accepted to be applicable to prestressed and partially prestressed concrete beams, opinions differ widely concerning the definition of the terms in the I_e equation. These are (*Tadros and Sulieman, 1983. Naaman, 1985. Harajili and Almeh, 1989*):

- The level of the externally applied moment (M_a) at which the I_e expression should be used as shown in Figure.(6.3).

- The value of cracking moment (M_{cr}) used in calculation: Different values were suggested (depending on the level of M_a) as follows:

$$M_{cr} = f_r \frac{I}{y_b} + \left(\frac{p_{ei}}{A}\right)\frac{I}{y_b} + p_{ei}e_i - M_d \qquad (6.5)$$

$$M_{cr} = f_r \frac{I}{y_b} + \left(\frac{p_{ei}}{A}\right)\frac{I}{y_b} + p_{ei}e_i \qquad (6.6)$$

$$M_{cr} = f_r \frac{I}{y_b} + \left(\frac{p_{ei}}{A}\right)\frac{I}{y_b} \qquad (6.7)$$

Or $\quad M_{cr} = f_r \frac{I}{y_b} \qquad (6.8)$

- The section axis about which I_{cr} is calculated, i.e., relative to the centroidal axis of the cracked transformed section, or relative to the neutral axis of bending assuming zero prestressing force (or equivalently infinite moment).

Also, in the case of an externally prestressed beam, the increase in stress of the external tendons is member dependent rather than section dependent and its eccentricity varies during loading. These add other difficulties in calculating the deflection of this type of beam.

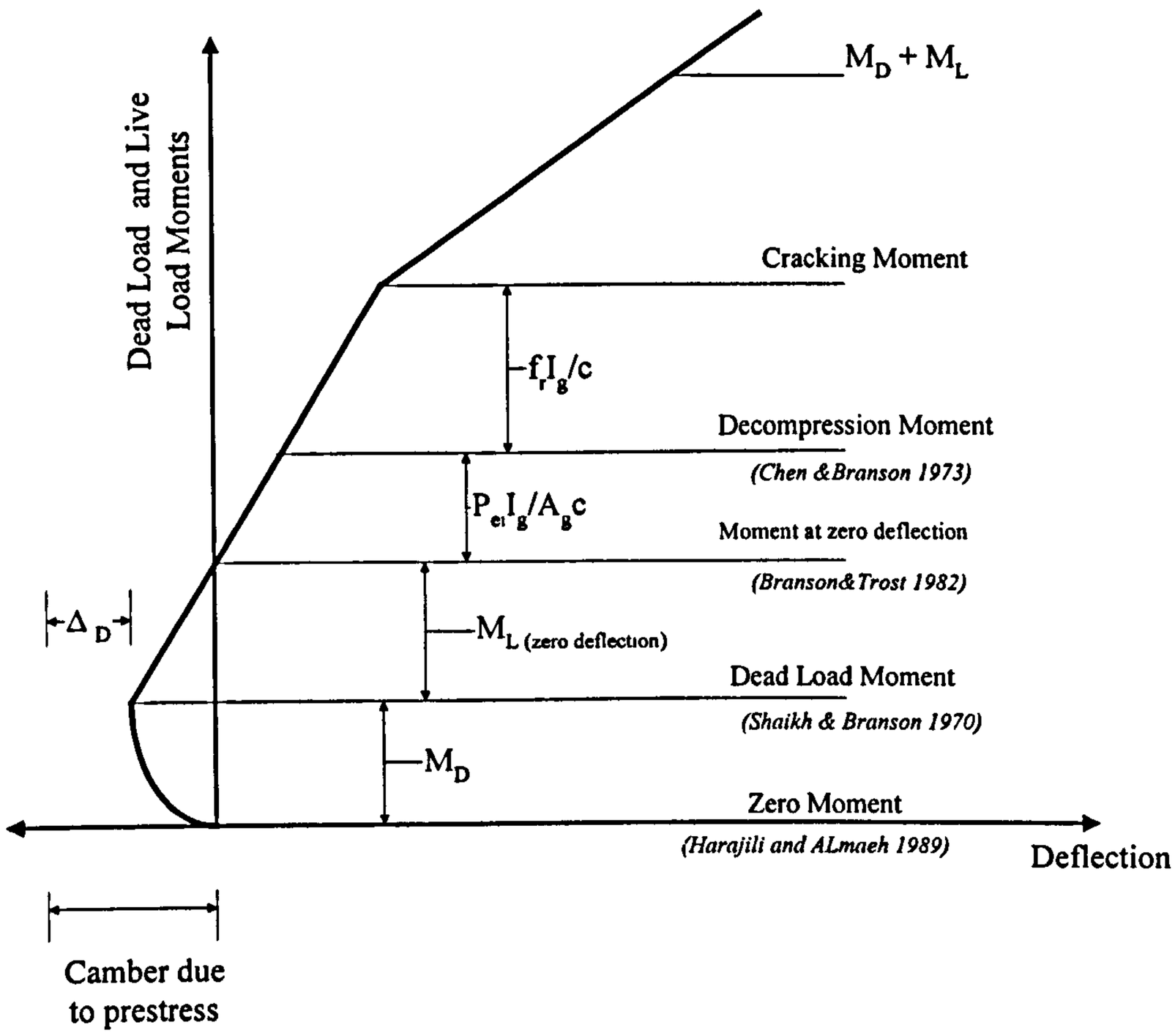

Figure (6.3): level of applied moment at which I_e should be used in different methods

Shaikh and Branson (1970), using the effective moment of inertia approach, suggested a *simplified* method to determine the deflection of the prestressed concrete members based on computing the live load deflection increment from the "prestress camber" minus "dead load deflection" point $(\Delta_P - \Delta_D)$ as seen in Figure (6.4) and calculate the effective inertia from the following equation:

$$I_e = \left(\frac{M_{cr}}{M_a}\right)^3 I_g + \left(1 - \left(\frac{M_{cr}}{M_a}\right)^3\right) I_{cr} \leq I_g \qquad (6.9)$$

where M_a = live load moment (M_L)

and $$M_{cr} = f_r \frac{I}{y_b} + \left(\frac{p_{ei}}{A}\right)\frac{I}{y_b} + p_{ei}e_i - M_d \qquad (6.10)$$

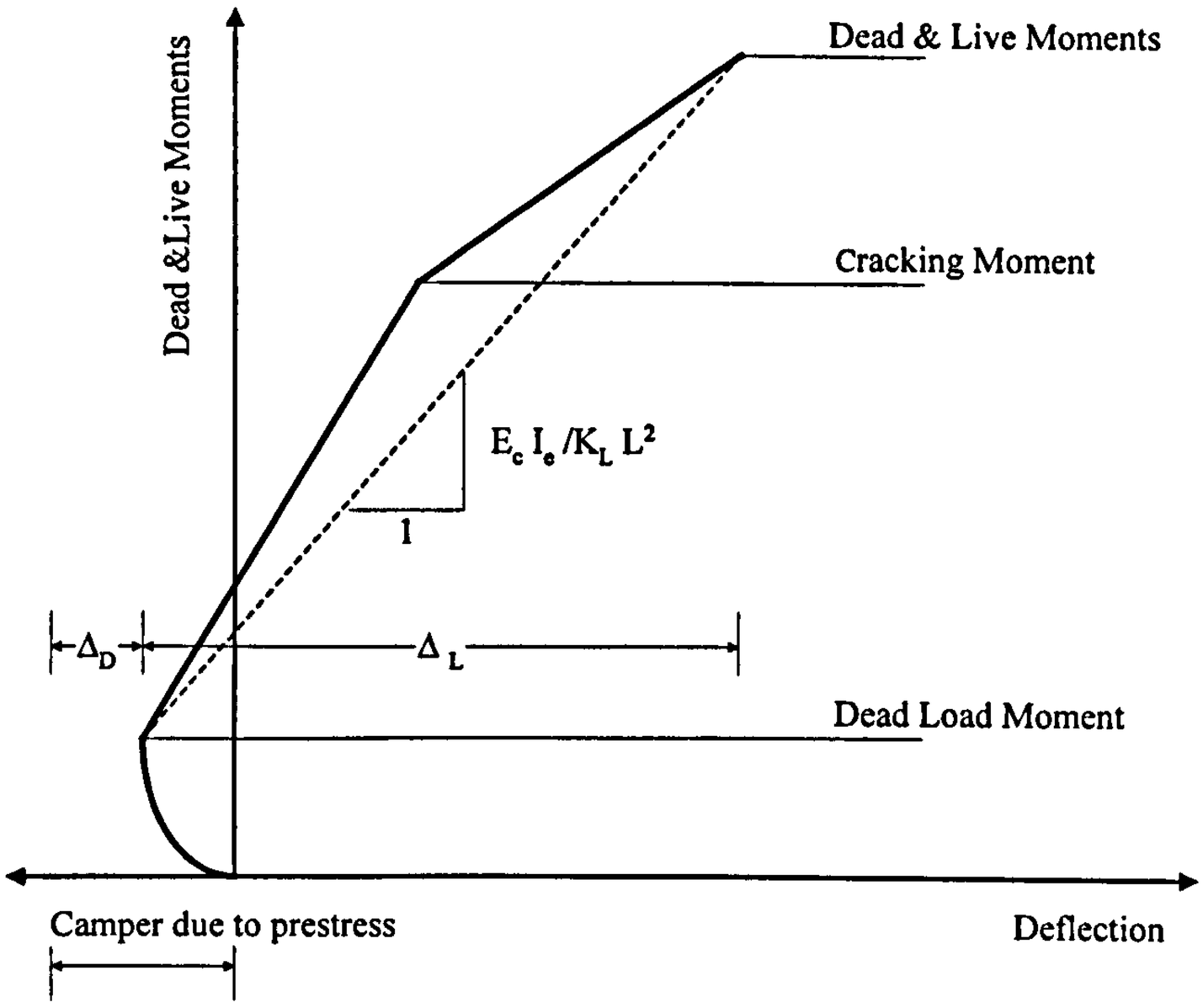

Figure (6.4): Idealization of load-deflection response of prestressed concrete beam
Shaikh and Branson (1970)

Branson (1977) in his book mentioned the slight improvement made by computing only the live load deflection above the "decompression" point, or point of zero bottom fibre stress as suggested by *Chen* in 1973, using the I_e formula as follows:

$$I_e = \left(\frac{M_{cr} - M_{dec}}{M_a - M_{dec}}\right)^3 I_g + \left(1 - \left(\frac{M_{cr} - M_{dec}}{M_a - M_{dec}}\right)^3\right) I_{cr} \leq I_g \qquad (6.11)$$

Where M_{dec} is the decompression moment (that moment leads to zero stress on precompressed concrete extreme fibres).

Branson and Trost (1982) suggested a unified I-effective formula to predict the short-time deflection of cracked reinforced and prestressed concrete members based on zero deflection as shown in Figure (6.3). They suggested calculating the live load deflection above the zero deflection, and treated the prestressed beam as a reinforced concrete beam. Details of this method can be seen in Figures (6.5 - 6.6) and can be explained as follows:

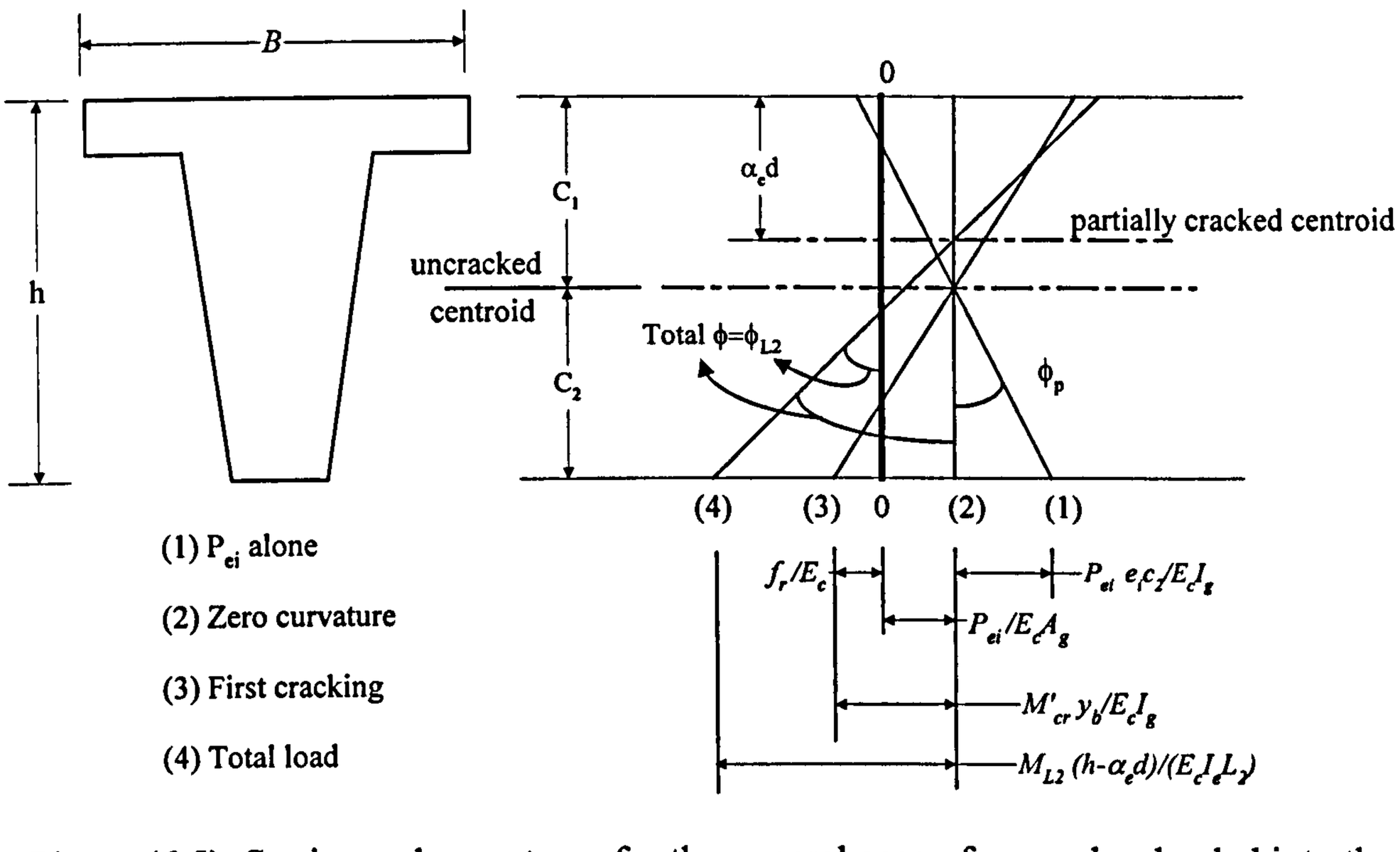

Figure (6.5): Strains and curvatures for the general case of a member loaded into the cracking range

From distribution line 1 in Figure (6.5), the deflection corresponding to the prestress curvature ϕ_p is given by

$$\Delta_p = \frac{K_p P_{ei} e_i L^2}{E_c I_g} \qquad (6.12)$$

and the dead load deflection is given by

$$\Delta_D = \frac{K_D M_D L^2}{E_c I_g} \qquad (6.13)$$

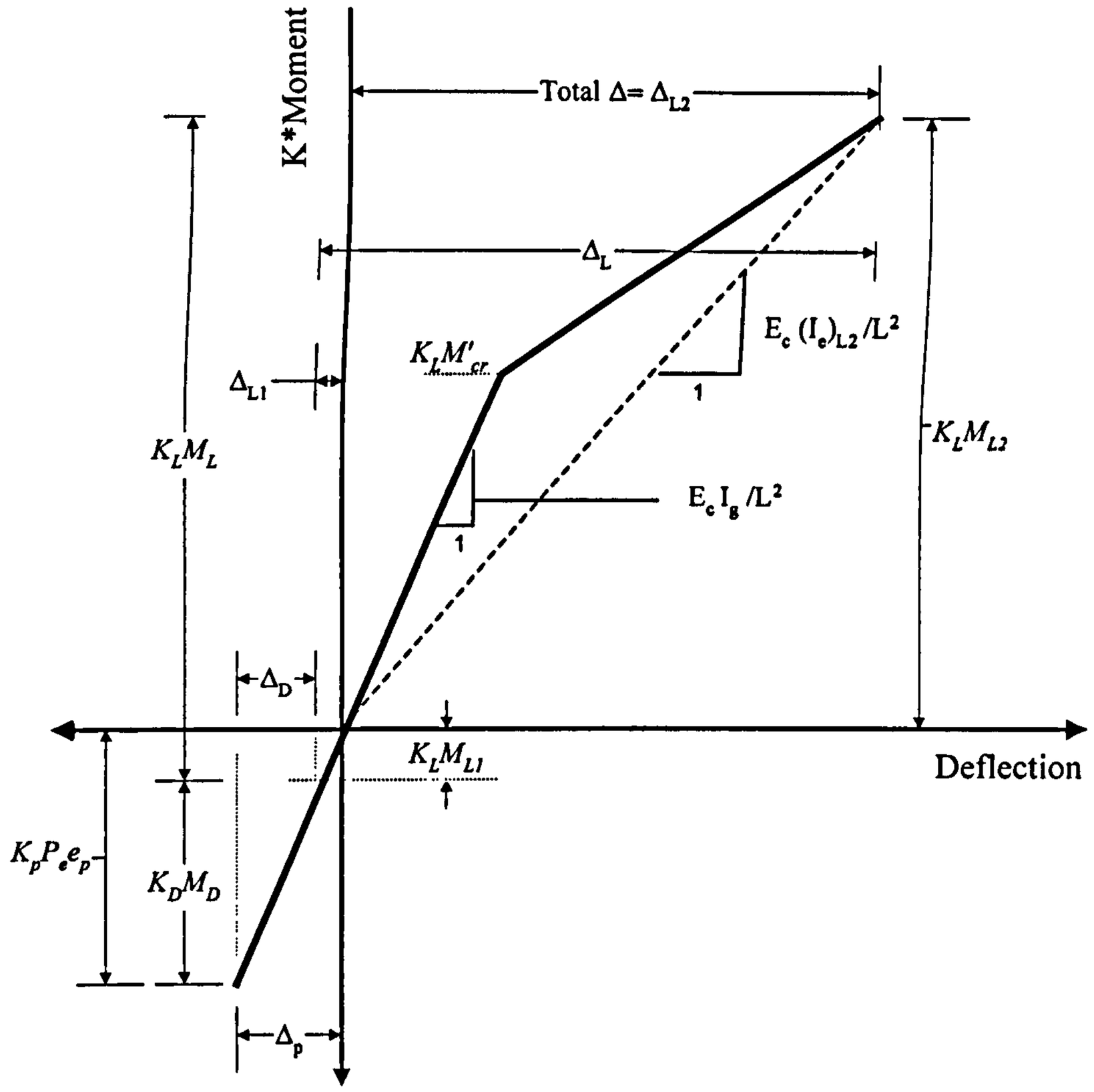

Figure (6.6): Idealization of load-deflection response of prestressed concrete beam

Branson and Trost (1982)

So the part of the live moment necessary to produce zero deflection as shown in Figure (6.6) can be calculated as follows:

$$K_L M_{L1} = K_P P_{ei} e_i - K_D M_D \qquad (6.14)$$

Or

$$M_{L1} = (K_P / K_L) P_{ei} e_i - (K_D / K_L) M_D \qquad (6.15)$$

and the deflection produced by M_{L1}

$$\Delta_{L1} = \frac{K_L M_{L1} L^2}{E_c I_g} \qquad (6.16)$$

The cracking moment M'_{cr} (refers to the moment above zero or the net positive moment) required to crack the section is obtained from:

$$f_r = \frac{M'_{cr}\, y_b}{I_g} - \frac{P_{ei}}{A_g} \tag{6. 17}$$

So,

$$M'_{cr} = \frac{f_r I_g}{y_b} + \frac{P_{ei} I_g}{A_g y_b} \tag{6. 18}$$

The total moment and the corresponding deflection are obtained as follows:

$$K_L M_L = K_{L1} M_{L1} + K_L M_{L2} \tag{6. 19}$$

$$M_{L2} = M_L - M_{L1} \tag{6. 20}$$

$$\Delta_{L2} = \frac{K_L M_{L2} L^2}{E_c (I_e)_{L2}} \tag{6. 21}$$

Where M_{L2} is the second part of the total live moment M_L, M'_{cr} as before and $(I_e)_{L2}$ computed from

$$(I_e)_{L2} = \left(\frac{M'_{cr}}{M_{L2}}\right)^3 I_g + \left(1 - \left(\frac{M'_{cr}}{M_{L2}}\right)^3\right) I_{cr} \le I_g \tag{6. 22}$$

Total $\quad \Delta = -\Delta_P + \Delta_D + \Delta_{L1} + \Delta_{L2} = \Delta_{L2}$ (6. 23

And $\quad \Delta_L = \Delta_{L1} + \Delta_{L2}$ (6. 24)

Also, *Branson and Trost* suggested modifying equation (6.22) in the case of an unbonded prestressed member with no bonded nonprestressed steel for crack control. Such a beam produces relatively fewer cracks than the normal bonded crack distribution, but the cracks tend to be larger, this results in greater tensile strains and deflections than in the case involving bonded steel. According to the previous remark, they suggested to modify equation (6.22) to be as follows:

$$(I_e)_{L2} = \left(\frac{M'_{cr}}{M_{L2}}\right)^4 I_g + \left(1 - \left(\frac{M'_{cr}}{M_{L2}}\right)^4\right) I_{cr} \le I_g \tag{6. 25}$$

This modification was checked by *Elzanaty and Nilson* (1982) who, on the basis of experimental results, concluded, " there is no need for such modification for deflection calculations of unbonded prestressed members if adequate bonded non prestressed reinforcement is provided".

Comparing the simplified method and the unified method with the experimental results, *Branson and Shaikh* (1985) concluded that "the results by the two I_e methods were shown to be in relatively close agreement". And they recommended use of the zero deflection method for the following reasons:

- Easy to use as the load corresponding to the zero mid-span deflection (for simply supported beam) will be unique, while that corresponding to the zero curvature or decompression may be different for different points along the span
- Can be used for prestressed and non prestressed concrete
- Can used to compute creep deflections from the zero elastic deflection point

Harajli and Alameh (1989) proposed a new equation to calculate the effective moment of inertia including the tension stiffening for partially prestressed concrete flexural members and calculate deflection as follows:

$$\Delta_t = \frac{M_a K_a}{E_c I_e^*} \tag{6.26}$$

Where:

Δ_t = total deflection due to the external applied moment (M_a)

$$I_e^* = I_g \qquad \text{if} \quad M_a < M_{cr} \tag{6.27}$$

$$I_e^* = \frac{I_{cra}}{1 - \frac{M_{cr}}{M_a}\left(1 - \frac{I_{cra}}{I_g}\right)} \qquad \text{if} \quad M_a \geq M_{cr} \tag{6.28}$$

$$M_{cr} = \frac{f_r I_g}{y_b} + \frac{P_i I_g}{A_g y_b} + P_i e_i \tag{6.29}$$

and

I_{cra} = inertia of the cracked section relative to the centroidal axis

$$I_{cra} = \frac{b_w y^3}{3} + \frac{b_w (c-y)^3}{3} + (B - b_w) h_f \left(\frac{y - h_f}{2}\right)^2 + \frac{(B - b_w) h_f^3}{12} + n_p A_p (d_p - y)^2 + n_s A_s (d_s - y)^2 \tag{6.30}$$

$$y = \frac{\frac{(B-b_w)h_f^{\,2}}{2} + \frac{b_w c^2}{2} + n_p A_p d_{p+} n_s A_s d_s}{(B-b_w)h_f + cb_w + n_p A_p + n_s A_s} \qquad (6.31)$$

and c = neutral axis depth for full cracked section

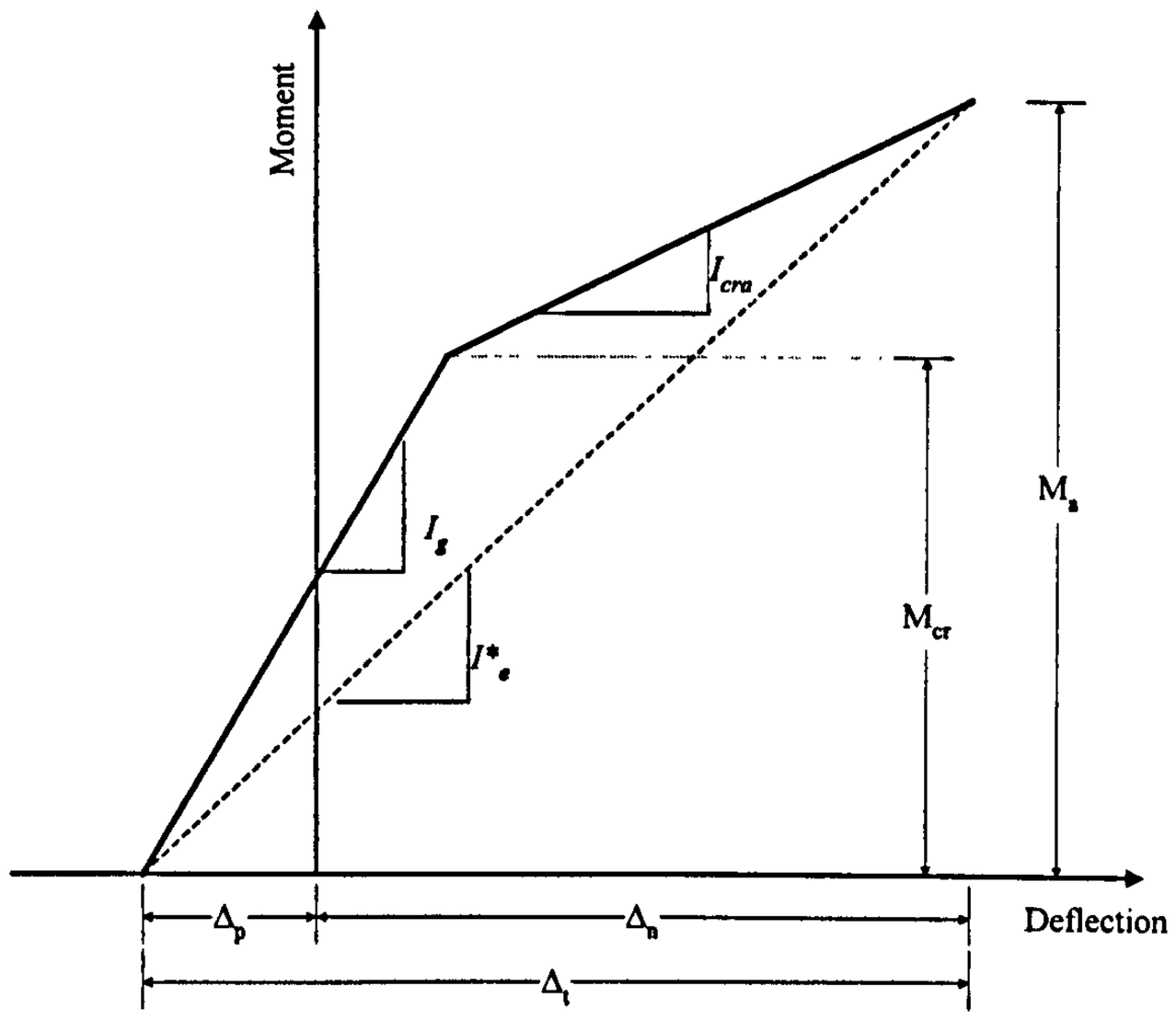

Figure (6.7): Idealization of load-deflection response of prestressed concrete beam (*Harajli and Alameh (1989*)

6.3.2 Deflection of Unbonded or External Prestressed Concrete Beams

Analysis of unbonded, prestressed or partially prestressed, concrete beams is more difficult than that with bonded tendons, as the stress increase in the tendons beyond the effective prestress due to external loading is member-dependent (depends on the deformation of the whole member) instead of being section-dependent. Thus, the increase in stress in unbonded tendons is assumed uniform at all sections and must be determined from the analysis of the deformation of the entire structure. This is true for the elastic, inelastic, and ultimate limit states (*Naaman and Alkhairi*, 1991 part 1&2).

However, before cracking the increase in stress of the unbonded tendon is small and can be neglected, while after cracking, the increase in tendon stress is significant and needs to be determined to calculate the properties of the cracked section.

Unbonded tendons can be treated as bonded tendons using a simple modification (a bond or strain reduction coefficient) as suggested by *Naaman* (1990). Thus, previous analytical solutions with bonded tendons could be used. The concept of bond reduction coefficient for the elastic uncracked and elastic cracked stages is explained next, while that for ultimate stage is discussed later.

6.3.2.1 Elastic uncracked stage

For the elastic uncracked section analysis, a bond reduction coefficient Ω was introduced and is defined as

$$\Omega = \frac{(\Delta\varepsilon_{psu})_m}{(\Delta\varepsilon_{psb})_m} = \frac{(\Delta\varepsilon_{psu})_{av}}{(\Delta\varepsilon_{cps})_m} \tag{6. 32}$$

Where $(\Delta\varepsilon_{psu})_m$ is the strain increase in the unbonded tendons, $(\Delta\varepsilon_{psb})_m$ is the strain increase in the equivalent bonded tendon, and $(\Delta\varepsilon_{cps})_m$ is the strain increase in the concrete at the level of tendon beyond effective prestress, all taken at the section of maximum moment (here considered to be the critical section for design). This last term $(\Delta\varepsilon_{cps})_m$ is the same as the strain increase in the bonded tendon. Note that the strain increase in the unbonded tendon is assumed to be the same at any section along the span (it is an average value of strain increase along the span), and that Ω=1 represents the case where the tendons are assumed fully bonded.

For simply supported beams with constant cross section, symmetrical loading, and symmetrical tendon profile, it can be shown that Ω can be calculated in the most general case from:

$$\Omega = \frac{2}{M_{\max}(e_0)_{\max}} L \int_0^{L/2} M(x)e_0(x)dx \tag{6. 33}$$

Where M_{max} and M(x) are, respectively, the change in bending moment at the critical section and at any section x along the span, and $(e_o)max$ and $e_o(x)$ are the corresponding eccentricities of the tendons at these sections. It is assumed that the change in the bending moment is taken with respect to a reference stage such as that corresponding to the effective prestress and dead load moment. The stress in the

tendon at the reference stage is assumed known and equal to the effective prestress f_{pe}.

The value of Ω was calculated by *Naaman* (1990) for most common loading and tendon profiles. Ω depends on the type of loading, the tendons profile, and the ratio of end eccentricity to maximum eccentricity as shown in Table (6.2)

Table (6. 2): *Value of strain reduction coefficient at uncracked stage*

Type of loading and tendon profile	***Strain reduction coefficient (uncracked stage)***
Uniform load and straight tendons	$\Omega = 2/3$
Uniform load and parabolic tendons	$\Omega = (8/15) + (1/4)(e_s/e_c)$
Third point load and straight tendons	$\Omega = 2/3$
Third point load and parabolic tendons	$\Omega = (44/81) + (10/81)(e_s/e_c)$
Concentrated midspan load and straight tendons	$\Omega = 0.5$
Concentrated midspan load and parabolic tendons	$\Omega = (5/12) + (1/12)(e_s/e_c)$

e_s = eccentricity at end supports; e_c = eccentricity at midspan

Also, Ω for third point loading and trapezoidal tendons is $\Omega = (2 + e_s/e_c)/9$

6.3.2.2 Elastic cracked stage

After cracking and within the elastic cracked stage, the increase in strain (stress) in the unbonded tendons can be calculated by introducing a bond reduction coefficient in the cracked stage Ω_{cr}. For simply supported beams with symmetrical loading and tendon profile and assuming a single crack occurs at the section of maximum moment, the value of Ω_{cr} can be calculated from the following general equation:

$$\Omega_{cr} = \Omega\frac{I_{cr}}{I_g} + \frac{2}{L}\left(1 - \frac{I_{cr}}{I_g}\right)\int_0^{L_c/2} \frac{M(x)e_0(x)}{M_{\max}(e_0)_{\max}}dx \qquad (6.34)$$

Where L_c is the width of the crack or the width of the smeared crack region. Values of Ω_{cr} were computed and given in detail by *Naaman* (1990) who suggested, if the value of L_c is small relative to the value of L, as is generally the case, Ω_{cr} can be taken as follows:

$$\Omega_{cr} \cong \Omega \frac{I_{cr}}{I_g} \tag{6. 35}$$

Another equation to calculate Ω_{cr} was derived by *Harajli and Kanj* (1992) based on the following assumptions:

- All beam sections follow a similar idealized moment-curvature relationship, as shown in Figure (6.8) (correct only for straight tendon profile)
- The neutral axis position is independent on the applied load (correct only for reinforced concrete members)

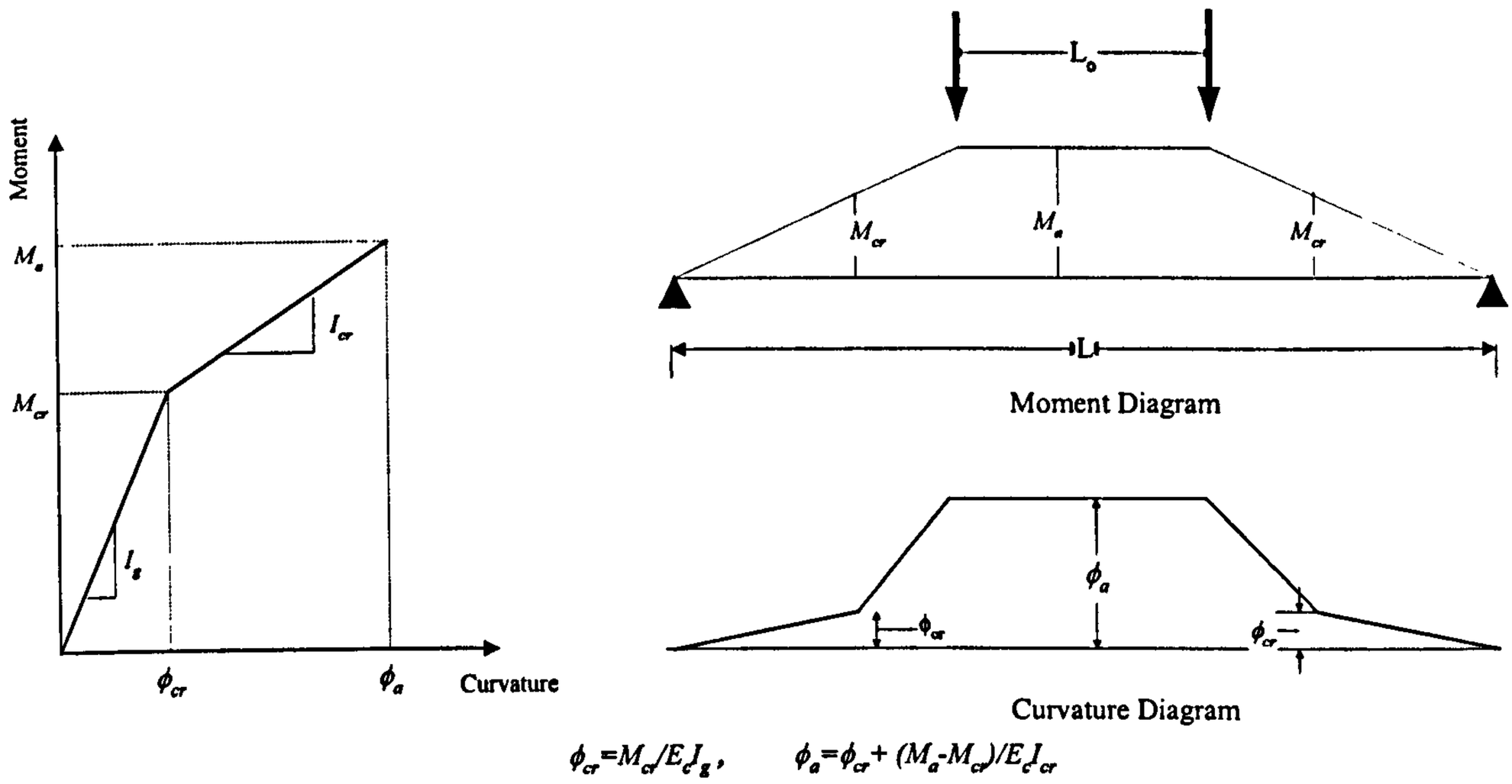

Figure (6.8): Assumed curvature distribution along span length

Based on these assumptions, the following approximate expression was derived:

$$\Omega_{cr} = \Omega - 0.5\left(1-\frac{L_o}{L}\right)\left(\frac{M_{cr}}{M_a} - \frac{1}{\left(\frac{M_{cr}}{M_a}-1\right)\frac{I_g}{I_{cr}}+1}\right) \tag{6. 36}$$

Where I_{cr} is calculated relative to the centroidal axis of the cracked section and Ω as given in equation (30).

Also, *Harajli and Kanj* (1992) stated that the strain reduction coefficient Ω_{cr} does not differ significantly from its value before cracking, as reducing the inertia after

cracking by 50%; I_{cr}/I_g =0.5 resulted in reducing Ω_{cr} by maximum 10% for the third-point loading and 17% for the single concentrated loading, compared to the magnitude of Ω_{cr} before cracking. Hence, they suggested, in order to simplify the analysis of the partially prestressed unbonded members, to assume that the strain reduction factor in the postcracking stage is equal to its exact value in the precracking stage as follows:

$$\Omega_{cr} = \Omega \tag{6. 37}$$

and deflection due to the total applied load can be calculated as given in equations (6.26 to 6.31) by replacing A_p by ΩA_p or $\Omega_{cr} A_p$.

6.3.3 Code Methods

6.3.3.1 Eurocode 2 (ENV 1992-1-1)

Two methods were suggested to calculate the deflection of both reinforced and prestressed concrete flexural members by the code, one rigorous and the other more approximate. In the more rigorous approach, the curvature is calculated at a reasonable number of sections along the beam and then the deflection is calculated by numerical integration.

In the approximate method, the deflection is calculated twice assuming the whole member be in the uncracked and fully cracked conditions and then employ the following equation:

$$\Delta = \zeta \Delta_{II} + (1 - \zeta)\Delta_{I} \tag{6. 38}$$

where

$$\zeta = 1 - B_1 B_2 (M_{cr}/M)^2 \tag{6. 39}$$

B_1 is a coefficient which takes account of the bond properties of the bars

= 0.5 for plain bars

= 1.0 for high bond bars

B_2 is a coefficient takes account of the duration of the loading or of repeated loading.

= 1 for a single short-term loading

$= 0.5$ for sustained loads or many cycles of repeated loading

Δ the deflection

Δ_I the deflection calculated on the basis of an uncracked section

Δ_{II} the deflection calculated on the basis of a cracked section

both Δ_I and Δ_{II} can be calculated from the general equation:

$$\Delta = K\frac{ML^2}{EI} \qquad (6.40)$$

I the inertia of either the cracked or the gross section relative to the bending moment.

However, it is not clear in the code the value of the cracking moment nor the applied moment at which this equation can be used. *Ghali and Favre* (1994) suggested using this equation after the decompression moment that produced zero stress at the bottom fibre (in the case of simple beam).

6.3.3.2 BS 8110-2 (1985)

Two methods were suggested to be used to calculate the deflection depending on the curvature. The first method is to calculate the deflection by integrating the curvature (as Eurocode *2*) and the second method (the simplified method) is to calculate the deflection directly from the following equation:

$$\Delta = kL^2\frac{1}{r_b} \qquad (6.41)$$

Where

k is a constant depending on the shape of the bending moment diagram.

$\frac{1}{r_b}$ is the curvature at mid span = $\frac{M}{E_C I}$

I is the inertia of either the cracked or the gross section relative to the bending moment.

However, BS8110 does not use a transition between the cracked and uncracked stages as actually should be.

6.3.3.3 ACI 318 (1999)

After cracking and due to the effect of tension stiffening, ACI 318 requires that a bilinear moment-deflection relationship be used to calculate instantaneous deflections. When the magnitude of tensile stress in service exceeds $6\sqrt{f'_c}$, I_g is used for the portion of moment not producing such tensile stress, while for the remaining portion of moment I_{cr} is used. The effective moment of inertia I_e for simply supported beams is given as follows:

$$I_e = \left(\frac{M_{cr}}{M_a}\right)^3 I_g + \left(1 - \left(\frac{M_{cr}}{M_a}\right)^3\right) I_{cr} \leq I_g \qquad (6.42)$$

Where

$$\left(\frac{M_{cr}}{M_a}\right) = \left(1 - \frac{f_{TL} - f_r}{f_L}\right) \qquad (6.43)$$

f_r = modulus of rupture = $7.5\sqrt{f'_c}$ psi

f_{TL} = total calculated stress in member

f_L = calculated stress due to live load

M_{cr} = moment due to that portion of unfactored live load moment M_a that causes cracking

M_a = maximum unfactored live load moment

6.3.4 Deflection of Externally Prestressed Concrete Beams

Table (6.3) shows the extension of the previous methods to introduce the effect of the external prestressing force in the deflection calculations. Also, Figures (6.9 and 6.10) show the relation between moment and deflection (actual and theoretical) of beams PG11 and PG32 including the deflection due to the internal and external prestressing forces.

From these figures, it can be seen that there is an increase in the actual deflection due to the prestressing force compared with that calculated using the ordinary

equations used in case of bonded or unbonded internally prestressed concrete beams. This can be attributed to the increase in the eccentricity of the external prestressing force during prestressing, rather than its original value, which was used in the calculation. So, in order to check the accuracy of the modified methods, actual and theoretical deflection due to the external applied moment only were compared. Figures (6.11 to 6.22) show the relation between the actual and the theoretical deflections and the external applied moment only. While Figures (6.23 to 6.29) show the relation between the actual and the theoretical deflection calculated using the modified methods.

It is also worth remarking that beam PG41 (strengthened after 0.36 P_{ult}) was calculated twice, first by assuming the modulus of rupture equal to zero ($f_r = 0$) and second by taking f_r as the code value. The second assumption gave better accuracy than the first, this may be because the cracks did not propagated or extended in the web and hence its stiffness was only slightly affected by such cracks and not as seriously affected as that of beam PG42 (strengthened after 0. 6 P_{ult}).

Table (6. 3): Extending the calculation deflection methods to include the effect of external prestressing force.

Method	*Cracking moment (M_{cr})*	*Effective inertia (Ie)*	*Deflection*
Shaikh & Branson (1970)	$M_{cr} = f_r \frac{I}{y_b} + \left(\frac{p_{ei} + p_{ex}}{A}\right)\frac{I}{y_b} + p_{ei}e_i + p_{ex}e_e - M_d$ using f_r in calculation	$I_e = \left(\frac{M_{cr}}{M_a}\right)^3 I_g + \left(1 - \left(\frac{M_{cr}}{M_a}\right)^3\right) I_{cr} \le I_g$ where M_a = live load moment (M_L)	$\Delta_L = \frac{K_L M_L L^2}{E_c (I_e)}$
Branson and Trost (1982)	$M_{cr} = \frac{f_r I_g}{y_b} + \frac{P_{ei} I_g}{A_g y_b} + \frac{P_{ex} I_g}{A_g y_b}$ using f_r in calculation	$(I_e)_{L2} = \left(\frac{M_{cr}}{M_{L2}}\right)^3 I_g + \left(1 - \left(\frac{M_{cr}}{M_{L2}}\right)^3\right) I_{cr} \le I_g$ where M_{L2} = part of live load moment after zero deflection	$\Delta_{L2} = \frac{K_L M_{L2} L^2}{E_c (I_e)_{L2}}$
Harajli and Kanj (1990)	$M_{cr} = \frac{f_r I_g}{y_b} + \frac{P_{ei} I_g}{A_g y_b} + P_{ei}e_i + \frac{P_{ex} I_g}{\Omega A_g y_b} + P_{ex}e_e$ using f_r in calculation	$I_e^* = \frac{I_{cra}}{1 - \frac{M_{cr}}{M_a}\left(1 - \frac{I_{cra}}{I_g}\right)}$ $I_{cra} = \frac{b_w y^3}{3} + \frac{b_w (c-y)^3}{3} + (B - b_w)h_f\left(\frac{y - h_f}{2}\right)^2 + \frac{(B - b_w)h_f^3}{12} + n_p A_{pS}(d_p - y)^2 + n_S A_s (d_s - y)^2 + \Omega n_e A_e (d_e - y)^2$	$\Delta_t = \frac{M_a K_a}{E_c I_e^*}$

$$I_{cr} = b_w c^3/3 + (B - b_w)h_f^{\,3}/12 + (c - h_f/2)^2 + n_p A_{ps}(d_p - c)^2 + n_s A_s (d_s - c)^2 + \Omega n_e A_e (d_e - c)^2$$

Method	*Cracking moment (M_{cr})*	*Effective inertia (I_e)*	*Deflection*
ACI-89	$\left(\frac{M_{cr}}{M_a}\right)=\left(1-\frac{f_{TL}-f_r}{f_L}\right)$ $f_{TL}=\frac{M_a y_b}{I_g}+\frac{M_D y_b}{I_g}-\frac{P_{ei}}{A_g}-\frac{P_{ei}e_i y_b}{I_g}-\frac{P_{ex}}{A_g}-\frac{P_{ex}e_e y_b}{I_g}$ $f_L=\frac{M_a y_b}{I_g}$ *and* $f_r=7.5\sqrt{f'_c}$	$I_e=\left(\frac{M_{cr}}{M_a}\right)^3 I_g+\left(1-\left(\frac{M_{cr}}{M_a}\right)^3\right)I_{cr}\le I_g$ where M_a = maximum live load moment	$\Delta_L=\frac{K_L M_L L^2}{E_c(I_e)}$
EC2	$M_{dec}=\frac{P_{ei}I_g}{A_g y_b}+P_{ei}e_i+\frac{P_{ex}I_g}{A_g y_b}+P_{ex}e_e$ $M_{cr}=\frac{f_{ctm}I_g}{y_b}$ using f_{ctm} instead of f_r	I = the inertia of either the cracked or the gross section relative to the bending moment. M_{L3} = part of live load moment after decompression	$\Delta=\zeta\Delta_{\Pi}+(1-\zeta)\Delta_I$ $\Delta_I=\frac{K_L M_{L3} L^2}{E_c(I_g)}$ $\Delta_{\Pi}=\frac{K_L M_{L3} L^2}{E_c(I_{cr})}$

- In all methods, I_{cr} relative to the neutral axis was used except in *Harjli and Kanj* method.
- In all methods (ΩA_e) replaced (A_e) in neutral axis and Inertia calculations.

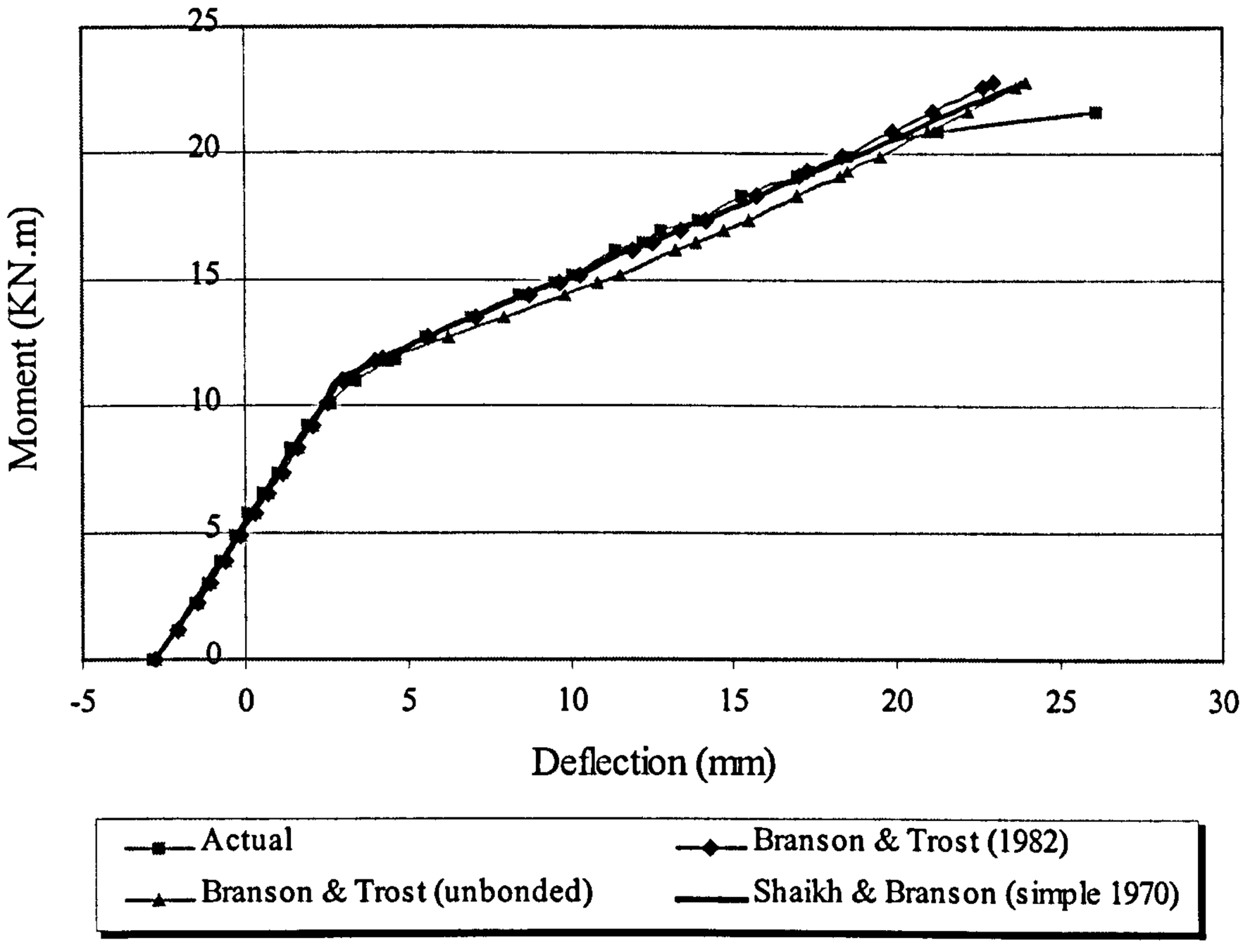

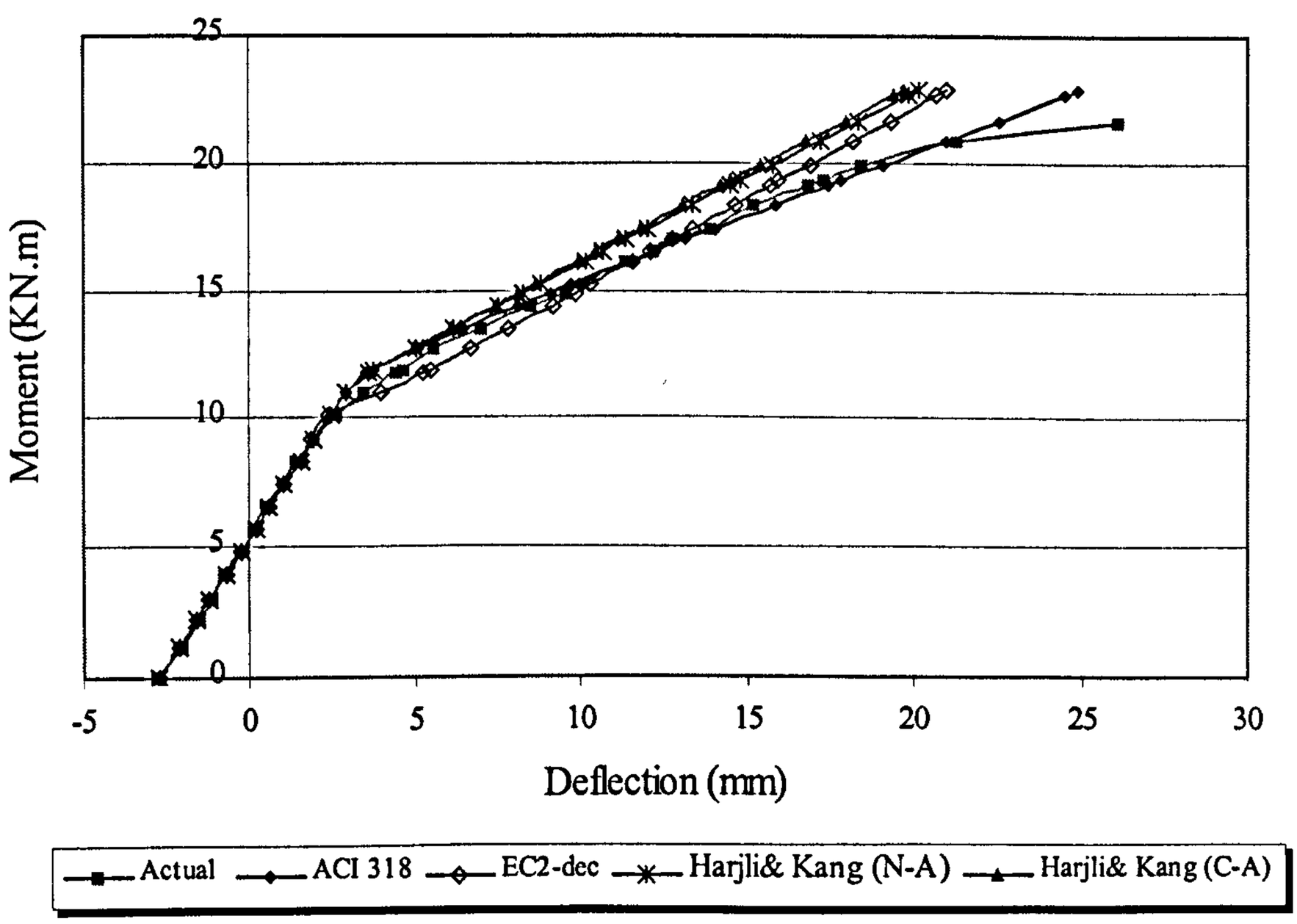

Figure (6.9): Comparison between actual and theoretical deflections of beam PG11

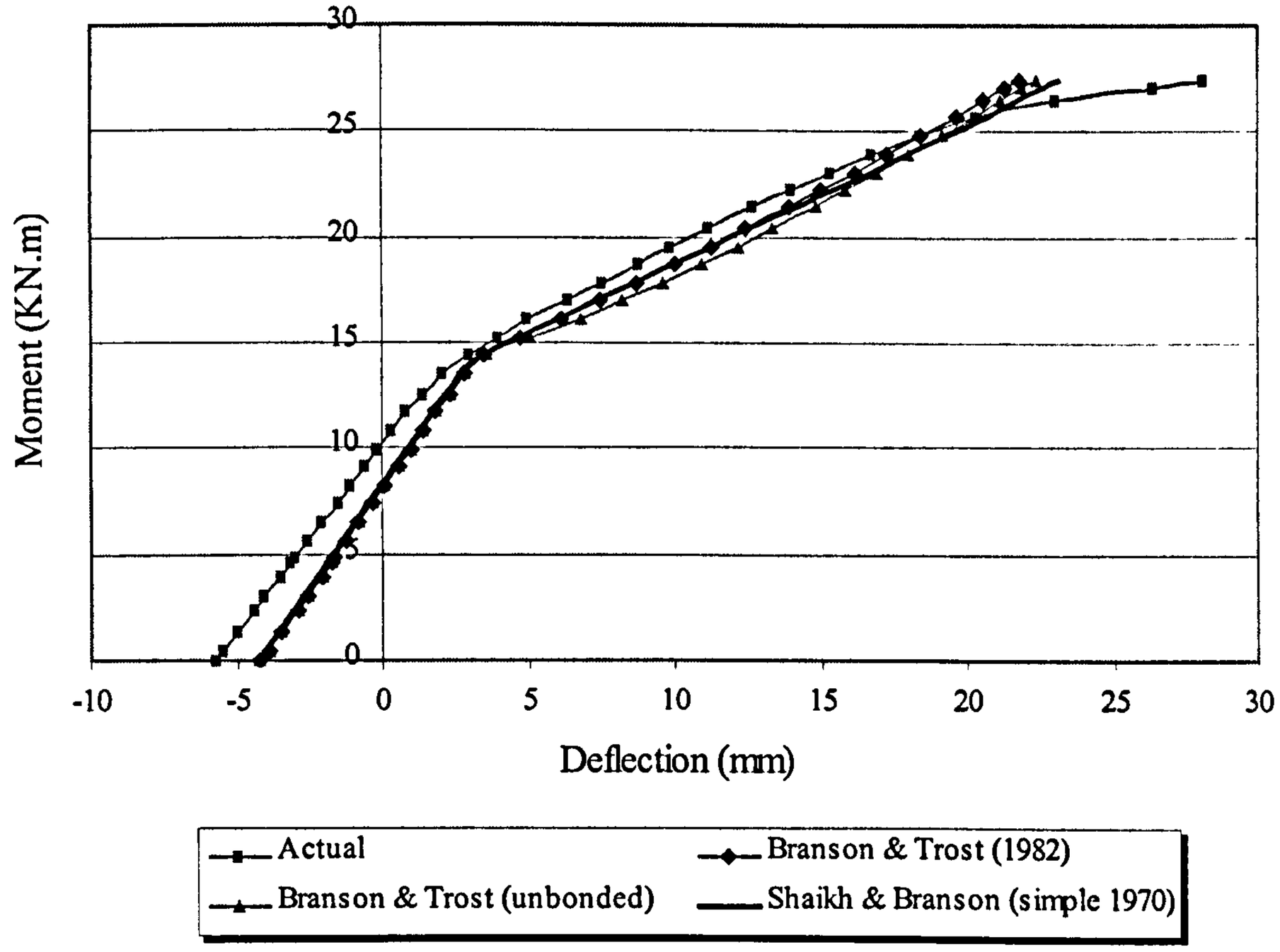

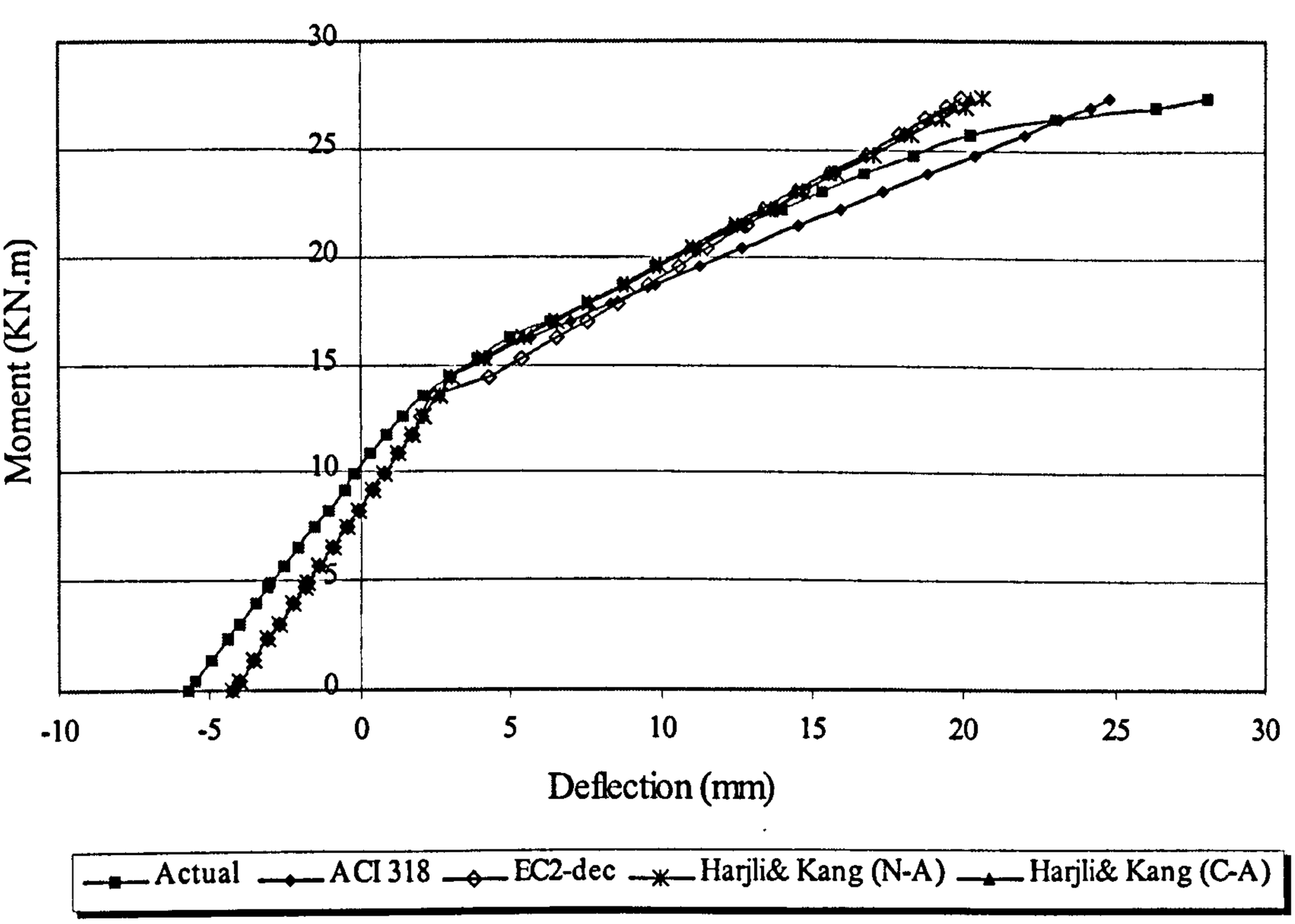

Figure (6.10): Comparison between actual and theoretical deflections of beam PG32

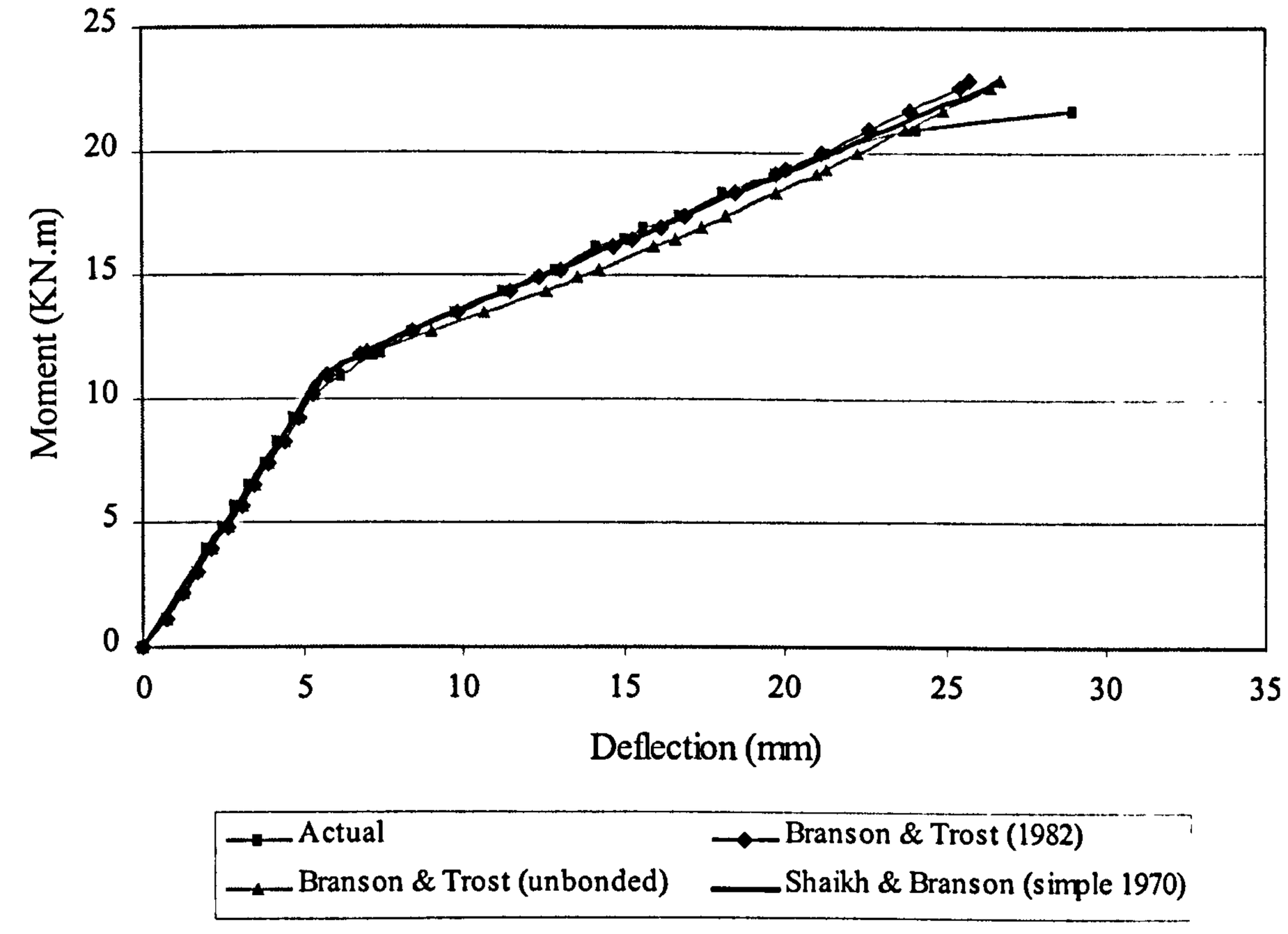

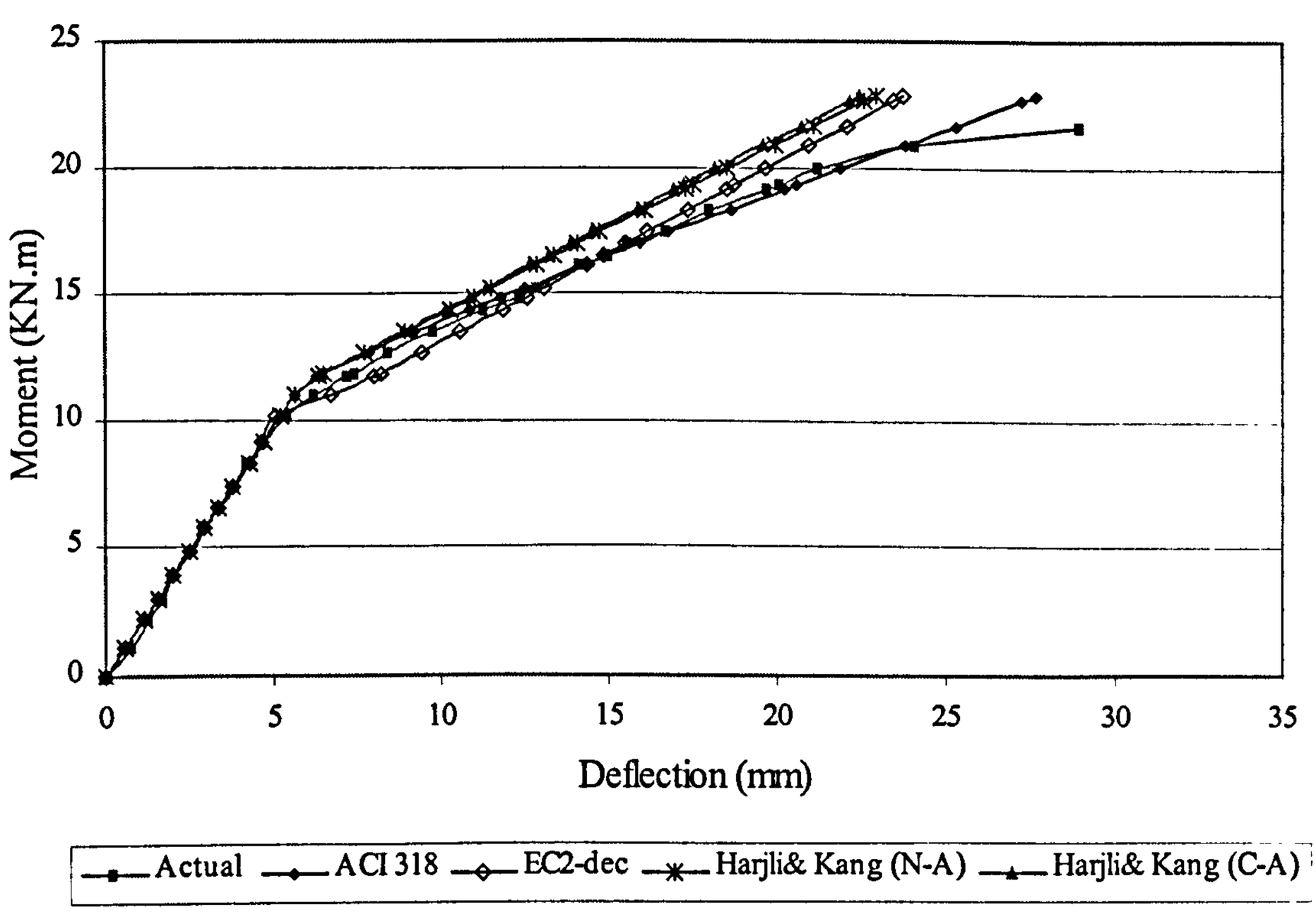

Figure (6.11): Comparison between actual and theoretical deflections due to live moment of beam PG11

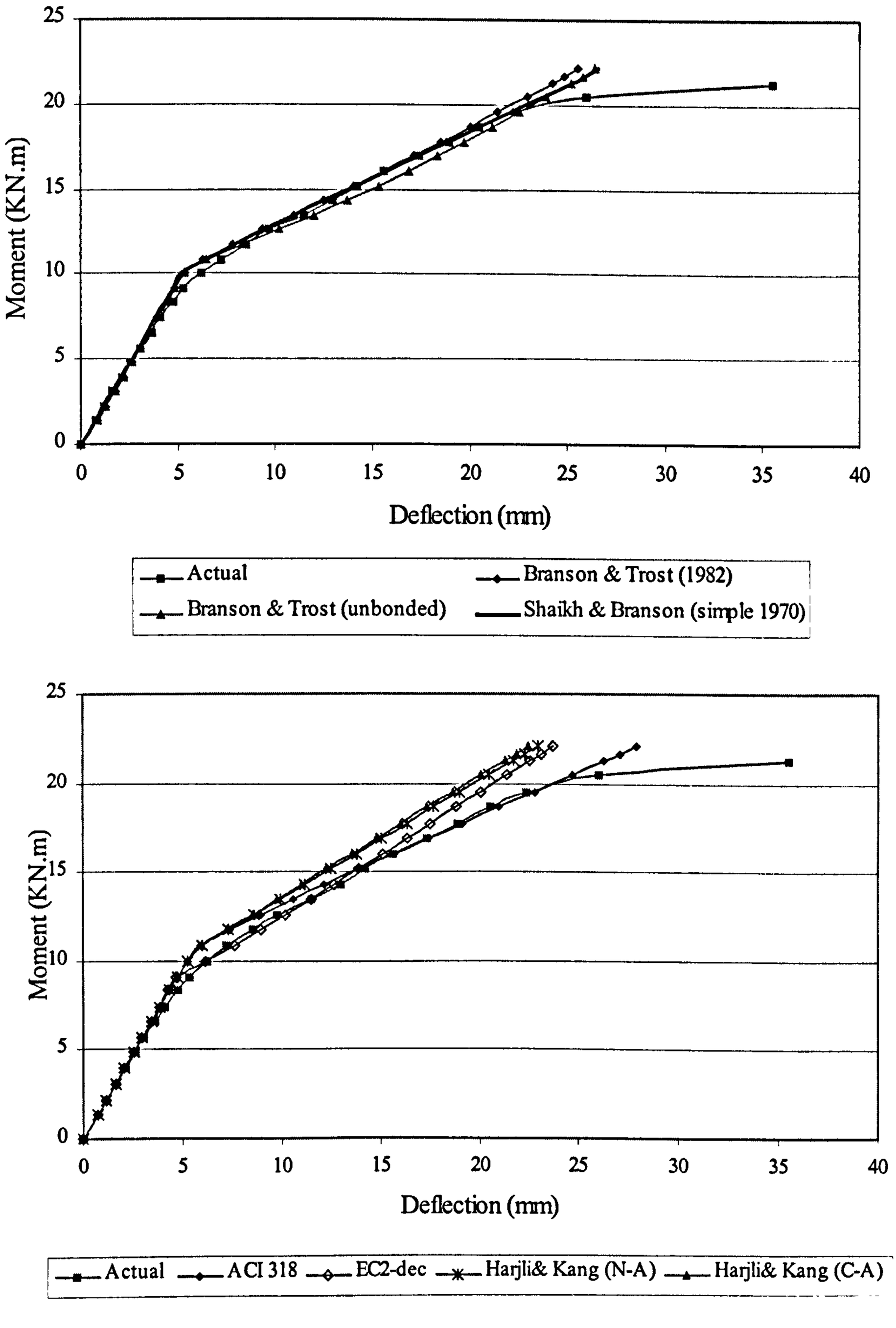

Figure (6.12): Comparison between actual and theoretical deflections due to live moment of beam PG12

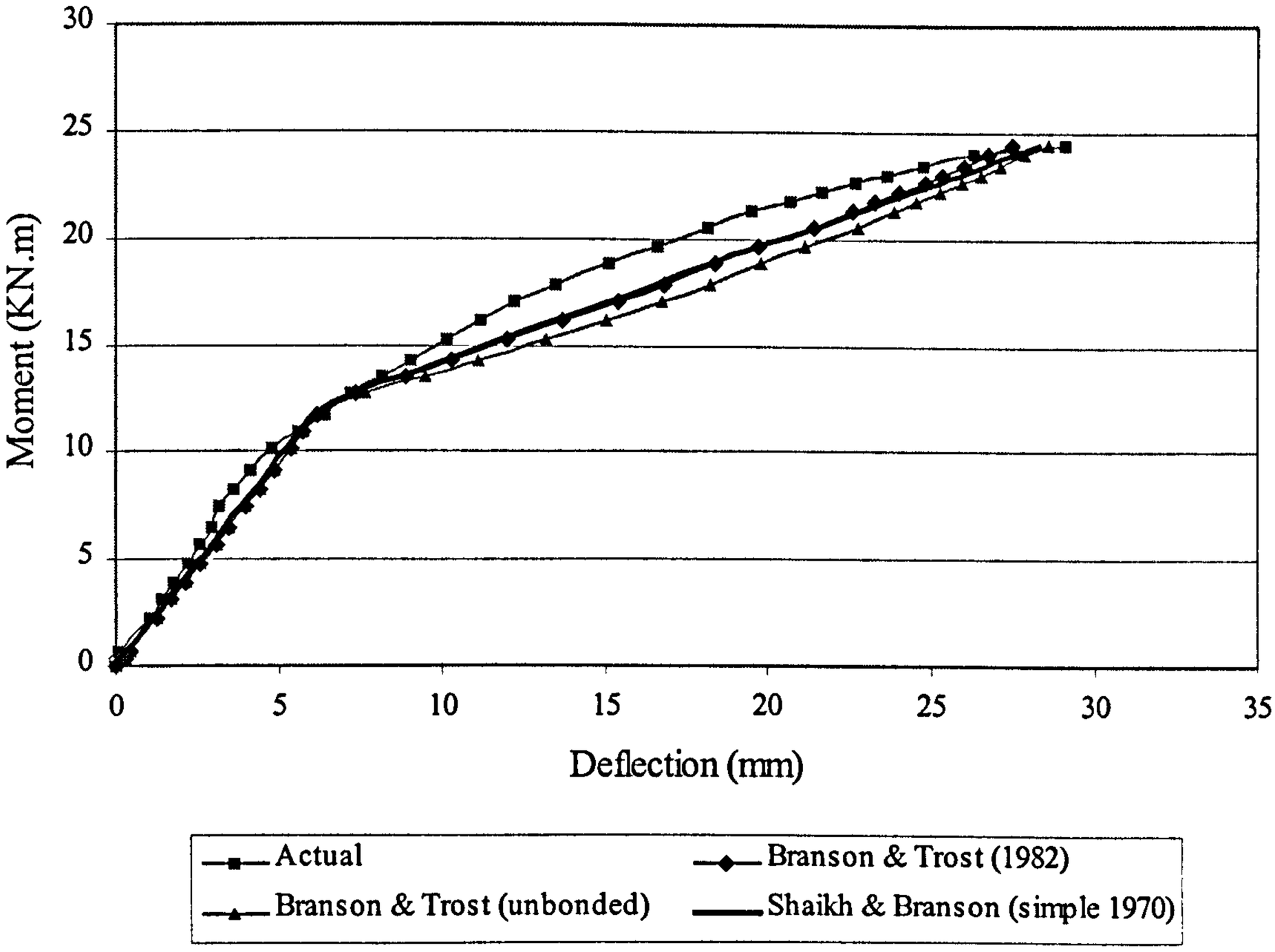

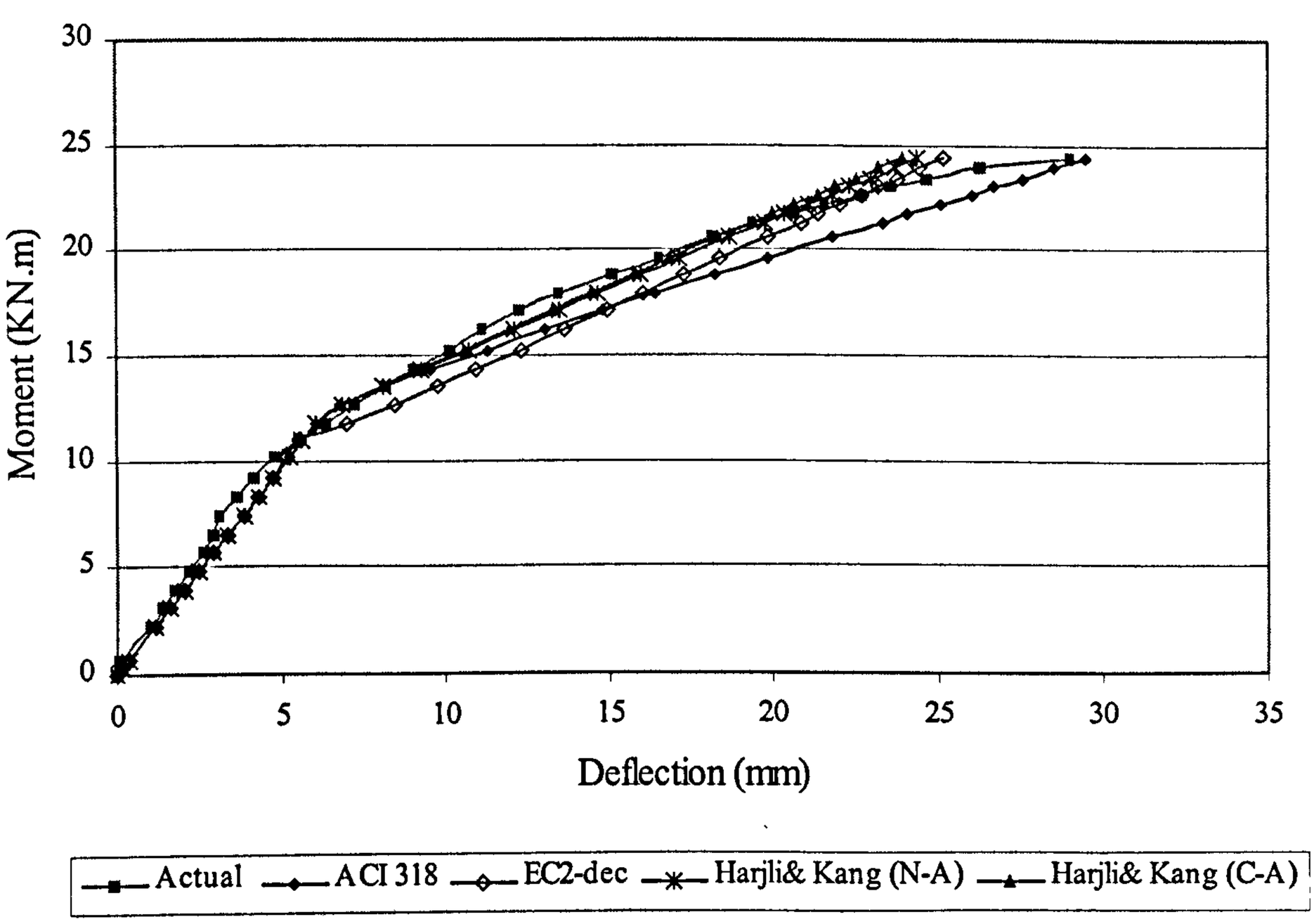

Figure (6.13): Comparison between actual and theoretical deflections due to live moment of beam PG13

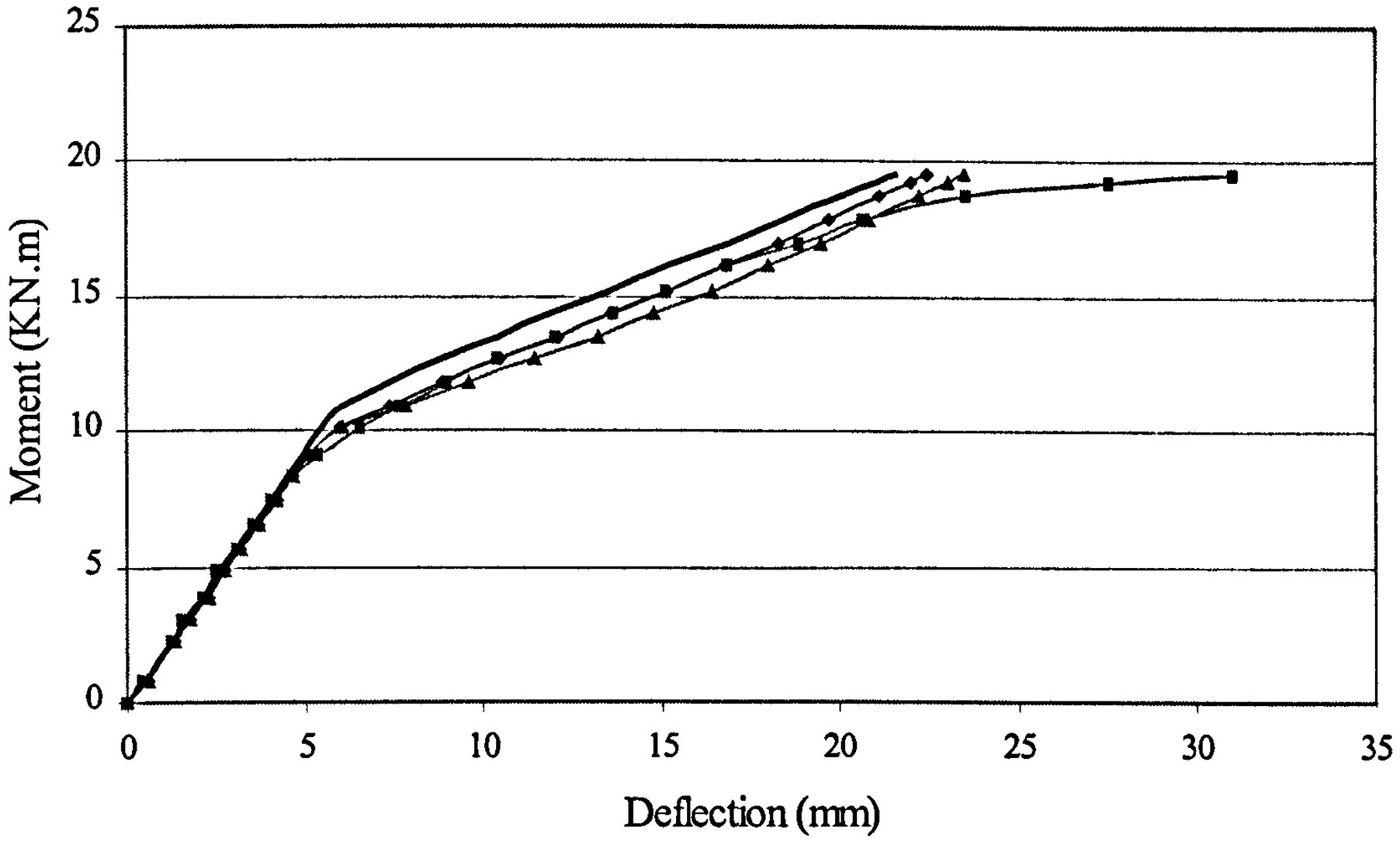

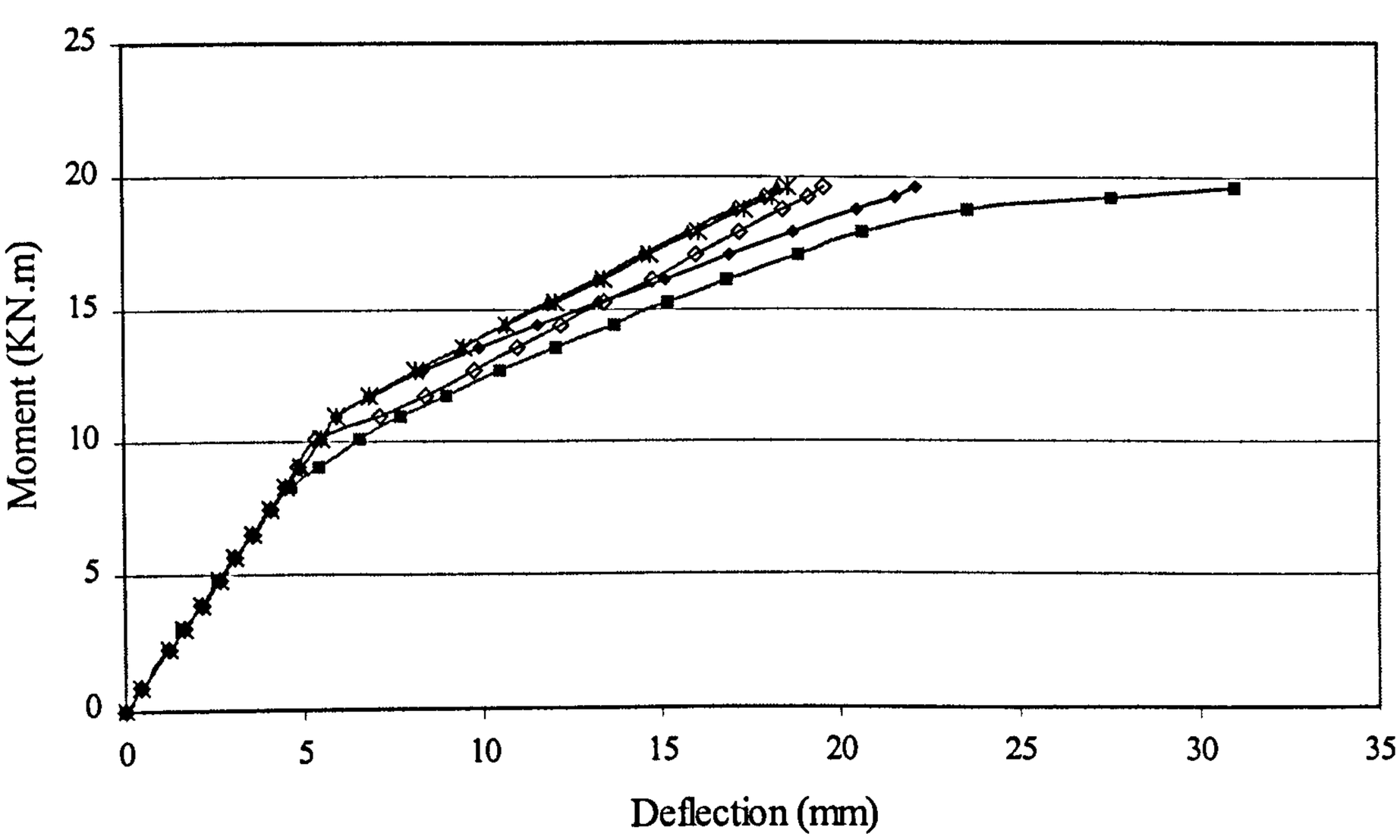

Figure (6.14): Comparison between actual and theoretical deflections due to live moment of beam PG21

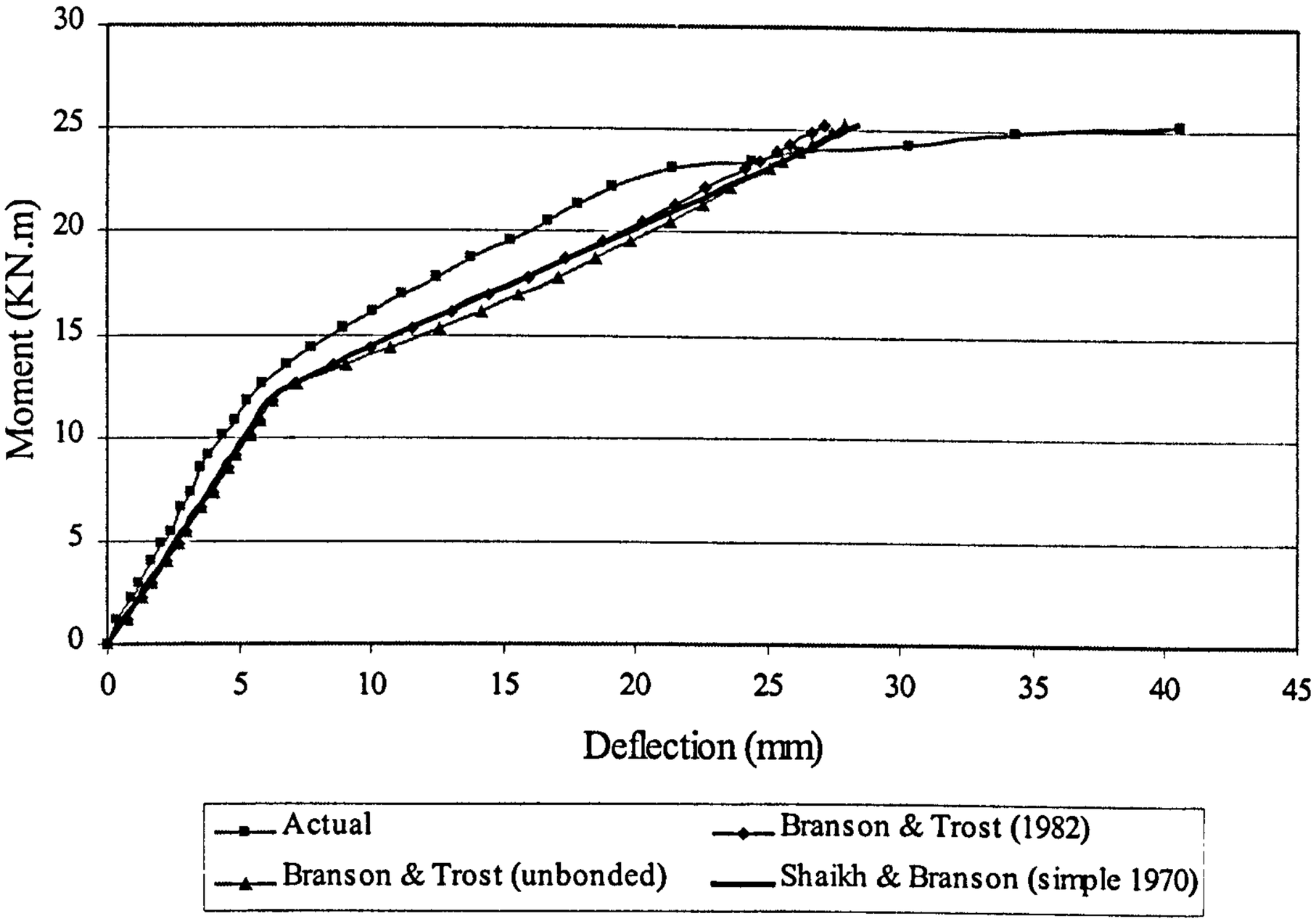

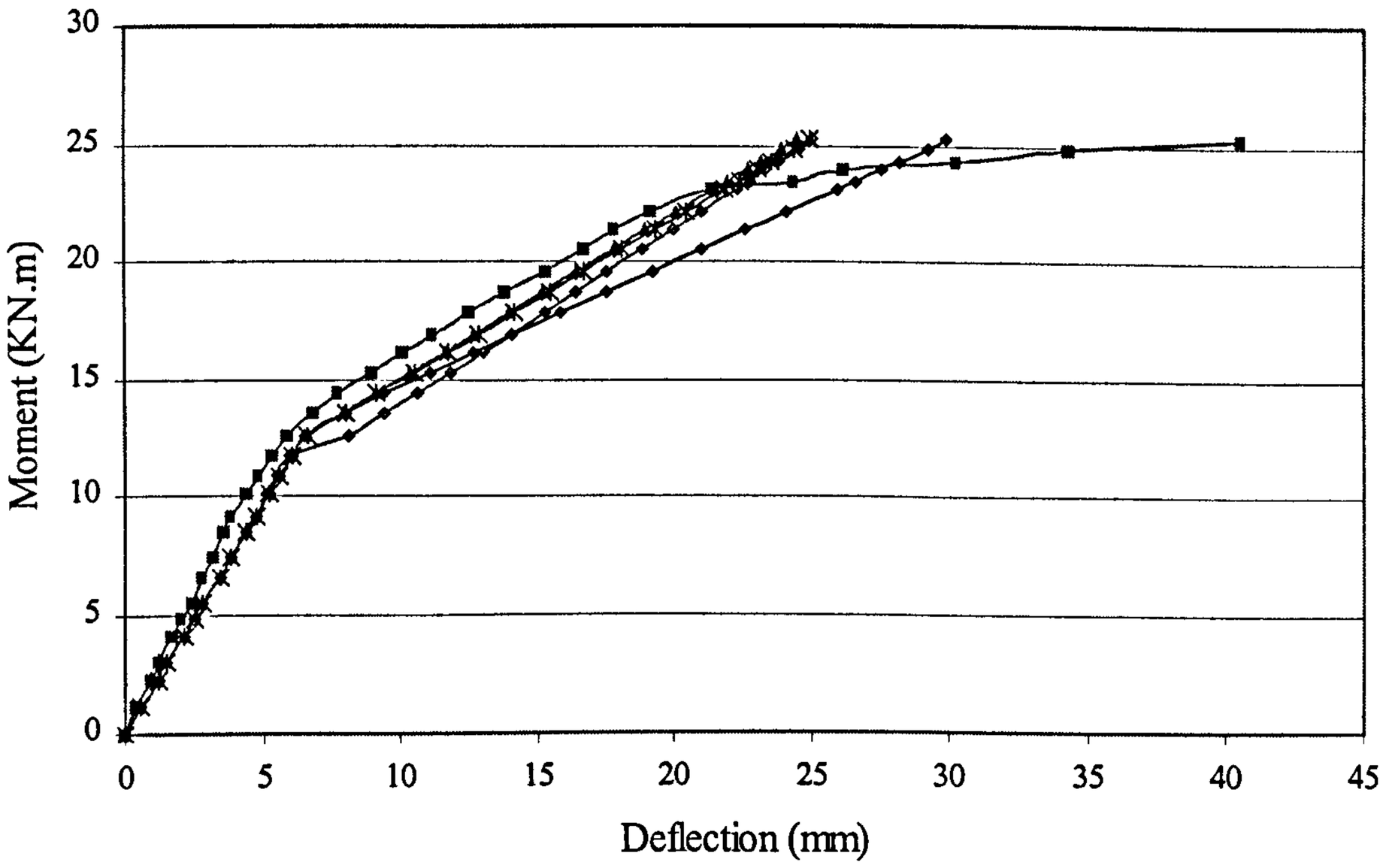

Figure (6.15): Comparison between actual and theoretical deflections due to live moment of beam PG31

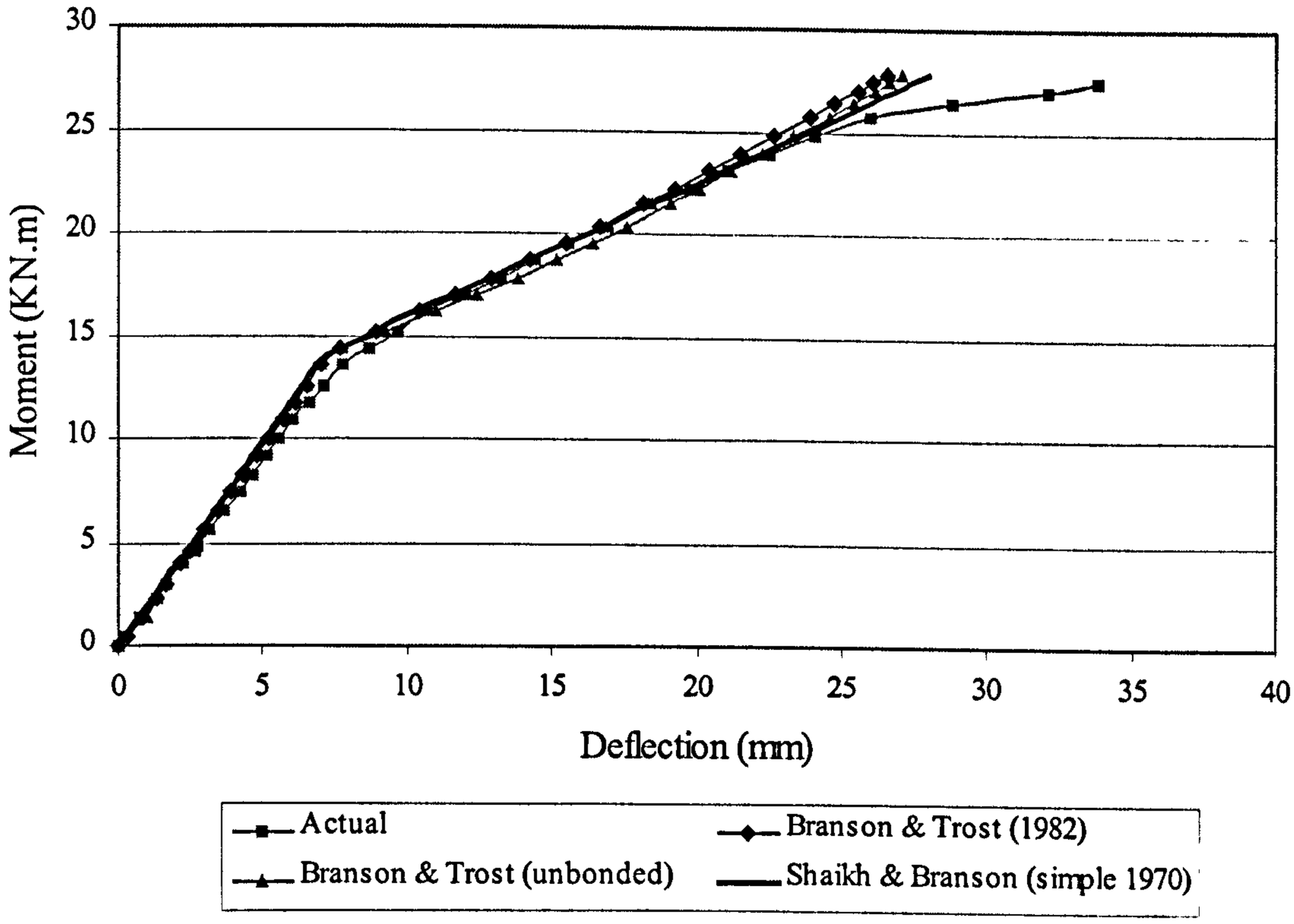

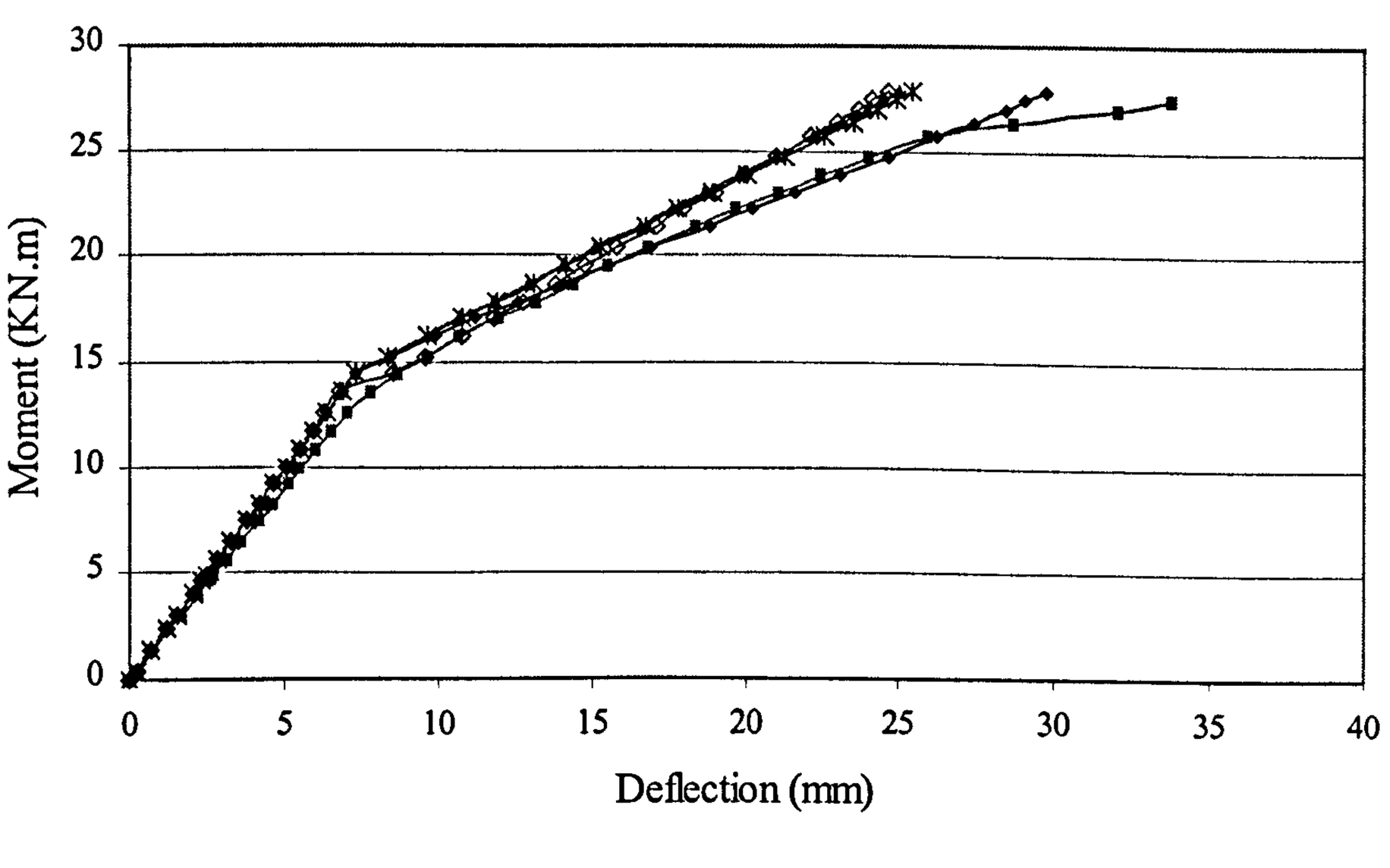

Figure (6.16): Comparison between actual and theoretical deflections due to live moment of beam PG32

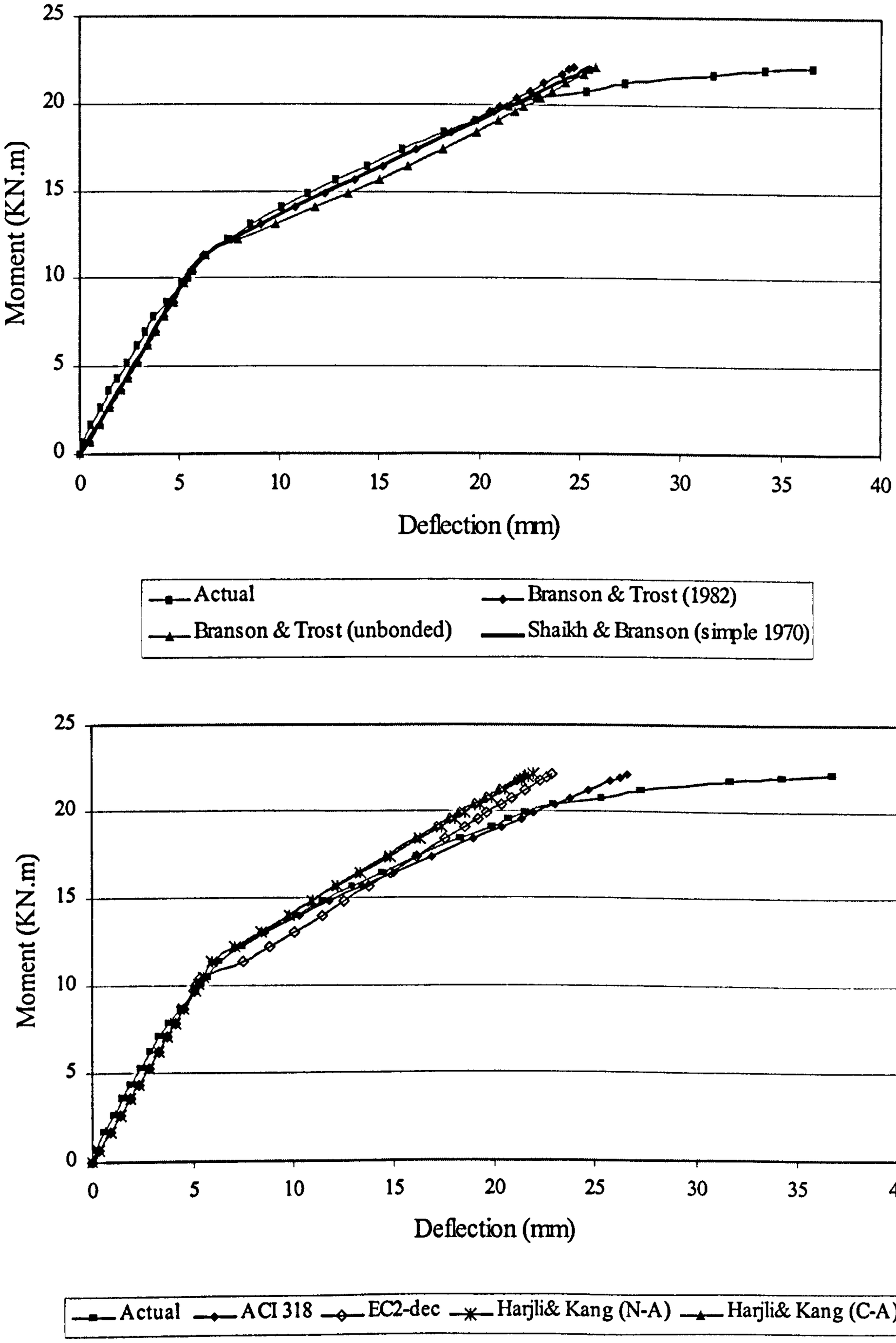

Figure (6.17): Comparison between actual and theoretical deflections due to live moment of beam PG41

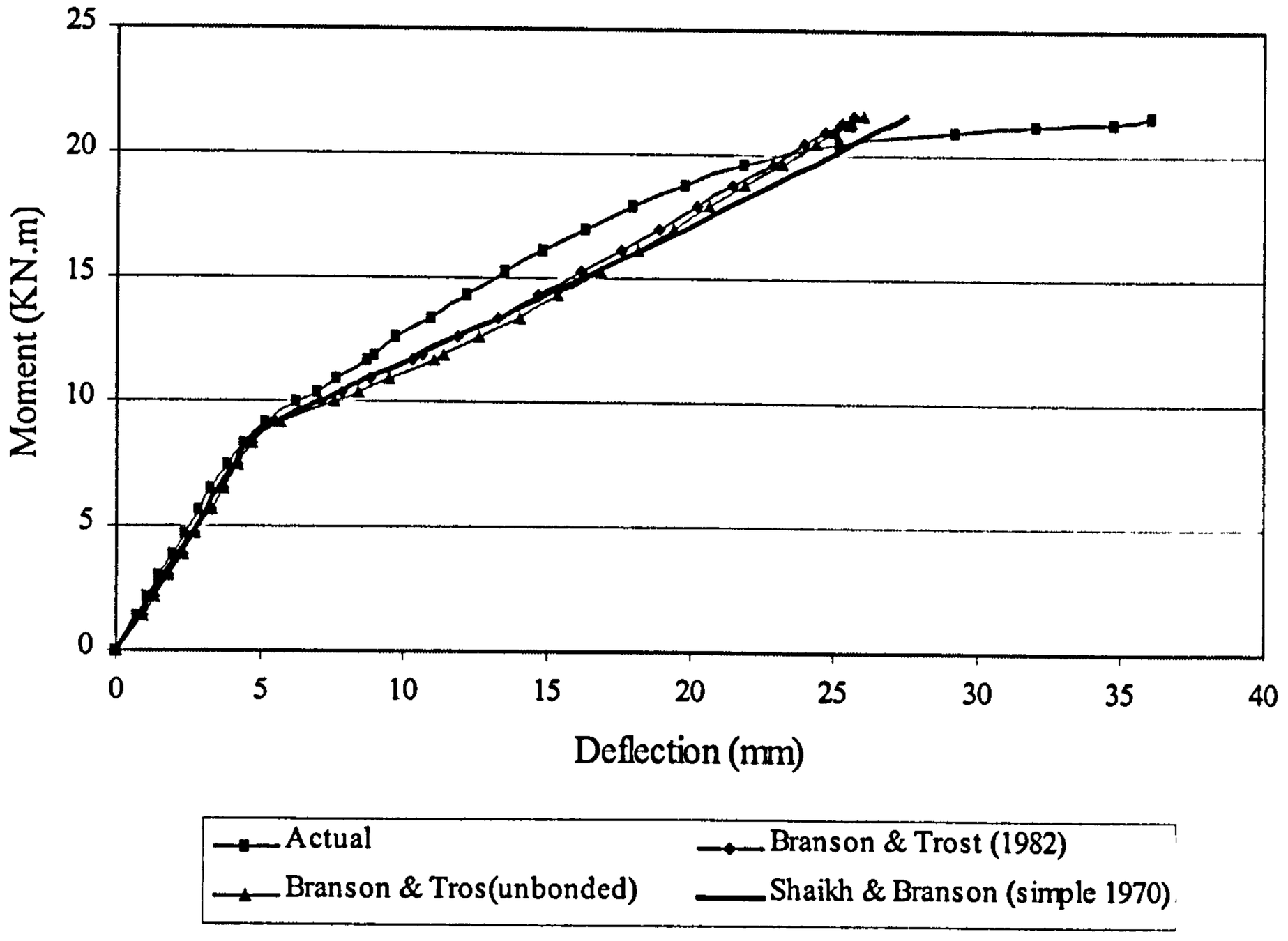

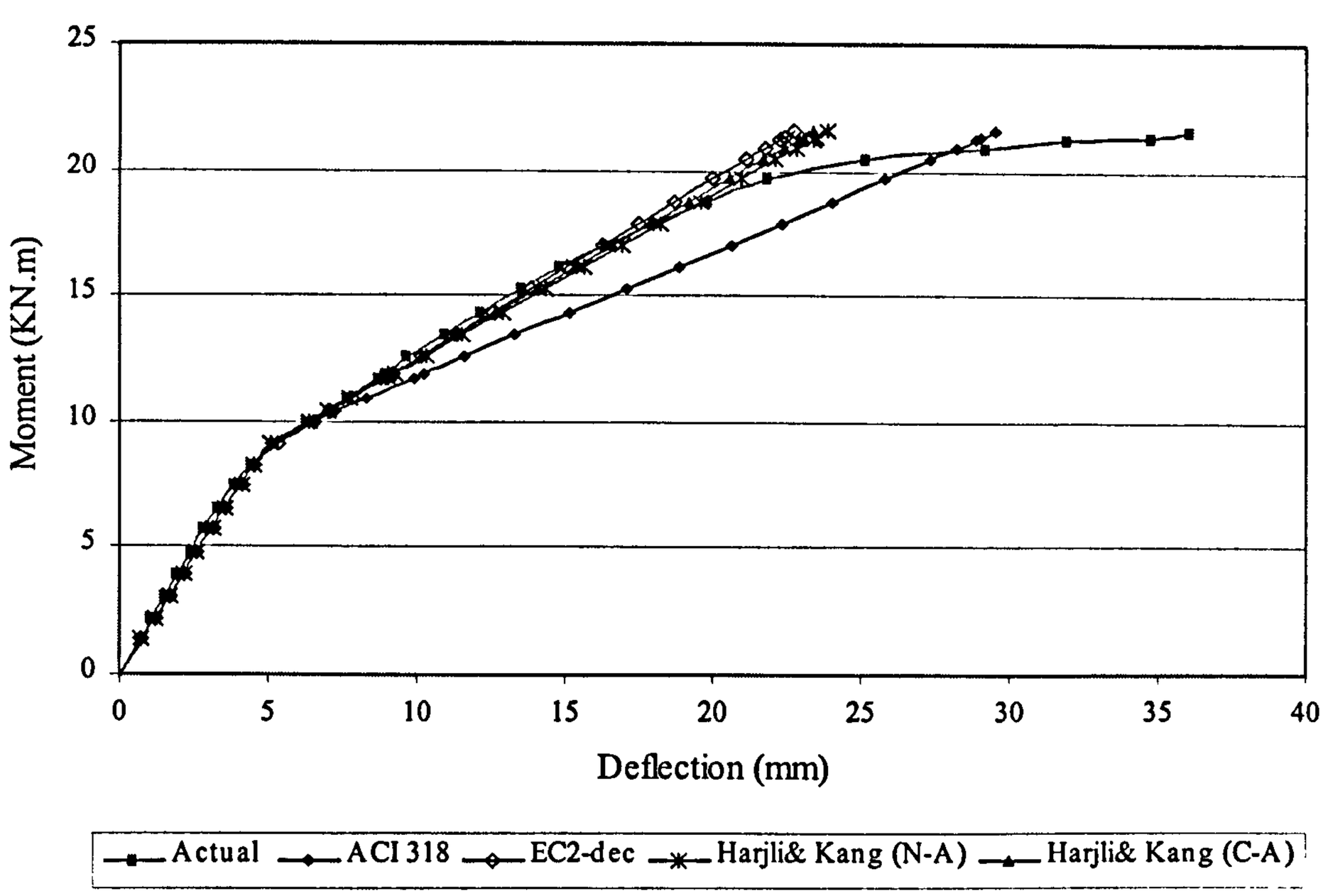

Figure (6.18): Comparison between actual and theoretical deflections due to live moment of beam PG42

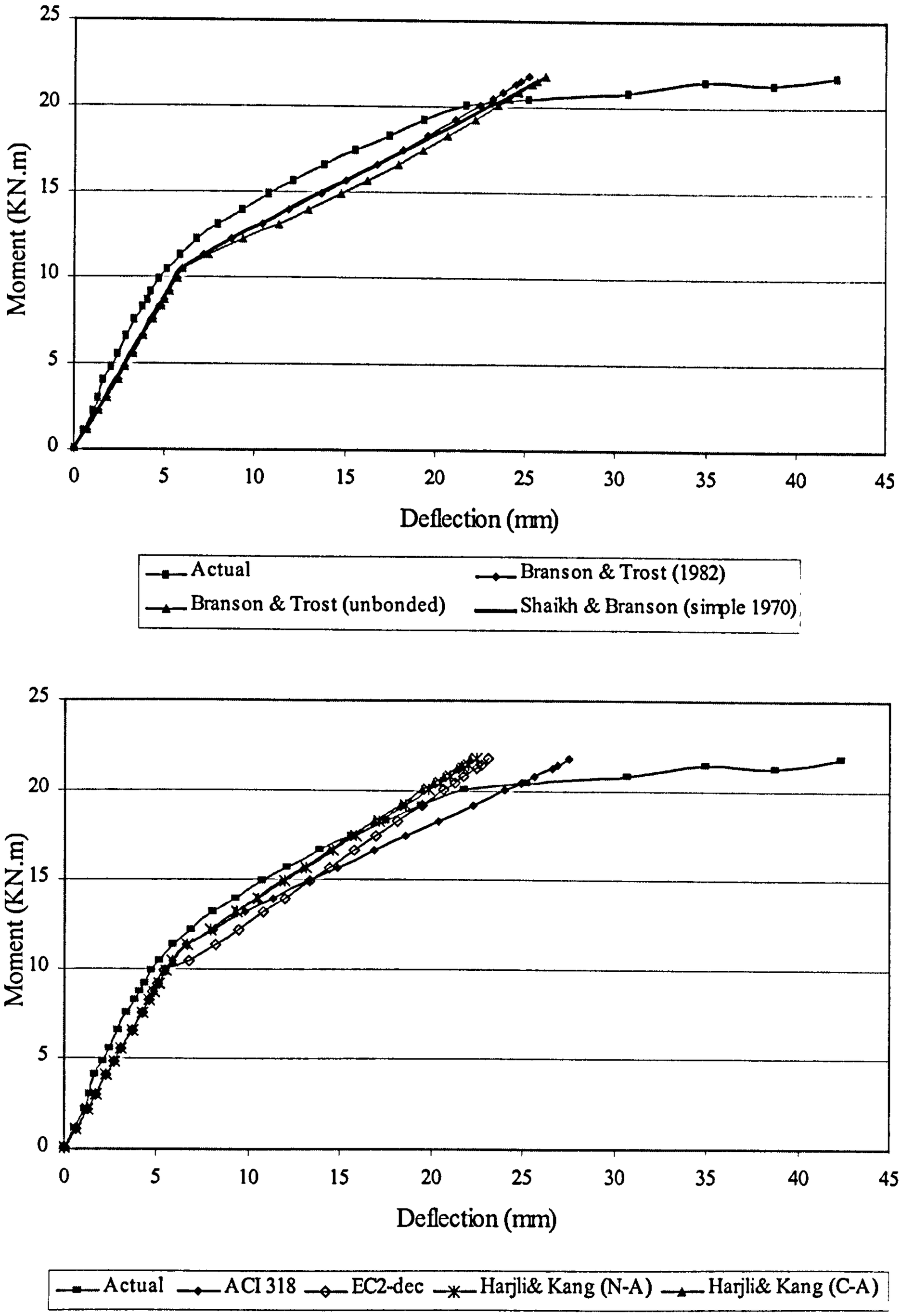

Figure (6.19): Comparison between actual and theoretical deflections due to live moment of beam PG51

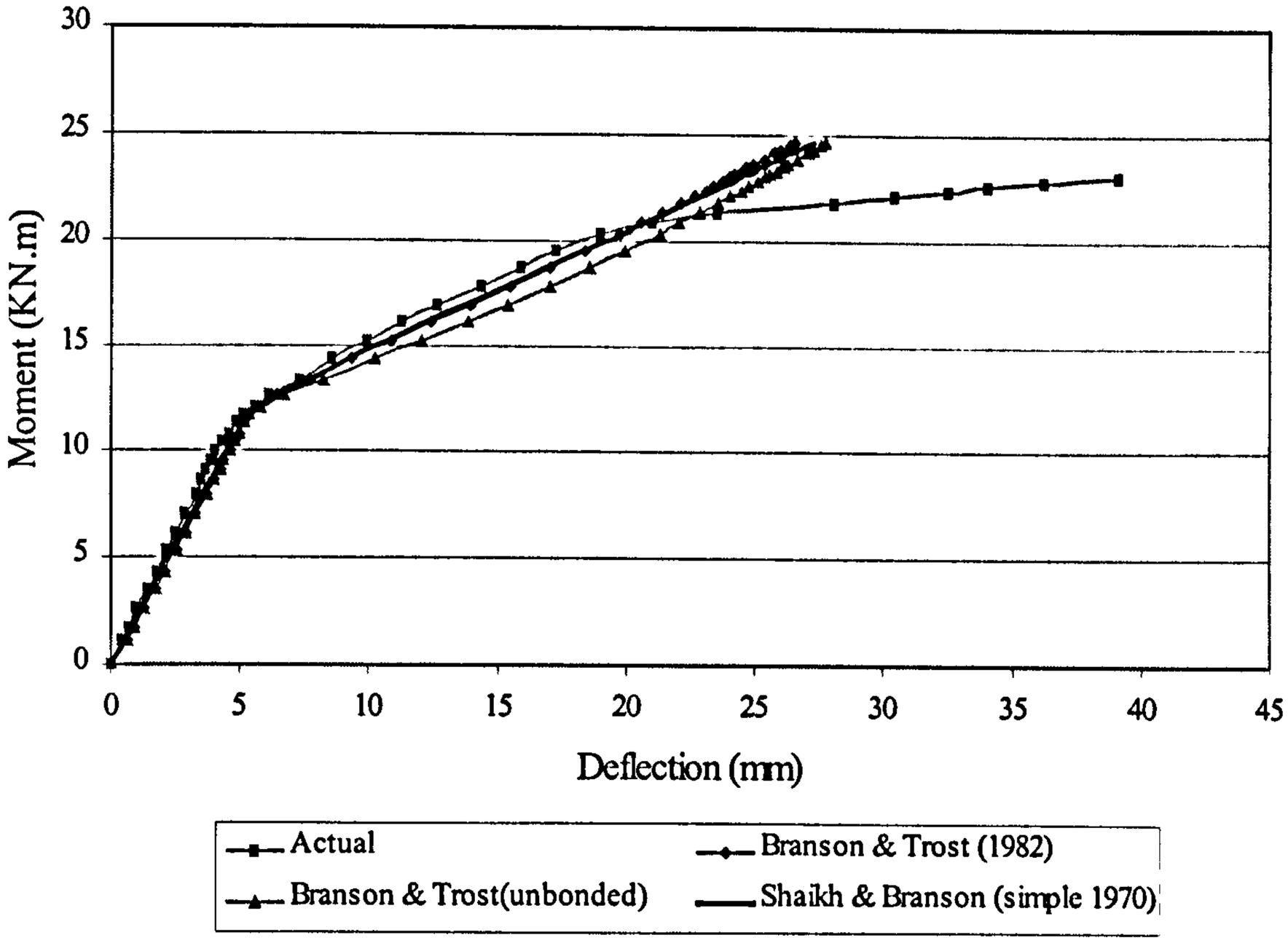

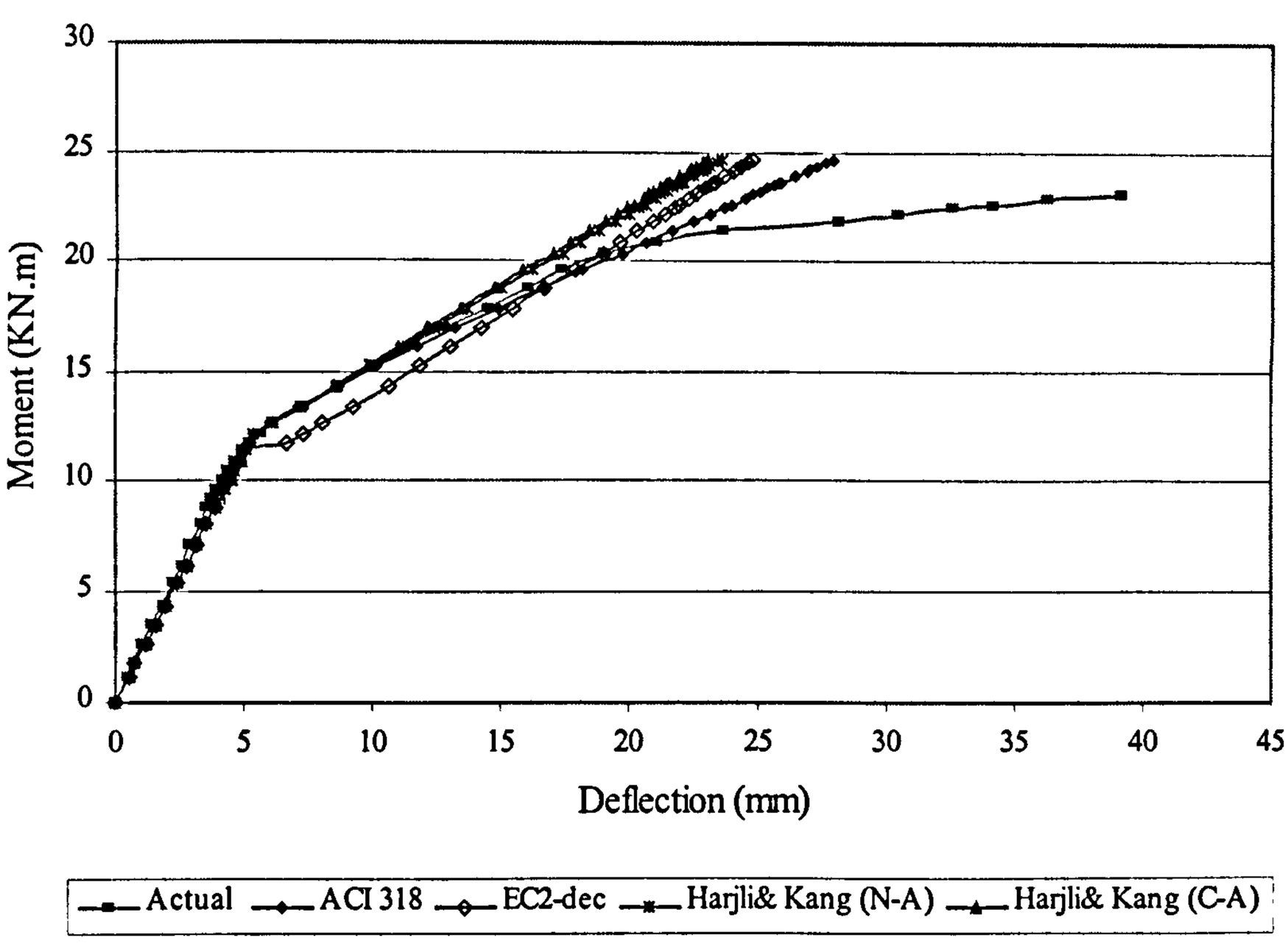

Figure (6.20): Comparison between actual and theoretical deflections due to live moment of beam PG52

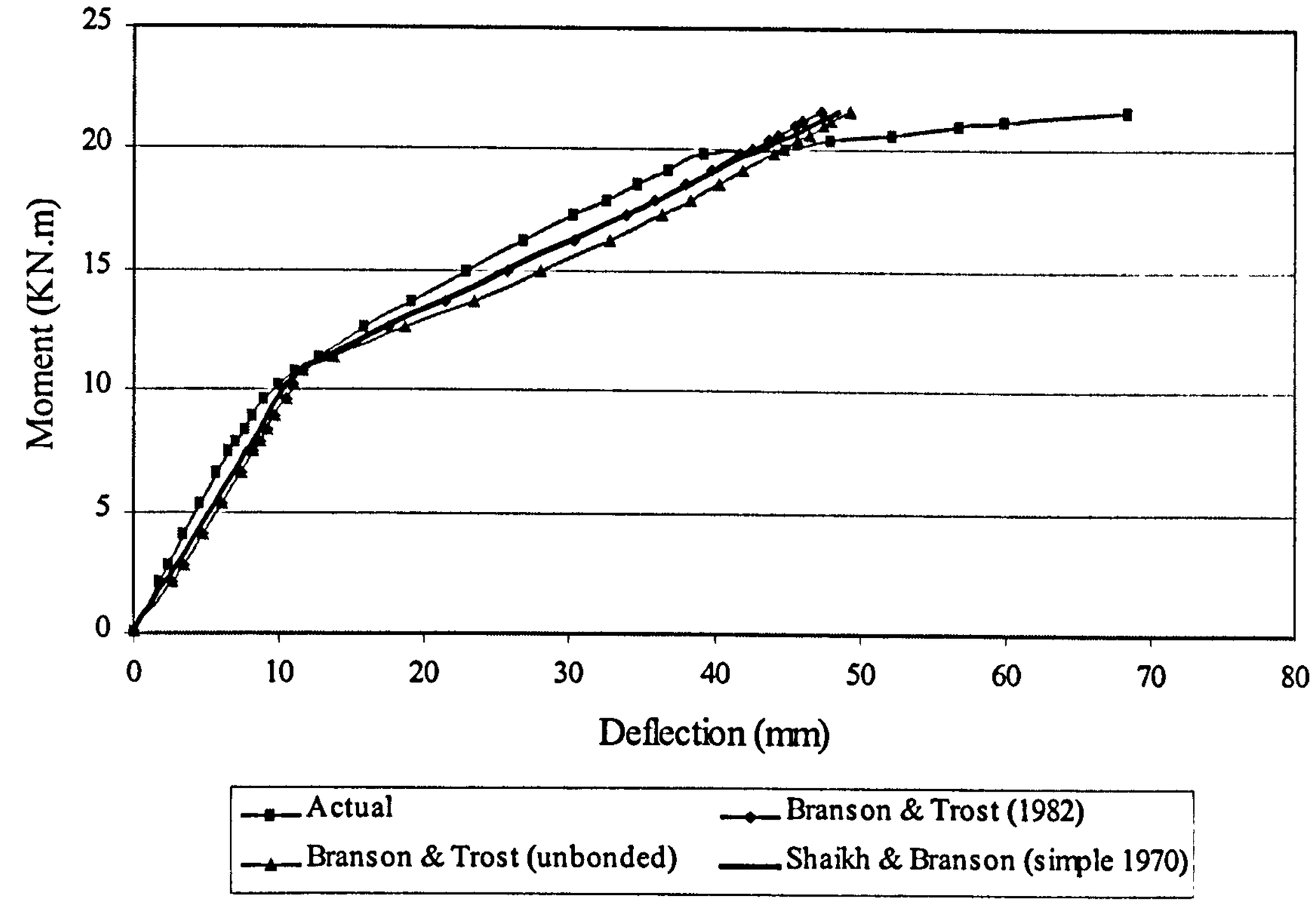

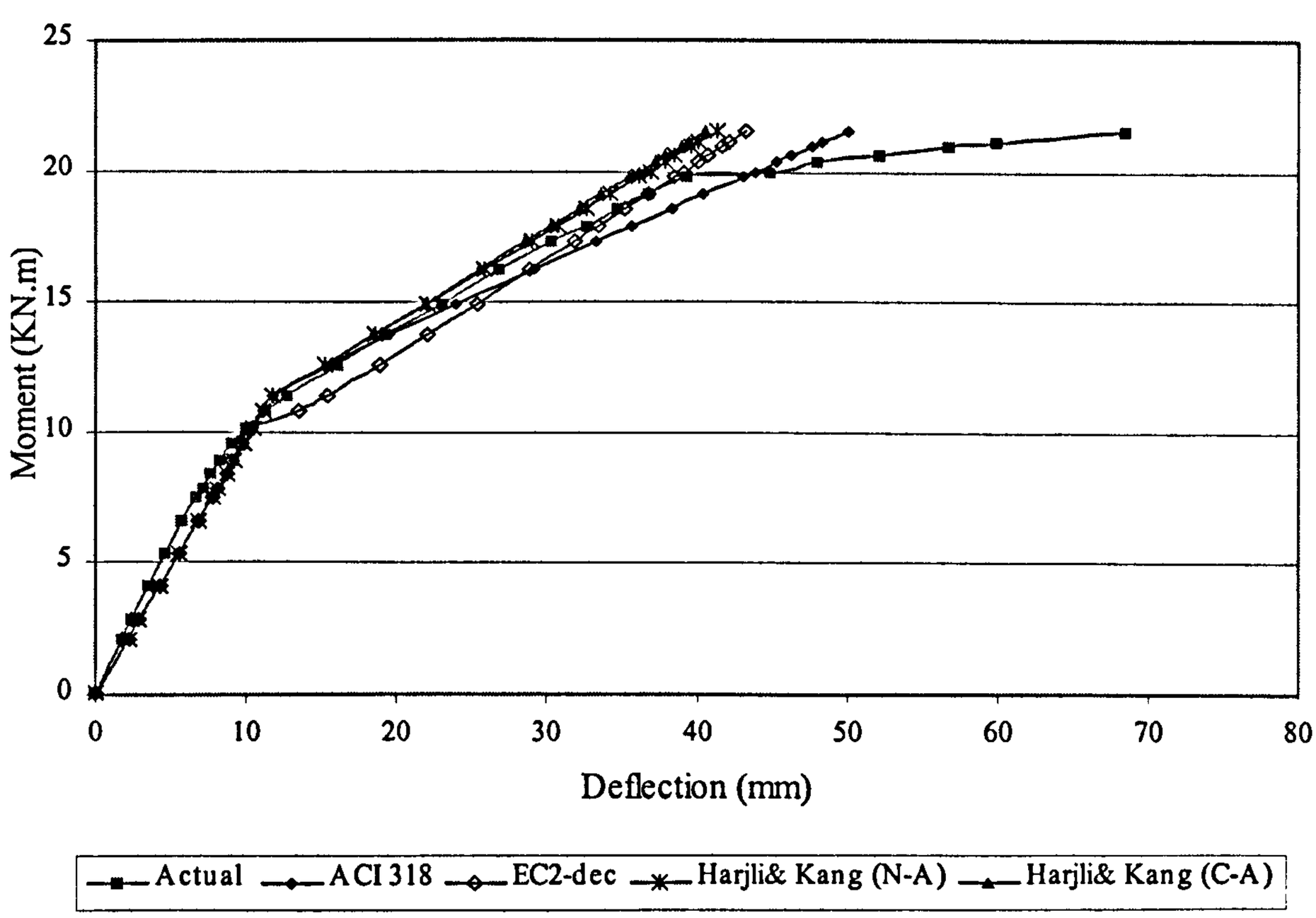

Figure (6.21): Comparison between actual and theoretical deflections due to live moment of beam PG61

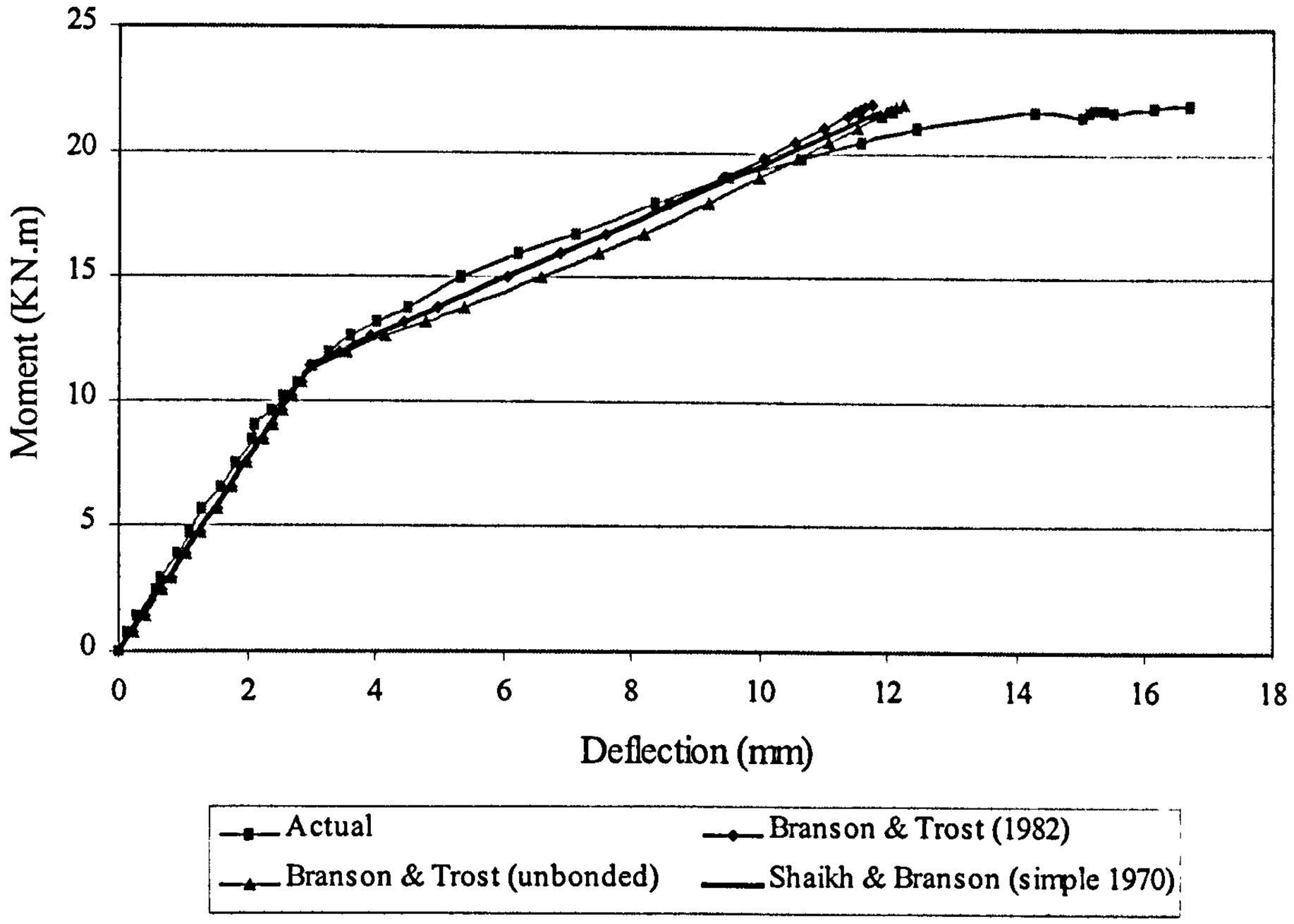

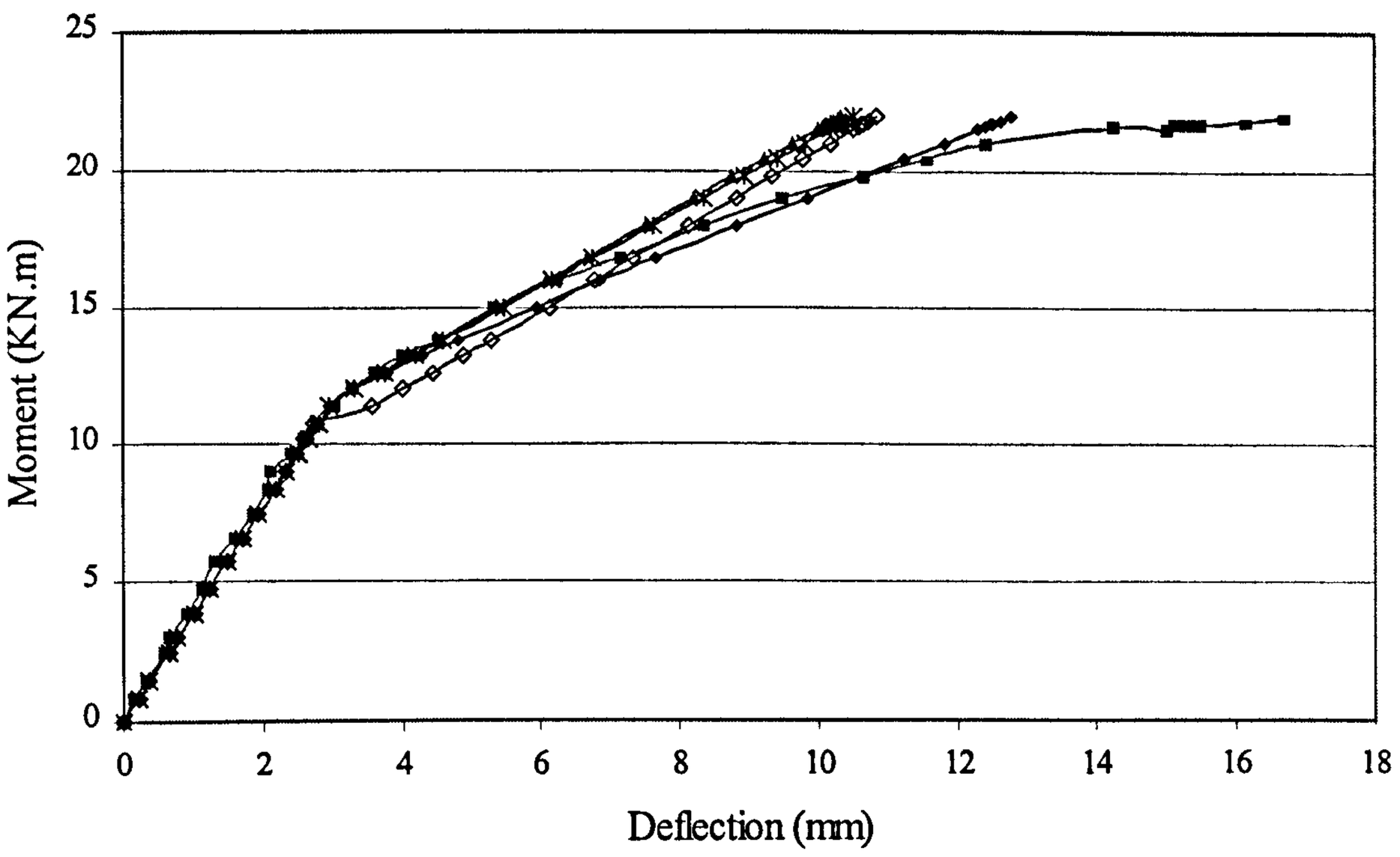

Figure (6.22): Comparison between actual and theoretical deflections due to live moment of beam PG62

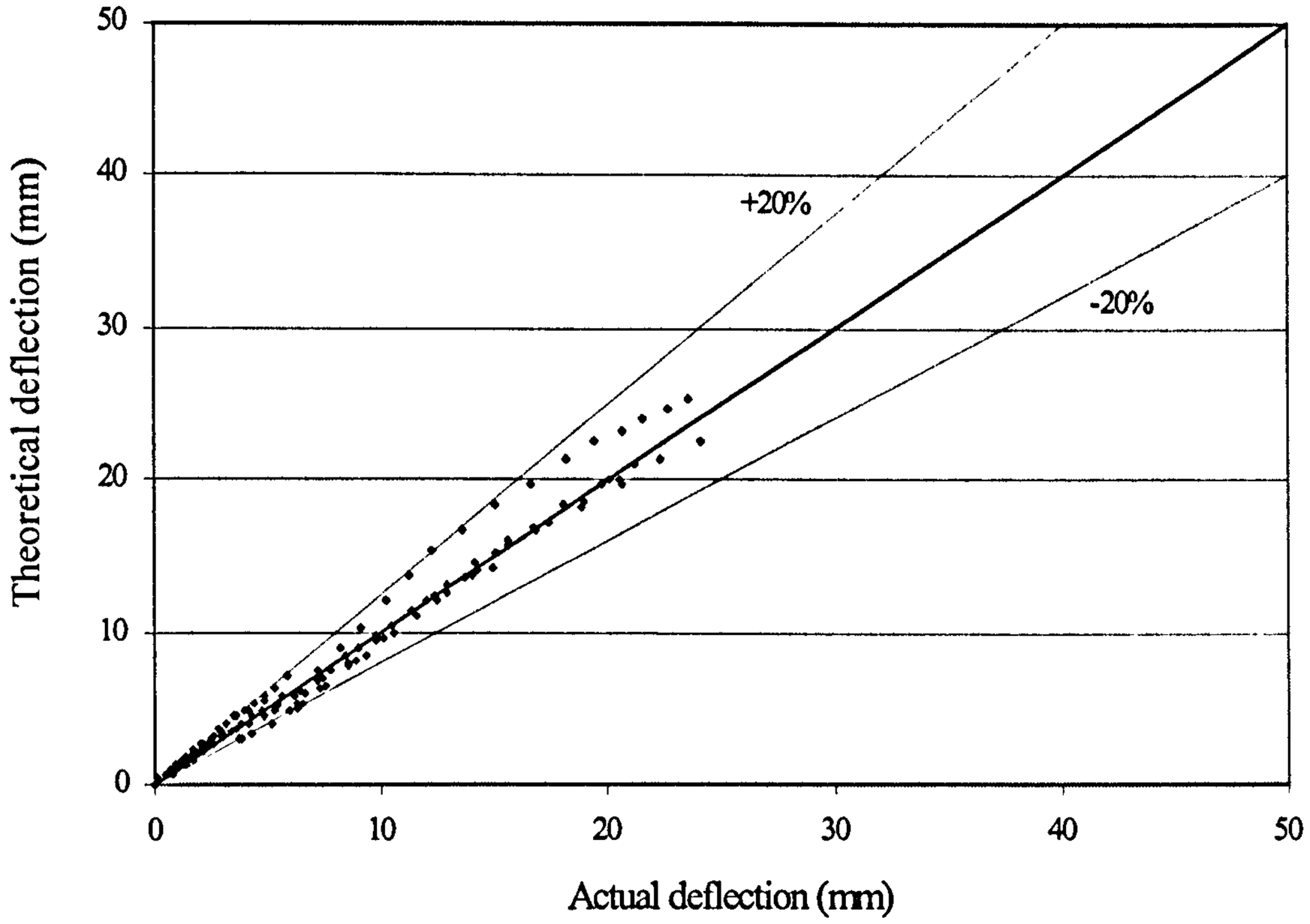

Figure (6.23): relation between actual deflection and theoretical deflection using *Branson & Trost* (1982) method

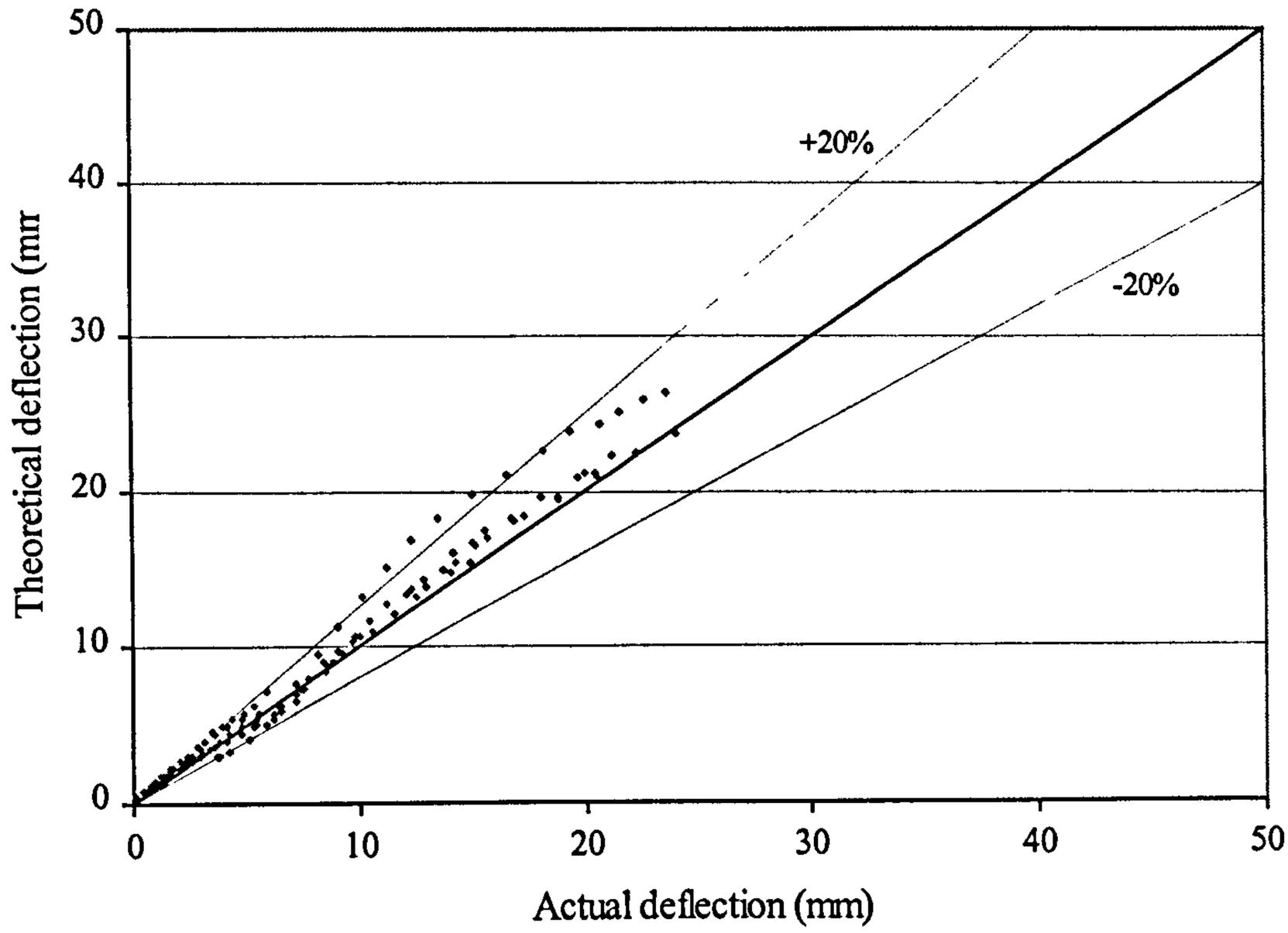

Figure (6.24): relation between actual deflection and theoretical deflection using *Branson & Trost* (1982) unbonded method

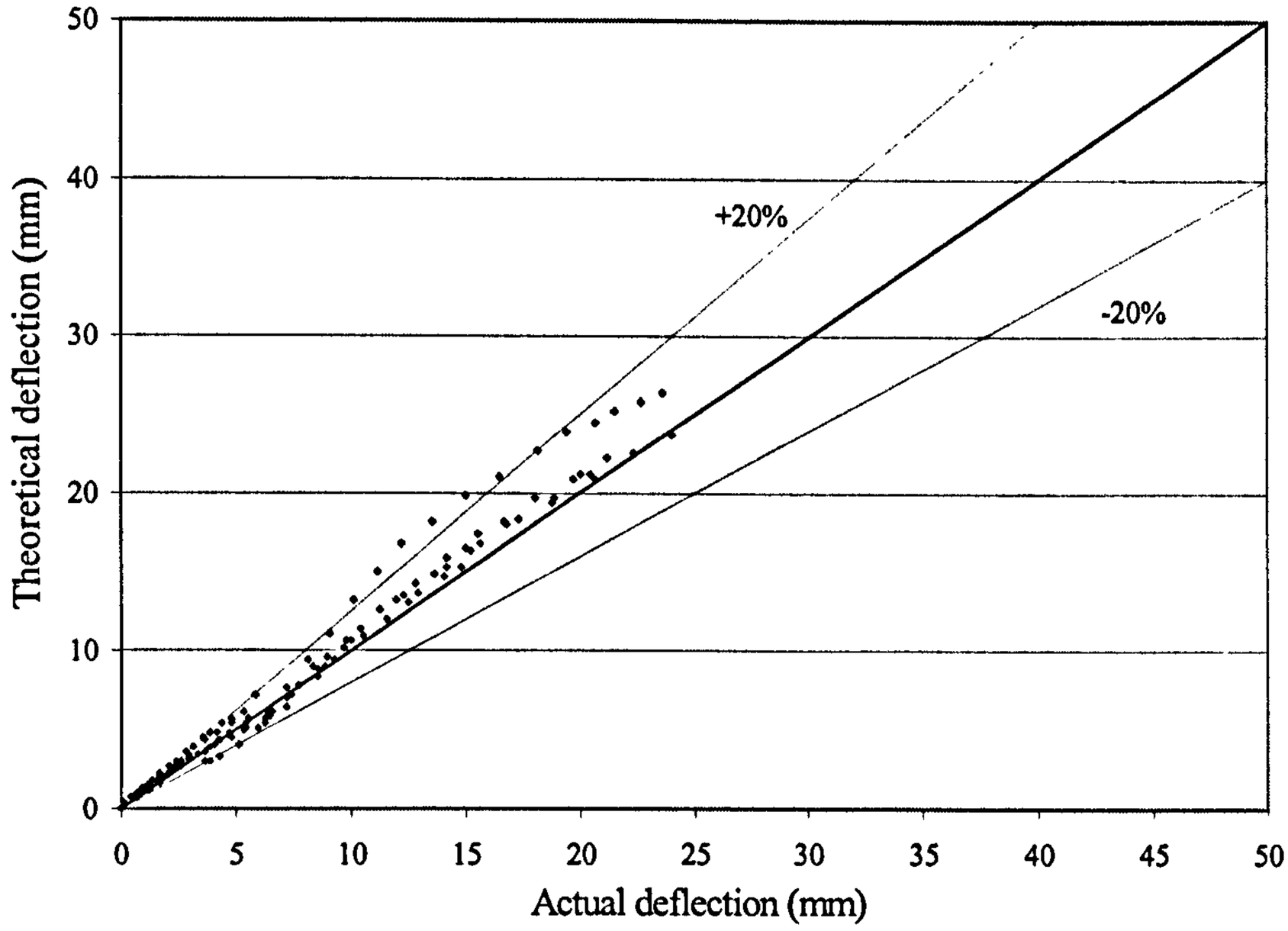

Figure (6.25): relation between actual deflection and theoretical deflection using *Shaikh & Branson* (1970)

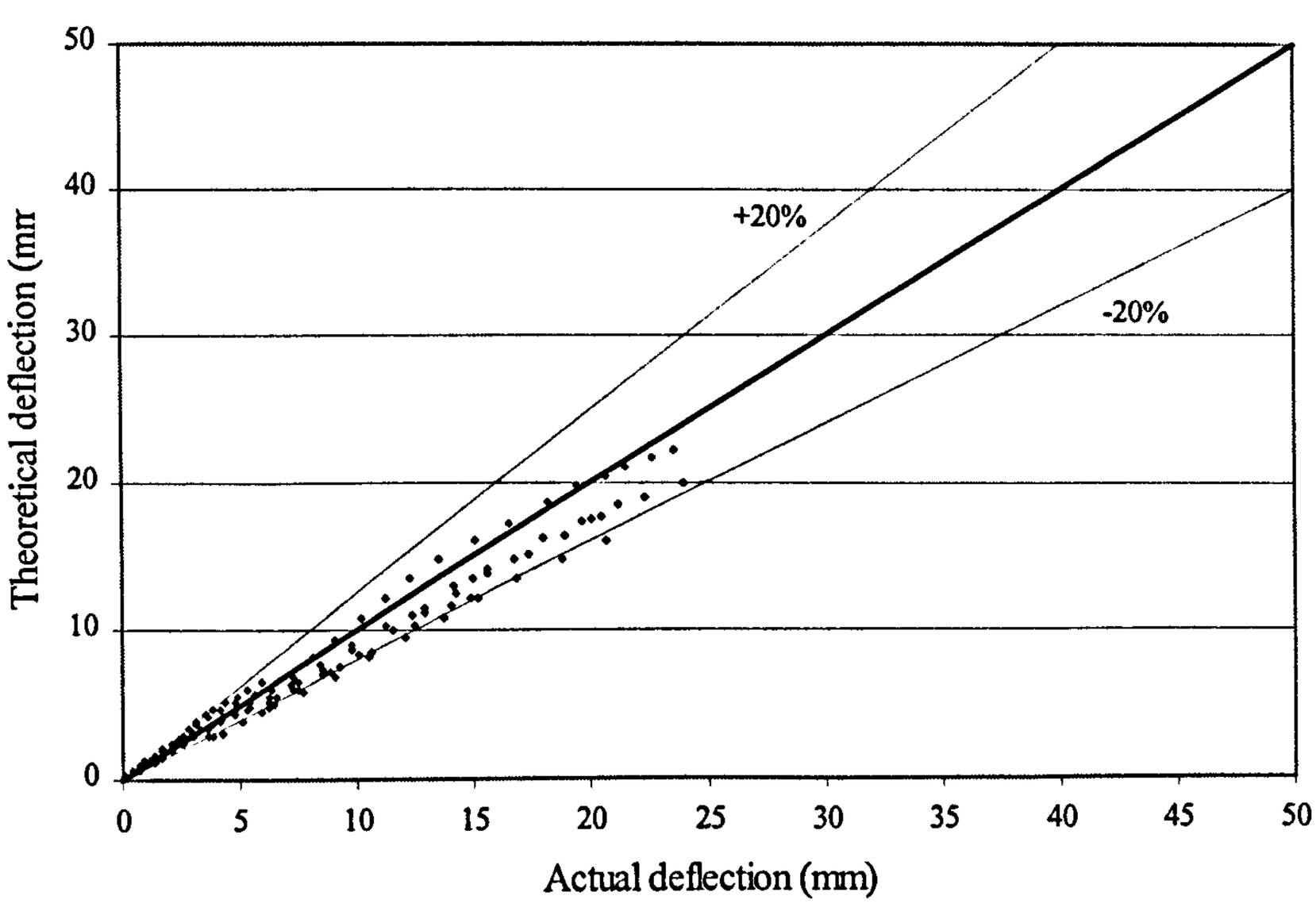

Figure (6.26): relation between actual deflection and theoretical deflection using *Harjili & Kanj* (neutral axis)

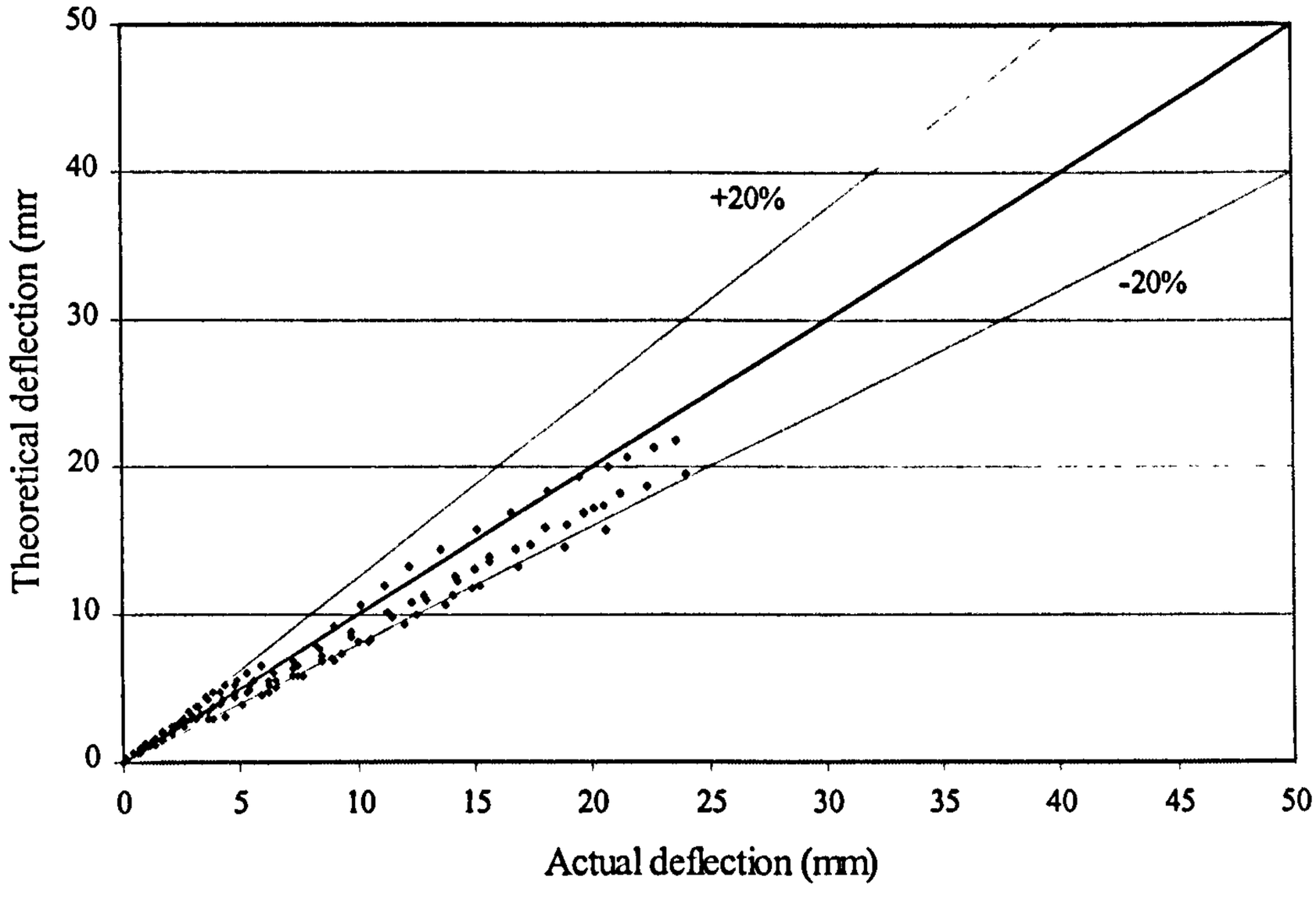

Figure (6.27): relation between actual deflection and theoretical deflection using *Harjili & Kanj* (centroidal axis)

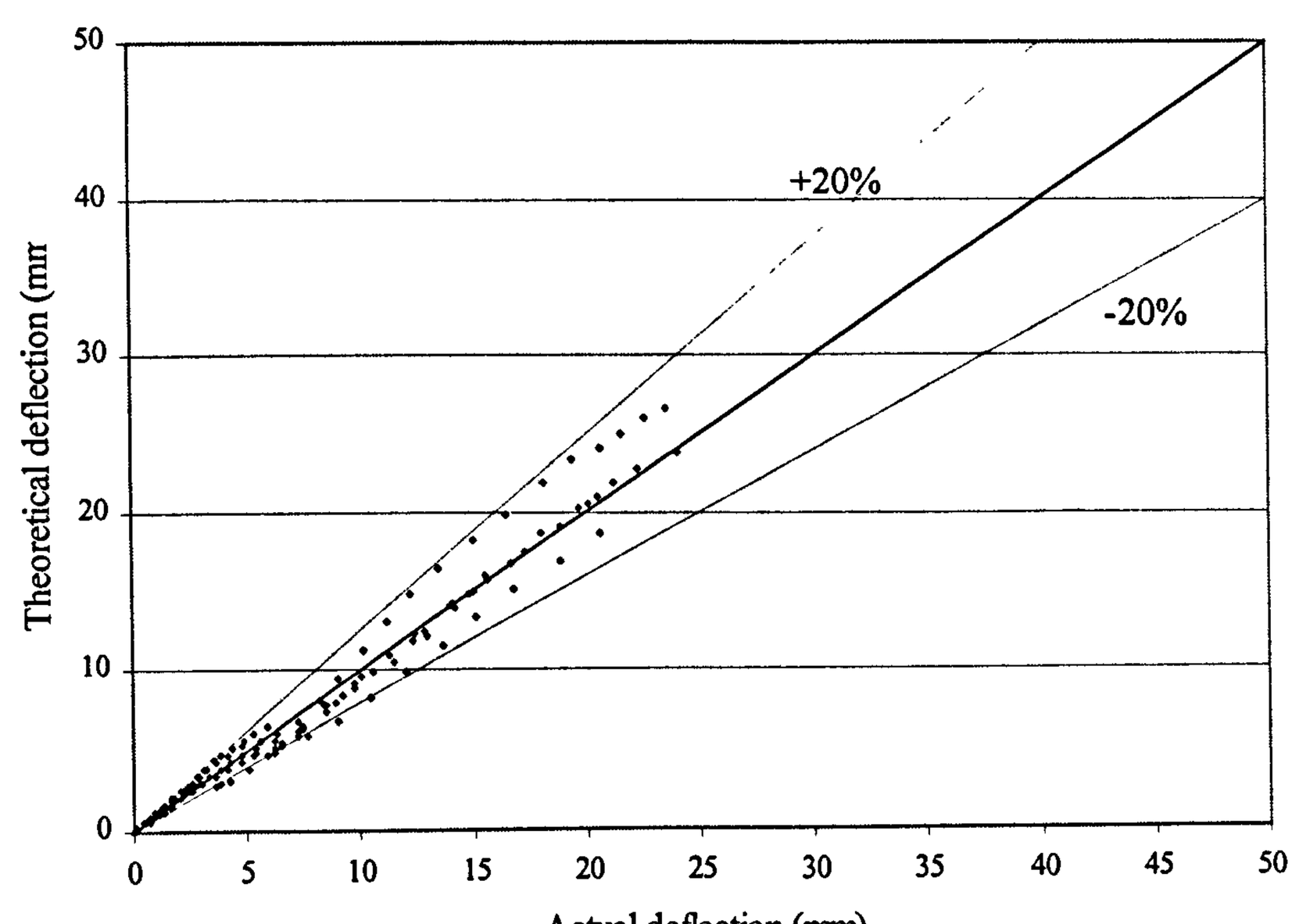

Figure (6.28): relation between actual deflection and theoretical deflection using ACI-318

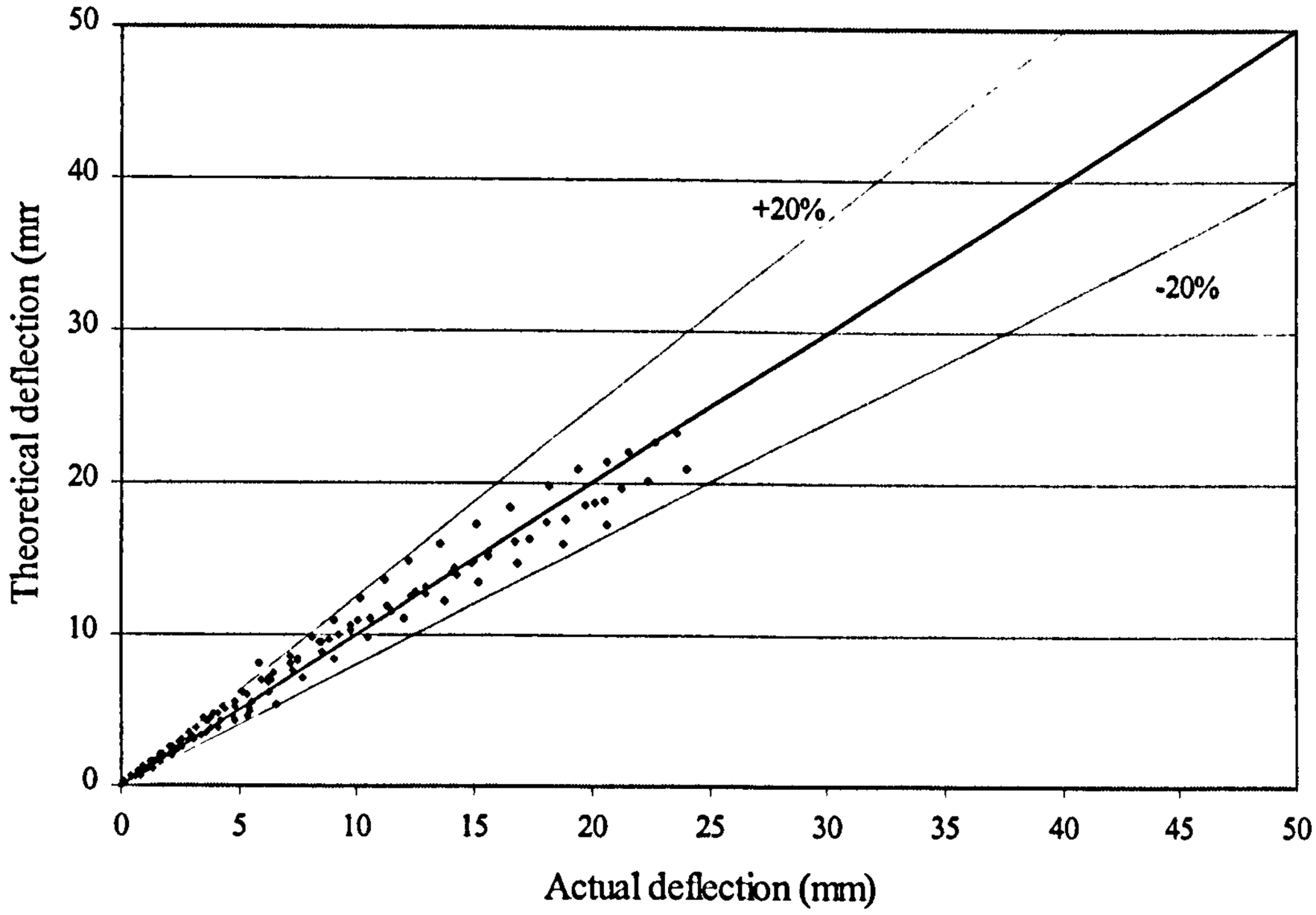

Figure (6.29): relation between actual deflection and theoretical deflection using EC-92 (decompression)

6.4 NOMINAL MOMENT STRENGTH OF PRESTRESSED BEAMS

For the analysis of prestressed concrete beams after strengthening externally using Parafil rope at ultimate, it is necessary to make certain assumptions and to know the complete stress-strain characteristics of concrete, steel, and Parafil rope. The following assumptions are those which are generally made for prestressed concrete sections:

- Plane sections remain plane during bending and perpendicular to the neutral axis after bending. Consequently, the strain distribution is assumed linear.
- Perfect bond exists between concrete and the internal steel. Hence, the strain in steel is the same as the strain in surrounding concrete before cracking.
- Concrete is weak in tension and therefore neglected in the flexural analysis and the tension reinforcement is assumed to take the total tensile force.

6.4.1 Nominal Bending Moment Strength of Flanged Section

For beam with T-cross section, calculation of the nominal moment strength depends on the position of the neutral axis at failure. First, if the neutral axis is located inside the compression flange ($c \leq h_f$) the section is considered as the rectangular section, while if it is out side the compression flange and the depth of the equivalent rectangular stress block is bigger than the flange thickness ($\beta_1 c > h_f$) it considered as the flanged section.

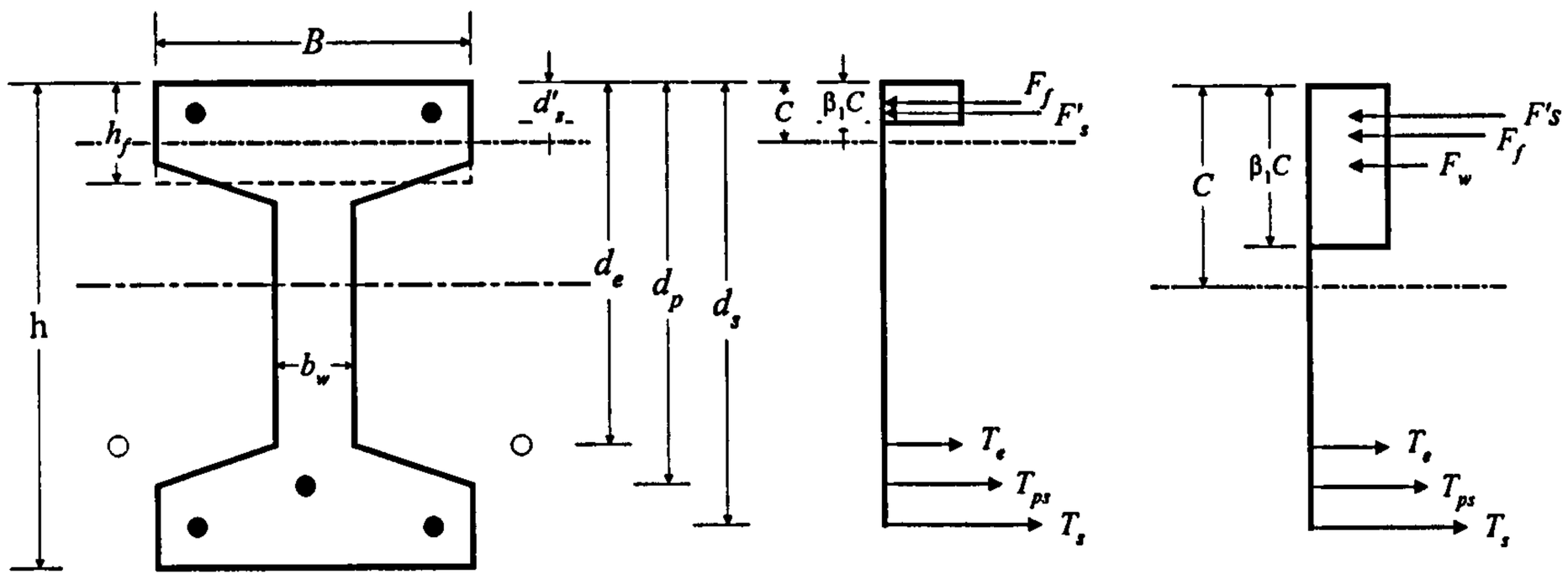

a) cross section b) stresses and forces for R-sec. c) stresses and forces for T-sec.

Figure (6.30): Possible stresses and forces at ultimate stage for I-sec.

Nominal moment strength of rectangle sections

From the equlibrium of the horizontal forces:

$$F_f + F'_s = T_s + T_{ps} + T_e \tag{6. 44}$$

Where

$$F_f = 0.67 f_{cu} B(\beta_1 c) \tag{6. 45}$$

$$F'_s = A'_s f'_s \tag{6. 46}$$

$$T_s = A_s f_s \tag{6. 47}$$

$$T_{pe} = A_{ps} f_{ps} \tag{6. 48}$$

$$T_e = A_e f_{pp} \tag{6. 49}$$

Substitute in Equation (6.44)

$$0.67 f_{cu} B^* \beta_1 c + A'_s f'_s = A_s f_s + A_{ps} f_{ps} + A_e f_{pp} \quad (6.50)$$

from which

$$c = \frac{A_s f_s + A_{ps} f_{ps} + A_e f_{pp} - A'_s f'_s}{0.67 f_{cu} B^* \beta_1} \quad (6.51)$$

and

$$M_n = A_{ps} f_{ps}\left(d_p - \frac{\beta_1 c}{2}\right) + A_e f_{pp}\left(d_{e-} \frac{\beta_1 c}{2}\right) + A_s f_s\left(d_{s-} \frac{\beta_1 c}{2}\right) - A'_s f'_s\left(d'_{s-} \frac{\beta_1 c}{2}\right) \quad (6.52)$$

Nominal moment strength of the flanged section

$$F_f + F_w + F'_s = T_s + T_{ps} + T_e \quad (6.53)$$

Where

$$F_w = 0.67 f_{cu} b_w (\beta_1 c) \quad (6.54)$$

$$F_f = 0.67 f_{cu} (B - b_w) h_f \quad (6.55)$$

F'_s, T_s, T_{ps} and T_e as before

From the equilibrium of the horizontal forces:

$$F_f + F_w + F'_s = T_s + T_{ps} + T_e \quad (6.56)$$

Substitute in Equation (6.56):

$$0.67 f_{cu} b_w * \beta_1 c + 0.67 f_{cu} (B - b_w) h_f + A'_s f'_s = A_s f_s + A_{ps} f_{ps} + A_e f_{PP} \quad (6.57)$$

From which

$$c = \frac{A_s f_s + A_{ps} f_{ps} + A_e f_{PP} - A'_s f'_s - 0.67 f_{cu} (B - b_w) h_f}{0.67 f_{cu} b_w * \beta_1} \quad (6.58)$$

$$M_n = A_{ps} f_{ps}\left(d_p - \frac{\beta_1 c}{2}\right) + A_e f_{pp}\left(d_e - \frac{\beta_1 c}{2}\right) + A_s f_s\left(d_s - \frac{\beta_1 c}{2}\right) - A'_s f'_s\left(d'_s - \frac{\beta_1 c}{2}\right) - 0.67 f_{cu} (B - b_w) h_f \left(\frac{h_f - \beta_1 c}{2}\right) \quad (6.59)$$

As can be seen from the previous equations, several unknowns should be determined first to calculate the nominal beam strength, namely:

- **Stress in the bonded tensile steel reinforcement**: That can be taken as yield stress of the steel.
- **Stress in the compression steel reinforcement**: This stress can reach the yield stress or less than it, depending on its position and strain value in the concrete at failure.
- **Stress in the internal prestressing wire**: As the high strength prestressing steel does not exhibit a yield stress plateau, so it can not be considered as an elasto-plastic material as the ordinary reinforcement steel (*Skogman et el.*, 1988).
- **Stress in external prestressing tendon**: Under loading, the increase in strain in the unbonded tendons is averaged (as no bond exists) over the whole length of the tendon, and thus is much smaller than the increase in strain of the bonded tendon taken at the section of maximum moment.
- **Effective depth of the external tendon**: As there is no bond between the rope and the concrete and the rope is attached to the concrete at the deviator points, its effective depth varies as the deflection increases.
- **Location of the neutral axis of T-beam at ultimate.**

Several investigations have beeen made to determine the stress in the internal bonded steel at ultimate in the prestressed concrete, less were made to determine the stress in the unbonded external prestressing strand, and a very few were made to determine the stress in both types in the same beam. In the following, a brief review of some of these equations can be found.

6.4.1.1 Stress in bonded prestressing steel

6.4.1.1.1 Naaman and Harajli (1985)

In 1985, *Naaman and Harajli* proposed the following equation to determine the stress in the prestressing steel. This equation was determined from the results obtained from a computer program using nonlinear analysis. The usual assumptions of

equilibrium of forces and compatibility of strains across the depth of the section were used. Also, a perfect bond between the concrete and the prestressing steel was assumed.

$$f_{ps} = f_{pu}(1-0.264\frac{c}{d_e}) \tag{6.60}$$

Where

c is the position of the neutral axis depth at nominal moment capacity of the section.

d_e is the effective depth from the extreme compression fibres to the centre of the resultant tension force.

$$d_e = \frac{A_{ps}f_{ps}d_p + A_s f_y d_s}{A_{ps}f_{ps} + A_s f_y} \tag{6.61}$$

From the previous equations and the equation of the force equilibrium, c and f_{ps} can be determined.

In order to simplify and shorten the analysis, *Naaman and Harajli* suggested two alternative equations in which the unknown variables, c and d_e, were replaced by easily calculated variables:

$$f_{ps} = f_{pu}(1-0.25\frac{c_u}{d_e}) \approx f_{pu}(1-0.25\frac{c_u}{d_u}) \tag{6.62}$$

Or

$$f_{ps} = f_{pu}(1-0.3\frac{c}{d_e}) \approx f_{pu}(1-0.3\frac{c}{d_u}) \tag{6.63}$$

Where c_u is the neutral axis depth calculated by assuming a stress f_{pu} in the tendons and f_y in the nonprestressed reinforcement.

$$d_u = \frac{A_{ps}f_{pu}d_p + A_s f_y d_s}{A_p f_{pu} + A_s f_y} \tag{6.64}$$

However, using d_u was rejected by *Loov* (1988) who said "there is no basis for this extra complication" and that "the correct parameter to use throughout is actually (d_p) the depth to the prestressing steel. This because the equations for f_{ps} have been

developed based on the assumption that the supplementary tension and compression reinforcement is strained beyond yield. Provided this restriction is met, the location of this reinforcement should have no effect on the stress in the prestressing steel. There is therefore no need to determine the location of the centroid of the tension force for calculating f_{ps}". Then, *Loov* proposed the following equation to calculate the steel stress of bonded prestressing steel assuming $f_{pe} \geq 0.6 f_{py}$:

$$\frac{f_{ps}}{f_{pu}} = \frac{(1 - k_h \frac{c_{sf}}{d_p})}{(1 - k_h \frac{c_{pu}}{d_p})} \tag{6.65}$$

Where

$$k_h = 2(1.04 - \frac{f_{py}}{f_{pu}}) \tag{6.66}$$

$$\frac{c_{sf}}{d_p} = \frac{c_s}{d_p} - \frac{c_{s'}}{d_p} - \frac{c_f}{d_p} \tag{6.67}$$

$$\frac{c_s}{d_p} = \frac{A_{ps} f_{ps}}{0.85 \beta_1 f'_c b_w d_p} \tag{6.68}$$

$$\frac{c_{s'}}{d_p} = \frac{A_{s'} f_{s'}}{0.85 \beta_1 f'_c b_w d_p} \tag{6.69}$$

$$\frac{c_f}{d_p} = \frac{0.85 f'_c (B - b_w) h_f}{0.85 \beta_1 f'_c b_w d_p} = \frac{(B/b_w - 1) h_f}{\beta_1 d_p} \tag{6.70}$$

And $$\frac{c_{pu}}{d_p} = \frac{A_{ps} f_{pu}}{0.85 \beta_1 f'_c b_w d_p} \tag{6.71}$$

Also, the neutral axis c can be calculated as follow

$$\frac{c_p}{d_p} = \frac{c_{pu}}{d_p} \frac{f_{ps}}{f_{pu}} \tag{6.72}$$

$$\frac{c}{d_p} = \frac{c_p}{d_p} + \frac{c_{sf}}{d_p} \tag{6.73}$$

Also, to insure yielding of the compression reinforcement c should satisfy the following condition:

$$c \geq \frac{d}{(1-\varepsilon_y/\varepsilon_c)} \tag{6.74}$$

Where

c = neutral depth

c_f = reduction of c produced by compression flange

c'_s = reduction of c produced by compression steel

c_p = depth to neutral axis required for tension steel

c_{sf} = neutral axis depth for combined effect of nonprestressed steel and flange

$c_{sf} = c_s - c'_s - c_f$

Depending on the previous equations, *Naaman* (1992,1995) suggested two equations to determine the stress in bonded prestressing steel - depending on the required accuracy- provided that $f_{pe} \geq 0.5 f_{pu}$ as follows:

1. Approximate conservative method for preliminary design

$$f_{ps} = f_{py} \tag{6.75}$$

2. Refined method

$$f_{ps} = f_{pu}(1 - k\frac{c}{d_p}) \tag{6.76}$$

Where $k = 2(1.04 - \frac{f_{py}}{f_{pu}})$ (6.77)

If any compression reinforcement is taken into account when calculating f_{ps}, the value of c should be larger than or equal to $3d'_s$ to insure yielding of the compression reinforcement, where d'_s is the depth from the extreme compression fibre to the centroid of the compression reinforcement (*Loov,* 1988. *Naaman,* 1992. Naaman, 1995,). If c is less than 3 d'_s , the contribution of the compressive reinforcement may be neglected.

6.4.1.1.2 ACI-318

According to (ACI 318-99) f_{ps} can be determined using strain compatibility method through the various loading and at ultimate if $f_{pe} < 0.5 f_{pu}$.

If $f_{pe} \geq 0.5 f_{pu}$ an approximate equation can be used to calculate f_{ps} as follows:

$$f_{ps} = f_{pu}\left(1-\frac{\gamma_p}{\beta_1}\left[\rho_p\frac{f_{pu}}{f'_c}+\frac{d}{d_p}(\omega-\omega')\right]\right) \qquad (6.78)$$

The term $\left[\rho_p\frac{f_{pu}}{f'_c}+\frac{d}{d_p}(\omega-\omega')\right]$ should not be less than 0.17 and d'_s should not be greater than 0.15 d_p. Also,

$\gamma_p = 0.55$ for $\frac{f_{py}}{f_{pu}} \geq 0.8$

$= 0.40$ for $\frac{f_{py}}{f_{pu}} \geq 0.85$)

$= 0.28$ for $\frac{f_{py}}{f_{pu}} \geq 0.9$

$\rho_i = \frac{A_{si}}{bd}$ and $\omega_i = \rho_i\frac{f_{yi}}{f'_c}$ for T-section b = flange width = B

Badie and Tadros (1999) stated that, the previous equation is not suitable in several situations such as, existence of large amount of compression steel, depth of the compression reinforcement is larger than 0.15 d_p, the value of $f_{pe} < 0.5f_{pu}$ and in cases of sections where the compression zone is other than a rectangular or T-section.

6.4.1.2 Stress in unbonded tendons

Stress increase in the unbonded tendons can be calculated from the bond reduction concept as previously explained, or by determining the tendon strain from the strain distribution of the concrete. Both methods are briefly discussed.

6.4.1.2.1 Bond Reduction Method

Stress in the unbonded tendons (f_{ps}) at ultimate can be predicted using the following equation

$$f_{ps} = f_{pe} + \Delta f_{ps} \qquad (6.79)$$

Naaman and Alkhairi (1991 part-1) made an evaluation on the existing equation to predict the stress in unbonded tendons. Then they concluded there is a room for

improvement not only in terms of accuracy but particularly in accounting for the variables that are found to influence most the value of f_{ps}.

Based on previous work made by *Naaman* (1990), a new equation was proposed by *Naaman and Alkhairi* (1991 part-2) to predict the stress in unbonded tendon at ultimate. A brief review of this method is as follow

Strain in unbonded tendons at ultimate can be obtained from the strain increase in bonded tendons using a bond reduction coefficient (Ω_u) defined as

$$\Omega_u = \frac{(\Delta\varepsilon_{psu})_m}{(\Delta\varepsilon_{psb})_m} \qquad (6.80)$$

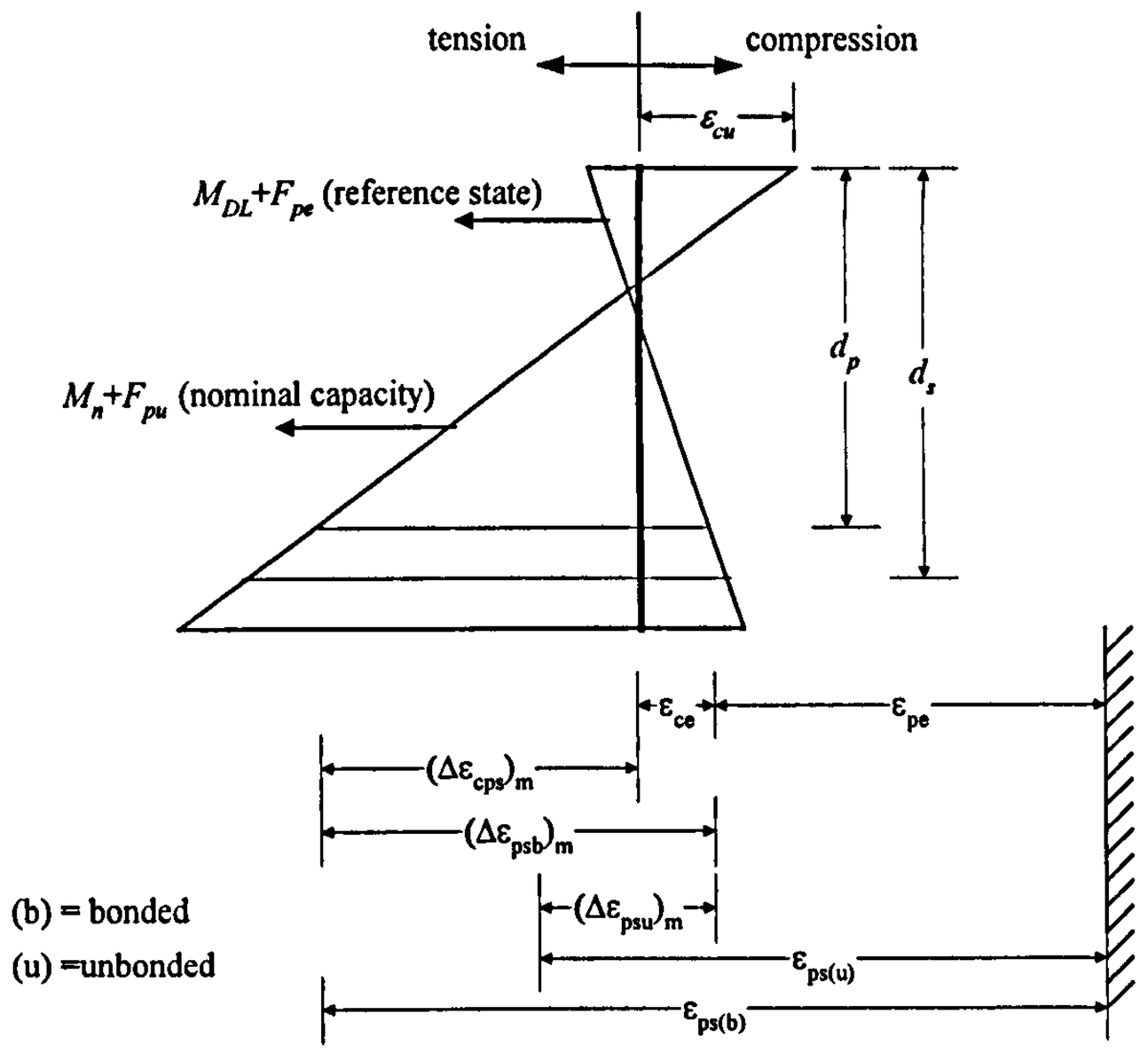

Figure (6.31): Strain distribution along section of maximum moment

Strain increase in the bonded tendon at the critical section can be calculated from the strain distribution at that section assuming perfect bond between concrete and steel. From Figure (6.31) the increase in strain in bonded steel can be calculated from

$$(\Delta\varepsilon_{psb})_m = \varepsilon_{ce} + (\Delta\varepsilon_{cps})_m = \varepsilon_{ce} + \varepsilon_{cu}\left(\frac{d_p}{c} - 1\right) \qquad (6.81)$$

Assuming the value of Ω_u were known, so the strain increase in the unbonded tendon could be determined from:

$$(\Delta\varepsilon_{cpu})_m = \Omega_u \varepsilon_{ce} + \Omega_u \varepsilon_{cu}\left(\frac{d_p}{c} - 1\right) \quad (6.82)$$

Assuming the stress in the unboded tendon remains in the elastic stage, so the stress change in unbonded tendons at nominal moment resistance can be obtained from

$$(\Delta f_{psu})_m = E_{ps}(\Delta\varepsilon_{psu})_m = \Omega_u E_{ps}\varepsilon_{ce} + \Omega_u E_{ps}\varepsilon_{cu}\left(\frac{d_p}{c} - 1\right) \quad (6.83)$$

the corresponding stress in the unbonded tendon is thus given by

$$f_{ps} = f_{pe} + (\Delta f_{psu})_m = f_{pe} + \Omega_u E_{ps}\varepsilon_{ce} + \Omega_u E_{ps}\varepsilon_{cu}\left(\frac{d_p}{c} - 1\right) \quad (6.84)$$

Generally, the value of ε_{ce} is negligible compared to the other terms and can be neglected. Hence, the previous equation becomes

$$f_{ps} = f_{pe} + (\Delta f_{psu})_m = f_{pe} + E_{ps}\Omega_u \varepsilon_{cu}\left(\frac{d_p}{c} - 1\right) \quad (6.85)$$

If the value of Ω_u can be determined, and by substituting the value of f_{ps} in the equation of force equilibrium, then the neutral axis depth (c) can be determined. Based on the data collected from 143 beam tests carried out by various investigators the, value of Ω_u was proposed as follow

$$\Omega_u = \frac{2.6}{L/d_p} \qquad \text{For one-point loading} \quad (6.86)$$

$$\Omega_u = \frac{5.4}{L/d_p} \qquad \text{For third-point or uniform loading} \quad (6.87)$$

For code purpose, *Naaman and Alkhairi* suggested the following equations:

$$f_{ps} = f_{pe} + (\Delta f_{psu})_m = f_{pe} + E_{ps}\Omega_u \varepsilon_{cu}\left(\frac{d_p}{c} - 1\right)\frac{L_1}{L_2} \qquad \leq 0.94 f_{py} \quad (6.88)$$

$$\Omega_u = \frac{1.5}{L/d_p} \qquad \text{For one-point loading} \quad (6.89)$$

$$\Omega_u = \frac{3.0}{L/d_p} \qquad \text{For third-point or uniform loading} \quad (6.90)$$

Where L_1 = length of loaded span or sum of lengths of loaded spans, affected by the same tendon

L_2 = length of tendon between end anchorages

The limitation of 0.94 f_{py} was selected to ensure that the stress in the steel remains as close as possible to the linear elastic range assumed in the analysis.

6.4.1.2.2 Concrete strain distribution method

During loading, the beam is considered to develop both elastic and inelastic zones as shown in Figure (6.32). The total deformation of the tendon between the anchorage ends can be taken as the summation of the concrete deformation at the tendon level in both the elastic and plastic zones. Also, as the concrete deformation in the elastic zone is small and can be neglected, so the total deformation can be assumed as that due to the plastic deformation occurred in the plastic zones.

This deformation can be considered as the extension in the tendon and then both strain and stress can be calculated.

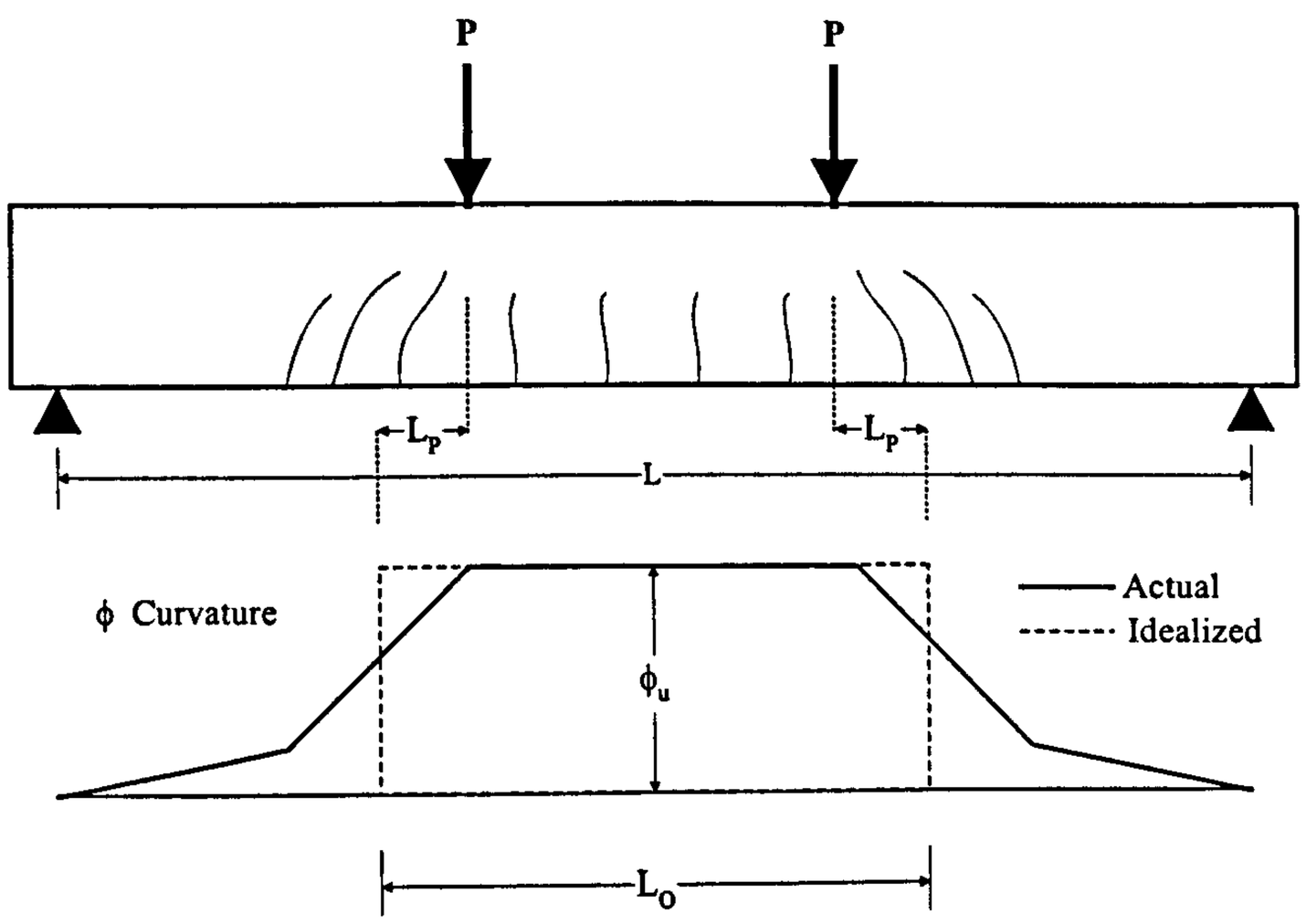

Figure (6.32): Curvature distribution along the simply supported beam length

Neglecting the deformation of the elastic zone was studied by *Harajli* (1990) who stated that "The predicted f_{ps} tends under this assumption to be a little conservative in comparison with the more accurate nonlinear analysis predictions at high reinforcement ratios. This is expected since high reinforcement ratios reduce the

ductility (ultimate curvature) of the member, which makes the contribution of the neglected portion of the curvature distribution relatively more significant"

In order to calculate the stress in the unbonded tendons at the ultimate strength, friction losses along the beam length were neglected and hence stress of the unbonded tendon can be considered constant along the beam length. Using this assumption tendon stress can be calculated as follows

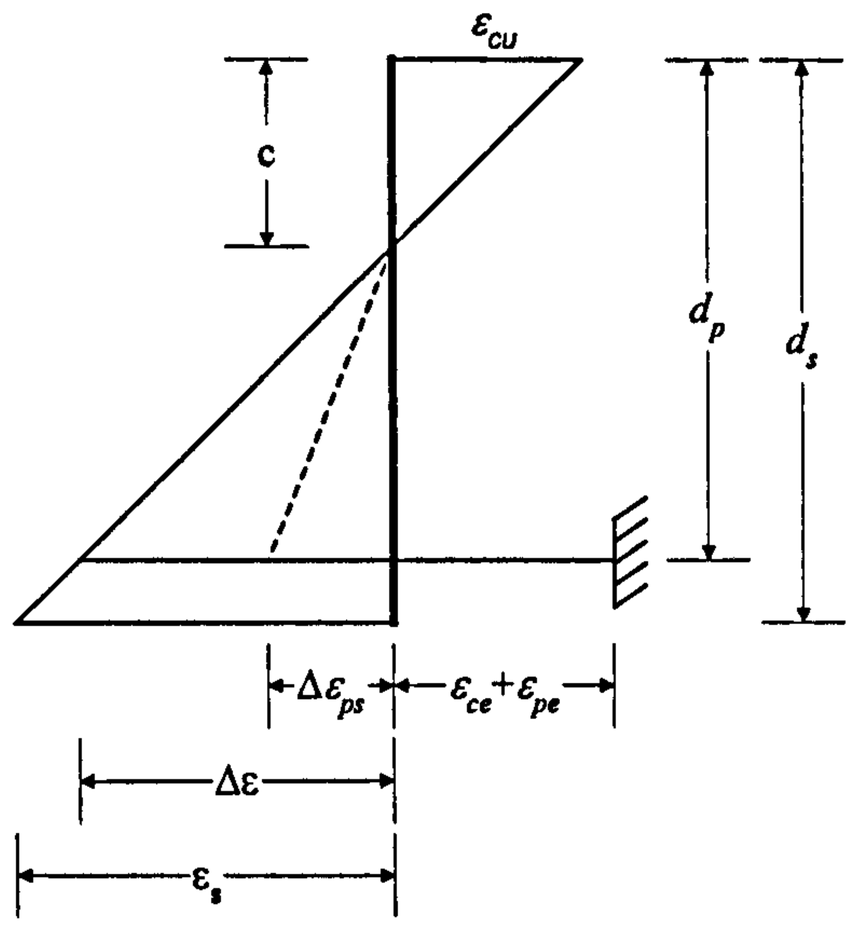

Figure (6.33) Strain distribution across the depth of unbonded prestresses concrete beam section

Increase in concrete strain at prestressing tendon level $\Delta\varepsilon = \frac{d_p - c}{c}\varepsilon_{cu}$ (6. 91)

The total increase in tendon elongation between the anchorage ends

$$\Delta L_{PS} = (\Delta\varepsilon + \varepsilon_{ce})L_o \quad (6.92)$$

ε_{ce} is very small and can be neglected. Hence,

$$\Delta L_{PS} = (\Delta\varepsilon)L_o = \frac{d_p - c}{c}\varepsilon_{cu}L_o \quad (6.93)$$

Increase in strain of prestressing tendon

$$\Delta\varepsilon_{ps} = \frac{\Delta L_{ps}}{L} = \frac{d_p - c}{c}\varepsilon_{cu}\left(\frac{L_o}{L}\right) \quad (6.94)$$

Tendon stress $f_{ps} = (\Delta\varepsilon_{ps} + \varepsilon_{pe})E_{ps} = \left(\varepsilon_{cu}\frac{d_p - c}{c}\left(\frac{L_o}{L}\right) + \varepsilon_{pe}\right)E_{ps}$ (6. 95)

From force equilibrium

$$0.67 f_{cu} b_w * \beta_1 c + 0.67 f_{cu}(B - b_w) h_f + A'_s f'_s = A_s f_y + A_{ps} f_{ps} \qquad (6.96)$$

Where

ε_{ce} = strain in the concrete at the level of prestressing steel due to prestressing.

L = total span length between the anchorage end.

L_o = the equivalent plastic length

L_a = distance between the two concentrated loads

Equations (6.95 & 6.96) included three unknowns (f_{ps} , c, L_o). If (L_o) is known , then by solving the previous equations, both (f_{ps} , c) can be determined.

In order to simplify the calculation several values for f_{ps} and c were suggested as follows:

BS8110

Depending on researches made by *Pannell* (1969) and *Pannell and Tam* (1976), BS8110 suggested (L_o) to be taken as 10 c. While for rectangular section or flanged section with a neutral axis depth less than 0.9 of the flange depth, BS8110 suggested the following equations to determine f_{ps} and c by taking ε_{cu} = 0.0035 and E_s =200 kN/mm^2

$$f_{ps} = f_{pe} + \frac{7000}{L/d}\left(1 - 1.7\frac{f_{pu}A_{ps}}{f_{cu}bd}\right) \qquad \leq 0.7 f_{pu} \qquad (6.97)$$

$$c = 2.47\left[\left(\frac{f_{pu}A_{ps}}{f_{cu}bd}\right)\left(\frac{f_{ps}}{f_{pu}}\right)d\right] \qquad (6.98)$$

These equations neglected the effect of tension reinforcement and assume (f_{ps}/f_{pu}) = 0.7 as a first assumption.

Harajli (1990)

Harajli (1990) followed the same assumption as BS8110 but taking L_o in a general form as follows:

$$L_o = L_a + 2L_p \qquad (6.99)$$

Where $2\,L_p$ is the equivalent plastic hinge length measured outside the constant moment region and equal to

$$L_p = 0.5\,d_p + 0.05\,Z \qquad (6.100)$$

In which Z is the shear span or the distance between the point of maximum moment and point of contraflexure.

Harajli (1990) suggested the following equation to calculate stress in the unbonded tendon

$$f_{ps} = f_{pe} + \left(10{,}000 + \frac{f'_c}{100\rho_p}\right)\left(0.4 + \frac{8}{L/d_p}\right) \quad \le f_{py} \quad \text{psi}$$

$$\text{or} \le f_{pe} + 60{,}000 \qquad (6.101)$$

f'_c and f_{pe} in psi

Equation (6.101) is for Rectangle section and neglects the effect of the nonprestresed compression and tension steel.

Lee *et al.* (1999)

Assuming $L_p = 0.5\,d_p$ and from moment equilibrium and global compatibility requirement *Lee et al.* (1999) suggested the following equation to calculate the unbonded steel stress

$$f_{ps} = 30{,}000 + 0.75 f_{se} + \frac{1}{12}\frac{(A'_s - A_s)f_y}{A_{ps}} + 82\sqrt{\frac{d_s}{d_p}\frac{f'_c}{\rho_p}\left(\frac{1}{f} + \frac{1}{L/d_p}\right)} \quad \text{psi}$$

$$\le f_{py} \quad or \quad f_{pe} + 10{,}000 \qquad (6.102)$$

ACI 318-1999

ACI-318 has suggested the following equation to determine stress in unbonded tendons depending on the span to depth ratio as approximate values.

- For a span-to- depth ratio of 35 or less

$$f_{ps} = f_{pe} + 70 + \frac{f'_c}{100\rho_p} \quad \leq f_{py} \quad \text{or} \quad (f_{pe} + 420) \quad \text{MPa} \qquad (6.103)$$

- For a span-to- depth ratio greater than 35

$$f_{ps} = f_{pe} + 70 + \frac{f'_c}{300\rho_p} \quad \leq f_{py} \quad \text{or} \quad (f_{pe} + 200) \quad \text{MPa} \qquad (6.104)$$

Where $\rho_p = \frac{A_{ps}}{bd}$ for T-section b = flange width = B

6.4.1.3 External unbonded tendons

The difference between the behaviour of externally prestressed beams and internally unbonded prestressed beams is mainly caused by the loss of tendon's eccentricity during loading namely "the second order effect".

Mutsuyoshi et al.(1995) observed from test results of internal and external unbonded beam with two deviators provided at different spacing that the reduction in flexural strength of beam with external tendons could be as high as 16% than that of internal beams. *Mutsuyoshi* stated that the second order effect should be taken into account, and hence introduced, as a result, the concept of depth reduction factor (R_d) that estimates the tendon eccentricity at ultimate. Based on parametric study and depending on Equation (6.85) proposed by *Naaman*, the following equation was proposed.

$$f_{ps} = f_{pe} + E_{ps}\Omega_u\varepsilon_{cu}\left(\frac{d_{pu}}{c} - 1\right) \qquad \leq f_{py} \qquad (6.105)$$

Where

$$\Omega_u = \frac{(1.47 + 10.3\frac{M_d}{L})}{(\frac{L}{d_e})} - 0.29(\frac{M_d}{L})(\frac{S_d}{L}) \qquad (6.106)$$

and the ultimate tendon position d_{pu} is given by

$$d_{pu} = R_d\, d_e$$

$$R_d = 1.0 - 0.022(\frac{L}{d_e} - 5)(\frac{S_d}{L} - 0.2) + 0.0186(\frac{L}{d_s})P_m \qquad (6.107)$$

$$P_m = \frac{A_S f_{sy}}{b d_s f'_c} \qquad (6.108)$$

Where

S_d = distance between deviators

Using a nonlinear analytical program *Aravinthan et al.* (1997) studied the effect of various factors (distance between deviators-to-span (S_d/L), loading span-to-span (L_p/L), span-to-effective prestressing depth (L/d_{ps}) bonded-to-total tendon area ratio ($A_{ps,int}/A_{ps,tot}$), prestressing steel ratio, reinforcing steel ratio) on the ultimate external tendon stress of simple prestressed beams strengthened using internal bonded and external unbonded tendons. Two equations were proposed to consider the effect of these factors on both the strain reduction coefficient Ω_u and the depth reduction factor (R_d) of the external tendon as follow

a) Strain reduction coefficient Ω_u

$$\Omega_u = \frac{0.21}{L/d_{ps}} + 0.04\left(\frac{A_{psi,\text{int}}}{A_{ps,tot}}\right) + 0.04 \qquad \text{for one-point loading} \qquad (6.109)$$

$$\Omega_u = \frac{2.31}{L/d_{ps}} + 0.21\left(\frac{A_{psi,\text{int}}}{A_{ps,tot}}\right) + 0.06 \qquad \text{for third-point loading} \qquad (6.110)$$

b) Depth reduction factor R_d

$$R_d = 1.14 - 0.005\left(\frac{L}{d_{ps}}\right) - 0.19\left(\frac{S_d}{L}\right) \quad \leq 1.0 \quad \text{for one-point loading} \quad (6.111)$$

$$R_d = 1.25 - 0.010\left(\frac{L}{d_{ps}}\right) - 0.38\left(\frac{S_d}{L}\right) \quad \leq 1.0 \quad \text{for two-point loading} \quad (6.112)$$

Then they concluded that

- The span-to-depth ratio was the most important factor influencing the ultimate tendon stress in the beam with external or unbonded tendons.
- The ultimate position of the external tendon is greatly influenced by the deviator distance-to-span ratio, thus affecting the ultimate flexural strength of such beams.

6.4.2 Analysis of internally-externally prestressed beams (test beams):

According to the writer's knowledge, there is no general equation from which the ultimate flexural strength of prestressed concrete beams, containing combination of internal bonded prestressing steel tendon and external unbonded prestressing FRP tendon can be calculated. So, in order to calculate the ultimate strength of such type of member from a simplified equation with a resonable accuracy, it is decided to use the former equations that used to calculate tendon stress at ultimate of both bonded and unbonded prestressing tendons after modification to be suitable for a mixture of steel and Parafil Rope as follows:

1. Stress of the internal prestressing tendons

From equations (6.76 and 6.77) steel stress can be calculated as a function in the neutral axis depth (c)

$$f_{ps} = f_{pu}(1 - k\frac{c}{d_{ps}}) \tag{6. 113}$$

$$k = 2(1.04 - \frac{f_{py}}{f_{pu}}) \tag{6. 114}$$

2. Stress of the external prestressing Parafil rope:

Equation (6.105) was modified to be suitable for Parafil rope as follows

$$f_{pp} = f_{pep} + E_{pp}\Omega_u\varepsilon_{cu}\left(\frac{d_{eu}}{c} - 1\right) \qquad \leq f_{ppy} \tag{6. 115}$$

Where

E_{pp} = Young's modulus of Parafil rope

$\varepsilon_{cu} = 0.0035$

$$\Omega_u = \frac{2.31}{L/d_e} + 0.21\left(\frac{A_{ps,\text{int}}}{A_{ps,tot}}\right) + 0.06 \qquad \text{for third-point loading} \tag{6. 116}$$

$$A_{ps.\text{int}} = A_{ps} + A_s\frac{f_{ys}}{f_{py}} \tag{6. 117}$$

$$A_{ps.tot} = A_{ps,\text{int}} + A_e \frac{E_{pp}}{E_{ps}} \tag{6.118}$$

$$R_d = 1.25 - 0.010\left(\frac{L}{d_e}\right) - 0.38\left(\frac{S_d}{L}\right) \qquad \leq 1.0 \quad \text{for two-point loading} \tag{6.119}$$

and f_{ys} and f_{py} are yield stress of non-prestressed steel and internal bonded prestressed steel respectively.

All test beams were analyzed using the previous suggested method. The sequence of the suggested method is shown in Figure (6.34), while a comparison between the actual and the analytical results is shown in Table (6.4) and Figure (6.35). From which it can be seen that:

- There is a good agreement between the actual and the analytical results, and the difference is less than 10%.

- The experimental results are higher than the analytical results except for beam PG32 that had the maximum (*e*/*h*). Therefore, using the suggested analytical method needs further investigation when used with eccentricity higher than the total beam height.

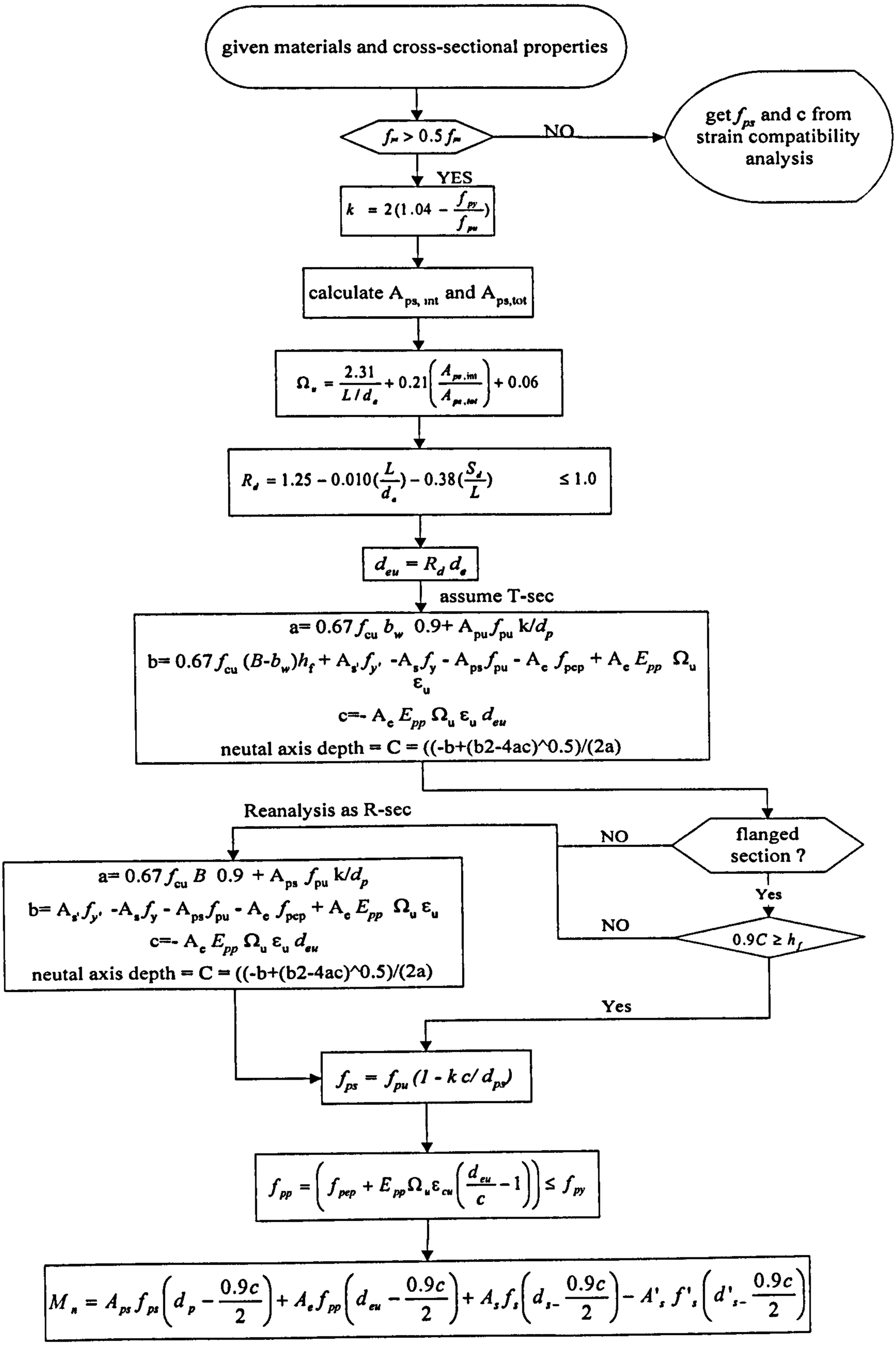

Figure (6. 34): Sequence of the suggested method

Table (6.4): *Actual and calculated ultimate moments.*

Beam no.	$M_{ult\ (act)}$	$M_{ult(theo)}$	$M_{ult(act)}/M_{ult(theo)}$
PG11	22.75	22.25	1.02
PG12	22.01	20.98	1.05
PG13	24.22	23.12	1.05
PG21*	19.46	19.55	1.00
PG31	24.74	24.23	1.02
PG32	27.68	28.86	0.96
PG41	22.62	21.95	1.03
PG42	21.50	21.38	1.01
PG51	21.67	21.05	1.03
PG52	24.52	23.89	1.03
PG61	21.6	20.52	1.05
PG62	22.95	22.53	1.02

* The ultimate moment of beam PG21 (one deviator at the middle) was calculated at the concentrated load (critical section) not at the middle.

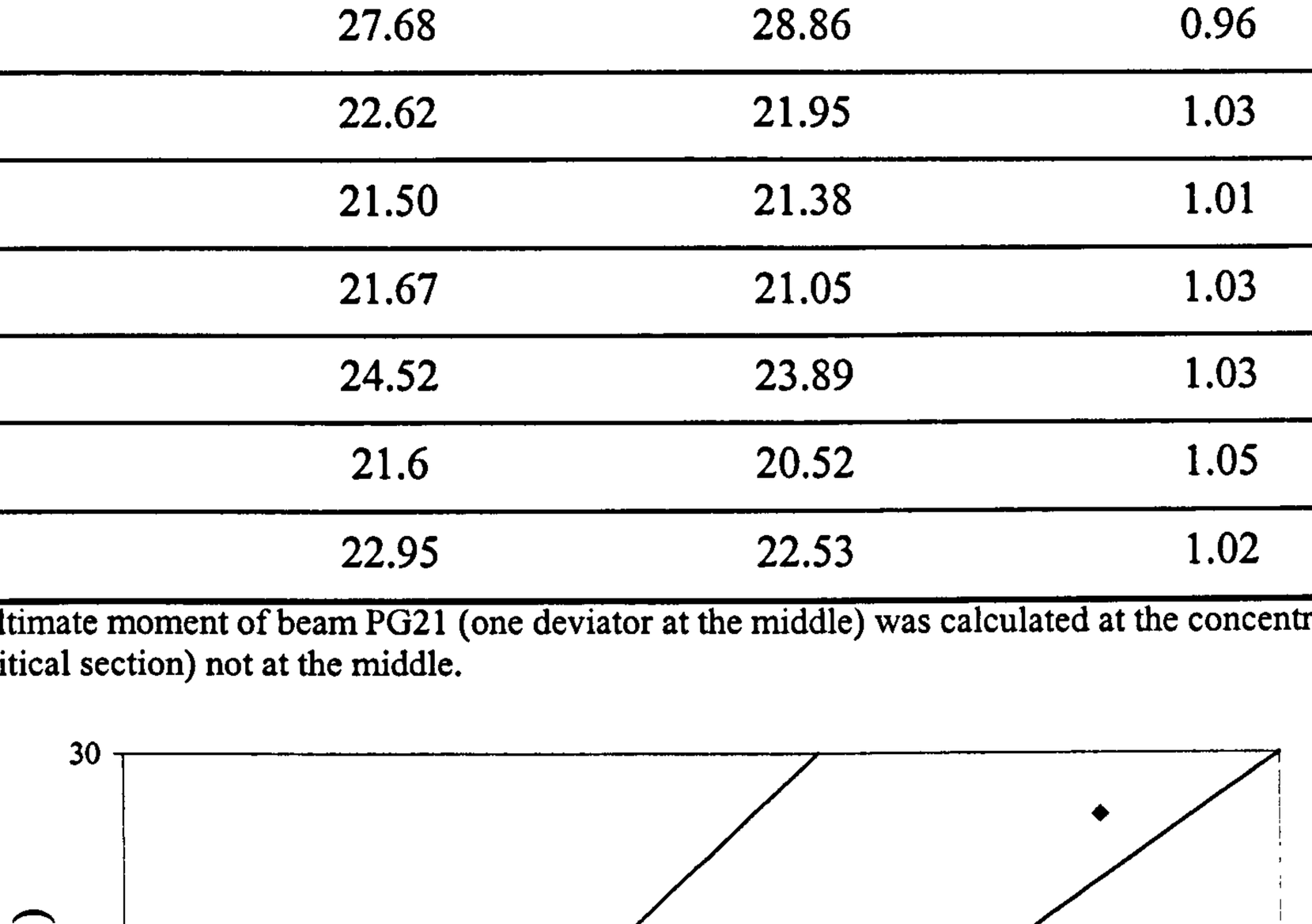

Figure (6.35): Relation between actual and theoretical nominal moment

Chapter 7

Conclusions and Future Work

7.1 INTRODUCTION

Many bridges in the world are classified as deficient and in need of rehabilitation or replacement. Some of them are deficient because their load-carrying capacity is inadequate for today's increased traffic load. To overcome this problem and increase their load capacity several methods can be used, one of them is the external prestressing. Also, to avoid the environmental attack and corrosion problem that faced this type of strengthening, Fibre Reinforced Plastics (FRP) can be used instead of steel tendons. Within the different types of FRP, Parafil Rope was established to be well suited for prestressing system, combining the benefits of light weight, high strength, easy handling and efficient anchorage system.

The benefit of using Parafil rope Type G as external prestressing tendons for strengthening or rehabilitation of prestressed concrete beams and the effect of several factors on the behaviour of prestressed concrete beams after externally strengthened were experimentally investigated. Thirteen prestressed beams, one with internal prestressing steel only, and the rest strengthened externally using Parafil Ropes Type G were tested up to failure. Six factors were studied to investigate their effect on the behaviour of strengthened beams. These factors are:

- Value of external prestressing force
- Number of deviators
- Effective depth of the external prestressing force
- Previous loaded stage before being externally strengthened
- Concrete strength (f_{cu})
- Effective span/depth ratio (L/h)

Also, analytical investigations were conducted to propose simple equations which could be used in the analysis of this beam type, regarding its deflection and flexural strength with an acceptable accuracy.

The main conclusions of study as well as suggestions for future work are presented in the following sections.

7.2 CONCLUSIONS:

Based on the results of the experimental and analytical investigations, the following conclusions are obtained:

7.2.1 General Conclusions

1) External prestressing using Parafil rope is a very powerful system for strengthening or rehabilitation of prestressed concrete structures, due to its light weight and flexibility, which make installation easy. Its corrosion resistance is also clearly highly beneficial.

2) Providing external prestressing force by a moderate amount improves the stiffness, and both cracking and ultimate flexural strength of prestressed concrete beams without a significant reduction in ductility even for cracked beams.

3) the camber of strengthened beams significantly increases as the eccentricity of the external prestressing force or (span/depth) ratio increases, and is slightly affected by an increase in the external prestressing force or in the concrete strength.

4) Although ductility is reduced in beams strengthened with external unbonded reinforcement, structural cracking gives ample warning of structural distress.

5) The error resulting from using the effective external prestressing force in flexural strength calculations during the uncracked stage can be neglected.

7.2.2 Effect of External Prestressing Force

1) The increase in the external prestressing force results in:

   - Reducing crack propagation
   - Improving stiffness after cracking and reducing deflection

2) Increase in the external prestressing force has a negligible effect on both stiffness and deflection before cracking while after cracking the increase in external prestressing force improves beam stiffness and reduces deflection (less ductile behaviour).

3) Increase in the external prestressing force can change the behaviour of strengthened beam at ultimate from ductile behaviour to brittle behaviour (beam acts as over-reinforced rather than under reinforced). Hence, the external prestressing force should be limited to avoid brittle failure.

4) The external prestressing force significantly increases both the cracking and ultimate moment compared to those before strengthening. However, the gain in the ultimate moment due to the increase in external prestressing force is relatively small.

5) The value of the initial external prestressing force has a negligible effect on the increase in external prestressing force at cracking, while at ultimate the rate of increase in the external prestressing force decreases as the initial prestressing force increases.

6) Losses of eccentricity of the external prestressing force significantly increases as the initial external prestressing force decreases.

7.2.3 Effect of Number of Deviators

1) Before cracking, deviator position has almost no effect on beam stiffness (ductility) while after cracking stiffness of beams strengthened using two

deviators at the third points of the span is higher than that strengthened using one deviator at the middle. Also, at ultimate it has more ductile failure.

2) The efficiency of using deviated tendon at mid span is controlled by the reduction in eccentricity of the external prestressing force at the concentrated load rather than at the mid span.

3) Because of the progressive reduction in the eccentricity of the tendons at the concentrated load when using one deviator at the mid span, external prestressing using a deviated profile at the middle was relatively less effective in increasing the flexural resistance than the deviated profile using two deviators at the third span.

4) Before cracking the position of the deviator has an effect on the increase of the rope load. But after cracking using two deviators at the third point of the span increases the external prestressing force at ultimate and hence increases the ultimate moment

7.2.4 Effect of Depth of The External Prestressing Force

1) Increasing the eccentricity of the external prestressing force results in:

   - Increasing shear resistance and reducing cracks propagation.
   - Higher stiffness after cracking.
   - Less ductile failure

2) Increasing eccentricity of the external prestressing force has a significant effect on both cracking and ultimate load; hence increasing the eccentricity of the prestressing force can be useful in cases where cracking is not allowed. Also, it can be considered as a main factor leading to increased beam strength.

3) The rope load after cracking is a function of the rope eccentricity and it increases as the eccentricity increases. However, the increase in eccentricity should be limited, otherwise the rope load could reach its maximum value with sudden fracture, though this did not happen in any of the tests reported here.

4) Increasing eccentricity of the external prestressing force reduces the loss in eccentricity of the external prestressing force at ultimate and enables the section to resist higher moments.

7.2.5 Previous Cracking Stage before Externally Strengthened

1) External prestressing can be used very effectively to control cracking and improve the service load deflections of cracked prestressed concrete beams, external prestressing was shown to:

   - Reduce the crack width or close the cracks completely
   - Lead to a stiffer service load – deflection response and hence, reduce the live load deflections.

2) After strengthening, the cracks completely closed and the full cross section can be used in deflection calculation whenever the bottom concrete stress is still in compression.

3) The cracking moment of pre-cracked beams after strengthening is significantly higher than before strengthening and can be calculated from the same equation used in bonded prestressed beams neglecting the concrete tensile strength.

4) The beam ductility decreases at failure as the ratio of pre-cracking increases.

5) The pre-cracked beam after strengthening can be analysed at ultimate in the same way as the uncracked strengthened beam if its internal reinforcement has not reached yield before strengthening.

6) The ultimate flexural strength after external prestressing is independent of the load history prior to strengthening, but depends mainly on the concrete strength and internal and external prestressing properties.

7) The degree of pre-loading and cracking reached before external prestressing has no effect on the increase in the external prestressing force in the uncracked and working stages, if the internal prestressing steel has not reached yield. However, the increase in the pre-cracking stage slightly decreases the increase in external prestressing force at ultimate.

7.2.6 Effect of Concrete Strength

1) The increase in concrete strength slightly increases beam stiffness and leads to less deflection in the uncracked and working stages, while at failure the beam with higher concrete strength has more ductile failure.

2) Increasing the concrete strength slightly increases cracking moment but significantly increases the ultimate moment.

3) Concrete strength has a slight effect on the increase in external prestressing force before cracking, while at ultimate, the increase in concrete strength can be considered as the main factor affects the increase of external prestressing force.

4) A beam with high concrete strength has a high loss in eccentricity at ultimate while the variation of concrete strength in the case of moderate strength has only a slight effect on the loss in eccentricity.

7.2.7 Span/ Depth Ratio:

1) The beam with a higher (L/h) ratio has lower stiffness in all loading stages.

2) Increasing (L/h) ratio increases deflection at cracking and significantly increases deflection at ultimate. Also, (L/h) can be considered the main factor affecting the deflection calculation, as would be expected.

3) Both the cracking and ultimate moments slightly decrease as the (L/h) ratio increases. However, the effect of the (L/h) ratio within the range taken in this investigation on the cracking and ultimate moments is small and less than 7%.

4) Between (span/depth) ratios (10-20) the increase in external prestressing force during loading is slightly affected by (span/depth) ratio.

5) The gain or loss in rope eccentricity increases as (L/h) ratio increases, slightly before cracking and highly at ultimate stage.

7.2.8 Analytical Investigation

7.2.8.1 Relation between external prestressing force and deflection

1) The relation between deflection and the external prestressing force can be presented by a bilinear relation, before and after cracking. Hence, all factors influencing the deflection have a similar effect on the external prestressing force.

2) The relation between deflection and external prestressing force at the working stage can be given from equation 5.2. This gave a good correlation between the actual and the theoretical increase in the external prestressing force.

3) The accuracy of equation 5.2 decreases as the eccentricity of the external prestressing force increases than about the section height (e/h>1.0). So, further research is needed to take the effect of the higher eccentricity (this equation is specific to the particular beam section used).

7.2.8.2 Analytical methods of deflection calculations

1) The suggested modifications for all the reviewed methods used in calculating deflection of bonded or unbonded prestressed concrete beams, to calculate the deflection of prestressed concrete beams containing both internal and external prestressing was found to give a fairly accurate results. This modification generalized these equations so that they may be used not only in bonded prestressed concrete (by putting A_e and P_{ex} = zero) or be used in the case of unbonded prestressed concrete (by using A_{ps} and P_{ei} = zero) but also when using FRP as external prestressing tendons.

2) The unbonded method suggested by *Branson & Trost* and the simple method suggested by *Shaikh and Branson* are less accurate than the other methods.

3) No significant improvement in accuracy was gained by using the inertia relative to the centroidal axis instead of relative to the neutral axis as suggested by *Harajli and Kanj*. So, using the later one will be less complicated and less time consumed without significant reduction in the accuracy.

4) Deflection calculated using *Harajli and Kanj's* method seems to be less than the actual deflection.

Bruggeling, C. J. (1988). Structural applications of type G Parafil. Symposium on Engineering applications of Parafil ropes. Burgoyne C. J. (editor). Department of civil engineering, Imperial college of science and technology. London, pp.39-47.

Burgoyne, C. J. Hobbs, R. E. & Strzemiecki, J. (1989). Tension bending and shear-bending fatigue of parallel lay ropes. Eighth International Congress on Offshore Mechanics and Arctic Engineering. The Hague, pp 691-698.

Burgoyne, C. J. (1993). Parafil ropes for prestressing tendons. In *Alternative materials for the reinforcement and prestressing of concrete*. Clarke, J. L. (editor). Blackie Academic & Professional. London, pp102-126.

Burgoyne, C. J. Campos, C. M. & Guimaraes, G. B. (1996). Behaviour of Beams with External Tendons. *FIP Symposium on Post-Tensioned Concrete Structures*, London, **2**, pp 865-871

Burgoyne, C. J. (1993). Should FRP be Bonded to Concrete!?. *International Symposium on Fiber-Reinforced-Plastic Reinforcement for Concrete Structures*. ACI SP-138. Nanni, A. & Dolan C. W. (editors), pp. 367-380.

Cairns, J. & Rafeeqi, F. (1997). Behaviour of reinforced concrete beams strengthened by external unbonded reinforcement. Construction and building materials, **11**(5-6), pp 309-317.

Chambers, J. J. (1988). Long term properties of Parafil. Symposium on Engineering applications of Parafil ropes. Burgoyne C. J. (editor). Department of civil engineering, Imperial college of science and technology. London, pp 21-27.

Chambers, J. J. (1986). Parallel-lay aramid ropes for use as tendons in prestressed concrete. PhD thesis. London university. UK.

Clark, L.A. & Toms, S. (1996). Shear strength of beam with unbonded or external tendons. *FIP Symposium on Post-Tensioned Concrete Structures*, London, **2**, pp 796-803.

Clements, L. L. (1998). Organic fibers. In *Hand book of composites*. Peters, S. T. (editor). Chapman & Hall. London. 2nd edition, pp 202-241.

Crasto, A. S. Kim, R. Y. & Mistretta, J. P. (1996). Rehabilitation of concrete bridge beams with externally-bonded composites plates. Part II. *Proceedings of 41st International SAMPE Symposium. and Exhibition*. G. Schmitt et al., (editors), pp. 1269–1279. (Bonacci, J. F. & Maalej M. (2000). Externally bonded FRP for service-life extension of RC infrastructure. *Journal of infrastructure systems*. **6** (1), pp. 41-51.

Dolan, C. W. (1990). Developments in non-metallic prestressing tendons. *PCI Journal*, **35**(5), pp 80-88.

Dolan, C. W. (1993). FRP development in the United States. In *Fiber-Reinforced-Plastic (FRP) Reinforcement for Concrete Structures: Properties and Applications,*

Nanni, A. (editor). Elsevier publishers B.V. pp 129-163.

DU PONT (1981). Characteristics and uses of kevlar 49 aramid high modulus organic fibre, Bulletin NO. K-5, September, 12pp. (Guimaraes, G. B. (1988). Short term propeerties of Parafil. *Symposium on Engineering applications of Parafil ropes*. Burgoyne, C. J. (editor), Department of civil engineering, Imperial college of science and technology. London, pp 13-19).

Eibl J. (1990). Externally Prestressed Bridges. In *External Prestressing in Bridges*. American Concrete Institute SP-120. Naaman, A. & Breen, J. (editors). Detroit, MI, USA pp 375-388.

Ehsani M. R. (1993). Glass-fiber reinforcing bars. In *Alternative materials for the reinforcement and prestressing of concrete*. Clarke. J. L. Blackie Academic & Professional. London, pp 34-54.

Ehsani, M. R. Saadatmanesh, H. & Tao, S. (1993). Bond of GFRP Rebars to Ordinary-Strength Concrete. *International Symposium on Fiber-Reinforced-Plastic Reinforcement for Concrete Structures*. ACI SP-138. Nanni, A. & Dolan C. W. (editors), pp 333-345.

Ehsani, M. R. Saadatmanesh, H. & Nelson, C. (1997). Transfer and flexural bond performance of aramid and carbon FRP tendons. *PCI Journal*, **42**(1), pp 76-86.

Elzanaty, A. & Nilson, A. (1982). Flexural behavior of unbonded post-tensioned partially prestressed concrete beams. Research report No.82-15. Cornell University, Department of Structural Engineering, New York, pp. 1-106.

Erki, M. A. Rrizkalla, S. H. (1993). A sample of the international production, FRP Reinforcement for concrete structures. *Concrete international*, **15**(6), pp 48-53.

Farkas, G. Akasha, A. M. (1998). Laboratory testing of post tensioned reinforced concrete beams. Proceedings of the XIII the FIP Congress on Challenges for concrete in the next millennium. Amsterdam, Netherlands. 23-29 May, **2**, pp 537-538.

Faza, S. S. & GangaRao, H. V. S. (1993). Glass FRP reinforcing bars for concrete. In *Fiber-Reinforced-Plastic (FRP) Reinforcement for Concrete Structures: Properties and Applications,* Nanni, A. (editor). Elsevier publishers B.V, pp. 167-188.

Gerritse A. (1993) Aramid-based prestressing tendons. In *Alternative materials for the reinforcement and prestressing of concrete*. Clarke. J.L. Blackie Academic & Professional. London, pp172-201.

Ghali, A. & Favre, R. (1994). Concrete structures stresses and deformations. 2nd edition, E & FN Spon. London.

Guimaraes, G. B. (1988). Short term properties of Parafil. Symposium on Engineering applications of Parafil ropes. Burgoyne C. J. (editor). Department of civil engineering, Imperial college of science and technology. London, pp 13-19.

PAGE NUMBERING AS ORIGINAL

REFRENCES

Abdalla, H. A. & Elbadry, M. M. (1997). Temperature effect on concrete members reinforced with FRP reinforcement. *Proceeding of Annual Conference of Canadian Society of Civil Engineering*. Sherbrooke,27-30 May, 6, pp. 171-180.

Abeles, P. W. Bardhan-Roy, B. K. & Turner F. H. (1976). Prestressed concrete designer's handbook. 2nd edition. Cement and Concrete Association, Slough, UK.

ACI 318 (1999). Building Code Requirements for Structural Concrete and Commentary. American concrete institute, Michigan, USA.

Alsayed, S., Al-Salloum, Y. & Almusallam, T. (2000) .Fibre-reinforced polymer repair materials—some facts.. *Civil Engineering,* **138**(8), pp131-134

Aravinthan, T. Mutsuyoshi, H., Fujioka & A. Hishiki Y. (1997). Prediction of the Ultimate Flexural Strength of Externally Prestressed PC Beams. *Transactions of the Japan Concrete Institute*, **19**, pp 225-230

Arnold, C. A. Hergenrother, P. M. & Mcgrath, J. E. (1991). An overviwe of organic polymeric matrix resins for composites. In *Composite application: The role of matrix, fiber, and interface*. Vigo, T. L. & Kinzig, B. J (Editors). New York Cambridge, VCH, pp 3-30.

Badie, S. & Tadros, M. (1999). Flexural strength according to AASHTO LRFD Specifications. *PCI Journal*, **44**(4), pp.122-127.

Bank, L. C. Puterman, M. & Katz, A. (1998). Effect of material degradation on bond properties of fiber reinforced plastic reinforcing bars in concrete. *ACI Materials Journal*, **95** (3), pp 232-243.

Bakht, B. Al-Bazi, G. Banthia, N. Cheung, M. Erki, M. Faoro, M. Machida, A. Mufti, A. Neale, K. & Tadros, G. (2000). Canadian bridge design code provisions for fiber-reinforced structures. *Journal of Composites for Construction*, **4**(1), pp3-15.

Bakis, C. E. (1993). FRP Reinforcement: Materials and Manufacturing. In *Fiber-Reinforced-plastic (FRP) Reinforcement for Concrete Structures: Properties and Applications*. Nanni, A. (editor). Elsevier publishers B.V., pp 13-57.

Bardhan-Roy, B. K. (1982). Fire resistance-design and detailing. In *Handbook of structural concrete*. Kong, F. K. Evans, R. H. Cohen & E. Roll F. (editors). Pitman. London, p.16.

BBR Systems Ltd. (2001). Prestressing products. http://www.bbrsystems.ch/. (visited 22/1/01 and 23/3/01)

BD 58/94 (1995). The design of concrete highway bridges and structures with external unbonded prestressing. In *Design manual for roads and bridges*. **1**, section 3, part 9. Highways agency. HMSO. London, 10pp.

Beeby, A.W. (1979). Cracking and Corrosion. Concrete in the oceans Technical Report 1, CIRIA/UEG.

Benmokrane, B. Zhang, B. Chennouf, A. & Masmoudi, R. (2000). Evaluation of aramid and carbon fibre reinforced polymer composite tendons for prestressed ground anchors. *Canadian Journal of Civil Engineering*, **27**(5), pp 1031-1045.

Benmokrane, B. Chaallal, O. & Masmoudi, R. (1995). Glass fibre reinforced plastic (GFRP) rebars for concrete structures. *Construction and Building Materials*, 9(6), pp. 353-364

Bennett, E. W. (1973). Structural Concrete Elements. Chapman and Hall Ltd., London, pp. 1-3

Branson, D. E. (1977). Deformation of concrete structures. McGraw-Hill. New York London.

Branson, D. E. & Trost, H. (1982). Unified procedures for predicting the deflection and centroidal axis location of partially cracked nonprestressed and prestressed concrete members. *ACI Journal*, **79**(2), pp 119-130.

Branson, D. E. & Trost, H. (1982). Application of the I-effective method in calculating deflections of partially prestressed members. *PCI Journal*, **27**(5), pp 62-77.

Branson, D. E. & Shaikh, A. F. (1985). Deflection of partially prestressed members. In Deflections of Concrete Structures. SP–86. American Concrete Institute. Detroit, MI, USA pp. 323-363

British Standards Institution (1983). BS 1881:1983. Testing concrete—Part 108: Method for making test cubes from fresh concrete. BSI, London, UK.

British Standards Institution (1985). BS8110 Structural use of concrete, Part 2: Code of practice for special circumstances. BSI, London, UK.

British Standards Institution (1992). DD-ENV 1992-1-1 Eurocode 2, Design of concrete structures, Part 1: General rules and rules for buildings. BSI London, UK.

British Standards Institution (1997). BS8110 Structural use of concrete, Part 1: Code of practice for design and construction. BSI, London. UK.

Bruggeling, A. S. G. (1990). External Prestressing – a state of the art. In *External Prestressing in Bridges*. American Concrete Institute SP-120. Naaman, A. & Breen, J. (editors). Detroit, MI, USA, pp 61-81.

Bruggeling, C. J. (1988). Structural applications of type G Parafil. Symposium on Engineering applications of Parafil ropes. Burgoyne C. J. (editor). Department of civil engineering, Imperial college of science and technology. London, pp.39-47.

Burgoyne, C. J. Hobbs, R. E. & Strzemiecki, J. (1989). Tension bending and shear-bending fatigue of parallel lay ropes. Eighth International Congress on Offshore Mechanics and Arctic Engineering. The Hague, pp 691-698.

Burgoyne, C. J. (1993). Parafil ropes for prestressing tendons. In *Alternative materials for the reinforcement and prestressing of concrete*. Clarke, J. L. (editor). Blackie Academic & Professional. London, pp102-126.

Burgoyne, C. J. Campos, C. M. & Guimaraes, G. B. (1996). Behaviour of Beams with External Tendons. *FIP Symposium on Post-Tensioned Concrete Structures*, London, **2**, pp 865-871

Burgoyne, C. J. (1993). Should FRP be Bonded to Concrete!?. *International Symposium on Fiber-Reinforced-Plastic Reinforcement for Concrete Structures*. ACI SP-138. Nanni, A. & Dolan C. W. (editors), pp. 367-380.

Cairns, J. & Rafeeqi, F. (1997). Behaviour of reinforced concrete beams strengthened by external unbonded reinforcement. Construction and building materials, **11**(5-6), pp 309-317.

Chambers, J. J. (1988). Long term properties of Parafil. Symposium on Engineering applications of Parafil ropes. Burgoyne C. J. (editor). Department of civil engineering, Imperial college of science and technology. London, pp 21-27.

Chambers, J. J. (1986). Parallel-lay aramid ropes for use as tendons in prestressed concrete. PhD thesis. London university. UK.

Clark, L.A. & Toms, S. (1996). Shear strength of beam with unbonded or external tendons. *FIP Symposium on Post-Tensioned Concrete Structures*, London, **2**, pp 796-803.

Clements, L. L. (1998). Organic fibers. In *Hand book of composites*. Peters, S. T. (editor). Chapman & Hall. London. 2nd edition, pp 202-241.

Crasto, A. S. Kim, R. Y. & Mistretta, J. P. (1996). Rehabilitation of concrete bridge beams with externally-bonded composites plates. Part II. *Proceedings of 41st International SAMPE Symposium. and Exhibitio*n. G. Schmitt et al., (editors), pp. 1269–1279. (Bonacci, J. F. & Maalej M. (2000). Externally bonded FRP for service-life extension of RC infrastructure. *Journal of infrastructure systems*. **6** (1), pp. 41-51.

Dolan, C. W. (1990). Developments in non-metallic prestressing tendons. *PCI Journal*, **35**(5), pp 80-88.

Dolan, C. W. (1993). FRP development in the United States. In *Fiber-Reinforced-Plastic (FRP) Reinforcement for Concrete Structures: Properties and Applications,*

Nanni, A. (editor). Elsevier publishers B.V. pp 129-163.

DU PONT (1981). Characteristics and uses of kevlar 49 aramid high modulus organic fibre, Bulletin NO. K-5, September, 12pp. (Guimaraes, G. B. (1988). Short term propeerties of Parafil. *Symposium on Engineering applications of Parafil ropes*. Burgoyne, C. J. (editor), Department of civil engineering, Imperial college of science and technology. London, pp 13-19).

Eibl J. (1990). Externally Prestressed Bridges. In *External Prestressing in Bridges*. American Concrete Institute SP-120. Naaman, A. & Breen, J. (editors). Detroit, MI, USA pp 375-388.

Ehsani M. R. (1993). Glass-fiber reinforcing bars. In *Alternative materials for the reinforcement and prestressing of concrete*. Clarke. J. L. Blackie Academic & Professional. London, pp 34-54.

Ehsani, M. R. Saadatmanesh, H. & Tao, S. (1993). Bond of GFRP Rebars to Ordinary-Strength Concrete. *International Symposium on Fiber-Reinforced-Plastic Reinforcement for Concrete Structures*. ACI SP-138. Nanni, A. & Dolan C. W. (editors), pp 333-345.

Ehsani, M. R. Saadatmanesh, H. & Nelson, C. (1997). Transfer and flexural bond performance of aramid and carbon FRP tendons. *PCI Journal*, **42**(1), pp 76-86.

Elzanaty, A. & Nilson, A. (1982). Flexural behavior of unbonded post-tensioned partially prestressed concrete beams. Research report No.82-15. Cornell University, Department of Structural Engineering, New York, pp. 1-106.

Erki, M. A. Rrizkalla, S. H. (1993). A sample of the international production, FRP Reinforcement for concrete structures. *Concrete international*, **15**(6), pp 48-53.

Farkas, G. Akasha, A. M. (1998). Laboratory testing of post tensioned reinforced concrete beams. Proceedings of the XIII the FIP Congress on Challenges for concrete in the next millennium. Amsterdam, Netherlands. 23-29 May, **2**, pp 537-538.

Faza, S. S. & GangaRao, H. V. S. (1993). Glass FRP reinforcing bars for concrete. In *Fiber-Reinforced-Plastic (FRP) Reinforcement for Concrete Structures: Properties and Applications,* Nanni, A. (editor). Elsevier publishers B.V, pp. 167-188.

Gerritse A. (1993) Aramid-based prestressing tendons. In *Alternative materials for the reinforcement and prestressing of concrete*. Clarke. J.L. Blackie Academic & Professional. London, pp172-201.

Ghali, A. & Favre, R. (1994). Concrete structures stresses and deformations. 2nd edition, E & FN Spon. London.

Guimaraes, G. B. (1988). Short term properties of Parafil. Symposium on Engineering applications of Parafil ropes. Burgoyne C. J. (editor). Department of civil engineering, Imperial college of science and technology. London, pp 13-19.

Guimaraes, G. B. & Burgoyne, C. J. (1992). Creep behaviour of a parallel-lay aramid rope. *Journal of materials science*, **27**, pp 2473-2489.

Harajli, M. H. & Alameh, A. S. (1989). Deflection of progressively cracking partially prestressed concrete flexural members. *PCI journal*, **34**(3), pp. 94-127.

Harajli, M. H. (1990). Effect of span-deth ratio on the ultimate steel stress in unbonded prestressed concrete members. *ACI structural journal*, **87**(3), pp 305-312.

Harajli, M. H. & Kanj, M. Y. (1992). Service load behavior of concrete members prestressed with unbonded tendons. *Journal of structural engineering*, **118**(9), pp. 2569-2589.

Harajli M. H. (1993). Strengthening of Concrete Beams by External Prestressing. *PCI journal*, **38**(6), pp 76-86.

Harajli, M. Khairallah, N. & Nassif, H. (1999). Externally Prestressed Members: Evaluation of Second-Order Effects. *Journal of Structural Engineering*, **125**(10), pp. 1151-1161.

Hollaway, L. (1993). Polymer composites for civil and structural engineering. Blackie Academic & Professional. London, pp.131-146.

Hutchinson, A. R. & Rahimi, H. (1996). Flexural strengthening of concrete beams with externally-bonded FRP reinforcement. *Proceeding of Advanced Composites Materials in Bridges and Structures*. El-Badry, M. (editor). Canadian Society for Civil Engineering, Montreal, pp. 519– 526.

ISIS Canada- Project 4.4 (1997). An Innovative Anchorage System for FRP Tendons. http://www.eng.ucalgary.ca/Civil/ISIS/isis_res2.html. November. (Visited 7/3/2001).

Issa, M. A. Sen, R. & Amer, A. (1993). Comparative study of transfer length in fiberglass and steel pretensioned concrete members. *PCI Journal*, **38**(6), pp. 52-63.

Jackson, P. (1996). Criteria for external and unbonded post-tensioning in design and strengthening. *FIP Symposium on Post-Tensioned Concrete Structures*, London, **2**, pp 865-871

Jang B. Z. (1994). Advanced Polymer Composites. ASM International. Materials Park, OH, pp12-13.

Jerrett, C. V. & Ahmad, S. H. (1996). Behavior of prestressed concrete beams strengthened by external FRP post-tensioned tendons. In *Proceeding of Advanced Composites Materials in Bridges and Structures*. El-Badry, M. (editor). Canadian Society for Civil Engineering, Montreal, pp. 305-312.

Karbhari, V. M. (1998). Use of composite materials in civil infrastructure in japan. International technology research institute. World technology (WTEC) division.

http://www.itri.loyola.edu/compce/toc.htm. (visited 2/2/01,3/4/01)

Katz, A. Berman, N. & Bank L. (1999). Effect of high temperature on bond strength of FRP rebars. *Journal of Composites for Constructio,* 3(2), pp 73-81.

Katz, A. (2000). Bond to Concrete of FRP Rebars after Cyclic Loading. *Journal of Composites for Construction,* 4(3), pp 137-144.

Khalifa, M. Kuska, S. B. & Krieger, J. (1993). Bridges constructed using fiber reinforced plastics. *Concrete international*, **15**(6), pp 43-47.

Kim, D. H. (1995). Composite Structures for Civil and Architectural Engineering. E. & F.N. Spon. London, pp.1-61.

Kingston, D. (1988). Development of parallel fibre tensile members. *Symposium on Engineering applications of Parafil ropes*. Burgoyne C. J. (editor). Department of civil engineering, Imperial college of science and technology. London, pp. 9-10.

Kondo, E. Mutsuyoshi, H. Takahashi, H. & Sano, M. (1994). Influence of External Prestressing Force on Shear Strength of PC Beams. *Transactions of the Japan Concrete Institute*, **16**, pp 395-402.

Lafdi, K. 7 Wright, M. (1998). Carbon fibers. In *Hand book of composites*. Peters S. T. (editor). Chapman & Hall. London. 2nd edition, pp. 169-201.

Lee, L. Moon, J. & Lim, J. (1999). Proposed Methodology for Computing of Unbonded Tendon Stress at Flexural Failure. *ACI Structural Journal*, **96**(6), pp. 1040-1048.

Linear Composite Limited (2000). Parafil ropes: Technical Note PF1. Issue **1**.UK.

Loov, R. (1988). A general equation for the steel stress for bonded prestressed concrete members. *PCI Journal*, **33**(6), pp 108-137.

MacGregor, J. G. Sozen, M. A. & Siess, C. P. (1960). Effect of draped reinforcement on behaviour of prestressed concrete beams. *ACI Journal*, **57**(6) pp 649-677.

Manjure, P. Y. (1996). Use of External Prestressing Technique - An Indian Experience. *FIP Symposium on Post-Tensioned Concrete Structures*. London, **2**, pp. 885-892.

Maruyama, T. & Honma, M. (1993). Experimental study on tensile strength of bent portion of FRP rods. *International Symposium on Fiber-Reinforced-Plastic Reinforcement for Concrete Structures*. ACI SP-138. Nanni, A. & Dolan, C. W. (editors), pp.163-176.

Matupayont, S. Tsuchida, K. Mutsuyoshi, H. & Machida, A. (1994). Loss of tendon's eccentricity in externally prestressed concrete beam. *Transactions of the Japan Concrete Institute*, **16**, pp. 403-410.

McKenna, C. J. & Chan, K. M. (1996). Externally post tensioned bridges route 3 country park section-hong kong. *FIP Symposium on Post-Tensioned Concrete Structures*, London, **2**, pp. 828-835.

Meier, U. (2000). Composite Materials in Bridge Repair. *Applied Composite Materials,* **7** (2), pp75–94.

Minosaku, K. (1991). Using FRP materials in prestressed concrete structures. *Concrete International*, **14**(8), pp 41-44.

Mochizuki, S. Matsuzzaki, Y. & Sugita, M. (1993). Evaluation Items and Methods of FRP Reinforcement as Structural Elements. *International Symposium on Fiber-Reinforced-Plastic Reinforcement for Concrete Structures*. ACI SP-138. Nanni, A. & Dolan, C. W. (editors), pp.117-131.

Mutsuyoshi, H. Tsuchida, K. Matupayont, S. & Machida, A. (1995). Flexural Behavior and Proposal of design Equation for Flexural Strength of Externally PC Members. *Proceedings of JSCE*, **26**(508), pp 67-77 (in Japanise).

Naaman, A. E. (1985). Partially prestressed concrete: Review and recommendations. *PCI Journal,* **30**(6), pp31-71.

Naaman, A. E. & Harajli, M. H. (1985). Evaluation of the ultimate steel stress in partially prestressed flexural members. *PCI Journal*, **30**(5), pp 54-81.

Naaman, A. E. (1990). New Methodology for the Analysis of beams Prestressed with External or unbonded Tendons. In *External Prestressing in Bridges*. American Concrete Institute SP-120. Naaman, A. & Breen, J. (editors). Detroit, MI, USA pp. 339-354.

Naaman, A. E. & Alkhairi, F. M. (1991). Stress at ultimate in unbonded post-tensioning Tendons: Part 1- Evaluation of the state-of-the-art. *ACI Structural Journal*, **88**(5), pp.641-651.

Naaman, A. E. & Alkhairi F. M. (1991). Stress at ultimate in unbonded post-tensioning Tendons: Part 2- Proposed Methodology. *ACI Structural Journal*, **88**(6), pp.683-692.

Naaman, A. E. (1992). Unified design recommendations for reinforced, prestressed, and partially prestressed concrete bending and compression members. *ACI Structural Journal*, **89**(2), pp 200-210.

Naaman, A. E. (1995). Unified bending strength design of concrete members: AASHTO LRFD code. *Journal of Structural Engineering*, **121**(6), pp 964-970.

Naani, A. Bakis, C. E. O'Neil, E. F. & Dixon, T. O. (1996). Performance of FRP tendon-anchor systems for prestressed concrete structures. *PCI Journal*, **41**(1), pp 34-43.

Pannell, F. N. (1969) .The ultimate moment of resistance of unbonded prestressed concrete beams. *Magazine of concrete research*, **21**(66), pp43-54.

Pannell, F. N. & Tam, A. (1976). The ultimate moment of resistance of unbonded partially prestressed reinforced concrete beams. *Magazine of concrete research*, **28** (97), pp 203-208.

Pendyala, R. Mendis, P. & Patnaikuni, I. (1996). Full-range behavior of high-strength concrete flexural members: comparison of ductility parameters of high and normal-strength concrete members. *ACI Structural Journal*, **93**(1), pp30-35.

Rahimi, H. & Hutchinson, A. (2001). Concrete Beams Strengthened with Externally Bonded FRP Plates. *Journal of Composites for Construction,* **5**(1), pp 44-56.

Rizkalla, S. and Labossiere, P. (1999). Structural engineering with FRP-in Canada. Concrete International, **21**(10), pp25-28.

Rostasy, F. S. (1993). FRP Tensile Elements for Prestressed Concrete- State of the Art, Potentials and Limits. *International Symposium on Fiber-Reinforced-Plastic Reinforcement for Concrete Structures*. ACI SP-138. Nanni, A. & Dolan, C. W. (editors), pp.347-365

Rowe, R. E. Somerville, G. Beeby, A. W. Menzies J. B. Forrest J. C. M. Harrison T. A. Moore J. F. A. Newman K. Taylor H. P. J. Threlfall A. J. and Whittle R. (1987). Handbook to British Standard BS 8110: 1985 Structural use of concrete. Palladian Publications, London, pp. 83-109.

Saadatmanesh, H. & Tannous, F. E. (1999). Long-term behavior of aramid fiber reinforced plastic (AFRP) tendons. *ACI Materials Journal*, **96**(3), pp 297-305.

Saeki, N. Horiguchi, T. & Ikeda T. (1993). Strengthening of damaged concrete beams by external prestressing of aramid fiber cable. *International Symposium on Fiber-Reinforced-Plastic Reinforcement for Concrete Structures*. ACI SP-138. Nanni, A. & Dolan, C. W. (editors), pp. 913-932.

Saito, J. & Yaginuma, Y. (1998). Ultimate strengths of PC precast block beams with external and internal cables. *Transactions of the Japan Concrete Institute*, **20**, pp 179-186.

Skogman, B. C. Tadros, M. K. & Grasmick, R. (1988). Ductility of reinforced and prestressed concrete flexural members. *PCI Journal*. **33**(6), pp. 94-107.

Shaikh, A. F. & Branson, D. E. (1970). Non-tensioned steel in prestressed concrete beams. *PCI Journal*, **15**(1), pp 14 –36.

Skogman, B. C. Tadros, M. K. & Grasmick, R. (1988). Flexural strength of prestressed concrete members. *PCI Journal*, **33**(5), pp.96-123.

Songkiat, M. Hiroshi, M. Kazuteru, T. & Atsuhiko, M. (1994). Loss of Tendon's Eccentricity in Externally Prestressed Concrete Beam. *Transactions of the Japan Concrete Institute*.**16**, pp. 403-410.

Tadros, M. K. & Sulieman, H. (1983). Comments on Application of the I-effective method in calculating deflections of partially prestressed members. by Branson D. E. and Trost H. (1982). *PCI Journal*, **28**(6), pp.131-136.

Tadros, M. K. Ghali, A. & Meyer, A. W. (1985). Prestresses loss and deflection of precast concrete members. *PCI Journal*, **30**(1), pp.114-136.

Taerwe, L. R. (1993). FRP Developments and applications in Europe. *International Symposium on Fiber-Reinforced-Plastic Reinforcement for Concrete Structures*. ACI SP-138. Nanni, A. & Dolan, C. W. (editors), pp.99-114.

Taerwe, L. R and Matthys, s. (1999). FRP for concrete construction. Concrete International, **21**(10), pp33-36.

Takewaka, K. & Khin, M. (1996). Deterioration and stress- rupture of FRP rods in alkaline solution simulating as concrete enviroment.. *Proceeding of Advanced Composites Materials in Bridges and Structures*. El-Badry, M. (editor). Canadian Society for Civil Engineering, Montreal, pp. 649-656.

Tan, K. & Ng, C. (1997). Effects of Deviators and Tendons Configuration on Behaviour of Externally Prestressed Beams. *ACI Structural Journal*, **94**(1), pp. 13-22.

Tighiouart, B. Benmokrane, B. & Gao, D. (1998). Investigation of bond in concrete member with fibre reinforced polymer (FRP) bars. *Construction and Building Materials*, **12**(8), pp. 453-462.

Uomoto, T. & Ohga, H. (1996). Performance of fiber reinforced plastics for concrete reinforcement. *Proceeding of Advanced Composites Materials in Bridges and Structures*. El-Badry, M. (editor). Canadian Society for Civil Engineering, Montreal, pp. 125-132.

Vaughan, D. J. (1998). Fiberglass reinforcement. In *Hand book of composites*. Peters S. T. (editor). Chapman & Hall. London. 2nd edition, pp. 131-155.

Vejvoda, M. F. (1992). Strengthening of existing structures with post-tensioning. *Concrete international*, **14**(9), pp 38-43.

Virlogeux, M. P. (1993). External prestressing: from construction history to modern technique and technology. *International Symposium on Fiber-Reinforced-Plastic Reinforcement for Concrete Structures*. ACI SP-138. Nanni, A. & Dolan, C. W. (editors), pp.1-59.

Whitaker, A. F. Finckenor, M. M. Dursch, H. W. Tennyson, R. C. & Young, P. R. (1998). Environmental effects on composites. . In *Hand book of composites*. Peters S. T. (editor). Chapman & Hall. London. 2nd edition, pp. 810-821.

Whiteway, P. (2000). Building a better bridge. American Metal Market. April 11. http://www.findarticles.com/cf_0/m3MKT/69_108/61643345/p1/article.jhtml?term=building+better+bridges. (Visited 29/3/01).

Wolff, R. & Miesseler, H. J. (1993). Glass-fibre Prestressing system. In *Alternative materials for the reinforcement and prestressing of concrete.* Clarke, J. L. (editor). Blackie Academic & Professional. London, pp.127-150

Yaginuma, Y. & Kitada, Y. (1988). Influence of Span on behaviour of partially prestressed concrete beams with exterior cables. *Transactions of the Japan Concrete Institute*, **10**, pp 409-416.

Yaginuma, Y. (1994). Flexural Behaviour of PRC Beam with both External and Internal Cables. *Transactions of the Japan Concrete Institute*. **16**, pp387-394.